

UNCLASSIFIED

AD NUMBER

AD348937

CLASSIFICATION CHANGES

TO: unclassified

FROM: confidential

LIMITATION CHANGES

TO:  
Approved for public release, distribution  
unlimited

FROM:  
Distribution authorized to U.S. Gov't.  
agencies and their contractors;  
Administrative/Operational Use; Nov 1963.  
Other requests shall be referred to Air  
Force Aero Propulsion Lab.,  
Wright-Patterson AFB, OH.

AUTHORITY

31 Dec 1972, GDS, DoD 5200.1-r per doc  
markings; AFWAL ltr, 9 Jun 1976

THIS PAGE IS UNCLASSIFIED

UNCLASSIFIED

AD NUMBER
AD348937
CLASSIFICATION CHANGES
TO
confidential
FROM
secret
AUTHORITY
31 Dec 1969, GDS, DoD 5200.1-r per doc markings

THIS PAGE IS UNCLASSIFIED

# GENERAL DECLASSIFICATION SCHEDULE

IN ACCORDANCE WITH  
DOD 5200.1-R & EXECUTIVE ORDER 11652

## THIS DOCUMENT IS:

CLASSIFIED BY \_\_\_\_\_

Subject to General Declassification Schedule of

Executive Order 11652-Automatically Downgraded at

2 Years Intervals- DECLASSIFIED ON DECEMBER 31, 1969

BY

1972

Defense Documentation Center

Defense Supply Agency

Cameron Station

Alexandria, Virginia 22314

UNCLASSIFIED

AD 348937

DEFENSE DOCUMENTATION CENTER

FOR

SCIENTIFIC AND TECHNICAL INFORMATION

CAMERON STATION, ALEXANDRIA, VIRGINIA



UNCLASSIFIED



NOTICE: When government or other drawings, specifications or other data are used for any purpose other than in connection with a definitely related government procurement operation, the U. S. Government thereby incurs no responsibility, nor any obligation whatsoever; and the fact that the Government may have formulated, furnished, or in any way supplied the said drawings, specifications, or other data is not to be regarded by implication or otherwise as in any manner licensing the holder or any other person or corporation, or conveying any rights or permission to manufacture, use or sell any patented invention that may in any way be related thereto.

NOTICE:

THIS DOCUMENT CONTAINS INFORMATION  
AFFECTING THE NATIONAL DEFENSE OF  
THE UNITED STATES WITHIN THE MEAN-  
ING OF THE ESPIONAGE LAWS, TITLE 18,  
U.S.C., SECTIONS 793 and 794. THE  
TRANSMISSION OR THE REVELATION OF  
ITS CONTENTS IN ANY MANNER TO AN  
UNAUTHORIZED PERSON IS PROHIBITED  
BY LAW.

SECRET

ASD-TDR-63-665, Part I

(Unclassified Title)

FEASIBILITY STUDY OF A HIGH CAPACITY DISTILLATION SEPARATOR  
FOR AN AIR ENRICHMENT SYSTEM  
(Experimental and Analytical Program)

TECHNICAL DOCUMENTARY REPORT ASD-TDR-63-665

November, 1963

AIR FORCE AERO PROPULSION LABORATORY  
Research and Technology Division  
Air Force Systems Command  
Wright-Patterson Air Force Base, Ohio

PROJECT NO. 3084, TASK NO. 308403

Downgraded at 3 year Intervals  
Declassified after 12 years  
DOD DIR 5200.10

(Prepared under Contract No. AF 33(657)-8722  
by Union Carbide Corporation, Linde Division  
Cryogenic Development Laboratory  
Tonawanda, New York)

63 ASRP-2391

SECRET

348937

## NOTICES

When Government drawings, specifications, or other data are used for any purpose other than in connection with a definitely related Government procurement operation, the United States Government thereby incurs no responsibility nor any obligation whatsoever; and the fact that the Government may have formulated, furnished, or in any way supplied the said drawings, specifications, or other data, is not to be regarded by implication or otherwise as in any manner licensing the holder or any other person or corporation, or conveying any rights or permission to manufacture, use, or sell any patented invention that may in any way be related thereto.

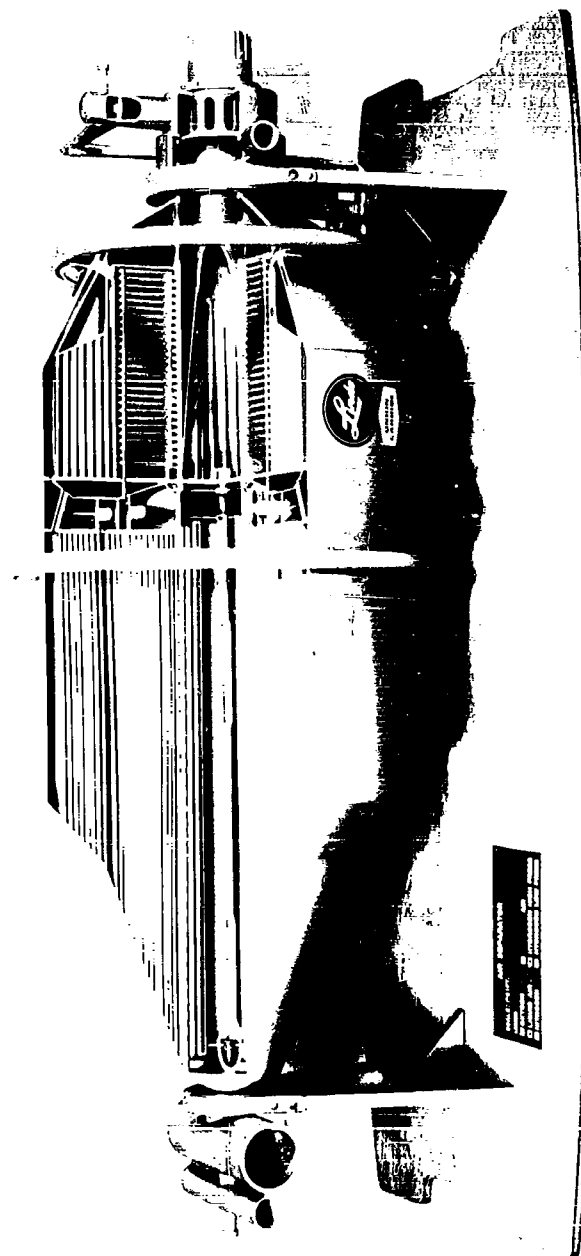
This document contains information affecting the National defense of the United States within the meaning of the Espionage Laws, Title 18, U.S.C., Sections 793 and 794. Its transmission or the revelation of its contents in any manner to an unauthorized person is prohibited by law.

Qualified requesters may obtain copies of this report from the Defense Documentation Center (DDC), (formerly ASTIA), Cameron Station, 5010 Duke Street, Alexandria, Virginia, 22314.

Copies of this report should not be returned to the Research and Technology Division unless return is required by security considerations, contractual obligations, or notice on a specific document.

CONFIDENTIAL

ASD-TDR-b3-665, Part I



ASD-TDR-b3-665, Part I

CONFIDENTIAL

**SECRET**

ASD-TDR-63-665, Part I

No. 54 of 63 Copies  
This document Consists of:  
218 SECRET Pages  
285 CONFIDENTIAL Pages  
132 UNCLASSIFIED Pages

OS-1023-54

FOREWORD

This report was prepared by Union Carbide Corporation, Linde Division, under USAF Contract No. AF 33(657)-8722. This contract was initiated under Project No. 3084, Task No. 308403. The contract was administered under the direction of the Air Force Aero Propulsion Laboratory, Research and Technology Division with Messrs. C. M. Donaldson, J. Leingang, and C. E. Ryan acting as Project Engineers.

Special acknowledgement is made to Messrs. K. E. Ackley, O. F. Allen, F. W. Bonnet, D. L. Close, A. M. Czikk, W. D. DeWitt, S. L. Fisher, R. J. Frainier (Project Manager), W. E. Goldstein, C. F. Gottzmann, M. O. Johnson, C. J. Linneball, J. R. Martin, L. C. Matsch, M. C. Noland, J. Notaro, P. S. O'Neill, W. J. Olzewski, R. S. Paul, O. P. Roberts, J. W. Sechler, W. L. Townsend, D. I-J Wang, D. W. Weiller, and E. F. Yendall of Union Carbide Corporation, Linde Division for their significant contributions in support of this program.

The associate contractor, General Dynamics/Astronautics, is acknowledged for providing the vehicle oriented information necessary for the performance of this contract.

This report is Part I of a two-part final report. Part I describes the experimental and analytical program conducted from May, 1962 to May, 1963. Part II reports the design and fabrication phases conducted from May 1, 1962 to March 1, 1964.

This report, excluding title, is classified "SECRET" because it contains design information which indicates the performance of a potential future aerospace system.

63 ASRP-2391

**SECRET**

# SECRET

ASD-TDR-63-665, Part I

## ABSTRACT

Realization of the full potential of recoverable air-breathing aerospace vehicles which utilize an air enrichment system, requires an efficient and reliable air enrichment unit of minimum weight and volume. The purpose of this study is to advance the technology of airborne air enrichment.

Initial steps in advancing the technology for airborne air enrichment were taken under Contracts AF 33(616)-7509 and AF 33(616)-7646. Results of these two contracts indicated that distillation in a rotating column offered the highest potential for meeting the propulsion system requirements. The studies described in this report were designed to advance the specialized technology for this distillation cycle in two areas: mass transfer and tray hydraulics, and boiling and condensing heat transfer. Mechanical component studies were also performed in support of the design of the cryogenic boilerplate air separator. A fourth program applied the results of these studies to the preliminary design of a full size flight-weight separator.

Results of these investigations have confirmed earlier, less sophisticated, studies that the airborne air enrichment unit can be designed within the prescribed goals. Mass transfer efficiencies and hydraulic performance of distillation trays have been determined from 50 to 500 g's. Heat transfer experiments performed on surfaces subjected to high gravitational fields from 75 to 400 g's produced an order of magnitude increase in performance by use of the special boiling surface and the porous condensing surface. Mechanical studies resulted in design information for a peripheral diffuser and seal, establishment of pressure drop correlations for two-phase flow in high gravitational fields and conception of a stable, internal liquid level control system for a rotating device. Results of these experimental programs have been utilized in the parametric studies of an airborne air separator. These studies provide the latest estimates of separator weight and volume as a function of inlet air pressure (180 to 245 psia), product purity (90 to 98 per cent oxygen by weight), and waste purity (96 to 98 per cent nitrogen by weight), all at a constant 56.5 psia waste gas pressure.

63 ASRP-2391

iii

# SECRET

**SECRET**

**ASD-TDR-63-665, Part I**

**TABLE OF CONTENTS**

<u>Section</u>	<u>Page</u>
1.0 INTRODUCTION	1
1.1 Review of Distillation	1
1.2 Review of Previous Studies	4
1.3 Current Program	5
2.0 SUMMARY	6
2.1 Conclusions	6
2.2 Recommendations	7
3.0 DISTILLATION EXPERIMENTAL AND ANALYTICAL PROGRAM	8
3.1 Introduction	8
3.2 Summary	11
3.3 Chronology of the Experimental Tray Program	14
3.3.1 Experimental Equipment	14
3.3.2 Initial Tray Experiments	14
3.3.3 Effect of Coriolis Acceleration Upon Tray Performance	22
3.3.4 An Operational Downcomer Tray	28
3.3.5 Circumferential Rotor Experiments	32
3.4 Analysis and Correlation of Data	32
3.4.1 Data Reported	32
3.4.2 Segmental Tray Data - Hydraulics	35
3.4.2.1 General Comments	35
3.4.2.2 The Dispersion Mechanism	36
3.4.2.3 Vapor Capacity	39
3.4.2.4 Liquid Capacity and Froth Heights	44
3.4.2.4.1 The Crest Equation	44
3.4.2.4.2 Miscellaneous Losses	48
3.4.2.5 Vapor Phase Pressure Drop	51
3.4.2.5.1 Theoretical Considerations	51
3.4.2.5.2 Discharge Coefficients of Perforated Plates	54
3.4.2.5.3 Volumetric Foam Density Data	58
3.4.2.6 Stability and Weeping	63
3.4.3 Segmental Tray Data - Mass Transfer	64
3.4.3.1 General Considerations Involving the Point Efficiency	64
3.4.3.2 The UCON Fluid Tray Efficiency Data	69

63 ASRP-2391

**SECRET**

# SECRET

## ASD-TDR-63-665, Part I

### TABLE OF CONTENTS (Continued)

<u>Section</u>	<u>Page</u>
3.4.4 Circumferential Tray Tests	74
3.4.4.1 Hydraulics	74
3.4.4.2 Mass Transfer	81
4.0 HEAT TRANSFER EXPERIMENTAL AND ANALYTICAL PROGRAM	82
4.1 Introduction	82
4.2 Summary	87
4.3 Pool Boiling at Normal Gravity and Elevated Pressures	88
4.3.1 Test Objectives	88
4.3.2 Pool Boiling Apparatus	89
4.3.3 Pool Boiling Results	92
4.4 Boiling and Condensing Studies in High-G Cryostat	97
4.4.1 Test Program	97
4.4.1.1 Condensation Inside Smooth Tubes - Test 1	99
4.4.1.2 Condensation Outside Smooth Tubes - Test 2	101
4.4.1.3 Condensation Inside Helical-Grooved Tubes - Test 3	101
4.4.1.4 Condensation Inside Copper and Aluminum Porous Condensing Surface Tubes - Tests 4 & 5	104
4.4.1.5 Condensation Inside Tubes with Non-wetted Surface - Test 6	108
4.4.1.6 Boiling On An Untreated Aluminum Surface - Test 7	109
4.4.2 High-G Cryostat Apparatus	110
4.4.3 High-G Cryostat Specimen	117
4.4.3.1 Specimen Size	117
4.4.3.2 Specimen Orientation	117
4.4.3.3 Specimen Materials of Construction	119
4.4.3.4 Specimen Design Details	119
4.4.4 High-G Cryostat Test Fluid	120
4.4.5 High-G Cryostat Data Reduction	120
4.4.5.1 Condensation Data Reduction	120
4.4.5.1.1 Calculation of Theoretical Condensing Coefficient	120
4.4.5.1.2 Calculation of Experimental Condensing Coefficient	125

63 ASRP-2391

v

# SECRET



**SECRET**

ASD-TDR-63-665, Part I

TABLE OF CONTENTS (Continued)

<u>Section</u>	<u>Page</u>
4.4.5.2 Boiling Data Reduction	131
4.4.6 High G Cryostat Results and Conclusions	131
4.4.6.1 Condensation Inside of Smooth Tubes - Test 1	131
4.4.6.2 Condensation Outside of Smooth Tubes - Test 2	131
4.4.6.3 Condensation Inside Helical Grooved Tubes - Test 3	136
4.4.6.4 Condensation Inside Tubes with Copper Porous Condensing Surface - Test 4	136
4.4.6.5 Condensation Inside Tubes with an Aluminum Porous Condensing Surface Test 5	143
4.4.6.6 Condensation Inside Tubes with a Non-Wetted Surface - Test 6	147
4.4.6.7 Boiling on an Untreated Aluminum Surface - Test 7	147
4.5 Pilot-Scale Reboiler-Condenser	155
4.5.1 Rotor Design	156
4.5.2 Dimensions and Configuration of Test Rotor	159
4.5.3 Instrumentation	160
4.5.4 Selection of Test Fluid	163
4.5.5 Experimental Data	168
4.5.6 Data Reduction	170
4.5.6.1 Mathematical Heat Transfer Model	170
4.5.6.2 Analysis of Experimental Heat Transfer Data	187
4.5.6.3 Comparison of Experimental Data with Theoretical Model	188
4.5.6.4 Fluid Flow	191
5.0 EXPERIMENTAL PROGRAM IN SUPPORT OF MECHANICAL DESIGN OF BOILERPLATE SEPARATOR	198
5.1 Introduction	198
5.2 Summary	198
5.3.1 Peripheral Seal Design Considerations	200
5.3.2 Peripheral Seal Experimental Apparatus	205
5.3.3 Peripheral Seal Experiments	208
5.3.4 Results	216

63 ASRP-2391

**SECRET**

**SECRET**

ASD-TDR-63-665, Part I

TABLE OF CONTENTS (Continued)

<u>Section</u>	<u>Page</u>
5.4 Peripheral Diffuser	216
5.4.1 Stationary Diffuser Study	216
5.4.1.2 Design and Operation	216
5.4.2 Rotating Diffuser Study	224
5.4.2.1 Peripheral Diffuser Design	224
5.4.2.2 Peripheral Diffuser Tests	235
5.4.2.2.1 Free Vortex Diffusion	235
5.4.2.2.2 Diffusion System With Eight Blades	235
5.4.2.2.3 Diffuser System as Designed - Type 1	240
5.4.2.2.4 Diffuser System Type 2 with Removal of Inside Blade Ends of Type 1	243
5.4.2.2.5 Diffuser System of Type 2 with Increase in Angle Between Diffuser Axis and Rotor Tangent	243
5.4.2.3 Rotating Diffuser Results	247
5.5 Pressure Drop in Two-Phase Flow Against a Gravitational Field	250
5.5.1 Analysis	250
5.5.2 Air-Water Experimental Program	252
5.5.3 UCON Fluid Experimental Program	260
5.5.4 Pressure Drop Results for Two Phase Flow	262
5.6 Internal Control System	262
5.6.1 Control System Description and Analysis	262
5.6.2 Detail Design of Control System for UCON Fluid Test	267
5.6.3 Design of UCON Fluid Control System Test Rotor	274
5.6.4 UCON Fluid Control System Tests	276
5.7 Instrumentation	277
5.7.1 Pressure Transducers	277
5.7.2 Experimental Work - Optical Systems	279
5.7.3 Vibration Monitor	282
5.8 Reboiler-Condenser Fabrication Problems	282
5.8.1 Basic Considerations	282
5.8.2 Foil Type Heat Exchanger Surface Program	284
5.8.3 Soldering Experiments	291
6.0 PRELIMINARY DESIGN AND ANALYSIS	293
6.1 Introduction	293
6.2 Summary	294

62 ASD-2391

**SECRET**

**SECRET**

ASD-TDR-63-665, Part I

TABLE OF CONTENTS (Continued)

<u>Section</u>	<u>Page</u>
6.3 Weight and Volume Analysis	297
6.3.1 General	297
6.3.2 Stationary System Cycle Studies	298
6.3.2.1 Parametric Trends in the Stationary System	298
6.3.2.2 Cycle Improvements for the Stationary System	302
6.3.3 Rotary System Studies	304
6.3.3.1 Process Description of Rotary Air Separator	304
6.3.3.2 Computer Analysis	308
6.3.3.3 Optimum Rotational Speed	308
6.3.3.4 Inlet Pressure Perturbation	309
6.3.3.5 Waste Purity Perturbations	314
6.3.3.6 Low Pressure Column Pressure Perturbation	314
6.3.3.7 Product Purity Perturbations	319
6.3.3.8 Optimum Arrangement of Components	326
6.3.3.9 Multiple Unit Assessment	329
6.3.4 Determination of System Weight and Volume	333
6.3.4.1 Component Process Stress Requirements	333
6.3.4.2 System Weight and Volume Mapping	337
6.3.4.3 Weight and Volume Confidence Level Estimates	346
6.3.4.4 Separator Design Optimization	355
6.3.4.5 Separator Heat Load and the Reflux Condenser	355
6.4 System Horsepower	357
6.5 Scaling Effects	358
6.5.1 General	358
6.5.2 Separator Size	359
6.5.3 Separator Performance	359
6.5.3.1 Cycle	359
6.5.3.2 Rotor	362
6.5.3.3 Low Pressure Column	362
6.5.3.4 High Pressure Column	363
6.5.3.5 Reboiler-Condenser	363
6.5.4 Weight and Volume	363
6.5.5 Reliability	364
6.6 Minor Constituent Effects	365
6.6.1 General	365
6.6.2 Water Vapor	365
6.6.3 Carbon Dioxide	365
6.7 Transient Study and Off-Design Performance	366

63 ASRP-2391

**SECRET**

**SECRET**

ASD-TDR-63-665, Part I

TABLE OF CONTENTS (Continued)

<u>Section</u>	<u>Page</u>
6.7.1 General	366
6.7.2 Start-up Performance	367
6.7.3 Off-Design Operation	367
6.7.4 Shutdown	372
6.8 Boiling Surface and Condensing Surface Treatments	372
6.8.1 General	372
6.8.2 Surface Treatment Evaluation	372
6.8.3 Reboiler-Condenser Sizing	374
6.9 Reliability	376
6.9.1 General	376
6.9.2 Product Reliability	377
6.9.2.1 General Design Requirements	377
6.9.2.2 Design Reliability of Components	379
6.9.2.3 Fabrication Reliability	380
6.9.3 Operation Reliability	381
6.9.4 Mission Reliability	382

63 ASRP-2391

**SECRET**

**SECRET**

ASD-TDR-63-665, Part I

LIST OF APPENDIXES

<u>Appendix</u>		<u>Page</u>
I	UCON Fluid Experimental Equipment and Segmental Tray Rotors	385
II	UCON Fluid Properties	395
III	Segmental Tray Data	405
IV	Circumferential Tray Data	433
V	Circumferential Tray UCON Fluid Test Rotor	435
VI	Derivation of Equation for Calculation of Condensate Drainage Blanketing	443
VII	Derivation of Condenser Tube Equation	447
VIII	Design and Fabrication of UCON Fluid Heat Transfer Test Rotor	451
IX	Computer Program for Integration of System of Four Differential Equations Describing Heat Transfer in UCON Fluid Rotor	459
X	Theoretical Discussion of the Centrifugal Seal	471
XI	Computer Program for Evaluation of Two Phase Pressure Drop Against a Gravitational Field	477
XII	Control Valve System	483
XIII	Stationary Column Results	495
XIV	Low Pressure Column Design Computer Program	513
XV	High Pressure Column Design Computer Program	519

63 ASRP-2391

x

**SECRET**

**SECRET**

**ASD-TDR-63-665, Part I**

**LIST OF APPENDIXES (Continued)**

<u>Appendix</u>		<u>Page</u>
XVI	Distillation Column Solution as a Function of Superficial Vapor Velocity	529
XVII	Air Separator - Weight, Volume, and Horsepower Computer Program and Sample Calculations	533
XVIII	Communications from General Dynamics/Astronautics	577

63 ASRP-2391

**SECRET**

**SECRET**

ASD-TDR-63-665, Part I

LIST OF FIGURES

<u>Figure No.</u>		<u>Page</u>
1	Fundamentals of Distillation	2
2	UCON Fluid Test Set Up	15
3	Test Series F, G, M-C, M-F Ripple Tray	18
4	Test Series H Ripple Tray	19
5	Run M-C-1 Ripple Tray Rotation	20
6	Run M-C-8 Ripple Tray Rotation	20
7	Test Series A, B, C Downcomer Tray	21
8	Test Series D Downcomer Tray	23
9	Test Series E Downcomer Tray	24
10		
11	Test Series S-A, S-B, S-C, S-D Flat Tray	27
12	Test Series M-A M-B Co-Rotational Flow Downcomer Tray	29
13	Test Series M-D, M-E Contra-Rotational Flow Downcomer Tray	30
14	Test Series S-E, S-F Contra-Rotational Flow Downcomer Tray	31
15	Circumferential Tray Configuration	33
16	Correlation Maximum Allowable Vapor Velocity	42
17	Comparison of Air Water and UCON Fluid Flooding Criteria	43
18	Tray Liquid Flow	44
19	Influence of Gravitational Field on Crest Height Using UCON Fluid	46
20	Influence of Liquid Rate on Crest Height Using UCON Fluid	47
21	Froth Height Correlation Using UCON Fluid	49
22	Foam Height Correlation Comparison Using Air- Water and UCON Fluid	50
23	Tray Pressure Drop	52
24	Orifice Coefficient versus Reynolds Number	56
25	Orifice Coefficient - Summary Correlation	57
26	Influence of System Variables Upon Tray Pressure Drop	59
27	Foam Density Correlation	61
28	Air Water UCON Fluid Foam Density Comparison	62
29	Tray Weeping	63
30	Tray Stability Criteria	65

63 ASRP-2391

**SECRET**

**SECRET**

**ASD-TDR-63-665, Part I**

**LIST OF FIGURES**

<u>Figure No.</u>		<u>Page</u>
31	Vapor-Liquid Equilibrium Data, UCON 12, UCON 114.	69
32	Efficiency Correlation UCON 12-114	73
33	Foam Height Correlation UCON 21-114	76
34	Flooding Correlation UCON 21-114	79
35	Weeping Correlation UCON 21-114	80
36	Efficiency Correlation UCON 21-114	83
37	Heat Transfer Surface and Headering	86
38	Pool Boiling Apparatus	90
39	Pool Boiling Test Specimen	91
40	Correlated Pool Boiling Data Linde Boiling Surface Applied To Copper	93
41	Correlated Pool Boiling Data at 1 atm. Linde Boiling Surface Applied to Aluminum	95
42	Correlated Pool Boiling Data at Elevated Pressure Linde Boiling Surface Applied to Aluminum	96
43	Cross Section of High G Cryostat	98
44	Heat Exchanger for Condensation Inside Smooth Tubes - Test No. 1	100
45	Heat Exchanger for Condensation Outside Smooth Tubes - Test No. 2	102
46	Typical Tube Condensation on Helical Weirs - Test No. 3	103
47	Porous Condensing Surface Flow	105
48	Specimen and Flange for Boiling on an Untreated Aluminum Surface - Test No. 7	111
49	High G Cryostat	112
50	Equipment Arrangement for High G Cryostat Transfer Tests (Boiling and Condensing)	113
51	Precision Device to Conduct Thermocouple EMF	115
52	Average Percent Blanketing Inside .250" I.D. Tube	118
53	Condensing Blanketing in Tubes	122
54	Nusselt Theoretical Condensing Film Coefficient Inside .250" I. D. Tube	126
55	Nusselt Theoretical Condensing Film Coefficient Inside .305" I. D. Tube	127
56	Nusselt Theoretical Condensing Film Coefficient Outside .375" O. D. Tube	128

63 ASRP-2391

xiii

**SECRET**



**SECRET**

ASD-TDR-63-665, Part I

LIST OF FIGURES

<u>Figure No.</u>		<u>Page</u>
57	Condensing Parameter Ratio for Nitrogen	129
58	Condensation Inside .250" I. D. Smooth Tubes	132
59	Condensation Outside .375" O. D. Smooth Tubes	134
60	Condensation Inside .250" I. D. Helical Grooved Tubes	137
61	Condensation Inside .250" I. D. Tubes Coated with a Porous Surface	139
62	Condensation Inside .305" I. D. Aluminum Tubes Coated with an Aluminum Porous Condensing Surface	144
63	Condensation Inside .305" I. D. Aluminum Tubes Coated with an Aluminum Porous Condensing Surface	145
64	Condensation Inside .250" I. D. Tubes coated with a Teflon Surface	148
65	Boiling $N_2$ on 2-7/8" Diameter Untreated Aluminum Disk	150
66	Comparison of $O_2$ - $N_2$ Boiling Data	151
67	Boiling Heat Transfer to Liquid Nitrogen	153
68	Boiling Heat Transfer to Liquid Oxygen	154
69	UCON Fluid Heat Transfer Disk after Brazing	161
70	Basic UCON Flow Circuit	162
71	Gibbs-Kelvin Boiling Parameter for Various UCON Fluids	165
72	Nusselt Condensing Parameter for Various UCON Fluids	166
73	Optimum Operating Pressures for UCON fluids	167
74	Pilot Scale Reboiler-Condenser, UCON fluid Test Rotor, Tube Configuration	171
75	Sketch of Tube Section	172
76	Relationship of Tube Angles	175
77	Theoretical Heat Transfer per Foot of tube in UCON Test Rotor vs. Transverse Acceleration	180
78	Theoretical Reduction of Heat Transfer in UCON Fluid Test Rotor due to Condensate Blanketing	181

63 ASRP-2391

xiv

**SECRET**

**SECRET**

**ASD-TDR-63-665, Part I**

**LIST OF FIGURES**

<u>Figure No.</u>		<u>Page</u>
79	Theoretical Mean Blanketing Angle in UCON Fluid Test Rotor Tubes	183
80	Determination of Exponent, m for theoretical Heat Transfer in Test Rotor	184
81	Determination of Exponent m for theoretical Heat Transfer in Test Rotor	185
82	Average Theoretical Heat Transfer in UCON Fluid rotors vs. Average Transfer accelera- tion and average overall temperature difference	186
83	Data Analysis on UCON Fluid Heat Transfer Rotor Ratio of Experimental to Predicted Performance	189
84	Pressure Buildup in Condensing Passage	192
85	Pressure Rise in the Boiling Passage vs. Boilup Vapor flow and average gravitational Field	194
86	Pressure Rise Transition Points for Two-Phase Flow in the Boiling Passage	196
87	Smoothed Data on Pressure Rise Through the Boiling Passage	197
88	Centrifugal Seal Configuration	202
89	Contact Type Peripheral Seal Design	203
90	Contact Type Peripheral Seal Design	204
91	Layout of Peripheral Diffuser and Rotary Seal Tester	206
92	Flow Circuit & Instrumentation For Seal and Diffuser Tests	207
93	Double Seal Packing Ring Type Contact Seal	209
94	Blade Type Centrifugal Seals	210
95	Centrifugal Seal Pressure Capability	212
96	Centrifugal Seal Power Consumption	213
97	Seal Leakage, 1/8 inch Blade Depth	214
98	Seal Leakage 1/16 inch Blade Depth	215
99	Centrifugal Seals Mounted on Rotor	217
100	Centrifugal Seals Mounted on Rotor	218
101	Flow Diagram Stationary Diffuser Test	220
102	Original Design of Stationary Diffuser	221
103	Final Stationary Diffuser Configuration	222
104	Stationary Diffuser Performance	223

63 ASRP-2391

XV

**SECRET**

**SECRET**

**ASD-TDR-63-665, Part I**

**LIST OF FIGURES**

<u>Figure No.</u>		<u>Page</u>
105	Rotary Tester for Peripheral Seal and Diffuser Tests	225
106	General Diffuser Configuration	224
107	Diffuser Configurations	228
108	Diffuser Passage Ring	229
109	Diffuser Exit	230
110	Diffuser Mounted on Tester	231
111	Diffuser Passage	232
112	Diffuser Passage	223
113	Ideal Kinetic Head in Diffuser Throat	234
114	Ideal Throat Reynolds Number	234
115	Vaneless, Free Vortex Diffusion (without inclusion of inlet exit expansion loss)	236
116	Vaneless Free Vortex Diffusion	237
117	Orifice Slot Propelling Blades	238
118	Modified Free-Vortex Diffuser (8 blades)	239
119	Diffuser Performance Configuration as Designated Type 1	241
120	High Loss Region at Orifice Slot	242
121	Inlet Conditions with Slip	242
122	Vector Representation of Slip	240
123	Diffuser Performance Configuration Type 2 Shortened Blade Ends	244
124	Pivoted Diffuser Blade Installation	245
125	Diffuser Performance Configuration Type 2 with Increase in Slip	246
126	Calculated Slip Characteristics Rotary Air-Water Tester	248
127	Orifice Slot Propelling Blades	249
128	Two Phase Flow Test Section	253
129	Two Phase Flow Test Section Schematic	254
130	Two Phase Flow	256
131	Two Phase Flow	257
132	Two Phase Volumetric Liquid Fraction $R_L$ Air Water Data	259
133	Two Phase Flow against Gravitational Field Predicted vs. Measured $\Delta P$ for UCON Fluid	261

63 ASRP-2391

**SECRET**

**SECRET**

ASD-TDR-63-666, Part I

LIST OF FIGURES

<u>Figure No.</u>		<u>Page</u>
134	Two Phase Volumetric Liquid Fraction- $R_L$ Air Water and UCON Fluid Data	263
135	Schematic of Kettle Liquid Level Control System	265
136	Response of Kettle Transfer Model to a Flow Impulse	266
137	Schematic of Modified Heater Design for UCON Fluid Rotor	268
138	Prototype Control Valve	270
139	Control Valve Orifice Opening vs. Signal Pressure Calibration Curve	271
140	Prototype Valve Flow Calibration with Water	272
141	Exploded View of Prototype Control Valve	273
142	UCON Fluid Control System Test Rotor Schematic	275
143	Schematic of Variable Reluctance Differential Pressure Transducer	278
144	Transducer Hookup Schematic	280
145	Calibration Curve for Pace P7 Transducer 0-50 psi in Liquid Nitrogen	281
146	Vibration Monitor Schematic	283
147	Stamped Foil Heat Exchanger	285
148	Die For Stamping Process	287
149	Foil Failure During Stamping	290
150	Effect of Plastic Deformation on Properties of Thin Gage Copper vs. Annealing Temperature	292
151	Double Column Air Separator	299
152	Preliminary Mass Flowsheet for Full Size Separator Cycle	305
153	Full Size Air Separator (Section View)	306
154	Optimum Rotational Speed	310
155	Inlet Pressure Perturbation - Low Pressure Column Trays	311
156	Inlet Pressure Perturbation - Reboiler- Condenser Heat Transfer Area	312
157	Inlet Pressure Perturbation - Heat Exchanger Duties	313

63 ASRP-2391

**SECRET**

**SECRET**

**ASD-TDR-63-665, Part I**

**LIST OF FIGURES**

<u>Figure No.</u>		<u>Page</u>
158	Waste Purity Perturbation - Low Pressure Column Trays	315
159	Waste Purity Perturbation - Reboiler-Condenser Heat Transfer Area	316
160	Waste Purity Perturbation - Heat Exchanger Duties	317
161	Sketch of Low Pressure Column Pressure Perturbation - Fixed Rotational Speed, Variable Waste Pressure - Low Pressure Column Trays and Reboiler Condenser Heat Transfer Area	318
162	Sketch of Low Pressure Column Pressure Perturbation - Fixed Rotational Speed, Variable Waste Pressure - Heat Exchanger Duties	318
163	Low Pressure Column Pressure Perturbation - Variable Rotational Speed, Fixed Waste Pressure - Low Pressure Column Trays	320
164	Low Pressure Column Pressure Perturbation - Variable Rotational Speed, Fixed Waste Pressure - Reboiler-Condenser Heat Transfer Area	321
165	Low Pressure Column Pressure Perturbation - Variable Rotational Speed, Fixed Waste Pressure - Heat Exchanger Duties	322
166	Product Purity Perturbation - Low Pressure Column Trays	323
167	Product Purity Perturbation - Reboiler-Condenser Heat Transfer Area	324
168	Product Purity Perturbation - Heat Exchanger Duties	325
169	Separate Component Weight Trend	328
170	Specific Weight and Volume of Single Separator versus Air Throughput Capacity	330
171	Specific Weight and Volume of Multiple Parallel Separators (including interconnecting piping)	332
172	Separator Weight - Product Oxygen Purity equals 90 per cent by Weight	338

63 ASRP-2391

xviii

**SECRET**

**SECRET**

ASD-TDR-63-665, Part I

LIST OF FIGURES

<u>Figure No.</u>		<u>Page</u>
173	Separator Weight - Product Oxygen Purity equals 95 per cent by Weight	339
174	Separator Weight - Product Oxygen Purity equals 98 per cent by Weight	340
175	Separator Volume	341
176	Separator Weight and Volume - Product Oxygen Purity equals 90 per cent by Weight	343
177	Separator Weight and Volume - Product Oxygen Purity equals 95 per cent by Weight	344
178	Separator Weight and Volume - Product Oxygen Purity equals 98 per cent by Weight	345
179	Pictorial View of Separator Weight and Volume - Surface Functions	347
180	Separator Weight and Volume - Waste Nitrogen Purity equals 96 per cent by Weight	348
181	Separator Weight and Volume - Waste Nitrogen Purity equals 97 per cent by Weight	348
182	Separator Weight and Volume - Waste Nitrogen Purity equals 98 per cent by Weight	349
183	Separator Weight and Volume - Separator Inlet Pressure equals 180 psia	349
184	Separator Weight and Volume - Separator Inlet Pressure equals 200 psia	350
185	Separator Weight and Volume - Separator Inlet Pressure equals 245 psia	350
186	Full Scale Flight Weight Air Enrichment Unit Estimated Unit Weight and Volume	353
187	Separator Payload Effect	356
188	UCON Fluid Test Rotor	388
189	UCON Fluid Test Rotor	389
190	Phase Equilibria of UCON 114-UCON21 at 54.5 psia (actual laboratory data)	399
191	Activity Coefficient vs. Mole Fraction 114 and X-Y Diagram $\pi = 60$ psia	400

63 ASRP-2391

xix

**SECRET**

**SECRET**

ASD-TDR-63-665, Part I

LIST OF FIGURES

<u>Figure No.</u>		<u>Page</u>
192	Vapor Pressure vs. Temperature, UCON Fluids	400
193	Liquid Viscosity, UCON Fluids	401
194	Vapor Viscosity @ 1 atm. UCON Fluids	401
195	Liquid Density, UCON Fluids	402
196	Vapor Density @ Saturation, UCON Fluids	402
197	Surface Tension vs. Temperature, UCON Fluids	403
198	Diffusion Coefficients, UCON 21-114	403
199	Diffusion Coefficients, UCON 12-114	404
200	Circumferential Tray UCON Test Rotor	436
201	Circumferential Tray Ring Assembly	438
202	Assembly Operation - Circumferential Tray	440
203	Final Assembly of Braze Tray Within Walls	441
204	Derivation of Condenser Tube Equation	448
205	UCON Heat Transfer Test Rotor	452
206	Distributor Orifice Configuration	453
207	Curved Heat Transfer Tube for UCON Test Rotor	457
208	Condenser Tube Section - UCON Fluid Tester	460
209	Solutions for Top of Tube	461
210	Solutions for Bottom of Tube	462
211	Crossplot of Solutions for Bottom of Tube	463
212	Computer for Integration of System of Four Differential Equations Describing Heat Transfer in UCON Fluid Test Rotor	466-467
213	Sketch of Centrifugal Seal	471
214	Centrifugal Seal - Rise in Casing Pressure	473
215	Computer Program for Evaluation of Two-Phase Pressure Drop Against a Gravitational Field	482
216	Block Diagram of Transfer Valve Control System	484
217	Kettle Schematic	485
218	Orifice Opening	489

63 ASRP-2391

XX

**SECRET**

**SECRET**

ASD-TDR-63-665, Part I

LIST OF FIGURES

<u>Figure No.</u>		<u>Page</u>
219	Low Pressure Column Design Computer Program	514-515
220	High Pressure Column Computer Program Flowsheet	520-521
221	High Pressure Column Computer Program Flow-sheet, Tray Equilibrium Subroutine	522

63 ASRP-2391

xxi

**SECRET**



**SECRET**

ASD-TDR-63-665, Part I

LIST OF TABLES

<u>Table No.</u>		<u>Page</u>
1	System Properties - Air-Water, UCON 12-114, UCON 21-114, and Liquid Air	12
2	Geometric Tray Configurations	17
3	Circumferential Tray Geometry	34
4	Orifice Coefficients of Sieve Trays	55
5	Flooding Points for Circumferential Trays	78
6	Condensation Inside Smooth Tubes - Test 1	133
7	Condensation Outside Smooth Tubes - Test 2	135
8	Condensation Inside Helical Grooved Tubes - Test 3	138
9	Condensation Inside Tubes with Copper Porous Condensing Surface - Test 4	140
10	Condensation Inside Tubes with Aluminum Porous Condensing Surface - Test 5	146
11	Condensation Inside Tubes Coated with a Teflon Surface - Test 6	149
12	Boiling Data for Liquid Nitrogen and Liquid Oxygen on a Smooth Aluminum Surface - Test 7	152
13	Pilot Scale Reboiler-Condenser Experimental Data	169
14	Theoretical Heat Transfer in UCON Fluid Test Rotor	178
15	Angle Between Fluid Velocity Vector and Rotor Tangent	227
16	Annealing Temperatures of Foil Samples	288
17	Experimental Data for First Drawing of Foil	288
18	Experimental Data for Second Drawing of Foil	289

63 ASRP-2391

xxii

**SECRET**

**SECRET**

**ASD-TDR-63-665, Part I**

**LIST OF TABLES**

<u>Table No.</u>		<u>Page</u>
19	Air Separator Cycle Study Summary (Non-Rotating System)	300
20	Weight and Volume Mapping Summary	342
21	Confidence Level Design Criteria	352
22	Final Confidence Level Estimates of Weight and Volume	354
23	Separator Size Comparison	360
24	Separator Performance Comparison	361
25	Theoretical Cycle Study with Separator Inlet Pressure Deviation	368
26	Separator Performance with Inlet Pressure Deviation	369
27	Theoretical Cycle Study with Separator Waste Pressure Deviation	371
28	Reboiler-Condenser Heat Transfer Characteristics	375
29	UCON Fluid Flow System Significant Sizes	391
30	Segmental Tray Data - Series A	405
31	Segmental Tray Data - Series B	406
32	Segmental Tray Data - Series C	408
33	Segmental Tray Data - Series D	410
34	Segmental Tray Data - Series E	411
35	Segmental Tray Data - Series F	412
36	Segmental Tray Data - Series G	414
37	Segmental Tray Data - Series H	416

63 ASRP-2391

**SECRET**

**SECRET**

ASD-TDR-63-665, Part I

LIST OF TABLES

<u>Table No.</u>		<u>Page</u>
38	Segmental Tray Data - Series S-A	417
39	Segmental Tray Data - Series S-B	419
40	Segmental Tray Data - Series S-C	421
41	Segmental Tray Data - Series S-D	423
42	Segmental Tray Data - Series S-E	425
43	Segmental Tray Data - Series S-F	427
44	Segmental Tray Data - Series M-A	429
45	Segmental Tray Data - Series M-B	430
46	Segmental Tray Data - Series M-C	430
47	Segmental Tray Data - Series M-D	431
48	Segmental Tray Data - Series M-E	432
49	Segmental Tray Data - Series M-F	432
50	Circumferential Tray - Hydraulic Data	433
51	Circumferential Tray - Efficiency Data	434
52	Experimental Air Water Data - Two Phase Flow Against a Gravitational Field, Series C	478
53	Experimental Air Water Data - Two Phase Flow Against a Gravitational Field, Series D	480
54	Experimental UCON-12 Fluid Data - Two Phase Flow Against a Gravitational Field	481
55	Stationary Column Results - Point No. 1	496
56	Stationary Column Results - Point No. 2	497
57	Stationary Column Results - Point No. 3	498
58	Stationary Column Results - Point No. 4	499
59	Stationary Column Results - Point No. 5	500
60	Stationary Column Results - Point No. 6	501

63 ASRP-2391

**SECRET**

**SECRET**

ASD-TDR-63-665, Part I

LIST OF TABLES

<u>Table No.</u>		<u>Page</u>
61	Stationary Column Results - Point No. 7	502
62	Stationary Column Results - Point No. 8	503
63	Stationary Column Results - Point No. 9	504
64	Stationary Column Results - Point No. 10	505
65	Stationary Column Results - Point No. 11	506
66	Stationary Column Results - Point No. 12	507
67	Stationary Column Results - Point No. 13	508
68	Stationary Column Results - Point No. 14	509
69	Stationary Column Results - Point No. 15	510
70	Stationary Column Results - Point No. 16	511
71	Stationary Column Results - Point No. 17	512
72	Enthalpy Coefficients as Linear Functions of Pressure	527

63 ASRP-2391

XXV

**SECRET**

~~SECRET~~

ASD-TDR-63-665, Part I

NOMENCLATURE

$a$	=	Acceleration, ft./hr. <sup>2</sup>
$a^\circ$	=	Function in High Pressure Column Program, tray equilibrium subroutine, dimensionless
$a_1$	=	Constant in determination of quality for two-phase flow, dimensionless
$a_2$	=	Power constant in determination of quality for two-phase flow, dimensionless
$a^*$	=	Coefficient expressing enthalpy as a linear function of pressure, Btu/lb.-mole
$A$	=	Area, ft. <sup>2</sup>
$A^\circ$	=	Constant orifice area of control valve, ft. <sup>2</sup>
$a_a$	=	Time function orifice area of control valve, ft. <sup>2</sup>
$A_{avg}$	=	Average total column flow area, ft. <sup>2</sup>
$A_b$	=	Boiling side heat transfer area, ft. <sup>2</sup>
$A_B$	=	Bellows area for control valve, ft. <sup>2</sup>
$A_c$	=	Condensing Side Heat Transfer Area, ft. <sup>2</sup>
$A_{CAS}$	=	Surface area of casing, ft. <sup>2</sup>
$A_i$	=	Inner total column flow area, ft. <sup>2</sup>
$A_o$	=	Outer total column flow area, ft. <sup>2</sup>
$A_s$	=	Active tray area, ft. <sup>2</sup>
AXIS	=	Length of outer casing major axis, in.
$A_\phi$	=	Fraction of reboiler-condenser heat transfer area made ineffective by blanketing, dimensionless
$A_e/A_t$	=	Ratio of diffuser exit area to throat area, dimensionless
$A/V$	=	Interfacial mass transfer area created per unit volume, ft. <sup>-1</sup>

63 ASRP-2391

xxvi

SECRET

**SECRET**

**ASD-TDR-63-665, Part I**

$b$	=	Width of tray or weir, ft.
$b^{\circ}$	=	Function in high pressure column program, tray equilibrium subroutine, dimensionless
$b^{*}$	=	Coefficient expressing enthalpy as a linear function of pressure, Btu/lb.-mole
$B$	=	Constant in equation for boiling side heat transfer coefficient, dimensionless
$b_a$	=	Average width between enriching section outer width and stripping section inner width, in.
$b_{avg}$	=	Average column width, in.
$b_i$	=	Column inner width, in.
$b_{iLPC}$	=	Inner width of low pressure column, in.
$b_k$	=	Width of kettle holdup chamber, ft.
$b_o$	=	Column outer width, in.
$b_{oHPC}$	=	Outer width of high pressure column, in.
$b_{oLPC}$	=	Outer width of low pressure column, in.
$b_s$	=	Width of kettle separator, in.
$C, c$	=	Constants, dimensionless
$c^{*}$	=	Coefficient expressing enthalpy as a linear function of pressure, Btu/lb.-mole
$C_1$	=	Unit length of circumferential fin, ft.
$C_2$	=	Coefficient in Chezy equation and expressed by the Manning Equation, $(lb_m\text{-ft.}/lb_s\text{-sec.})^{1/2}$
$C_3, C_4, C_5, C_6, C_7, C_8, C_9$	=	Constants

63 ASRP-2391

**SECRET**

**SECRET**

**ASD-TDR-63-665, Part I**

$C_1^\circ$	=	Constant multiplying factor in equation for calculation of foam height, dimensionless
$C_2^\circ$	=	Constant multiplying factor in equation for calculation of the number of gas phase mass transfer units $(NTU)_g$ , dimensionless
$C_3^\circ$	=	Constant multiplying factor in equation for calculation of the number of liquid phase mass transfer units $(NTU)_L$ , dimensionless
$C_D$	=	Drag coefficient, dimensionless
$C_{HP}$	=	Constant to convert separator horsepower requirement to drive weight, lbs./hp
$C_i$	=	Design stress cryogenic improvement factor, dimensionless
$C_v$	=	Orifice coefficient, dimensionless
$C_x$	=	Constant equal to 0.9 and used in equation for calculation of tray frictional pressure drop, eliminating the iteration on foam density, dimensionless
$C_Y$	=	Ratio of dry plate pressure drop to hydrostatic pressure drop, dimensionless
$d$	=	Diffuser throat diameter, ft.
$d_1, d_2$	=	Constants, $\text{lbs}/\text{ft}^3$ , $\text{lb}_m/\text{ft}^3/\text{lb}_f/\text{ft}^2$
$d^*$	=	Coefficient expressing enthalpy as a linear function of pressure, $\text{Btu}/\text{lb} \cdot \text{mole}$
$D$	=	Pipe diameter, ft.
$D_b$	=	Bubble diameter, ft.
$dF$	=	Differential force, $\text{lb}_f$
$D_g$	=	Gas phase diffusion coefficient, $\text{ft}^2/\text{sec}$ .
$D_L$	=	Liquid phase diffusion coefficient, $\text{ft}^2/\text{sec}$ .
$dm$	=	Differential element of mass, lbs.
$D_o$	=	Perforation diameter, ft.
$D_p$	=	Droplet diameter, ft.
$D_{si}$	=	Shaft inner diameter, in.

63 ASRP-2391

xxviii

**SECRET**

**SECRET**

**ASD-TDR-63-665, Part I**

$D_{so}$	=	Shaft outer diameter, in.
$d_t$	=	Inside diameter of reboiler-condenser tube, in.
$e$	=	Natural Logarithm Base, or control system error signal, dimensionless, ft.
$e^*$	=	Coefficient expressing enthalpy as a linear function of pressure, Btu/lb.-mole
$E$	=	Point efficiency, dimensionless
$E^\circ$	=	Tray efficiency after enhancement, dimensionless
$E_{mv}$	=	Murphree point efficiency, dimensionless
$\Sigma E^\circ$	=	Summation of enhanced tray efficiencies, dimensionless
$f$	=	Free area fraction of the tray, dimensionless
$f^*$	=	Coefficient expressing enthalpy as a linear function of pressure, Btu/lb.-mole
$f_1, f_2, f_3, f_4$	=	Functions in UCON test rotor heat transfer computer program, $^\circ R/rad.^2$ , $^\circ R/rad.$ , ft./rad., Btu/hr./ft. tube/rad.
$F$	=	Frictional energy loss in axial condensate flow through condenser tube, ft.-lb <sub>f</sub> /lb <sub>m</sub>
$F^\circ$	=	Ratio of experimental heat transfer rate in UCON test rotor to theoretical heat transfer rate, dimensionless
$F_1$	=	Separator feed air flow rate, lb-moles/lb-mole feed air
$g$	=	Normal acceleration of gravity, ft./sec. <sup>2</sup>
$G$	=	Molar gas rate, moles/sec.
$G_1$	=	Mass velocity, lb./ft. <sup>2</sup> sec.
$g_c$	=	Newton's conversion factor, lb <sub>m</sub> -ft/lb <sub>f</sub> -sec. <sup>2</sup>
$G_D$	=	Diffuser fluid flow rate, gal./min.
$G$	=	Gas flow in two-phase tester, lbs./sec.
$G_L^c$	=	Seal leakage flow rate, lbs./sec., or liquid flow in two-phase tester, lbs./sec.
$G_T$	=	Total exiting flow from periphery, lbs./sec.
$h$	=	Column shell thickness, in.

63 ASRP-2391

xxix

**SECRET**



**SECRET**

ASD-TDR-63-665, Part I

$H, H'$	=	Disengagement space or spray height, ft., in.
$H_1$	=	Distance between inner radius of high pressure column and inner radius of foam on first tray, in.
$h_b$	=	Boiling side film coefficient, Btu/ft. <sup>2</sup> hr.°R
$h_c, h_c'$	=	Crest Height, ft., in.
$hc_1$	=	Condensing side film coefficient, Btu/ft. <sup>2</sup> hr.°R
$(h_c)_{EXP}$	=	Experimental condensing side film coefficient, Btu/ft. <sup>2</sup> hr.°R
$h_{CM}$	=	Calculated condensing side film coefficient for full scale unit, Btu/ft. <sup>2</sup> hr.°R
$(h_c)_{THEO}$	=	Theoretical condensing side film coefficient, Btu/ft. <sup>2</sup> hr.°R
$h_f, h_f'$	=	Foam height, ft., in.
$h_{feed}$	=	Enthalpy of separator feed, Btu/lb.-mole
$h_k$	=	Kettle separator shell thickness, in.
$h_{K_1}$	=	Enthalpy of kettle liquid leaving high pressure column, Btu/lb.-mole
$h_L^o, h_L^o'$	=	Constant liquid holdup at kettle periphery of high pressure column, ft., or peripheral column liquid holdup, in.
$H_L$	=	Liquid enthalpy, Btu/lb.-mole
$h_{LC}$	=	Enthalpy of high pressure liquid stream leaving reboiler-condenser, Btu/lb.-mole
$h_{LK}$	=	Kettle separator liquid holdup, in.
$h_L(t)$	=	Liquid level in column as a function of time, ft.
HPB	=	Bearing friction horsepower loss, hp
HPF	=	Total fluid acceleration horsepower required, hp
$HP_{H-T}$	=	Hydrogen turbine horsepower output, hp
$HP_{LPC-T}$	=	Low pressure column turbine horsepower output, hp

63 ASRP-2391

xxx

**SECRET**

**SECRET**

ASD-TDR-63-665, Part I

$HP_{NET}$	=	Net air separator horsepower (excess or deficiency), hp
$HP_{OUTPUT}$	=	Total air separator horsepower output, hp
$HP_{RBC-T}$	=	Recirculation turbine horsepower output, hp
$HP_{REQ}$	=	Total air separator horsepower requirement, hp
$HPS$	=	Seal fluid horsepower loss, hp
$HPW$	=	Windage horsepower loss, hp
$h_{SEAL}$	=	Difference between inner radius of seal fluid and inner radius of column peripheral liquid, ft.
$h_{tL}$	=	Liquid holdup at kettle periphery of high pressure column as a time function, ft., or peripheral column liquid holdup, in.
$H_v$	=	Vapor enthalpy, Btu/lb.-mole
$h_{vRBC}$	=	Enthalpy of high pressure vapor stream entering reboiler-condenser, Btu/lb.-mole
$\Delta h_D$	=	Dry plate head loss, ft.
$\Delta H_T$	=	Turbine enthalpy drop, Btu/lb.
$i$	=	Index on evaluation of functions in computer programs, dimensionless
$J$	=	Index on evaluation of functions in computer programs, dimensionless
$k$	=	Thermal conductivity, Btu/ft.hr.°R, and index on evaluation of functions in computer programs, dimensionless
$k_1, k_2, k_3, k_4$	=	Equations resulting from control valve system analyses, lb <sub>m</sub> /ft., lb <sub>m</sub> /ft. <sup>2</sup> sec., dimensionless, ft. <sup>-1</sup>
$k_1^o, k_2^o, k_3^o, k_4^o, k_5^o, k_6^o$	=	Constants used to express enthalpy as a linear function of pressure, Btu/lb.-mole/psig
$K$	=	Vapor-liquid equilibrium constant, dimensionless
$K_1$	=	Kettle liquid flow rate, lb.-moles/lb-mole feed

63 ASRP-2391

xxxi

**SECRET**

~~SECRET~~

ASD-TDR-63-665, Part I

$K_0^\circ, K_1^\circ, K_2^\circ,$ $K_3^\circ, K_4^\circ$	=	Functions in high pressure column program, tray equilibrium subroutine, dimensionless
$k_b$	=	Bellows constant for control valve, lb <sub>f</sub> /ft.
$k_f$	=	Thermal conductivity of condensate film, Btu/ft.hr.-°R
$k_{g1}$	=	Gas phase mass transfer coefficient, ft./hr.
$k_L$	=	Thermal conductivity of liquid, Btu/ft.hr.-°R
$k_{L1}$	=	Liquid phase mass transfer coefficient, ft/hr.
$k_m$	=	Thermal conductivity of metal, Btu/ft.-hr.°R
$k_s$	=	Spring constant for control valve, lb <sub>f</sub> /ft.
$k_t$	=	Stress concentration factor due to tray perfor- ations, dimensionless
$l$	=	Index on evaluation of functions in computer programs, dimensionless
$L$	=	Molar liquid rate, moles/sec.
$L_1$	=	Circumferential distance between downcomers on first tray in high pressure column, in.
$L^\circ$	=	Length of flow path, ft.
$L^\square, L^\square_1$	=	Liquid flow rate, lb-moles/lb-mole feed, lbs/lb feed
$L^\square^\circ$	=	Liquid flow rate after enhancement, lb-moles/ lb-mole feed
$L_c$	=	Flow rate of high pressure liquid leaving reboiler- condenser, lb-moles/lb-mole feed
$L_{EXT}$	=	Total shaft extension beyond reboiler and reflux condensers, in.
$LHTA$	=	Length of reboiler-condenser heat transfer area, ft.
$L^\square_{LPC}$	=	Flow of liquid leaving low pressure column, lb-moles/ lb-mole feed

63 ASRP-2391

xxxii

SECRET

**SECRET**

ASD-TDR-63-665, Part I

$L_m$	=	Liquid flow rate or hydrogen liquid flow through reflux-condenser, lb-moles/lb-mole feed
$L_R$	=	Length of shaft between reboiler condenser and and reflux condenser, in.
$L_{RBC}^{\square}$	=	Flow of liquid leaving reboiler condenser, lb-moles/lb-mole feed
LRC	=	Length of reflux condenser, in.
$L_S$	=	Length of shaft, in.
$L/A$	=	Feet of length per square foot of heat transfer area, $ft^{-1}$
$L/V$	=	Liquid to vapor flow ratio, dimensionless
$m$	=	Power coefficient in equation, $Q_{\Delta T_O} = Q_{10^{\circ}} \left( \frac{\Delta T_O}{10} \right)^m$ , dimensionless
$M$	=	Index on evaluation of functions in computer programs, dimensionless
$Ma$	=	Molecular weight of air, lbs/lb-mole
$M_H$	=	Molecular weight of hydrogen, lbs/lb-mole
$M_{L,g}$	=	Liquid and vapor phase molecular weight, lbs/lb-mole
$M_{LPC}$	=	Molecular weight of liquid leaving low pressure column, lbs/lb-mole
$M_{RBC}$	=	Molecular weight of liquid leaving reboiler condenser, lbs/lb-mole
$n$	=	Roughness factor in Chezy Formula, dimensionless, or power coefficient in general boiling equation, dimensionless
$n_1$	=	Number of tray downcomers, dimensionless
$N$	=	Rotational speed, RPM
$N_1$	=	Number of radial segments in two-phase flow computer program, dimensionless

63 ASRP-2391

xxxlii

**SECRET**

**SECRET**

ASD-TDR-63-665, Part I

$N_a$	=	Number of actual column trays, dimensionless (In high pressure column computer program, $k-1$ equals $N_a-1$ , the number of actual column trays required, and $k^o-1$ is the interpolated number of actual column trays.)
$N_{DSI}$	=	Number of diffuser passage blade sides, dimensionless
$N_g$	=	Number of gravities ( $\frac{R\omega^2}{g}$ ) at superficial rotor speed, dimensionless
$N_{g^o}$	=	Number of gravities for tray fluid relative to rotor ( $N_g - s/\alpha$ ), dimensionless
$\overline{N_{g_b}}$	=	Average gravitational field for reboiler-condenser boiling passage, dimensionless
$N_{g_{flood}}$	=	Number of gravities at the column superficial vapor flooding velocity, dimensionless
$N_{g_p}$	=	Number of gravities parallel to reboiler-condenser tube axis, dimensionless
$N_{g_T}$	=	Number of gravities transverse to reboiler-condenser tube axis, dimensionless
$\overline{N_{g_T}}$	=	Average transverse acceleration, dimensionless
$N_{P^*}$	=	Number of theoretical trays, dimensionless
$N_{ssi}$	=	Number of peripheral seal sides, dimensionless
$NTU$	=	Number of mass transfer units, dimensionless
$(NTU)_g$	=	Number of gas phase mass transfer units, dimensionless
$(NTU)_L$	=	Number of liquid phase mass transfer units, dimensionless
$(NTU)_O$	=	Number of overall mass transfer units, dimensionless
$N_{vi}$	=	Viscosity group, dimensionless
$P, P'$	=	Pressure, $lb_f/ft.^2$ , psig or total pressure, $lb_f/ft.^2$ , psia

63 ASRP-2391

xxxiv

**SECRET**

**SECRET**

ASD-TDR-63-665, Part I

$P_{\square}, P^*$	=	Pressure, psia
$P^{\circ}$	=	Perforation pitch, ft.
$P_b$	=	Boiling pressure, psig
$P_c$	=	Condensing pressure, psig
$P_{CAS}, P'_{CAS}$	=	Casing pressure, $lb_f/ft.^2$ , psia
$P_{COL}$	=	Column pressure, $lb_f/ft.^2$
$P_{ENV}$	=	Environmental pressure surrounding outer casing, psia
$P_f, P'_f$	=	Peripheral high pressure column feed air pressure, psig, $lb_f/ft.^2$
$P_{fl}$	=	Final pressure at periphery of low pressure column section, psia
$P_I, P'_I$	=	Inlet pressure, psia, $lb_f/ft.^2$
$P_K$	=	Kettle high pressure column pressure, psig
$P_L, P'_L$	=	Liquid pressure, $lb_f/ft.^2$ , psia
$P_P$	=	Peripheral pressure minus casing pressure, psia
$P_s$	=	Shelf high pressure column pressure, psig
$P_{START}$	=	Starting pressure for high pressure column computer program and equal to average reboiler-condenser condensing pressure, psig, or pressure at inner radius of low pressure column section for low pressure column computer program, psia
$P^*_{tray}$	=	Tray pressure level, psig
$P_v, P'_v$	=	Vapor pressure, $lb_f/ft.^2$ , psia
$\Delta P$	=	Pressure drop or change, psi or $lb_f/ft.^2$
$\Delta P_D, \Delta P'_D$	=	Dry plate pressure drop, $lb_f/ft.^2$ , psi

63 ASRP-2391

xxxv

**SECRET**

**SECRET**

ASD-TDR-63-665, Part I

$\Delta P_{\text{DIFF}}$	=	Pressure drop across diffuser, psi
$\Delta P_f$	=	Tray frictional pressure drop, psi
$\Delta P_H, \Delta P'_H$	=	Hydrostatic pressure drop, $\text{lb}_f/\text{ft.}^2$ , psi
$\Delta P_{\text{LIQ}}$	=	Liquid phase pressure drop, psi
$\Delta P_o$	=	Observed pressure drop, $\text{lb}_f/\text{ft.}^2$
$\Delta P_s$	=	Static pressure change due to gravitational field, psi
$\Delta P_{\text{SEAL}}$	=	Pressure head across centrifugal seal, $\text{lb}_f/\text{ft.}^2$
$\Delta P_T$	=	Experimental tray pressure drop, psi
$\Delta P_{\text{TP}}, \Delta P'_{\text{TP}}$	=	Two-phase pressure drop, $\text{lb}_f/\text{ft.}^2$ , psi
$\Delta P_V$	=	Pressure drop across control valve, $\text{lb}_f/\text{ft.}^2$
$Q, Q'$	=	Heat transfer, Btu/hr., Btu/sec.
$Q_1$	=	Heat duty, Btu/lb-mole feed
$\bar{Q}, \bar{Q}^1$	=	Mean heat transfer, Btu/hr/ft-tube, Btu/min/ft-tube
$Q_C$	=	Reflux condenser heat duty (air separator system heat load), Btu/lb-mole feed
$Q_{\text{ELECTRICAL}}$	=	Electrical heat input to condensing side of High-G Cryostat, watts
$Q_{\text{HEAT LEAK}}$	=	Heat leak input to condensing side of High-G cryostat, watts
$Q_L, Q'_L$	=	Liquid flow rate, $\text{ft.}^3/\text{sec.}$ , Gal./min.
$\bar{Q}_L$	=	Superficial column liquid rate, $\text{ft.}^3/\text{ft.}^2\text{-sec.}$
$Q_R$	=	Reboiler-condenser heat duty, Btu/lb-mole feed
$Q_S$	=	Product subcooling heat duty, Btu/lb-mole feed
$Q_{\text{TK}}$	=	System heat loss due to kettle stream expansion, Btu/lb-mole feed

63 ASRP-2391

xxxvi

**SECRET**

~~SECRET~~

ASD-TDR-63-665, Part I

$QTS$	=	System heat loss due to shelf stream expansion, Btu/lb-mole feed
$Q/A$	=	Heat flux, Btu/ft <sup>2</sup> -hr.
$Q/A_b$	=	Boiling side heat flux, Btu/ft <sup>2</sup> -hr.
$Q/A_c, (Q/A_c)'$	=	Condensing side heat flux, Btu/ft <sup>2</sup> -hr, Btu/ft <sup>2</sup> -sec.
$\bar{Q}_L/b$	=	Volumetric liquid flow per foot of weir, ft <sup>3</sup> /sec/ft weir
$r, R, r', R'$	=	Radius, ft., in.
$R^\circ$	=	Nusselt pressure correction term for physical properties, dimensionless
$R^*$	=	Radius, in.
$R_{avg}$	=	Average column radius, in.
$R_b$	=	Bubble radius, ft.
$R_c$	=	Gas constant, ft-lb <sub>f</sub> /lb-mole/°R
$R_D$	=	Diffuser passage blade radial depth, in.
$Re$	=	Reynolds' number, dimensionless
$r'_{fic}, r'_{fic}$	=	Reboiler-condenser inner radius where tube axis coincides with radius vector, ft., in.
$R_H, R'_H$	=	Hydraulic radius, ft., in.
$r_1, r'_1$	=	Inner radius of reboiler-condenser tubes, ft., in.
$R_i$	=	Inner radius, in.
$R_I$	=	Inlet radius, in.
$R_{iHPC}$	=	Inner radius of high pressure column, in.
$r_{1seal}, r'_{1seal}$	=	Inner radius of centrifugal seal fluid, ft., in.
$R_k$	=	Radius of kettle stream inlet to low pressure column, in.
$r_l$	=	Inner radius of column liquid holdup, ft.

63 ASRP-2391

xxxvii

SECRET



~~SECRET~~

ASD-TDR-63-665, Part I

$R_L$	=	Volumetric liquid fraction, dimensionless
$r_{\text{mean}}, r'_{\text{mean}}$	=	Radius at point of average transverse acceleration in full-scale reboiler condenser, ft., in.
$r_o, r'_o$	=	Outer radius of reboiler-condenser tubes, ft., in.
$R_o, R'_o$	=	Outer radius of rotor or column, ft., in.
$r_{ok}$	=	Radius of kettle periphery in high pressure column, ft.
$R_{\text{orf}}$	=	Orifice radius in control valve, ft.
$R_p$	=	Radius of collector pipe, in.
$r_t$	=	Tube inside radius, ft.
$R_{\text{tray}}$	=	Tray radius, in.
$\Delta R$	=	Change in radius, in.
$s$	=	Laplacian operator, dimensionless
$S, S'$	=	Length of reboiler-condenser tube, ft., in.
$S^\circ$	=	Ratio of slope of liquid-vapor Y-X equilibrium line to column liquid-vapor ratio $(\frac{KG}{L})$ , dimensionless
$S_1$	=	Stress, psi
$S^\circ_1$	=	Shelf liquid flow rate, lb-moles/lb-mole feed
$S_p$	=	Signal pressure for control valve, $\text{lb}_f/\text{ft}^2$ , in. Hg
$t, t'$	=	Tray thickness, ft., in.
$t_1$	=	Time, sec.
$t^\circ_1, t^\circ_2, t^\circ_3,$ $t^\circ_4, t^\circ_5, t^\circ_6$	=	Power coefficients in equation for calculation of number of liquid phase mass transfer units, dimensionless
$T, T'$	=	Temperature, °R, °K
$T^\circ$	=	Tortuosity factor, dimensionless

63 ASRP-2391

xxxviii

SECRET

~~SECRET~~

ASD-TDR-63-665, Part I

$T_l$	=	Time constant for control valve system analysis, sec.
$T^*$	=	Index on heat transfer computer program printout, dimensionless
$T_b$	=	Boiling temperature, °R
$T_c$	=	Condensing temperature, °R
$t_{cas}$	=	Thickness of outer casing shroud, in.
$t_D$	=	Diffuser passage blade wall thickness, in.
$t_{ks}$	=	Kettle separator side thickness, in.
$T_L$	=	Liquid temperature, °R
$t_s$	=	Column side thickness, in.
$t_{seal}$	=	Seal wall thickness, in.
$t_t, t_t'$	=	Reboiler-condenser tube wall thickness, in.
$T_V$	=	Vapor temperature, °R
$t_w$	=	Wall temperature, °R
$\Delta T$	=	Temperature difference, °R
$\Delta T_b$	=	Boiling side temperature difference, °R
$\Delta T_c$	=	Condensing side temperature difference, °R
$\Delta T_o$	=	Overall reboiler-condenser temperature difference, °R
$U$	=	Rotor tangential velocity, ft./sec.
$U_o$	=	Overall heat transfer coefficient, Btu/ft <sup>2</sup> -hr.°R
$v$	=	Volumetric vapor rate, ft <sup>3</sup> /sec, or control system set point, ft.
$V, V'$	=	Velocity, ft/sec, ft/hr, or velocity imparted to vapor by rotor, ft/sec.

63 ASRP-2391

xxxix

SECRET

**SECRET**

ASD-TDR-63-665, Part I

$V^*$	=	New fluid velocity for diffuser with change in angle $\phi^\circ$ to $\phi^{*\circ}$ , ft/sec.
$V_1$	=	Volumetric flow rate, ft <sup>3</sup> /sec.
$V, V^{\square^\circ}$	=	Vapor flow rate, lb-moles/lb-mole feed, lbs/lb. feed
$V^{\square^\circ}$	=	Vapor flow rate after enhancement, lb-moles lb-mole feed
$V_{ac}$	=	Volume of air separator inlet air side truncated cone, ft <sup>3</sup>
$V_{AS}$	=	Total air separator volume, ft <sup>3</sup>
$V_{cyl}$	=	Volume of air separator cylindrical section, ft <sup>3</sup>
$V_f$	=	Froth velocity ( $\frac{QL}{\alpha b h_f}$ ), ft/sec.
$V_f^\circ$	=	Radial fluid velocity vector for diffuser, ft/sec.
$V_L$	=	Superficial liquid velocity or liquid velocity, ft/sec.
$V_{LI}$	=	Liquid inlet velocity, ft/sec.
$V_m$	=	Vapor flow rate, lb-moles/lb-mole feed
$V_M$	=	Molar volume, ft <sup>3</sup> /lb-mole
$V_O$	=	Perforation velocity, ft/sec.
$V_s$	=	Superficial column vapor velocity based upon active tray area, ft/sec.
$V_{s_{flood}}, V_{s_{max}}$	=	Superficial vapor velocity at the flooding point, ft/sec.
$V_{SL}$	=	Specific volume of liquid, ft <sup>3</sup> /lb.
$V_{SV}$	=	Specific volume of vapor, ft <sup>3</sup> /lb.
$\Delta V_s$	=	Incremental change in superficial vapor velocity for computer program column solutions, ft/sec.
$W, W'$	=	Stream flow rate, lbs/sec., lbs/min.
$W^\circ$	=	Temperature function in high pressure column computer program, tray equilibrium subroutine, dimensionless

63 ASRP-2391

xl

**SECRET**

**SECRET**

ASD-TDR-63-665, Part I

$W_a$	=	Separator inlet air flow rate, lbs/sec.
$W_{AS}$	=	Total air separator weight, lbs.
$W_{blades-c}$	=	Weight of low pressure column diffuser blades, lbs.
$W_{blades-r}$	=	Weight of reboiler-condenser diffuser blades, lbs.
$W_{CAS}$	=	Weight of outer casing, lbs.
$W_{coll-c}$	=	Weight of low pressure column diffuser collectors, lbs.
$W_{coll-r}$	=	Weight of reboiler-condenser diffuser collectors, lbs.
$W_D$	=	Downcomer weight, lbs.
$W_{DIFF-LPC}$	=	Weight of low pressure column diffuser system, lbs.
$W_{DIFF-RBC}$	=	Weight of reboiler-condenser diffuser system, lbs.
$W_{DRIVE}$	=	Total weight of air separator drive, lbs.
$W_e$	=	Weber number, dimensionless
$W_{HTA}$	=	Weight of heat transfer area, lbs.
$W_{HPC}$	=	Total high pressure column weight, lbs.
$W_{ks}$	=	Total kettle separator weight, lbs.
$W_{ksh}$	=	Kettle separator shell weight, lbs.
$W_{ksi}$	=	Kettle separator sides weight, lbs.
$W_L$	=	Reboiler-condenser low pressure liquid holdup, lbs.
$W_{LPC}$	=	Total low pressure column weight, lbs.
$W_o$	=	Constant design flow rate for control valve, lbs/sec.
$W_{PS}$	=	Weight of low pressure column pressure shell, lbs.
$W_{RBC}$	=	Total reboiler-condenser weight, lbs.

63 ASRP-2391

**SECRET**

**SECRET**

ASD-TDR-63-665, Part I

$W_{rsh}$	=	Reboiler-condenser shell weight, lbs.
$W_{rsi}$	=	Reboiler-condenser sides weight, lbs.
$W_{seal-c}$	=	Weight of low pressure column centrifugal seal blades, lbs.
$W_{seal-r}$	=	Weight of reboiler-condenser centrifugal seal blades, lbs.
$W_{sh}$	=	Column shell weight, lbs.
$W_{shaft}$	=	Shaft weight, lbs.
$W_{si}$	=	Column sides weight, lbs.
$W_T$	=	Tray weight, lbs.
$w_v$	=	Time function flow through control valve, lbs/sec.
$W_v$	=	Stream flow rate through control valve, lbs/sec.
$W_v^\circ$	=	Constant stream flow rate through control valve, lbs/sec.
$x$	=	Length of tube where condensation occurs, ft.
$x^\circ$	=	Control valve operator position, ft.
$X$	=	Vapor quality, mass fraction
$X_1, X_2$	=	Mole fraction of more volatile and less volatile component, mole fraction
$X_A$	=	Liquid Argon purity, mole fraction
$X_A^\circ$	=	Enhanced liquid Argon purity, mole fraction
$x_c^\circ$	=	Constant control valve operator position, ft.
$X_{KA}$	=	Argon purity of kettle liquid stream, mole fraction
$X_{KN}$	=	Nitrogen purity of kettle liquid stream, mole fraction
$X_{KO}$	=	Oxygen purity of kettle liquid stream, mole fraction

63 ASRP-2391

xl11

**SECRET**

# SECRET

## ASD-TDR-63-665, Part I

$X_N$	=	Liquid Nitrogen purity, mole fraction
$X_N^\circ$	=	Enhanced liquid Nitrogen purity, mole fraction
$X_{NF1}$	=	Final Nitrogen liquid purity in stream leaving periphery of low pressure column section, mole fraction
$X_{Ni}$	=	Nitrogen purity of liquid stream entering low pressure column section, mole fraction
$X_O$	=	Liquid Oxygen purity, mole fraction
$X_O^\circ$	=	Enhanced liquid Oxygen purity, mole fraction
$X_{OF1}$	=	Final Oxygen liquid purity in stream leaving periphery of low pressure column section, mole fraction
$X_{O1}$	=	Oxygen purity of liquid stream entering low pressure column section, mole fraction
$X_{OLC}$	=	Oxygen purity of high pressure liquid stream leaving reboiler-condenser, mole fraction
$X_{SA}$	=	Argon purity of shelf liquid stream, mole fraction
$X_{SN}$	=	Nitrogen purity of shelf liquid stream, mole fraction
$X_{SO}$	=	Oxygen purity of shelf liquid stream, mole fraction
$x_t^\circ$	=	Time function control valve operator position, ft.
$y$	=	Thickness of porous condensing surface, ft.
$y^\circ$	=	Height of rise of fluid in a capillary, ft.
$Y$	=	Condensing film thickness, ft.
$Y_1, Y_2$	=	Mole fractions of more volatile and less volatile components, mole fraction
$Y_1^\circ, Y_2^\circ, Y_3^\circ, Y_4^\circ, Y_5^\circ, Y_6^\circ$	=	Power coefficients in equation for calculation of foam height, dimensionless
$Y_A$	=	Vapor Argon purity, mole fraction
$Y_A^\circ$	=	Enhanced vapor Argon purity, mole fraction

63 ASRP-2391

xlili

# SECRET

# SECRET

## ASD-TDR-63-665, Part I

$Y_{FA}$	=	Argon purity of separator feed air, mole fraction
$Y_{FN}$	=	Nitrogen purity of separator feed air, mole fraction
$Y_{FO}$	=	Oxygen purity of separator feed air, mole fraction
$Y_N$	=	Vapor Nitrogen purity, mole fraction
$Y_N^\circ$	=	Enhanced vapor Nitrogen purity, mole fraction
$Y_{NF1}$	=	Final Nitrogen purity in vapor stream entering at periphery of low pressure column section, mole fraction
$Y_{N1}$	=	Nitrogen purity in vapor stream leaving low pressure column section, mole fraction
$Y_O$	=	Vapor Oxygen purity, mole fraction
$Y_O^\circ$	=	Enhanced vapor Oxygen purity, mole fraction
$Y_{OF1}$	=	Final Oxygen purity in vapor stream entering at periphery of low pressure column section, mole fraction
$Y_{O1}$	=	Oxygen purity in vapor stream leaving low pressure column section, mole fraction
$Y_{OVRBC}$	=	Oxygen purity of high pressure vapor stream entering reboiler-condenser, mole fraction
$Z$	=	Circumferential temperature gradient in wall of theoretical heat transfer model $\left(\frac{d\Theta^\circ}{d\Phi_1}\right)_{\text{wall}}$ , $^\circ\text{R}/\text{rad.}$ , or index on low pressure column computer program computation, dimensionless
$Z'$	=	Number of final purities per low pressure column program run, dimensionless
$\alpha$	=	Volumetric foam density, dimensionless
$\alpha^\circ$	=	Angle between plane normal to tube axis and the radius vector, deg.
$\alpha_1$	=	Constant in control valve analysis, dimensionless

63 ASRP-2391

xliv

# SECRET

# SECRET

## ASD-TDR-63-665, Part I

$\alpha_0^o, \alpha_1^o, \alpha_2^o,$ $\alpha_3^o, \alpha_4^o, \alpha_5^o$	=	Constants in high pressure column computer program correlation for enhancement in tray efficiency, dimensionless
$\alpha_{AO}$	=	Relative volatility, argon-oxygen, dimensionless
$\alpha_{NO}$	=	Relative volatility, nitrogen-oxygen, dimensionless
$\alpha_r$	=	Relative volatility, dimensionless
$\beta$	=	Angle between plane normal to radius vector and the direction of condensate flow, deg.
$\beta_0, \beta_1, \beta_3,$ $\beta_4, \beta_5, \beta_6$	=	Constants in high pressure column computer program correlation to correct $X_A$ as a function of enhancement in $X_O$ , dimensionless
$\gamma$	=	Angle between radius vector and direction of condensate flow, deg.
$\gamma^*$	=	Activity coefficient, dimensionless
$\gamma_0, \gamma_1, \gamma_2$ $\gamma_3, \gamma_4, \gamma_5$	=	Constants in high pressure column computer program to correct $Y_A$ as a function of enhancement in $Y_O$ , dimensionless
$\delta$	=	Quantity, $\frac{2\omega}{\gamma h_f} \left( \frac{Q_L}{b} \right)$ , dimensionless
$\delta^o$	=	Capillary diameter, ft.
$\delta_1$	=	Downcomer multiplying factor, dimensionless
$\delta_2$	=	Tray plus downcomer multiplying factor, dimensionless
$\Delta$	=	Output of holdup chamber function, lbs/sec.
$\epsilon$	=	Contact angle in porous condensing surface capillaries, deg.
$\eta^o$	=	Fugacity coefficient at system temperature and pure component vapor pressure, dimensionless
$\eta'_d$	=	Diffuser efficiency, percent
$\eta_g$	=	Composite of vapor phase dynamic mass transfer variables, dimensionless

63 ASRP-2391



# SECRET

## ASD-TDR-63-665, Part I

$\eta_L$	=	Composite of liquid phase dynamic mass transfer variables, dimensionless
$\eta_o$	=	Overall diffuser recovery of theoretical kinetic energy with inclusion of diffuser expansion loss, percent.
$\eta_v$	=	Fugacity coefficient at system temperatures and total pressure, dimensionless
$\Theta$	=	Angular direction of reboiler-condenser tubes, rad.
$\Theta^\circ$	=	Condensing side temperature difference in theoretical heat transfer model, $^\circ R$
$\Theta_1$	=	Mass transfer boundary layer renewal time, hr.
$\Theta_1^\circ, \Theta_2^\circ, \Theta_3^\circ, \Theta_4^\circ, \Theta_5^\circ, \Theta_6^\circ, \Theta_7^\circ, \Theta_8^\circ, \Theta_9^\circ$	=	Calculated and input values for low pressure column computer program, expression of liquid and vapor densities as functions of composition and pressure, lb./ft. <sup>3</sup> /psia, lb./ft. <sup>3</sup> /psia, dimensionless, lb./ft. <sup>3</sup> /psia, lb./ft. <sup>3</sup> , lb./ft. <sup>3</sup> psia, lb./ft. <sup>3</sup> , dimensionless, lb./ft. <sup>3</sup>
$\Theta_D$	=	One half of diffuser divergence angle ( $2\Theta_D$ ), deg.
$\Theta_s^\circ$	=	Condensing side temperature difference in theoretical heat transfer model at point where circumferential temperature gradient is zero, $^\circ R$
$\lambda$	=	Heat of vaporization, Btu/lb.
$\mu, \mu'$	=	Viscosity, lb./ft.-hr., lb./ft.-sec.
$\mu_L, \mu_L'$	=	Liquid viscosity, lb./ft.-hr., lb./ft.-sec.
$\mu_v$	=	Vapor viscosity, lb./ft.-sec.
$\rho, \rho'$	=	Density, lb./ft. <sup>3</sup> , lb./in. <sup>3</sup>
$\rho_L$	=	Liquid density, lb./ft. <sup>3</sup>
$\rho_{L_I}$	=	Inlet liquid density, lb./ft. <sup>3</sup>
$\rho_{L_{II}}$	=	Outlet liquid density, lb./ft. <sup>3</sup>
$\rho_{L_{MAX}}$	=	Maximum liquid density, lb./ft. <sup>3</sup>

63 ASRP-2391

# SECRET

## ASD-TDR-63-665, Part I

$\rho_{L_N}$	=	Nitrogen liquid density, lb./ft. <sup>3</sup>
$\rho_{L_O}$	=	Oxygen liquid density, lb./ft. <sup>3</sup>
$\rho_m$	=	Metal density, lb./ft. <sup>3</sup>
$\rho_p$	=	Pore density, ft. <sup>-2</sup>
$\rho_{TP}$	=	Actual two-phase density at radial location (r), lb./ft. <sup>3</sup>
$\rho_v$	=	Vapor density, lb./ft. <sup>3</sup>
$\rho_{v_I}$	=	Inlet vapor density, lb./ft. <sup>3</sup>
$\rho_{v_N}$	=	Nitrogen vapor density, lb./ft. <sup>3</sup>
$\rho_{v_O}$	=	Oxygen vapor density, lb./ft. <sup>3</sup>
$\sigma$	=	Surface tension, lb <sub>f</sub> /sec. <sup>2</sup> , dynes/cm
$\sigma'$	=	Surface, tension, lb <sub>f</sub> /ft.
$\sqrt{\sum (\Delta_i)^2}$	=	Square root of sum of squares of deviation of UCON properties from oxygen properties, dimensionless
$\tau$	=	Length of radial arc across reboiler-condenser tube, ft.
$\tau_i$	=	Contact time of mass transfer phases, hr.
$\gamma$	=	Correlating parameter in two-phase pressure drop correlation, dimensionless
$\phi, \phi'$	=	Condensate blanketing angle, rad., deg.
$\phi_1, \phi'_1$	=	Angle around tube circumference, deg., rad., and angle around orifice circumference, rad.
$\phi^\circ$	=	Angle between fluid rotor exit velocity vector and rotor tangent for diffuser, deg.
$\phi_1^\circ, \phi_2^\circ, \phi_3^\circ, \phi_4^\circ, \phi_5^\circ, \phi_6^\circ$	=	Constants used to express enthalpy as a linear function of pressure, Btu/lb.-mole
$\bar{\phi}, \bar{\phi}'$	=	Average condensate blanketing angle, rad., deg.
$\psi$	=	Angle between tube axis and radius vector, deg.
$\omega, \omega'$	=	Angular velocity, rad./sec., rad./hr.

63 ASRP-2391

**SECRET**

**ASD-TDR-63-665, Part I**

**1.0 INTRODUCTION**

Several concepts of future aerospace vehicles employ a propulsion system which requires air collection, enrichment, liquefaction and storage for propulsive use later in the vehicle mission. All such systems require an efficient airborne air enrichment unit of minimum weight and volume. During the past four years Union Carbide Corporation, Linde Division, has contributed to the technology required for airborne air enrichment with particular emphasis on the low temperature distillation process. This introduction will review the fundamentals of distillation, review the results of the two previous contracts, and finally present the scope and organization of this present study.

**1.1 Review of Distillation**

Fractional distillation utilizes the difference in equilibrium compositions of vapor and liquid phases of fluid mixtures, resulting from differences in vapor pressures of individual components, to effect separation in a series of contacting stages. In the fractional distillation process most widely used for the separation of air, streams of vapor are brought into continuous, intimate, countercurrent contact with streams of liquid in rectifying columns. Each column contains several contacting stages or trays arranged in series.

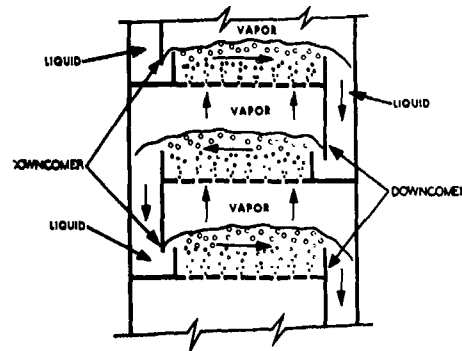
Figure 1-a shows a schematic detail of a tray section within a column. The liquid is seen to flow across a perforated contacting tray from downcomer to downcomer while vapor enters via openings in the plate and bubbles through the liquid. It is evident that as vapor issues from the perforations it achieves close contact with the liquid and forms a more or less homogeneous two-phase dispersion which in the case of standard trays takes the form of froth or foam consisting of numerous bubbles of vapor dispersed throughout the liquid. By virtue of the intimate contact of liquid and vapor on the trays the vapor and liquid leaving an individual tray will be nearly at phase equilibrium. As a consequence the rising vapor becomes progressively richer in lower boiling (more volatile) nitrogen while the descending liquid becomes richer in higher boiling oxygen.

To illustrate the basic distillation process the equilibrium diagram for the oxygen-nitrogen system is shown on Figure 1-b. The equilibrium line indicates that the vapor is always richer in nitrogen than its

63 ASRP-2391

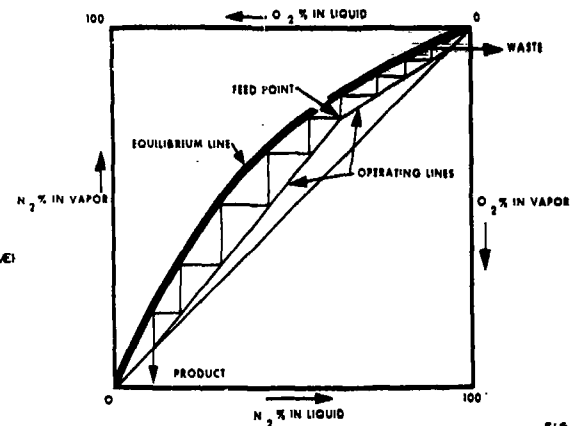
**SECRET**

ASD-TDR-63-665, Part I



STATIONARY TRAYS

FIG. 1A



LIQUID VAPOR EQUILIBRIUM AND DISTILLATION DIAGRAM

FIG. 1B

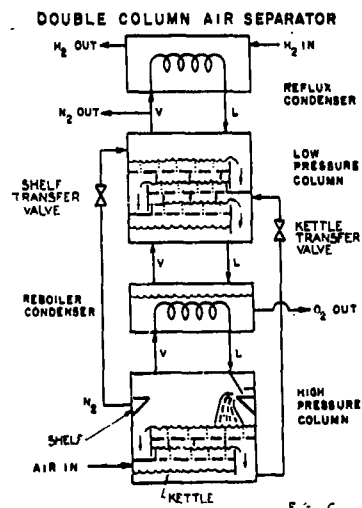


FIG. 1C

FUNDAMENTALS OF DISTILLATION FIG. 1

63 ASRP-2391

**SECRET**

**ASD-TDR-63-665, Part I**

corresponding equilibrium liquid. The steps between the equilibrium and operating lines demonstrate the separating action of the trays. The operating lines are graphical expressions for the mass balances required because in steady state condition the amounts of oxygen and nitrogen entering and leaving an individual tray must be the same. For many systems the ratios of liquid to vapor mass flow are almost constant for a column section and it can be shown that the slopes of the operating lines are equal to the liquid to vapor flow ratios. The number of steps indicates the number of theoretical (or 100% efficient) contacting stages required to effect the desired separation. It is evident that the location and slope of the operating lines have a great effect on the number of steps required. Also, it can be seen easily that as high product and waste purities are approached separation steps become successively smaller. In other words, high purities demand considerably more trays than moderate purities.

Figure 1-c shows the double column cycle conceived for producing liquid oxygen in the Aerospaceplane propulsion cycle. Except for the method of supplying refrigeration to the system, this cycle is very similar to the one used in most commercial oxygen producing plants. Saturated air vapor is fed to the bottom of the high pressure column where the first phase of the distillation process separates the air into nitrogen (condensed at the top of the high pressure column), and a liquid containing about 32% oxygen (withdrawn at the bottom or kettle). The liquid nitrogen from the top is split into two streams, one serves as reflux for the high pressure column, the other, called the shelf stream, is transferred to the top of the low pressure column to provide part of the reflux in this column. Here the main distillation process takes place at a lower pressure. The liquid stream from the kettle of the high pressure column is throttled and introduced into the low pressure column at a point where column equilibrium compositions correspond to those of the transferred feed stream. Liquid oxygen is produced at the bottom (stripping section) and nitrogen gas at the top (enriching section) of the low pressure column. The function of the reboiler-condenser is to condense nitrogen at the top of the high pressure column and to provide boil-off for the low pressure column. To make up refrigeration deficiencies, part of the waste nitrogen is condensed by a reflux condenser, and returned to the column. Refrigeration for the reflux condenser is furnished by a liquid hydrogen stream.

63 ASRP-2391

**SECRET**

# SECRET

## ASD-TDR-63-665, Part I

### 1.2 Review of Previous Studies

The initial step in the advancement of airborne air enrichment was taken in the first study, Contract No. AF 33(616)-7509 under sub-contract to General Dynamics/Astronautics, where the fractional distillation process showed promise for an airborne separator. This theoretical and experimental program was reported in ASD TR-61-412.

The theoretical study demonstrated distillation cycles which could be compatible with the propulsion cycle. That is, within the limitations of the inlet pressure and limited hydrogen refrigeration, separation could be achieved in a reasonable number of stages or theoretical trays and the waste nitrogen still could be recompressed to expel it overboard through the engines.

The experimental program showed that the rotating column principle would indeed be feasible, since reasonable mass transfer (tray) efficiencies could be expected. This substantiated theoretical predictions that a high gravity force field would permit considerably higher vapor velocities through the contacting stages, thus providing a smaller device.

Based on the above work the expanded feasibility study program was undertaken. This second study was also under sub-contract to General Dynamics/Astronautics on Contract No. 33(616)-7646 and reported in ASD TR-61-699 Part II Vol. 2. Much of the work was concurrent with the first study but of much broader scope.

Different methods of air separation (including permeation, adsorption, chemical separation, cocurrent contactors, sequential spray chambers, wetted wall separators, and vortex separators) were examined but only the rotating tray-type distillation showed immediate promise. It offered a thermodynamically efficient process. Because of the low temperature and high pressure the fluid densities are fairly high. Consequently the volume occupied by the distillation system is smaller than that required by other schemes which usually operate at higher temperatures. The chemical technique offered the advantage of slightly smaller heat exchangers, and therefore was recommended for further study, even though the estimated weight of reactant exceeded the design goal.

Stationary cocurrent and rotating counter-current distillation contactors were studied. The rotating counter-current contactor was

63 ASRP-2391

**SECRET**

**ASD-TDR-63-665, Part I**

found more attractive and additional tests were conducted to demonstrate enrichment by counter-current distillation in a rotating device.

A parallel experimental effort in boiling and condensing heat transfer showed that the reboiler-condenser of the distillation separator could be improved. An order of magnitude increase in the overall heat transfer coefficient seemed possible.

**1.3 Current Program**

Having been successful in the initial steps of the program by experimentally confirming the basic theories of a rotating air separator, a more detailed analytical and experimental program was organized along functional lines exploring the columns, the reboiler-condenser, and thirdly the mechanical design areas requiring applied research. These were combined in the fourth area, - preliminary design and analysis of a full size flight-weight separator.

The first area was distillation. This program developed the necessary tray hydraulic data and mass transfer efficiencies to permit rational design of a rotating distillation column. Although distillation was a well developed science for stationary (normal gravity) columns, the knowledge of rotating (50-500 g) counter-current vapor - liquid contactors was extremely meager at the inception of this project. This program consisted of three phases. In the first, several types of sieve tray segments were explored visually, and limited brief hydraulic measurements were taken. The second phase developed the hydraulic data and mass transfer efficiencies in depth for the more promising tray types. Thirdly, a complete column (full circumference) containing four trays was tested to demonstrate the uniform tray hydraulics over the full circumference.

The second area of research and development was in heat transfer as applied to the reboiler-condenser. Referring back to Figure 1-c it can be seen that all of the air (saturated vapor) must be condensed by the reboiler-condenser since the two streams leaving the high-pressure column are liquid. Condensation is achieved by rejecting heat to the liquid oxygen from the low pressure column. Thus, is shown the strong incentive for improvement in boiling and condensing coefficients to handle these large quantities of air. It was estimated a 40-fold increase in unit heat flux was needed over commercial practice to produce a separator within the target weight goals. This program consisted of

63 ASRP-2391

**SECRET**

**SECRET**

**ASD-TDR-63-665, Part I**

three phases. The first phase was to determine the boiling coefficient for the special Linde boiling surface in oxygen at elevated pressures. The second phase reaffirmed that the "g" field would be advantageous in improving the condensing film coefficient on a smooth tube and the third was to extend this improvement by investigating various novel condensing surfaces. The fourth phase was to demonstrate the performance of the most promising boiling and condensing surfaces in the ambient temperature test facility using UCON fluorocarbon fluids. This last phase was accomplished by testing two small heat transfer discs to develop the full circumferential flow pattern of both fields.

The third area of experimental work included mechanical development in support of the design of a 1/20 scale cryogenic boilerplate separator. This section included peripheral seal and diffuser tests, two-phase flow experiments in a high gravitational field, instrumentation and control valve development, and some fabrication development for design of the reboiler-condenser.

The fourth and last area of study was solely analytical in the preliminary design and analysis of a full size flight-weight separator. In this section all experimental results are combined into a complete design. This work was divided into six phases. The predominant area was a parametric study of weight and volume, as of function of inlet pressure, and product and waste purities. Other studies included scaling effects, minor constituent effects, transient study and off-design performance, heat transfer study and reliability.

**2.0 SUMMARY**

**2.1 Conclusions**

In general, it is concluded that an airborne air separator is feasible for the Aerospaceplane concept. It was shown that distillation is practicable in the rotating column, since increased vapor velocities are possible without sacrificing mass transfer efficiency. Sufficient data are available to design one preferred tray configuration, although it likely is not the optimum design.

Heat transfer experiments have yielded more than an order of magnitude increase in performance as expected. The special boiling surface has been proven beneficial also in the high gravitational field. Condensing experiments have yielded an order of magnitude increase

63 ASRP-2391

**SECRET**



**SECRET**

**ASD-TDR-63-665, Part I**

in film coefficient due to the high gravitational forces of a rotating system. A porous condensing surface offers even greater improvement. It is superior to the other condensing surfaces tested. Operation of these surfaces was demonstrated in UCON fluids proving that one design is available for the high performance rotating reboiler-condenser.

Several experiments conducted in two-phase flow in pipes and control valves in high gravitational fields have indicated that the fluid transfer can be accomplished within the rotor. Data has been accumulated for the design of the first cryogenic unit. Seal tests and diffuser tests have substantiated theoretical predictions that the kinetic energy of the liquid leaving the rotor can be recovered with acceptable efficiencies.

The preliminary design and analysis shows that the target weight can be achieved in a flight-weight full size design. Volume will slightly exceed the goal, but the weight equivalent penalty for excess volume is acceptable.

Scaling effect studies show the minimum specific weight occurs between 1000 and 2000 lb./sec. flow rate, and the 100 lb./sec. cryogenic boilerplate model can be scaled up to 2000 lb./sec. Other studies also confirmed the full scale design as a practicable apparatus.

**2.2 Recommendations**

The program to date has yielded a column design and a reboiler-condenser design which appear capable of demonstrating feasibility of the airborne air separator. However, these are not optimized, and further study will likely permit a more compact design.

In distillation, the mass transfer may be improved by investigating the optimum flow length and weir height for the trays. This program will determine the enhancement in tray efficiency possible in a rotating column. In a more general sense it can be stated that deeper understanding of the phase contact mechanism is required. Particle sizes, phase continuity, and specifications of the microhydraulic mechanism by which mass transfer is controlled, all remain largely unknowns. Admittedly it is not necessary to know these to design columns, but substantial breakthrough most often follows a deeper understanding of the physical processes. Thus, to improve the degree of success in this program, this study is recommended.

63 ASRP-2391

**SECRET**

# SECRET

## ASD-TDR-63-665, Part I

The improvement in condensing heat transfer made under this contract should be explored under additional studies to optimize the pore size, pore geometry, coating thickness and orientation to the "g" field. Other improvements in heat transfer may be presented through additional study but this area appears most promising at this time.

Considerable further mechanical research efforts in the areas of fluid mechanics, internal separator fluid transfer controls, mechanical elements and particularly fabrication techniques is required before design of a flight-weight separator can be approached. Examples for proposed studies are supplemental two-phase flow tests, refinement of control valves to accommodate the variable flow conditions expected in the ultimate propulsion system, peripheral liquid seals and diffusers, and/or peripheral liquid transfer pumps. Special emphasis is recommended for the area of fabrication where available techniques for construction of large thin gauge structures are inadequate for the precision and dynamic balance required in a flight-weight separator. In conjunction with the proposed research effort, design and construction of a scale light-weight separator is recommended for test in the 100 lb./sec. facility at the earliest possible date. Such a device would bring into focus many of the mechanical problems facing design of a flight-weight unit and demonstrate feasibility of the rotating distillation separator concept from mechanical as well as functional points of view.

As the experimental results are accumulated they should be related to the final product, a flight-weight full size separator. A preliminary design function is required to present the latest estimate of reliability, weight, and volume of the airborne unit. Separation cycles must also be studied on a continuing basis to accomplish the most efficient integration with the propulsion system.

### 3.0 DISTILLATION EXPERIMENTAL AND ANALYTICAL PROGRAM

#### 3.1 Introduction

Distillation is defined as the separation of a mixture of gases or miscible liquids into the various components utilizing their difference in volatility. Volatility is defined as the tendency of a liquid to vaporize. This type of separation occurs within the temperature range required by the highest boiling temperature of the least volatile component and the lowest condensing temperature of the most volatile component. An excellent treatise on distillation can be found in Reference 1.

63 ASRP-2391

# SECRET

# SECRET

## ASD-TDR-63-665, Part I

In air separation, distillation occurs in the cryogenic temperature range where the upper temperature limit is determined by the oxygen component and the lower temperature limit by the nitrogen component. The technology for air separation has been well established, but improvements through research and development still continue. Technological advances in areas of conventional air separation have been primarily geared toward intrinsically higher cycle efficiencies and thus a correspondingly lower consumption of energy (lower vapor velocities and pressure drop.) Overall plant and production costs are therefore of prime importance whereas system weight and volume assume secondary position.

However, in design of an airborne air separation system, especially when a flow rate of 2000 lb./sec. is considered, a different approach is necessary. This flow rate is approximately 70% of the rated throughput of the combined U.S. oxygen producing plants. Thus, based on weights and volumes of commercial oxygen plants, this approach is obviously unrealistic for the Aerospaceplane.

To solve the problem it was proposed that the distillation be performed in a very high gravitational field, which is developed by rotating the distillation unit. The advantage of this approach is that it permits considerably higher vapor velocities and thus smaller column cross sections. In the conventional distillation column the vapor flows upward counter to liquid which is propelled downward by normal gravity. In the rotating system, gravitational force again propels liquid, in this case radially outward, counter-current to the vapor. However, the much larger forces now acting on the liquid permit much higher velocities of the vapor flowing in the opposite direction without disrupting the general counter flow of the two phases - which would mean a breakdown of the distillation process. This high vapor velocity is achieved at the expense of power in the form of pressure drop in the vapor stream as it moves through the high "g" liquid. It turns out that this high pressure drop dissipated on the "froth" on the trays causes such an intimate contact between liquid and vapor that it greatly aids mass transfer on the trays. This will be amplified by further discussion throughout the report.

As shown in Figure 1-c a heat exchanger is necessary between the high and low pressure columns. A prime concern is to make available the largest possible temperature difference across this exchanger to minimize its size and weight. Because this temperature difference is determined by the condensing and boiling pressures in the exchanger, the pressure drop in the high and low pressure columns must be minimized.

63 ASRP-2391

# SECRET

## ASD-TDR-63-665, Part I

This shows the essence of the design of the airborne distillation unit. Pressure drop must be optimumly distributed between columns to minimize system weight since there is a counter trend between column and heat exchanger weight. Pressure drop is also a function of rotational speed, therefore providing a second consideration in optimization.

To accomplish this optimization, the distillation process was explored analytically and experimentally. Specific goals were to establish the critical design factors such as minimum tray areas (maximum superficial vapor velocity), minimum tray spacing, mass transfer efficiency and pressure drop.

Early in the air-water program (Ref. 2) it was established that a rotating contactor might readily accommodate vapor velocities in excess of 30 ft./sec. at accelerations of less than 500 Ng. It was, nevertheless, equally apparent that under these circumstances the liquid handling capacity of standard downcomer configurations was not nearly in proportion to their vapor throughput capabilities. As a result, emphasis was at first placed upon the use of ripple trays which seemingly offered substantially greater liquid throughputs than did downcomer trays. Generally speaking the prime purpose of this initial program was, however, demonstration of basic functional feasibility rather than the development of an optimum tray geometry. The latter was to be accomplished to some degree as part of the subsequent UCON fluoro-carbon fluid experiments (Ref. 3) which were planned so as to provide a much closer simulation of liquid air physical properties than had been possible with air and water. It was then learned that high free area ripple trays, as they were first conceived, left much to be desired from a point of view of stability and separation efficiency. Also, with the UCON fluid system there appeared to be a general shift in acceptable throughput from what had been found earlier. At a given tray acceleration both the column vapor handling capacity and the pressure drop were noticeably below their anticipated values, a trend that could only be attributed to the differences in certain physical properties between the two systems.

As a result of these findings, the program reported herein comprises three phases: (1) development of an operable tray geometry, (2) the detailed evaluation of the hydraulic and mass transfer performance of this configuration employing relatively small, segmental trays, and (3) confirmation of the latter technology with a complete circumferential tray to prove the hydraulic stability of such a geometry. Parts one and two were conducted using UCON 12 and UCON 114 as the test fluids,

63 ASRP-2391

# SECRET

# CONFIDENTIAL

ASD-TDR-63-665, Part I

whereas in part three, for reasons of system capacity, UCON 21 and UCON 114 were employed. The degree to which these experiments simulated future liquid air conditions is shown in Table 1, where the earlier air and water operation has also been summarized. Much in contrast to the air-water system, the UCON fluids are seen to duplicate the physical properties of liquid air very closely with the exception of liquid density. It is felt that this property difference may, however, be adequately accounted for without the necessity of actual variations of the test fluids. Of the remaining physical properties, surface tension appears, for reasons to be discussed in a subsequent section, to bear an important influence upon the performance of a rotary distillation column as it is described here. It may be seen from Table 1 that this parameter was particularly well simulated with the present fluid systems.

Based upon the experimental results one may, therefore, proceed with considerable confidence to design a cryogenic test rotor without the expense and difficulties associated with the development of the overall tray technology at cryogenic temperatures.

## 3.2 Summary

The UCON fluid mass transfer program, executed under AF 33(657)-8722, is reported here. Also earlier findings from air-water experiments made during previous subcontracts under AF 33(616)-7509 and AF 33(616)-7646 are included for comparison. These findings constitute our knowledge of the performance of distillation trays operated in high centrifugal force fields.

This program consisted of three phases. In the first, several types of sieve trays were briefly studied by means of hydraulic measurements and visual observations made of single 3 x 4 inch trays operated over a range of 50 to 500 Ng. Second phase experiments studied thoroughly the most promising types. These were the same size but were installed four in tandem to increase the accuracy of the mass transfer measurements. In the third phase of the program a four-tray column was tested, with each tray extending around the entire rotor circumference. This demonstrated the applicability of the earlier findings to a tray configuration approximating the final configuration.

Data taken from the first two phases of the program has been correlated to predict design factors such as minimum tray areas and

63 ASRP-2391

# CONFIDENTIAL

# CONFIDENTIAL

ASD-TDR-63-665, Part I

TABLE I  
SYSTEM PROPERTIES

PROPERTY	Air-Water		Ucon 12-114		Ucon 21-114		Liquid Air	
	Min.	Max.	Min.	Max.	Min.	Max.	Min.	Max.
$V_s - \frac{\text{Ft.}}{\text{sec.}}$	8.97	47.2	4.25	26.4	5.26	7.70	4.0	10.0
$\rho_v - \frac{\text{Lb.}}{\text{Ft.}^3}$	.150	1.43	1.32	3.74	0.89	1.27	.76	4.07
$\rho_L - \frac{\text{Lb.}}{\text{Ft.}^3}$	62.0	62.0	78.4	90.0	81.5	84.7	38.7	60.6
$\rho_v/\rho_L$	.00242	.0231	.0169	.0416	.0109	.0150	.0196	.0672
$Q_{L/b} - \frac{\text{Ft.}^2}{\text{sec.}}$	.010	.149	0	.188				
$N_g$	8	400	29	504	12.6	212	125	505
$h_f - \text{In.}$	0.9	3.0	0.3	3.0	0.1	1.8	0.8	1.5
$\mu_v - \text{cp.}$	.018	.018	.012	.013	.012	.012	.008	.008
$\mu_L - \text{cp.}$	1.0	1.0	.260	.330	.279	.332	.080	.150
$\sigma - \frac{\text{Dynes}}{\text{CM}}$	72	72	~5	~11	15	17	4	11
$\sigma/\mu_v$	4000	4000	416	846	1250	1420	667	1375
$Dg - \frac{\text{Ft.}^2}{\text{sec.}}$	$6.2 \times 10^{-6}$	$7.6 \times 10^{-5}$	$4.6 \times 10^{-6}$	$6.6 \times 10^{-6}$	$3.3 \times 10^{-5}$	$3.8 \times 10^{-5}$	$2.3 \times 10^{-6}$	$7.0 \times 10^{-6}$
$D_L - \frac{\text{Ft.}^2}{\text{sec.}}$	$1.2 \times 10^{-8}$	$2.3 \times 10^{-8}$	$3.9 \times 10^{-8}$	$5.1 \times 10^{-8}$	$2.3 \times 10^{-5}$	$3.0 \times 10^{-5}$	$5 \times 10^{-8}$	$11 \times 10^{-8}$

NOTE: UCON is a registered trademark of Union Carbide Corporation. In these experiments the following UCON fluorocarbon fluids were used.

UCON 12 - dichlorodifluoromethane  $\text{C Cl}_2 \text{ F}_2$

UCON 21 - dichlorofluoromethane  $\text{C H Cl}_2 \text{ F}$

UCON 114 - dichlorotetrafluoroethane  $\text{C Cl F}_2 - \text{C Cl F}_2$

63 ASRP-2391

## CONFIDENTIAL

### ASD-TDR-63-665, Part I

spacings, mass transfer efficiency, and pressure drop. These are reported as functions of the physical properties of the fluids, relevant changes in tray geometry, liquid and vapor flow rates, and centrifugal force.

The following conclusions summarizing the results of this section are:

a. Tray type distillation columns operating in a centrifugal force field are, hydraulically, an entirely feasible way of decreasing the required vapor flow area (and hence volume and weight) of the column. Over the range of accelerations tested (50 to 500 Ng), the required flow area varied inversely as the square root of the acceleration.

b. Mass transfer and vapor velocity of the preferred tray design both increase with centrifugal acceleration. However, the inverse dependency of NTU upon vapor velocity limits the extent to which it is beneficial to increase the acceleration field.

c. Frictional pressure drop (a measure of the mass transfer power requirement) varies with the  $1/2$  to  $2/3$  power of the acceleration. (The exact relation can be specified if the tray length is known. An optimization of this latter variable was beyond the capabilities of the present program.)

d. A recommended sieve tray configuration is presented as Figure 14. This configuration was evolved by observation of the performance of a succession of partially successful designs with corrections made at each step to eliminate observed operational inadequacies.

e. Extensive data was taken on the effect of geometric and operating variables upon the performance of the recommended configuration. This is presented in the form of tables, graphs, and equations for the convenience of the developmental designer.

f. A circumferential tray rotor was designed according to the above recommendations and tested with a different fluid. Its operation was in agreement with the predictions of the earlier data correlations. Equally important, it was observed that there were no liquid distribution problems, flow instabilities, or mechanical vibrations.

The following presents recommendations for future work:

63 ASRP-2391

# CONFIDENTIAL

## ASD-TDR-63-665, Part I

a. For the recommended tray configuration the greatest present uncertainty is the variation in performance with tray length. This has two aspects. First, an increased length results in more separation per tray by decreasing the amount of mixing between liquids entering and leaving the tray. This is countered by the possibility of froth gradients causing maldistribution of flows and higher pressure drops. It is believed these detrimental factors can be minimized, however, by proper design. The theoretical promise of efficiency enhancement is substantial, indicating it should certainly be explored experimentally.

b. In a more general sense one may say that much remains to be done before we understand the details of the phase contact mechanism. Particle sizes, phase continuity, and specification of the microhydraulic mechanism by which mass transfer is controlled, all remain unknown. While it is admittedly not necessary to know these to design columns, or to discover improvements, substantial breakthroughs most often follow a deeper understanding of physical processes. Thus, to the degree that an improved distillation process can improve over-all program success, basic research is recommended in this area.

### 3.3 Chronology of the Experimental Tray Program

#### 3.3.1 Experimental Equipment

A flow circuit has been constructed to allow simulation of either the low or high pressure sections of a rotary air distillation column and to permit both tray and hydraulic and subsequent reboiler-condenser heat transfer tests to be conducted. Figure 2 is a simple schematic of the flow loop which, in this instance, was designed to deliver a maximum fluid rate of about 6 lb./sec. of UCON fluid at pressures up to 150 psig and liquid to gas ratios either greater or less than unity. The test columns could be rotated at speeds of up to 120 rad./sec. yielding average accelerations of over 500 times those of normal gravity. A more detailed description of the entire flow circuit and its components, including the test rotor, is given in Appendix 1.

#### 3.3.2 Initial Tray Experiments

From the outset it appeared that a comparative evaluation of downcomer and ripple trays in UCON fluid service would be most desirable. In addition, it was decided that the majority of hydraulic

63 ASRP-2391

CONFIDENTIAL



UConn Fluid Test Series

15

# CONFIDENTIAL

## ASD-TDR-63-665, Part I

experiments be confined to single tray tests on account of reduced fabrication time and ease of data reduction. Table 2 represents a summary of the pertinent geometric tray variations that have been examined in approximately the chronological order in which the experiments occurred. All but the series M - A through M - F runs were conducted with single trays.

With respect to the ripple tray configurations it was noted that they were generally quite susceptible to phase maldistribution and liquid channeling effects; factors primarily responsible for their limited rangeability. Figures 3 and 4 are representations of the two basic ripple tray layouts as well as typical views of their actual operating behavior in what might be described as stable range. It is worth noting that while in both instances the major portion of the liquid flow occurred via the depressed regions, there is also evidence of a certain amount of weeping at the "trailing edge" of the plate. It will be shown later that this phenomenon is directly attributable to Coriolis acceleration effects. The latter are also thought to be, to a great degree, responsible for the maldistribution problems encountered in many multiplate ripple tray experiments, as shown, for instance, in Figure 5. By contrast, Figure 6 represents a more stable operation.

It is apparent from these photographs that this ripple tray column acts more like a continuous counter-current contactor rather than as a tray contactor. This observation was borne out later during a series of efficiency experiments which showed the separation efficiencies to be independent of the number of trays in a given contacting section. Unfortunately, the efficiencies were also considerably lower than those measured with downcomer tray columns.

Thus, the downcomer trays appeared to be most favorable on the basis of schedule and cost for the current development effort. It is possible that future work could lead to the development of a high performance ripple tray. However, since downcomer trays appeared to provide the best performance at present, they are emphasized in this study.

The downcomer trays did at first present a number of difficulties never before experienced in air-water service. Figure 7 represents a view of the first tray layout and its stable operation. In order to conserve as much active area as possible, the inlet weir had been deleted during series A experiments. The results were excessive weeping and tray instability near the inlet section. It was concluded that the

63 ASRP-2391

# CONFIDENTIAL

# CONFIDENTIAL

ASD-TDR-63-665, Part I

TABLE 2

## GEOMETRIC TRAY CONFIGURATIONS

Test Series	Tray Type	Free Area %	Perf. Dia. In.	Inlet Weir In.	Outlet Weir In.	Active Area %	Tray Flow Path	Ripple Dimensions			Total Test Points
								Depth In.	Width In.	Shape	
A	Dwncmr	22.0	0.041	-	0.625	0.719	C-R				6
B	Dwncmr	22.0	0.041	0.375	0.625	0.625	C-R				76
C	Dwncmr	34.0	0.033	0.375	0.625	0.625	C-R				62
D	Dwncmr	28.7	0.036	0.250	0.625	0.625	B-R				25
E	Dwncmr	45.0	0.038	0.250	0.625	0.625	B-R				29
F	Ripple	45.0	0.038	0.250	-	0.810	C-C	0.500	0.500	✓	70
G	Ripple	34.0	0.033	0.250	-	0.810	C-C	0.500	0.500	✓	74
H	Ripple	45.0	0.038	0.250	-	0.810	C-C	0.250	0.500	✓	31
S-A	Flat	22.0	0.041	0.375	0.375	0.810	C-R				97
S-B	Flat	28.7	0.036	0.375	0.375	0.810	C-R				87
S-C	Flat	22.1	0.035	0.375	-	0.910	C-R				110
S-D	Flat	34.0	0.033	0.375	-	0.910	C-R				93
S-E	Dwncmr	22.1	0.035	0.437	-	0.690	C-R				89
S-F	Dwncmr	14.0	0.036	0.406	-	0.625	C-R				70
M-A	Dwncmr	20.0	0.033	0.500	0.250	0.660	B-R				19
M-B	Dwncmr	20.0	0.033	0.500	0.250	0.660	B-R				14
M-C	Ripple	45.0	0.038	-	-	1.00	C-C	0.500	0.500	✓	9
M-D	Dwncmr	20.0	0.033	0.375	0.250	0.660	C-R				18
M-E	Dwncmr	26.0	0.037	0.437	-	0.625	C-R				40
M-F	Ripple	34.0	0.033	-	-	1.00	C-C	0.625	0.625	✓	2
										Total	1011

Note: C-R - Counter Rotational Liquid Flow  
B-R - Bi-Rotational Liquid Flow  
C-C - Counter Current Liquid Flow

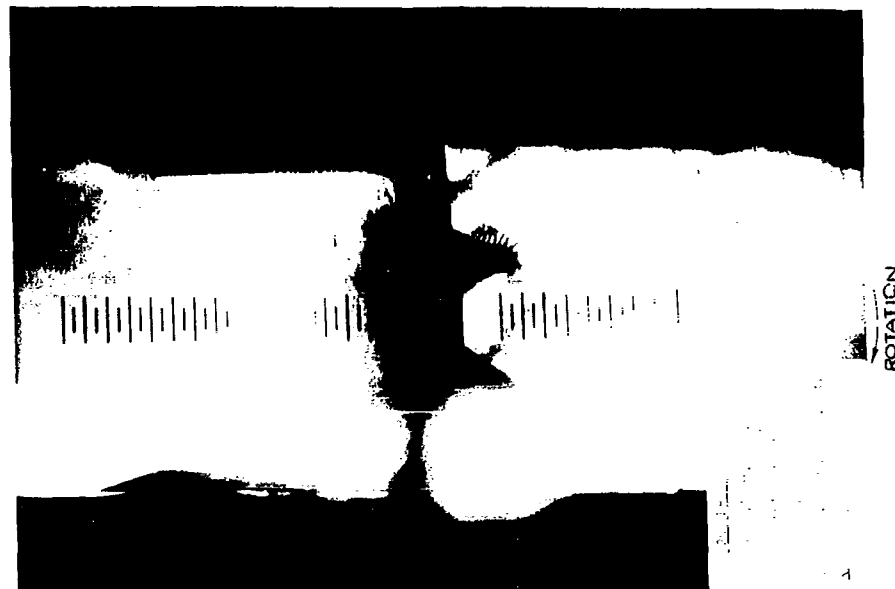
CONFIDENTIAL

**O**

TEST WEIR

TEST WEIR

TEST WEIR

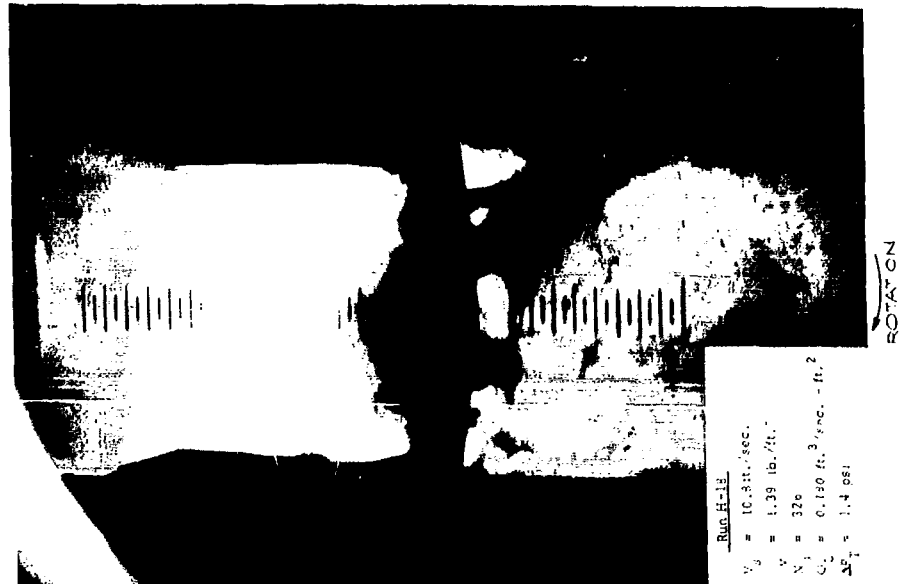
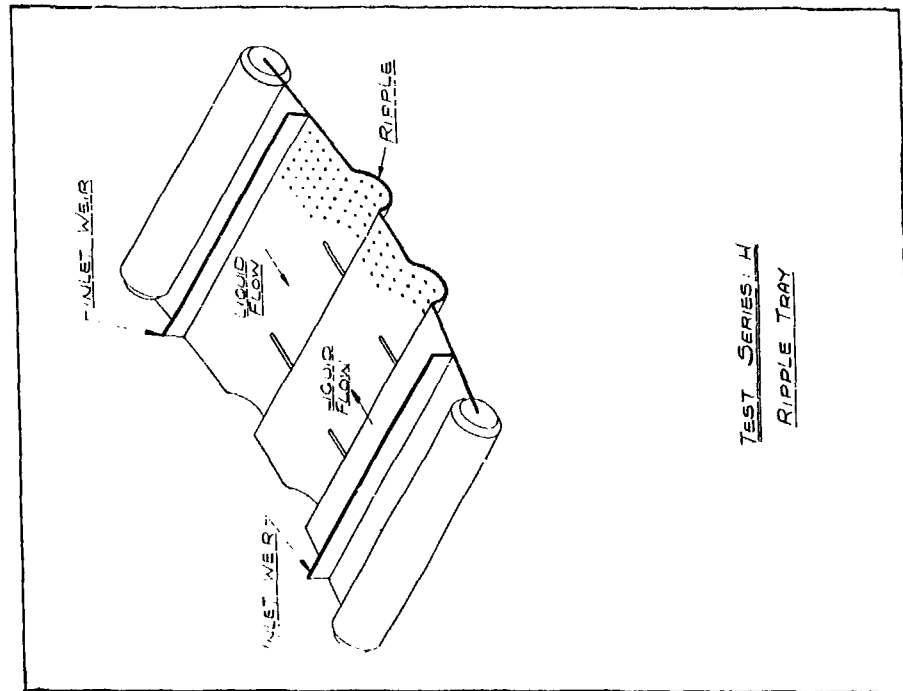


63 ASRP-2391

**CONFIDENTIAL**

# CONFIDENTIAL

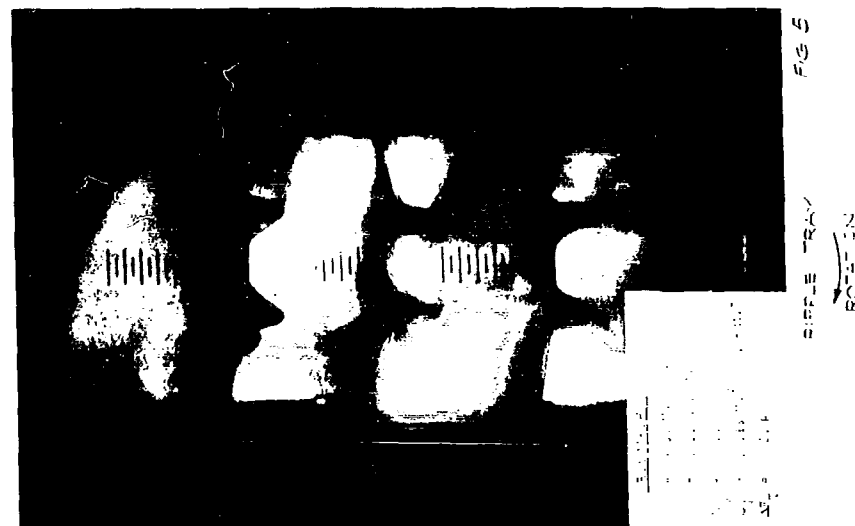
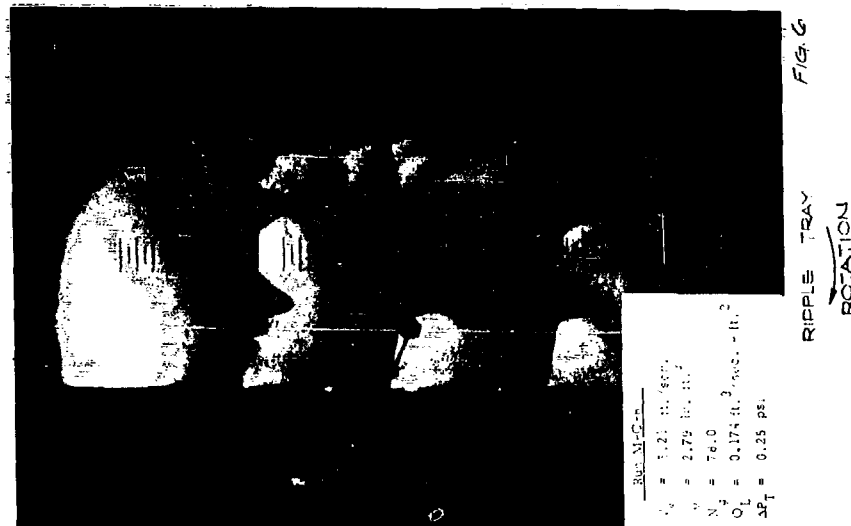
ASD-TDR-63-665, Part I



63 ASRP-2391 4

# CONFIDENTIAL

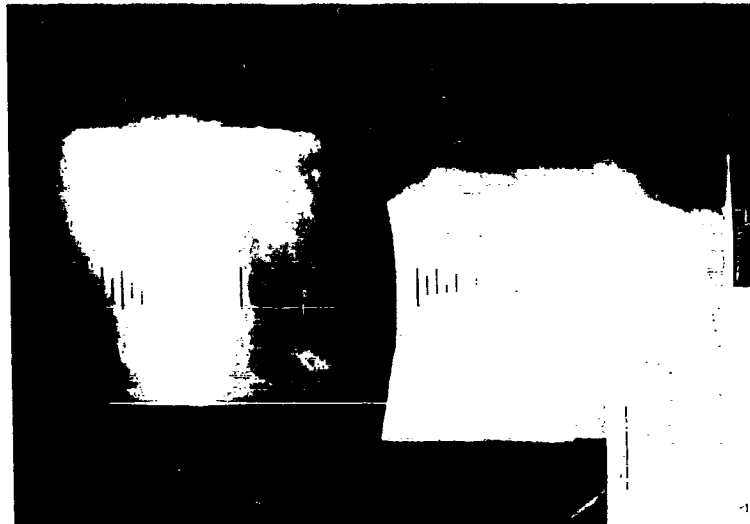
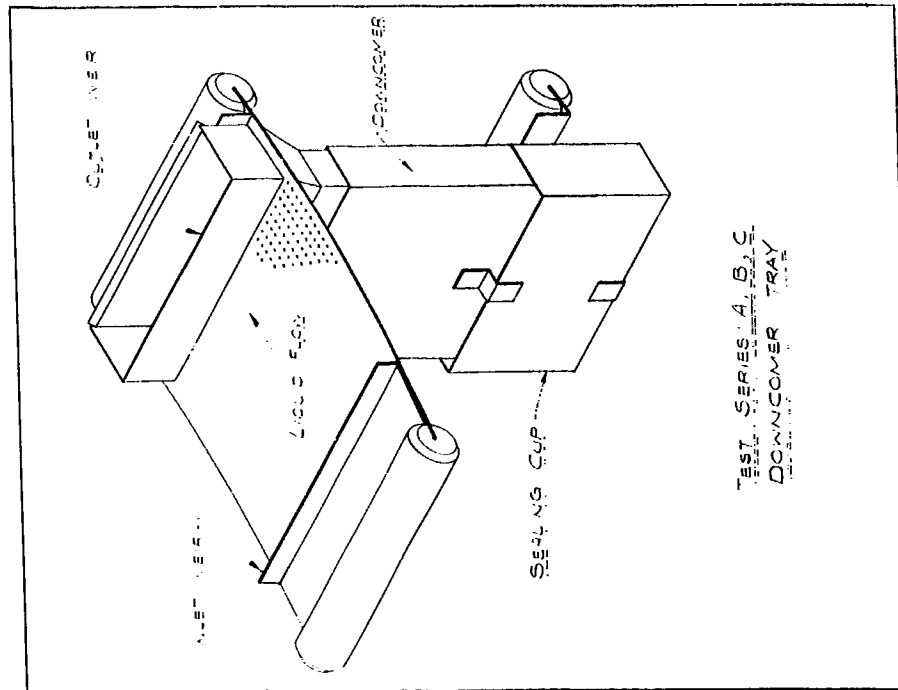
ASD-TDR-63-665, Part I



63 ASRP-2391

CONFIDENTIAL

ASD-TDR-63-665, Part I



63 ASRP-2391

CONFIDENTIAL<sup>21</sup>

# CONFIDENTIAL

ASD-TDR-63-665, Part I

introduction of liquid directly onto a perforated section makes it difficult for the vapor to flow in this region and that consequently some means of initiating the bubbling is required. The problem is caused by the high gravities and the low permissible dry plate losses of the tray. It was found that this difficulty could be eliminated by a small inlet weir, which apparently allows adequate dispersion of the liquid stream before it reaches the tray surface.

During the succeeding series of experiments other weeping and maldistribution effects were found. These were first brought to light by the seemingly inconsistent nature of the experimental data. Another indication of the difficulty was given by series D and E experiments where the downcomers were located in the center of the tray, as shown in Figures 8 and 9, and liquid flowed both with and against the rotation. The extreme maldistribution effects apparent from these photographs prompted a re-examination of acceleration forces acting upon the liquid. Also, a series of downcomerless or flat plate experiments were initiated specifically to study the weeping behavior.

### 3.3.3 Effect of Coriolis Acceleration Upon Tray Performance

The results of these developments led to the conclusion that Coriolis acceleration exerts a major influence upon the froth behavior and may even lead to inoperable column conditions, especially at low dry plate pressure drops. For the moment let us briefly examine this acceleration in a very simple fashion according to Figure 10 which follows.

63 ASRP-2391

CONFIDENTIAL



CONFIDENTIAL

ASD-TDR-63-665, Part I

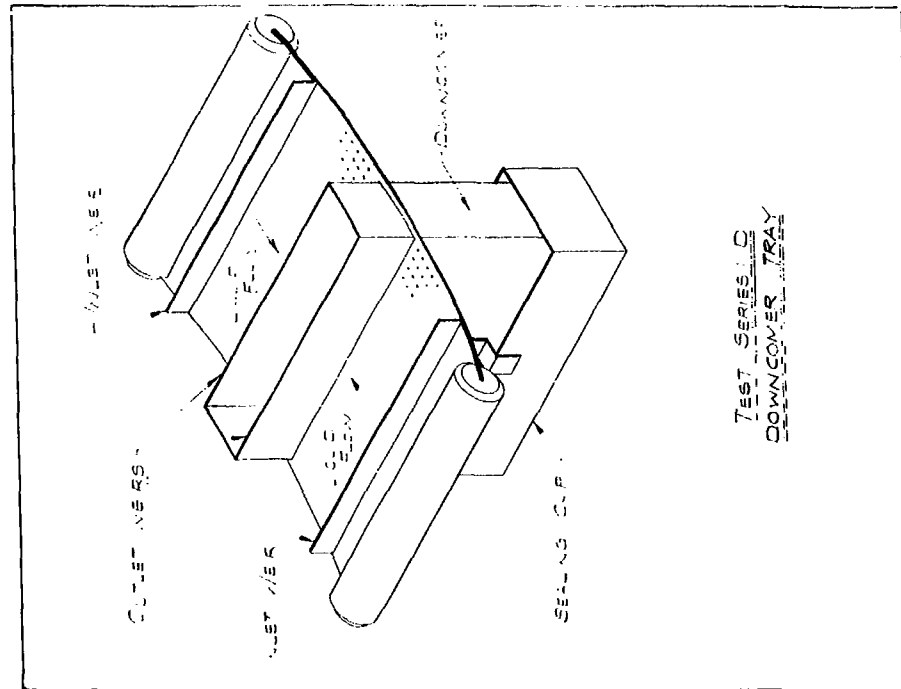


FIG. 8

63 ASRP-2391

CONFIDENTIAL

## 3

— 20 —

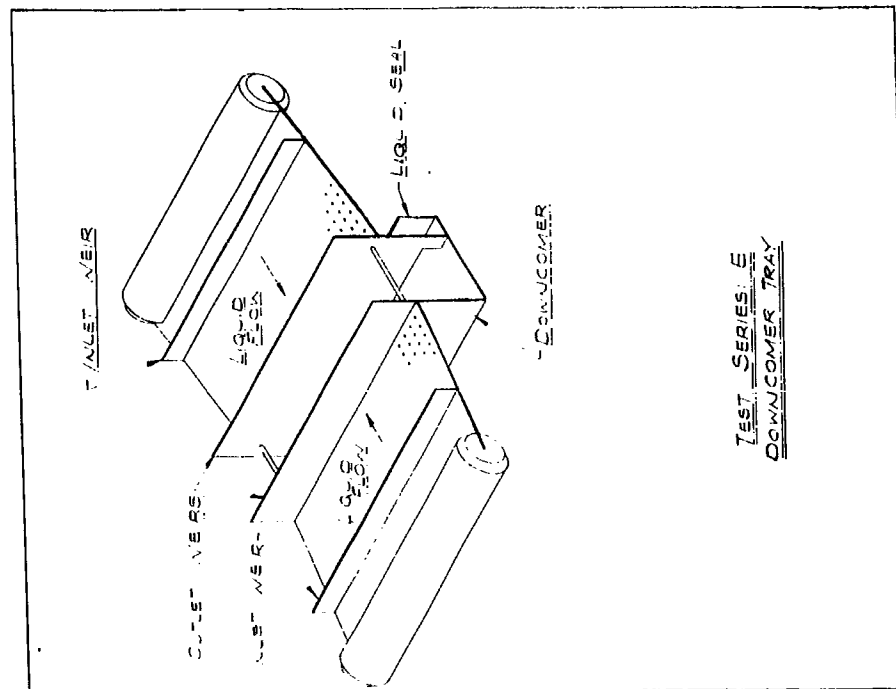


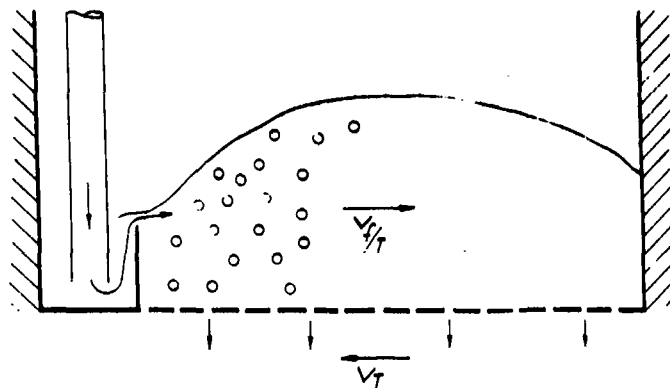
Fig 9

63 ASRP-2391

**CONFIDENTIAL**

# CONFIDENTIAL

ASD-TDR-63-665, Part I



EXAMINATION OF CORIOLIS ACCELERATION

FIG. 10

In relation to a stationary reference frame let the tangential velocity of the tray be  $V_T = R\omega$  as indicated. The gravitational field experienced by it is then given by  $Ng = R\omega^2/g$ . Flow of the liquid on the other hand, occurs against the direction of rotation. The following is the superficial froth velocity relative to the tray:

$$V_{f/T} = (1/b) (Q_L / \alpha h_f) \quad (1)$$

The absolute velocity of the froth (aerated liquid) in reference to a stationary frame, is then given by:

$$V_f = V_T - V_{f/T} \quad (2)$$

Therefore the aerated liquid on the tray experiences a centrifugal acceleration of

$$Ng^o = \frac{(R\omega - \frac{1}{b} [\frac{Q_L}{\alpha h_f}])^2}{R} \quad (3)$$

or

$$Ng^o = R\omega^2 - \frac{2}{b} (\frac{Q_L}{\alpha h_f}) \omega + (\frac{1}{b} \frac{Q_L}{\alpha h_f})^2 \frac{1}{R} \quad (4)$$

63 ASRP-2391

## CONFIDENTIAL

ASD-TDR-63-665, Part I

The second term in the above equation is recognizable as a Coriolis acceleration. It may be shown that within the framework of the experiments, froth velocities in excess of 10ft. per second were not uncommon, leading to a Coriolis component of up to 25%. At the same time, the influence of the third term is usually negligible so that in general one may approximate the effective gravitational acceleration of the froth as it moves along the tray by:

$$Ng^{\circ} \approx (Ng)_c = \frac{R\omega^2 - \frac{2}{b} \left( \frac{Q_L}{\alpha h_f} \right) \omega}{g} \quad (5)$$

By similar reasoning it is, of course, evident that the Coriolis component would be additive if the liquid flow direction were reversed; or in other words, if the path were co-rotational. Under these circumstances the dispersed phase then experiences an acceleration greater than does the tray.

By now, operation of the "flat" or downcomerless trays had already confirmed early speculation as to the importance of this acceleration effect. Figure 11 represents a view of such a tray including a typical operating condition. Here liquid flows counter to the rotation and, while it is flowing, the effective gravitational field might be approximated by equation 5. Upon contact with the wall at the right of the picture it is, however, re-accelerated to the tangential velocity of the rotor, since now  $V_f/T = 0$ . The resultant increase in potential head which includes the increase brought about by the conservation of liquid momentum, causes weeping in the immediate vicinity of the wall, or in this instance, just prior to the dummy outlet weir. This potential head is, of course, counteracted by the upward forces exerted on account of pressure drop across the tray, so that at conditions of high dry plate head losses, the weeping may actually disappear.

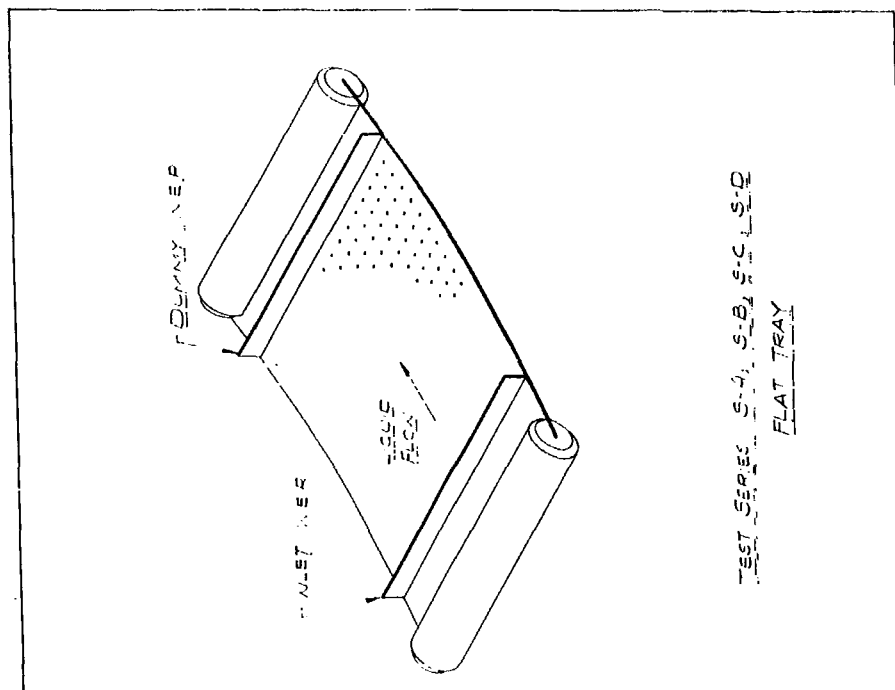
The above reasoning was substantiated by several hundred weeping experiments conducted with "flat", downcomerless trays of various free areas. The construction simplicity and weight advantages of such a tray configuration may in themselves prove to be of major advantage to future designs.

63 ASRP-2391

## CONFIDENTIAL

CONFIDENTIAL

ASD-TDR-63-665, Part I



63 ASRP-2391

CONFIDENTIAL

# CONFIDENTIAL

ASD-TDR-63-665, Part I

## 3.3.4 An Operational Downcomer Tray

These developments now pointed toward two prerequisites for an operational downcomer tray:

For one, the liquid flow direction should be contra-rotational at all times. The resultant Coriolis acceleration effect may then be looked upon as promoting the tray activity at the inlet where the transition from clear to dispersed liquid might otherwise cause weeping. Liquid radial acceleration at the exit, in turn, facilitates froth disengagement and drainage into the downcomer.

Secondly, the use of an outlet weir as such is an ineffective method of froth height control and generally leads to weepage upstream of the weir. A weir or flow barrier must be provided behind the downcomer to accelerate the liquid and thereby to aid the froth disengagement. In a segmental rotor this barrier is, of course, furnished by the confining chamber walls whereas a peripheral contactor must be provided with special flow barriers that are roughly equal in height to that of the froth.

The initial series of multitray experiments were, nevertheless, conducted with a bi-directional liquid flow arrangement as shown in Figure 12. In spite of a sloped inlet section on the two trays with co-rotational flow, the maldistribution effects are very evident from the photograph. While this condition might have been rectified by resizing the tray, reversing the froth flow seemed better. Thus complete contra-rotational liquid flow was chosen for the next two series of multitray experiments as well as for two subsequent series of single tray runs. As seen from Figures 13 and 14, the use of small tubes made this possible even in a segmental column. The vast improvement in tray performance is apparent. In these as well as the prior experiments, outlet weeping was eliminated through use of very low weirs or their elimination altogether.

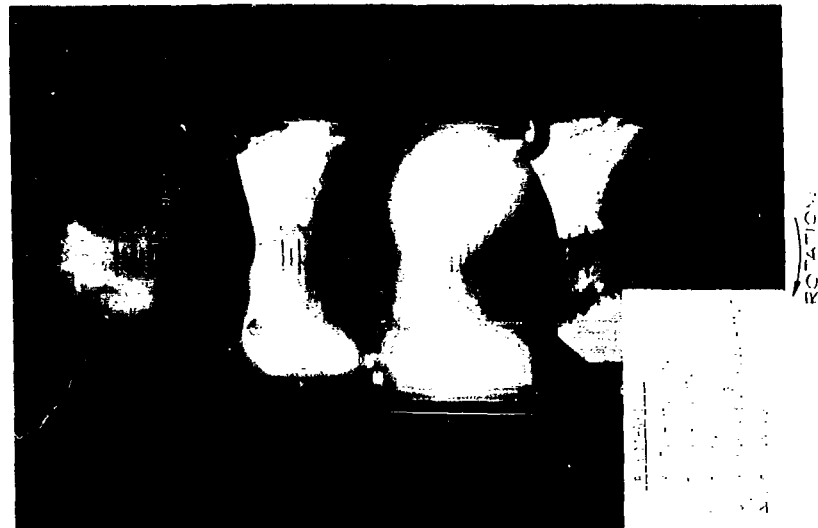
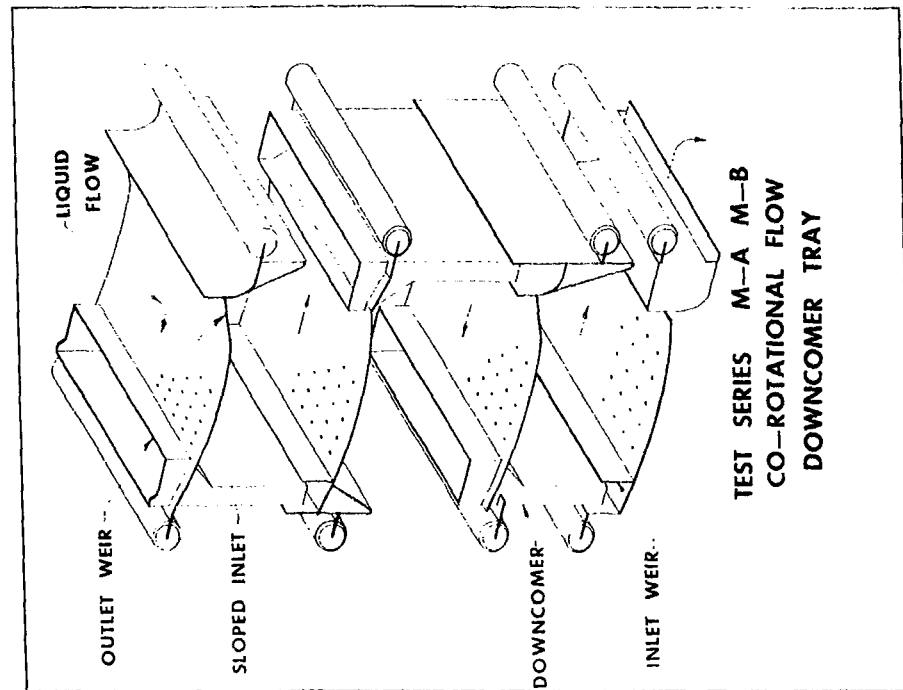
It is this particular tray arrangement which thus represents the end result of the second phase of our development program. Proof testing of this design was subsequently undertaken during a third test phase employing a four-tray circumferential rotor.

63 ASRP-2391

# CONFIDENTIAL

CONFIDENTIAL

ASD-TDR-63-665, Part I

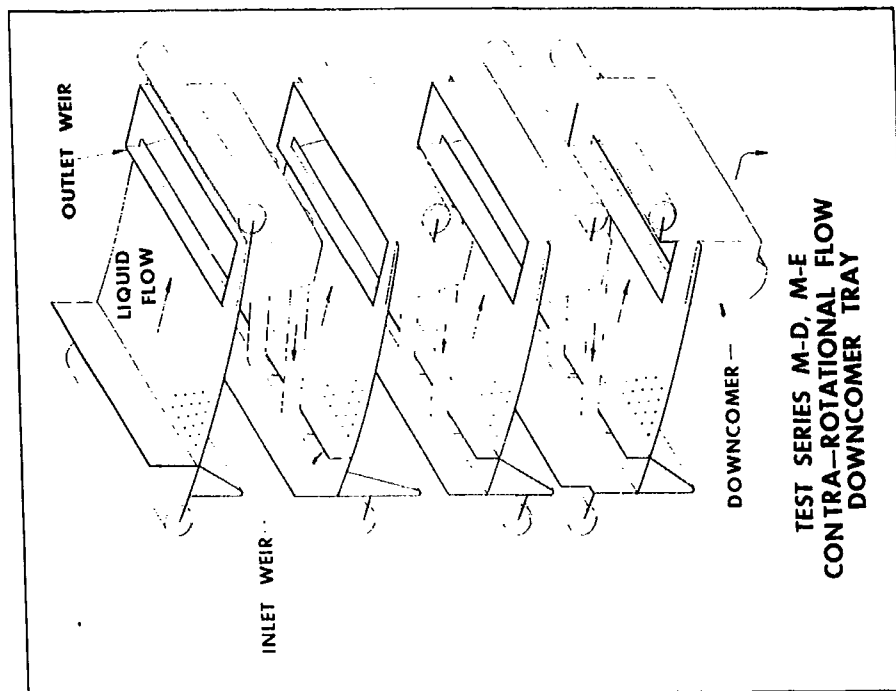


63 ASRP-2391

CONFIDENTIAL

CONFIDENTIAL

ASD-TDR-63-665, Part I



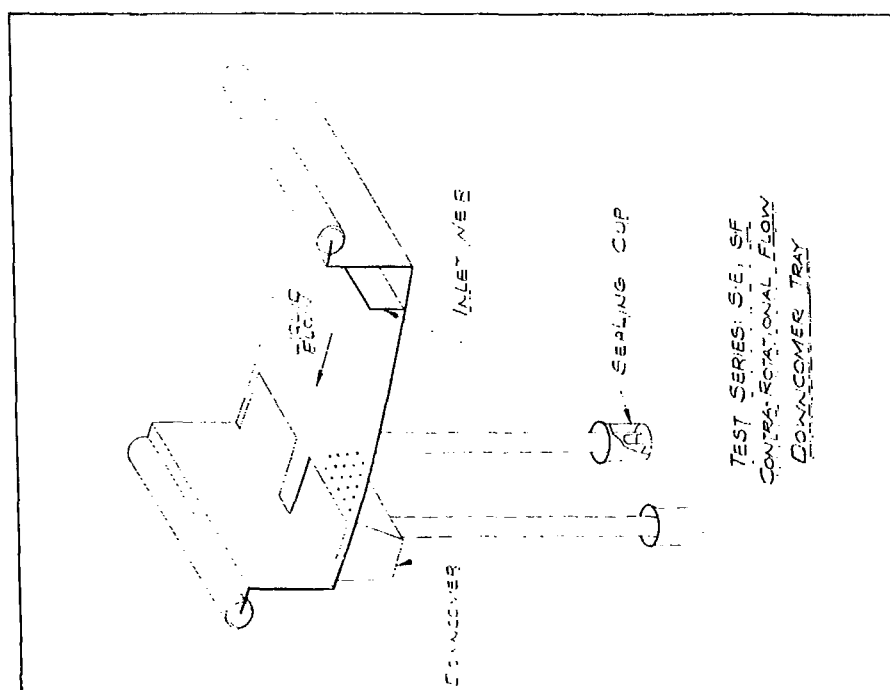
63 ASRP-2391

CONFIDENTIAL



CONFIDENTIAL

ASD-TDR-63-665, Part I



63 ASRP-2391

CONFIDENTIAL

# CONFIDENTIAL

ASD-TDR-63-665, Part I

## 3.3.5 Circumferential Rotor Experiments

To simulate the cryogenic unit, the UCON fluid system was modified, as described in Appendix 1, to provide higher flow rates. UCON 21 was chosen as an operating fluid because its low gas density would yield higher vapor velocities than any other common fluid while it still exhibited physical properties not too different from liquid air.

The tray configuration and a typical operating condition can be seen in Figure 15. During fabrication of the trays, an acid cleaning step was used which resulted in an increase in hole diameter from 0.030 inches to 0.037 inches. This etching increased the free area of the trays from 20% to 24% which caused concern about tray operation. It was shown in the segmental tests that if the dry plate pressure drop was less than 0.3 times the hydrostatic head, the trays could weep excessively. Since it appeared that this would happen with the increased free area, it was decided to block off 3/16 of an inch from both sides of the trays by laying a bead of solder along the edges, thus decreasing the width. This procedure effectively increased the dry plate pressure drop to enable stable tray operation, but caused minor problems in the correlation of the data as discussed later in this report. Table 3 summarizes the geometry of the circumferential trays.

It might be pointed out that the reasons for offsetting the downcomers in the manner shown center around the question of weeping. The arrangement chosen for this column prevents liquid bypassing of more than one contacting stage if weeping occurs, as it usually does, at either the inlet or the outlet of the tray.

The test program demonstrated that the operation of a rotor of this type is both hydraulically and mechanically stable, and that its performance may be predicted correctly by the segmental tray correlations.

## 3.4 Analysis and Correlation of Data

### 3.4.1 Data Reported

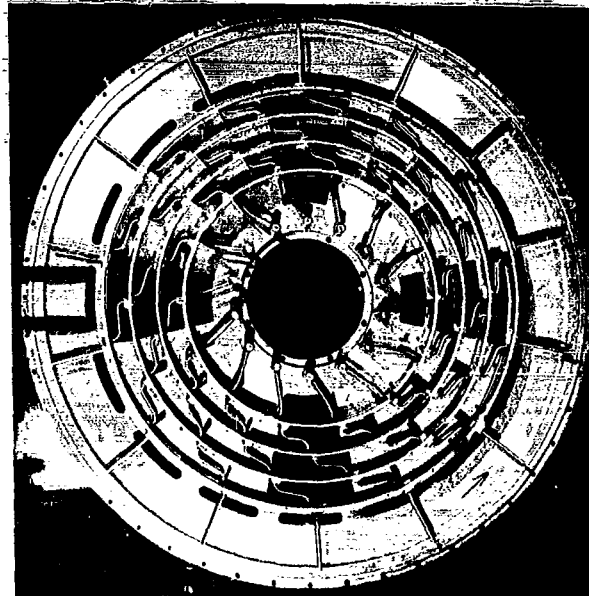
In line with the preceding discussion one might categorize the UCON fluid experiments according to tray type roughly as follows:

63 ASRP 2391

CONFIDENTIAL

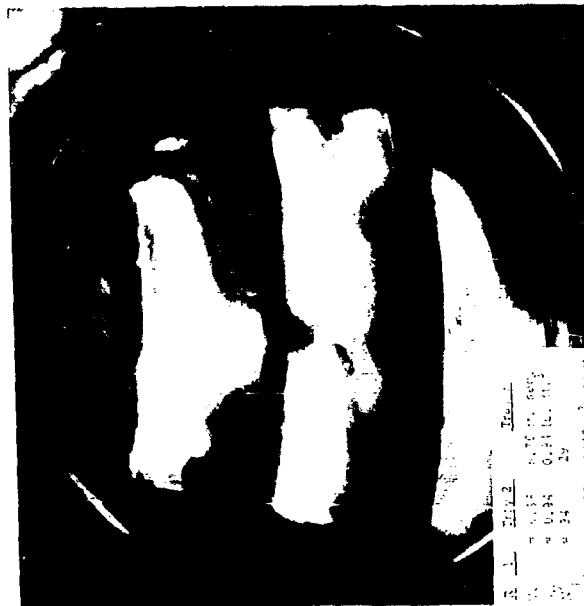
CONFIDENTIAL

ASD-TDR-63-665, Part I



ROTATION

CIRCUMFERENTIAL TRAY  
CONFIGURATION



ROTATION

Fig. 15

63 ASRP-2391

CONFIDENTIAL

CONFIDENTIAL

ASD-TDR-63-665, Part I

TABLE 3

CIRCUMFERENTIAL TRAY GEOMETRY

Tray No.	Radius	b, tot	b, act	L <sub>act</sub>	L <sub>inactive</sub>	A <sub>gross</sub>	A <sub>act</sub>	A <sub>segment</sub>	$\frac{A}{A_g}$	$C_{Ng}^*$ ( $\times 10^{-4}$ )
1	15.25 in	1.50 in.	1.13 in.	5.03 in.	1.81 in.	143.7 in. <sup>2</sup>	79.6 in. <sup>2</sup>	5.68 in. <sup>2</sup>	0.554	4.33
	1.271 ft.	0.125 ft.	0.094 ft.	0.419 ft.	0.151 ft.	0.998 ft. <sup>2</sup>	0.553 ft. <sup>2</sup>	.0394 ft. <sup>2</sup>		
2	13.25 in.	1.72 in.	1.35 in.	4.35 in.	1.59 in.	143.1 in. <sup>2</sup>	82.2 in. <sup>2</sup>	5.87 in. <sup>2</sup>	0.574	3.76
	1.104 ft.	0.143 ft.	0.112 ft.	0.363 ft.	0.133 ft.	0.994 ft. <sup>2</sup>	0.571 ft. <sup>2</sup>	.0408 ft. <sup>2</sup>		
3	11.25 in.	2.03 in.	1.66 in.	3.61 in.	1.44 in.	143.6 in. <sup>2</sup>	83.9 in. <sup>2</sup>	5.99 in. <sup>2</sup>	0.584	3.19
	0.938 ft.	0.169 ft.	0.138 ft.	0.301 ft.	0.120 ft.	0.997 ft. <sup>2</sup>	0.583 ft. <sup>2</sup>	.0416 ft. <sup>2</sup>		
4	9.25 in.	2.48 in.	2.11 in.	2.84 in.	1.31 in.	144.4 in. <sup>2</sup>	83.9 in. <sup>2</sup>	5.99 in. <sup>2</sup>	0.581	2.62
	0.771 ft.	0.207 ft.	0.175 ft.	0.236 ft.	0.109 ft.	1.003 ft. <sup>2</sup>	0.583 ft. <sup>2</sup>	.0416 ft. <sup>2</sup>		

$$* N_g = (C_{Ng})^2 \text{ (RPM)}^2$$

63 ASRP-2391

CONFIDENTIAL

# CONFIDENTIAL

## ASD-TDR-63-665, Part I

- a. Downcomer trays with outlet weirs; contra-rotational as well as co-rotational liquid flow.
- b. Ripple trays; totally counter-current contacting.
- c. Flat plate trays without downcomers; parallel contra-rotational liquid flow path.
- d. Downcomer trays without outlet weirs; contra-rotational liquid flow path.

Experimental results obtained with these various segmental tray geometries are reported in Appendix III. Subsequent circumferential tray data is, in turn, given in Appendix IV while the pertinent physical and thermodynamic fluid properties utilized in the reduction of laboratory data are included in Appendix II. Since the last of the above configurations was established as most suitable for the boilerplate cryogenic air separator, detailed analysis of the data was almost exclusively confined to these trays. Referring to Table 2 this would include test series S-E, S-F, M-A, M-B, M-D, and M-E, covering free areas of from 14 to 26%. The discussion to follow describes the results of this effort.

### 3.4.2 Segmental Tray Data - Hydraulics

#### 3.4.2.1 General Comments

The liquid and vapor phases traverse a downcomer tray in crossflow, liquid flowing for a certain distance along a concentric tray element before being guided via downcomer tubes to the next stage. Vapor, on the other hand, flows in a radially inward direction along a curvilinear path governed in part by the Coriolis forces exerted upon it. In so doing, it is brought into repeated contact with liquid on the trays and forms a more or less homogeneous two-phase dispersion. It is important that, the vapor, be adequately disengaged from the liquid before entering the next tray. The liquid flow across the tray thus represents a complex case of two-phase open channel flow. The crest height at the outlet weir and the resultant froth height establish the minimum spacing between successive trays at a given column operation and are influenced greatly by the prevailing gravitational field. The latter also plays a significant role in the reduction of hydraulic gradients which might normally be expected at the high liquid loadings in question and for trays of any appreciable flow path length.

63 ASRP-2391

# CONFIDENTIAL

## ASD-TDR-63-665, Part I

0

The overall operation of a tray is, in simple terms, bounded by serious liquid entrainment or flooding on the one hand and by weeping or dumping on the other. Since both weeping and entrainment generally occur to some extent at almost all conditions, one can evaluate such factors only in terms of the detrimental effects their existence has upon overall column performance, in particular, upon the tray efficiency. Accurate weeping or entrainment criteria should, therefore, be based upon rate measurements which, of course, are almost impossible to obtain for a rotating assembly of trays. Fortunately, it has been found that at conditions where these effects begin to seriously reduce the tray performance they are also relatively easily discernible by means of visual observations. Weeping and flooding criteria have, therefore, been established for rotating sieve trays in a somewhat arbitrary fashion but have proved to be quite valid for the operating conditions in question.

### 3.4.2.2 The Dispersion Mechanism

Before proceeding with a discussion of the experimental data, it may be worthwhile to speculate as to the dispersion mechanism which governs the hydraulic behavior as well as the mass and momentum transfer characteristics of rotary distillation trays.

In conventional columns the two-phase dispersion takes the form of a froth or foam consisting of numerous bubbles distributed throughout the liquid. At the surface, however, where the bubbles burst, one generally finds a spray extending into the disengagement space, consisting of a multitude of liquid particles of varying sizes. It may also be noted that on conventional cryogenic trays more spray is generated than on an air-water tray. A multitude of visual and photographic observations of rotary sieve trays coupled with some qualitative reasoning has, furthermore, led to the speculation that at the high velocities and gravitational fields in question, the bulk of the two-phase mixture consists of liquid particles dispersed within the gas phase. In part such reasoning is also based upon the work that has been reported in the open literature covering the stability of liquid globules or sheets in turbulent gas streams.

For instance, one may visualize that vapor jets issuing from the perforations at velocities ranging as high as 120 ft./sec. will first disrupt the adjacent liquid layer into numerous fluid ligaments. In so doing, the vapor transfers momentum to the liquid and in essence resumes the superficial column velocity it had prior to entering the plate perforations. The initial liquid filaments are, however, unstable under the

63 ASRP-2391

CONFIDENTIAL

**CONFIDENTIAL**

**ASD-TDR-63-665, Part I**

influence of this turbulent motion and they in turn disintegrate further into globules of progressively smaller sizes. Inasmuch as these seem to depend upon many not readily controllable conditions, it is at present practically impossible to predict theoretically the final size distribution of this or any other dispersion coming about by way of a "chaotic" disintegration process. Based upon available theory one may, however, draw some conclusions as to the factors governing formation of the maximum stable droplets.

Miesse (Ref. 4) and later Fraser (Ref. 5) have dealt with the disintegration of and the droplet formation from moving liquid sheets. It has been shown that small perturbances on the surface created by the action of aerodynamic forces will tend to grow and set up oscillations of the sheet. Under conditions where the aerodynamic forces exceed the interfacial tension forces, unstable waves, either sinous or dilational, are set up and propagate at the same velocity as the sheet and with exponentially increasing amplitude. The result is a disintegration of the sheet into small droplets.

In his study of the disintegration of liquid jets, Miesse (Ref. 4) made the observation that liquid nitrogen data did not at all agree with that of higher surface tension fluids, notably water. He concluded that here the final size distribution of the liquid phase was determined primarily by factors governing secondary atomization processes, that is, the further and more chaotic disintegration of particles originally formed from the jet. In this instance, the original stream could not sustain itself at all but broke up into droplets almost immediately upon leaving the nozzle.

The secondary disintegration of these liquid globules is, of course, once again governed by the interaction of aerodynamic forces tending to deform them and of surface forces acting so as to hold them together. Those tending to deform a particle have a tangential component caused by viscous effects and a normal component caused by the velocity pressures of the ambient fluid stream. Based upon potential flow theory and neglecting viscous forces, Hinze (Ref. 6) devised a stability criterion for spherical particles exposed to a gas stream which takes into account the pressure profile across their surface. He found that splitting of a particle occurs if the Weber number, often defined as

63 ASRP-2391

**CONFIDENTIAL**

# CONFIDENTIAL

## ASD-TDR-63-665, Part I

$$W_e = \frac{D_p \rho_v V^2}{\sigma}$$

exceeds a certain critical value. He proceeded to show in a later paper (Ref. 7) that the value of this critical Weber number is greatly dependent upon both the prevailing flow conditions as well as at times the viscosities of the fluid phases. Three cases were treated:

- a. Deformation in viscous flow.
- b. Breakup in an air stream.
- c. Emulsification in turbulent flow.

Of these, categories b. and c. might well apply to the present situation. In the latter case, dispersion is thought to occur on account of the velocity fluctuations taking place in a turbulent flow field, the pattern of which is, for the special case of isotropic turbulence, solely determined by the energy dissipation per unit time and mass.

Let us assume for the moment that we are, in the case of a rotary distillation tray, dealing with a dispersion mechanism similar to that governing liquid injection into a vapor stream (category b.). Hinze has shown that for a globule in its final stages of disintegration the critical Weber number may then be expressed by the relation:

$$(W_e)_c = C [1 + \phi (N_{v1})] \quad (6)$$

where  $\phi (N_{v1})$  represents a function of a dimensionless viscosity group

$$(N_{v1} = \frac{\mu_L}{\sqrt{\rho_L \sigma D_p}}) \text{ and it approaches zero as } N_{v1} \rightarrow 0.$$

In this form, C is the value of the critical Weber number for a vanishing viscosity effect. The latter condition can be shown to exist in both the UCON fluid and the liquid air systems where now the critical Weber number may, according to Hinze, be taken as equal to  $\sim 13$ . Lane (Ref. 8) also confirmed the direct dependence of the maximum stable droplet size upon surface tension by means of variations in this parameter between 28 and 475 dynes/cm. (.00016 and .0027 lbs.<sub>f</sub>/in.)

Assuming now a typical tray operation at,  $V_s = 10$  ft./sec.,  $\rho_v = 2.2$  lb./ft.<sup>3</sup> and  $\sigma = 8$  dynes/cm, one may estimate that the maximum stable droplet size lies at around 300 microns. Based upon drag

63 ASRP-2391



## CONFIDENTIAL

### ASD-TDR-63-665, Part I

coefficients measured by Ingebo (Ref. 9) in turbulent gas streams, it has been determined that at 260 Ng's, particles of around 26 microns or greater should not be entrained by vapor flowing at the superficial column velocity. As a result of these conjectures one might, therefore, speculate that at this particular operating condition the particle size spectrum might be between 26 and 300 microns. These figures are, incidentally, consistent with pressure drop and total available energy considerations. Assuming the "froth" to consist of uniform spherical droplets and that the entire hydrostatic head loss is reflected in the creation of surface, it may be shown that the minimum diameter is given by the relation:

$$D_{\min} = \frac{6 Q_L \sigma}{v \Delta P g_c} \quad (7)$$

For the operation in question this yields a value of ~ .20 microns; well below the estimated size range. For a pressure atomizer, Consiglio and Slepceovich (Ref. 10) found that the conversion of compression energy to surface energy appears to be constant at approximately .1%. This, of course, leads to an average particle size of 200 $\mu$  for the condition described here, a value that is close to the average one might expect.

As a result of these considerations one would estimate that for the air-water system the droplet spectrum was, for reasons of the higher surface tension, generally shifted toward larger sizes. The effect should then be reflected in somewhat different tray operating characteristics as was indeed found to be the case.

Attempts to resolve this entire question further by way of high speed photographic observations (flash duration 1/2 microsecond) have not been successful so far, mostly because of poor optical conditions. It should also be pointed out that whatever mechanism may prevail at higher gravitational fields and throughputs will most likely not be the same at lower Ng, say around 25 or 50.

#### 3.4.2.3 Vapor Capacity

In general, the vapor capacity of a given tray will be governed by the entrainment of liquid droplets in the gas stream. Under normal tray operation the droplet phase exhibits a clearly visible interface or froth height relative to the vapor space above, much in the same manner as does a solid-gas fluidized bed. At this condition, entrainment occurs by way of two possible mechanisms

63 ASRP-2391

# CONFIDENTIAL

## ASD-TDR-63-665, Part I

controlled either by vapor drag or simply by the droplet ballistics. In the latter case, droplets are visualized as being torn away from the bulk fluid and hurled up into the disengagement space between trays at an initial velocity  $V_D$ . They would then reach a height given by:

$$H = \frac{V_D^2}{2 N g} \quad (8)$$

If it is further assumed that at high vapor velocities,  $V_D$  is proportional to  $V_s$ , then, for a given disengagement space  $H$ , the allowable gas throughput would tend to increase with the square root of the gravitational field.

In terms of the alternate entrainment mechanism, the particles at the surface of the froth are thought to be swept along by vapor as soon as the drag exerted upon them exceeds the gravitational forces tending to keep them on the tray. In terms of a single droplet of mean diameter  $\bar{D}_p$  suspended in an infinite gas medium, this model yields an equation for the maximum allowable vapor velocity of the form:

$$V_s(\max) = \sqrt{\frac{4}{3} \frac{g_c \bar{D}_p}{C_D} N g \frac{(\rho_L - \rho_v)}{\rho_v}} \quad (9)$$

Here again, allowable vapor velocity increases with  $\sqrt{N g}$ . From the previous discussion concerning the dispersion mechanism it is apparent that a value of  $\bar{D}_p$  cannot be computed with reasonable certainty. One may, nevertheless, conclude that of the pertinent physical properties the surface tension could play the most important role in determining the mean particle diameter. The drag coefficient,  $C_D$ , is similarly a rather difficult quantity to ascertain for a multi-particulate system in turbulent gas flow. Based upon data presented by Dryden (Ref. 11) and by Torobin (Ref. 12), fluid turbulence may, for instance, have a significant effect upon its value. Their results have shown that on account of high turbulence intensities,  $C_D$  may be reduced appreciably below what it is for single spheres in a laminar gas stream; at times even lower than the value of .4 commonly accepted in the Newtonian range.

Experimentally, the maximum permissible vapor velocity was established as that condition where the column is essentially incapable of sustaining counter-current flow of the phases and where the liquid phase is at the verge of total entrainment. At a given vapor velocity, density and a minute liquid flow rate, this point was found by lowering the tester speed until the liquid just hovered on the tray. Any further reduction then resulted in total entrainment or complete flooding of the column.

63 ASRP-2391

## CONFIDENTIAL

### ASD-TDR-63-665, Part I

In this limit, the entrainment is normally drag controlled and should correlate accordingly. Figure 16 represents the data obtained during runs conducted with trays from 14 to 34% free area where the latter effect was apparently of little or no significance. The drag mechanism seems to be confirmed by this correlation although the question of particle diameter and  $C_D$  are sidestepped for the moment. The maximum allowable vapor velocity may then be obtained as:

$$V_{s \max.} = 0.14 \sqrt{Ng \frac{(\rho_L - \rho_v)}{\rho_v}} \quad (10)$$

Although this type of data was not taken directly during air-water experiments, a similar flooding criterion could be derived from the available information as shown in Figure 17. Actual operating points that were closest to flooding are plotted here for the UCON as well as the air-water systems. The differences in performance are indeed quite startling, pointing toward substantially higher throughput capabilities with the latter system.

The exact reasons for this difference are difficult to ascertain. Based upon earlier discussions of the dispersion mechanism one can, of course, speculate that the discrepancy results from a variation in the size distribution of the liquid particles on the tray as brought on mainly by differences in physical properties. Of these, the surface tension might play a most significant role. If the entire shift in operation were attributed to surface tension differences, then the maximum allowable vapor velocity would tend to depend upon this parameter as:

$$V_s \approx \sigma^{1/3}$$

For purposes of predicting the performance of a liquid air separator it is, nevertheless, recommended that the UCON fluid data be used directly and without a surface tension correction. It essentially covers a range in the latter parameter nearly identical to that expected in cryogenic service. (See Table 1)

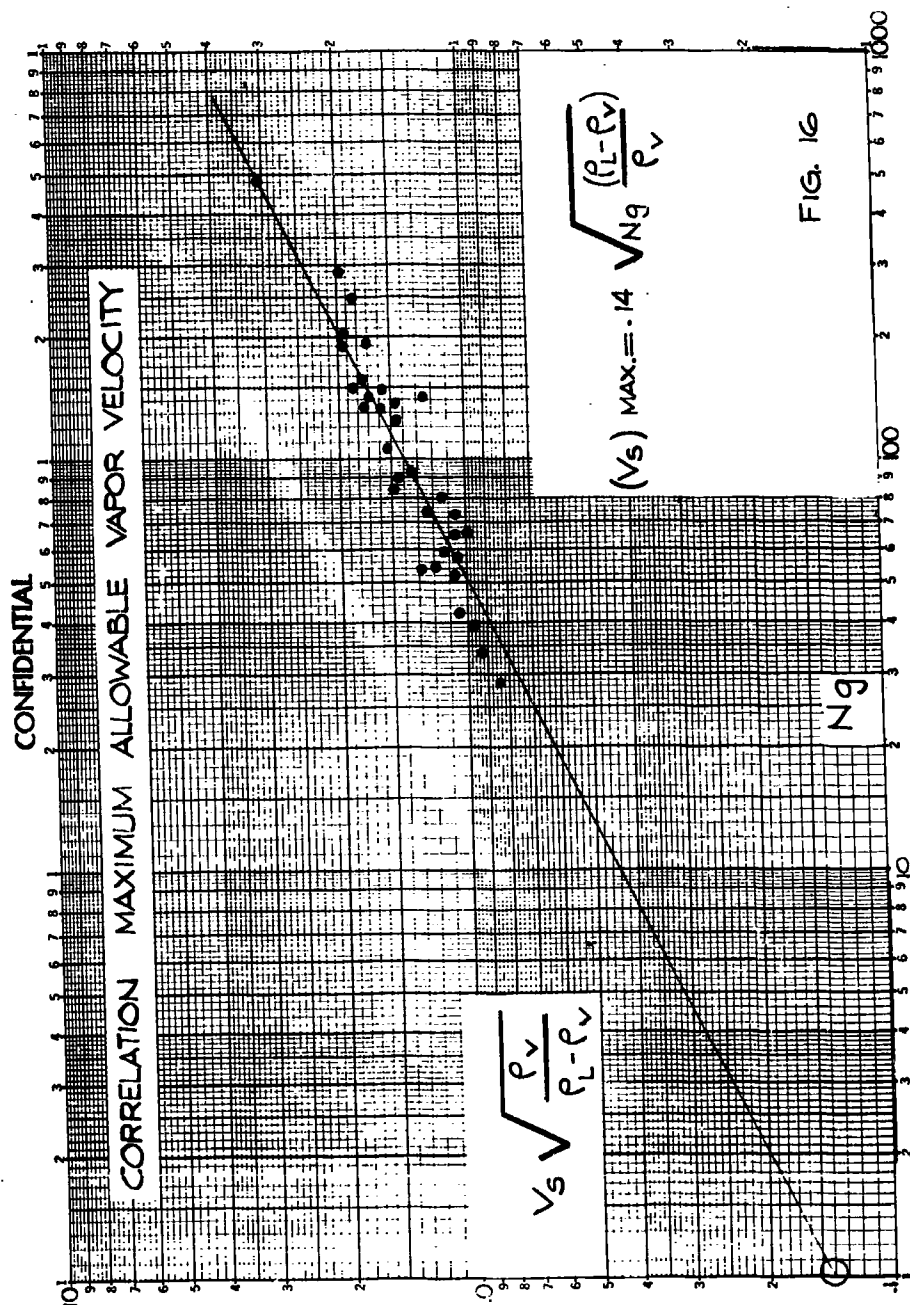
At column accelerations substantially higher than those resulting in flooding as defined by equation 10, there appears to be negligible entrainment; negligible from the point of view that it seems of no detriment to the tray efficiency. This was found to be the case at

63 ASRP-2391

## CONFIDENTIAL

CONFIDENTIAL

ASD-TDR-63-665, Part I



63 ASRP-2391

CONFIDENTIAL

CONFIDENTIAL

ASD-TDR-63-665, Part I

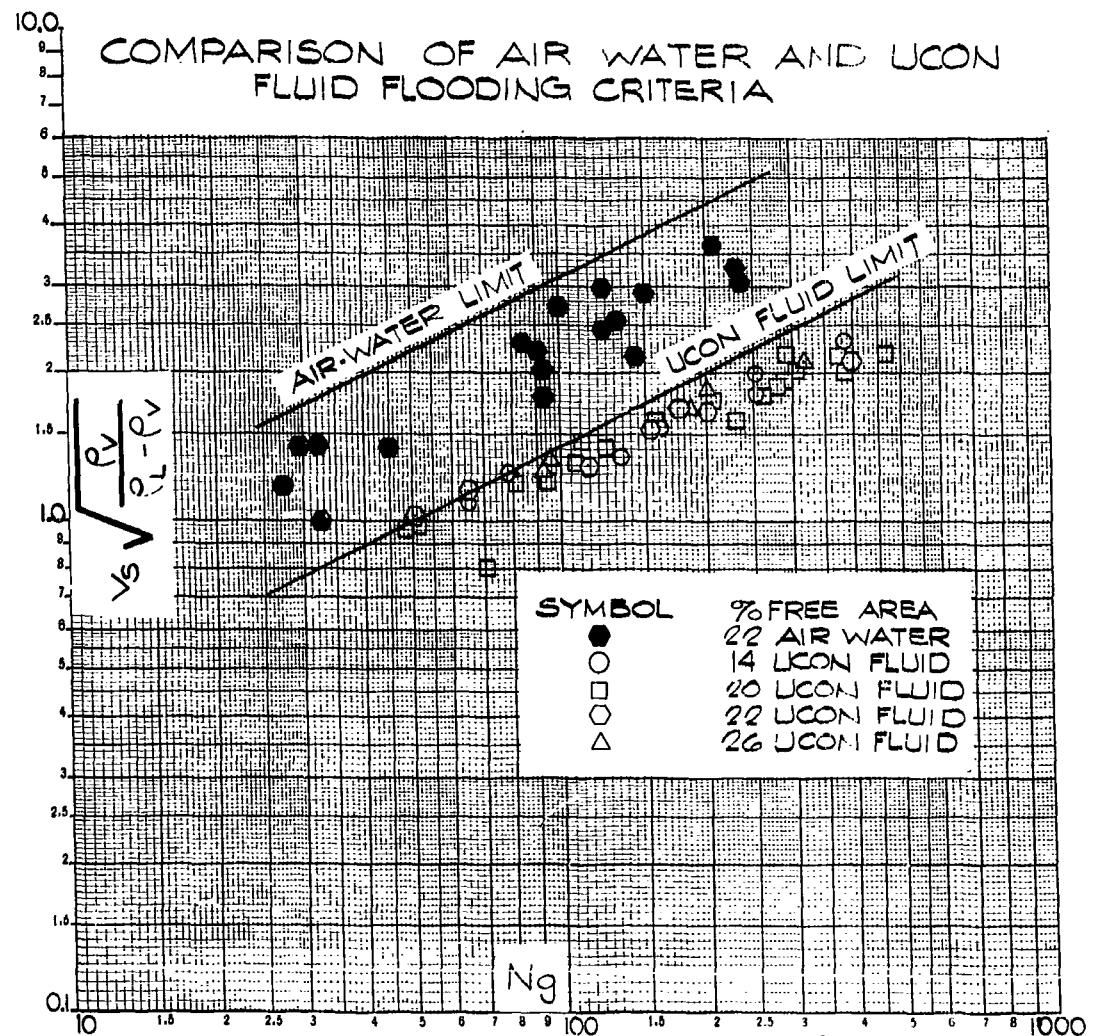


FIG. 17

CONFIDENTIAL

# CONFIDENTIAL

ASD-TDR-63-665, Part I

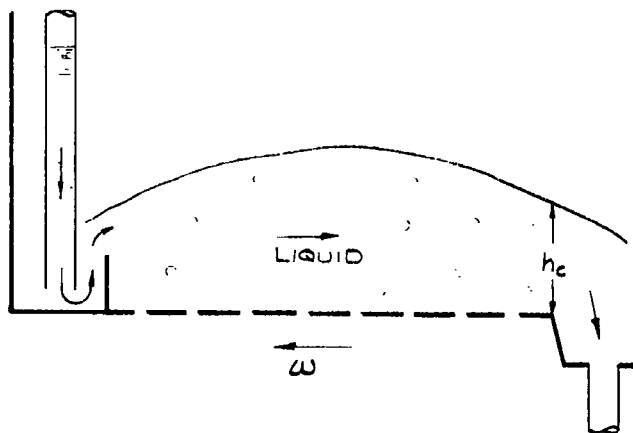
disengagement spaces as low as 1/4 inch. One reason may be the fact that the majority of liquid droplets are much too large to be entrained on account of vapor drag and that they are not hurled to any appreciable height ballistically. Examination of over a hundred tray photographs has led to the conclusion that existing perturbances at the froth interface are, nevertheless, most likely due to some minor ballistic entrainment. This data has been found to correlate roughly according to the latter model which is also recommended for purposes of establishing the required disengagement space.

$$\text{Thus, } H = .05 \frac{V_s^2}{Ng} \quad (11)$$

## 3.4.2.4 Liquid Capacity and Froth Heights

### 3.4.2.4.1 The Crest Equation

The vapor rate alone is, however, not the sole capacity criterion of a rotary distillation column. At the high loadings to be expected in an air-borne air separation plant, the ability of a tray to handle large liquid quantities is equally important. Thus, liquid has to flow through downcomer tubes, across an inlet weir, over the tray segment and back into the downcomer of the next tray as shown in Figure 18



TRAY LIQUID FLOW

FIG. 18

63 ASRP-2391

CONFIDENTIAL

# CONFIDENTIAL

## ASD-TDR-63-665, Part I

The crest height equals the height of the tray foam measured from the top of the outlet weir while the froth height equals the height of the tray foam measured from the perforated tray. If there is no outlet weir as in the case of the finally chosen downcomer tray, the crest height equals the froth height so the terms can be used interchangeably.

Of the resistances offered to this transport of liquid, those attributed to the flow of aerated fluid generally control in a high gravitational field. The foam or crest height established at the outlet of the tray is, in turn, the prime factor determining the required tray spacing. As of this date no theoretical treatment is available which describes the complex fluid dynamics of two-phase open channel and weir flow as it exists on a distillation tray. Based upon extensions of single phase theory, a number of semiempirical approaches are commonly employed which are, nevertheless, still not directly applicable to the present situation. Consequently, a digital computer and linear regression techniques were employed in establishing a workable correlation. The froth height was thought to be governed by the following independent variables:

$$h_f = \phi \left[ V_s, Ng, \frac{\rho_v}{\rho_L - \rho_v}, \frac{Q_L}{b}, f \right]$$

where their sequence as shown here corresponds roughly to the order of their significance. Figure 19 shows the effect of the gravitational field upon the froth height at various operating conditions; the overall effect being a decrease in  $h_f$  with increasing values of  $Ng$ . Figure 20 points to the relatively minor influence of liquid rate upon the froth height. There is no complete explanation available as to why the liquid velocity is less significant in foam flow than it is in single phase liquid flow where, for instance, the Francis weir equation predicts a dependence of  $h_c$  upon  $\left(\frac{Q_L}{b}\right)$  to the 2/3 power. Close examination of Figure 20 does however point to an interesting yet unconfirmed finding as to the possible influence of perforation velocity upon the liquid rate. In these as well as in a number of similar but constant free area runs, there appears to be a slight increase in the power of  $\frac{Q_L}{b}$  at lower perforation velocities; the value of 2/3 being approached as a limit. This effect could, however, not be substantiated completely on account of the basic inaccuracies that are involved in measurements of froth height.

63 ASRP-2391

# CONFIDENTIAL

CONFIDENTIAL

ASD-TDR-63-665, Part I

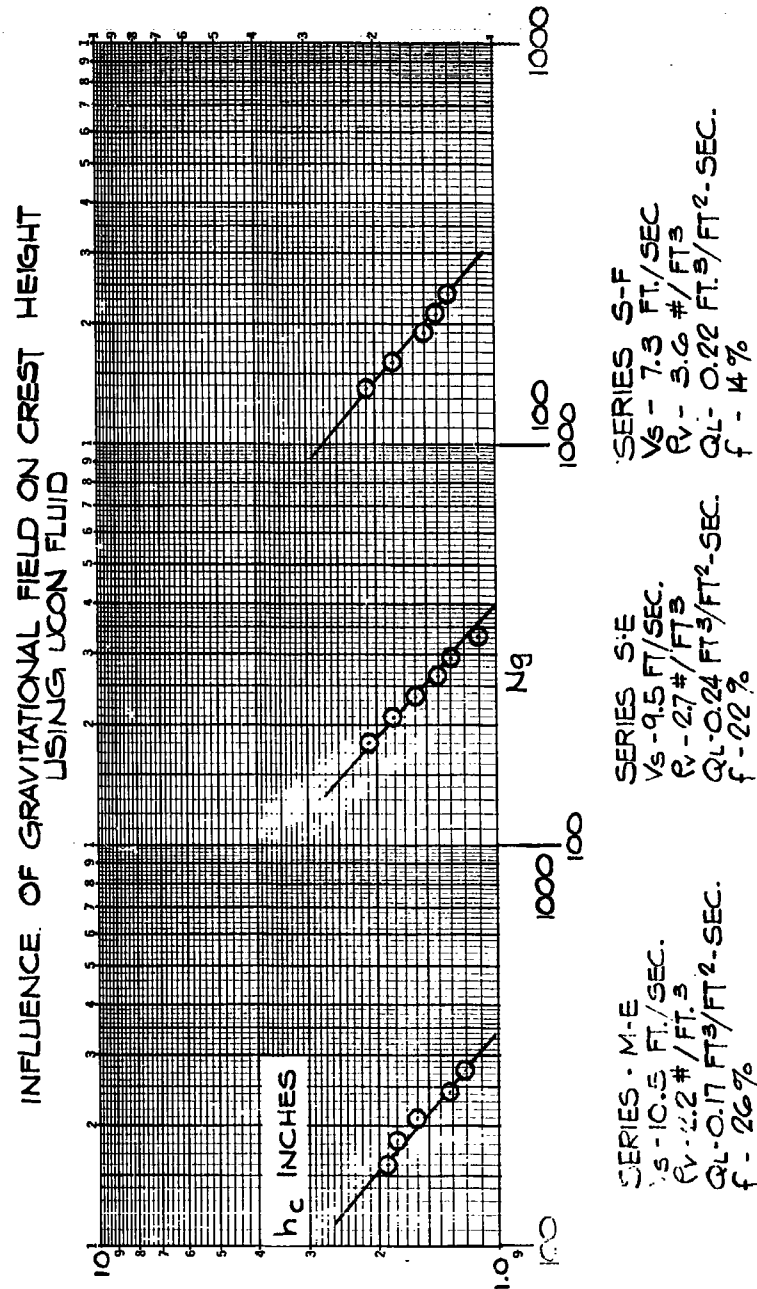


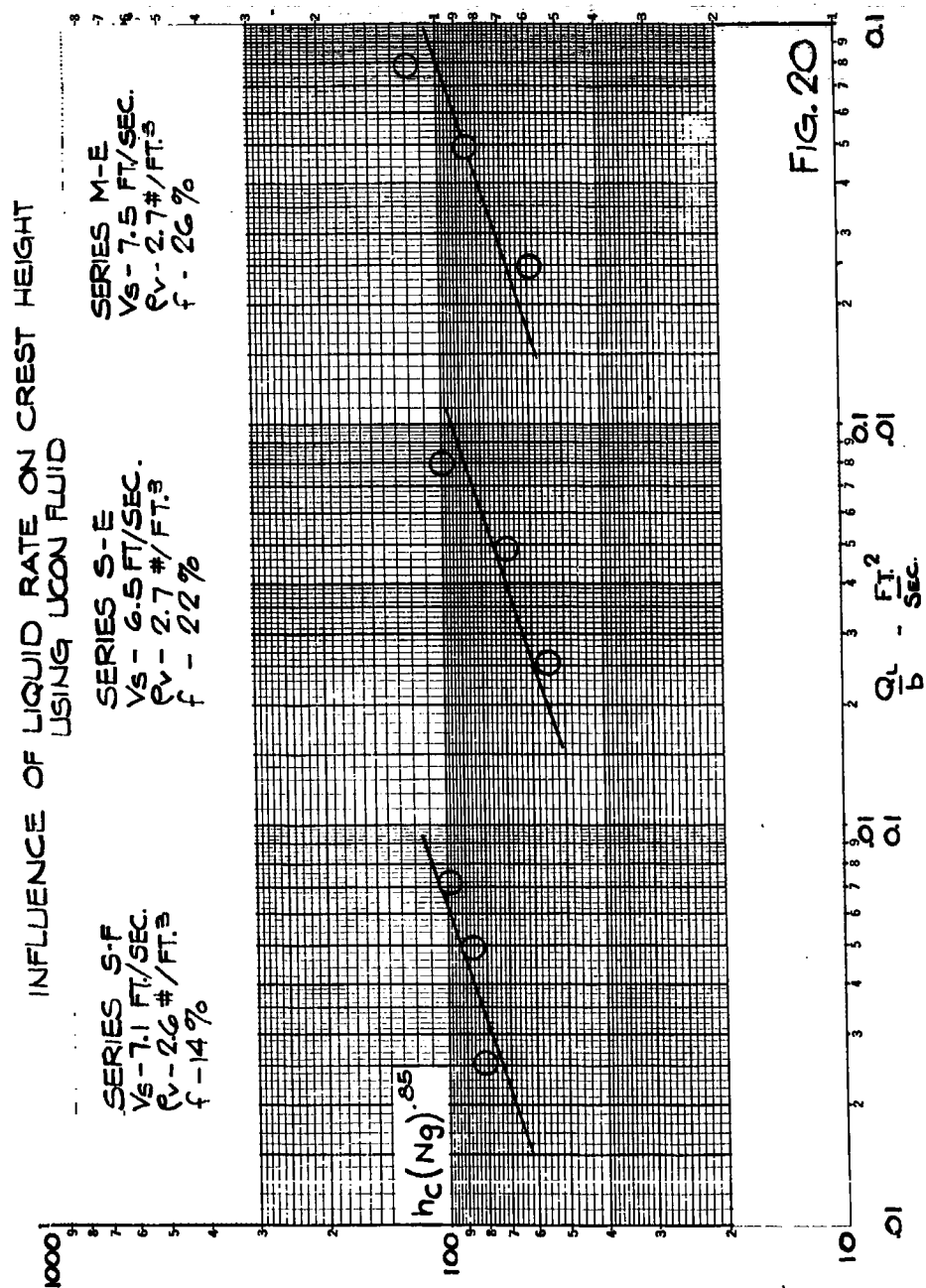
FIG. 19

CONFIDENTIAL



CONFIDENTIAL

ASD-TDR-63-665, Part I



CONFIDENTIAL

# CONFIDENTIAL

## ASD-TDR-63-665, Part I

Figure 21 summarizes the final correlation as established for downcomer trays from 14 to 26% free area and at perforation velocities up to 120 ft./sec.

$$h'_c \text{ (inches)} = \frac{48.7 \left( \frac{Q_L}{b} \right)^{1/3} V_s^{1.6} \left( \frac{\rho_v}{\rho_L - \rho_v} \right)^{1/2}}{(Ng)^{.85} f^{.13}} \quad (12)$$

The above equation represents all the data to within a standard deviation of .22 inches and 95% of the points to within .174 inches. In comparison to this, an analysis of the available tray photographs and their consequent comparison to visually determined foam heights yielded a standard difference of about .18 inches.

Once more re-evaluation of the air-water data seemed to be in order. The results are shown in Figure 22 and are also based upon an analysis made by linear regression. Again the data is seen to correlate well according to the overall functional relationships established in UCON fluid service, yet there is a similar displacement toward higher throughputs as was the case with flooding data. For a liquid air design it is, nevertheless, recommended that use be made only of the UCON fluid correlation and that no further physical property adjustment be made at this time.

### 3.4.2.4.2 Miscellaneous Losses

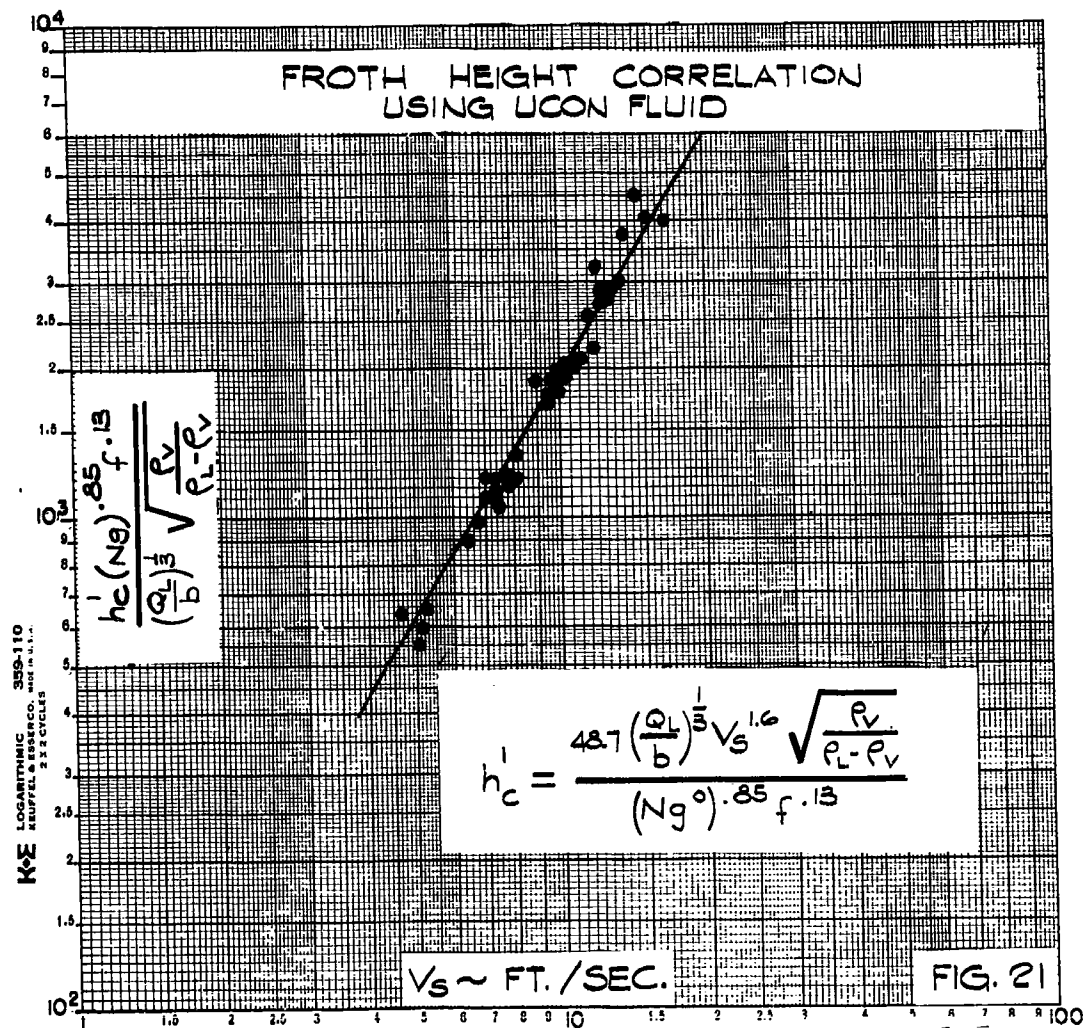
In flowing from one stage to the next, the liquid stream encounters a number of additional resistances other than that represented by the foam crest at the tray exit. These so called liquid phase head losses are, for instance, due to downcomer tube friction, flow reversal at the inlet receiving cup, introduction of liquid into the froth layer and then also the flow resistance offered by the tray channel itself. In combination with the equivalent gas phase head loss between two stages they are characterized by the level at which liquid will stand in the downcomer tubes. It is evident that the tray spacing, in turn, must be greater than this sum total of these losses so as to prevent flooding of the column by liquid accumulating in the downcomer.

In computing the magnitude of these various flow resistances, conventional column technology must be extended. One of the more difficult quantities to ascertain, however, involves the hydraulic gradient to be expected on longer tray elements. The data obtained so far has unfortunately not been able to shed much light upon the subject since neither the segmental nor the circumferential tray tests closely simulated the anticipated

63 ASRP-2391

CONFIDENTIAL

ASD-TDR-63-665, Part I



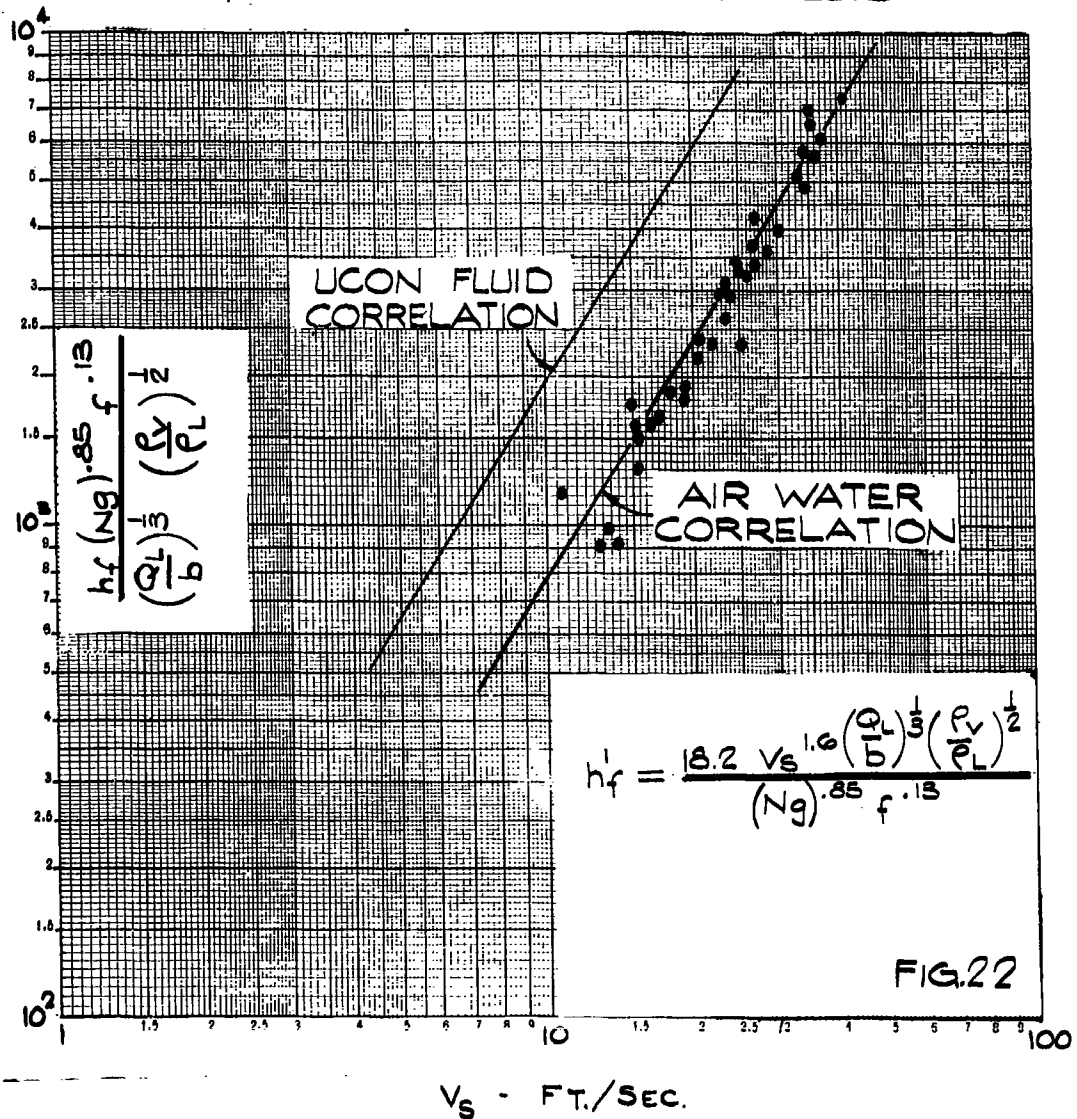
CONFIDENTIAL

CONFIDENTIAL

ASD-TDR-63-665, Part I

0

FOAM HEIGHT CORRELATION COMPARISON  
USING AIR-WATER AND UCON FLUID



CONFIDENTIAL

# CONFIDENTIAL

## ASD-TDR-63-665, Part I

low temperature conditions. Based upon available column technology it has been estimated that for tray lengths of less than two feet, hydraulic gradients are negligible. Considering, on the other hand, the present lack of substantiating data, it is recommended that the lengths be maintained below one foot. As a general rule one might propose, furthermore, that the individual trays be designed so as to not make their spacing limited by the liquid phase losses described here.

### 3.4.2.5 Vapor Phase Pressure Drop

#### 3.4.2.5.1 Theoretical Considerations

In passing through a contacting stage vapor undergoes two major types of pressure drop, static and frictional. The static pressure drop is due to the "weight" of the vapor itself and, though large enough in centrifugal columns to be of prime importance to a designer, will not concern us here. The so-called frictional pressure drop (which includes liquid body forces and changes in vapor momentum) is derived from experimental data and hence will now be discussed.

Vapor in passing through a contacting stage will undergo a two-fold frictional pressure drop, that on account of the tray perforations, and that due to the presence of the liquid dispersion above the tray. This vapor phase head loss plays a critical role in establishing the power requirement of an air separation cycle and was, therefore, measured directly by means of a transducer located within the rotor. (The experimental  $\Delta P$  values do not include the static head of vapor across a radial increment between the trays.)

The tray as shown in Figure 23 is examined in conjunction with an overall force balance around a given control volume bounded radially by the inward surface of the tray and the top of the froth.

63 ASRP-2391

# CONFIDENTIAL

**CONFIDENTIAL**

ASD-TDR-63-665, Part I

TRAY PRESSURE DROP

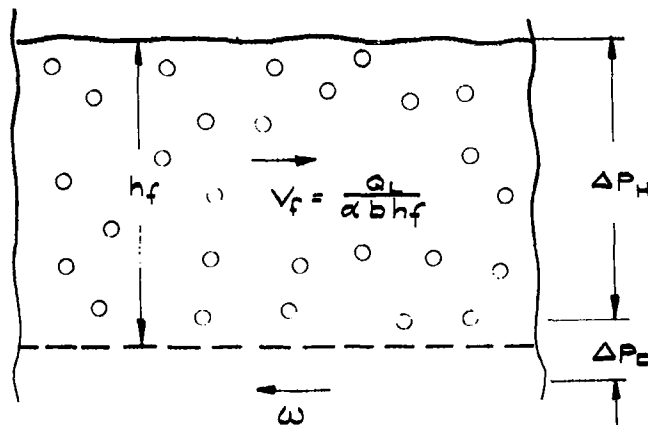


FIG. 23

Neglecting time dependent changes of momentum within the control volume, the following summation of body, surface and momentum forces applied:

$$\Sigma F_b + \Sigma F_s + \Sigma F_m = 0 \quad (13)$$

Assuming the momentum transport across the lateral boundaries as algebraically zero, the above forces may then be defined further as:

$$\Sigma F_b = h_f Ng [\alpha \rho_L + (1-\alpha) \rho_v] \quad (14)$$

where  $\alpha$  represents the volumetric liquid fraction of the froth on the tray. The surface force at the tray is equal to  $P$ , whereas that near the upper boundary is  $P - \Delta P_h$ . Thus,

$$\Sigma F_s = P_1 - P_2 = \Delta P_h \quad (15)$$

The momentum of the gas entering the control volume is:

$$\frac{\rho_v V_s^2}{g_c f}$$

63 ASRP-2391

**CONFIDENTIAL**

# CONFIDENTIAL

## ASD-TDR-63-665, Part I

while, under the assumption of a uniform velocity profile, that leaving is:

$$\frac{\rho_v}{g_c} V_s^2$$

As a result:

$$\Sigma F_m = \frac{\rho_v V_s^2}{g_c} \left( \frac{1}{f} - 1 \right) \quad (16)$$

Similarly, the observed pressure drop may be written as follows:

$$\Delta P_o = \Delta P_D + \Delta P_h - \rho_v h_f Ng \quad (17)$$

Here,  $\Delta P_D$  is the pressure drop suffered by vapor in passing through the plate perforations. It is defined as,

$$\Delta P_D = \frac{1}{C_v^2} \frac{\rho_v}{2g_c} \left( \frac{V_s^2}{f} \right) \quad (18)$$

Substitution of these equations into equation (17) yields the following equation for the frictional pressure drop through a given contacting stage:

$$\Delta P_o = \left[ \left( 1 - \frac{1}{f} \right) + \frac{1}{2C_v^2 f^2} \right] \frac{\rho_v V_s^2}{g_c} + \alpha Ng h_f (\rho_L - \rho_v) \quad (19)$$

To be exact, the value of  $Ng$  should be the gravitational field actually experienced by the dispersion within the control volume and as such must include the effect of liquid flow direction. For a contra-rotational liquid passage, it was shown earlier that:

$$Ng^o \approx Ng - \frac{2 \omega}{g_c h_f} \left( \frac{Q_L}{\alpha b} \right) \quad (20)$$

Substitution of this expression into equation (19) finally yields:

$$\Delta P_o = \left[ \left( 1 - \frac{1}{f} \right) + \frac{1}{2C_v^2 f^2} \right] \frac{\rho_v V_s^2}{g_c} + \left( \alpha - \frac{\delta}{Ng} \right) h_f Ng (\rho_L - \rho_v) \quad (21)$$

63 ASRP-2391

# CONFIDENTIAL

ASD-TDR-63-665, Part I

where  $\delta$  is now defined as:

$$\frac{2 \omega}{g_c h_f} \left( \frac{Q_L}{b} \right)$$

There are two unknown quantities in the above equation, namely  $C_v$  and  $\alpha$ . The latter could only be derived from experimental pressure drop measurements and a known value of  $C_v$ . Thus, by rearrangement of equation (21) the same can be used to define the volumetric froth density as follows:

$$\alpha = \frac{\Delta P_o - \frac{\rho_v V_s^2}{g_c} \left[ \left(1 - \frac{1}{f}\right) + \frac{1}{2 C_v^2 f^2} \right]}{N g h_f (\rho_L - \rho_v)} - \frac{2 \omega}{N g g_c h_f} \left( \frac{Q_L}{b} \right) \quad (22)$$

From these relations, it would also appear that under conditions where the upward momentum force equals the body forces or the hydrostatic head, the froth should once again just hover on the tray or lie at the verge of fluidization. Such a situation might then constitute another performance limit not to be exceeded. It has been found, however, that in practice trays will still operate at conditions where  $\Sigma F_m > \Sigma F_b$ , but that such operation is most undesirable. Extreme jetting and slugging of liquid will generally occur, resulting in considerable ballistic entrainment and reduced mass transfer efficiencies. It may be shown that, fortunately, such a situation seldom, if ever, arises at high gravities and that normally skin and form drag represent the true operating limit.

## 3.4.3.5.2 Discharge Coefficients of Perforated Plates

The determination of  $\alpha$  by way of Equation (22) requires rather accurate knowledge of the orifice coefficient  $C_v$ . Inasmuch as there exist widely differing values for this quantity, it was decided that some measurements be made in conjunction with the flat plate experiments and directly within the rotary test chamber. This then allowed the use of UCON 114 as the gas phase in addition to providing a means of testing the reliability of the transducer system through measurements conducted at various rotational speeds.

Orifice coefficients were determined with four different tray specimens according to Equation (18). Compressibility effects may

63 ASRP-2391



# CONFIDENTIAL

## ASD-TDR-63-665, Part I

be shown as negligible under present circumstances. The value of  $C_v$  was not only found to be closer to unity than first expected but was evidently not a function of the perforation Reynolds number. Instead, there seemed to be a stronger dependence upon the plate characteristics. A brief search of the literature led to the work of Kolodzie & vanWinkle (Ref. 13) who conducted an extensive investigation of this particular subject using a multitude of different plate configurations. In general, the coefficient of discharge was found to be a function of the following dimensionless groupings:

$$C_v = \phi \left[ \left( \frac{D_o V_o \rho_v}{\mu} \right), \frac{D_o}{P_o}, \frac{t}{D_o} \right]$$

Figure 24 is a sample reproduction of their results showing the influence of Reynolds number at various plate thickness to orifice diameter ratios. The present data, all at  $(Re)_o$  values greater than 20,000, is in essential agreement with these findings. Figure 25 represents a summary correlation as reported by Kolodzie and as now recommended for the design of rotary sieve plate columns. In passing, it should also be mentioned that a marked reduction in coefficient was reported by these authors when the active tray area fell below 50%. Fortunately, such conditions seldom, if ever, exist in actual distillation practice.

Table 4 summarizes the pertinent tray dimensions as chosen for this development program, showing the computed and experimental discharge coefficients.

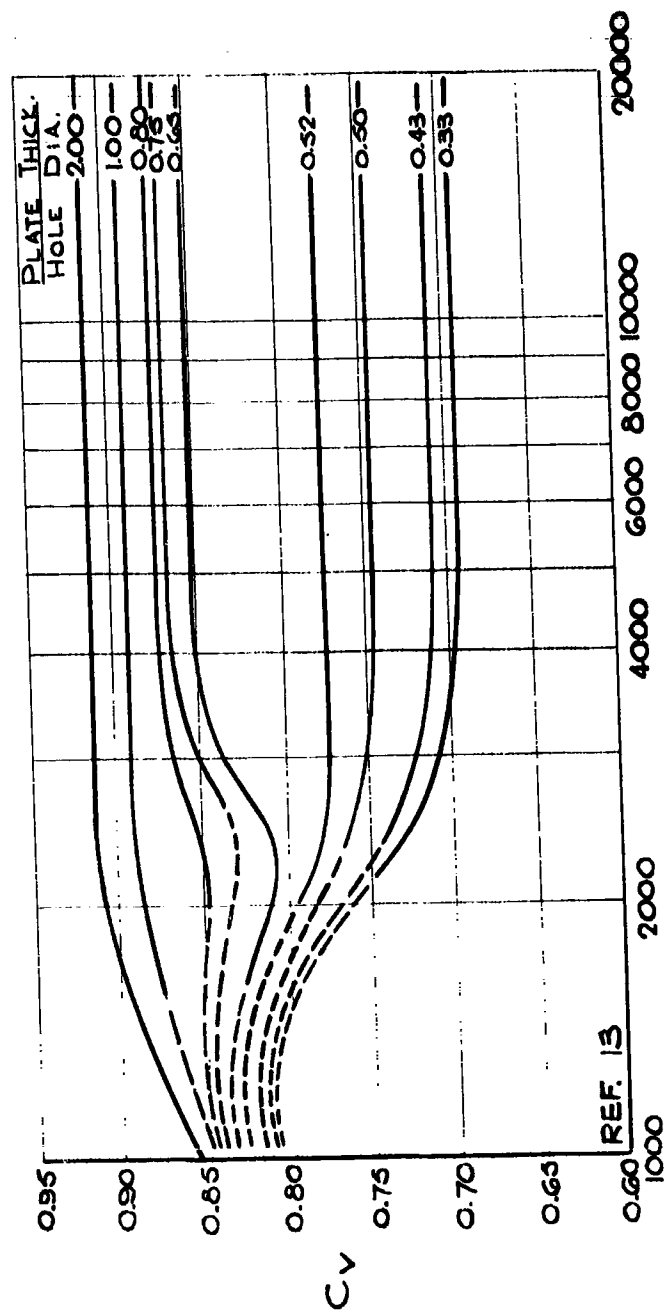
Table 4

### Orifice Coefficients of Sieve Trays

% Free Area	$\frac{D_o}{P_o}$	$\frac{t}{D_o}$	$C_v$ (computed)	$C_v$ (exper.)
14	.423	1.14	.880	----
20	.500	.576	.820	----
22	.482	.951	.885	.912
22.1	.506	.621	.840	.833
26	.500	1.05	.895	----
28.7	.563	.917	.900	.945
34	.500	.727	.861	.800
45	.576	.842	----	----

63 ASRP-2391

ORIFICE COEFFICIENT VERSUS REYNOLD'S NUMBER



$$Re_o \sim \left( \frac{P^o}{D_o} = 2 \right)$$

Fig 24

ORIFICE COEFFICIENT - SUMMARY CORRELATION

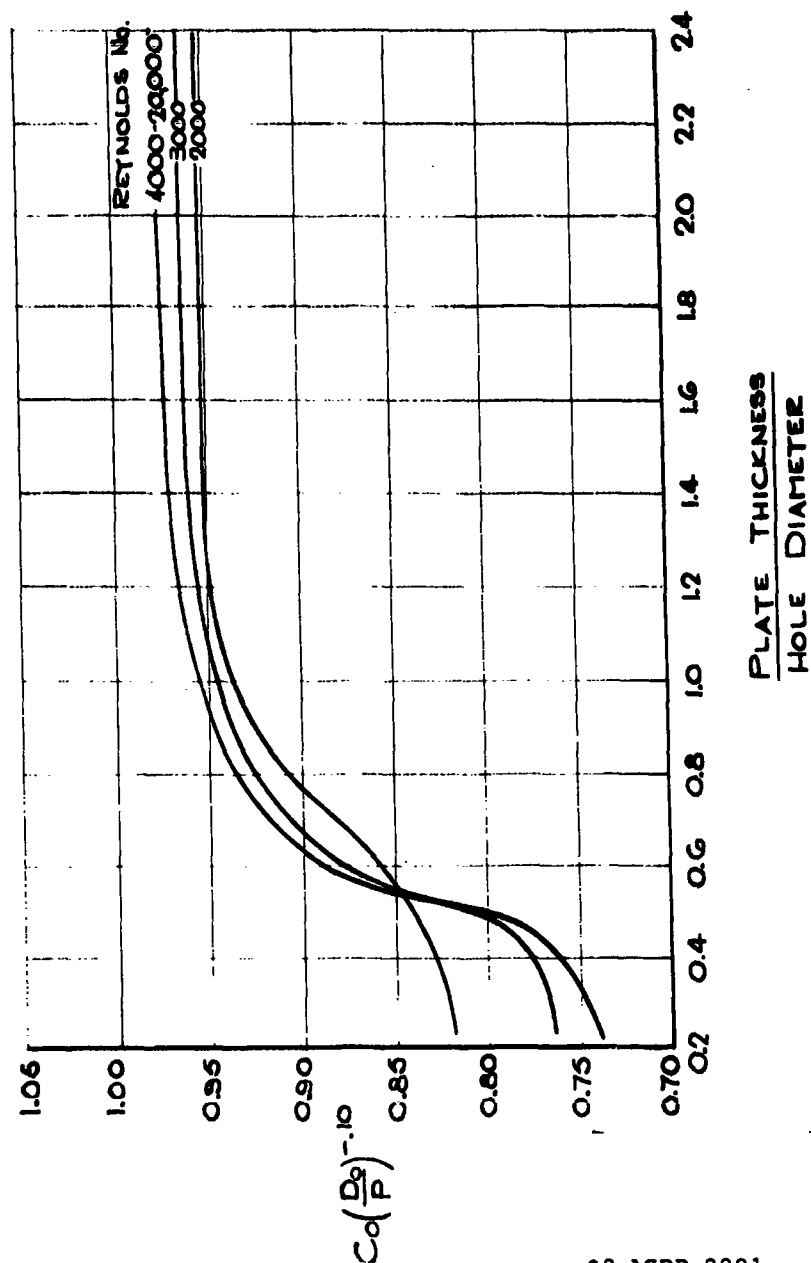


FIG. 25

63 ASRP-2391

# CONFIDENTIAL

## ASD-TDR-63-665, Part I

### 3.4.2.5.3 Volumetric Foam Density Data

With the aid of equation (22) and computed perforation discharge coefficients, values of  $\alpha$  were computed for 244 data points. Closer scrutiny of this as well as the basic pressure drop data now revealed an anomaly which could not be accounted for by the model as outlined here. It is evident from equation (21) that the total frictional pressure drop across a tray should, at constant  $\alpha$ , be almost independent of liquid rate or, at best, just decrease slightly with increasing values of  $\frac{Q_L}{h}$ . Furthermore, a plot of  $\Delta P$  versus froth height should be linear, intersecting the ordinate at:

$$\left[ \left( 1 - \frac{1}{f} \right) + \frac{1}{2 C_v^2 f^2} \right] \frac{\rho_v v_s^2}{g_c}$$

A representative sampling of the data is shown in Figure 26 from which it is evident that above velocities of 9 ft./sec. there appears a change in the basic pressure drop behavior as reflected by a nonlinearity at lower froth heights. It must be assumed that this is the result of interactions between vapor and liquid which are not accounted for in the present treatment and which might be due to either high speed transient conditions on the tray or a net transfer of momentum across the lateral boundaries of the control volume.

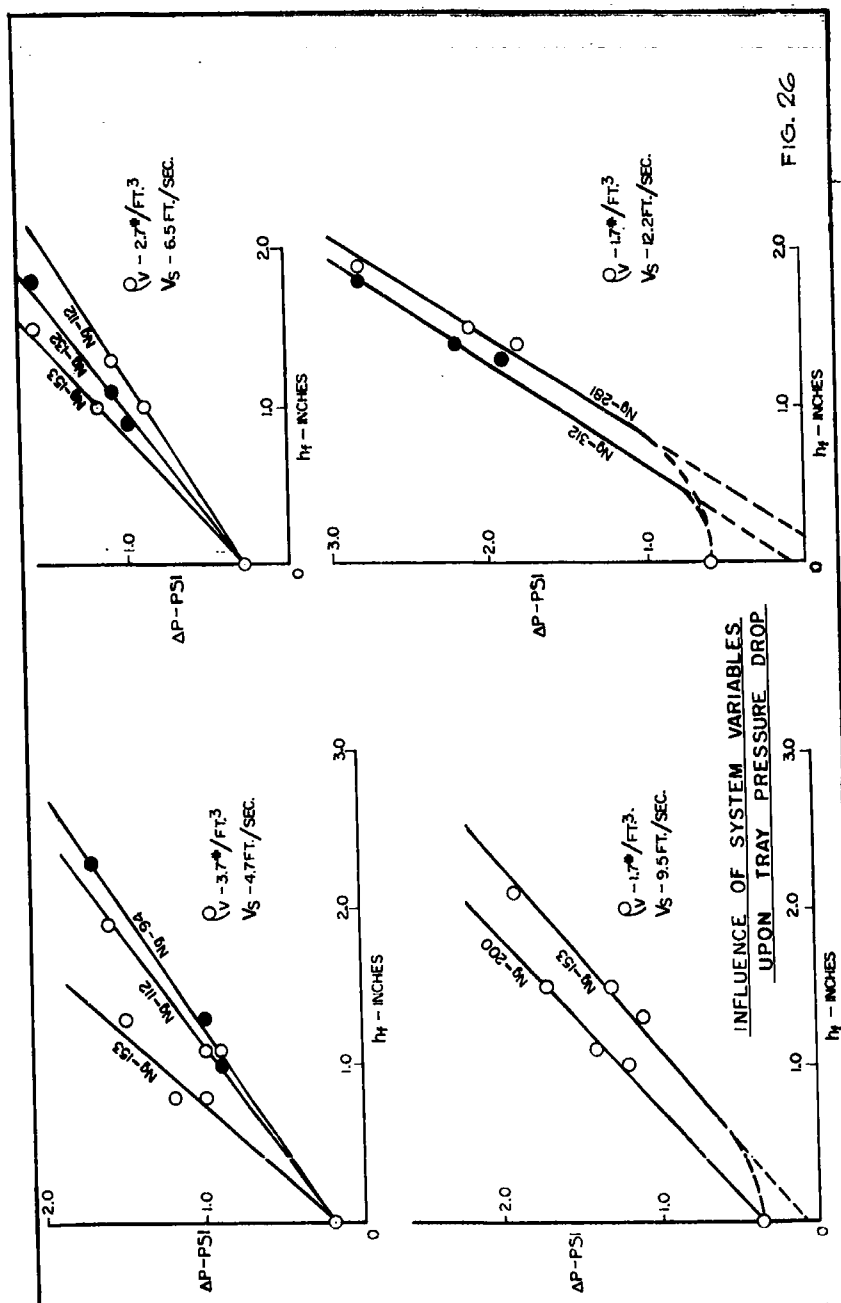
According to the analysis presented here, such behavior manifests itself as an increase in the volumetric foam density with increasing liquid velocity and may, in a gross sense, be taken into account by the  $\alpha$  correlation. A similar approach was taken with respect to the influence of free area; the value of  $\alpha$  having been found to increase at lower free areas. Inasmuch as the latter trend is generally associated with higher perforation velocities, it might be reasonable to assume that there is some connection between this effect and that due to liquid velocity.

Since it was not possible to pursue questions of the momentum transfer mechanism further within the framework of this program, it was decided that an empirical correlation of the volumetric foam density data might once again be most suitable. As was the case earlier with respect to the foam height correlation, use was made of a computer in analyzing the data by linear regression. The following functional dependence of  $\alpha$  was assumed to hold:

63 ASRP-2391

CONFIDENTIAL

ASD-TDR-63-665, Part I



63 ASRP-2391

CONFIDENTIAL

**CONFIDENTIAL**

ASD-TDR-63-665, Part I

$$\frac{1-\alpha}{\alpha} = \phi \left[ V_s, Ng, \frac{\rho_v}{\rho_L - \rho_v}, \frac{Q_L}{b}, f \right]$$

where in this instance  $Ng$  is the gravitational field corrected for the effect of liquid flow direction, Equation (20).

The final correlation is shown in Figure 27. The general scatter reflects, at least in part, the difficulties associated with measurements of this type, wherein the foam density is computed from overall tray pressure drop data. In equation form, the correlation reads:

$$\frac{1-\alpha}{\alpha} = 8.1 \left( \frac{\rho_v}{(\rho_L - \rho_v)Ng} \right)^{1/2} V_s^2 \left( \frac{fb}{Q_L} \right)^{.2} \quad (23)$$

The above correlation described all pressure drop measurements to within a standard deviation of about 25%, and 85% of the data to within 15%. The greatest scatter, in turn, occurred at high velocities and at correspondingly high accelerations. Note should also be made of the fact that the analysis presented here assumes no weeping on the tray. There were undoubtedly a number of runs where this was not the case and where as a result the effective dry plate pressure drop was higher than has been calculated. This would then lead to computed  $\alpha$  values somewhat greater than actual.

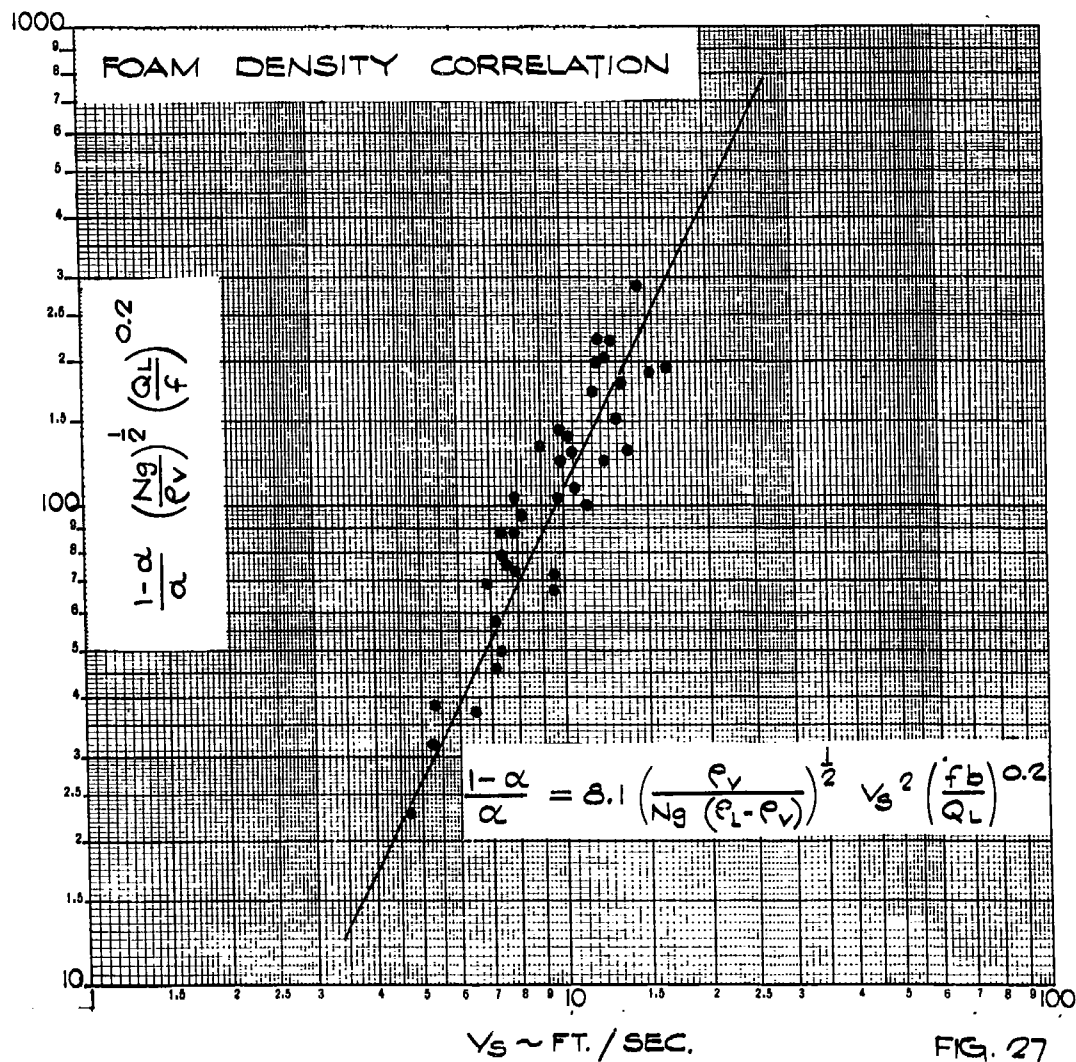
Attempts to derive a suitable correlation which would at the same time be dimensionally consistent met with little success. From dimensional analysis, one would expect the froth density to be a function of inertial, viscous, gravitational and possibly surface forces. A crude comparison of air-water to UCON fluid data leads, once more, to the conclusion that most likely surface forces do play a significant role in establishing the value of  $\alpha$ . This is shown in Figure 28 where, for purposes of comparison, the UCON fluid data was correlated according to the one-third power of  $Ng$  and  $\rho_v$ . From this plot, it would appear that the froth density is, more than any other parameter, influenced by the properties of the fluid phases. The existing data does not warrant a more detailed analysis at this time. In addition, it should be remembered that the  $\alpha$  values as computed with air and water were obtained from overall pressure drop measurements across the tester and under the assumption that they are independent of liquid rate.

63 ASRP-2391

**CONFIDENTIAL**

CONFIDENTIAL

ASD-TDR-63-665, Part I

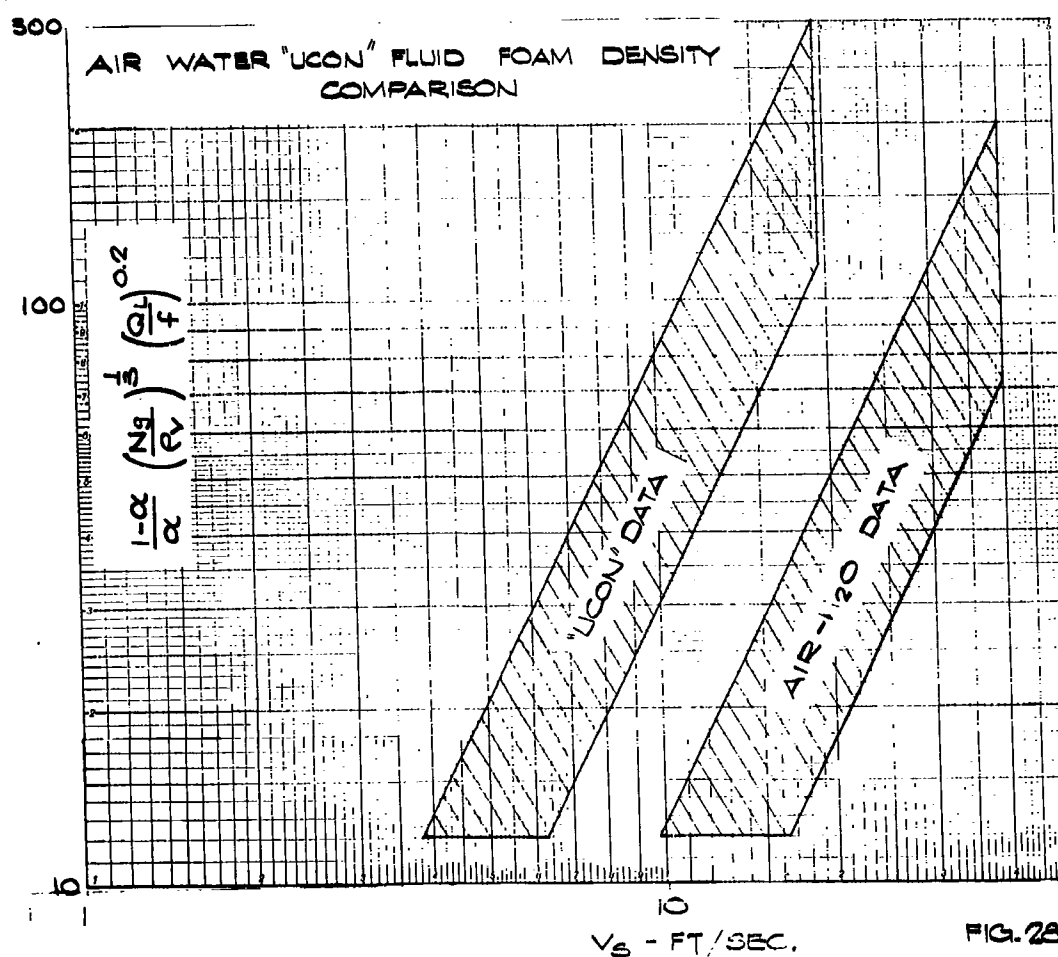


CONFIDENTIAL

CONFIDENTIAL

ASD-TDR-63-665, Part I

0



CONFIDENTIAL



# CONFIDENTIAL

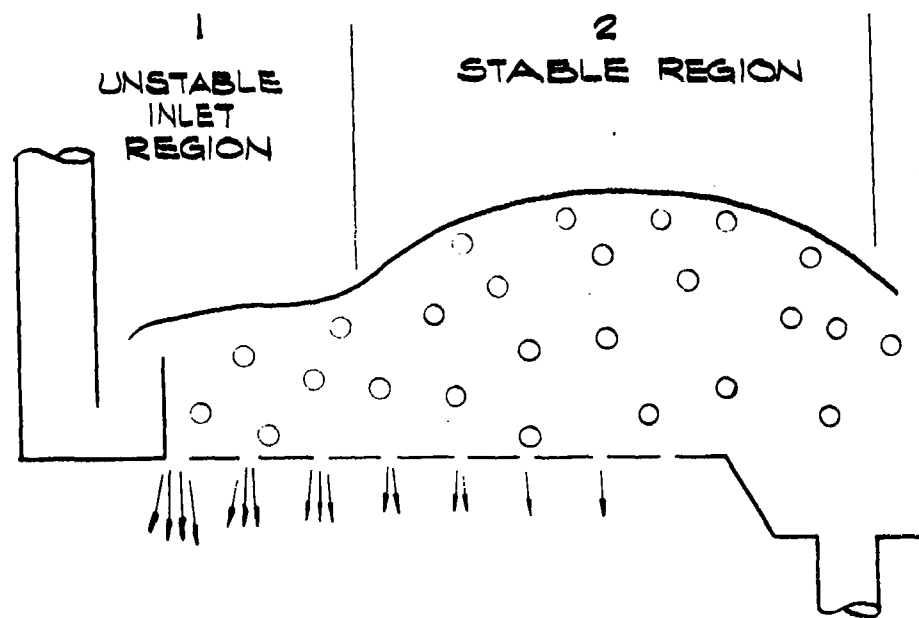
ASD-TDR-63-665, Part I

## 3.4.2.6 Stability and Weeping

A rotating sieve tray will, like its counter part at normal gravity, generally exhibit some weeping over a considerable range in operation. This causes concern, however, only where the tray efficiency begins to deteriorate noticeably. Lacking actual rate data, one must, therefore, establish a further operating criterion describing in a sense the upper limit to which a given tray can be accelerated without causing serious weepage. By its very definition such a limit is, once again, somewhat arbitrary especially since it is based upon difficult and uncertain visual observations.

A distinction should normally be made between weeping on a stable tray and that caused by instabilities as shown in Figure 29.

### TRAY WEEPING



63 ASRP-2391 FIG. 29

# CONFIDENTIAL

## ASD-TDR-63-665, Part I

From conventional column technology it may be shown that for region 1 a stability criteria should, in its simplest form, reduce to a critical ratio of hydrostatic head to dry plate pressure drop,

$$\frac{\Delta h_D}{h_s} \geq C.$$

The value of C might, furthermore,

lie in the vicinity of 0.50. Experimentally it was, however, quite difficult to distinguish between weeping which occurred on account of this inactivity at the tray inlet and that which may normally take place even in totally active regions. This latter weeping can be ascribed to momentary pressure fluctuations at various points on the tray, fluctuations resulting in more or less random seepage of liquid through the perforations where, at the moment, the hydrostatic head exceeds an allowable maximum value. For a given fluid system and approximately constant perforation diameters it is postulated that a point of serious weeping or dumping can be defined in terms of a simple ratio of dry plate to hydrostatic head loss.

Data which according to visual and photographic observations presented either moderate or serious weeping has been plotted in Figure 30. It is seen that evidently no weeping occurred above  $\frac{\Delta h_D}{h_s}$  values of 0.5 and that instances of serious weeping were generally confined to values of  $\frac{\Delta h_D}{h_s}$  less than 0.3. It should be mentioned that these latter points are of considerable uncertainty since neither the dry plate nor the hydrostatic head can be defined in this case and extrapolation of the data is necessary.

All of the series M-E efficiency runs fell into a range  $\frac{\Delta h_D}{h_s}$  between 0.30 and 0.50, yet in spite of a moderate amount of weeping no serious reduction in mass transfer occurred. As a result, it is recommended that in the interest of reduced pressure drops the following criterion be used as a lower limit of operation:

$$\frac{\Delta h_D}{h_s} \geq 0.3 \quad (24)$$

### 3.4.3 Segmental Tray Data-Mass Transfer

#### 3.4.3.1 General Considerations Involving the Point Efficiency

In the case of the most distillation systems, the resistance to mass transfer lies in both the liquid and gas phase. Under the

63 ASRP-2391

CONFIDENTIAL

ASD-TDR-63-665, Part I

TRAY STABILITY CRITERIA

SYMBOL	% FREE AREA
○	22
□	20
△	26

NOTE  
OPEN POINTS INDICATE MODERATE WEEPING  
DARK POINTS INDICATE SEVERE WEEPING

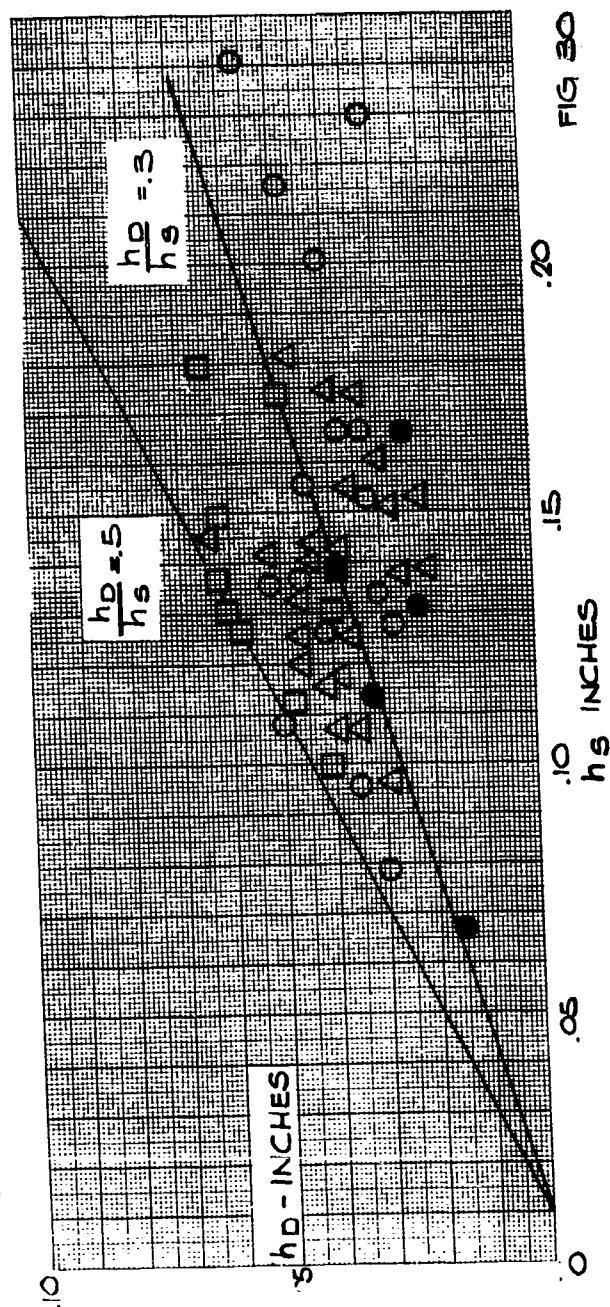


FIG 30

63 ASRP-2391

CONFIDENTIAL

# CONFIDENTIAL

## ASD-TDR-63-665, Part I

assumption of a linear equilibrium line in addition to uniform liquid composition on the tray, an expression for the local point efficiency may be derived from two film theory. This efficiency, defining the degree to which vapor leaving a tray has reached equilibrium with the bulk liquid on the tray, is then written in terms of two series conductance terms for the gas and liquid phase as follows:

$$-\ln (1 - E) \triangleq NTU = \frac{1}{\frac{1}{(NTU)_g} + \frac{1}{(NTU)_L}} \quad (25)$$

The quantities  $(NTU)_g$  and  $(NTU)_L$  are, in turn, related to transfer coefficients in the respective phases:

$$(NTU)_L = \left( \frac{k_L'}{\epsilon_1} \right) \left( \frac{A}{V} \right) (\tau') \quad (26)$$

$$(NTU)_g = \left( k_g' \right) \left( \frac{A}{V} \right) (\tau') \quad (27)$$

Therefore:

$R_g', R_L'$  = gas and liquid phase mass transfer coefficients respectively. The term  $\epsilon$  stems directly from the material balance equations which have to hold, and as such are defined by the equation:

$$\epsilon_1 = \frac{M_L \rho_v K}{M_g \rho_L}$$

Here:

$\rho_L, \rho_v$	=	Liquid and vapor phase density
$M_L, M_g$	=	Liquid and vapor phase molecular weight
$K$	=	Slope of the vapor-liquid equilibrium line

Equations (26) and (27) are seen to contain a common factor  $(A/V) \tau'$  which is primarily influenced by fluid dynamic system parameters. Thus,  $A/V$  represent the interfacial area that is created per unit volume of vapor in the froth whereas  $\tau'$  defines the contact time of the phases.

The respective mass transfer coefficients  $k_L$  and  $k_g$  are, on the other hand, like their counterparts in heat transfer, strongly influenced by both the fluid dynamic characteristics and the molecular

63 ASRP-2391

# CONFIDENTIAL

0

## ASD-TDR-63-665, Part I

transport properties. Various models have been devised to formulate expressions for  $k$  in terms of those variables. On the basis of one concept, the penetration theory, it is postulated that in the course of gas passing through a layer of froth the thin liquid film surrounding the gas is renewed a number of times due to the relative shear between the phases. Higbie (Ref. 14) has shown that, for a constant renewal function, this leads to a liquid phase mass transfer coefficient as follows:

$$K_{L1} = 2 \sqrt{\frac{D_L}{\pi \theta_1}}$$

Here:

$D_L$  = diffusion coefficient

$\theta_1$  = boundary layer renewal time

If it is further assumed that  $\theta_1$  is solely dependent upon the system dynamics, Equation (26) may then be rearranged to yield:

$$\frac{(NTU)_L \epsilon_1}{\sqrt{D_L}} = f(\eta_L) \quad (28)$$

where:  $f(\eta_L)$  represents a composite of all the dynamic variables. Geddes (Ref. 15) derived an analogous equation assuming a froth comprising bubbles of uniform diameter  $D_b$ . In this case, he showed that:

$$f(\eta_L) = 12 \frac{\tau_1}{D_b \sqrt{\theta_1}} \quad (29)$$

On the basis of similar reasoning, we may write the following empirical function for the gas phase:

$$(NTU)_g = \phi(D_g, \eta_g) \quad (30)$$

where  $D_g$  equals a gas phase diffusion coefficient and  $\eta_g$ , once again, the respective dynamic system parameter.

It is evident that evaluation of the aforementioned dynamic factors may best be accomplished experimentally. Furthermore, conditions should normally be chosen such that the two resistances

63 ASRP-2391

# CONFIDENTIAL

# CONFIDENTIAL

## ASD-TDR-63-665, Part I

are separable, thereby allowing the determination of both the gas and liquid phase parameters. During earlier air-water experiments (Ref. 2) this was accomplished by adding trace "impurities" to the bulk phases; "impurities" either very soluble in water for studies involving a gas phase controlling system, or only minutely soluble where the liquid phase resistance was to predominate. Methanol and carbon dioxide were chosen for this purpose and injected at concentrations generally less than 1% by weight. Concerning the UCON-12 UCON-114 as well as the liquid air-systems, it cannot be ascertained directly whether the rate of mass transfer is determined by either the gas or the liquid phase resistance. Based upon the air-water correlations and conventional column data one would estimate that both of the above systems are gas phase controlled. This is, of course, not too surprising for the dispersion as postulated; that is, fine particles of liquid distributed in a vapor stream.

### 3.4.3.2 The UCON Fluid Tray Efficiency Data

Mass transfer experiments were initiated only after the hydraulic behavior of rotary sieve trays was well understood and could be predictably controlled. With the aid of the binary system UCON-12 UCON-114, tray efficiencies were determined from concentration differences across a four tray column using either a McCabe-Thiele graphical tray counting procedure or the Fenske equation. The latter is applicable in this instance where operation is confined to the lower concentration ranges of the more volatile component, that is, between about 6 and 35% UCON-12. As a result, the number of theoretical trays are:

$$N_p^* = \frac{\ln \left( \frac{Y_2}{1-Y_2} \right) \left( \frac{1-Y_1}{Y_1} \right)}{\ln \alpha_r} \quad (31)$$

Here  $\alpha_r$  is the relative volatility. (It is interesting to note that this particular distillation system is almost ideal; also, it resembles liquid air closely in its vapor-liquid equilibrium characteristics as seen from Figure 31.

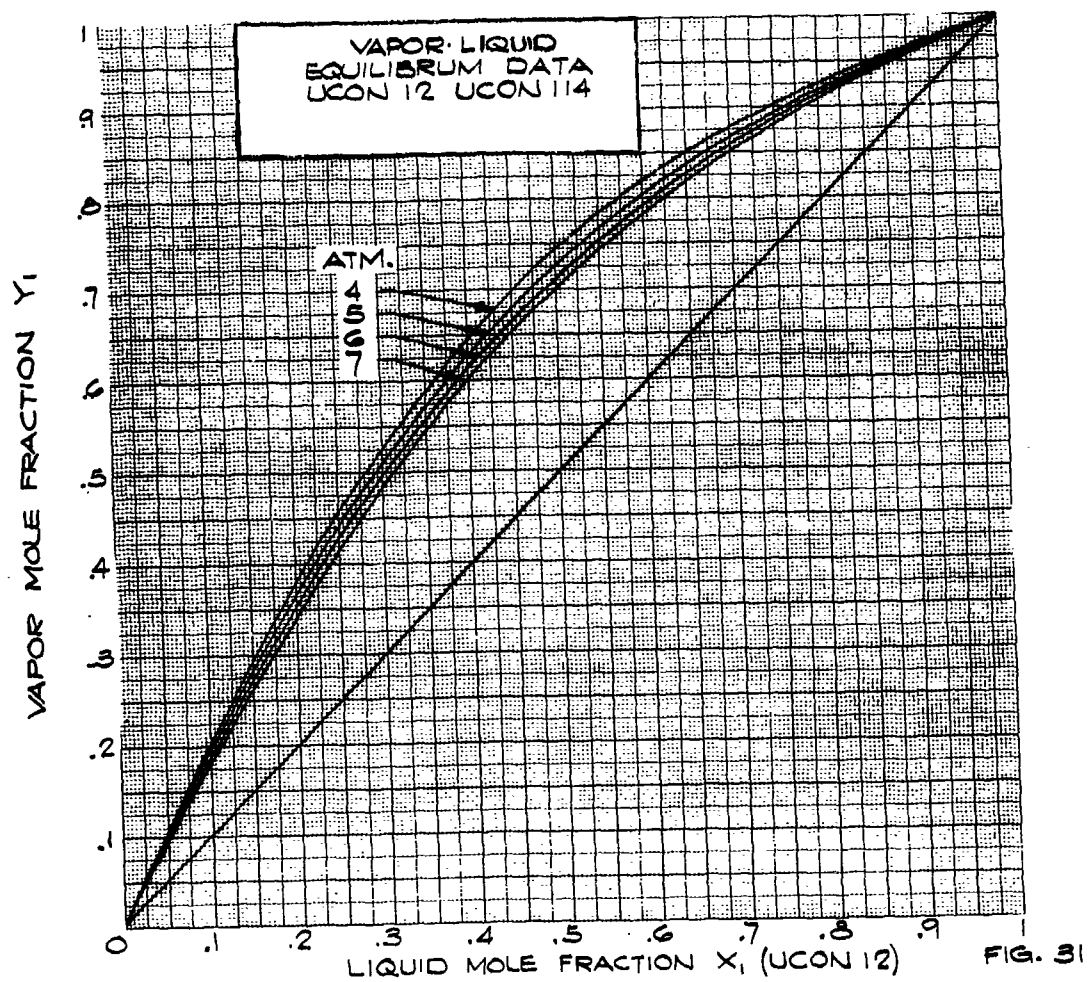
The average column efficiency is then equal to:

$$E_c = \frac{N_p^*}{N_a} = \frac{N_p^*}{4} \quad (32)$$

63 ASRP-2391

CONFIDENTIAL

ASD-TDR-63-665, Part I



CONFIDENTIAL

# CONFIDENTIAL

## ASD-TDR-63-665, Part I

Since in this range of operation both the operating and equilibrium lines are straight, the latter of slope K, one may proceed to compute the Murphree plate efficiency as:

$$E_{mv} = \frac{(S^\circ)^{E_c} - 1}{(S^\circ) - 1} \quad (33)$$

where:

$$S^\circ = K \frac{G}{L} \triangleq K \text{ (at total reflux)}$$

It must now be assumed that no enhancement is achieved on these small trays and that in essence the liquid is completely mixed. The Murphree plate efficiency then equals the point efficiency and in accordance with equation (25) the number of overall transfer units, based upon gas phase composition changes, may be written as:

$$(NTU) = \ln(1 - E_{mv})$$

Efficiency data was obtained with three different column configurations, defined earlier as series M-B, M-D, and M-E. In the first of these, liquid flowed in opposite directions on successive trays. Although the hydraulic performance of this column was poor as described before, the effects of the same upon tray efficiency were relatively minor, being mostly reflected in a wider data scatter. The second of these test series comprised the preferred counter-rotational flow arrangement yielding more consistent and reproducible data. Both of these experiments involved trays of 20% free area and operation outside the weeping range. As a result, the third set of experiments was conducted with trays of 26% free area but with a column configuration otherwise identical to that employed during the series M-D tests. Although a minor amount of weeping could generally be detected during these experiments  $(.5 \geq \frac{\Delta h_D}{h_s} \geq .3)$

there appeared to be only a slight reduction in tray efficiency; small enough to be within the scatter of the final correlation.

As mentioned earlier, it is not possible to determine exactly which of the phases controls the mass transfer rate. Based upon all available data including conventional column correlations, it would appear that the gas phase resistance predominates. Consequently it is assumed that,

63 ASRP-2391



**CONFIDENTIAL**

ASD-TDR-63-665, Part I

$$NTU \approx (NTU)_g = \phi (D_g \eta_g)$$

Over the pressure range investigated (from 4.5 to 7.8 atmospheres) it was not possible to establish exactly the dependence of NTU upon the gas phase diffusion coefficient. Resort was, therefore, taken to the prior methanol and acetone-water data where the dependence had been reported as  $NTU \sim D_g^{2/3}$ . Careful re-evaluation of those results

seemed, however, to point to an even greater effect, such as  $D_g^{.8}$ .

The immediate question, of course, arises as to how such a relation might be justified since it indicates almost laminar behavior. Again the answer appears to lie in the dispersion mechanism. If it is assumed, for instance, that the latter does indeed involve small liquid globules suspended in a turbulent gas stream, then one might expect the gas phase mass transfer coefficient to be of the form:

$$\frac{k_g D_p}{D_g} = 2 + c \left( \frac{D_p V \rho}{\mu_v} \right)^{1/2} \left( \frac{\mu_v}{D_g \rho} \right)^{1/3} \quad (\text{Ref. 16})$$

In the limit one would thus expect the mass transfer coefficient to be directly dependent upon the gas phase diffusion coefficient, provided, of course, the pertinent Reynolds number becomes sufficiently small. At high Reynold's numbers the dependence would in turn be to the  $2/3$  power.

As had been the case throughout the centrifugal contactor program, it was again found that merely increasing the rotational speed of the tester did not affect the tray efficiency (up to the point, of course, where dumping occurs). Inasmuch as the froth height decreases, however, with increasing  $Ng$ , one might in the simplest sense assume, therefore, that (see equation 12):

$$NTU \approx h_f (Ng)^{.85}$$

63 ASRP-2391

**CONFIDENTIAL**

# CONFIDENTIAL

## ASD-TDR-63-665, Part I

Figure 32 represents a summary plot of all the efficiency data according to these functional dependencies. The steep velocity dependence is somewhat misleading since it must be remembered that the froth height is also strongly influenced by  $V_s$ . In summary, the following equation is recommended for estimating the efficiency of a rotating liquid air distillation tray:

$$(NTU)_g = 1.5 \times 10^5 D_g^{.8} \frac{h_f^i (Ng)^{.85}}{V_s^3} \quad (34)$$

In an effort to determine whether the possibility existed that these measurements did not constitute point efficiencies, two additional experiments were conducted at L/G ratios greater than one. According to Lewis (Ref. 17) the plate efficiency should decrease as KG/L decreases at a given value of point efficiency where the liquid on the tray is incompletely mixed. Since a typical liquid air column will generally operate at  $KG/L \approx 1.0$ , one would, in this case expect lower plate efficiencies than presently measured for ( $KG/L \approx 1.9$ ), i.e.,  $L/V = 1$ ,  $K = 1.9$  for UCON fluid. The following measured E's obtained from special Runs M-E 6 and M-E 12, at  $KG/L \approx 1.0$  and at correspondingly higher liquid rates, indicate just the opposite when compared to values calculated by equation (34).

<u>Run</u>	<u><math>V_s</math></u>	<u><math>h_f^i</math></u>	<u><math>Ng</math></u>	<u>E meas.</u>	<u>E calc.</u>
M-E 6	10.5	1.8	223	.845	.610
M-E 12	7.8	1.8	121	.950	.780

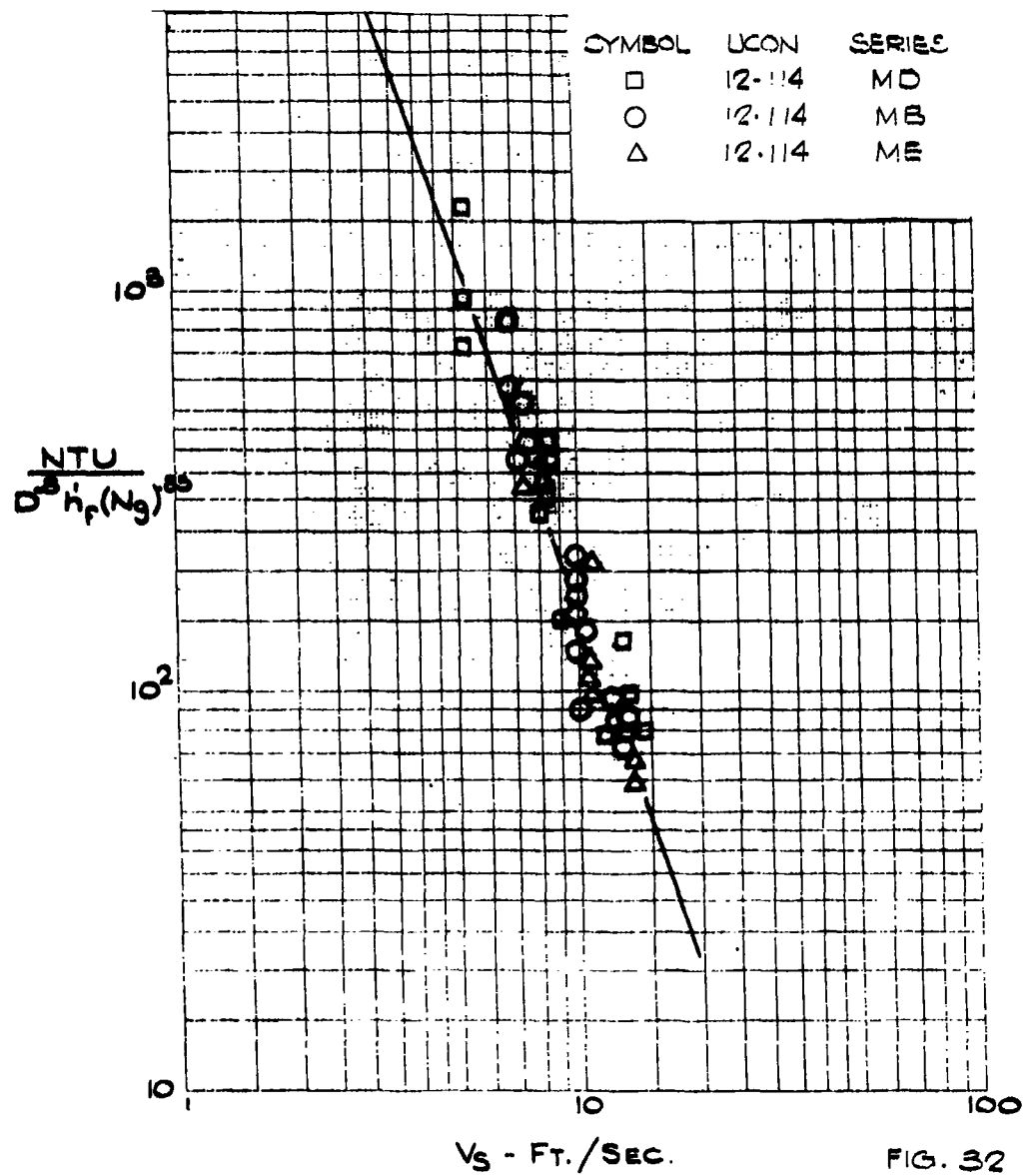
From this it would appear that liquid mixing was complete and that there might once again be a secondary effect of liquid velocity which has not been accounted for.

63 ASRP-2391

CONFIDENTIAL

ASD-TDR-63-665, Part I

EFFICIENCY CORRELATION  
UCON 12-114



63 ASRP-2391

CONFIDENTIAL

# CONFIDENTIAL

ASD-TDR-63-665, Part I

## 3.4.4 Circumferential Tray Tests

This program was designed as a logical, intermediate step between the segmental tray tests and the 100 lb./sec. cryogenic unit. Its main purpose was to test the empirical design criteria developed in the previous air-water and UCON fluid test programs with a tester in which the geometry more closely resembles that of the cryogenic unit. The program was thus regarded as "proof test" and was, as such, entirely successful. The design and fabrication of the circumferential tray test rotor is presented in Appendix V.

It was found that the fluid handling circuitry had a relatively narrow operating range as can be seen in Table 1, under UCON 21-114. When the vapor feed rate was increased, for instance, the tester pressure rose accordingly due to the difficulty in condensing the increased amount of vapor. Thus, the vapor density increased and vapor velocity remained relatively constant. Secondly, at any set of operating conditions only a small change in gravitational force was possible between flooding and dumping conditions. Consequently, only 20 "runs" were required to cover the achievable range of operation of the fluid circuit. Similarly, the efficiency tests covered as wide a range as possible and further testing was felt to be unnecessary. Each section of the hydraulic and efficiency correlations will be discussed separately.

### 3.4.4.1 Hydraulics

Due to the fluid circuit limitations noted in the previous paragraph, all of the data taken were at lower velocities and rotational speeds relative to the data from the segmental tester. Although this data covered the operating range of the equipment as discussed above, it does not cover a wide enough range of the variables to justify the development of new empirical relationships or changes in previous correlations. For this reason, the data will be examined to see whether or not it is reasonably consistent with the correlations developed in both the air-water and the segmental tray UCON fluid studies.

The configuration of the tester windows was such that foam height observations were limited to the middle trays, numbered 2 and 3. Because of the vapor flow past the outside of the windows and because some liquid was

63 ASRP-2391

# CONFIDENTIAL

**CONFIDENTIAL**

**ASD-TDR-63-665, Part I**

continually splashing against them, the visual aspects of the tester were far from perfect. However, several photographs were taken and the observed foam heights were compared to these photographs and corrected where necessary. A typical photograph has been included for illustrative purposes (Fig. 15). Two data points were obtained for each set of conditions and the 20 hydraulic and 6 efficiency runs thus yielded 52 data points. These are tabulated in Appendix IV.

An empirical relation between foam height and the independent variables effecting the tray operation was derived from the previous tests and reported in the preceding section on Figure 22 as:

$$h_f' = C \frac{(V_s)^{1.6} \left(\frac{Q_L}{b}\right)^{1/3} \left(\frac{\rho_v}{\rho_L - \rho_v}\right)^{1/2}}{(Ng)^{.85} (f)^{0.13}}$$

The decision to block off a portion of each tray to increase the dry plate pressure drop and thus increase the operating range of the column was discussed previously. This blocked off section, however, created some problems in calculating liquid and vapor velocities since there were actually two "active areas" which could be used. The area based on the column width before the trays were blocked was used because it is more reasonable to assume that this width determines velocities rather than the smaller, blocked off width of the trays themselves. Since some channeling of the liquid along the edges of the tray might well have occurred, the blocking of the trays might account for some of the deviations between predicted and actual foam heights.

If the above equation holds for the circumferential trays, a

$$\log - \log \text{ plot of } h_f \text{ versus } \frac{V_s^{1.6} \left(\frac{Q_L}{b}\right)^{1/3} \left(\frac{\rho_v}{\rho_L}\right)^{1/2}}{Ng^{.85} f^{.13}}$$

must, by definition, fall on a straight line with a slope of 1.0. Figure 33 is such a plot and shows the previously determined correlations for air-water and UCON fluid as well as the actual data points for the circumferential trays. It is evident that the data does indeed fall very well onto or near a line with a slope of 1.0, located between the previous correlations. There are several factors, in particular surface tension and tray geometry, that could account for the displacement of the three systems from one another.

63 ASRP-2391

**CONFIDENTIAL**

**CONFIDENTIAL**

ASD-TDR-63-665, Part I

**FOAM HEIGHT CORRELATION**  
"UCON" 21-114

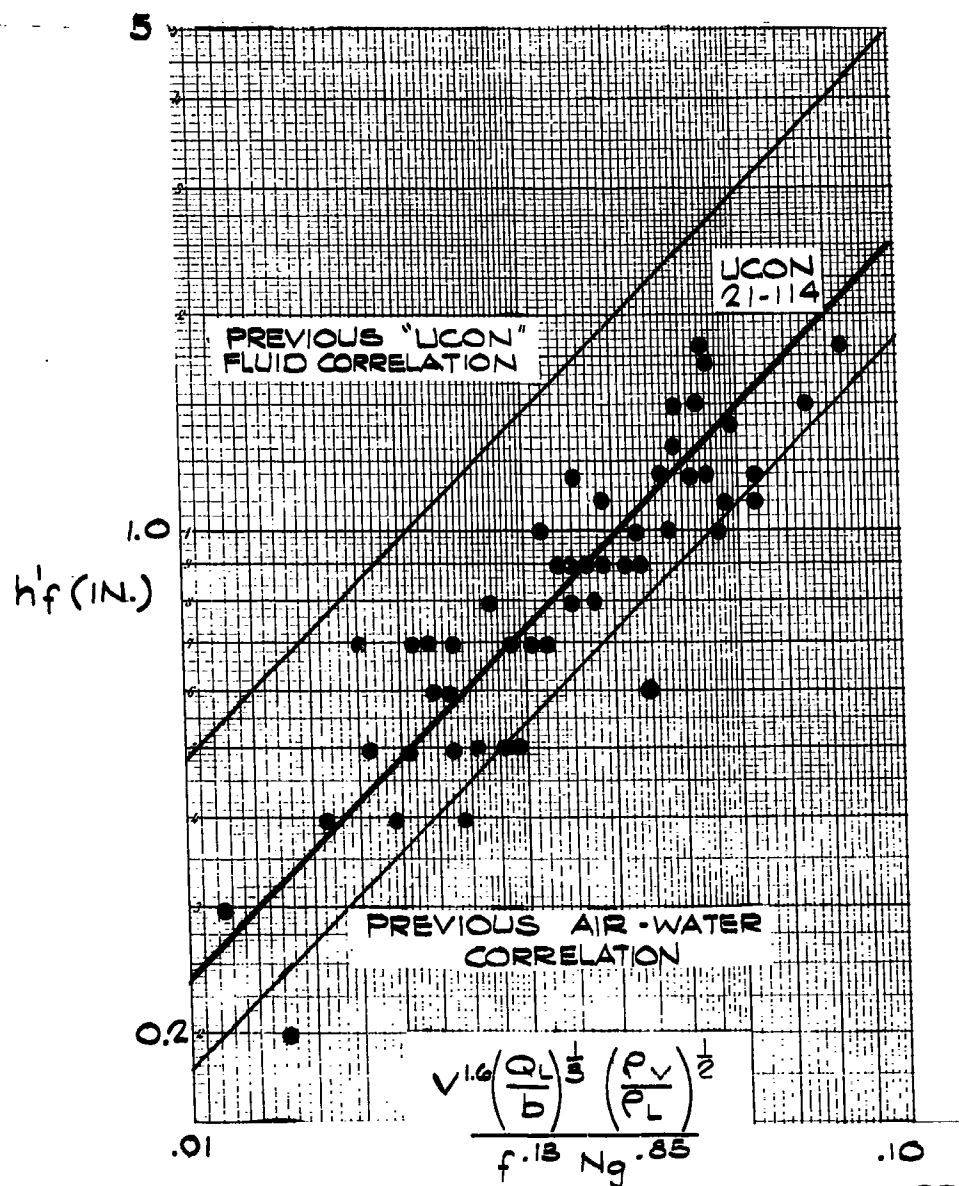


FIG. 33

63 ASRP-2391

**CONFIDENTIAL**

**CONFIDENTIAL**

**ASD-TDR-63-665, Part I**

In addition, one should point out that the tester operation was confined to gravitational fields below 100 Ng and, therefore, generally outside the range where previous segmental tray experiments had been conducted.

In other respects the hydraulic performance of this rotor was completely satisfactory. Earlier doubts as to phase maldistribution and the resultant rotor unbalances and vibrations proved to be unfounded even at conditions where partial inactivity and weeping occurred on the trays. Although there appeared to be no evidence of hydraulic gradients it is, nevertheless, impossible to draw any definite conclusions from the data obtained so far. Not only was the column operation outside a range where serious gradients would have been expected, but the tray lengths were still less than 6 inches, making foam gradient measurements difficult and unrealistic.

Two differential pressure transducers were used to measure the pressure drops across the trays. One was placed across Tray No. 2, the other across all four trays. The results indicate that their value was marginal since the data was inconsistent at times, i.e., the pressure drop read across the single tray being often about the same as that across all four trays. Secondly, the instrument zero shifted significantly during each series of runs, making all readings questionable.

A direct comparison of foam density measurements would, therefore, appear to be of little value. It may be stated, however, that the available pressure drops seemed to once again place the data between that of air-water and of UCON-12 - UCON-114 as described previously and as shown in Figure 28.

For three different vapor velocities, the rotational speed was cut back until the foam height reached 2 inches which is the tray spacing. These flooding points, listed in Table 5, were plotted on Figure 34 as a log - log plot of

$$v_s \sqrt{\frac{\rho_v}{\rho_l}} \text{ versus } Ng$$

Again, it is evident that the present system falls between the other UCON fluid and air-water correlations.

Even though the pressure drops were scattered a plot of  $h_D$  was made in Figure 35, where

$$h_D = \text{dry plate pressure drop}$$

63 ASRP-2391

**CONFIDENTIAL**

**CONFIDENTIAL**

ASD-TDR-63-665, Part I

TABLE 5

FLOODING POINTS FOR CIRCUMFERENTIAL TRAYS

$\frac{\rho}{L}$	$\frac{\rho}{V}$	$\frac{V}{s}$	$Nq$
83.7	1.26	6.45	8
81.5	1.08	7.56	16
83.9	1.11	5.5	12.5

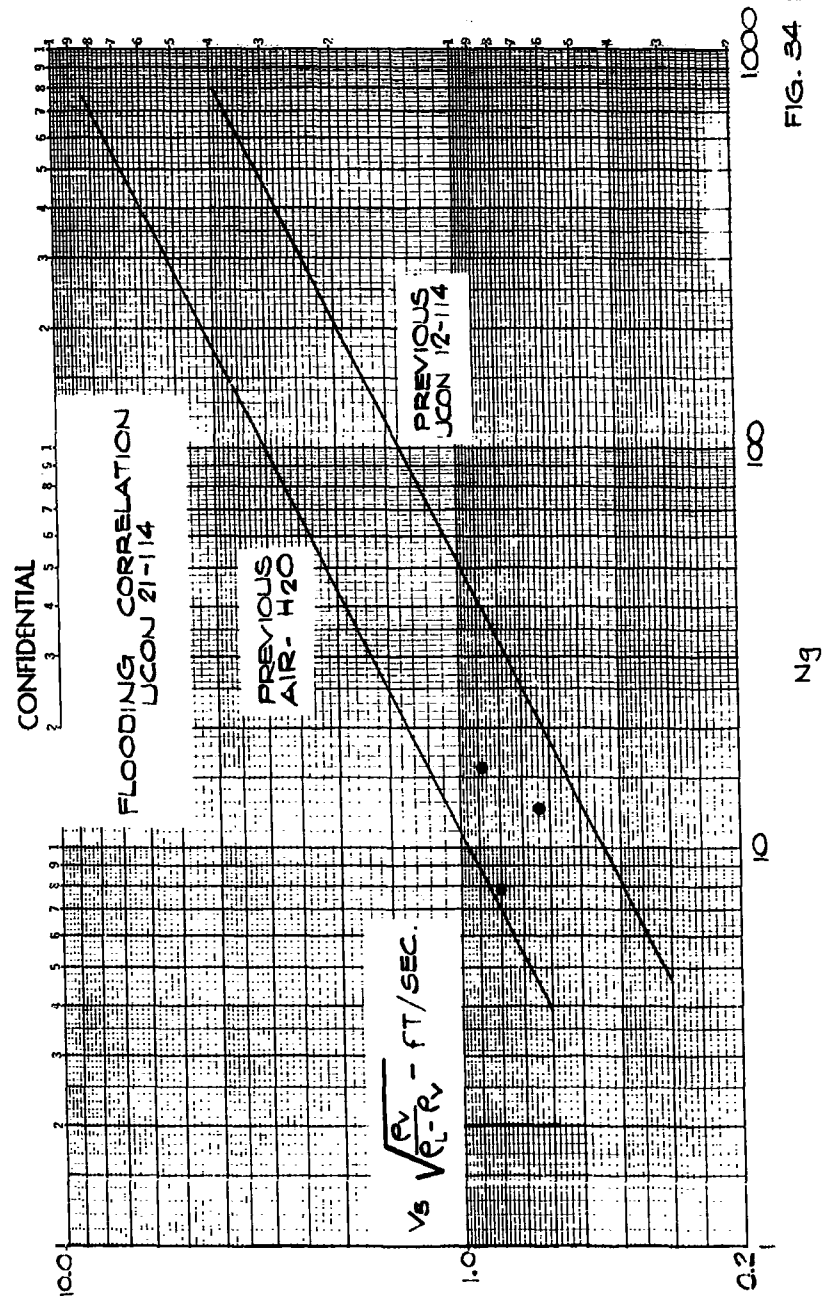
63 ASRP-2391

**CONFIDENTIAL**



CONFIDENTIAL

ASD-TDR-63-665, Part I



CONFIDENTIAL

CONFIDENTIAL

ASD-TDR-63-665, Part I

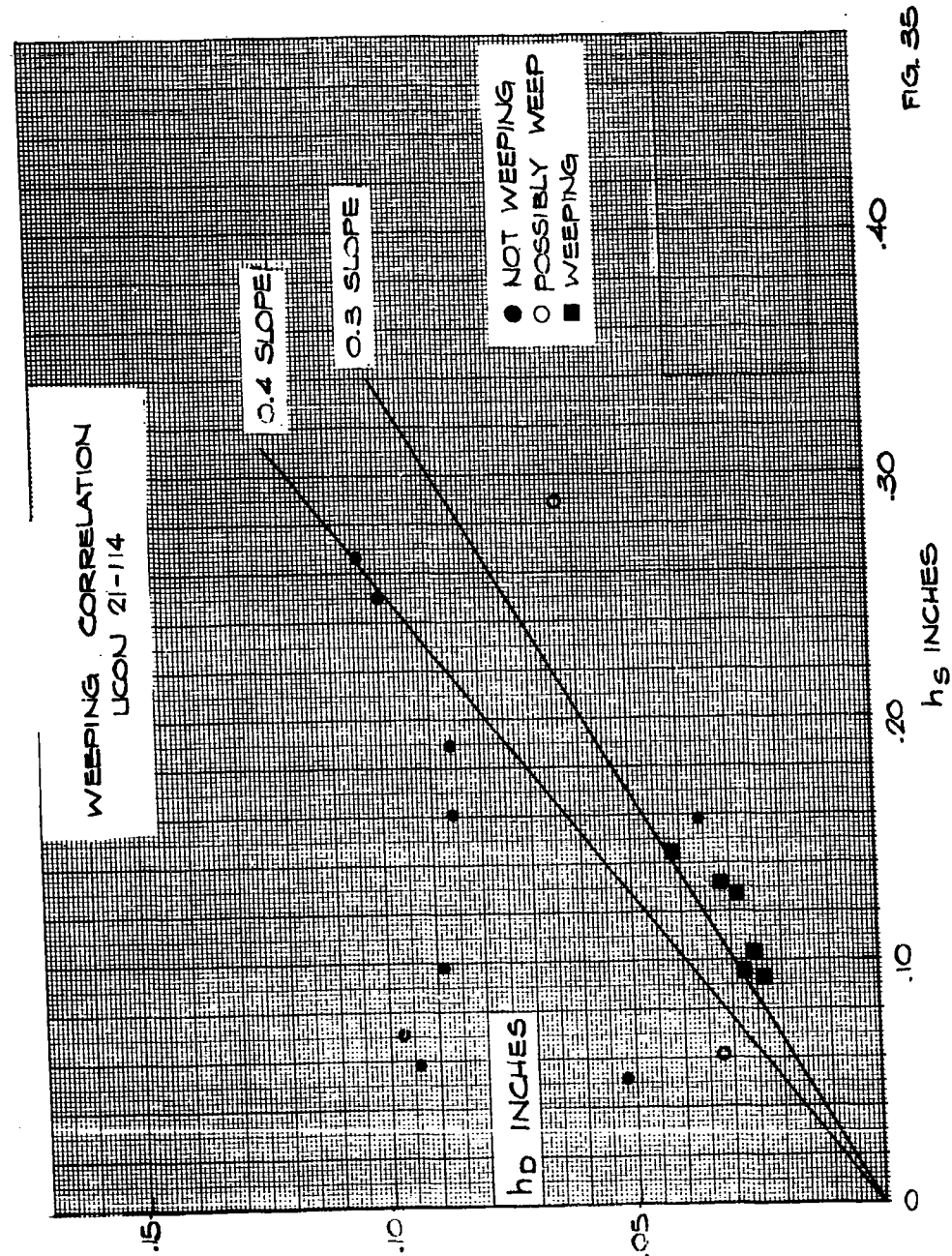


FIG. 35

CONFIDENTIAL

# CONFIDENTIAL

ASD-TDR-63-665, Part I

$$\frac{1}{C_v^2} \frac{\rho_v}{\rho_L} \left( \frac{V_s}{f} \right)^2$$

$$h_s = \text{hydrostatic head} = \alpha h_f N g (\rho_L - \rho_v)$$

and

$$h_s + \Delta h_D = \frac{\Delta P_o \times 144 \frac{g_c}{g}}{\rho_L}$$

It is reported in the segmental tray test section of this report that the trays would start weeping when

$$\frac{\Delta h_D}{h_s} = 0.3 \rightarrow 0.5 \text{ and that the trays will dump at}$$

$$\frac{\Delta h_D}{h_s} = 0.3 \text{ or less. About the only comment which can be}$$

made is that these numbers, particularly the first, might be somewhat conservative.

## 3.4.4.2 Mass Transfer

A total of 6 runs were made using a mixture of UCON 21 and UCON 114 as discussed in an earlier section of this report. After operation had steadied out for each set of operating conditions, the vapor feed and the exit vapor were analyzed. Since the system was operated at total reflux, the composition of the exit vapor was necessarily the same as that of the liquid feed and the composition of the liquid discharge equaled that of the vapor feed.

The compositions were then used as end points of a McCabe-Thiele analysis wherein the number of theoretical plates (NTP) were stepped off on an x-y, liquid-vapor equilibrium plot. The column efficiency,  $E_c$ , was then calculated by dividing the NTP by 4, the actual number of trays. Column efficiency was converted to Murphree tray efficiency by,

63 ASRP-2391

# CONFIDENTIAL

# CONFIDENTIAL

ASD-TDR-63-665, Part I

$$E_{mv} = \frac{K^{Ec} - 1}{K - 1}$$

where:

$E_{mv}$  = Murphree vapor efficiency  
 $K$  = average slope of the equilibrium line

and the number of transfer units, (NTU), were then calculated from the definition:

$$(NTU) = \ln(1 - E_{mv})$$

Figure 36 is a log - log plot of NTU divided by  $D_g^{.8}$  ( $D_g$  = Gas Phase Diffusion Coefficient),  $h_f'$  and  $(Ng)^{.85}$  versus  $V$ . This relation, reported in the segmental UCON<sup>f</sup> test section, utilized data for several different tray geometries and was an excellent fit. As is evident in Figure 36, the UCON 21-114 data also falls very well within the predicted range. Since many of the uncorrelated parameters, such as surface tension, and the tester geometry were different in the circumferential tests, it is quite reasonable to expect that the liquid air performance can be predicted by this relationship.

## 4.0 HEAT TRANSFER EXPERIMENTAL AND ANALYTICAL PROGRAM

### 4.1 Introduction

As described in the introduction, the distillation system incorporates a heat exchanger for transfer of heat from the high pressure column to the low pressure column. This heat exchanger called the reboiler-condenser is shown schematically in Figure 1-c.

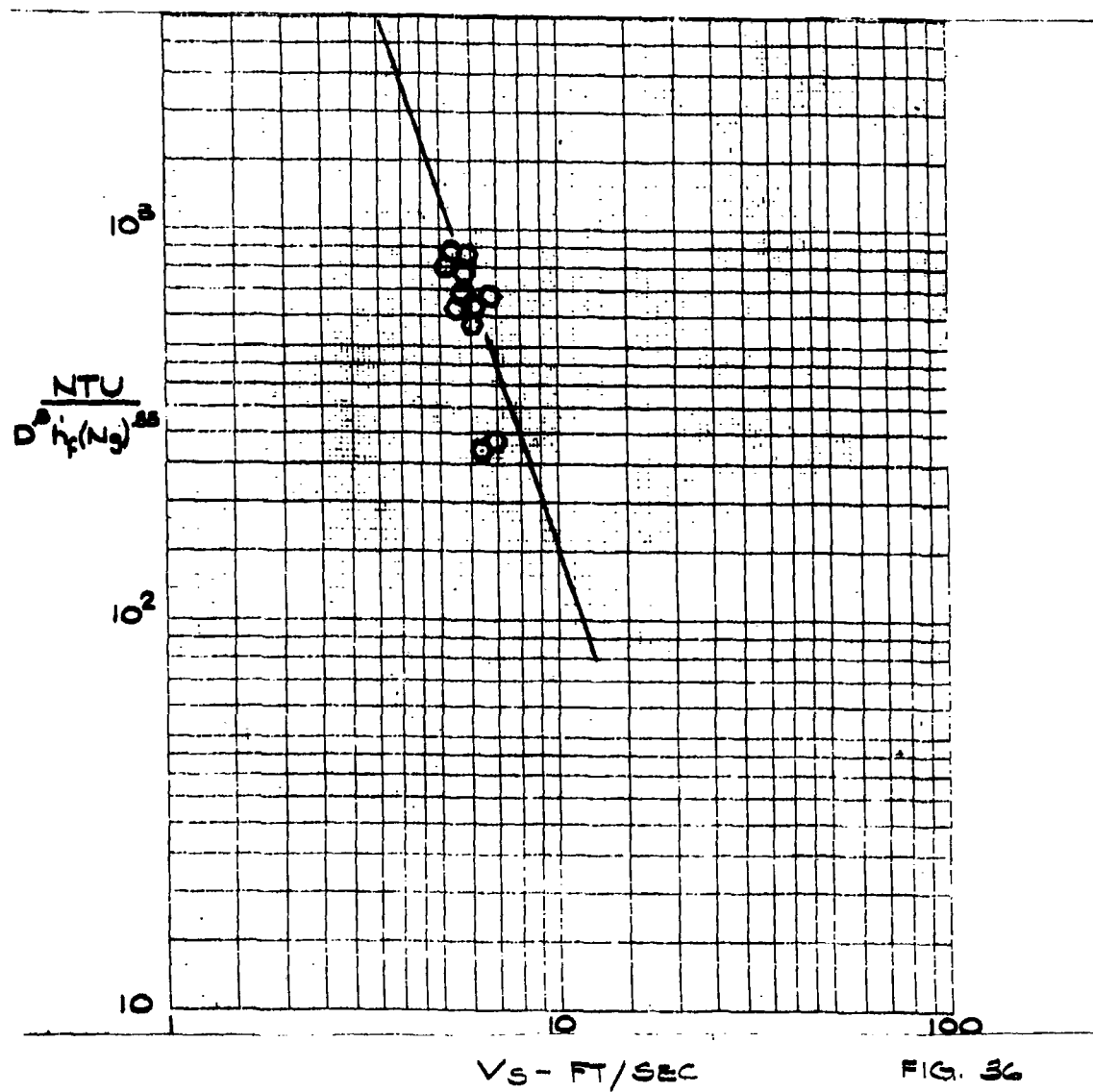
The experimental and analytical program reported in this section was selected to develop a reboiler-condenser configuration that would promote maximum unit heat flux. It was previously shown that if feed gas and waste gas pressures are fixed the  $\Delta T$  across the reboiler-condenser is controlled by column pressure drop. Thus, minimum column pressure drop means maximum  $\Delta T$  and hence maximum unit heat flux. The other factor determining unit heat flux is the overall heat transfer coefficient which is comprised of individual resistances. This program concentrated on improving the boiling and condensing coefficients where the maximum resistances occur.

63 ASRP-2391

CONFIDENTIAL

ASD-TDR-63-665, Part I

EFFICIENCY CORRELATION  
LCON 21-114



CONFIDENTIAL

**SECRET**

**ASD-TDR-63-665, Part I**

Linde, prior to participation in the airborne air separation research program, found that very high boiling heat transfer coefficients could be achieved with specially prepared surfaces. These studies were limited to operation under normal gravitational conditions. Work performed under Contract No. AF 33(616)-7646 later showed that these specially prepared boiling surfaces exhibited no loss of performance at several hundred Ng. At this point the condensing heat transfer resistance was controlling.

Preliminary studies on condensation showed that the best chance of increasing the condensing heat transfer coefficients was to use the high acceleration field that could be generated by rotating the reboiler-condenser. The total resistance to heat transfer during condensation of a single component vapor is in the film of condensate on the surface. Any reduction in the thickness of this film will proportionately decrease the heat transfer resistance. To increase the coefficient, an acceleration parallel to the condensing surface is needed. It is also helpful to make the condensing surface short; this keeps the film thin by reducing accumulated condensate. A quantitative measure of these effects is shown by the Nusselt analysis (Ref. 18) of film condensation. The Nusselt analysis for a vertical surface predicts that:

$$h_c = 0.943 \left( \frac{k_L^3 \rho_L^2 \lambda}{\mu_L \Delta T_c} \right)^{1/4} \left( \frac{a}{L^0} \right)^{1/4} \quad (35)$$

This equation predicts that the condensing heat transfer coefficient is proportional to the acceleration and inversely proportional to the length of the condensing surface, both to the 1/4 power. These relations were confirmed in the test program conducted on a subcontract under Air Force Contract No. AF 33(616)-7646. In that program, condensing coefficients were measured on a 3-inch diameter disk, oriented perpendicular to the gravitational field, and milled with 1/16 inch deep, 45 degree vee grooves.

The objective of the present test program, conducted under Air Force Contract AF 33(657)-8722, was to develop and demonstrate, on a small scale, a sufficiently compact and lightweight prototype reboiler-condenser. This unit would utilize the special boiling surface and high acceleration fields in order to meet the performance requirements. Fulfillment of this objective required a series of preliminary tests to aid in the development of the design of the prototype unit. These tests were to be followed by a demonstration or proof test of a prototype element of the best reboiler-condenser design evolved from the basic  
63 ASRP-2391

**SECRET**

**SECRET**

**ASD-TDR-63-665, Part I**

heat transfer studies. (This prototype element is the UCON fluid test rotor in Section 4.5 of the report.)

The preliminary test phase (basic heat transfer studies) was necessary to:

- a. Establish the effect of pressure on the boiling performance of the special surface; all results to date were for performance at atmospheric pressure.
- b. Reaffirm the conclusion that high gravitational fields and short condensate stripping lengths (short flow path for condensate) could be advantageously used to increase the condensing heat transfer coefficient, especially in a practical reboiler-condenser configuration, such as inside small diameter, smooth tubes.
- c. Investigate possible means of increasing the condensing heat transfer coefficient inside tubes above that attainable with smooth tubes and high gravitational fields. It was a prerequisite that any technique evolved be compatible with configurational requirements dictated by strength considerations for the reboiler-condenser.
- d. Provide boiling performance curves on an untreated aluminum surface in a high gravitational field. A comparison of this data with that for the special boiling surface would show clearly the advantages offered by these special surfaces.

Tests to satisfy the first item of the preliminary test phase were conducted in an apparatus operating at normal gravity. Tests to satisfy Items 2, 3, and 4 were conducted in the high G cryostat constructed under Contract No. AF 33(616)-7646.

The basic element of the prototype reboiler-condenser is a rotating disk, as shown in Figure 37. This disk is made of curved tubes, brazed together, and rotates about its axis of symmetry. The complete reboiler-condenser consists of many of these disks, stacked with a common axis of rotation. All tubes are headered together at their inlets at the inner annular boundary of the disks, and also at their outlets at the outer boundary. The high pressure fluid, the condensing stream, is contained within the tubes so as to minimize tube wall thickness and thus, weight. The condensate, which is formed

63 ASRP-2391

**SECRET**

**CONFIDENTIAL**

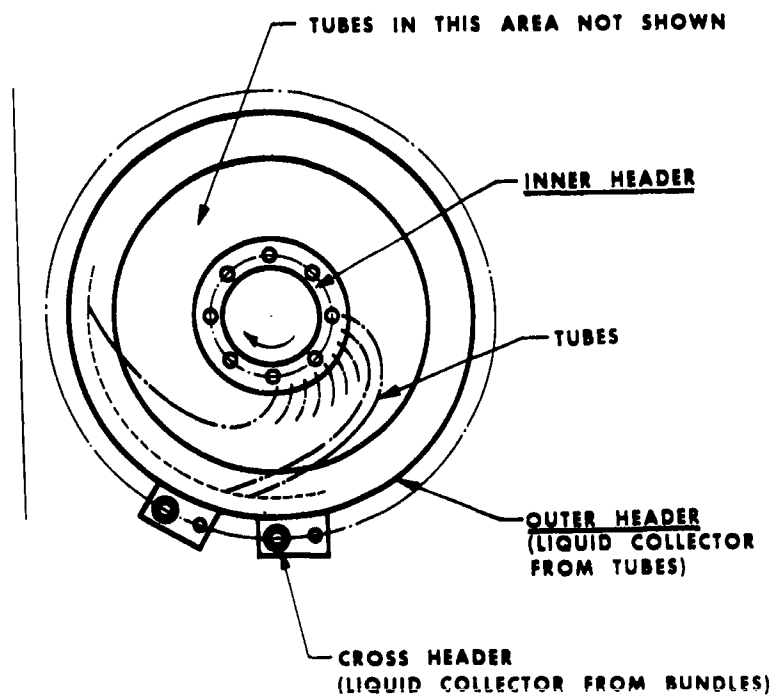
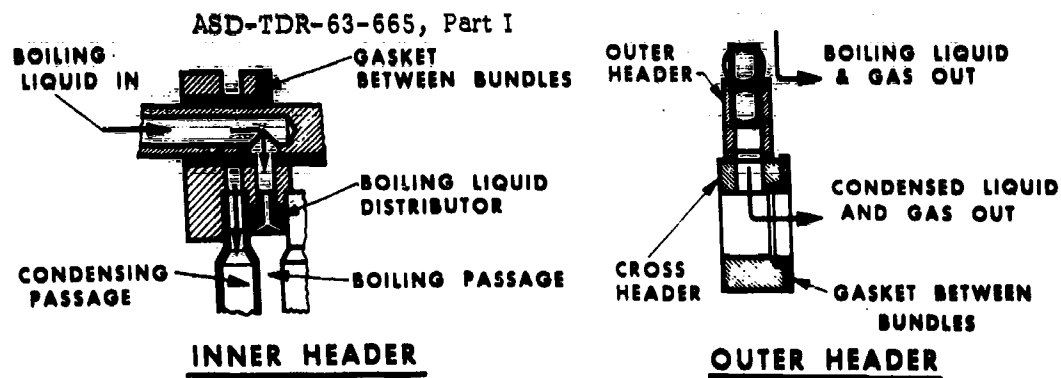


**FIG. 37**

**HEAT TRANSFER SURFACE & HEADERING**

63 ASRP-2391

**CONFIDENTIAL**



**SECRET**

**ASD-TDR-63-665, Part I**

on the walls of the tube, flows radially outward under the influence of the centrifugal acceleration (slightly modified by Coriolis acceleration.) Due to the curvature of the tubes, this radial flow is essentially transverse to the tube axis over most of the area of the rotor. The condensate eventually accumulates on the side of the tube which is radially outward and flows out of the tube in response to that component of the acceleration which is parallel to the tube axis. On the average, the latter component is quite small compared to the total acceleration. The boiling fluid occupies the small space between adjacent disks and flows radially outward.

This configuration was established for the reboiler-condenser on the basis of feasible construction and maximum use of the gravitational field. The development of equations describing heat transfer behavior in the reboiler-condenser are presented in this section and the application of these equations toward actual design will be shown in the Preliminary Design and Analysis Section (Section 6) of this report.

The air enrichment device also requires development of a compact and lightweight reflux condenser. The function of this unit is to provide means for efficient exchange of heat between a low pressure condensing nitrogen stream and a super-critical hydrogen stream. In contrast to the reboiler-condenser, the reflux-condenser design calls for condensation on the outer surface of the exchanger tubes since the condensing stream is the lower pressure stream in this instance. Nitrogen condensation tests on the outer surface of small diameter tubes were included in the aforementioned preliminary test phase to provide the heat transfer information needed to develop the design of the reflux condenser.

#### 4.2 Summary

Of the several methods investigated to reduce the condensing side heat transfer resistance (use of a non-wetting surface, helical grooves and porous surfaces), porous surfaces proved to be the most attractive. Condensing side coefficients well in excess of the often discussed  $2500 \text{ Btu}/(\text{ft}^2) (\text{hr.}) (^\circ\text{R})$  figure can be obtained, the exact quantity depending on condensing side temperature difference and rotational speed.

Boiling tests on a normal (flat, untreated) surface have shown that the special boiling surface retains a substantial advantage over the

63 ASRP-2391

**SECRET**

**SECRET**

**ASD-TDR-63-665, Part I**

conventional boiling surface at all heat fluxes and accelerations of interest. With both types of boiling surfaces, high pressure operation increased heat transfer coefficients.

Consequently, an aluminum porous condensing surface in combination with the special boiling surface shows promise of markedly reducing the volume and weight of the reboiler-condenser. The Preliminary Design and Analysis Section (Section 6) of this report converts the porous condensing and special boiling surface performances into weight and volume estimates.

The proposed reboiler-condenser design with smooth condensing surfaces has performed functionally as expected in the prototype tests with UCON fluids. Operation proved to be smooth and trouble-free. The improvement in condensing side heat transfer on a smooth tube as indicated by tests in the high G cryostat was verified by the tests in the UCON fluid prototype reboiler-condenser.

Future experimental work is recommended to optimize the design of the reboiler-condenser. Parameters affecting the porous condensing surface, such as pore size and surface thickness, and condensing fluid property parameters, such as condensate pressure, should be studied. Two-phase flow of the boiling fluid should be examined in detail since this has a strong bearing on the boiling side temperature, and hence on  $\Delta T$ .

Future work should also include the investigation of the porous condensing surface on the outside of tubes. If the same high performance can be obtained as with condensation inside tubes, porous coatings could be advantageously applied to the reflux-condenser. Test results for condensation on the outer surface of a smooth-walled tube agreed reasonably well with predictions made using a Nusselt-type analysis by Hassan and Jacob (Ref. 19). Efforts in this area would lead to future design work on a reflux-condenser.

This summary illustrates the important strides that have been made in the heat transfer area. The work presented in the Preliminary Design and Analysis Section of this report will illustrate the tremendous influence of the reboiler-condenser on system weight and volume. Thus, it is important that work continue in this area.

**4.3 Pool Boiling at Normal Gravity and Elevated Pressures**

**4.3.1 Test Objectives**

The purpose of this phase of the basic heat transfer program was to evaluate the effect of pressure on performance of the special boiling

63 ASRP-2391

**SECRET**

# CONFIDENTIAL

## ASD-TDR-63-665, Part I

surface. All previous data had been taken at atmospheric pressure. Data at elevated pressures with UCON fluids and oxygen were needed to evaluate performance of the UCON fluid test rotor, and to allow accurate assessment of the performance of the proposed cryogenic reboiler-condenser. In both cases, the pressure on the boiling side would be about 70 psia.

The three fluids whose boiling performance was measured as a function of pressure were UCON 12, UCON 22, and oxygen. Oxygen and UCON 12 were chosen because they were the fluids most likely to be used in the two previously mentioned experimental heat exchangers. UCON 22 was tested because it was still being considered as a possible alternate test fluid for the non-cryogenic test rotor. It was necessary that the boiling data be obtained experimentally, since there is no completely reliable method of estimating the effect of the fluid physical properties on boiling performance.

### 4.3.2 Pool Boiling Apparatus

The test apparatus is shown in Figure 38. It consisted of a large reservoir (25 gallon capacity) of the boiling liquid, with the test piece submerged in it. The test piece was mounted on the end of a long stainless steel rod, which entered the insulated container through the flanged closure. The reservoir was charged with liquid prior to each run. The large volume of liquid made it unnecessary to add liquid during the run.

The pressure inside the test apparatus was controlled manually by a vapor vent valve and measured by a Laboratory test gauge. Steady pressures were easily achieved because the large vapor volume had a dampening influence on fluctuations. The vent valve and test gauge are not shown on Figure 38.

The test piece used in this apparatus is shown in Figure 39. It was a cylinder with an overall length of 7-9/32 inches. The active heat transfer length (that is, the length which is wetted by the test fluid, and on which boiling can occur) was 6-5/8 inches. Specimens were 1 inch in diameter. Both copper and aluminum specimens were tested. A cartridge heater inside the cylinder supplied heat to the boiling surface. Alternating current real power to this heater was measured by a watt meter. Heat leak into the test piece was negligible since the long, thin stainless steel support rod conducted heat at a very low rate. The little heat that was conducted along the support rod was absorbed by the liquid in the reservoir before it could reach the test piece.

63 ASRP-2391

# CONFIDENTIAL

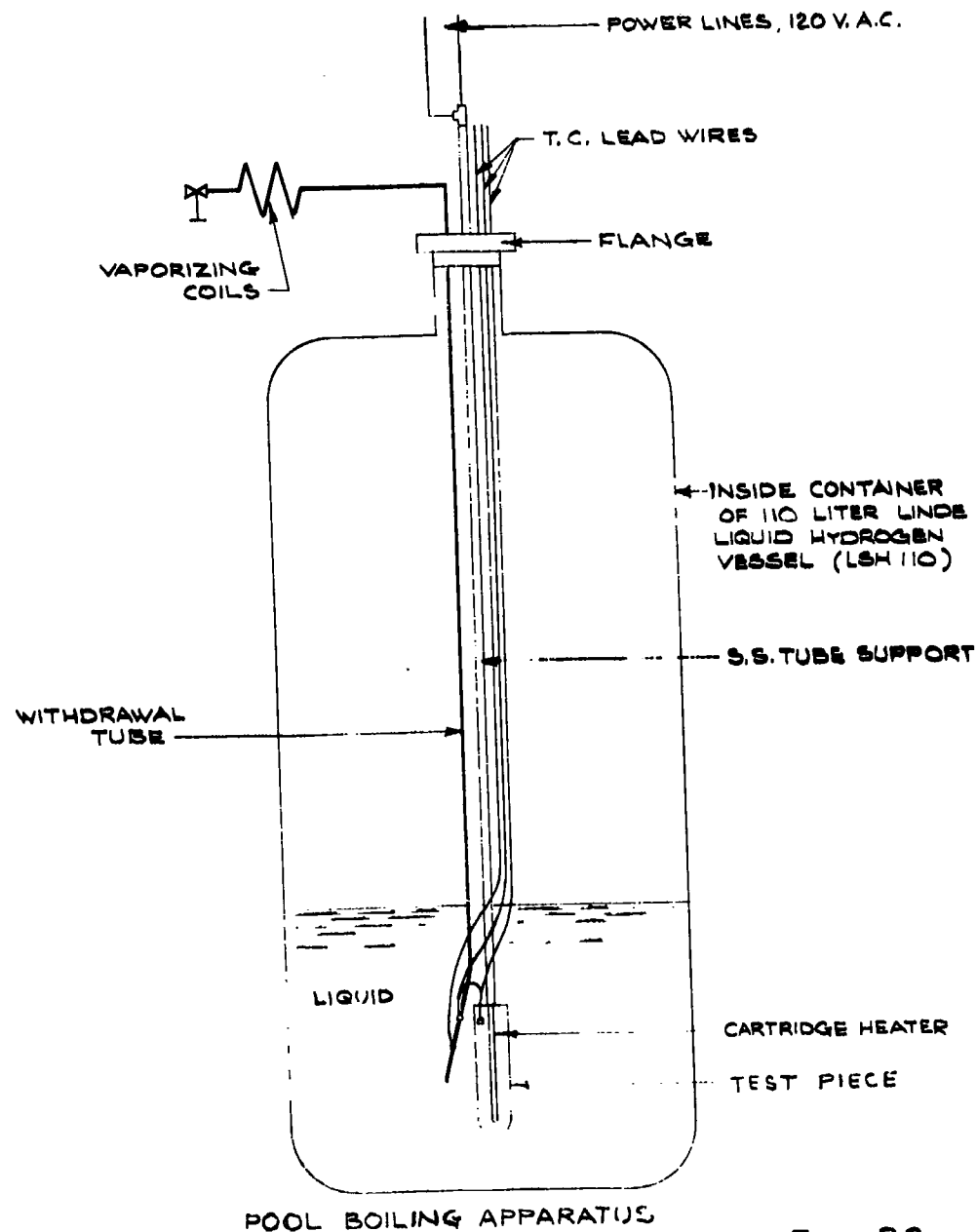
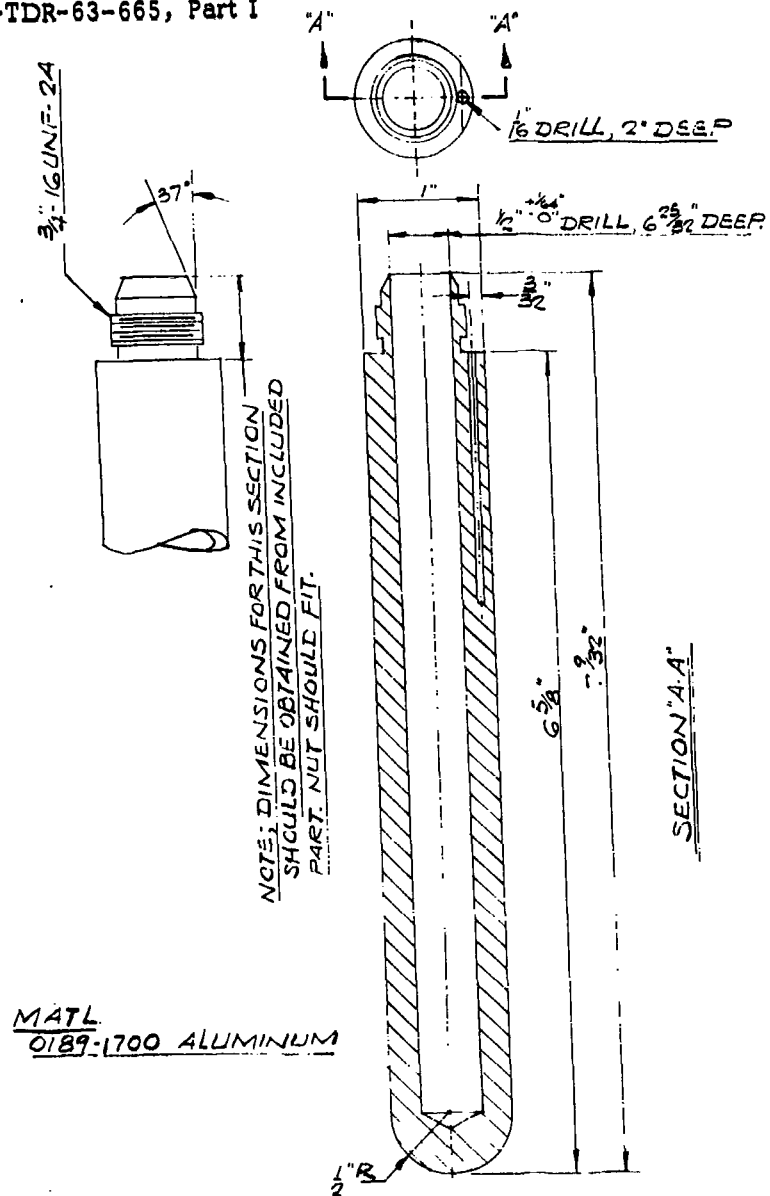


FIG. 38

63 ASRP-2391

ASD-TDR-63-665, Part I



POOL BOILING TEST SPECIMEN

FIG. 39

63 ASRP-2391

# CONFIDENTIAL

## ASD-TDR-63-665, Part I

A copper-constantan thermocouple was used to measure the  $\Delta T$  between the test piece and the boiling fluid. One junction was located in a hole 1/16" in diameter and about 2 inches deep, just underneath the surface of the test specimen. This junction was cemented in place, using a high thermal conductivity cement. The other junction was in the bulk of the test fluid. The boiling side  $\Delta T$  ( $\Delta T_b$ ) was found by subtracting the conductive temperature drop ( $\Delta T_m$ ), between the thermocouple hole and the outside surface of the test specimen, from the overall  $\Delta T$  measured by the thermocouple. Thus, all the data needed to construct a heat flux versus  $\Delta T_b$  curve was directly obtainable.

### 4.3.3 Pool Boiling Results

The results for boiling UCON 12, UCON 22, and oxygen on the special boiling surface applied to copper are shown in Figure 40. The boiling coefficient is plotted as a function of the heat flux multiplied by the parameter  $(\lambda \rho \sqrt{\sigma T_b})$ . The use of this parameter takes into account the significant physical properties of the boiling fluids and thus allows generalization of the test data to yield a useful correlation for all three fluids.

The significance of this parameter is shown by the following derivation.

The pressure inside a vapor bubble of small diameter is greater than in the surrounding liquid, because of surface tension forces. The surface tension force acting on the equator of the hemisphere is:

$$F_1 = 2\pi R_b \sigma$$

The opposing pressure force is:

$$F_2 = (P_v - P_L) \pi R_b^2$$

where  $R_b$  is the bubble radius, and  $P_v$  and  $P_L$  are the vapor and liquid pressures, for equilibrium  $F_1 = F_2$ . Therefore:

$$\Delta P = (P_v - P_L) = \frac{2\sigma}{R_b}$$

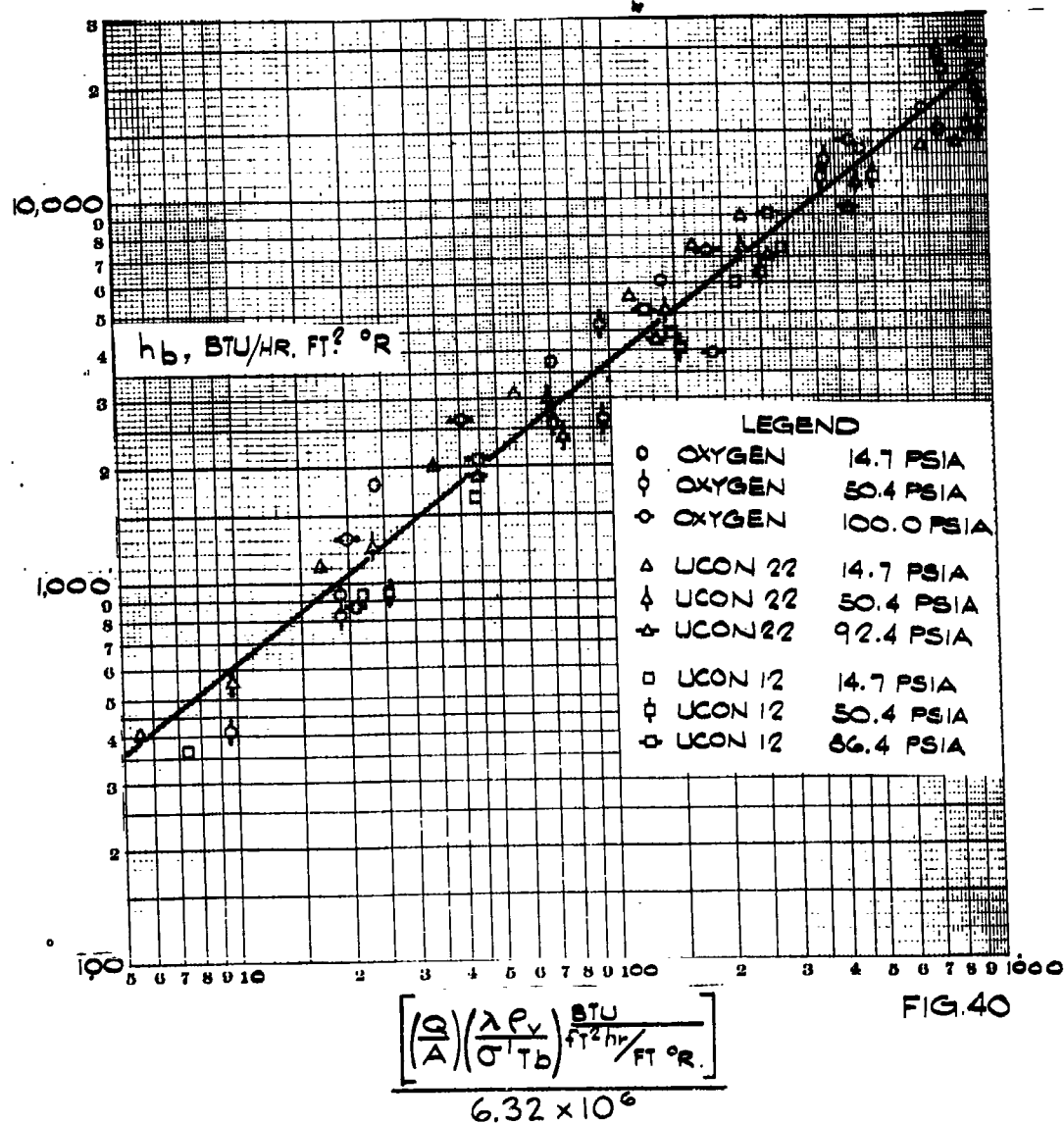
63 ASRP-2391

# CONFIDENTIAL

CONFIDENTIAL

ASD-TDR-63-665, Part I

CORRELATED POOL BOILING DATA  
SPECIAL BOILING SURFACE APPLIED TO COPPER



63 ASRP-2391

CONFIDENTIAL

# CONFIDENTIAL

## ASD-TDR-63-665, Part I

If the bubble is assumed to be at thermal equilibrium,  $T_v = T_L$ . The superheat can be calculated using the Clausius-Clapeyron equation:

$$\frac{dP}{dT_b} = \frac{\lambda}{T_b (1/\rho_v - 1/\rho_L)} = \frac{\lambda \rho_L \rho_v}{T_b (\rho_L - \rho_v)}$$

For small changes in  $T_b$ , the vapor pressure curve can be assumed linear and:

$$\frac{dP}{dT_b} = \frac{\Delta P}{\Delta T_b} = \frac{\lambda \rho_L \rho_v}{T_b (\rho_L - \rho_v)}$$

Therefore:

$$\Delta P = \frac{\lambda \rho_v \rho_L \Delta T_b}{T_b (\rho_L - \rho_v)} = \frac{2 \sigma'}{R_b}$$

Rearranging, and noting that at modest pressure  $\rho_L / (\rho_L - \rho_v) \approx 1.0$

$$\frac{1}{\Delta T_b} \approx \frac{\lambda \rho_v R_b}{2 \sigma' T_b}$$

If we assume that  $R_b$  is the characteristic size of an active site on the Linde boiling surface, then  $\Delta T_b$  would be the minimum temperature difference necessary to start vapor bubbles growing from an active site. Thus, for boiling of a variety of fluids on a given surface,

$$\frac{h_b}{Q/A_b} = \frac{1}{\Delta T_b} \approx \frac{\lambda \rho_v R_b}{2 \sigma' T_b}$$

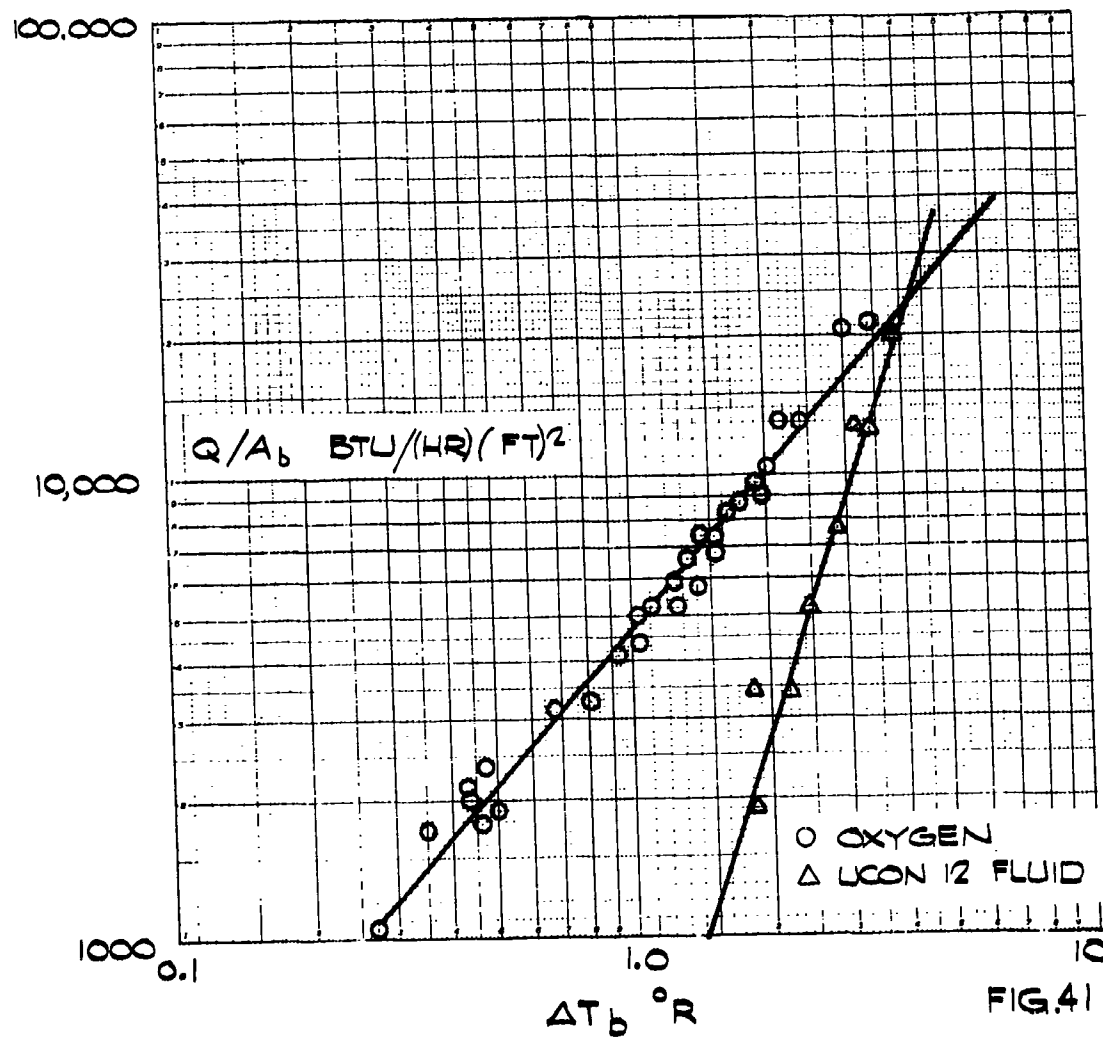
$$(h_b) \approx (Q/A_b) \left( \frac{\lambda \rho_v}{2 \sigma' T_b} \right) R_b \quad (36)$$

Qualitatively, the result is that the boiling coefficient for a fluid increases with increase in pressure.

The results for boiling of UCON 12 and oxygen on the Linde boiling surface applied to aluminum are shown in Figures 41 and 42. The heat flux  
63 ASRP-2391



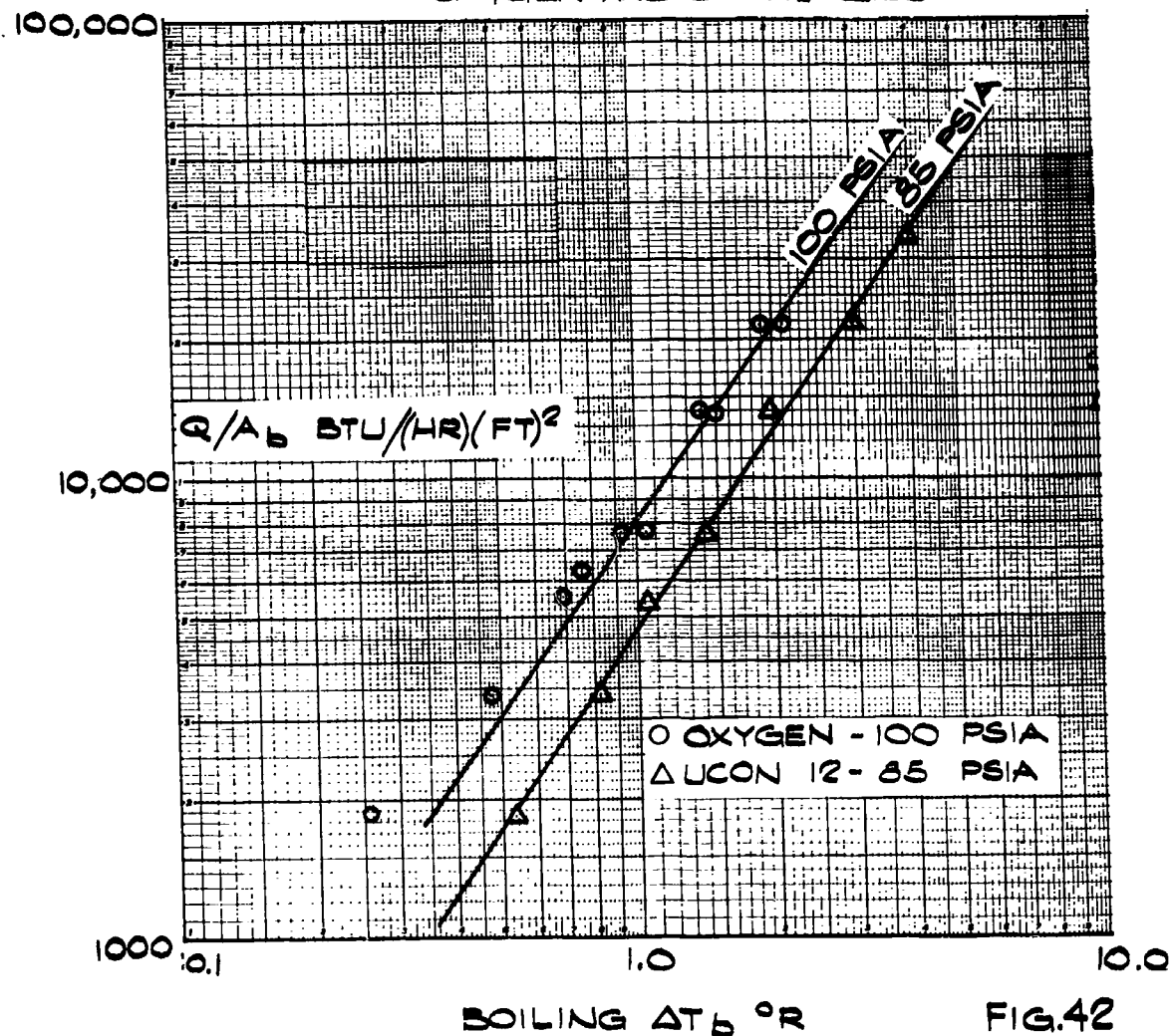
CORRELATED POOL BOILING DATA AT 1 ATM.  
SPECIAL BOILING SURFACE APPLIED TO ALUMINUM



# CONFIDENTIAL

ASD-TDR-63-665, Part I

CORRELATED POOL BOILING DATA AT ELEVATED  
PRESSURE SPECIAL BOILING SURFACE APPLIED TO  
ALUMINUM  
PRESSURE ABOVE 1ATM  
OXYGEN AND UCON 12 FLUIDS



63 ASRP-2391

# CONFIDENTIAL

## ASD-TDR-63-665, Part I

on this surface is shown as a function of temperature difference between the metal wall and the boiling fluid. Unfortunately, these results did not correlate in the same way as those on the copper surface. This is attributed to the special boiling surface on the aluminum not being applied as uniformly as that on copper. With sufficient care in preparation, an aluminum surface that is comparable in performance to a copper surface, and which would conform to the proposed correlation could be prepared.

The effect of pressure on the boiling performance was qualitatively the same as that noted on the copper surface. A smaller  $\Delta T$  was required to produce a given heat flux at high pressures than at low pressures. Thus, the boiling coefficient improved as the pressure was increased. A linear interpolation of  $\Delta T_b$  with pressure is recommended for estimating the boiling side  $\Delta T$  at a given heat flux and intermediate pressure for the aluminum surface.

In these experiments the values for heat of vaporization ( $\lambda$ ) and vapor density ( $\rho_v$ ) for oxygen were taken from Reference (20) and the values for the surface tension of oxygen from Reference (21). Use of Reference (20) will also give saturation temperature versus pressure values for oxygen.

The properties for UCON fluids were obtained from Reference (22) except the surface tension at pressures above one atmosphere was obtained by use of the Eötvös equation, Reference (23).

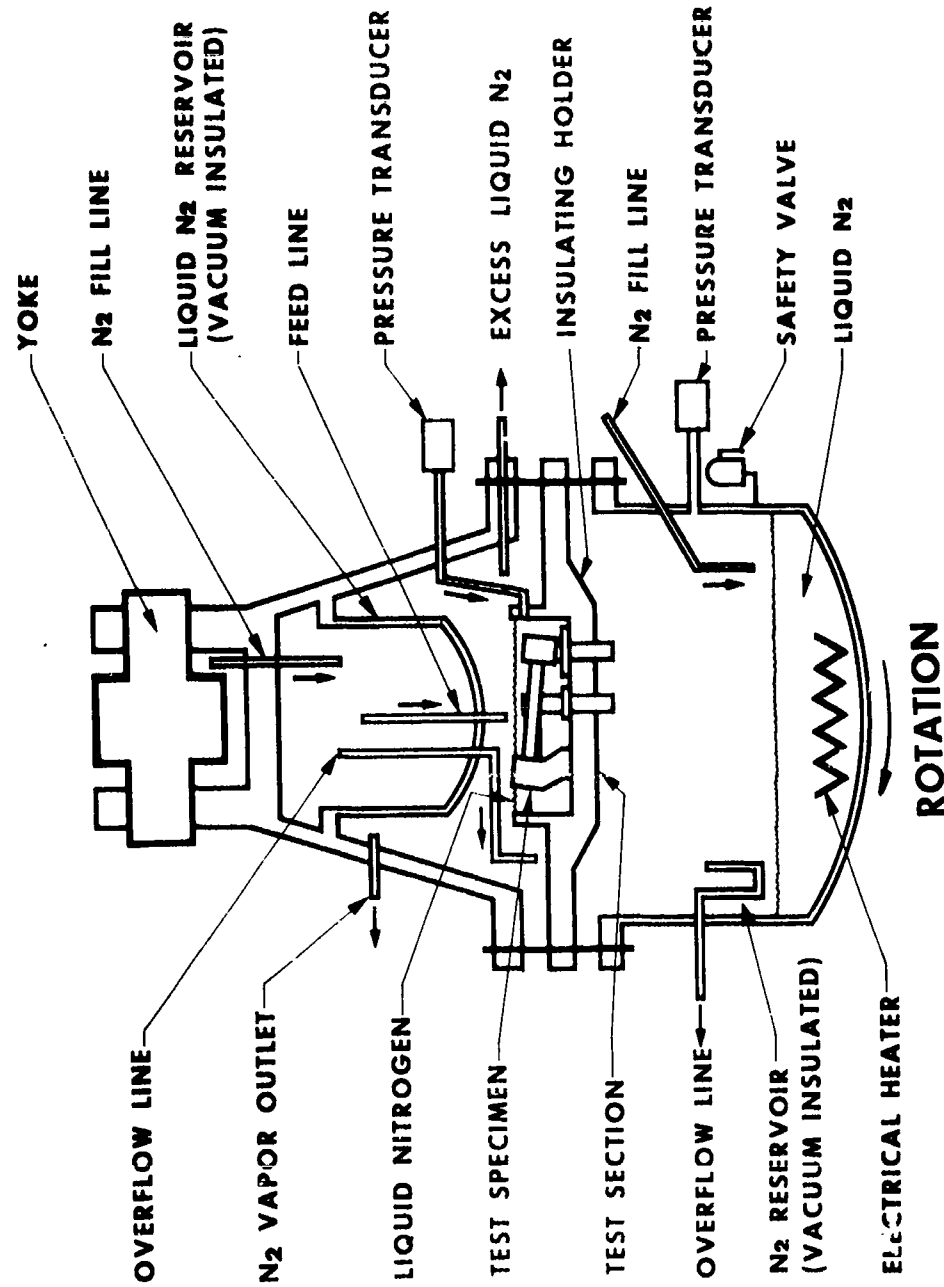
### 4.4 Boiling and Condensing Studies in High-G Cryostat

#### 4.4.1 Test Program

Seven specimens were required to satisfy the program for basic heat transfer studies in high gravitational fields. The first six tests were condensation experiments while the seventh was a boiling experiment.

Five of the six condensation experiments were for condensation inside tubes where different surfaces were tested on the heat transfer specimen. (Tests 1, 3, 4, 5, and 6). These five specimens each consisted of four heat exchanger tubes headered at both ends into stainless steel manifolds which distributed vapor and collected condensate. The manifolds were connected to the condensing and boiling chambers, respectively, by stainless steel tubes passing through a micarta flange, which divided the cryostat, Figure 43, into two separate chambers. Nitrogen was used as the heat transfer medium on both sides of the exchanger. The condensing side was a closed system; the heat load was therefore the sum of the electrical energy to the reboiler and the heat leak. Boiling and condensing side pressures were

63 ASRP-2391



CROSS SECTION OF HIGH G CRYOSTAT

FIG. 43

63 ASRP-2391

# CONFIDENTIAL

## ASD-TDR-63-665, Part I

measured by pressure transducers and the overall  $\Delta T$  was then calculated from the vapor pressure curves giving the difference between the boiling and condensing fluid saturated temperatures. The condensing side  $\Delta T$  was found by subtracting the wall temperature drop and the boiling side  $\Delta T$  from the overall  $\Delta T$ . All six condensing experiments were performed with the boiling side treated with the special boiling surface. The boiling side  $\Delta T$  was known from previous Linde studies at normal gravity, since the work done under Contract AF 33(616)-7646 showed that a high gravitational field had no effect on heat transfer on a special boiling surface in the range of heat fluxes of interest. Since the heat transfer area was known, the average condensing coefficient was directly computable.

Test specimens 3, 4, 5, and 6 were used to investigate means of increasing the condensing coefficient above the smooth surface values of test specimen 1. Since the resistance on the condensing side was the major resistance to heat transfer, any improvement in condensing performance could be directly translated into a reduction in heat transfer area requirements, temperature difference requirements, or a combination of both. All configurations investigated were applied inside the tubes. Schemes tested were (1) helical grooves, (2) a porous surface (two test specimens) and (3) a nonwetted surface. These specimens were constructed and tested identically as in test 1. The only difference was the alteration of the condensing surface in an attempt to get improved condensing heat transfer coefficients.

Test 2 was designed to measure condensation outside smooth tubes and therefore the previously discussed tube manifolds supplied liquid and removed a two-phase stream of vapor boiloff and excess liquid. The condensing side  $\Delta T$  was measured directly with a thermocouple.

The last specimen (test 7) measured boiling on a smooth surface in a high gravitational field. It will be discussed in detail later in section 4.4.1.6.

### 4.4.1.1 Condensation Inside Smooth Tubes - Test 1

This test was designed to measure condensing heat transfer coefficients inside smooth copper tubes to provide condensing performance data for the reboiler-condenser where small diameter, smooth tubes are used. The test specimen is shown in Figure 44.

63 ASRP-2391

TEST NO. 1  
HEAT EXCHANGER FOR CONDENSATION INSIDE SMOOTH TUBES

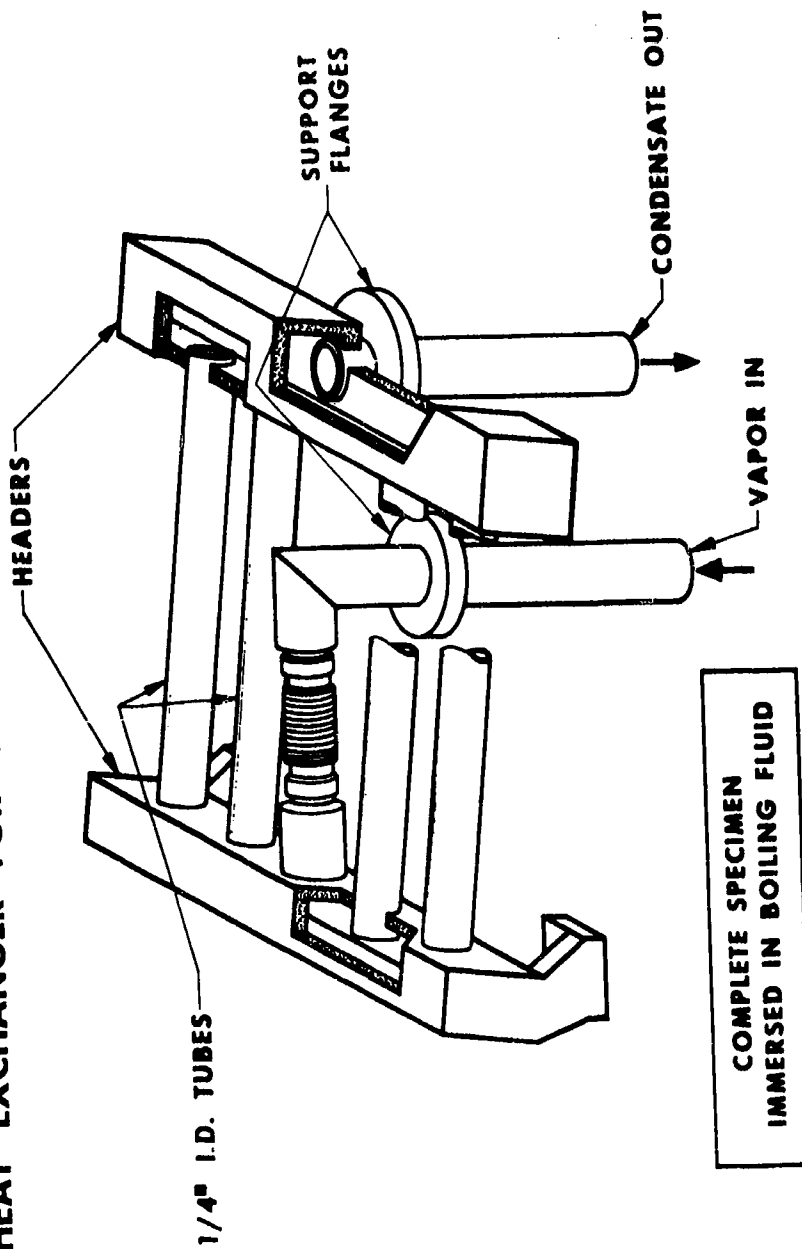


FIG. 44

63 ASRP-2391

**CONFIDENTIAL**

**ASD-TDR-63-665, Part I**

**4.4.1.2 Condensation Outside Smooth Tubes - Test 2**

This test was designed to measure condensing heat transfer coefficients outside smooth copper tubes to provide condensing performance data for the reflux condenser where, as in the case of the reboiler-condenser, small diameter, smooth tubes are used. The test specimen is shown in Figure 45.

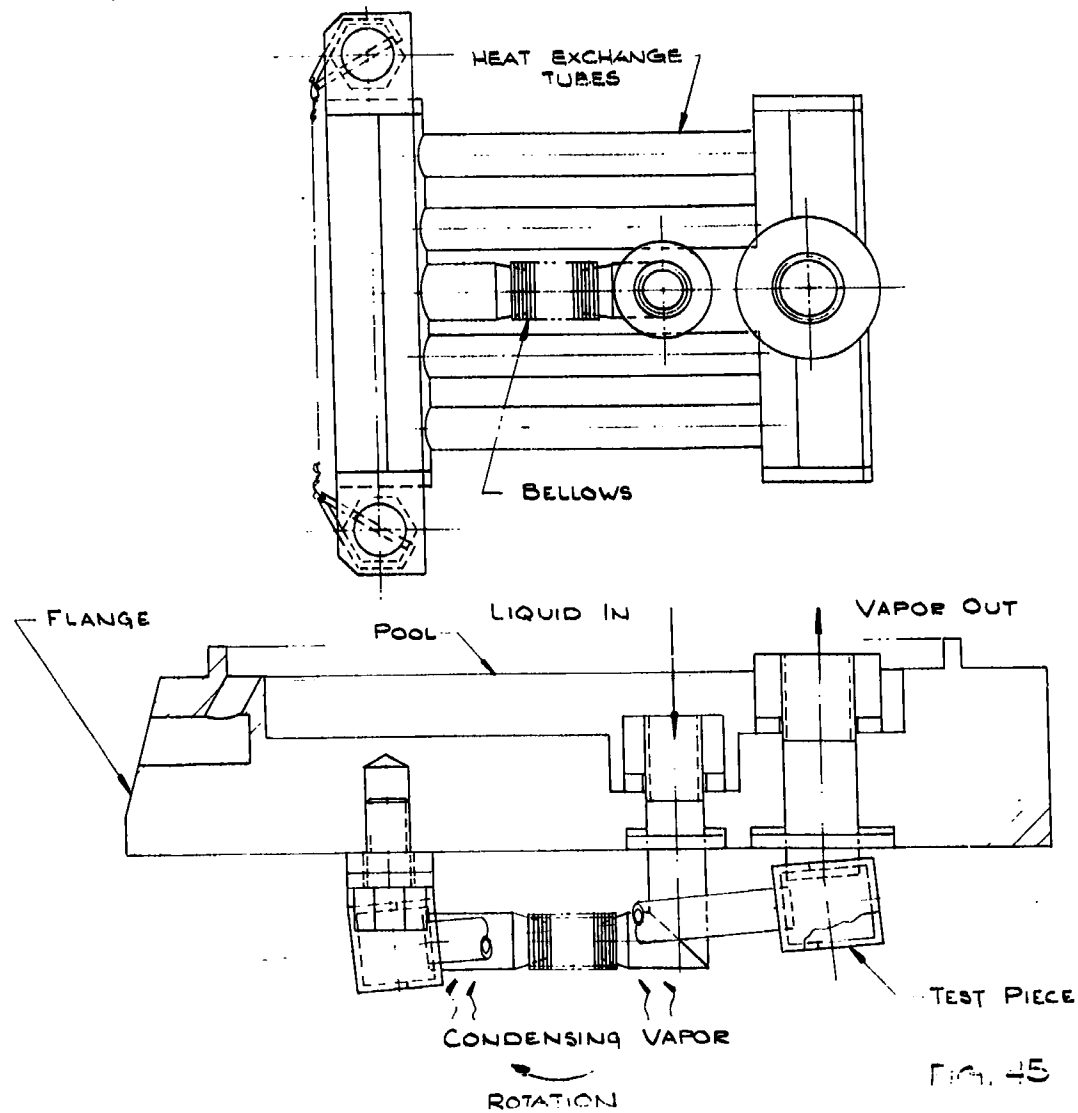
**4.4.1.3 Condensation Inside Helical-Grooved Tubes - Test 3**

A tap was run through the copper tubes of the test piece prior to welding them into the headers. This cut a helical thread with a pitch of 1/18 inch, and a 60° groove angle. A reamer was then run through the tube to shave the peaks off the threads. A 25 mil wide flat resulted. The remaining groove was 20 mil deep. A sketch of a typical tube is shown in Figure 46. It was expected that this profile would improve the condensing coefficient on the radially-inward portion of the tube by providing ridges towards which the condensate would run, and from which the condensate would be easily removed as droplets by the high gravitational field. Film flow around the circumference of the tube would then be circumvented. The sides of the grooves in the radially-inward portion of the tube would be relatively bare of condensate, and the stripping length would be reduced from one-half the tube circumference to the length of the sides of the grooves. The expected improvement in coefficient would be 2.03 times, since the condensing heat transfer coefficient varies with the length to the one-quarter power. On the radially-outward portion of the tube, the condensate was expected to preferentially accumulate in the troughs of the grooves, and be held there by gravitational and surface tension forces. The condensate would then drain to the most radially-outward position of the tube by way of the troughs. The flats, having lost most of their condensate by flow into the troughs, would have a thinner film than if no troughs were present, and hence a higher coefficient. The portion of the heat transfer area that would be rendered ineffective (the flats on the radially-inward portion of the tube and the sides of the troughs on the radially-outward portion of the tube) because of heavy accumulations of condensate would be more than compensated for by the higher coefficients prevailing on the rest of the area.

63 ASRP-2391

**CONFIDENTIAL**

TEST N° 2 HEAT EXCHANGER FOR CONDENSATION OUTSIDE SMOOTH TUBES

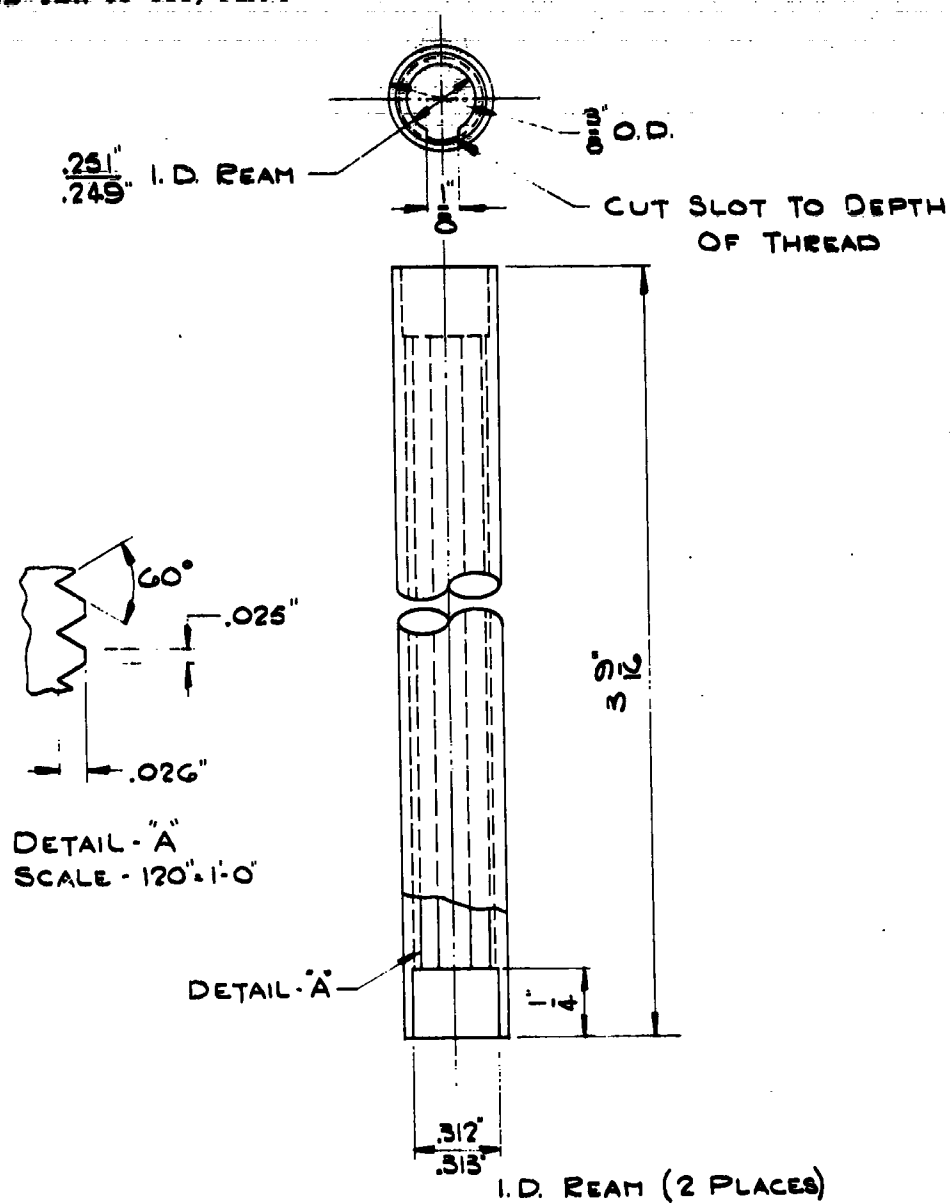


63 ASRP-2391



0

ASD-TDR-63-665, Part I



TEST N°3 - TYPICAL TUBE CONDENSATION  
ON HELICAL WEIRS

FIG. 46

63 ASRP-2391

**CONFIDENTIAL**

ASD-TDR-63-665, Part I

4.4.1.4 Condensation Inside Copper and Aluminum Porous Condensing Surface Tubes - Tests 4 and 5

The first porous surface test specimen was prepared with a 7-10 mil thick porous layer sintered on the inside of the copper tubes. It was composed of 325 mesh copper particles, which were roughly spherical in shape. The porosity of the resulting surface was about 40%. The second porous condensing surface specimen was physically identical to the first except that 3003 aluminum was used as the tube, manifold, and nozzle material, and the I.D. of the tubes was 0.305 inches instead of 0.250 inches. A porous surface 7-10 mil thick, composed of 270-400 mesh aluminum particles was sintered onto the inside of the tubes.

The principle of the porous surface was that the condensate would be drawn into the capillaries of the porous surface by surface tension forces, and would flow to the "bottom" of the tube through the capillaries within the porous structure under the influence of the high artificial gravitational forces. "Bottom" refers to radially outward from the rotor axis, and "top" to radially inward toward the rotor axis. The high heat transfer resistance of the condensate would thus be effectively short circuited by the porous layer, which would have a high equivalent heat transfer coefficient (about 100,000 Btu/(ft.)<sup>2</sup> (hr.) (°R). This value is obtained from the assumption that the porous surface would completely absorb the condensate film so that the limitation on the film coefficient would be the thermal conductivity of the metal of the porous surface itself. The accumulated condensate would drain along the bottom of the tube, parallel to the tube axis, in response to the minor component of the acceleration in that direction. This is shown schematically in Figure 47. For the sake of convenience, the tube section shown there is taken perpendicular to the tube axis, and the actual condensate radial path acted upon by  $N_g$  must be compensated by diminishing the force motivating flow in the capillaries by the amount  $\cos \alpha^\circ$ . Thus the acceleration acting in the direction perpendicular to the tube axis is  $(N_g) (\cos \alpha^\circ)$ .

The two necessary conditions for adequate functioning of the porous surface, referring to the pressure balances shown in Figure 47, are as follows:

Condition 1

$$\frac{4 \sigma'}{y \delta^\circ} \geq \frac{\rho L g}{g_c \cos \epsilon} N_g \cos \alpha^\circ \cos \phi_1, \quad (37)$$

63 ASRP-2391

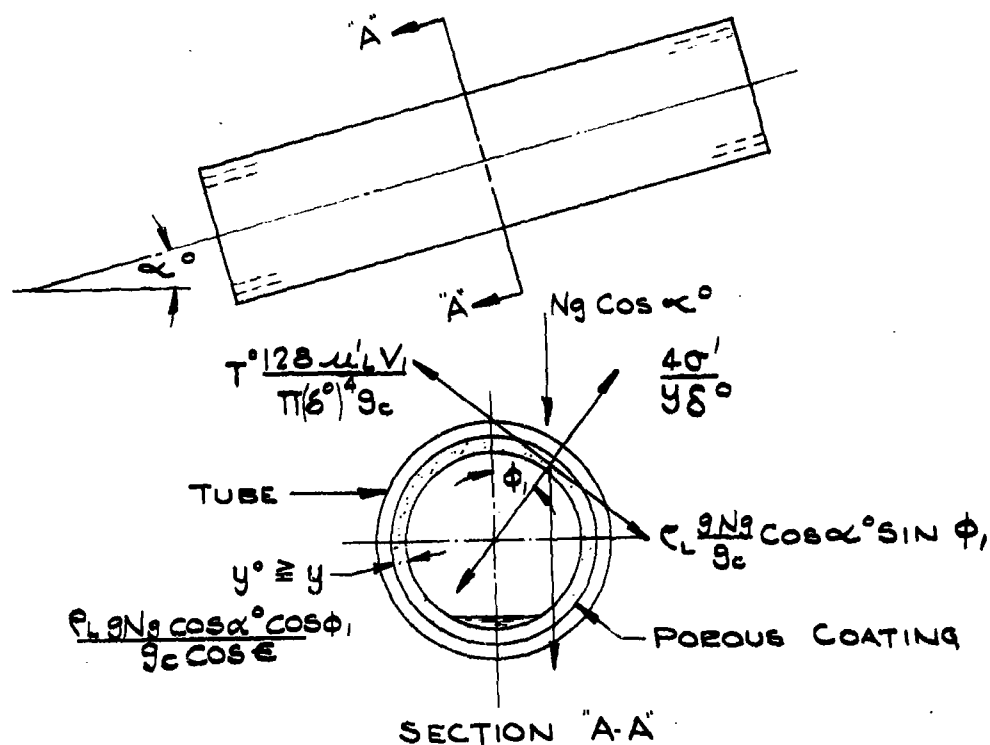
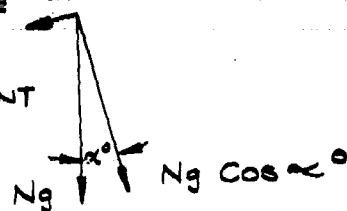
**CONFIDENTIAL**

C

ASD-TDR-63-665, Part I

$$N_g \sin \alpha^\circ =$$

DRAINAGE  
COMPONENT



$y$  = THICKNESS OF POROUS COATING  
 $V_1$  = FT<sup>3</sup>/HR. OF CONDENSATE  
 FLOW IN ONE CAPILLARY  
 $T^\circ$  = TORTUOSITY FACTOR

POROUS CONDENSING SURFACE FLOW

FIG. 47

63 ASRP-2391

**CONFIDENTIAL**

**ASD-TDR-63-665, Part I**

This was derived from the equation for the height of rise of a fluid in a capillary,

$$y^{\circ} = \frac{4 g_c \sigma' \cos \epsilon}{g \delta^{\circ} (\rho_L - \rho_v)} \quad (\text{Ref. 23})$$

Here the height  $y^{\circ}$  is the height of rise of the liquid,  $\epsilon$  is the contact angle between fluid and porous surface wall and  $\delta^{\circ}$  is the capillary diameter.

In order for the fluid to be retained in the porous surface,  $y^{\circ}$  must be greater than or equal to  $y$ , the thickness of the porous surface. That is: the capillary rise, radially, must equal or exceed the thickness of the porous surface. Thus:

$$\frac{g_c 4 \sigma' \cos \epsilon}{g \delta^{\circ} (\rho_L - \rho_v)} \geq y$$

Assuming that  $(\rho_L - \rho_v) \approx \rho_L$ , and incorporating  $Ng \cos \alpha^{\circ} \cos \phi_i$ , to get the component of the acceleration field in the direction perpendicular to the porous surface,

$$\frac{4 g_c}{g Ng \cos \alpha^{\circ} \cos \phi_i} \frac{\sigma'}{\delta^{\circ}} \frac{\cos \epsilon}{\rho_L} \geq y$$

or

$$\frac{4 \sigma'}{\delta^{\circ} y} \geq \frac{\rho_L g Ng \cos \alpha^{\circ} \cos \phi_i}{g_c \cos \epsilon}$$

63 ASRP-2391

**CONFIDENTIAL**

**CONFIDENTIAL**

ASD-TDR-63-665, Part I

Condition 2.

$$\frac{\rho_L g N g}{g_c} \cos \alpha^\circ \sin \phi_i \geq \frac{128 T^\circ V_i \mu'_L}{\pi g_c (\delta^\circ)^4} \quad (38)$$

This condition expresses the fact that the force motivating fluid drainage through the capillaries of the porous surface must be greater than the retarding resistance to flow. In other words, the hydrostatic head of liquid drainage must be greater than the frictional pressure drop.

The frictional pressure drop for the porous surface capillaries can be derived from the Hagen-Poiseuille equation as follows:

$$\Delta P = \frac{32 L^\circ V_i \mu'_L}{g_c (\delta^\circ)^2}$$

The frictional pressure drop per unit length of capillary is:

$$\frac{\Delta P}{L^\circ} = \frac{32 V_i \mu'_L}{g_c (\delta^\circ)^2}$$

multiplying by A/A (A = area)

$$\frac{\Delta P}{L^\circ} = \frac{32 V A \mu'_L}{g_c (\delta^\circ)^2 A}$$

calling V A the volumetric flow rate V, in one capillary and substituting

$$\frac{\pi (\delta^\circ)^2}{4} \text{ for } A$$

$$\frac{\Delta P}{L^\circ} = \frac{32 V_i \mu'_L}{g_c (\delta^\circ)^2 \left[ \frac{\pi (\delta^\circ)^2}{4} \right]} = \frac{128 V_i \mu'_L}{\pi g_c (\delta^\circ)^4}$$

63 ASRP-2391

**CONFIDENTIAL**

# CONFIDENTIAL

## ASD-TDR-63-665, Part I

Since the porous surface is not an ideal capillary, a dimensionless quantity called the tortuosity factor ( $T^\circ$ ) must be inserted to account for the increase in pressure drop due to the irregularity of the flow path. (Ref. 24)

$$\therefore \frac{\Delta P}{L^\circ} = \frac{128 T^\circ V_1 \mu'_L}{\pi g_c (\delta^\circ)^4}$$

Thus in order that the condensate drains through the capillaries at a sufficient rate to prevent flooding

$$\rho_L \frac{g}{g_c} \cos \alpha^\circ \sin \phi_i \geq \frac{128 T^\circ V_1 \mu'_L}{\pi g_c (\delta^\circ)^4}$$

The condensate flow rate,  $V_1$ , may be calculated from the heat flux  $Q/A_c$  and pore density at the point on the circumference of the tube indicated by  $\phi$  in Figure 47.

$$\frac{(Q/A_c) r_t \phi_i}{\lambda \rho_L Y \rho_P} = V_1$$

The two necessary conditions were calculated to be satisfied within the range of the proposed heat flux and gravitational field variations at nearly all points on the tube circumference if 325 mesh copper particles were used to form a porous coating 3 mil thick. The small fraction of the area where  $\cos \phi_i$  is small (near the top of the tube) would obviously require infinite coating thickness, since there is no acceleration component to promote flow at that point, but this can be neglected. A somewhat thicker coating was applied to provide a reasonable safety factor.

### 4.4.1.5 Condensation Inside Tubes with Non-wetted Surface - Test 6

A non-wetting surface or one where the angle  $\epsilon$ , previously defined is greater than  $90^\circ$ , was desired to promote dropwise condensation. The incentive was that it might offer a means of getting high condensing heat transfer coefficients at relatively low  $Ng$  values. This, coupled with the Linde boiling surface whose performance is little affected by  $Ng$  values up to at least several hundred, offered the possibility of a high performance

63 ASRP-2391

**CONFIDENTIAL**

**ASD-TDR-63-665, Part I**

reboiler-condenser at low  $N_g$ . Furthermore, the realization of dropwise condensation would be highly advantageous due to the small weight penalty it would incur compared to other methods. The advantages are obvious. The probability of finding a surface with low enough surface energy to promote dropwise condensation of nitrogen (surface tension of 7 dynes/cm) was expected to be low.

A review of the literature indicated that dropwise condensation could be induced for fluids other than water by the use of a coating of a low surface energy material such as Teflon. Bobco (Ref. 25) reported dropwise condensation of iso-octane ( $\sigma = 50.81$  dynes/cm), carbon disulfide, ( $\sigma = 40.3$  dynes/cm), and ethanol ( $\sigma = 17.67$  dynes/cm). Topper and Baer (Ref. 26) observed dropwise condensation of ethylene glycol ( $\sigma = 37.8$  dynes/cm), nitrobenzene ( $\sigma = 33.3$  dynes/cm), and aniline ( $\sigma = 32.5$  dynes/cm). They found filmwise condensation with benzene ( $\sigma = 21.3$  dynes/cm), however. No reference was found citing dropwise condensation with such a variety of vapors for any material other than Teflon. For this reason, the sixth specimen was coated with a 5,000 Angstrom (app. .02 mil) thick Teflon film. It was prepared by diluting DuPont Teflon primer liquid 5 to 1 by weight with distilled water. This suspension was filtered and poured into the tubes to be coated. When thorough wetting had been accomplished, the tube was drained and air dried. The Teflon was fused by heating to 600°F, leaving a thin, clear film of obvious non-wetting characteristics when tested with water.

The thickness of the Teflon coating was determined by treating a pieced aluminum foil in the same manner that the tubes were coated. The thickness of the film was calculated from the increase in weight of the foil. The thickness of the Teflon on the tube was assumed to be the same as the thickness of the film on the foil. The determination of the thickness of the Teflon on the foil was reliable, since the increase in weight due to coating was a good percentage of the weight of the foil. The coating was 3 to 5 mil thick. A control sample showed that the increase in weight could not be caused only by oxidation at the 600°F. temperature.

**4.4.1.6 Boiling On An Untreated Aluminum Surface - Test 7**

This test was made to verify the advantage of the special boiling surface, over an untreated boiling surface, for the heat fluxes and gravitational fields of interest.

63 ASRP-2391

**CONFIDENTIAL**

# CONFIDENTIAL

## ASD-TDR-63-665, Part I

A disk shaped test piece (Fig. 48) was used for the boiling test. It was made of 3003 aluminum and care was taken to preserve the "mill finish" on the boiling face. This was done by mounting the disk in a protective holder during the machining operations. Resistance wire was wound in the grooves in the base of the piece to form a heater element. Two crisscrossed layers (imbedded in a high thermal conductivity ceramic cement) were required so that adequate heat fluxes could be reached without danger of overheating the wire. Two copper-constantan thermocouples were installed in 1/32 inch diameter holes about 1/16 inch (the exact distances were known) under the boiling surface. One inch of immersion of the leads in the holes was deemed sufficient to prevent heat leak along the thermocouple leads from influencing the junction temperature. One thermocouple hot junction was near the edge of the piece and the other near the axis. The cold junctions were in the boiling pool near the pressure tap. The overall boiling side  $\Delta T$  was directly determined by correcting the measured  $\Delta T$  for the conduction drop through the metal. The heat input to the heater was measured with a watt meter. The heat flux versus  $\Delta T$  curve for the test piece was thus readily determined. The pressure tap was required to establish the absolute pressure at a known point in the pool. The voltage gradient of the copper-constantan differential thermocouple,  $dE/dT$  emf/degree was a function of temperature, so that it was necessary to know the temperature in the pool to reduce the data accurately. Measurement of a hydrostatic head of liquid at this point also insured that the test surface was adequately covered with liquid.

The test piece was cemented into the flange with epoxy resin. The resin bonded tightly to the mica flange and the aluminum, and prevented liquid from boiling on the sides of the disc. The heat flux lines in the piece were thereby kept straight and parallel.

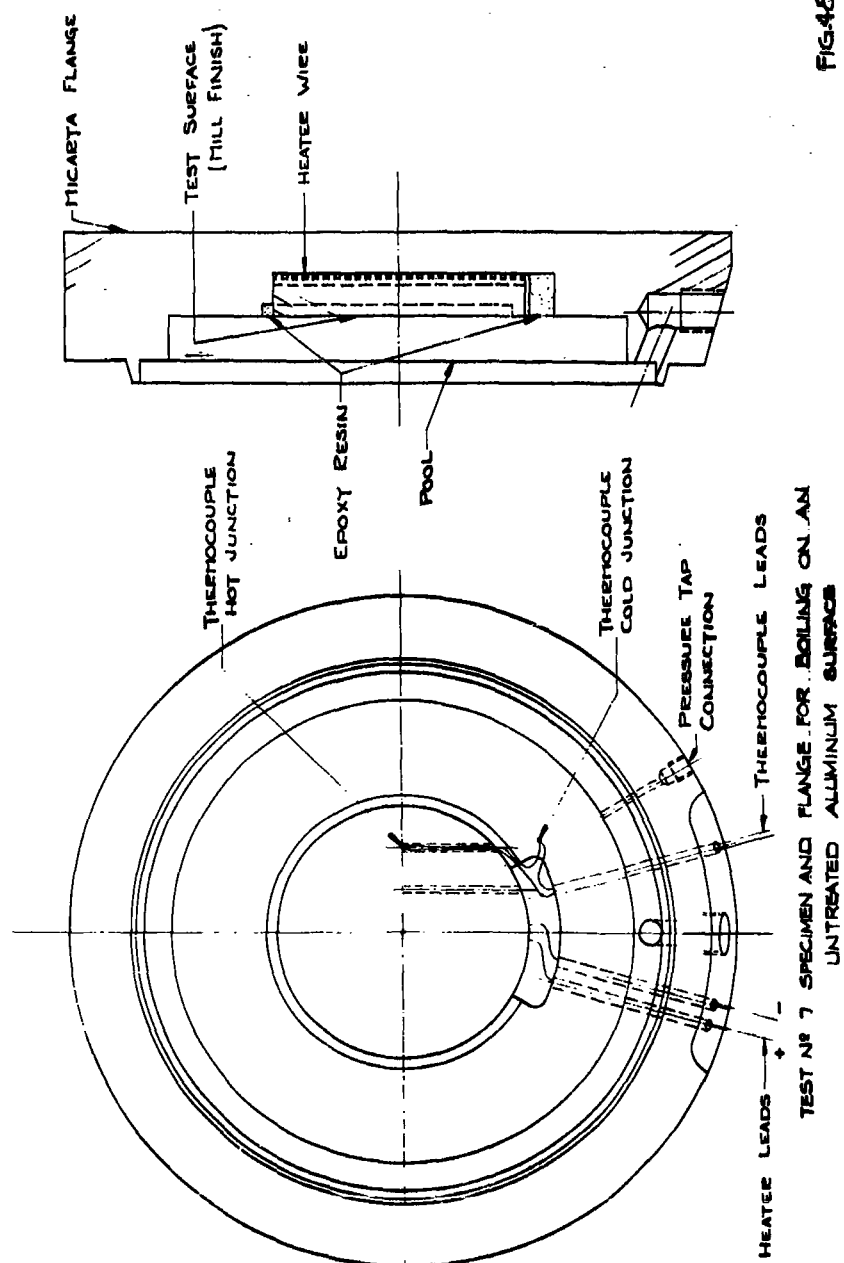
### 4.4.2 High-G Cryostat Apparatus

The centrifuge used to produce the rotary motion was similar to that used by Merte and Clark (Ref. 27). Figure 49 is a photograph of the cryostat; Figure 50 shows the apparatus in a schematic diagram. The test piece was mounted in the cryostat at one end of the rotating arm. A counterweight at the opposite end of the arm was used to balance the rotor. The cryostat and counterweight were swivel mounted, and assumed a position compatible with the resultant of the artificial accelerational field and the earth's gravitational field. The lowest acceleration attainable was 20 Ng and the maximum was about 400 Ng. Both values were for locations at the test piece radius, which was about 18 inches.

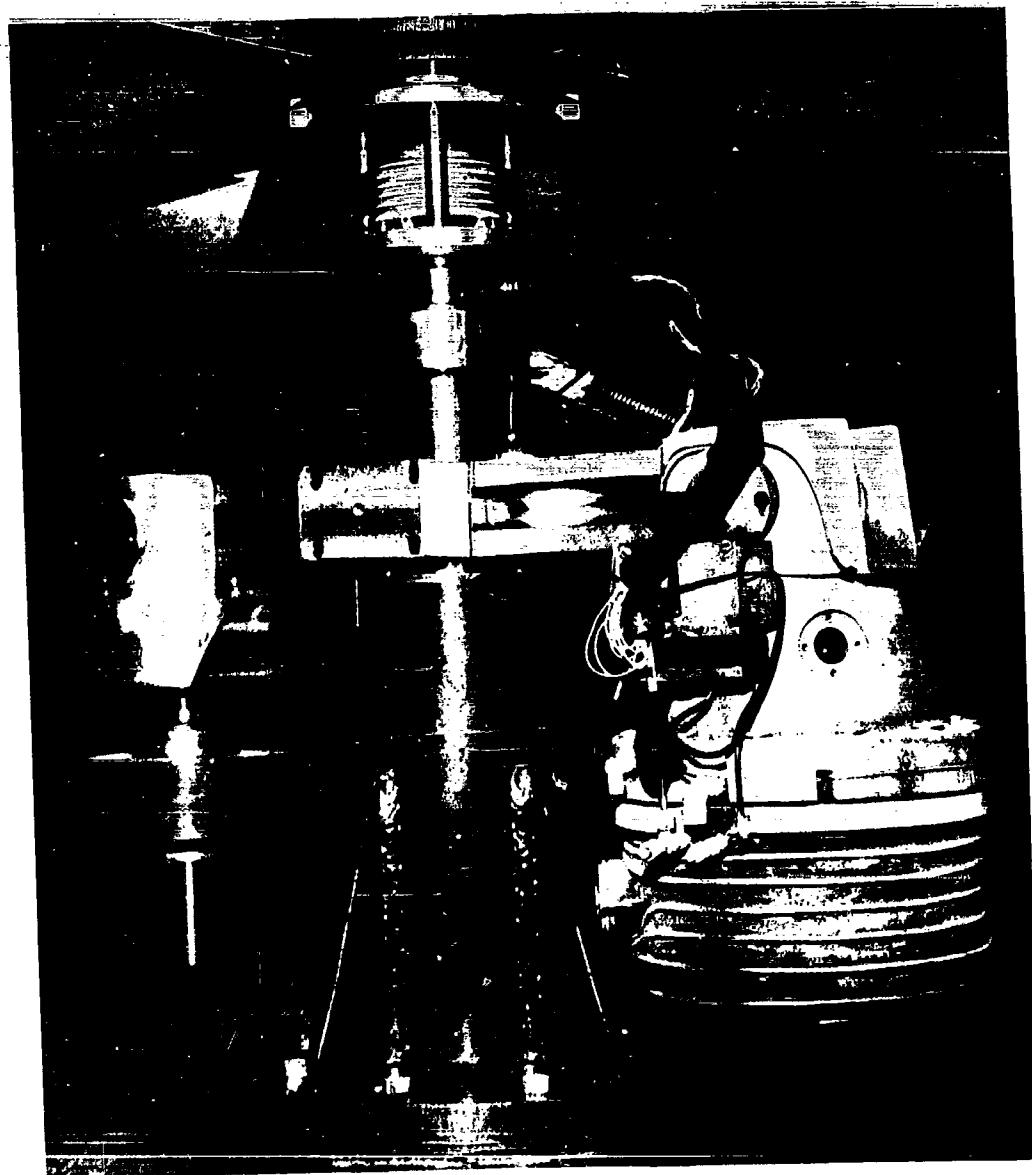
63 ASRP-2391



FIG. 48



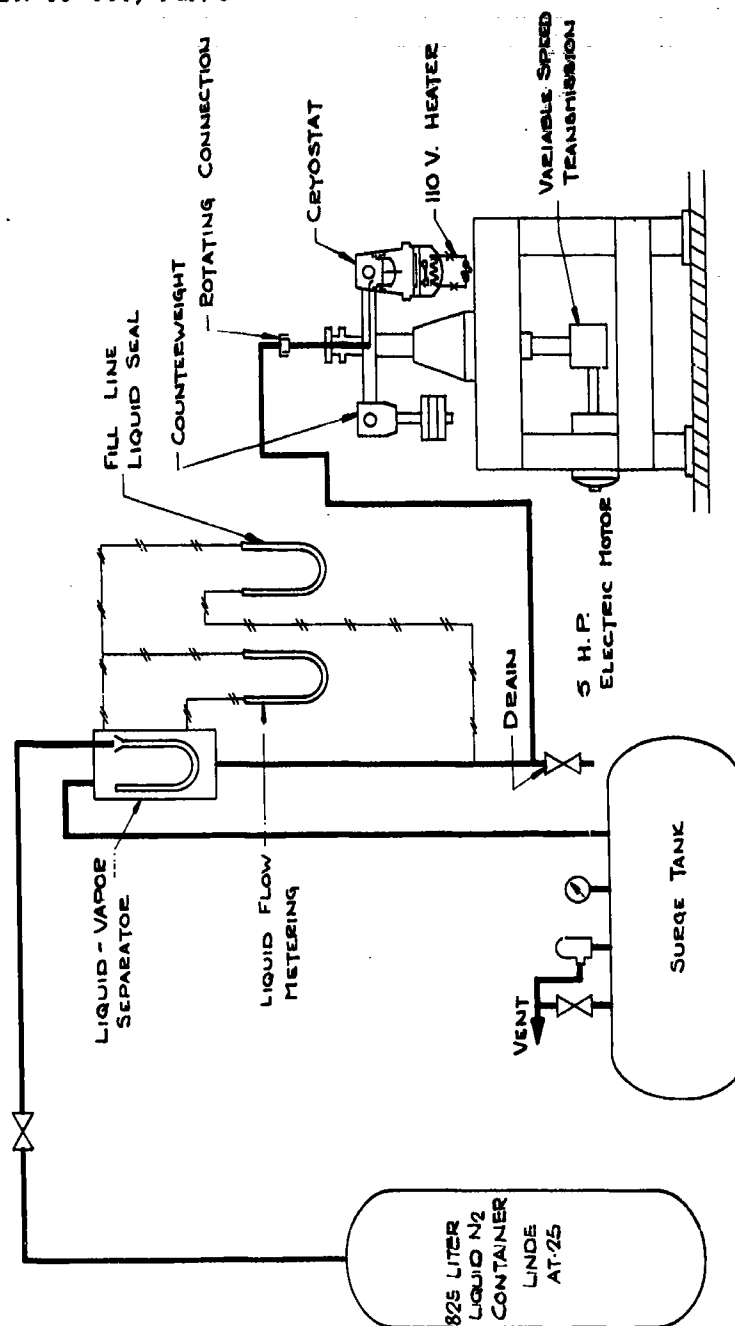
63 ASRP-2391



HIGH G CRYOSTAT

FIG. 49

63 ASRP-2391



EQUIPMENT ARRANGEMENT FOR HIGH G CRYOSTAT TRANSFER TESTS  
(BOILING AND CONDENSING)

FIG. 50

63 ASRP-2391

# CONFIDENTIAL

## ASD-TDR-63-665, Part I

The rotor was driven by an electric motor, coupled to a variable speed drive. Adjustment of the RPM at the instrument panel was made possible by an extension of the adjusting shaft on the variable speed drive. The adjustment mechanism was calibrated, using a strobotac, in terms of the gravitational field produced at the test piece radius, so that the desired value of the gravitational field could be set exactly for each run.

The liquid which was ultimately boiled was supplied to the cryostat from a stationary tank through vacuum insulated lines, and entered the cryostat through rotating seals. An air activated valve controlled from the instrument panel admitted the liquid from the tank to a separator. Vapor flashoff due to throttling and vapor generated by heat leak were vented from the separator via the surge tank and a second valve, located on the surge tank. This valve was also controlled from the panel, and was used to adjust the system pressure at this point. The liquid flowed from the separator into a flow cup which was a multiple orifice type meter for measuring liquid flow. No flashoff occurred in the orifices since the liquid entering was slightly subcooled and the pressure drop was very small. (Generally, it was less than 4 psi.)

The amount of liquid entering the cryostat was adjusted in response to the anticipated need through the combined operation of the two valves. Waste due to overflow was thereby minimized. Vapor was prevented from entering the apparatus by having a six-foot U-shaped liquid trap in the supply line. The presence of a liquid seal, as indicated by a manometer, showed that no vapor was being passed.

Separate systems were used to convey the transducer and thermocouple emf's from the rotor to the stationary frame. Copper slip rings were used for the transducer inputs and outputs. In these instances, the emf's in question were much larger than the electrical background noise associated with slip rings, or any thermal emf's which might have arisen at the contacts or junction blocks. Transducer excitation was about 5 volts, and typical signals were greater than 1 millivolts. Unwanted emf's were probably less than 50 microvolts. Hence, there was no significant loss of accuracy when slip rings were used in these circuits. Conversely, the emf of the differential thermocouples was in the microvolt range. Evidently, a high precision device was needed here. This condition was satisfied by a pair of mercury-kerosene baths, a sketch of which is shown in Figure 51. In these baths, platinum knife edges rotated in separate mercury channels and constituted the method whereby the transition was made from a rotating to a stationary frame of reference.

63 ASRP-2391

# CONFIDENTIAL

THERMOCOUPLE WIRING  
FOR MERCURY SLIP-RING

EMF

CU

CU

PT

PT

SHAFT ROTATION

NEUTRALIZATION BATH (KERO.)

ROTATING

STATIONARY

MERCURY SLIP-RING

Hg

HOT JUNCTION

COLD JUNCTION

CONSTANTAN

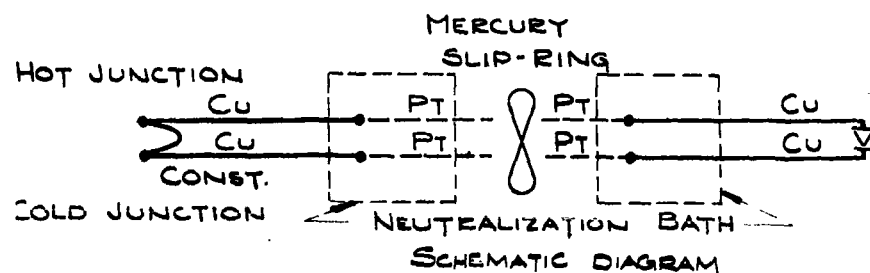


FIG. 51

115

# CONFIDENTIAL

## ASD-TDR-63-665, Part I

Both the knife edges and their corresponding pickups in the bottom of the channels were platinum since other materials were adversely affected by mercury. The purpose of the kerosene baths was to neutralize the effect of the intermediate metal (platinum) in the copper circuit. In a given thermocouple circuit, where there are two wires, four copper to platinum junctions exist. By locating each of these junctions in the kerosene bath, isothermal conditions were insured between junctions and net stray emf's (generated by each junction acting as a thermocouple) were prevented. A Leeds Northrup K-3 potentiometer and an electronic galvanometer were used to take all pressure transducer and thermocouple data. This system is accurate to  $\pm 0.5$  microvolts. Electronic recorders were used to follow the transducer outputs when the system was operating but data was not being taken. These were less sensitive but more suitable for this purpose.

The cryostat itself consisted of two sections which bolted together and formed two isolated chambers separated by the micarta flange. The lower or radially outward chamber was double walled and vacuum insulated. It enclosed the condensing side of the test heat exchanger and was charged with liquid nitrogen which could be continuously boiled up by an electrical heater. The vapor condensed on the condensing surface of the heat exchanger. This chamber was protected by a safety valve set at 100 psi, although the chamber could stand 400 psi if desired. Several 1/8 inch lines of stainless steel tubing led into the chamber. They served as pressure transducer taps, connections for liquid charging, and vapor vent-off lines during charging or at the completion of a run.

The upper, or radially inward, portion of the cryostat which always remained connected to the rotating arm was not insulated and was open to the atmosphere. During operation it was constantly supplied with liquid from the liquid storage tank to make up for the boiloff and overflow.

Micarta had several desirable characteristics which warranted its choice as the material for the flange which separated the two chambers and which also served as the base for holding the test specimen. It had low thermal conductivity, thus preventing heat transfer between the two sections of the cryostat, and it had high strength (and no brittleness) over the entire temperature range. (Micarta is a laminate of glass cloth with an epoxy binder.) It was quite machineable although precautions had to be taken against the silicate dust and could be shaped into parts which mated well with other smooth surfaces to give leak tight seals. A different flange was used for each of the three basic test specimen designs, condensing inside tubes, condensing outside tubes, and boiling.

63 ASRP-2391

# CONFIDENTIAL

# CONFIDENTIAL

## ASD-TDR-63-665, Part I

### 4.4.3 High-G Cryostat Specimen

#### 4.4.3.1 Specimen Size

Seven individual test specimens were required to obtain the needed data. Their design evolved mainly from considerations of the characteristics and limitations of the cryostat. The cryostat itself did not permit the use of a very large specimen. However, in order to minimize errors, it was desirable to provide as much heat transfer area as possible, so that the electrical heat input could be much larger than the heat leak. This made it necessary to have at least 4 tubes, approximately 3 inches long, 0.375 inches O.D., and 0.250 inches I.D. Additional tubes would disproportionately increase the fabrication costs due to crowding of the tubes.

The inner diameter of the tubes (0.250 inches) was chosen as follows. Condensation theory predicts higher coefficients as the tube diameters decrease. The limit to which this could be carried was governed by the fact that the percent of the tube area made inoperative for heat transfer by accumulated condensate rose sharply as the diameter was decreased. A 0.250 inch diameter best satisfied these conflicting considerations.

#### 4.4.3.2 Specimen Orientation

Figure 43 shows that the inclination of the tubes for the condensing tests could not be very large. It was necessary to have some slope, however, so that the condensate would drain from the tubes, and not cover too much of the heat transfer area. It was found that a slope of  $5^\circ$  from the normal to the gravitational field would be satisfactory, using the Chezy formula for flow in partially filled channel (See Appendix VI). The process whereby heat transfer area was made inoperative by a layer of accumulated condensate may be referred to as blanketing. A plot of the average percent of the area blanketed as a function of the controlling parameter  $(Ng)/(Q/A_c)^2$  is shown in Figure 52. The worst condition was at high heat flux and low  $Ng$ , where 13.4% of the area was blanketed at a heat flux of  $36,000 \text{ Btu}/(\text{ft.})^2(\text{hr.})$  and an acceleration of  $80 Ng$ . It was arbitrarily decided to orient the test piece in the cryostat in such a direction that the earth's gravitational field aided in the drainage of the condensate. That is, the tubes were perpendicular rather than parallel to the plane of rotation of the rotor. The procedure for calculation of the average blanketing angle is presented in section 4.4.5.

63 ASRP-2391

AVERAGE PERCENT BLANKETING INSIDE .250" I.D. TUBE 3/4" LONG  
AND INCLINED 5° FROM NORMAL TO GRAVITATIONAL FIELD FOR N<sub>2</sub>  
AT 1 ATM.

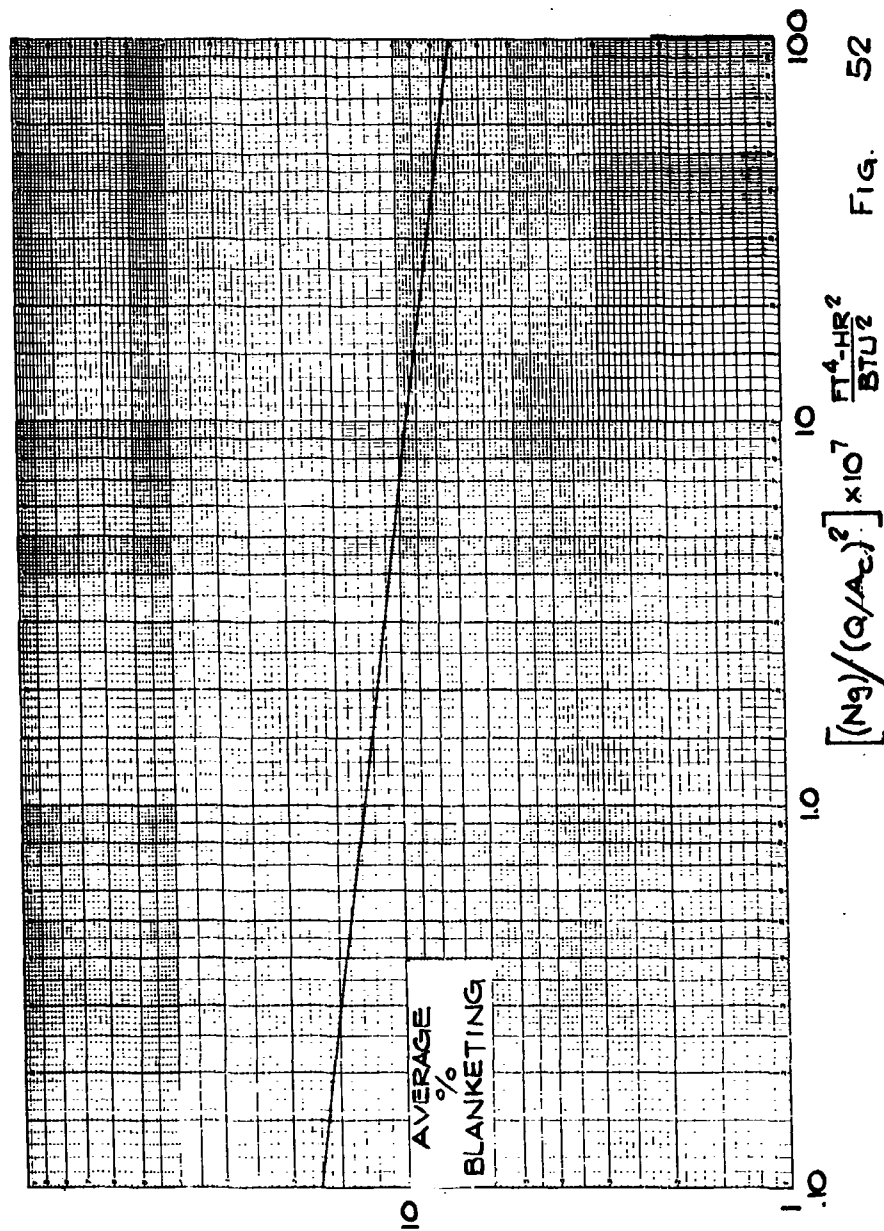


Fig. 52

63 ASRP-2391



**CONFIDENTIAL**

**ASD-TDR-63-665, Part I**

**4.4.3.3 Specimen Materials of Construction**

The heat transfer tubes in condensing tests 1, 2, 3, 4, and 6 were made of copper. The use of the special boiling surface reduced the  $\Delta T$  on the boiling side to less than 1/10 of the overall  $\Delta T$ . Utilization of copper for the tubes reduced the  $\Delta T$  through the wall to tolerable levels, because of its high thermal conductivity. This avoided the undesirable situation of subtracting large  $\Delta T$ 's to get a relatively small condensing side  $\Delta T$  during reduction of the data. The particular type of copper used for a specimen depended on availability and time. Whenever possible, OFHC copper was used because it is easily welded to stainless steel, the manifold material, and has a high thermal conductivity. It was sometimes necessary to use phosphorous deoxidized copper, however, which has a lower thermal conductivity, but is equally weldable.

The remainder of each test specimen was made of 304 stainless steel because of strength considerations. If copper had been used throughout, it would have had to be excessively thick to prevent deformation. No special difficulties were encountered in Heliarc welding copper to stainless steel. The welding was done in a dry box filled with  $N_2$  gas to prevent degradation of the copper tube surface by oxidation.

The fifth and seventh test specimens (condensing on a porous aluminum surface, and boiling on an untreated aluminum surface) were both made of 3003 aluminum. Special care was taken to preserve the boiling surface "mill finish" on the boiling specimen since the boiling curve is influenced by surface conditions (i.e., the lack or presence of pits, scratches, grooves, etc.). 3003 alloy was required for the fifth specimen, since the technique for applying a porous aluminum surface had not been successful on other alloys.

**4.4.3.4 Specimen Design Details**

All the condensation test specimens had a bellows between the two lines passing through the micarta flange. Its purpose was to allow for contraction of the test piece on cooling to cryogenic temperatures. The micarta contracted much less than either copper or aluminum, and severe stresses would have resulted if no bellows were used. These stresses could potentially be sufficient to break the welds at the tube to manifold connections.

63 ASRP-2391

**CONFIDENTIAL**

# CONFIDENTIAL

## ASD-TDR-63-665, Part I

Pressure drop calculations showed that there was negligible pressure drop through the tubes in specimens 1 through 5. Also, the vapor velocity was so low that it could not influence the drainage of condensate or the condensate film.

All the outside area of the heat exchangers except the tube area was insulated with a 1/4 inch thick layer of foamed-in-place polyurethane foam. This prevented heat transfer in unwanted areas by introducing a large heat transfer resistance.

### 4.4.4 High G Cryostat Test Fluid

Liquid nitrogen was used on both the boiling and condensing sides of the test heat exchangers. Nitrogen was chosen for the condensing fluid because it will be the fluid condensed in the cryogenic boilerplate unit. The use of liquid nitrogen instead of liquid oxygen on the boiling side eliminated the safety hazard due to fire or explosion. The pressure on the condensing side required to give a certain  $\Delta T$  was also much lower when nitrogen was used on the boiling side. Nitrogen has to be brought to a pressure of 38 psig just to reach the normal boiling point of liquid oxygen. This pressure would reach 100 psig when heat was being transferred. With nitrogen to nitrogen heat exchange, condensing pressures rarely exceeded 50 psig.

The boiling coefficients for liquid nitrogen and liquid oxygen on the special boiling surface were similar, so that in no sense could the substitution of nitrogen for oxygen have influenced the test results, particularly since the appropriate boiling side  $\Delta T$  was always subtracted from the overall  $\Delta T$  in determining the condensing side  $\Delta T$ . The use of liquid nitrogen boiling data was therefore deemed acceptable.

### 4.4.5 High G Cryostat Data Reduction

#### 4.4.5.1 Condensation Data Reduction

##### 4.4.5.1.1 Calculation of Theoretical Condensing Coefficient

The first task is calculation of per cent blanketing of tube area

63 ASRP-2391

CONFIDENTIAL

# CONFIDENTIAL

## ASD-TDR-63-665, Part I

where blanketing refers to the relatively thick sector of condensate at the bottom of the tube. This condensate continually runs off in a direction parallel to the tube axis, but effectively insulates the area it covers. (See Figure 53). The Chezy formula (Ref. 23, p. 377-384) for flow in an open channel was used to calculate the size of this sector of condensate expressed in terms of  $\phi$ , the angle subtended by the condensate.

$$f(\phi) = \frac{\phi^{4/3}}{[\frac{\phi}{2} - \cos \frac{\phi}{2} \sin \frac{\phi}{2}]^{10/3}} = \left(\frac{1.486}{.011}\right)^2 \frac{g}{g_c}$$

$$Ng \cos \psi \frac{\rho L^2 r_t^{16/3}}{W^2}$$

The derivation of this formula is given in Appendix VI.

The flow rate of condensate can be related to the heat flux by the following relationships for steady state:

$$W \lambda = \left(\frac{Q}{A_c}\right)^1 A_c$$

$$W \lambda = \left(\frac{Q}{A_c}\right)^1 (2 \pi r_t x)$$

$$\therefore W = \left(\frac{Q}{A_c}\right)^1 \left(\frac{2 \pi r_t x}{\lambda}\right)$$

substituting in the  $f(\phi)$  equation =

$$f(\phi) = \frac{\phi^{4/3}}{[\frac{\phi}{2} - \cos \frac{\phi}{2} \sin \frac{\phi}{2}]^{10/3}} = \left(\frac{1.486}{.011}\right)^2 \left(\frac{g}{g_c} Ng \cos \psi\right)$$

$$\frac{\rho L^2 r_t^{16/3}}{[ \left(\frac{Q}{A_c}\right)^1 ]^2 \left(\frac{2 \pi r_t x}{\lambda}\right)^2}$$

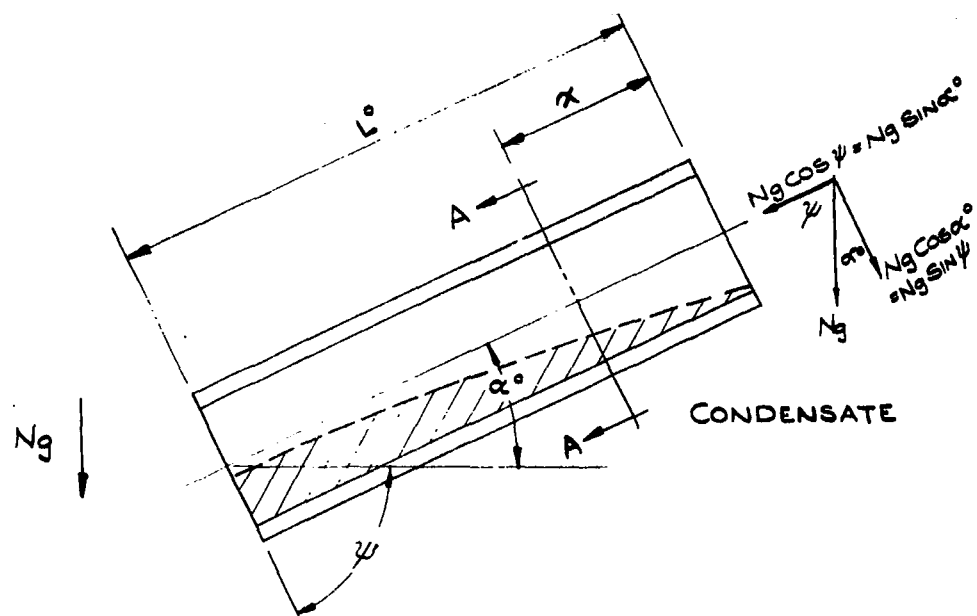
combining terms:

$$f(\phi) = \frac{\phi^{4/3}}{[\frac{\phi}{2} - \cos \frac{\phi}{2} \sin \frac{\phi}{2}]^{10/3}} = \left(\frac{1.486}{.011}\right)^2 \frac{1}{4 \pi^2} \left(\frac{g}{g_c} Ng \cos \psi\right)$$

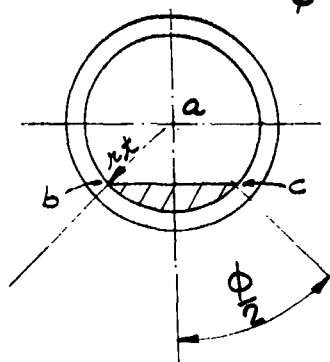
$$\frac{\rho L^2 r_t^{10/3} (\lambda)^2}{[ \left(\frac{Q}{A_c}\right)^1 ]^2 x^2}$$

$$[ \left(\frac{Q}{A_c}\right)^1 ]^2 x^2$$

63 ASRP-2391



$\phi$  = BLANKETING ANGLE



SECTION A-A

CONDENSATE BLANKETING IN TUBES

FIG. 53

63 ASRP-2391

# CONFIDENTIAL

ASD-TDR-63-665, Part I

Let

$$K_o = \left( \frac{1.486}{.011} \right)^2 \frac{1}{4\pi^2} \left( \frac{g}{g_c} \cos \psi \right) \rho_L^2 r_t^{10/3} (\lambda)^2$$

$$\therefore f(\phi) = \frac{\phi^{4/3}}{\left[ \frac{\phi}{2} - \cos \frac{\phi}{2} \sin \frac{\phi}{2} \right]^{10/3}} = K_o \left[ \frac{Ng}{\left( \frac{Q}{Ac} \right)^2} \right] x^2 \quad (39)$$

Thus,  $Ng/[(Q/Ac)^2]$  is a parameter controlling  $\phi$  for a given value of  $x$ .

The average value of  $\phi$  as a function of  $x$  is given by the following:

$$\bar{\phi} = \frac{1}{L} \int_0^L (\phi) dx$$

$\bar{\phi}$  was evaluated and tabulated for a series of values of the parameter,  $Ng/[(Q/Ac)^2]$ . Graphical integration was used (Ref. 23) since  $f(\phi)$  cannot be solved analytically for  $\phi$ . The calculated values are given below, with  $\phi$  converted to per cent of area blanketed.

$Ng/(Q/Ac)^2$ $(Ft.)^4 (Hr)^2 / Btu^2$	$\left( \frac{\bar{\phi}}{360} \right) (100)$ % Blanketed Area
$77.2 \times 10^{-7}$	7.4%
$7.72 \times 10^{-7}$	9.7%
$0.772 \times 10^{-7}$	13.1%

Figure 52 is a plot of this relationship.

Strictly, this plot pertains only to those specimens whose tubes have an 0.250 inch inside diameter. However, little error will be incurred if these values are used for the fifth test specimen (condensation on a porous aluminum surface) which had an inside diameter of 0.305 inches.

63 ASRP-2391

# CONFIDENTIAL

## ASD-TDR-63-665, Part I

Hassan and Jacob (Ref. 19) showed that the average condensing film coefficient at any location along a round, smooth-wall tube, except in a very short entrance region, is:

$$(h_c)_{\text{THEO}} = C_o \left[ \left( \frac{k_L^3 \rho_L^2 \lambda}{3 \mu_L r_t} \right) (g) (\cos \alpha) \right]^{1/4} [\Delta T_c]^{-1/4}$$

Since this is modified by the artificial gravitational field, multiply it by  $(Ng)^{1/4}$ . Thus, since  $Q/Ac = (h_c)_{\text{THEO}} \Delta T_c$ :

$$(h_c)_{\text{THEO}} = C_o^{4/3} \left[ \left( \frac{k_L^3 \rho_L^2 \lambda}{3 \mu_L r_t} \right) (Ng) (g) (\cos \alpha) \right]^{1/3} [Q/Ac]^{-1/3}$$

$C_o$  is a function of the portion of the circumference of the tube on which condensation is occurring. For the entire circumference,  $C_o = 0.8047$ .  $C_o$  arises from an integration of the film thickness around the active (or unblanketed) circumference of the tube to get the average film thickness (and hence, condensing coefficient). Thus, the general equation for the average condensing coefficient inside a tube with an average blanketing angle  $\Phi$  which has been

previously defined is shown on the following page.

63 ASRP-2391

**CONFIDENTIAL**

ASD-TDR-63-665, Part I

$$(h_c)_{\text{THEO}} = C_o^{4/3} \left[ \left( \frac{k_L^3 \rho_L^2 \lambda}{3 \mu_L r_t} \right) (Ng)(g) (\cos \alpha) \right]^{1/3} \left[ Q/A_c \right]^{-1/3} \left[ 1 - \frac{\bar{\Phi}}{360} \right] \quad (40)$$

where  $C_o$  is consistent with  $\bar{\Phi}$ . The resulting equation, for  $N_2$  at 1 atmosphere, corresponding to test specimens 1, 3, 4, and 6, is plotted on Figure 54. Figure 55 is for specimen 5, which has an I.D. of 0.305 inches instead of 0.250 inches.

A similar set of curves was calculated for specimen 2, where condensation occurs outside the tubes. In this case, however, there was no blanketing, and the constant  $C_o$  was determined for the entire circumference. These curves are shown in Figure 56. The condensing coefficients on Figure 54, 55, and 56 can be converted to pressures other than atmospheric by multiplying by the factors on Figure 57, which are defined as:

$$R^o = \frac{\left[ \frac{k_L^3 \rho_L^2 \lambda}{\mu_L} \right]^{1/3} P}{\left[ \frac{k_L^3 \rho_L^2 \lambda}{\mu_L} \right]^{1/3} P=1 \text{ atm.}} \quad (41)$$

This enables the theoretical coefficient and experimental coefficient to be compared at the same pressure,  $P$ . In most cases, the experimental condensing coefficients were corrected to the values they would have at 1 atmosphere by the above process.

#### 4.4.5.1.2 Calculation of Experimental Condensing Coefficients

The equation for the experimental average condensing coefficient at pressure  $P$  is:

$$(h_c)_{\text{EXP}} = \frac{(Q_{\text{ELECTRICAL}} + Q_{\text{HEAT LEAK}}) (3.41)}{(A_c) (\Delta T_c)} = \frac{(3.41) (\Sigma Q)}{(A_c) (\Delta T_c)} \text{ Btu/(ft.)}^2 \text{ (hr.) (}^\circ\text{R)}$$

63 ASRP-2391

**CONFIDENTIAL**

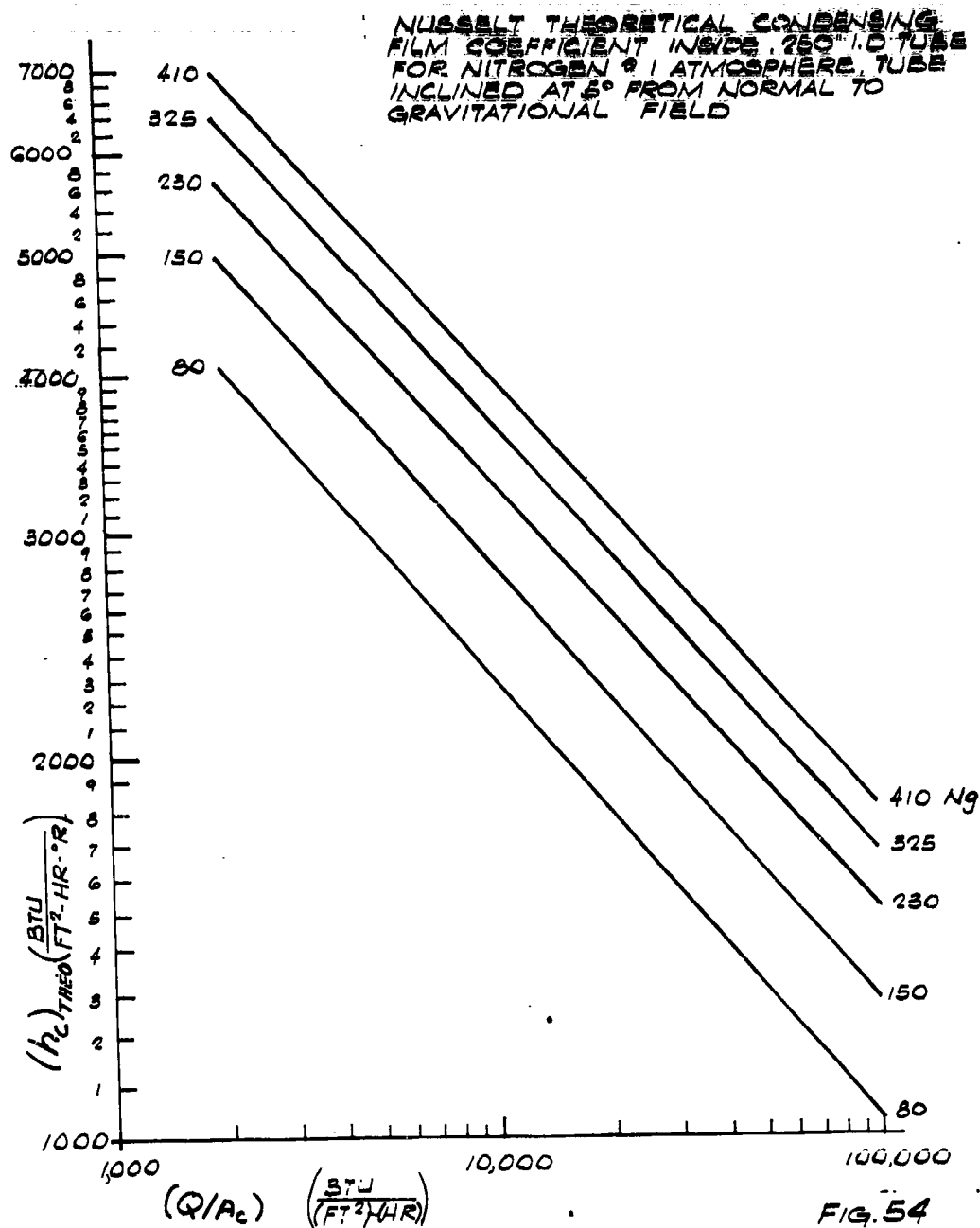


FIG. 54

63 ASRP-2391



ASD-TDR-63-665, Part I

NUSSELT THEORETICAL CONDENSING FILM COEFFICIENT INSIDE  
 .305" I.D. TUBE  
 (FOR NITROGEN @ 1 ATMOSPHERE, TUBE INCLINED AT 5° FROM  
 NORMAL TO GRAVITATIONAL FIELD)

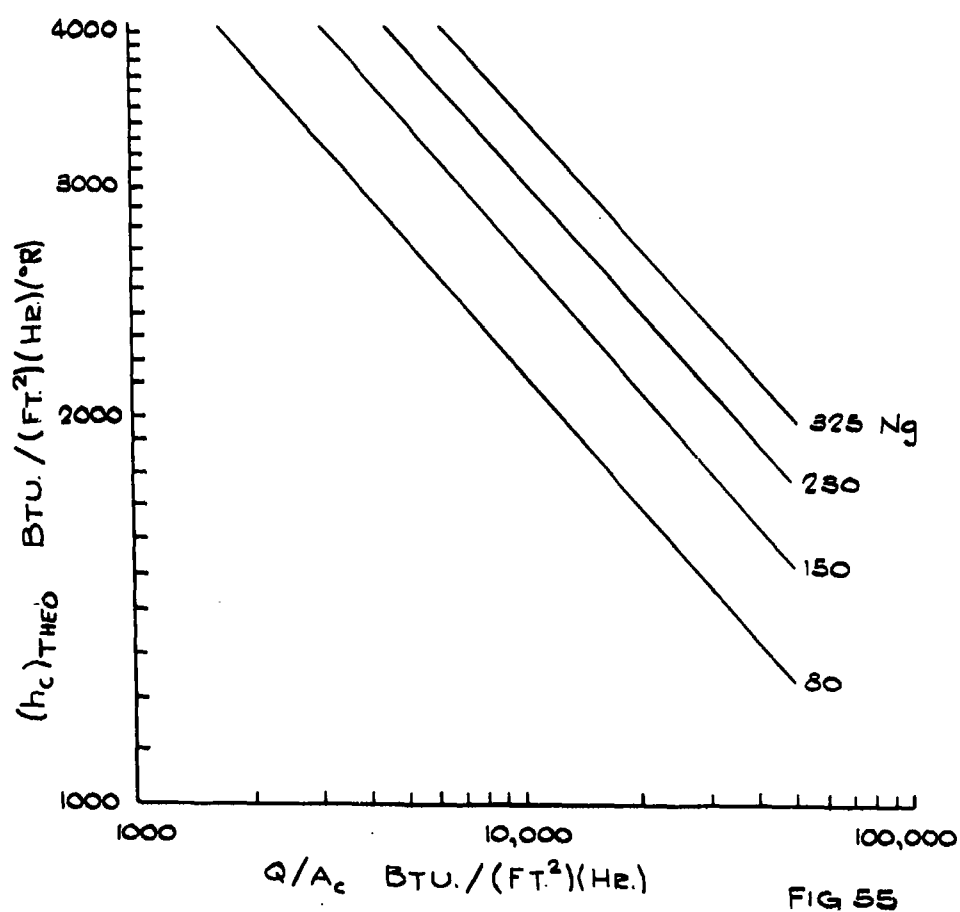


FIG 55

63 ASRP-2391

NUSSELT THEORETICAL CONDENSING FILM COEFFICIENT  
OUTSIDE .875" O.D TUBE (FOR NITROGEN AT ONE  
ATMOSPHERE, TUBE INCLINED 5° FROM NORMAL  
TO GRAVITATIONAL FIELD)

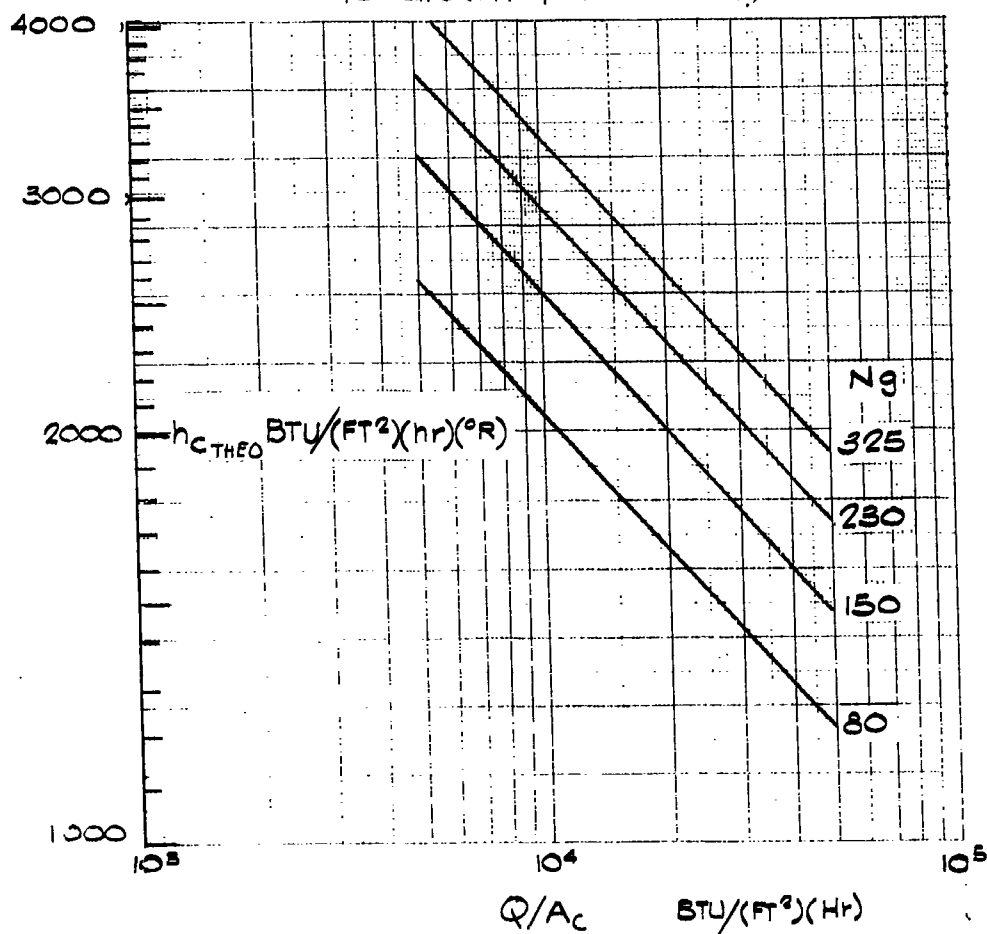


FIG.56

ASD-TDR-63-665, Part I

CONDENSING PARAMETER  
RATIO FOR NITROGEN

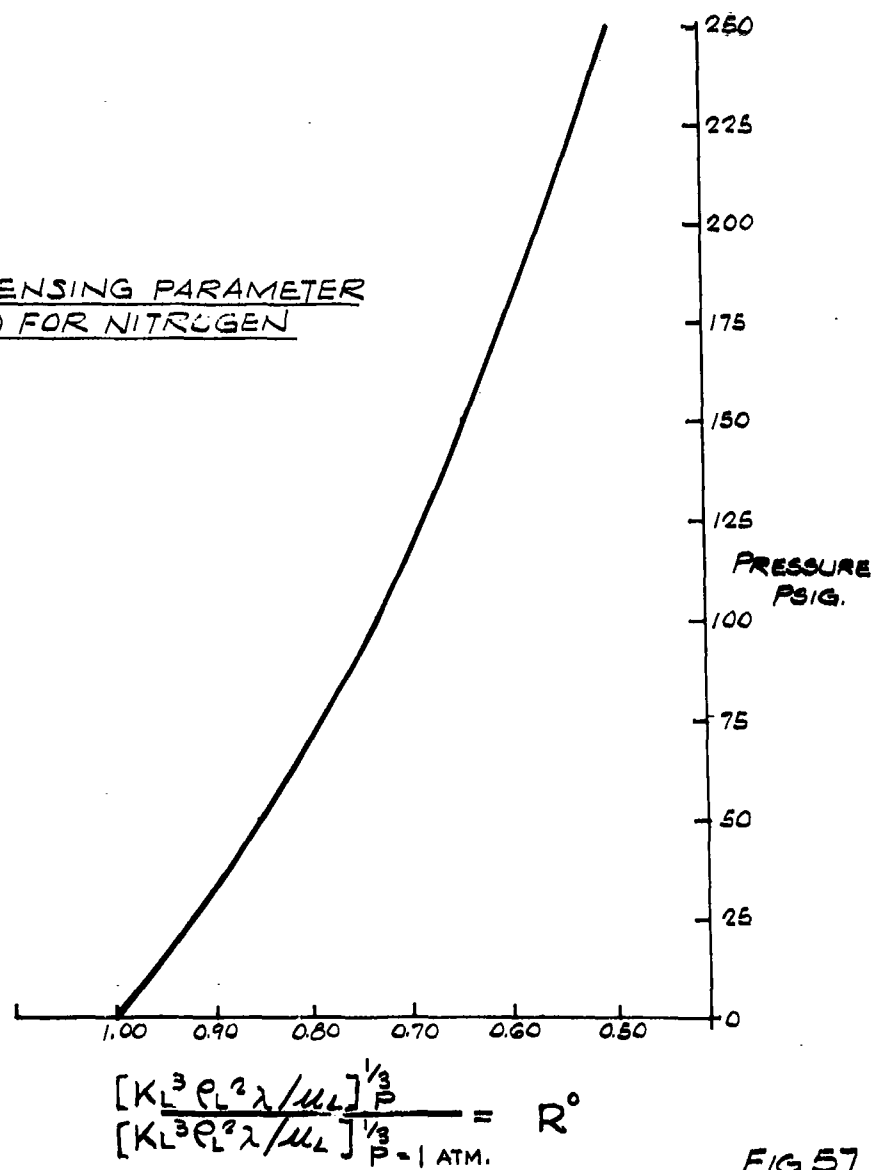


FIG. 57

63 ASRP-2391

# CONFIDENTIAL

## ASD-TDR-63-665, Part I

with  $Q$  in watts. For those tests (1, 3, 4, 5, and 6) where the overall  $\Delta T$  ( $\Delta T_o$ ) was determined by pressure transducer measurements of the boiling and condensing pressures, with appropriate corrections for barometric pressure, hydrostatic head of vapor in transducer lines, and hydrostatic head of boiling liquid between the pressure tap location, and the average height of the tubes.

$$(\Delta T_c) = \Delta T_o - \Delta T_{wall} - \Delta T_b$$

$\Delta T_b$  was taken from a plot of experimentally determined  $Q/A_b$  versus  $\Delta T_b$  curve for the special boiling surface at the  $Q/A_b$  corresponding to  $(\Sigma Q) (3.41) A_b$ . This plot was obtained from work under Contract No. AF 33(616)-7646 previously discussed in Section 4.4.1.  $\Delta T_{wall}$  was calculated from the equation for conductive heat transfer.

In test 2, a thermocouple measured  $\Delta T_c$  directly. Thus,  $(h_c)_{EXP}$  can be directly computed if  $Q_{HEAT LEAK}$  is known. Since accurate values of  $Q_{HEAT LEAK}$  were unavailable, it was necessary to assume a heat leak. The test of a proper assumption was that the values of

$$(h_c)_{EXP} / (h_c)_{THEO} \text{ @ 1 atm}$$

calculated for the points with electrical heat input and without electrical heat input would follow a consistent pattern, when plotted as a function of  $(Q/A_c)$ .

Data with zero electrical heat input was available from tests 1, 2, 3, and 6 for condensation on tubes with a non-porous condensing surface. In the runs with electrical heat input the function

$$\frac{(h_c)_{EXP}}{(h_c)_{THEO}} \text{ @ 1 atm vs. } \frac{Q_{ELECTRICAL} + Q_{HEAT LEAK}}{(A_c)}$$

was considered where  $Q_{HEAT LEAK}$  and the ratio  $(h_c)_{EXP} / (h_c)_{THEO}$  were unknown. A heat leak value was assumed and  $(h_c)_{EXP} / (h_c)_{THEO}$  was calculated for data in tests 1, 2, 3 and 6, as a function of  $(Q/A_c)$ .  $(h_c)_{EXP} / (h_c)_{THEO}$  @ 1 atm. vs.  $Q_{HEAT LEAK} / A_c$  was then plotted.

Closeness of fit of the zero electrical input film coefficient ratio with the coefficient ratio for points with electrical heat input was the criteria of acceptance of the heat leak value assumed for each test series. If excessive deviations existed for most of the points, a new heat leak value was assumed and the procedure repeated.

63 ASRP-2391

# CONFIDENTIAL

## ASD-TDR-63-665, Part I

Thus, the correct smooth, continuous correlation curve evolved, as typified by Figure 58 (Test 1). The heat leaks determined by this method were always within the range which would be expected by calculating the conductive and convective heat transfer into the cryostat by conventional means and are only significant in regions of low heat flux. They varied because they were functions of two uncontrolled parameters - the liquid level in the condensing chamber and the amount of frost on the outside of the cryostat.

### 4.4.5.2 Boiling Data Reduction

The reduction of the boiling side data for Test 7 was straightforward. The electrical heat input was converted to heat flux. No heat leak was assumed because heat transfer through the micarta flange is negligible. The boiling side  $\Delta T$  was found by subtracting the wall  $\Delta T$  from the overall  $\Delta T$  as measured by the thermocouples. No analytical equation for predicting boiling performance has yet been advanced that is adequate for comparison purposes. The effect of surface conditions, which can drastically alter the heat flux versus  $\Delta T$  curve, seems to be the most difficult aspect to resolve. For this reason, the experimental data was compared only with other experimental results.

### 4.4.6 High G Cryostat Results and Conclusions

#### 4.4.6.1 Condensation Inside of Smooth Tubes - Test 1

The experimental heat transfer coefficients were identical with the theoretical coefficients at low heat fluxes (5,000 - 10,000 Btu/(ft.)<sup>2</sup>(hr.)) at all gravitational levels. The experimental coefficients were better than the predicted coefficients at heat fluxes above 10,000 Btu/(ft.)<sup>2</sup>(hr.).  $[(h_c)_{EXP}/(h_c)_{THEO}]$  @ 1 atm. reached a value of 1.26 at a heat flux of 50,000 Btu/(ft.)<sup>2</sup>(hr.). This was attributed to rippling of the condensate film, which resulted in a lower average film thickness for a given condensate flow rate than laminar film flow theory would predict. This caused the condensing coefficient to increase above the predicted value. These results are shown in Figure 58 and Table 6.

#### 4.4.6.2 Condensation Outside of Smooth Tubes - Test 2

The results for this test specimen are presented in Figure 59 and Table 7.  $[(h_c)_{EXP}/(h_c)_{THEO}]$  @ 1 atm. approached 1.0 (within the

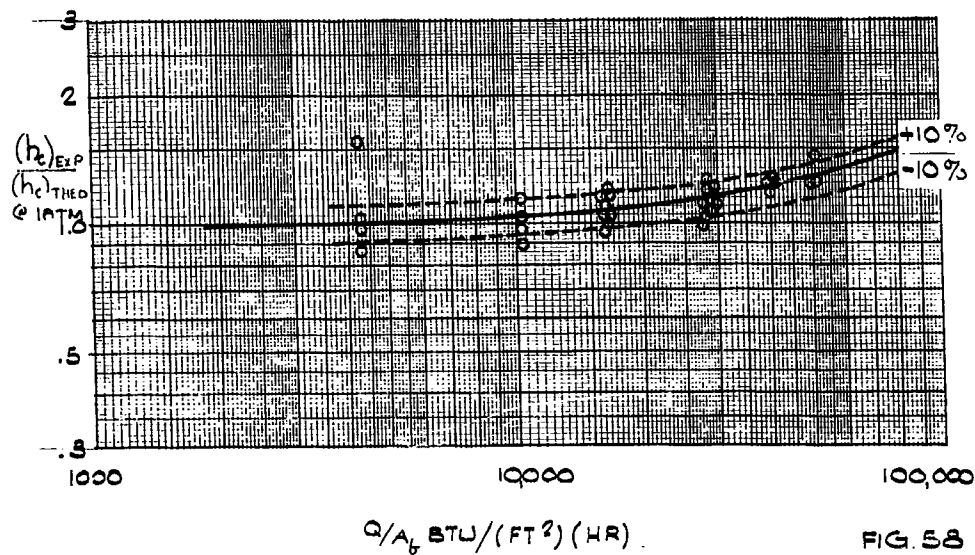
63 ASRP-2391

# CONFIDENTIAL

CONFIDENTIAL

ASD-TDR-63-665, Part I

CONDENSATION INSIDE .250" I.D. SMOOTH TUBES INCLINED  
5° FROM NORMAL TO GRAVITATIONAL FIELD  
PRESSURE = 1 ATMOSPHERE



CONFIDENTIAL

**CONFIDENTIAL**

ASD-TDR-63-665, Part I

TABLE 6

CONDENSATION INSIDE SMOOTH TUBES - TEST 1

(Basis: Inside Area)

Pressure = 1 Atmosphere

Run	N <sub>g</sub>	(Q/A <sub>c</sub> ) Btu/(ft) <sup>2</sup> (hr)	(h <sub>c</sub> ) EXP @139.3°R Btu/(ft) <sup>2</sup> (hr)°R	(h <sub>c</sub> ) THEO@139.3°R Btu/(ft) <sup>2</sup> (hr)°R	(h <sub>c</sub> ) EXP (h <sub>c</sub> ) THEO Dimensionless
1	230	16,050	2999	2820	1.06
2	230	27,800	2388	2330	1.025
3	80	10,150	2033	2300	.882
4	80	16,050	1970	1950	1.01
5	80	27,800	1828	1620	1.13
6	80	39,600	1783	1410	1.26
7	80	51,500	1581	1290	1.22
8	150	10,150	2716	2850	.952
9	150	16,050	2289	2400	.954
10	150	27,800	2052	1990	1.03
11	150	39,600	2082	1780	1.17
12	150	51,500	1946	1610	1.21
13	230	10,150	3337	3310	1.01
14	230	16,050	3165	2820	1.12
15	230	27,800	2468	2330	1.06
16	230	39,600	2666	2080	1.28
17	230	51,500	2591	1810	1.43
18	325	10,150	4230	3701	1.14
19	325	16,050	3733	3150	1.18
20	325	27,800	3197	2600	1.23
21	325	32,600	3120	2460	1.27
22	80	16,050	2028	1950	1.04
23	80	27,800	2017	1620	1.24
24	80	16,050	2093	1950	1.06
25	80	16,050	2294	1950	1.17
26	150	27,800	2236	1990	1.12
<u>AVERAGE VALUE OF RUNS WITH NO ELECTRICAL HEAT INPUT</u>					
	80	4,250	3040	3100	.98
	150	4,250	3350	3850	.87
	230	4,250	7090	4420	1.60
	325	4,250	5230	5000	1.045

63 ASRP-2391

**CONFIDENTIAL**

CONFIDENTIAL

ASD-TDR-63-665, Part I

CONDENSATION  
OUTSIDE OF .375" OD. SMOOTH TUBES INCLINED 5°  
FROM NORMAL TO GRAVITATIONAL FIELD  
(PRESSURE = 1 ATMOSPHERE)

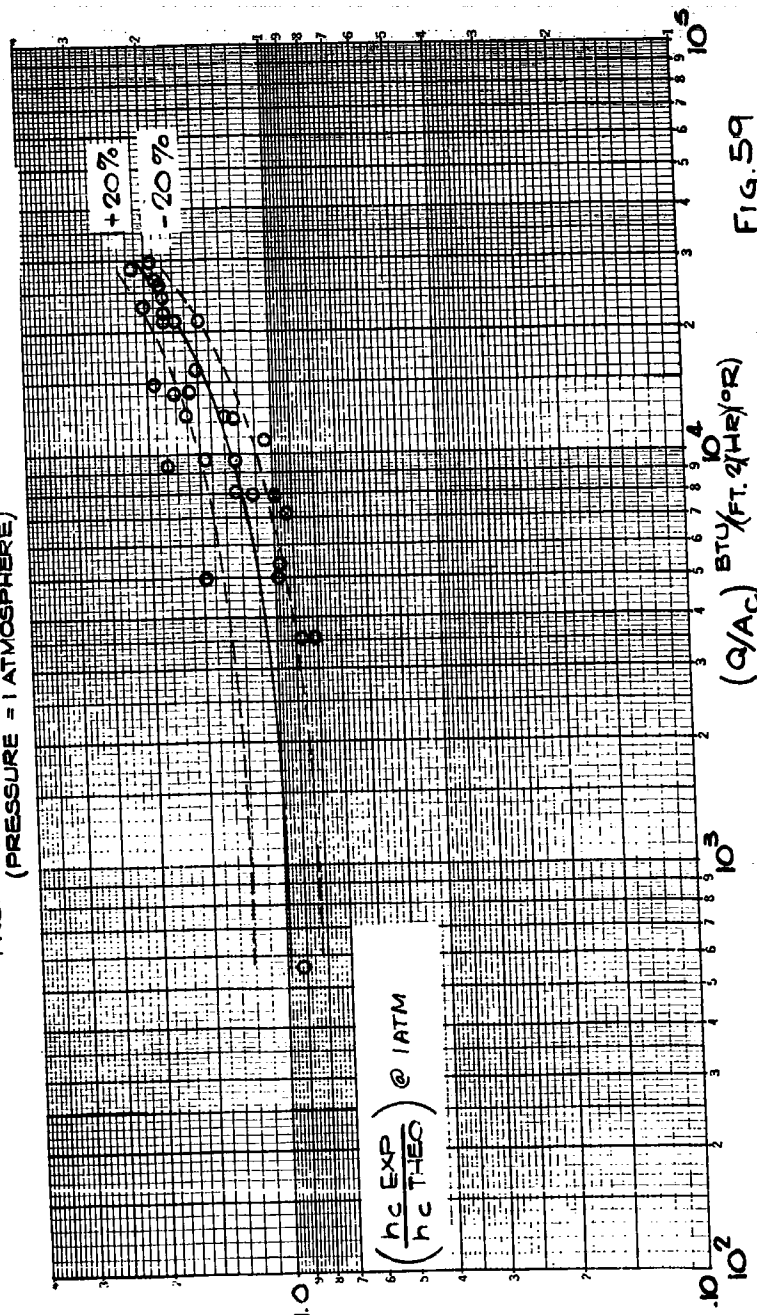


FIG. 59

63 ASRP-2391

CONFIDENTIAL



**CONFIDENTIAL**

ASD-TDR-63-665, Part I

TABLE 7  
CONDENSATION OUTSIDE SMOOTH TUBES - TEST 2

(Basis: Outside Area)

Pressure = 1 Atmosphere

Run	No	$(Q/A_s)$ Btu/(ft) <sup>2</sup> (hr)	$(h_c)_{EXP}$ @139.3°R Btu/(ft) <sup>2</sup> (hr)°R	$(h_c)_{THEO}$ @139.3°R Btu/(ft) <sup>2</sup> (hr)°R	$\frac{(h_c)_{EXP}}{(h_c)_{THEO}}$ @139.3°R Dimensionless
1	1	5,001	903	605	1.493
2	1	9,435	894	488	1.832
3	1	14,756	833	435	1.915
4	80	8,087	2527	2225	1.136
5	80	12,521	2504	1938	1.292
6	80	21,388	2718	1620	1.678
7	80	8,087	2216	2225	.996
8	80	12,521	2417	1938	1.247
9	80	21,388	2425	1620	1.497
10	80	24,935	2216	1525	1.453
11	80	8,087	2808	2225	1.262
12	80	12,521	3115	1938	1.607
13	80	21,388	2966	1620	1.831
14	80	26,709	2820	1490	1.893
15	150	9,896	3152	2558	1.232
16	150	14,330	3574	2255	1.585
17	150	23,197	3467	1915	1.810
18	150	9,896	3693	2558	1.444
19	150	14,330	3926	1915	1.741
20	150	23,197	3899	1200	2.036
21	150	28,518	3849	1780	2.162
22	230	11,776	2872	2790	1.029
23	230	16,210	3832	2505	1.530
24	230	25,077	3918	2140	1.831
25	230	30,398	3969	2030	1.955
<u>AVERAGE VALUES OF RUNS AT ZERO ELECTRICAL HEAT INPUT</u>					
	1	566	1155	1260	.918
	80	3,653	2255	2810	.802
	150	5,462	3034	3060	.992
	230	7,342	2891	3192	.906
	325	5,179	3923	3996	.982

63 ASRP-2391

**CONFIDENTIAL**

**CONFIDENTIAL**

**ASD-TDR-63-665, Part I**

limits of experimental error) at low heat fluxes, and reached a value of 2.0 at a heat flux of 30,000 Btu/(ft)<sup>2</sup>(hr). The reason for this more radical departure from theoretical performance is not known although it may be attributed to the increased tendency for condensate rippling when the condensate is not confined, as in a tube. This was the only condensing specimen whose performance was measured directly with a thermocouple. (The hot junction was soldered to the bottom of the tube midway along its length, and the cold junction was referenced to the condensing vapor.) Calculations indicated that this should be a reliable measuring method.

**4.4.6.3 Condensation Inside Helical Grooved Tubes - Test 3**

The condensing heat transfer coefficients on this surface parallel the behavior of the condensing coefficients on the smooth surface. They were better, however, by a factor of 1.75 times when  $[(h_c)_{EXP}/(h_c)_{THEO}]$  @ 1 atm. and  $(Q/A_c)$  were based on the projected area of the tubes. (See Figure 60 and Table 8). Most of this may be attributed to the fact that the true area was 1.48 times the projected area, hence the apparent increase when the projected area was used. The difference between 1.75 and 1.48 may be attributed to the beneficial film disrupting influence of the grooves themselves, as was previously theorized. The inherent weight penalty of such a surface (0.020 inches of extra wall thickness) does not make this scheme appear attractive, when it is remembered that the cryogenic reboiler-condenser will have tubes with less than 0.010 inch thick walls.

**4.4.6.4 Condensation Inside Tubes with Copper Porous Condensing Surface  
Test 4**

The porous condensing surface showed no advantage over a smooth surface at 80 Ng at any heat flux. However, at 150, 230, and 325 Ng, encouraging results were obtained.  $[(h_c)_{EXP}/(h_c)_{THEO}]$  had values of 1.31, 1.78 and 2.40 at 150, 230, and 325 Ng respectively, at a heat flux of 20,000 Btu as shown on Figure 61 and Table 9. The comparable value for a smooth surface was 1.09. As with the helically grooved specimen, any improvement attributed to the porous surface must be diminished by the extra weight it adds. A 10 mil coating with 50 per cent void space is equivalent to 5 mils of solid metal. If the reboiler-condenser has 0.010 inch thick tube walls,  $[(h_c)_{EXP}/(h_c)_{THEO}]$  must be at least 1.5 to break even. This would require an average

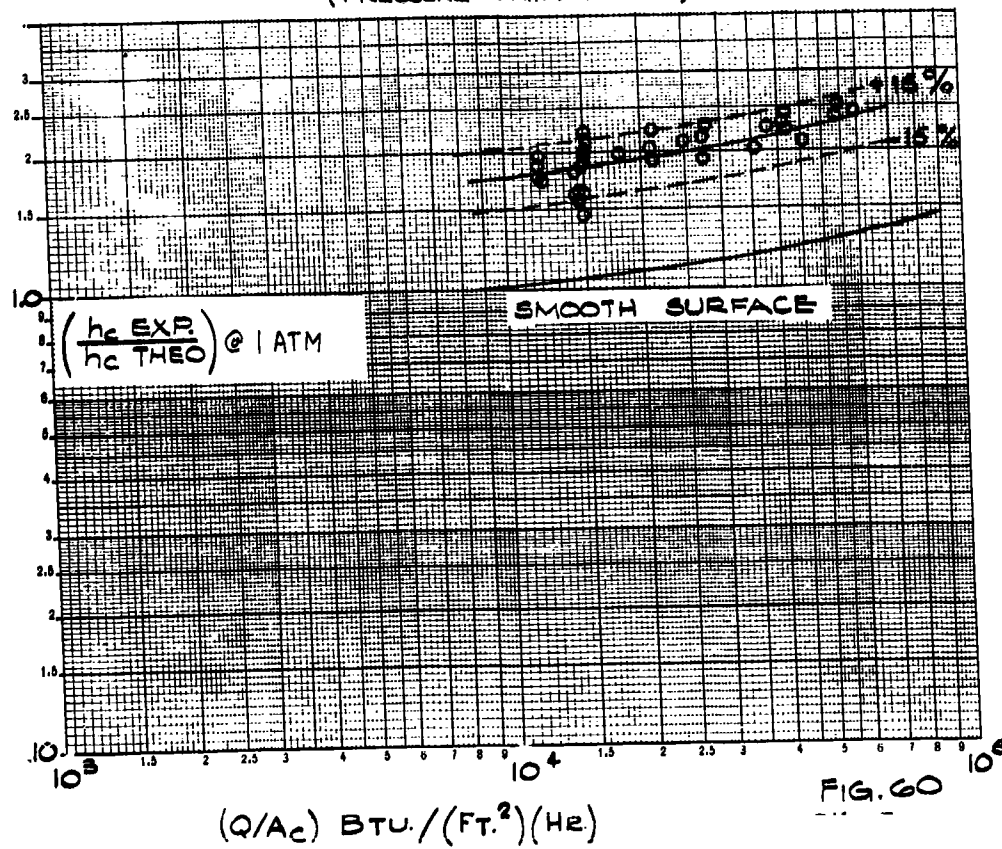
63 ASRP-2391

**CONFIDENTIAL**

**CONFIDENTIAL**

ASD-TDR-63-665, Part I

CONDENSATION INSIDE .250" I.D. HELICAL GROOVED TUBES  
INCLINED 5° FROM NORMAL TO GRAVITATIONAL FIELD  
(PRESSURE = 1 ATMOSPHERE)



63 ASRP-2391

**CONFIDENTIAL**

**CONFIDENTIAL**

**ASD-TDR-63-665, Part I**

**TABLE 2**  
**CONDENSATION INSIDE HELICAL GROOVED TUBES - TEST 1**

(Basis: Inside Area)

Pressure = 1 Atmosphere

Run	No.	$(Q/A_c)$ Btu/(ft) <sup>2</sup> (hr)	$(h_c)$ EXP @ 139.3°R		$(h_c)$ THEO @ 139.3°R Dimensionless
			$Btu/(ft)^2(hr)^\circ R$	$Btu/(ft)^2(hr)^\circ R$	
1*	80	11,879	4243	2165	1.96
2	80	18,391	3664	1845	1.99
3*	80	11,879	3869	2165	1.79
4	80	24,904	3543	1670	2.12
5*	80	11,879	3869	2165	1.79
6	80	37,929	3273	1435	2.28
7*	80	11,879	4034	2165	1.87
8	80	50,954	3173	1300	2.44
9*	150	14,953	5517	2470	2.23
10	150	21,465	4889	2175	2.25
11*	150	14,953	4984	2470	2.02
12	150	27,978	4579	1985	2.31
13*	150	14,953	4951	2470	2.00
14	150	41,003	4188	1735	2.41
15*	150	14,953	5052	2470	2.05
16	150	54,023	3938	1575	2.50
17*	230	14,484	5936	2910	2.04
18	230	20,996	5249	2565	2.05
19*	230	14,484	5267	2910	1.81
20	230	27,509	5038	2345	2.15
21*	230	14,484	4800	2910	1.65
22	230	40,534	4730	2055	2.30
23*	230	14,484	4613	2910	1.59
24	230	53,559	4467	1860	2.40
25*	325	14,692	6147	3240	1.90
26	325	21,205	5451	2845	1.92
27*	325	14,692	5285	3240	1.63
28	325	27,717	5021	2605	1.93
29*	325	14,692	4724	3240	1.46
30	325	35,532	4820	2390	2.02
31*	325	14,692	6122	3240	1.89
32	325	40,742	5217	2290	2.28
33*	325	14,692	5323	3240	1.64
34	325	45,952	4604	2185	2.11

\* Denotes runs with no electrical heat input

63 ASRP-2391

**CONFIDENTIAL**

CONFIDENTIAL

ASD-TDR-63-665, Part I

CONDENSATION INSIDE .250" ID TUBES COATED WITH A  
POROUS SURFACE AND INCLINED 5° FROM NORMAL TO  
GRAVITATIONAL FIELD

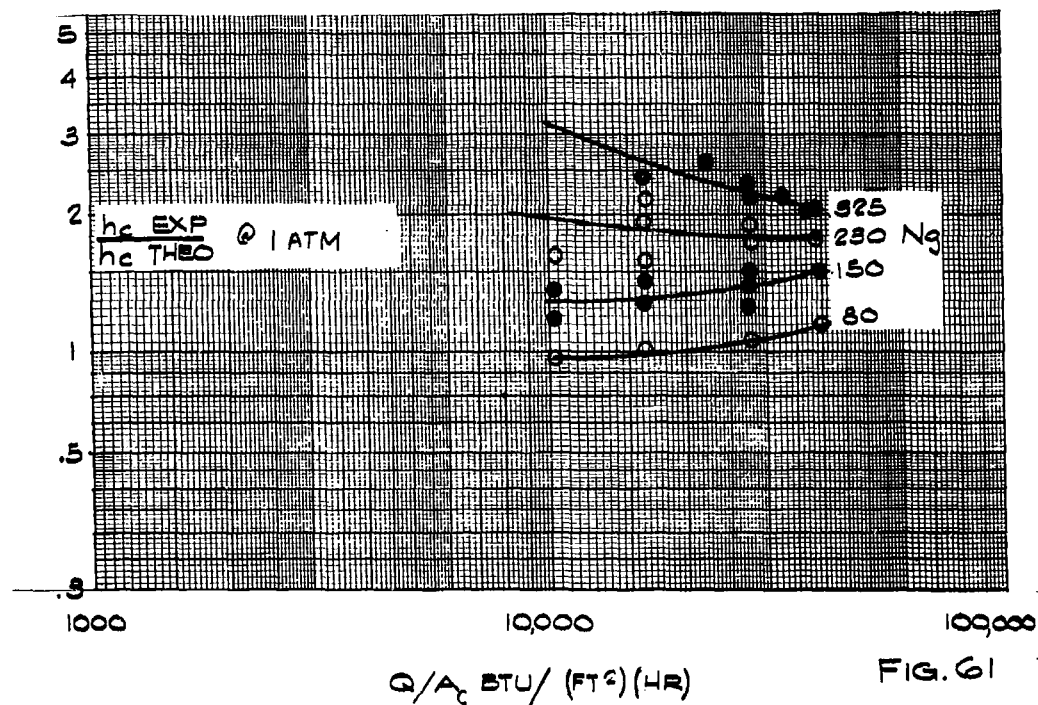


FIG. 61

CONFIDENTIAL

**CONFIDENTIAL**

**ASD-TDR-63-665, Part I**

TABLE 9  
CONDENSATION INSIDE TUBES WITH COPPER  
POROUS CONDENSING SURFACE - TEST 4

(Basis: Inside Area)  
Pressure ~ 1 Atmosphere

Run	N <sub>g</sub>	$(Q/A_c)$ Btu/ft <sup>2</sup> -hr.	$(h_c)$ EXP Btu/ft <sup>2</sup> -hr-°R.	$(h_c)$ THEO @139.3°R. Btu/ft <sup>2</sup> -hr-°R.	$(h_c)$ EXP @ 139.3°R $(h_c)$ THEO Dimensionless
1	80	10,150	2180	2300	.95
2	80	16,050	1935	1950	.99
3	80	27,800	1685	1620	1.04
4	80	39,600	1605	1410	1.14
5	150	10,150	3270	2850	1.15
6	150	16,050	3000	2400	1.25
7	150	27,800	2450	1900	1.23
8	150	39,600	2670	1780	1.50
9	230	16,050	7290	2820	2.58
10	230	10,150	4650	3310	1.40
11	325	16,050	7570	3150	2.40
12	325	27,800	6110	2600	2.35
13	230	10,150	5310	3310	1.61
14	230	16,050	4420	2820	1.57
15	230	27,800	4020	2330	1.73
16	150	10,150	3870	2850	1.36
17	150	16,050	2730	2400	1.44
18	150	27,800	2730	1990	1.37
19	325	23,100	7410	2800	2.56
20	325	27,800	5620	2600	2.16
21	325	32,500	5330	2450	2.18
22	325	39,600	4650	2320	2.00
23	325	37,300	4490	2350	2.00
24	230	16,050	5460	2820	1.94
25	150	27,800	2950	1990	1.48
26	230	27,800	4430	2330	1.89
27	230	16,050	6160	2820	2.18
28	230	39,600	3586	2660	1.74
<u>POINTS WITH NO ELECTRICAL HEAT INPUT</u>					
29	80	4,250	2540	3100	.82
30	80	4,250	2640	3100	.83
31	150	4,250	4400	3810	1.15
32	150	4,250	4050	3810	1.06
33	230	4,250	10,100	4200	2.41

63 ASRP-2391

**CONFIDENTIAL**

**CONFIDENTIAL**

**ASD-TDR-63-665, Part I**

acceleration in the reboiler-condenser tubes of about 200 Ng. The derivation of average acceleration will be presented in a later section. Consideration must also be given to the fact that the porous condensing surface tested was undoubtedly not the optimum one. There is potentially a wide variation in the possible required thickness and porosities of a functional porous condensing surface which would result in substantially less coating weight and increased values of  $(h_c)_{EXP} / (h_c)_{THEO}$ . This would enhance the attractiveness of the porous condensing surface.

In both Test 4 and 5  $(h_c)_{THEO}$  was calculated using the Nusselt equation in the form of Hassan and Jakob with physical properties consistent with 1 atm. (139.3°R.) However,  $(h_c)_{EXP}$  was not corrected to 1 atm. to account for the effect of pressure on the physical properties because the correlation describing this effect on the condensing heat transfer coefficient on porous surfaces is not known. Thus, the coefficient measured at some pressure other than one atmosphere cannot be corrected to one atmosphere by a correction term similar to  $R^\circ$  in Figure 57, which is for a smooth surface. For this reason, the results for condensation on porous surfaces are presented in terms of the ratio  $(h_c)_{EXP} / (h_c)_{THEO}$  where  $(h_c)_{EXP}$  is at the condensing pressure  $P$  ( $P > 1$  atm.) and  $(h_c)_{THEO}$  is evaluated at one atmosphere. Since the condensing pressures in Tests 4 and 5 were close to one atmosphere, the ratio  $(h_c)_{EXP} / (h_c)_{THEO}$  may be taken as a one atmosphere value with introduction of less error than the experimental scatter.

The problem now faced is how to use this ratio at higher pressures such as required for the cryogenic boilerplate unit requiring condensing pressures near 15 atmospheres. Obviously, further experimental work is needed to evaluate this ratio at higher pressures. Since estimates are needed now, it is assumed that the film coefficient ratio determined at approximately one atmosphere could be multiplied by the Nusselt coefficient evaluated at the appropriate pressure level of approximately 15 atmospheres to give the proper coefficient.

$$(h_c)_P = \left[ \frac{(h_c)_{EXP}}{(h_c)_{THEO}} @ \sim 1 \text{ atm} \right] (h_c)_{THEO}_P \quad (42)$$

This was taken to be a sound approach based on the following:

63 ASRP-2391

**CONFIDENTIAL**

**CONFIDENTIAL**

ASD-TDR-63-665, Part I

As shown previously,  $\left[ \frac{(h_c)_{EXP}}{(h_c)_{THEO}} \right]$  for smooth tubes increases from 1.0 as higher heat fluxes are approached. This may be attributed to rippling of the much thicker condensate film. This is not accounted for in the Nusselt equation for  $(h_c)_{THEO}$ , which assumes the mode of condensate flow is laminar without rippling effects. The effect of pressure on the film coefficient should be considered in terms of rippling. Rippling, in turn, is a function of the Reynolds number. In Reference 24, the following is indicated:

4 < Re < 25 laminar flow, no rippling  
25 < Re < 1000-2000 laminar flow with rippling

Assuming a constant heat flux and heat exchanger geometry, Reynolds number varies with pressure in the following manner:

$$\frac{Re_P}{Re_{1 \text{ atm}}} = \frac{\left( \frac{DV \rho_L}{\mu'_L} \right)_P}{\left( \frac{DV \rho_L}{\mu'_L} \right)_{1 \text{ atm}}} = \frac{\left( \frac{DW}{A \mu'_L} \right)_P}{\left( \frac{DW}{A \mu'_L} \right)_{1 \text{ atm}}} \quad \text{since } V = \frac{W}{\rho_L A}$$

At constant heat flux:

$$\frac{Q'}{A} = \left( \frac{W \lambda}{A} \right)_P = \left( \frac{W \lambda}{A} \right)_{1 \text{ atm}}$$

$$\therefore (W)_P = \frac{Q'}{(\lambda)_P} \quad \text{and} \quad (W)_{1 \text{ atm}} = \frac{Q'}{(\lambda)_{1 \text{ atm}}}$$

63 ASRP-2391

**CONFIDENTIAL**



**CONFIDENTIAL**

ASD-TDR-63-665, Part I

$$\therefore \frac{(Re)_P}{(Re)_{1 \text{ atm.}}} = \frac{Q' \left[ \frac{D}{A \mu'_L \lambda} \right]_P}{Q' \left[ \frac{D}{A \mu'_L \lambda} \right]_{1 \text{ atm.}}} = \frac{\left[ \mu'_L \lambda \right]_{1 \text{ atm.}}}{\left[ \mu'_L \lambda \right]_P} \quad \text{since } D \text{ \& } A \text{ are constant.}$$

For  $P = 15 \text{ atm.}$ ,  $\frac{(Re)_P}{(Re)_{1 \text{ atm.}}} = 3.09$ , indicating a three-fold increase in

Reynolds Number. Thus, the effect of pressure on rippling is to increase it slightly. Since the experimental film coefficient is expected to improve with rippling, it should tend to be slightly better at higher pressures. The calculation procedure used to get  $h_c @ P$  should be valid and very slightly conservative.

#### 4.4.6.5 Condensation Inside Tubes with an Aluminum Porous Condensing Surface - Test 5

The condensing coefficients on the aluminum porous condensing surface were slightly better than those on the copper porous condensing surfaces. The experimental results are presented in Figures 62 and 63 and Table 10. The theoretical condensing coefficient has previously been presented in Figure 55. The experimental condensing coefficient has been correlated in terms of the heat flux ( $Q/A_c$ ) and the gravitational field ( $Ng$ ). It was found that  $(h_c)_{EXP}$  varied as  $(Q/A_c)^{-0.6}$  and  $(Ng)^{.75}$ . The advantage of presenting the data in this form is that the condensing heat transfer coefficient may be calculated directly. There is no need to consider both  $(h_c)_{EXP}/(h_c)_{THEO}$  as a function of  $(Q/A_c)$  and  $(h_c)_{THEO}$  as a function of  $(Q/A_c)$  although plots of these relationships are shown in Figures 63 and 55 to achieve consistency with the previous method of data presentation.

Figure 62 shows that  $(h_c)_{EXP}$  has a value of  $5920 \text{ Btu/(ft}^2\text{)(hr)(}^\circ\text{R)}$  at a heat flux of  $20,000 \text{ btu/(ft}^2\text{)(hr)}$  and  $150 Ng$ .  $(h_c)_{EXP}$  on a smooth surface at the same conditions would be  $2420 \text{ Btu/(ft}^2\text{)(hr)(}^\circ\text{R)}$ . The use of the aluminum porous surface causes a 2.42 times increase in the average condensing coefficient. This is a 1.63 times increase in overall performance if the porous coating increases the weight of the reboiler-condenser by 50%. The use of a porous aluminum surface would thus appear to be attractive for the reboiler-condenser.

The reason for the better performance of the aluminum porous condensing surface is not known, although it was noted that the aluminum

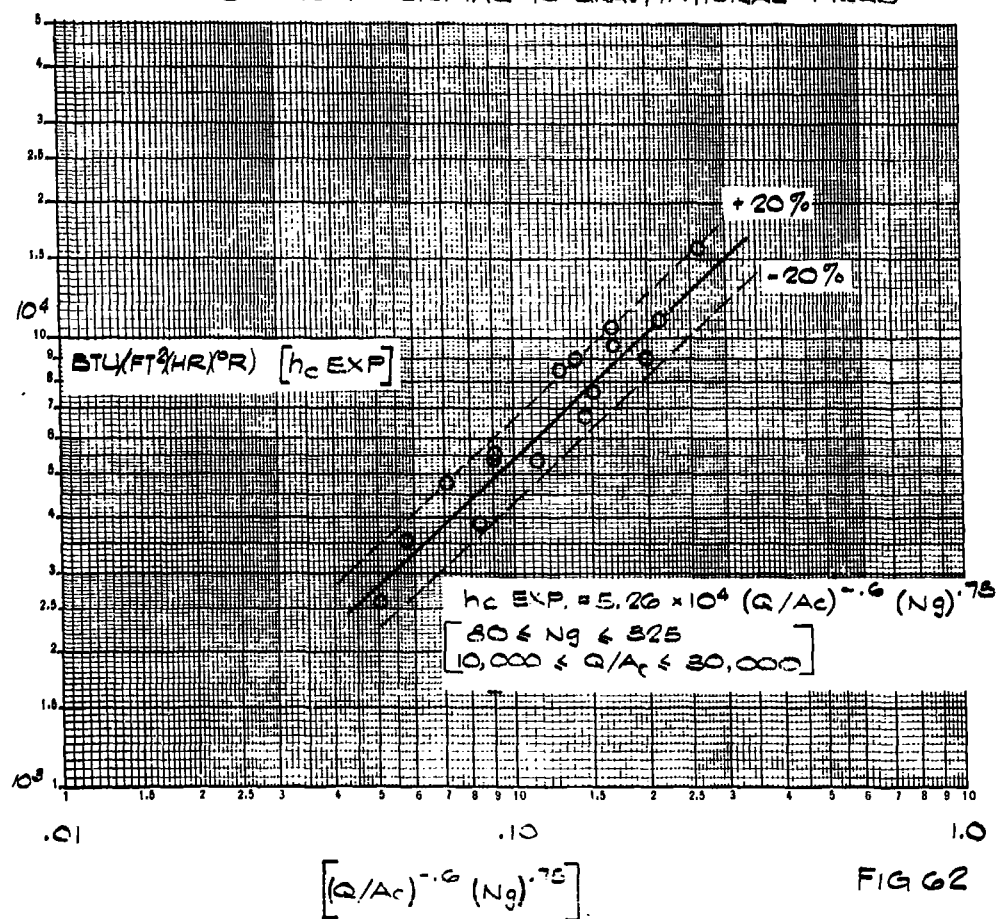
63 ASRP-2391

**CONFIDENTIAL**

CONFIDENTIAL

ASD-TDR-63-665, Part I

CONDENSATION INSIDE .205 I.D. ALUMINUM TUBES COATED  
WITH AN ALUMINUM POROUS CONDENSING SURFACE AND  
INCLINED 5° FROM NORMAL TO GRAVITATIONAL FIELD



CONFIDENTIAL

CONFIDENTIAL

C

ASD-TDR-63-665, Part I

CONDENSATION INSIDE .805" I.D. ALUMINUM TUBES COATED  
WITH AN ALUMINUM POROUS CONDENSING SURFACE AND  
INCLINED 5° FROM NORMAL TO GRAVITATIONAL FIELD

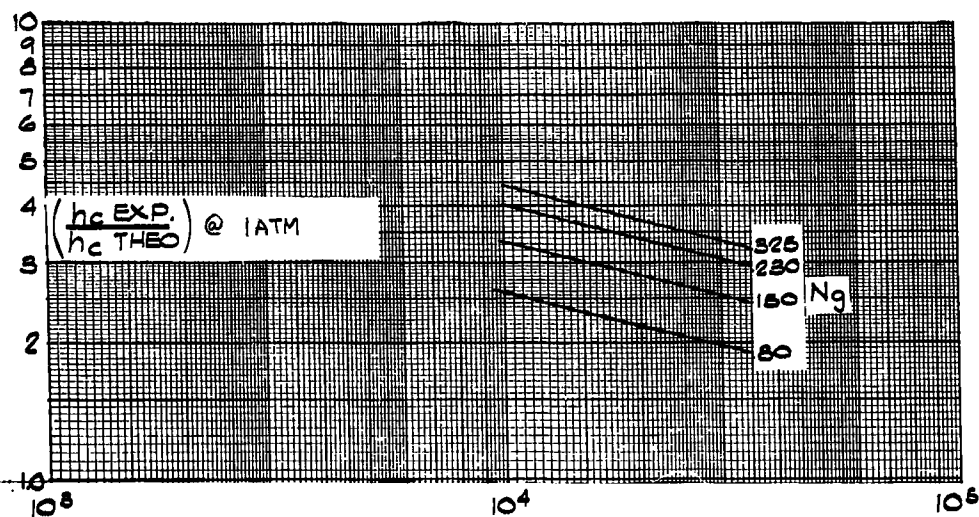


FIG. 63

$Q/A_c \text{ BTU}/(\text{FT.}^2)(\text{HR.})$

CONFIDENTIAL

CONFIDENTIAL

ASD-TDR-63-665, Part I

TABLE 10

CONDENSATION INSIDE TUBES WITH ALUMINUM

POROUS CONDENSING SURFACE - TEST 5

(Basis: Inside Area)

Pressure ~ 1 Atmosphere

<u>Run</u>	<u>Ng</u>	<u>(Q/A<sub>c</sub>) Btu/ft<sup>2</sup>-hr.</u>	<u>(h<sub>c</sub>) EXP Btu/ft<sup>2</sup>-hr-°R.</u>
1	325	13,200	15,172
2	325	18,100	11,240
3	325	27,950	10,627
4	325	33,900	7,722
5	325	37,800	9,153
6	230	13,200	8,980
7	230	18,100	9,731
8	230	27,950	8,627
9	230	33,900	5,433
10	150	13,200	6,839
11	150	18,100	6,830
12	150	27,950	5,601
13	150	33,900	3,924
14	80	13,200	5,455
15	80	18,100	4,827
16	80	27,950	3,634
17	80	33,900	2,665

63 ASRP-2391

CONFIDENTIAL

# CONFIDENTIAL

## ASD-TDR-63-665, Part I

porous condensing surface had larger capillary radii than the copper porous condensing surface previously tested.

### 4.4.6.6 Condensation Inside Tubes with a Non-Wetted Surface - Test 6

The non-wetted Teflon condensing surface was ineffectual in promoting high condensing heat transfer coefficients. In fact, as Figure 64 and Table 11 show, the performance is even worse than on a smooth surface. The effect is particularly noticeable at low heat fluxes where the condensing coefficient is large. At high heat fluxes, the condensing coefficient is strongly controlling, so that performance asymptotically approaches the smooth surface value. This is a result of a contact resistance between the Teflon film and the tube wall. The Teflon film is too thin to account for this increased resistance itself, since the equivalent coefficient of a 5000 Angstrom (.02 mil) thick Teflon film is 86,000 Btu/(ft.)<sup>2</sup>(hr)(°R). The contact coefficient has a value of 7150 Btu/(ft)<sup>2</sup>(hr)(°R). Such a contact resistance could arise if the Teflon coating trapped pockets of air in the micro roughness of the tube wall during the coating fusion process. The peak to valley roughness of a reamed surface such as that inside the tubes is 63-125 micro inches. A 75 micro inch gap would have an equivalent coefficient of 7150 Btu/(ft)<sup>2</sup>(hr)(°R) if filled with air. The Teflon coated surface obviously should not be considered for use in the reboiler-condenser.

### 4.4.6.7 Boiling on an Untreated Aluminum Surface - Test 7

Figure 65 shows the boiling curves obtained for N<sub>2</sub> boiling on the test specimen surface. The heat flux is plotted against the average temperature difference between the metal surface and the boiling N<sub>2</sub> at various Ng. Figure 66 shows the boiling curve obtained for boiling oxygen at normal gravity on this specimen, compared with the nitrogen boiling curve obtained under the same conditions. The data for these curves are listed on Table 12. Figures 67 and 68 show, for reference, boiling curves for nitrogen and oxygen on various surfaces at normal gravity as reported in the literature, or obtained by the Union Carbide Corp., Linde Division in previous work. (Ref. 28, 29, 30, 31, 32, 33, 34, 35).

The influence of the gravitational field on boiling performance is shown by the N<sub>2</sub> data in Figure 65. There was no gravitational field effect at high heat fluxes; however, at low heat fluxes, where

63 ASRP-2391

# CONFIDENTIAL

# CONFIDENTIAL

ASD-TDR-63-665, Part I

CONDENSATION INSIDE .250" I.D. TUBES  
COATED WITH A TEFLON SURFACE AND  
INCLINED 5° FROM NORMAL TO THE GRAVITATIONAL  
FIELD

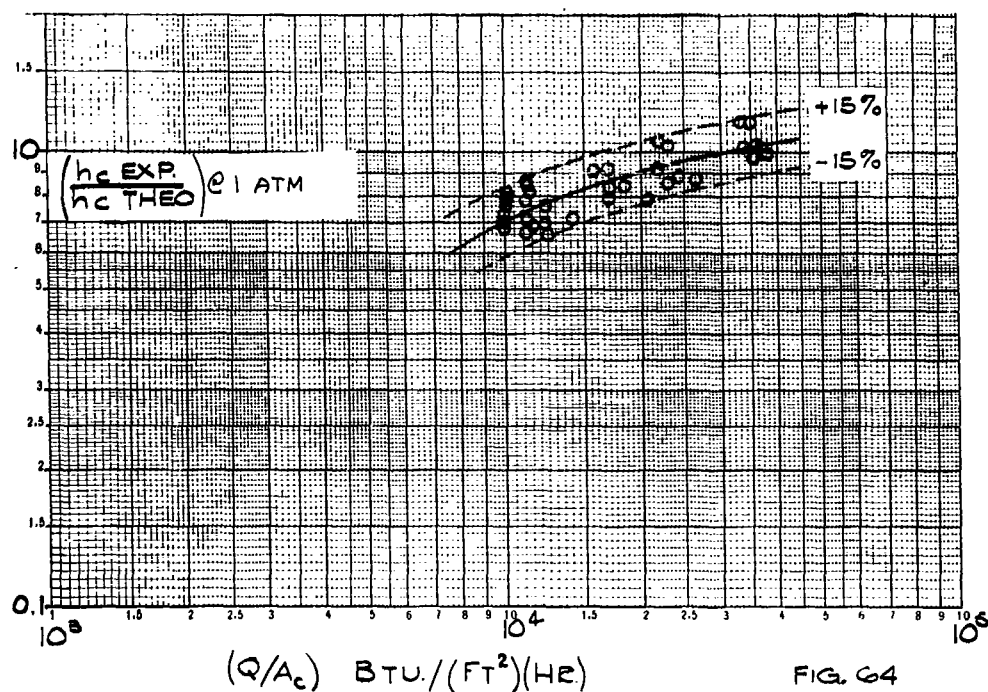


FIG. 64

# CONFIDENTIAL

## ASD-TDR-63-665, Part I

TABLE II  
CONDENSATION INSIDE .250 IN. I.D. TUBES  
COATED WITH A TEFLON SURFACE - TEST 6

(Basis: Inside Area)

Pressure = 1 Atmosphere

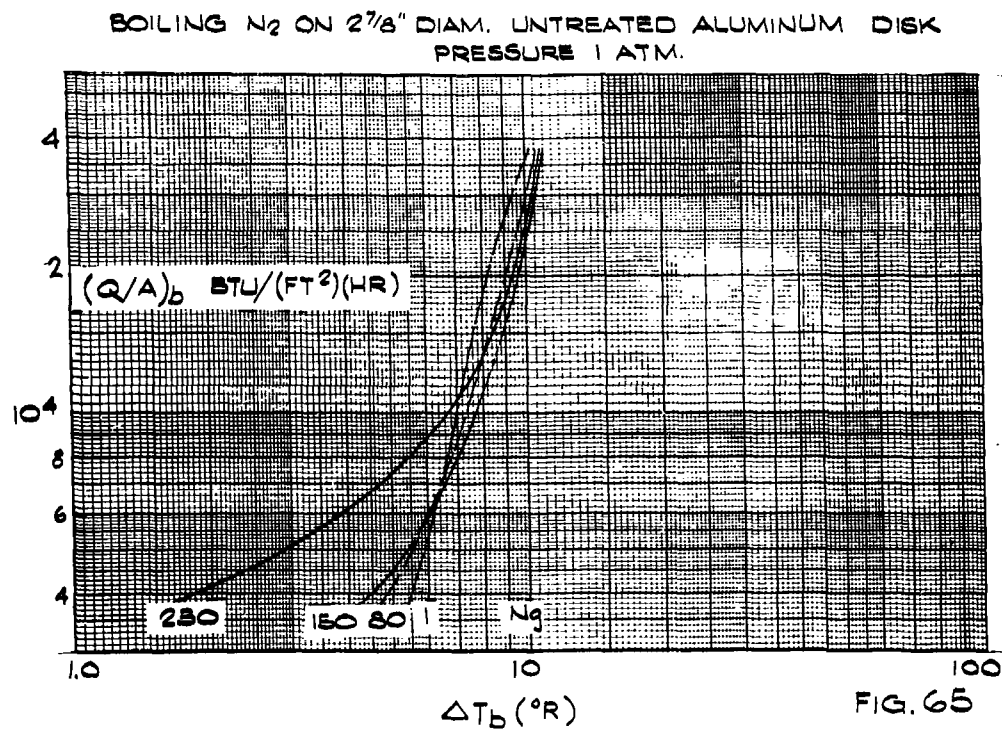
Run	No.	$(Q/A_s)$ Btu/(ft <sup>2</sup> -hr.)	$(h_c)_{EXP @ 139.3^\circ R}$		$(h_c)_{THEO @ 139.3^\circ R}$	Dimensionless
			Btu/(ft <sup>2</sup> -hr.-°R)	Btu/(ft <sup>2</sup> -hr.-°R)		
1*	80	9,905	1707	2340	.729	
2	80	15,690	1604	2066	.841	
3*	80	9,905	1737	2340	.742	
4	80	21,680	1572	1882	.933	
5*	80	9,905	1748	2340	.746	
6	80	33,450	1456	1679	1.045	
7*	150	11,080	1941	2800	.694	
8	150	16,975	1822	2495	.793	
9*	150	11,080	1899	2800	.678	
10	150	22,850	1780	2289	.865	
11*	150	11,080	1897	2800	.678	
12	150	34,650	1692	2042	.983	
13*	80	9,905	1830	2340	.782	
14	80	15,690	1753	2059	.916	
15*	80	9,905	1917	2340	.819	
16	80	21,680	1791	1870	1.057	
17*	150	11,080	2410	2800	.861	
18	150	16,975	2114	2482	.915	
19*	150	11,080	2233	2800	.792	
20	150	22,850	2137	2275	1.032	
21*	150	11,080	2217	2800	.791	
22	150	34,650	2016	2018	1.157	
23*	230	12,255	2400	3125	.768	
24	230	18,150	2240	2841	.854	
25*	230	12,255	2159	3125	.691	
26	230	24,050	2110	2631	.890	
27*	230	12,255	2098	3125	.672	
28	230	35,820	2116	2352	1.047	
29*	325	14,130	2437	3380	.721	
30	325	20,040	2250	3149	.782	
31*	325	14,130	2250	3380	.666	
32	325	25,930	2313	2920	.881	
33*	325	14,130	2181	3380	.646	
34	325	37,760	2442	2624	.997	
35*	80	9,905	1806	2340	.686	
36	80	33,450	1629	1661	1.156	

\* Denotes points with no electrical heat input.

63 ASRP-2391

CONFIDENTIAL

ASD-TDR-63-665, Part I



63 ASRP-2391

CONFIDENTIAL



CONFIDENTIAL

ASD-TDR-63-665, Part I

COMPARISON OF  $O_2$ - $N_2$  BOILING DATA AT 1 NG  
AND 1 ATM ON AN UNTREATED ALUMINUM DISK

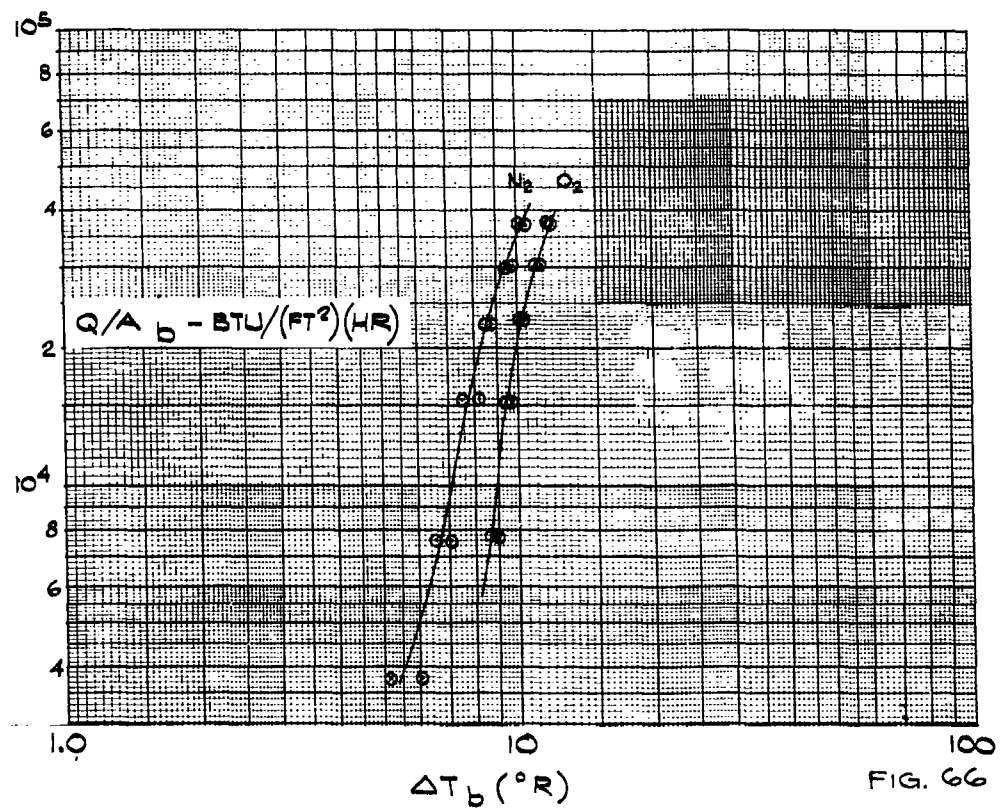


FIG. 66

CONFIDENTIAL

# CONFIDENTIAL

ASD-TDR-63-665, Part I

TABLE 12  
BOILING DATA FOR LIQUID NITROGEN AND LIQUID OXYGEN  
ON A SMOOTH ALUMINUM SURFACE - TEST 7  
Pressure = 1 Atmosphere

Run	(Q/A <sub>b</sub> ) Btu/(ft <sup>2</sup> -hr.)	<u>Liquid Nitrogen</u>		Ng
		$\Delta T_1$ Center T.C. °R	$\Delta T_2$ Edge T.C. °R	
1	7,570	7.53	5.92	150
2	15,500	9.45	8.58	150
3	22,710	10.32	9.54	150
4	30,280	11.00	10.20	150
5	37,850	11.20	10.32	150
6	3,785	4.61	3.65	150
7	39,430	10.52	10.43	80
8	30,280	9.61	9.46	80
9	22,710	9.12	9.06	80
10	15,500	8.39	8.00	80
11	7,570	6.75	6.19	80
12	3,785	5.01	4.41	80
13	37,850	10.56	10.52	230
14	30,280	10.56	10.20	230
15	22,710	10.15	9.30	230
16	15,500	8.64	8.10	230
17	7,570	5.32	4.84	230
18	3,785	1.90	1.76	230
19	37,700	10.12	10.02	1
20	30,280	9.60	9.35	1
21	22,610	8.69	8.48	1
22	15,500	7.96	7.54	1
23	7,570	6.96	6.54	1
24	3,785	5.89	5.15	1
		<u>Liquid Oxygen</u>		
25	7,570	8.93	8.65	1
26	15,500	9.50	9.45	1
27	22,710	10.36	10.30	1
28	30,280	11.08	11.20	1
29	37,850	11.60	11.70	1

CONFIDENTIAL

BOILING HEAT TRANSFER TO LIQUID NITROGEN  
AT 1 NG, 1 ATM (REFERENCE DATA)

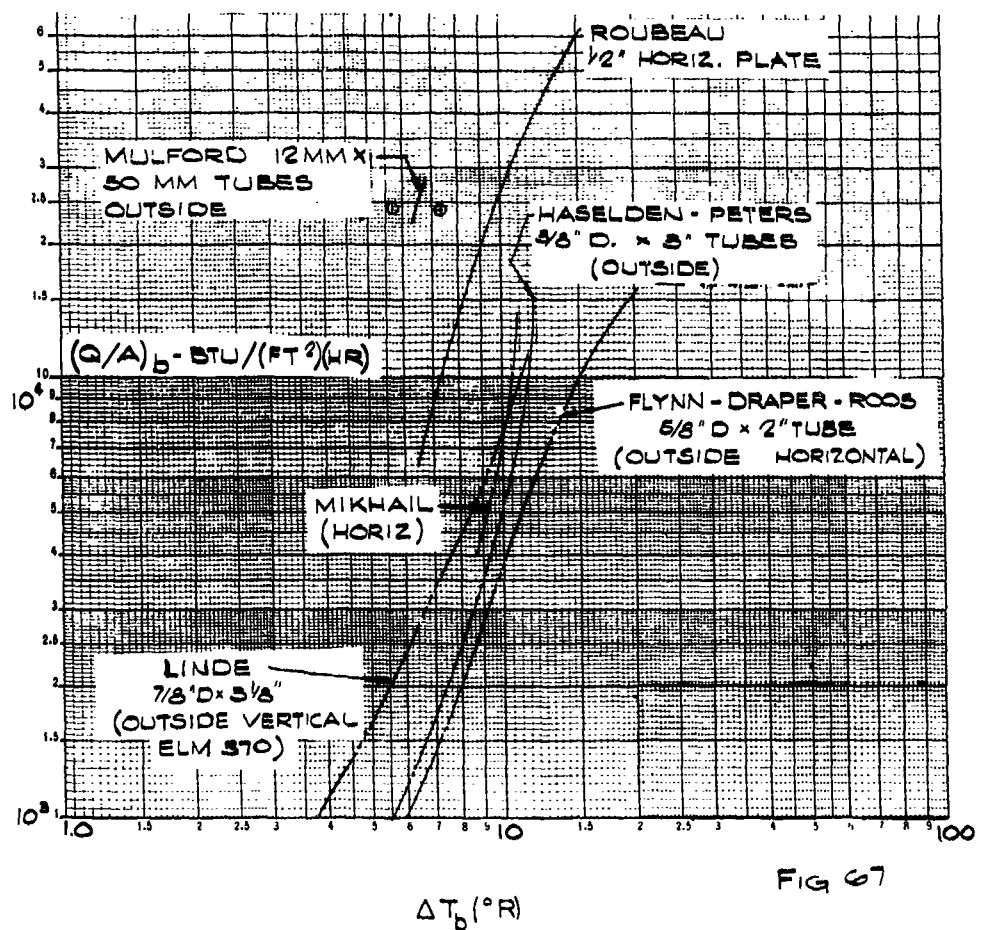


FIG 67

BOILING HEAT TRANSFER TO LIQUID OXYGEN  
AT 1 N<sub>2</sub>, 1 ATM. REFERENCE DATA

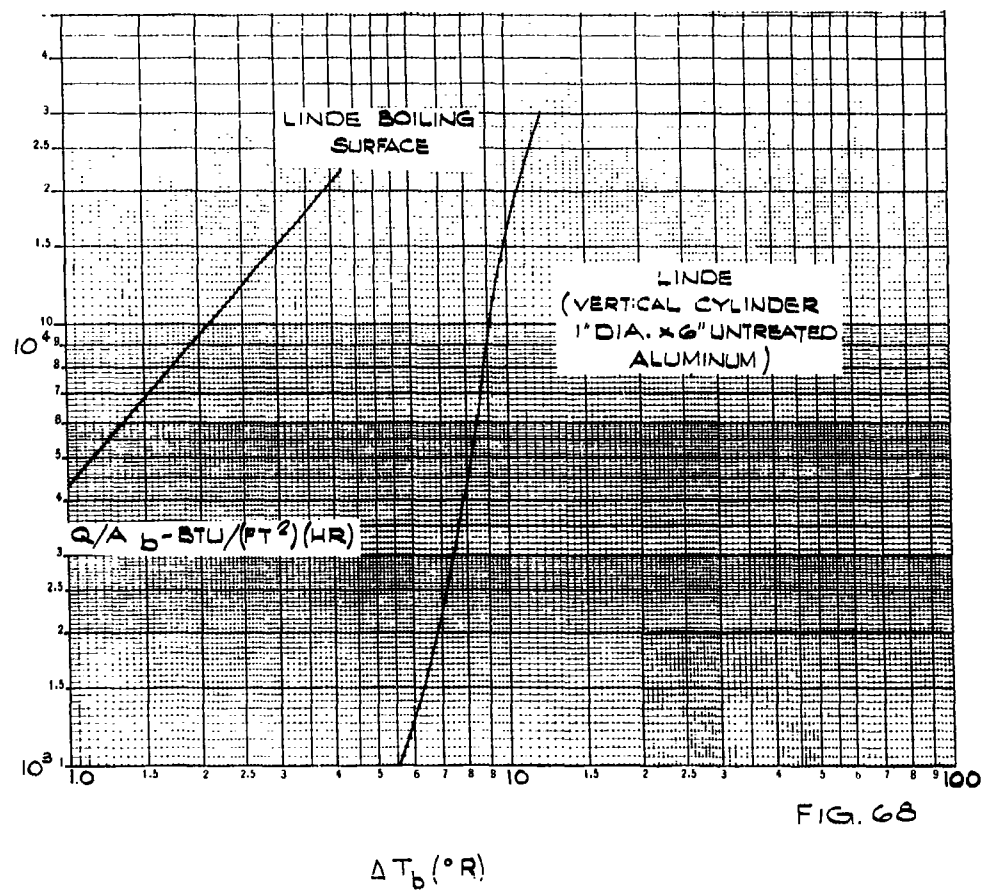


FIG. 68

# CONFIDENTIAL

## ASD-TDR-63-665, Part I

convective heat transfer can be substantial, an appreciable gravitational field effect was noticed. Similar results were obtained for boiling on a special surface as reported in the Summary Report on "Heat Transfer Studies", Contract AF 33(616)-7646. Since the reboiler-condenser would operate at heat fluxes where gravitational field has no influence on the boiling curve, it may be concluded that the special surface retains heat transfer advantage over a conventional boiling surface at all gravitational fields for all heat fluxes of interest.

The effect of the boiling fluid on the boiling curve is shown by comparison of the  $O_2$  and  $N_2$  data at normal gravity (Figure 66) where the boiling performance decreases as the normal boiling point of the test fluid increases. This is consistent with previous experience in the nucleate boiling of cryogenic fluids.

In comparison of performance with other untreated surface data, the data obtained with this specimen compares well with literature data and other Linde data. Figure 67 shows the results of six previous investigations of boiling heat transfer to liquid  $N_2$ . Although the heat transfer coefficients obtained in the present work were somewhat greater than the average coefficients previously obtained, differences in surface characteristics and specimen configuration could account for this variation. No attempt was made to polish our surface to remove any of the nucleating sites, as others may have done, since it was desired to test a mill finished surface, untreated in any way. Surface roughness is known to have a pronounced effect on the nucleate boiling heat transfer coefficient.

The  $O_2$  data compares well with previously obtained Linde data for boiling on an untreated aluminum surface (See Figure 68). The surface of the previous specimen was machined on a lathe, and thus may have had nucleating sites comparable in number to those on our test piece, hence the good agreement.

### 4.5 Pilot-Scale Reboiler-Condenser

The objective of the second phase of the heat transfer test program was to demonstrate or proof test a small scale reboiler-condenser utilizing the concepts and information that evolved from the basic heat transfer studies. A further criterion established for this phase of the test program was that the experimental apparatus should be geometrically similar to the design of the full scale reboiler-condenser in all respects except size. In accordance with these objectives, design

63 ASRP-2391

# CONFIDENTIAL

# CONFIDENTIAL

## ASD-TDR-63-665, Part I

parameters were established, "efficiencies" defined, and the performance of the unit predicted by mathematical analysis. The experimental model then was fabricated and the resulting test data evaluated in terms of the aforementioned criteria.

### 4.5.1 Rotor Design

As described earlier, the basic component of the reboiler-condenser was a rotating disk made of curved tubes, brazed together. In order to braze the disk, the tubes must be in lateral contact everywhere along their lengths. This also served to pack the maximum area into a disk of given dimension. It was also necessary that the tubes be oriented so that the major component of the acceleration should act in a direction transverse to the tube axis over most of the length of each tube. Such an orientation strips the condensate from the walls of the tube into a small drainage trough on the side of the tube which is radially outward.

To simplify the headering at the inner annular boundary of the disk, the tubes at this location were made parallel to the disk radius. The derivation of the equation for a single tube in lateral contact everywhere along its length is given in Appendix VII. The equation for one of these tubes in polar coordinates is:

$$\Theta = \arccos \frac{r_i}{r} - \sqrt{\left(\frac{r}{r_i}\right)^2 - 1} \quad (43)$$

where  $r$  is the length of the radius vector and  $\Theta$  is the angle between the radius vector and the polar axis. The length of each tube is given by the following derivation:

$$\text{From Appendix VII,} \quad \frac{ds}{dr} = \frac{r}{r_i}$$

$$\therefore \int_0^s ds = \int_{r_i}^{r_o} \frac{r}{r_i} dr$$

and

$$S = \frac{1}{2 r_i} (r_o^2 - r_i^2) \quad (44)$$

The efficiency with which these tubes were oriented to the available centrifugal acceleration was determined by comparison with a fictitious

63 ASRP-2391

# CONFIDENTIAL

ASD-TDR-63-665, Part I

optimum orientation. Obviously, if all tubes were perpendicular to the radius of the rotor at every point, the total centrifugal acceleration would be utilized in stripping the condensate from the walls of the tube. With no component parallel to the tubes the condensate would not drain and the tubes would flood with liquid, which makes the heat transfer optimum fictitious. However, retaining it as a standard of comparison, the following considerations apply. The centrifugal acceleration at any point on the rotor was  $r \omega^2$ . The component of this centrifugal acceleration perpendicular to the axis of the tube was  $\omega^2 r \sin \psi$ , where  $\psi$  is the angle between the radius vector and the axis of the tube and is the complement of the angle  $\alpha^\circ$  defined in the previous section. The efficiency of orientation is defined as the integral of the perpendicular component of the centrifugal acceleration along the length of the tube divided by the integral of the total centrifugal acceleration along the tube. This efficiency was

$$\text{Orientation efficiency} = \frac{\int_{r_1}^{r_0} r \sin \psi \, ds}{\int_{r_1}^{r_0} r \, ds}$$

where:

$$\frac{dr}{ds} = \cos \psi = \frac{r_1}{r} \quad (\text{See Appendix VII})$$

$$ds = \frac{r}{r_1} \, dr$$

$$\sin \psi = \frac{\sqrt{r^2 - r_1^2}}{r}$$

substituting:

$$\text{Orientation efficiency} = \frac{\int_{r_1}^{r_0} (r) \left( \frac{\sqrt{r^2 - r_1^2}}{r} \right) \left( \frac{r}{r_1} \right) dr}{\int_{r_1}^{r_0} r \left( \frac{r}{r_1} \right) dr}$$

$$= \frac{\int_{r_1}^{r_0} \frac{r}{r_1} \sqrt{r^2 - r_1^2} \, dr}{\int_{r_1}^{r_0} \frac{r^2}{r_1} \, dr}$$

63 ASRP-2391

# CONFIDENTIAL

# CONFIDENTIAL

ASD-TDR-63-665, Part I

The integration yielded:

$$\text{Orientation Efficiency} = \frac{\left[ \frac{r_o^2 - r_i^2}{r_o^3 - r_i^3} \right]^{3/2}}{r_o^3 - r_i^3} \quad (45)$$

The Nusselt analysis as formulated by Hassan and Jakob for inclined circular cylinders (Ref. 19) indicates that the heat transfer coefficient is directly proportional to the acceleration perpendicular to the axis of the cylinder raised to the 1/4 power. Therefore, the perpendicular component of the centrifugal acceleration raised to the 1/4 power was integrated along the length of the tube and an efficiency again defined as previously. This efficiency, based on the heat transfer potential, was:

$$= \frac{\int_{r_i}^{r_o} (r \sin \psi)^{1/4} ds}{\int_{r_i}^{r_o} r^{1/4} ds} = \frac{(r_o^2 - r_i^2)^{9/8}}{r_o^{9/4} - r_i^{9/4}} \quad (46)$$

The condensate accumulates on the side of the tube which is radially outward and flows out of the tube under the influence of that component of the acceleration parallel to the tube axis. Because of the low condensate fluid velocity, the Coriolis force effect was found to be negligible. The tube with a profile given by equation (43) had a constant acceleration parallel to the axis of the tube at every point along its length and its magnitude was defined by the following equation:

$$\frac{\omega^2 r \cos \psi}{g} = \frac{\omega^2 r_i}{g} = Ng_p \quad (47)$$

63 ASRP-2391



# CONFIDENTIAL

## ASD-TDR-63-665, Part I

### 4.5.2 Dimensions and Configuration of Test Rotor

The heat transfer test rotor consisted of two tube disks, Fig. 69, forming one boiling passage flanked by two condensing passages. The outer side of each condensing passage was not exposed to the boiling fluid. The inner and outer radii of these disks were  $r_i = 6$  inches and  $r_o = 18$  inches. Each disk or tube sheet consisted of 121 type 3003 aluminum tubes of 0.280 inches I.D. and 0.016 inches wall. The length of each tube as determined by equation (44) was 2 feet. The orientation efficiency calculated from equation (45) was 0.870. This meant that 87% of the total centrifugal acceleration available was perpendicular to the axis of the tube. The efficiency based on the heat transfer potential, calculated by means of equation (46), was 0.957. From this, the conclusion can be made that if all the tubes were mounted circumferentially on the rotor (fictitious optimum) there could only be an increase of 4.3% in the heat transfer when compared with the orientation selected.

The two tube plates were separated in the axial direction by a space of 3/16 inches (minimum spacing between crests of opposed tubes) to serve as the boiling passage. No vanes or restrictions were placed in this passage. Under high acceleration any significant depth of liquid on a vane would cause an appreciable increase in the hydrostatic pressure of the liquid with a corresponding rise in its saturation temperature. Since the reboiler-condenser must operate at low overall temperature differences, this hydrostatic pressure rise would significantly reduce the temperature difference available for heat transfer. The liquid completely wetted the walls of the tube disks which banned its passage. Over most of the operating range, the liquid flowed as a film on the disk surface, and the vapor flowed cocurrently as a segregated core in the center of the passage. Under certain conditions, non-segregated two-phase flow occurred.

The vapor header at the entrance to the tubes consisted of a manifold connecting all the tubes together. Bushings were passed through the vapor manifold to conduct liquid to the boiling passage. This liquid was distributed by an orifice ring, which included 242 orifices, which sprayed the liquid onto the disk surfaces, half the orifices facing one disk and half, the other.

At the outer periphery of the rotor twelve cross headers equally

63 ASRP-2391

# CONFIDENTIAL

## ASD-TDR-63-665, Part I

spaced were provided to join the two disks and collect the condensate. A liquid seal maintained an elevated pressure on the tube side. The condensed liquid passed through this liquid seal, and was discharged freely into the stationary casing surrounding the rotor. The excess, or unvaporized, liquid from the boiling passage was also collected at the outer periphery and discharged freely to the casing. This was possible because, as shown below, the same fluid was used for both condensing and boiling streams, a pressure difference providing the temperature driving force. In the actual air separator application, of course, suitable exit headers would be required. A seal was maintained on the excess boiling passage liquid to prevent discharge of vapor to the casing. The boilup vapor was passed through holes at the periphery of the rotor into an annular passage and returned to the center of the rotor, where a rotating seal was provided for an exit from the casing. The configuration of the tube disks along with the inner and outer headers is shown in Figure 37. A photograph of the brazed tubes comprising one rotor disk is shown in Figure 69.

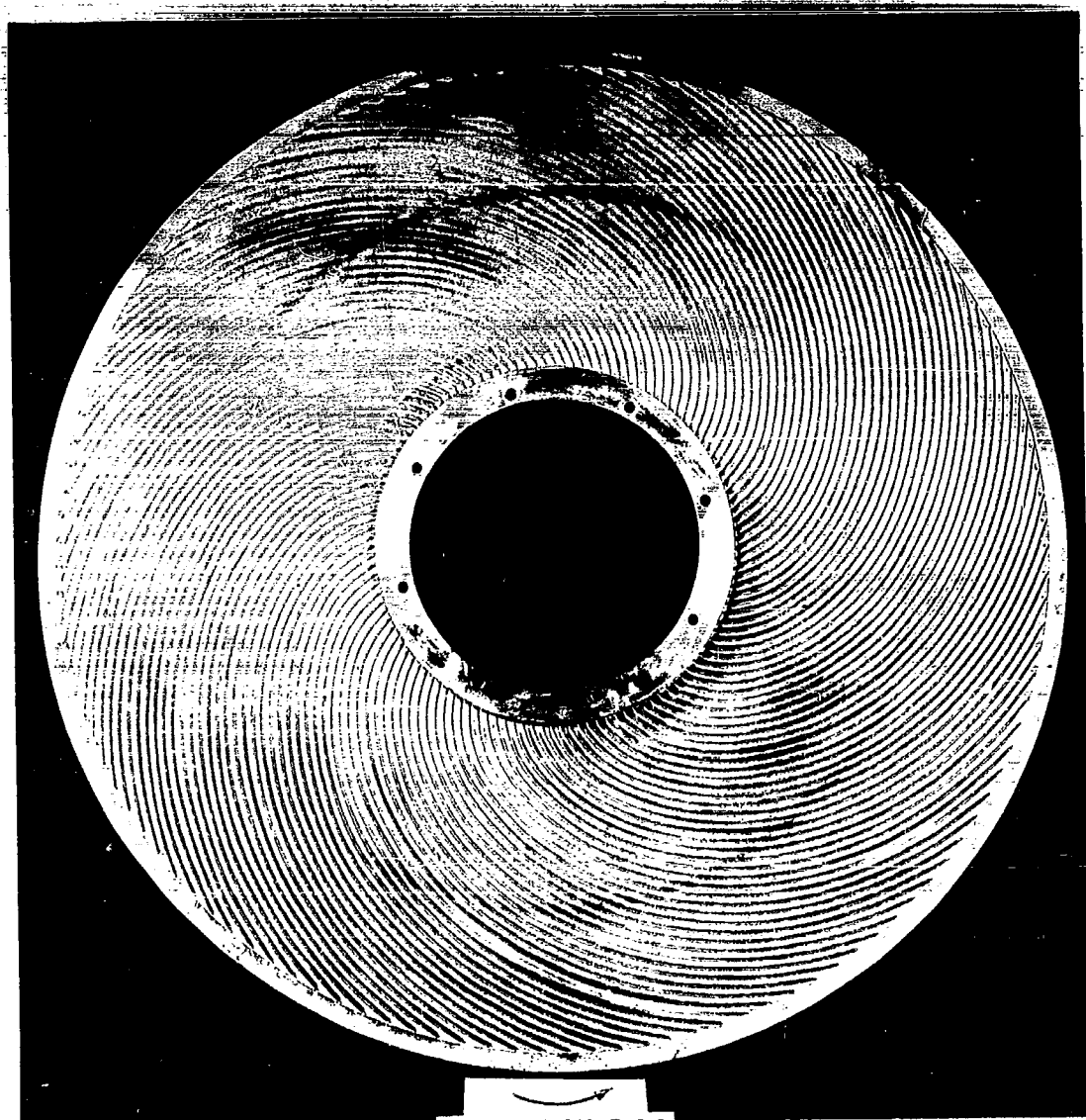
### 4.5.3 Instrumentation

The auxiliary apparatus for providing saturated vapor and liquid to the test rotor was a closed loop cycle consisting of a reboiler and condenser, high pressure pumps, vapor separators, heat exchangers, storage tanks, and the necessary piping. The storage vessels and piping were designed to operate at pressures up to 150 psig. A schematic of the circuit is shown in Figure 70. This flow circuit was basically the same as that used under Contract AF 33(616)-7509, and a complete description is included in that report. The only modification required was the addition of another fluid line with a metering device, between the storage tank and the condenser, (broken line in Figure 70). The inlet and exit streams to the rotor were metered and their temperatures and pressures controlled and measured.

Three Statham, strain gauge, differential pressure transducers were mounted on the rotor. The high pressure ports on these pressure transducers were connected to the tube side of the disks while the low pressure ports or references were connected to the annular boiling passage. The three transducers were located at radial locations of 6 in., 12 in., and 18 in., respectively. The pressure ports were located after the inlet headers and orifices and before the exit headering. This assured that no pressure drops across the headering arrangements were measured and the pressure phenomena measured corresponded to that occurring in the active heat transfer area. The output from these transducers was

63 ASRP-2391

ASD-TDR-63-665, Part I



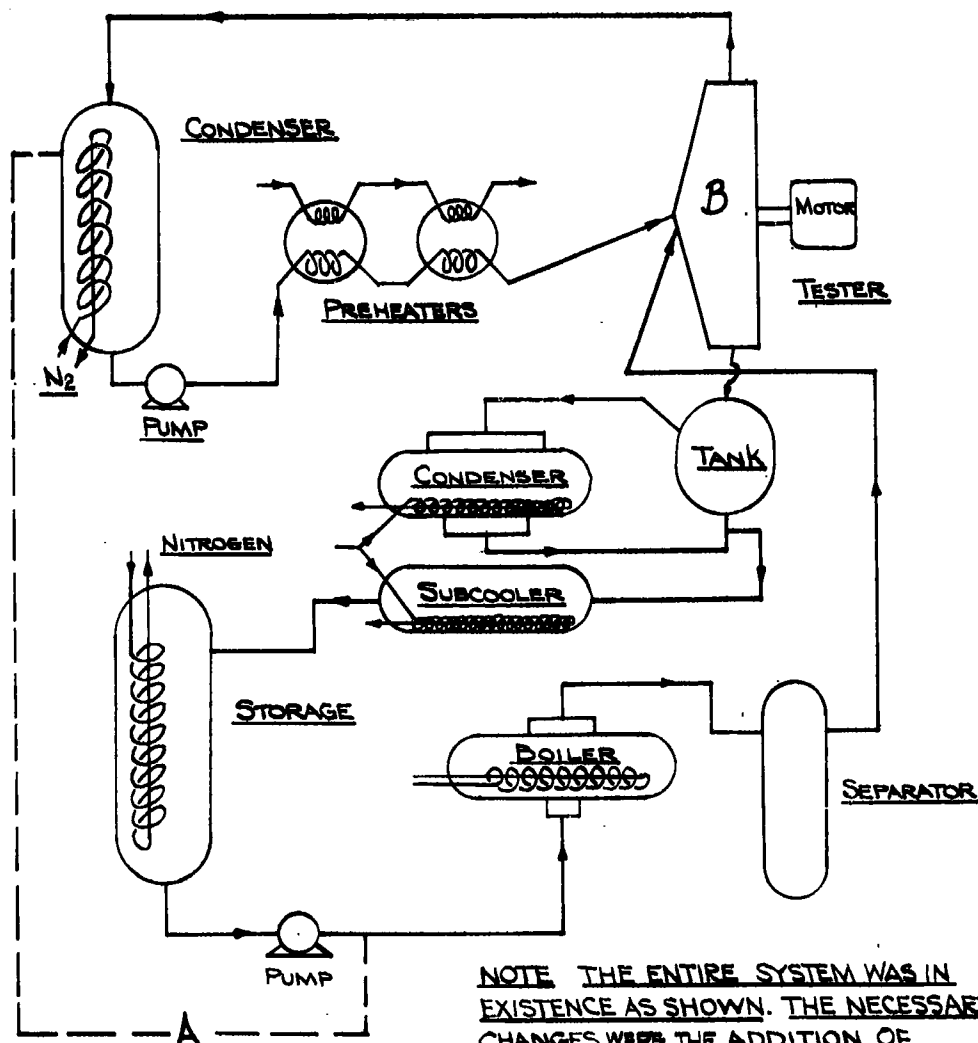
ROTATION

UCON FLUID HEAT TRANSFER DISK  
AFTER BRAZING

FIG. 69

63 ASRP-2391

BASIC UCON FLOW CIRCUIT



NOTE THE ENTIRE SYSTEM WAS IN EXISTENCE AS SHOWN. THE NECESSARY CHANGES WERE THE ADDITION OF BY-PASS LINE A AND AN ENTIRELY DIFFERENT ROTOR FOR TESTER B

FIG. 70

**CONFIDENTIAL**

**ASD-TDR-63-665, Part I**

recorded and gave a direct indication of the local pressure differences existing between the streams at the three different locations along the tube. From the pressures as measured experimentally, the overall temperature difference between the boiling and condensing fluids could be determined.

The heat flux was determined with the aid of the external metering devices and a mass balance on the basis of known area, measured flow rates and determined heat of vaporization. Independent checks on the overall mass balance could be determined by individual mass balances around each storage tank and the rotor. The agreement between the calculated and measured quantities was always within a few per cent.

**4.5.4 Selection of Test Fluid**

The basic functional study of heat transfer in this novel configuration would have been complicated by secondary problems if cryogenic oxygen and nitrogen had been used. Those problems would be the design of suitable low temperature seals, the need for separate flow circuits for each fluid, and the hazardous nature of liquid oxygen. Further, the test loop suitable for UCON fluids could not be adapted for cryogenic use.

It was necessary to choose a single UCON fluid to simulate both oxygen and nitrogen. The following similarity criteria were accepted, as work by Martinelli and Lockhart (36) showed that the following physical property ratios affect two-phase flow:

$$\frac{\rho_v}{\rho_L}, \frac{\mu_v}{\mu_L}, \frac{\rho_L}{\mu_L}, \frac{\rho_v}{\mu_v}$$

Boiling heat transfer on the special surface is controlled by the Gibbs-Kelvin parameter:

$$\frac{\sigma' T_b}{\lambda \rho_v} \quad (\text{Refer to section 4.3.3})$$

Condensing heat transfer is controlled by the Nusselt parameter;

$$\left[ \frac{k_L^3 \rho_L^2 \lambda}{\mu_L} \right]^{1/4}$$

63 ASRP-2391

**CONFIDENTIAL**

**CONFIDENTIAL**

**ASD-TDR-63-665, Part I**

The six similarity criteria were evaluated for UCON 12, UCON 22, UCON 113, and UCON 114. The Gibbs-Kelvin parameter and the fluid flow criteria were also evaluated for oxygen and the condensing parameter for nitrogen at the saturation pressures expected in the reboiler-condenser. Values for UCON fluid and oxygen properties can be found in Ref. 19, 20 and 37. Figure 71 shows the deviation of the Gibbs-Kelvin parameter of the four UCON fluids from that of oxygen at 85 psig as a function of the UCON fluid pressures. Figure 72 shows the deviation of the Nusselt parameters from that of nitrogen at 250 psig. Similar plots were made for the four fluid flow criteria as shown in Figure 73 where the square root of the sum of the squares of the deviations of the UCON fluid flow parameters from those of oxygen at 85 psig are plotted as a function of UCON pressure. This method is valid, as statistically it is the evaluation of the standard deviation of the UCON parameters from the mean defined as the calculated value of the parameters for oxygen at 85 psig. (Ref. 38)

The symbol  $\sqrt{\Sigma \Delta_i^2}$  is composed of the following:

$$\sqrt{\Sigma \Delta_i^2} = \left( \left[ \left( \frac{\rho}{\mu} \frac{v}{L} \right)_u - \left( \frac{\rho}{\mu} \frac{v}{L} \right)_o \right]^2 + \left[ \left( \frac{\mu}{\mu_v} \frac{L}{u} \right) - \left( \frac{\mu}{\mu_v} \frac{L}{o} \right) \right]^2 + \left[ \left( \frac{\rho}{\mu} \frac{L}{u} \right) - \left( \frac{\rho}{\mu} \frac{L}{o} \right) \right]^2 + \left[ \left( \frac{\rho}{\mu_v} \frac{v}{u} \right) - \left( \frac{\rho}{\mu_v} \frac{v}{o} \right) \right]^2 \right)^{1/2} \quad (48)$$

The location of the minimum standard deviation for each UCON fluid on Figure 73 is based on the minima location of a function as defined by calculus (Ref. 23 p. 82).

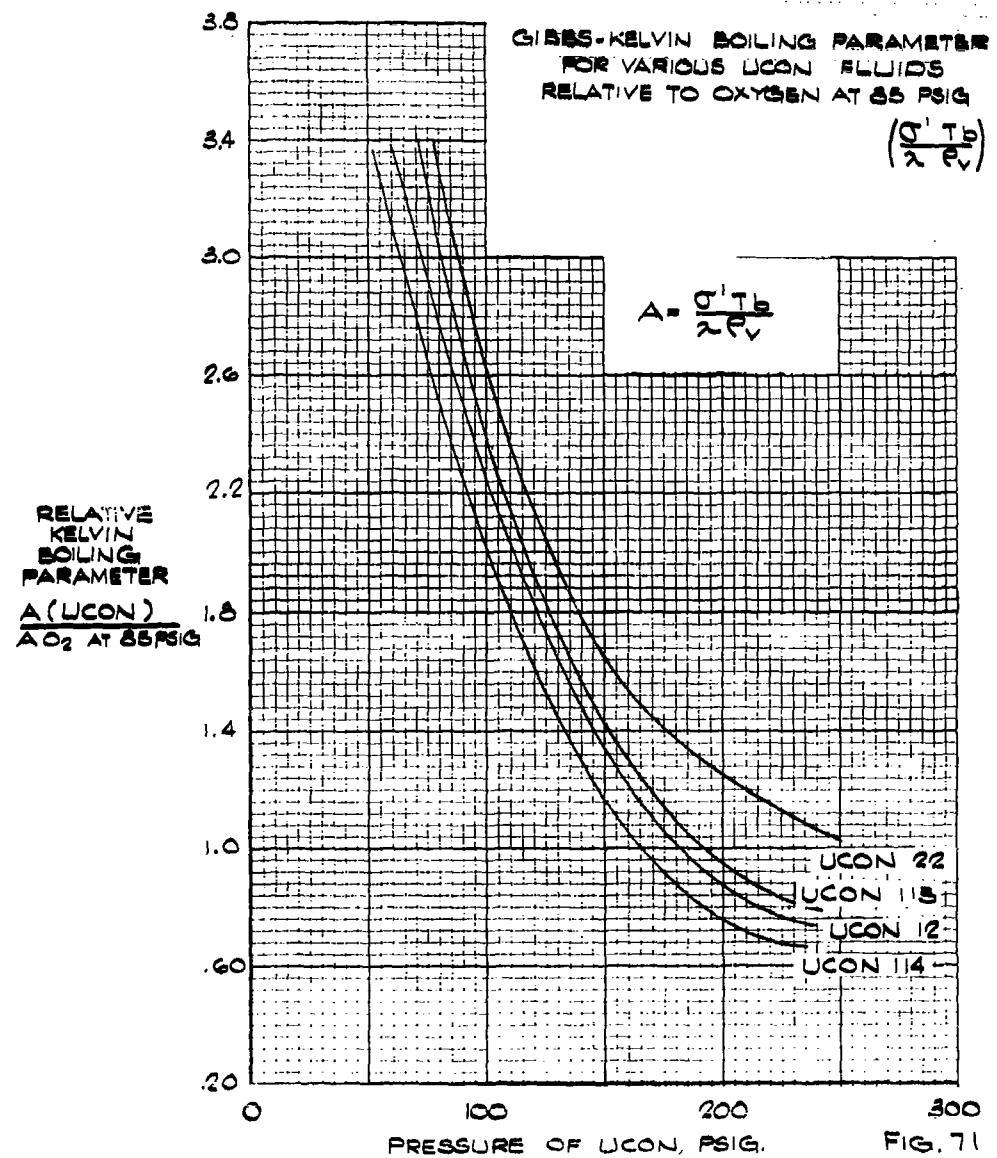
For a particular UCON fluid, the location of the minimum standard deviation is at the UCON pressure where:

$$\frac{\partial (\sqrt{\Sigma \Delta_i^2})}{\partial P} = 0.$$

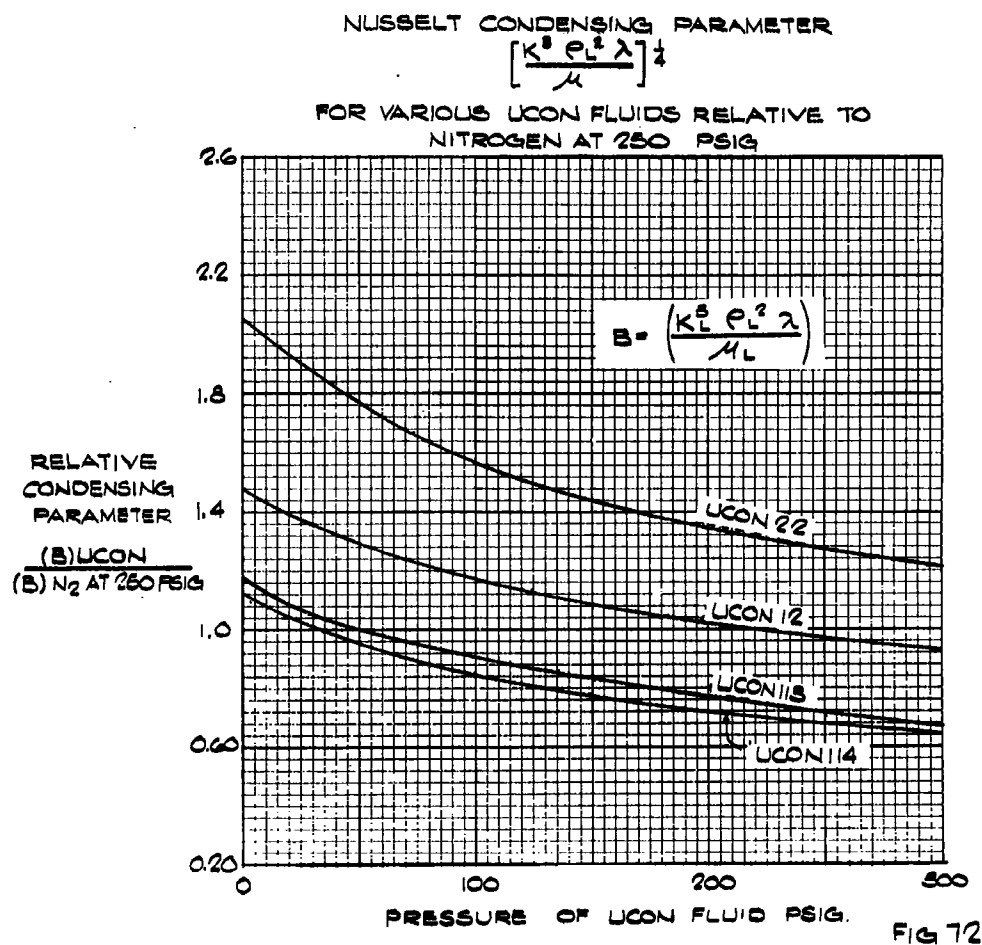
63 ASRP-2391

**CONFIDENTIAL**

ASD-TDR-63-665, Part I



63 ASRP-2391





SQUARE ROOT OF  
THE SUM OF THE SQ.  
OF DEVIATION OF  
FLUID FLOW PARA-  
METERS

$\frac{P_v}{P_L} \frac{\mu_v}{\mu_L} \frac{P_L}{P_v} \frac{P_v}{\mu_v}$   
OF UCONS  
RELATIVE TO OXYGEN

$$\sqrt{\sum \Delta^2}$$

OPTIMUM OPERATING PRESSURES  
FOR UCON FLUIDS RELATIVE TO OXYGEN  
AT 85 PSIG

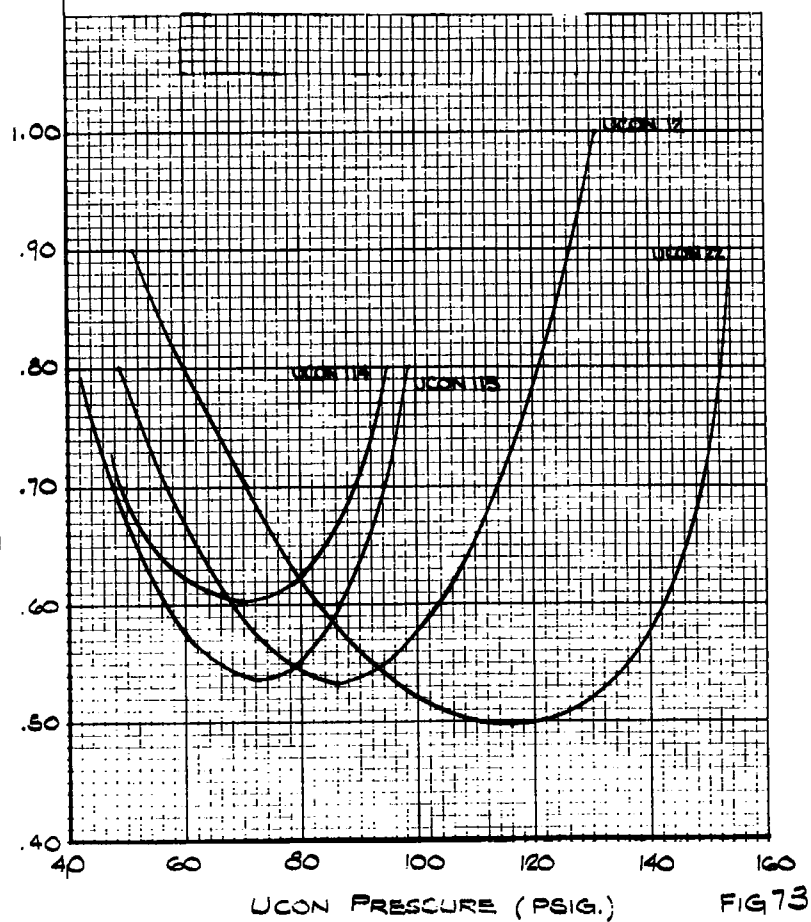


FIG 73

**CONFIDENTIAL**

**ASD-TDR-63-665, Part I**

Examination of these figures showed that UCON 12 gave the best overall match with the pair of cryogenic fluids. The two-phase flow parameters were the least predictable and thus were given preference to the boiling and condensing parameters which can be predicted. UCON 12 is also convenient in that it gives a good match with oxygen at pressures where the UCON 12 saturation temperature is near ambient, minimizing heat leak problems. Finally, suitable temperature driving forces of about 10°F were obtained at conditions consistent with similarity with the cryogenic fluids. A typical operating condition with UCON 12 was 75 psig on the boiling side and 90 psig on the condensing side.

**4.5.5 Experimental Data**

A total of 68 data points were taken. All the data taken is presented in Table 13. A wide range of the operating variables was covered. Rotational speeds varied over the range of 500-1100 RPM (52-115 rad./sec.) or an integrated average transverse acceleration between 80 Ng and 388 Ng. The parallel acceleration along the tube (that utilized for drainage of the tube) varied between 42.5 Ng and 206 Ng.

The average transverse acceleration along a tube can be calculated from the following: (Refer to Appendix VII and Section 4.5.1)

$$\begin{aligned}\overline{Ng_T} &= \frac{\int Ng \sin \psi ds}{\int ds} \\ \overline{Ng_T} &= \frac{\int \frac{r\omega^2}{g} \sin \psi ds}{\int ds} \\ \text{Since } ds &= \frac{r}{r_1} dr \text{ and } \sin \psi = \left( \frac{r^2 - r_1^2}{r^2} \right)^{1/2} \\ \overline{Ng_T} &= \frac{\frac{\omega^2}{g} \int \frac{r}{r_1} (r^2 - r_1^2)^{1/2} \left( \frac{r}{r_1} \right) dr}{\int \frac{r}{r_1} dr}\end{aligned}$$

63 ASRP-2391

**CONFIDENTIAL**

**CONFIDENTIAL**

**ASD-TDR-63-665, Part I**

TABLE 13

PILOT SCALE REBOILER-CONDENSER EXPERIMENTAL DATA

Run	R. P. M.	Ngr	W vap. lbs./min.	Q Btu/min.	Q/A Btu/hr.ft. of tube	P cond. psig.	6" Psi	12" Psi	18" Psi	ΔT °R	% Recycle	Γ°
13	710	161.8	33.5	2041	253.1	71.2	8.09	8.12	8.67	6.51	52.6	0.703*
14	710	161.8	56.0	3581	444.0	76.0	10.55	10.40	10.59	7.95	44.0	1.028*
15	905	262.9	69.2	4349	539.3	80.0	11.33	11.40	12.47	8.96	43.1	1.025*
16	910	265.8	32.6	2041	253.1	69.2	4.49	4.22	4.94	3.54	60.9	1.162
17	1000	321	32.0	1960	243.0	69.2	4.18	3.87	4.55	3.27	60.6	1.169
18	1100	388.4	31.7	1933	240	69.8	4.26	3.89	4.48	3.26	57.9	1.132
19	750	180.6	32.3	2049	254.1	69.0	4.69	4.03	4.99	3.55	60.6	1.232
20	490	77.1	32.2	1998	247.8	68.6	5.56	4.46	3.32	3.96	62.7	1.245
21	800	205.4	51.9	3385	419.7	74.8	8.02	7.95	8.75	6.22	48.1	1.173
22	905	262.9	51.6	3277	406.3	74.6	7.76	7.60	8.58	6.04	48.2	1.122
23	1000	321	51.5	3284	407.2	74.7	7.50	7.43	8.08	5.79	47.7	1.122
24	1100	388.4	51.3	3226	400	74.5	7.04	7.10	7.90	5.55	47.2	1.125
25	595	113.6	51.4	3295	408.6	74.1	8.66	8.51	6.46	6.55	48.9	1.215
26	500	80.3	50.9	3269	405.3	73.2	8.89	8.20	5.55	6.56	49.8	1.27
27	480	74.0	70.5	4473	554.7	80.0	12.45	13.79	15.05	10.17	38.7	1.18
28	600	115.6	70.7	4492	557.0	79.5	12.45	12.81	9.91	9.32	39.0	1.197
29	700	157.3	70.8	4497	557.6	79.7	11.51	12.04	8.53	8.66	39.0	1.205
30	800	205.4	70.7	4494	557.3	79.6	11.00	11.48	7.14	8.24	38.7	1.19
31	900	260	70.8	4492	557.0	80.0	10.97	11.19	6.93	8.10	38.5	1.166
32	1000	321	70.7	4487	556.4	80.0	10.85	10.75	11.59	8.08	38.2	1.127
33	1100	388.4	70.8	4492	557.0	80.2	10.15	10.32	11.32	7.72	37.9	1.14
34	1100	388.4	94.6	5658	701.6	86.5	14.20	14.40	9.50	10.04	37.0	1.12
35	800	205.4	70.6	4256	527.7	79.2	11.10	10.82	6.76	8.06	40.0	1.159
36	800	205.4	51.7	3161	392	74.0	7.48	7.38	7.11	5.53	46.4	1.224
37	700	157.3	33.2	2034	252.2	68.5	4.33	4.20	4.42	3.39	56.5	1.31
38	800	205.4	51.8	3152	390.8	73.0	7.60	7.41	7.85	5.82	50.7	1.164
39	600	115.6	32.0	1940	240.6	69.0	5.99	6.01	6.46	4.85	48.9	.932*
40	600	115.6	30.4	1846	228.9	68.0	5.56	5.25	5.99	4.47	63.4	.964*
41	600	115.6	32.6	1978	245.3	68.5	5.67	5.43	5.99	4.50	70.8	1.027*
42	600	115.6	31.6	1912	237.1	67.7	5.35	5.16	5.41	4.23	77.1	1.066*
43	900	260	31.0	1880	233.1	68.0	4.59	4.79	4.76	3.73	76.5	1.02*
44	900	260	32.3	1956	242.5	68.8	5.27	5.64	5.82	4.65	58.8	.858*
45	900	260	55.3	3578	443.7	75.0	8.71	--	9.58	7.18	44.0	1.04*
46	900	260	56.3	3672	455.3	75.2	8.92	--	9.81	7.10	56.5	1.078
47	900	260	55.9	3460	429.0	75.2	8.71	--	9.81	7.01	28.9	1.03**
48	900	260	54.4	3343	414.5	76.3	--	10.40	10.28	7.79	13.9	.899**
49	1100	388.4	57.8	3556	440.9	76.8	8.34	9.23	9.91	6.82	22.5	1.015**
50	1100	388.4	57.2	3496	433.5	77.8	9.83	10.21	10.41	7.51	14.2	.909**
51	1000	321	57.0	3410	422.8	77.0	9.87	10.19	11.36	7.83	14.0	.880**
52	990	318.1	76.8	4773	591.9	83.3	14.66	14.63	13.33	10.24	10.8	.962**
53	990	318.1	61.3	3886	581.9	77.8	9.42	9.73	10.50	7.31	42.6	1.107
54	600	115.5	32.2	1975	244.9	69.0	7.49	7.39	7.99	6.04	57.9	.778*
55	600	115.5	33.5	2032	252	68.8	6.90	6.55	7.52	5.56	65.1	.866*
56	600	113.5	69.7	4316	535.2	79.2	14.87	14.78	12.81	10.56	41.2	1.024*
57	700	157.3	70.9	4465	553.7	79.8	13.86	13.82	11.12	9.53	43.7	1.093
58	800	205.4	70.8	4472	554.5	79.4	12.63	12.84	9.49	9.43	44.9	1.051
59	900	260	71.3	4512	559.5	79.2	11.44	12.07	9.58	8.67	43.0	1.10
60	1000	321	69.9	4424	548.6	79.0	10.71	11.35	12.02	8.35	30.0	1.072
61	1100	388.4	69.6	4399	545.5	79.6	10.38	11.13	11.78	8.13	29.6	1.063
62	1100	388.4	68.4	4391	544.5	79.2	10.22	10.82	11.55	7.98	41.2	1.08
63	900	260	69.5	4400	545.6	78.5	10.91	11.26	9.22	8.22	41.6	1.128
64	900	260	69.7	4394	544.9	80.0	12.79	12.78	10.05	9.42	20.9	.991*
65	900	260	59.2	4378	542.9	79.0	10.97	11.35	10.52	8.06	44.8	1.142
66	900	260	82.4	5172	641.3	82.2	13.43	13.94	9.34	9.94	41.7	1.11
67	1000	321	81.3	5100	632.4	82.3	12.75	13.10	12.83	9.41	40.9	1.11
68	1100	388.4	82.3	5442	675.7	82.8	12.68	13.14	14.0	9.57	40.4	1.127
69	800	205.4	83.0	5203	645.2	82.3	14.12	14.18	9.81	10.54	42.2	1.106
70	700	157.3	83.5	5224	647.8	82.8	15.14	15.07	11.36	10.97	41.1	1.127
71	600	115.6	83.7	5258	652.1	82.5	15.62	16.39	13.16	11.70	41.6	1.138
72	500	80.3	83.7	5242	650	82.4	16.56	16.21	14.46	12.04	39.0	1.176
75	600	115.6	50.6	3250	403	73.0	8.88	8.73	8.58	6.71	48.9	1.167
76	1100	388.4	94.8	5713	708.4	86.0	14.65	15.55	15.78	10.86	31.6	1.052
77	1000	321.0	94.9	5719	709.0	86.0	15.10	15.71	11.49	10.91	31.4	1.087
78	900	260.0	55.2	2722	339.6	86.0	15.46	16.06	11.46	11.23	31.4	1.102
79	800	205.4	94.6	5698	706.6	85.8	16.14	16.40	12.75	11.60	31.7	1.113
80	690	152.8	96.1	5787	717.6	86.3	17.28	17.54	14.85	12.42	31.1	1.126
81	600	115.6	96.6	5804	719.7	87.2	18.51	18.61	15.28	13.27	30.7	1.125
82	500	80.3	96.0	5750	713.0	88.0	20.0	19.64	18.61	14.10	30.5	1.122

\* Data taken within 2 hours of startup

\*\* Low recycle data

63 ASRP-2391

**CONFIDENTIAL**

**CONFIDENTIAL**

ASD-TDR-63-665, Part I

$$\frac{Ng_T}{g} = \frac{\frac{\omega^2}{g} \int_{r_1}^{r_o} r (r^2 - r_1^2)^{1/2} dr}{\int_{r_1}^{r_o} r dr}$$

$$\therefore Ng_T = \frac{\frac{2\omega^2}{3g} (r_o^2 - r_1^2)^{3/2}}{r_o^2 - r_1^2} = \frac{2\omega^2}{3g} (r_o^2 - r_1^2)^{1/2} \quad (49)$$

As shown before in Section 4.5.1, equation (47) the parallel acceleration is:

$$\frac{r_1 \omega^2}{g}$$

The recycle, or excess liquid to the boiling side over that required for boilup, was varied between 75% and 10%. The heat flux was not uniform around the circumference of a given tube due to the nature of the test apparatus as the tube side not facing the boiling fluid acted as a fin conducting heat to the boiling fluid and an approximately adiabatic surface with respect to the test apparatus adjacent to it. The major portion of the heat transfer took place on the side of the tube which contacted the boiling fluid as on this side of the tube the highest heat flux corresponded to approximately 19,000 Btu/(ft.)<sup>2</sup> (hr.). The lowest heat flux at which it was possible to obtain reliable data was approximately 5,000 Btu/(ft.)<sup>2</sup> (hr.). These heat fluxes corresponded to vapor flow rates to the rotor of 95 and 30 lb./min. respectively. The vapor-liquid seal on the condensing side required an equivalent head of liquid of 5 psi. In order to generate this head with the height of liquid provided in the rotor, the unit must operate at no less than 52 rad./sec. Consequently, no data could be taken below this rotational speed.

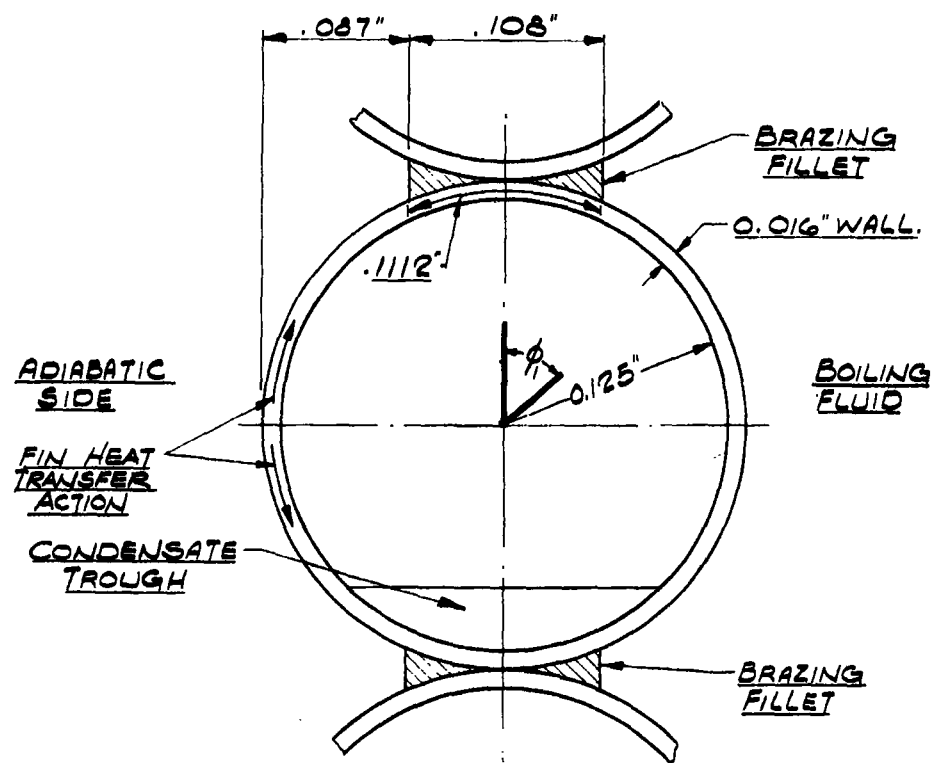
#### 4.5.6 Data Reduction

##### 4.5.6.1 Mathematical Heat Transfer Model

Since only half of each condenser tube was exposed to boiling refrigerant, there was a considerable fin effect as condensation occurred on the unexposed portion of the tube. Due to this fin effect, there was

63 ASRP-2391

**CONFIDENTIAL**



PILOT SCALE REBOILER CONDENSER, UCON FLUID  
TEST ROTOR, TUBE CONFIGURATION

FIG. 74

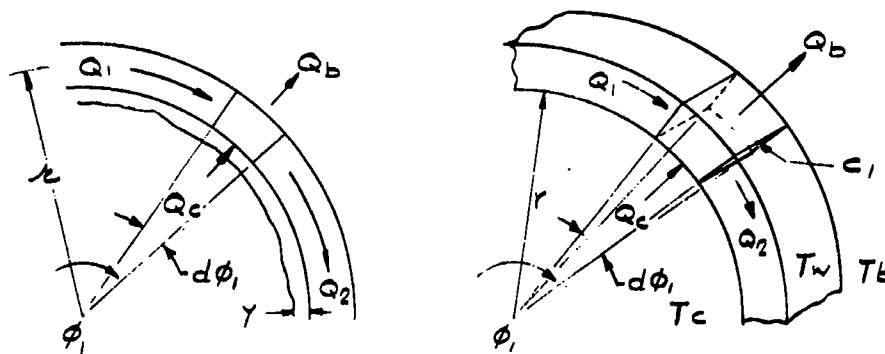
**CONFIDENTIAL**

ASD-TDR-63-665, Part I

a variable wall temperature around the circumference of each tube. In order to interpret the data taken in the test, it was necessary to be able to calculate the heat transferred as a function of the overall temperature difference between the boiling and condensing passages, taking into account the variable wall temperature. One of the condenser tubes with its unsymmetrical environment is depicted in Figure 74.

The analytical equations describing the situation are too complicated to be used conveniently because of the unsymmetrical heat transfer configuration. To define the heat transfer inside the tube, it is necessary to calculate local values of the condensing side  $\Delta T$ , the condensing film thickness and the heat flux. There are two types of heat transfer area within each tube. One type is a fin with one insulated side while the other side is experiencing heat transfer by condensation. The other is primary heat transfer surface, with condensation on one side and boiling on the other. Even with the primary surface, a fin effect occurs, due to the unsymmetrical environment of the tube.

Expressions for the pertinent variables in mathematically describing the situation within a tube in the heat transfer rotor were obtained by starting with a heat balance on an element of the wall of the tube with unit length along the tube, as shown in Figure 75. The mathematical analysis follows:



SKETCH OF TUBE SECTION

FIG. 75

63 ASRP-2391

**CONFIDENTIAL**

**CONFIDENTIAL**

ASD-TDR-63-665, Part I

$$Q_1 + Q_c = Q_b + Q_2$$

$$- \frac{k_m A dt_w}{r d \phi_1} + h_c C_1 (T_c - t_w) r d \phi_1 = h_b C_1 (t_w - T_b) r d \phi_1 - k_m A \left( \frac{dt_w}{r d \phi_1} + \frac{d^2 t_w}{r^2 d \phi_1^2} r d \phi_1 \right)$$

where  $\frac{dt_w}{r d \phi_1}$  is the circumferential temperature gradient.

$$\text{or } -k_m A \frac{d^2 t_w}{r^2 d \phi_1^2} = h_c C_1 (T_c - t_w) - h_b C_1 (t_w - T_b)$$

$$\text{Letting } T_c - t_w = \Theta^\circ \quad \therefore \frac{d(T_c - t_w)}{r d \phi_1} = - \frac{dt_w}{r d \phi_1} = \frac{d \Theta^\circ}{r d \phi_1}$$

Since

$$- \frac{d^2 t_w}{r^2 d \phi_1^2} = \frac{d^2 \Theta^\circ}{r^2 d \phi_1^2}$$

$$k_m A \frac{d^2 \Theta^\circ}{r^2 d \phi_1^2} = h_c C_1 \Theta^\circ - h_b C_1 (t_w - T_b)$$

solving for  $\frac{d^2 \Theta^\circ}{r^2 d \phi_1^2}$  and substituting  $T_c - \Theta^\circ$  for  $t_w$

$$\frac{d^2 \Theta^\circ}{r^2 d \phi_1^2} = \frac{h_c C_1}{k_m A} \Theta^\circ - \frac{h_b C_1}{k_m A} (T_c - \Theta^\circ - T_b)$$

$$\therefore \frac{d^2 \Theta^\circ}{d \phi_1^2} = r^2 \left[ \frac{h_c C_1}{k_m A} \Theta^\circ - \frac{h_b C_1}{k_m A} (T_c - \Theta^\circ - T_b) \right] \quad (50)$$

where  $h_b = B (t_w - T_b)^n$  as shown by Figures 40 and 41

For the case where heat transfer is taking place on one side only (no

63 ASRP-2391

**CONFIDENTIAL**

# CONFIDENTIAL

ASD-TDR-63-665, Part I

boiling fluid in contact with the wall of the tube) the differential equation becomes:

$$\frac{d^2 \Theta}{d \phi^2} = r^2 \frac{h_c C_i}{k_m A} \Theta$$

Assuming that heat transfer through the condensate film is by conduction, the relation between the condensing heat transfer coefficient and this film thickness is given by:

$$h_c = \frac{k_f}{Y}$$

The derivation for Y, the condensing film thickness, is obtained from Hassan and Jakob (Ref. 19) with the following alterations: For conduction through the liquid film of condensed fluid of thickness Y and unit length ( $C_i$ ) along the tube:

$$dQ = k_f \frac{\Theta}{Y} r d\phi$$

Furthermore from the latent heat supply:  $\frac{dQ}{C_i} = d(Y V' \cos \delta \rho \lambda)$  Btu/ft.hr. for unit length along tube.

The angle  $\delta$  and its complement  $\beta$  are shown in Figure 76, along with the relationship to angles  $\alpha$  and  $\psi$ , previously defined. As shown,  $V' \cos \delta$  is the condensate velocity component in the radial direction. It can be shown that  $V'$  is expressed by the following relation (Ref. 19):

$$V' = \frac{\rho Y^2 g N g \sin \beta}{3 \mu}$$

where  $\beta$  is the angle between the flow path and the plane normal to the radius vector.

Substituting:

$$dQ = d \left[ \left( \frac{\rho^2 g N g \lambda}{3 \mu} \right) \sin \beta \cos \delta Y^3 \right]$$

63 ASRP-2391

# CONFIDENTIAL



C

ASD-TDR-63-665, Part I

RELATIONSHIP OF TUBE ANGLES

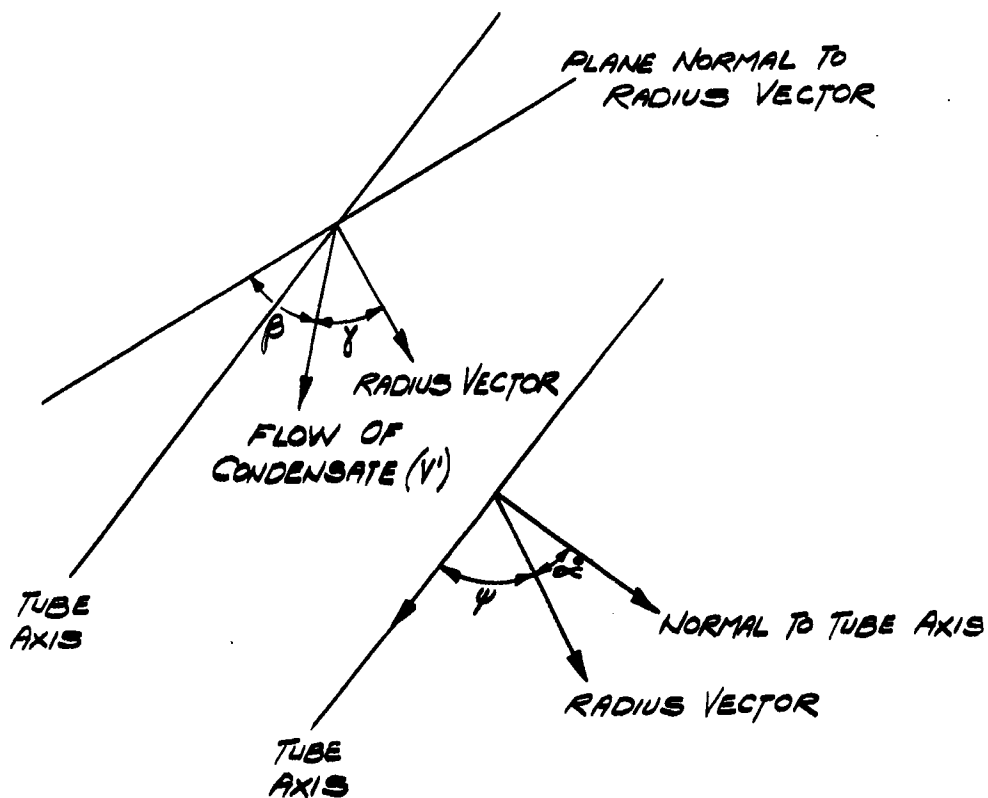


FIG. 76

63 ASRP-2391

**CONFIDENTIAL**

ASD-TDR-63-665, Part I

Jakob has shown

$$\sin \beta \cos \gamma = \cos \alpha^\circ \sin \phi_i \quad (\text{Ref. (19)})$$

where  $\alpha^\circ$  is the angle between the direction of the acceleration field and the normal to the tube axis. Substituting this expression:

$$dQ = d \left( \frac{\rho^2 g N g \lambda}{3 \mu} \cos \alpha^\circ \sin \phi_i Y^3 \right)$$

Performing the differentiation

$$\frac{dQ}{d\phi_i} = \frac{\rho^2 g N g \lambda}{3 \mu} \cos \alpha^\circ \left( \sin \phi_i 3Y^2 \frac{dY}{d\phi_i} + Y^3 \cos \phi_i \right)$$

also

$$\frac{dQ}{d\phi_i} = r k_f \frac{\Theta^\circ}{Y}$$

Solving for the rate of change of the film thickness with respect to the angular distance around the tube:

$$\frac{dY}{d\phi_i} = \frac{\mu k_f r}{\rho^2 g N g \lambda \cos \alpha^\circ} \frac{\Theta^\circ}{Y^3 \sin \phi_i} - \frac{Y}{3} \cot \phi_i \quad (51)$$

The expression for Q, the heat flux, can be written directly from the considerations involved in deriving the film thickness differential equation:

$$\frac{dQ}{d\phi_i} = r \frac{k_f}{Y} \Theta^\circ \quad (52)$$

Equations 50, 51 & 52 form a system of equations which can be integrated simultaneously. The Runge-Kutta numerical integration procedure (Ref. 39) was used as the basis for a computer program (Burroughs 205) by making the following substitution in Equation 50.

63 ASRP-2391

**CONFIDENTIAL**

**CONFIDENTIAL**

ASD-TDR-63-665, Part I

Letting  $\frac{d\Theta^\circ}{d\phi_1} = Z$

$$\therefore \frac{d^2\Theta^\circ}{d\phi_1^2} = \frac{dZ}{d\Theta^\circ}$$

The analysis has produced a system of four first order ordinary differential equations, to which the Runge-Kutta procedure is applicable. In essence the system is:

$$\frac{d\Theta^\circ}{d\phi_1} = f_1$$

where  $f_n = f(\phi_1, \Theta^\circ, Y)$

$$\frac{dZ}{d\phi_1} = f_2$$

$$\frac{dY}{d\phi_1} = f_3$$

$$\frac{dQ}{d\phi_1} = f_4$$

This set of equations is a boundary value problem; therefore, a system of trial and error is necessary to determine the solution. The computer program is described in detail in Appendix IX.

The computer program was used to calculate heat transfer within the rotors for eleven different cases. The pertinent parameters for these cases were obtained from average conditions at which the experimental data was subsequently taken. The parameters common to all the cases were the following:

63 ASRP-2391

**CONFIDENTIAL**

# CONFIDENTIAL

ASD-TDR-63-665, Part I

<u>Physical Properties</u>	<u>Tube Parameters</u>
$P_b = 65 \text{ psig}$ $T = 526^\circ\text{R}$	$r = 0.01233 \text{ ft.}$
$P_c = 78.4 \text{ psig}$ $T = 536^\circ\text{R}$	$A_{fin} = 0.001333 \text{ ft.}^2$ (wall thickness of 16 mil.)
$\lambda = 59.5 \text{ Btu/(lb.)}$	$C_l = 1 \text{ ft.}$
$\rho_L = 92.0 \text{ lb./(ft.)}^3$	$k_m = 93 \text{ Btu/(hr.)(ft.)(}^\circ\text{R)}$ (aluminum)
$\mu_L = 0.620 \text{ lb./(ft.)(hr.)}$	
$k_L = 0.0498 \text{ Btu/(hr.)(ft.)(}^\circ\text{R)}$	
$h_b = 4100 (\Delta T_b)^{.54} \text{ Btu/ft.}^2\text{hr.}^\circ\text{R}$	

Cases 1 - 4 determined the effect of variations in the transverse acceleration; cases 5 - 7, the effect of the condensate blanketing angle; and cases 8 - 11, the effect of changing the overall  $\Delta T$ . Table No. 14 lists the results of these computer calculations. The heat transfer calculated in Btu/ft.hr. per tube is the total heat transfer of the tube per foot of length.

TABLE 14

## THEORETICAL HEAT TRANSFER IN UCON FLUID TEST ROTOR

<u>Case</u>	<u><math>\overline{N}_{gt}</math></u>	<u><math>\overline{\phi}</math> degrees</u>	<u><math>\Delta T_o</math> <math>^\circ\text{R}</math></u>	<u><math>\overline{Q}</math> Btu/(hr.)(ft.) per tube</u>
1	75	10°	10	480.4
2	174	10°	10	556.9
3	275	10°	10	603.7
4	400	10°	10	644.3
5	275	20°	10	597.8
6	275	30°	10	591.4
7	275	50°	10	572.6
8	75	10°	5	252.8
9	275	10°	5	312.3
10	75	10°	15	691.9
11	275	10°	15	874.3

63 ASRP-2391

# CONFIDENTIAL

# CONFIDENTIAL

## ASD-TDR-63-665, Part I

Figure 77 plots cases 1-4, showing the effect of variation in the transverse acceleration. The effect of varying the condensate blanketing is shown in Figure 78 (cases 3, 5-7). A blanketing angle of  $50^\circ$  corresponds to 13.9% of the circumference of the tube, but results in only 5.2% reduction of the heat transfer when compared to the standard case of a blanketing angle of  $10^\circ$ . This is reasonable since the condensate trough is formed over that portion of the tube where the film on the walls is the thickest. The relationship between the blanketing angle and the relative rates of heat transfer as shown in Figure 78 was assumed to apply at all values of  $Ng$  and  $\Delta T_{\text{overall}}$ .

The magnitude of the blanketing angle as a function of the condensate flow rate and the acceleration directed parallel to the condenser tubes (calculated by means of equation (47), Section 4.5.1) was determined by the Chezy formula. This derivation is given in Appendix VI. Point values of the angle subtended on the circumference of the tube by accumulated condensate were calculated by the Chezy formula and plotted as a function of the flow rate of condensate for rotational speeds of 500, 700, 900, and 1100 rpm (52.3, 73.3, 94.2, 115.2 rad./sec.). With the assumption that the condensate flow rate changes linearly along the length of the tube, the average blanketing angle was obtained as the integrated values over the length of tube.

Given the curves for calculated point values of  $\phi'$  versus  $Ng$  and flow rate and that:  $w = \text{constant (s)}$  ( $w = 0$  at beginning of tube).

$$\bar{\phi}' = \frac{\int \phi' dw}{\int dw}$$

Now,

$$dw = \text{constant (ds)}$$

$$\therefore \bar{\phi}' = \frac{\text{constant} \int \phi' ds}{\text{constant} \int ds} = \frac{\int \phi' ds}{\int ds}$$

Therefore:

$$\bar{\phi}' = \frac{\int \phi' dw}{\int dw} = \frac{\int \phi' ds}{\int ds}$$

so integration of the  $\phi'$  curves given, in the above fashion, for each rotational speed will yield a proper  $\bar{\phi}'$  over the tube length. This integration is performed graphically. (Ref. 23, p.90) 63 ASRP-2391

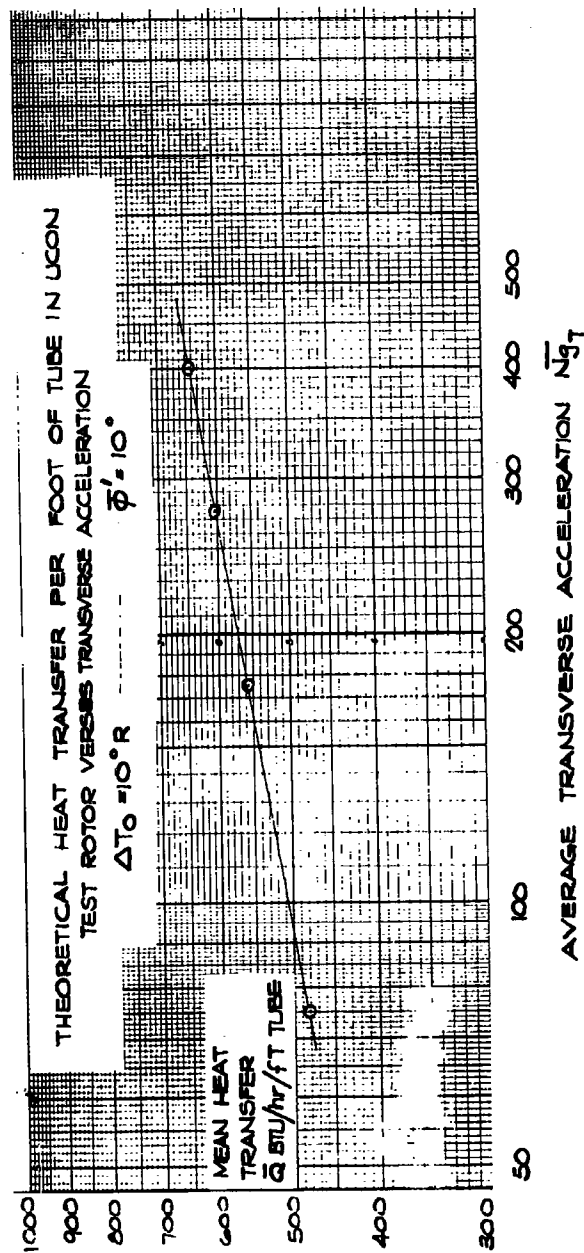


FIG. 77

63 ASRP-2391

ASD-TDR-63-665, Part I

THEORETICAL REDUCTION OF HEAT TRANSFER IN UCON  
FLUID TEST ROTOR DUE TO CONDENSATE BLANKETING.  
AVERAGE TRANSVERSE ACCELERATION  $\bar{N}_g = 275$

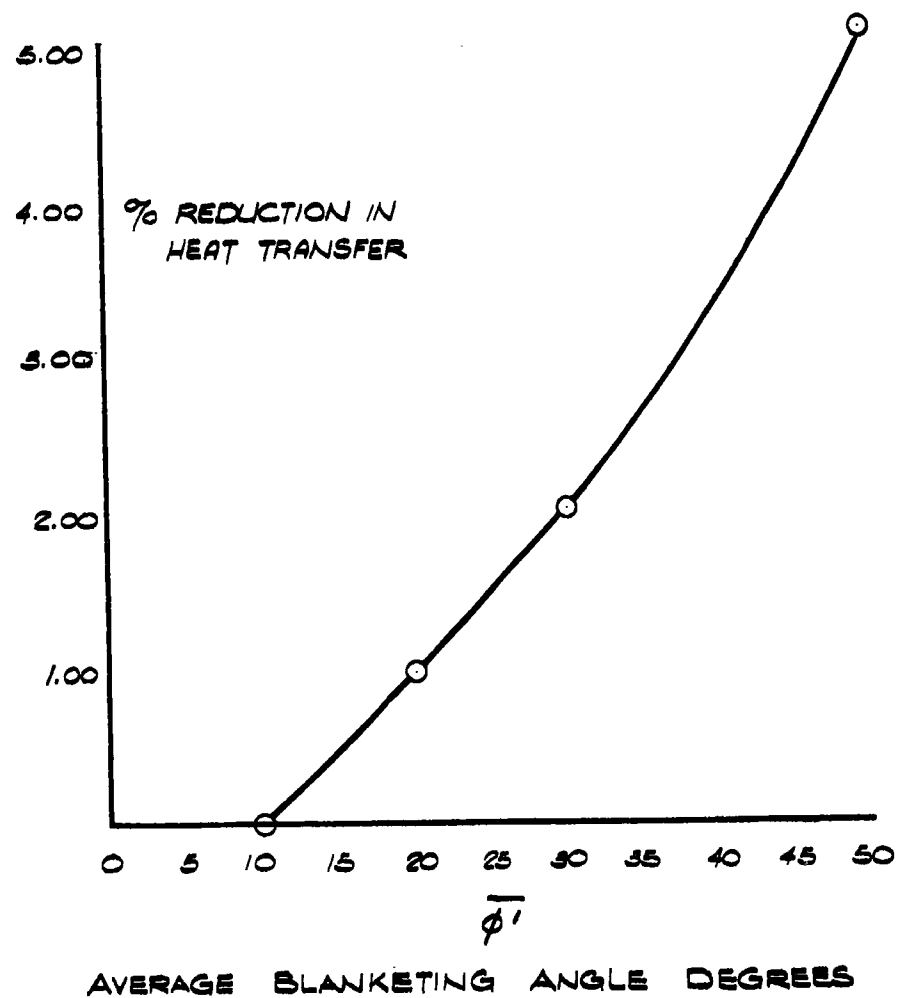


FIG. 78

63 ASRP-2391

# CONFIDENTIAL

ASD-TDR-63-665, Part I

The results of these calculations are shown in Figure 79.

The variation of heat flow in the UCON rotor as a function of the total temperature difference between boiling and condensing fluids depends upon the fraction of the total temperature difference split between the two resistances on the condensing and boiling sides. The Nusselt correlation for condensing heat transfer indicated the rate of heat transfer within the tube was proportional to the temperature difference between the vapor and the walls of the tube raised to the 3/4 power since the film coefficient is a function of  $\Delta T^{1/4}$ . However, the rate of heat transfer on the exterior of the tubes was proportional to the temperature difference between the wall and the fluid raised to the 1.54 power. This relation was determined from data taken on the special boiling surface with UCON - 12 at elevated pressures. This data was represented by the following equation: which defines a curve (not shown) on Figure 42 for boiling at the pressures (65-70 psi) deduced from Table 13.

$$Q/A_b = 4100 (\Delta T)_b^{1.54} \quad (53)$$

The results of the computer calculations (cases 1, 3, 8 - 11) dealing with the effect of the overall temperature difference on  $Q$ , were expressed in terms of Equation 54.

$$\bar{Q}_{\Delta T_o} = \bar{Q}_{10^\circ} \left( \frac{\Delta T_o}{10} \right)^m \quad (54)$$

$\bar{Q}_{10^\circ}$  was the heat flow at a  $\Delta T_o = 10^\circ$ ,  $\bar{\phi}' = 10^\circ$  and a given  $N_{gt}$ .  $\bar{Q}_{\Delta T}$  was the heat flow at identical conditions except for  $\Delta T_o$ .  $\bar{Q}_{10^\circ}$  is shown in Figure 77. The computer results, as shown in Figure 80, indicated that  $m$  in equation (54) varied between 0.90 and 0.96. The same results are cross plotted in Figure 81.

63 ASRP-2391

CONFIDENTIAL



THEORETICAL MEAN BLANKETING ANGLE IN UCON  
FLUID TEST ROTOR TUBES

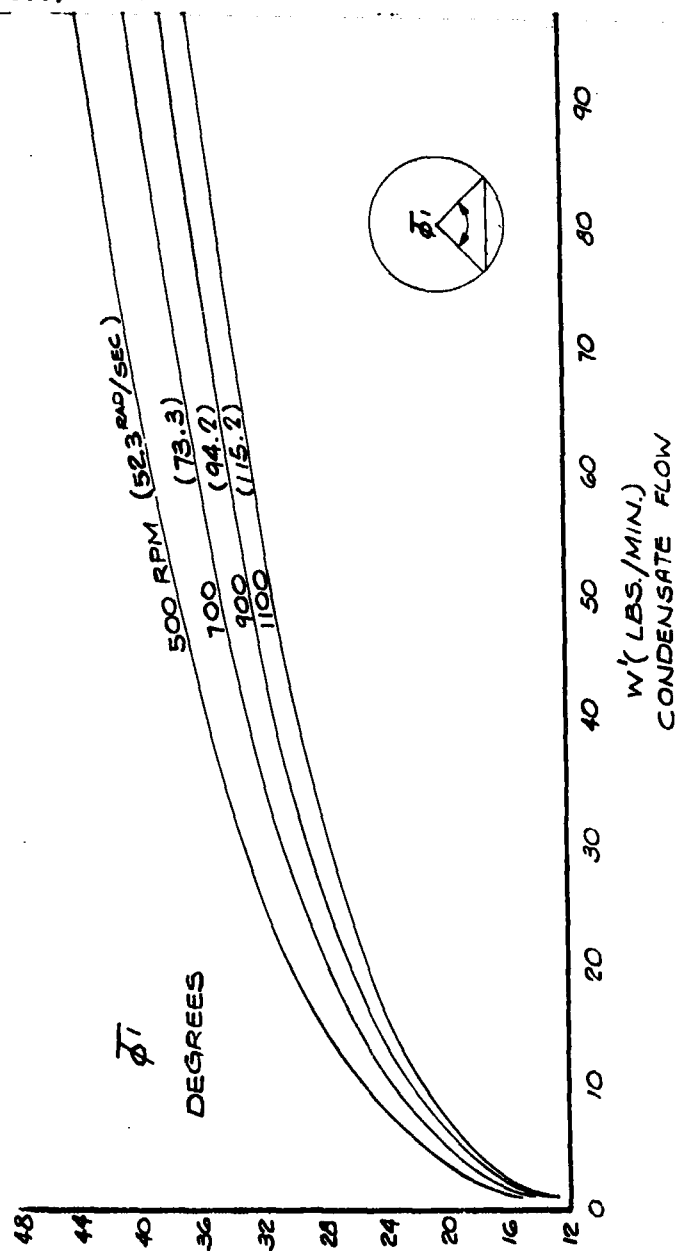
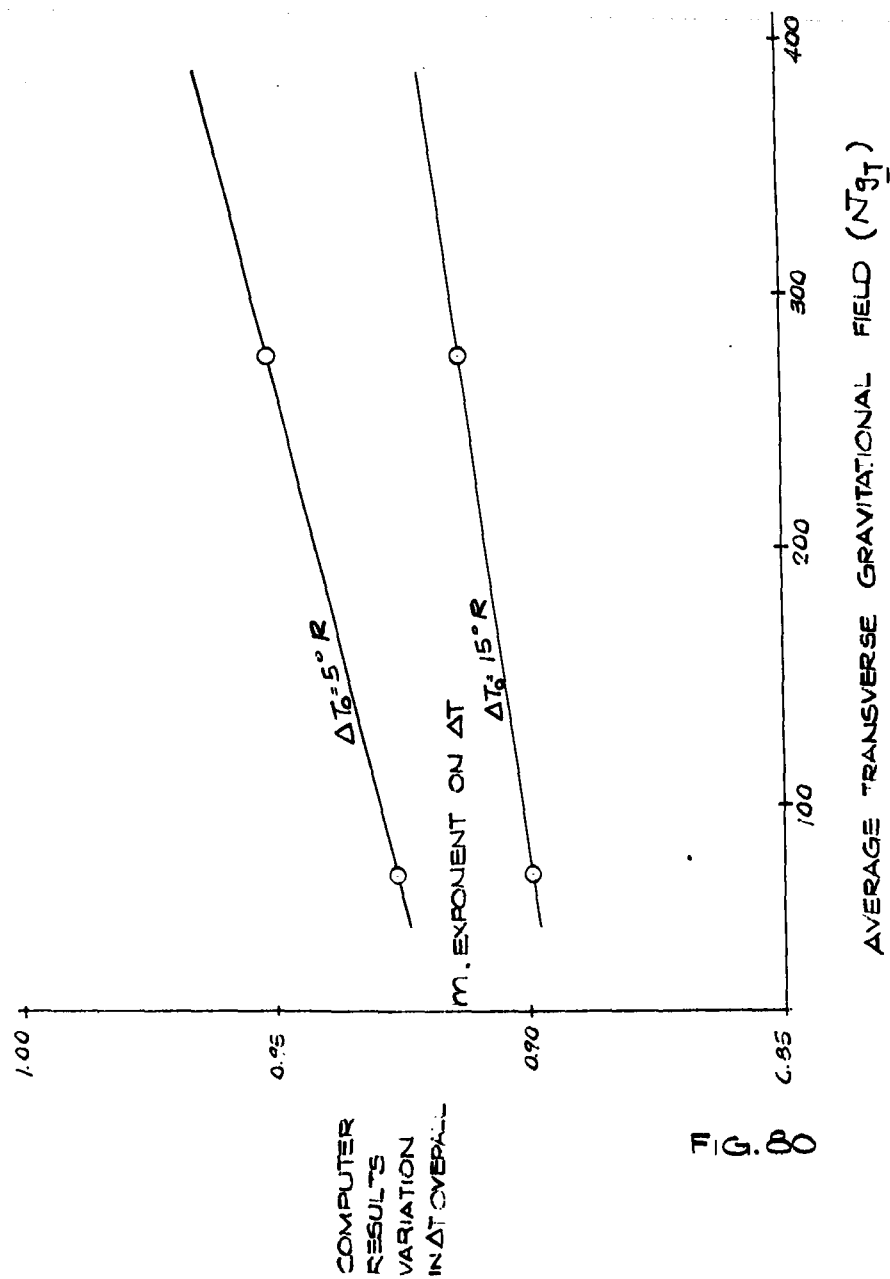


FIG. 79

63 ASRP-2391

DETERMINATION OF EXPONENT,  $m$ , FOR THEORETICAL  
HEAT TRANSFER IN TEST ROTOR WHERE  $\overline{Q}_{\Delta T_0} = \overline{Q}_{\Delta T_0} \left( \frac{\Delta T_0}{10} \right)^m$   
AND  $\phi = 10^\circ$



DETERMINATION OF EXPONENT  $m$  FOR  
THEORETICAL HEAT TRANSFER IN TEST ROTOR

WHERE:  $\bar{Q}_{\Delta T_0} = \bar{Q}_{10} \cdot \left(\frac{\Delta T_0}{10}\right)^m$

AND:  $\phi = 10^\circ$

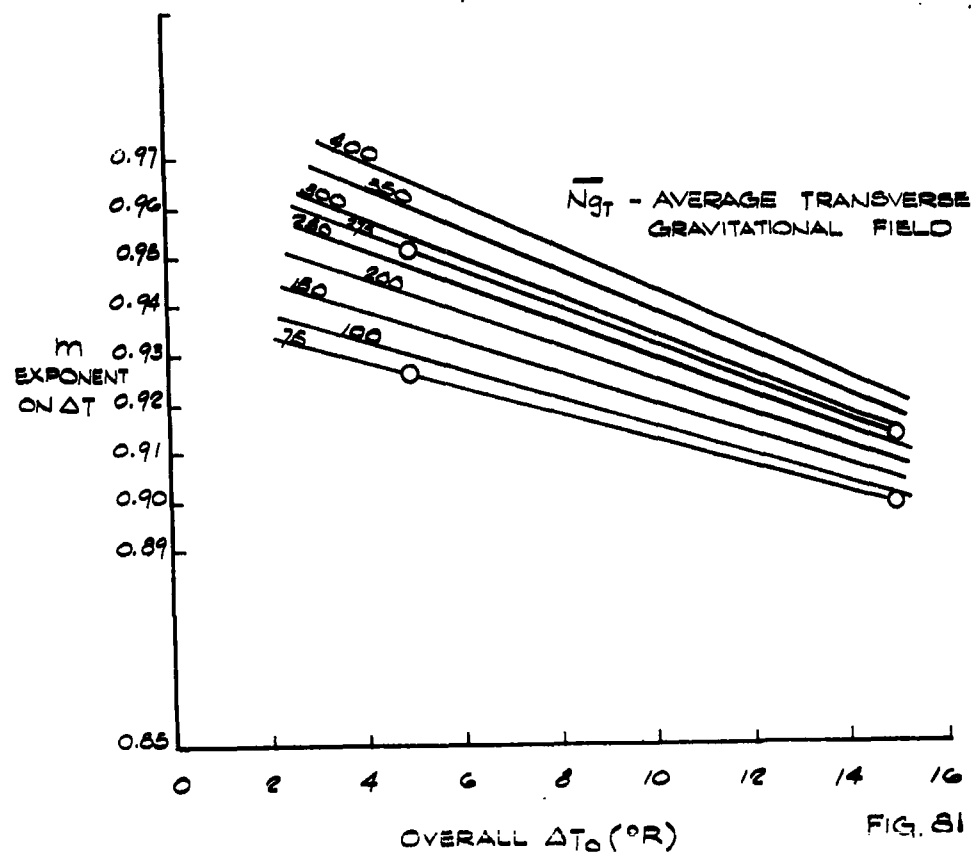


FIG. 81

ASD-TDR-63-665, Part I

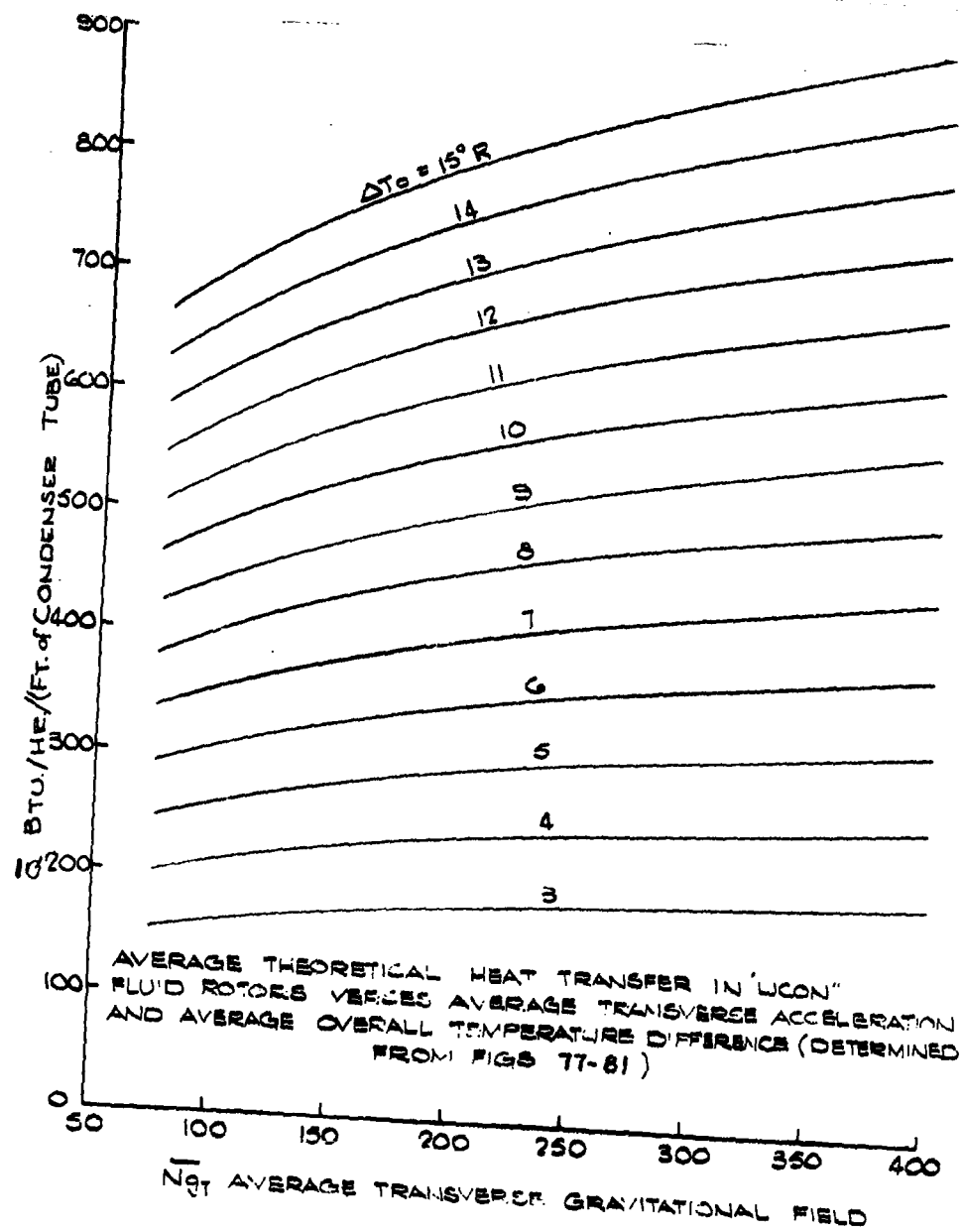


FIG. 82

63 ASRP-2391

CONFIDENTIAL

ASD-TDR-63-665, Part I

Figure 82 shows the mean heat flow in the UCON reboiler-condenser,  $\bar{Q}$ , as a function of the average temperature difference  $\Delta T_o$  and average transverse acceleration  $\bar{N}g_t$ . The mean blanketing angle was a function of  $\Delta T_o$  and  $\bar{N}g_t$  as shown in Figure 79 where  $\Delta T_o$  is represented by the condensate flow rate.

Figure 82 was developed as follows:

In Figure 77  $\bar{Q}_{10^\circ R} = \text{Function}(\bar{N}g_t)$  where  $\Delta T_o = 10^\circ R$ ,  $\bar{\Phi}' = 10^\circ$ ,  $\bar{Q}$  is the average heat transfer per foot of tube.

From Figure 81,  $\bar{Q}_{\Delta T_o}$  was calculated, as here  $\bar{Q}_{\Delta T_o} = \bar{Q}_{10^\circ R} \left(\frac{\Delta T_o}{10}\right)^m$ . Thus for a given  $\bar{N}g_t$ ,  $\bar{Q}_{10^\circ R}$  is known from Figure 77, and  $m$  is known for each  $\Delta T_o$  selected, so therefore,  $\bar{Q}_{\Delta T_o}$  is known.

The flow of condensate could then be calculated as  $W' = \frac{\bar{Q}_{\Delta T_o} S}{\lambda}$  where  $\lambda$  and tube length ( $S$ ) are known.

Using Figure 79, the mean condensate blanketing angle  $\bar{\Phi}'$ , could be determined for each  $\bar{N}g_t$  and the condensate flow rate.

Using Figure 78,  $\bar{Q}_{\Delta T_o}$  was corrected for condensate blanketing. The flow of condensate is determined again, then the blanketing angle  $\bar{\Phi}'$ , and  $\bar{Q}_{\Delta T_o}$  is corrected again. This procedure is continued until no further correction on  $\bar{Q}_{\Delta T_o}$  is necessary.

#### 4.5.6.2 Analysis of Experimental Heat Transfer Data

The computer program gave a rigorous prediction of the local rate of heat transfer when the local values of acceleration, overall temperature difference and level of accumulated condensate were specified. This program could be used to calculate the average rate of heat transfer in a rigorous way, by numerical or graphical integration using a number of radial increments, each calculated using the correct local values of the variables. However, the results reported herein were obtained by using the computer program with average values of the acceleration, temperature difference, and

63 ASRP-2391

CONFIDENTIAL

**CONFIDENTIAL**

ASD-TDR-63-665, Part I

condensate level. Estimates of the difference between the two methods indicated that the agreement was good, making it unnecessary to apply the more lengthy method to each run.

The average acceleration for each run was determined by integration of the centrifugal component perpendicular to the tube axis along the length of the tube. This integral divided by the total length of the tube resulted in the integrated average transverse acceleration utilized for stripping the condensate from the walls of the tube. For convenience, a mean radius on the rotor was defined such that the total centrifugal acceleration at that point was equal to this average transverse acceleration over the whole length of the tube.

$$\omega^2 r_m = \frac{\int_{r_1}^{r_o} \omega^2 r \sin \psi ds}{s} = \omega^2 \frac{2}{3} \sqrt{r_o^2 - r_1^2} \quad (11)$$

Since

$$r_o = 3 r_1 = 18"$$

$$r_m = 11.31"$$

(The derivation of this equation is shown in section 4.5.5)

The average temperature difference was determined for each run by assuming the liquid and vapor were saturated at all points along the rotor. The three transducers located at 6 in., 12 in., and 18 in. radial locations indicated the pressure difference between the condensing and boiling fluids. These transducer readings were averaged and the corresponding  $\Delta T$  obtained from the vapor pressure-temperature relationship of UCON-12. For those runs where the  $\Delta T$  decreased at the outer periphery the average of the two inner readings was used. The procedure was followed because the decrease in the temperature difference occurred near the periphery of the rotor and was not representative of much of the active heat transfer area.

4.5.6.3 Comparison of Experimental Data with Theoretical Model

The experimental data are shown in Table 13. The final results are reported as the ratio of experimental to calculated heat transfer rates. This ratio, which in essence is an improvement factor applied to Nusselt's analysis for condensation of UCON fluid inside a tube, is presented in Figure 83, as a function of the average transverse gravitational field. This factor varies between approximately 1.21 and 1.10 over the range of accelerations equal to 75-400 Ng. Figure 83 presents experimental proof

63 ASRP-2391

**CONFIDENTIAL**

CONFIDENTIAL

C

ASD-TDR-63-665, Part I

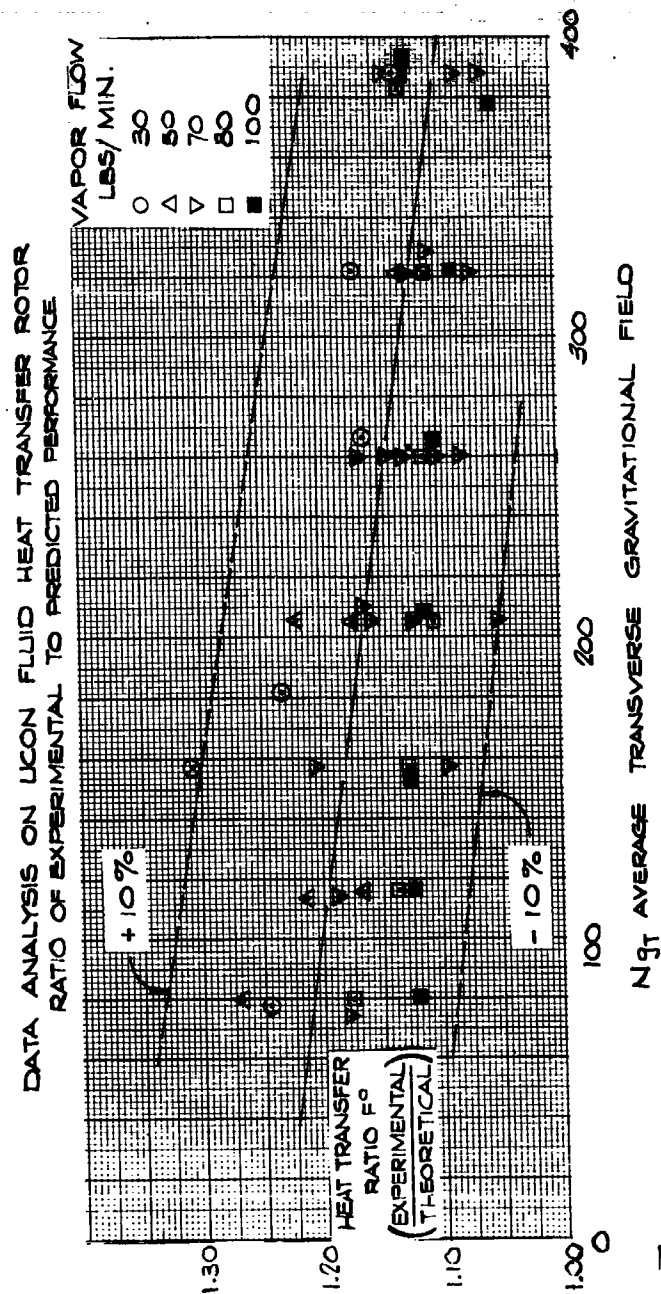


FIG. 83

63 ASRP-2391

CONFIDENTIAL

**CONFIDENTIAL**

**ASD-TDR-63-665, Part I**

of the value of the special boiling surface and condensation at high  $Ng$ . Of the 68 data points taken on the rotor, 48 are presented on this graph. The other 20 points are not presented on the plot of the performance for the following reasons. It was observed that the heat transfer performance improved after startup, taking about two hours to reach steady state.

This effect can be observed in runs 39-42 where data taking was started shortly after liquid was introduced to the rotor. With no change in the operating condition the  $F^\circ$  factor increased from 0.93 to 1.07 over a period corresponding to approximately one hour. On several subsequent days data was taken during this initial period to determine the duration and magnitude of the transient effect. It was concluded that after two hours there was no further change in performance. There did not appear to be a hysteresis effect. Tests were made in which the over-all  $\Delta T$  was increased, followed by a return to the previous value with no increase in performance over that expected from the interval of time elapsed. Whether the cryogenic reboiler-condenser would require an induction period will be determined in a future experimental program. The data points taken less than 1-1/2 hours after startup were Run No. 13-15, 39-45, and 54-56.

The recycle rates (the liquid supplied in excess of the boilup, expressed as a percentage of the total liquid) was varied from 10 to 75 per cent. When the recycle liquid dropped below 30 per cent, the performance dropped off. It was expected that there would be a lower limit on the allowable recycle liquid. There are several factors that could explain the poorer performance at low recycle. Portions of the boiling surface may actually have run dry due to imperfections in the liquid distribution. With a higher percentage of excess liquid, slight maldistribution of the liquid would not be harmful. There also could be deposition of oil or grease on the boiling surface since there was only a small quantity of liquid left at the outer portion of the rotor, in which the nonvolatiles would be concentrated. Those data points taken with a recycle rate of less than 30 per cent are runs 47-52 and 64.

Since, as shown in Section 4.5.4, UCON-12 was chosen to best simulate  $O_2-N_2$  conditions, it is expected that the same results obtained in the UCON heat transfer rotor studies would prevail in a cryogenic rotating air separator reboiler-condenser.

The UCON test rotor heat transfer studies were undertaken to verify the improvement shown in the pool boiling and high-G cryostat studies. Figure 83 provides verification of this improvement.

63 ASRP-2391

**CONFIDENTIAL**



**CONFIDENTIAL**

**ASD-TDR-63-665, Part I**

Since the UCON test rotor experiments were made for verification purposes, design work should use the film coefficient correlations for boiling on the special boiling surface and the condensing film coefficient improvement curves for the porous condensing surfaces along with the basic Nusselt equation for a condensing film coefficient corrected for blanketing angle and gravitational field. Section 6, the Preliminary Design and Analysis section of this report, will present a procedure for use of heat transfer equations in design of a cryogenic reboiler-condenser.

**4.5.6.4 Fluid Flow**

Three strain gauge differential pressure transducers were located along the UCON heat transfer disks at three different radial locations as discussed previously. The high pressure ports were connected to the inside of the condenser tubes at these radial locations. The low pressure or reference chambers were connected to the 3/16 in. annular space between the rotors. With this arrangement a direct reading of the pressure difference between the inside and outside of the condenser tubes was obtained at three different locations along the length of the tube. The pressure profile on the interior of the tubes was calculated for different UCON fluid pressures. This pressure rise through the condenser tubes was caused by the hydrostatic head of the vapor under high gravitational fields. At the maximum flow rates of vapor encountered in the experimental work, the frictional drop through the tubes was negligible. Similarly, the pressure drop due to conversion of the liquid to vapor and the resulting increase in velocity, was negligible. The calculated pressure rise within the tubes is shown in Figure 84. The angular velocity of the vapor was known at all points along the tubes since the vapor is brought to the rotational speed of the rotor at all points by the tubes.

The pressure rise in the annular space between the tube disks between the inlet and outlet was obtained from the pressure transducers mounted at the 6 in. and 18 in. radial location. The pressure rise in the boiling passage was derived by calculating the condensing side pressures at each end of the tube and correcting to boiling side pressure with the transducer  $\Delta P$  measurements. The condensing side  $\Delta P$  can be calculated since it is a single phase fluid - the boiling fluid is a two-phase mixture.

63 ASRP-2391

**CONFIDENTIAL**

PRESSURE BUILDUP IN  
CONDENSING PASSAGE

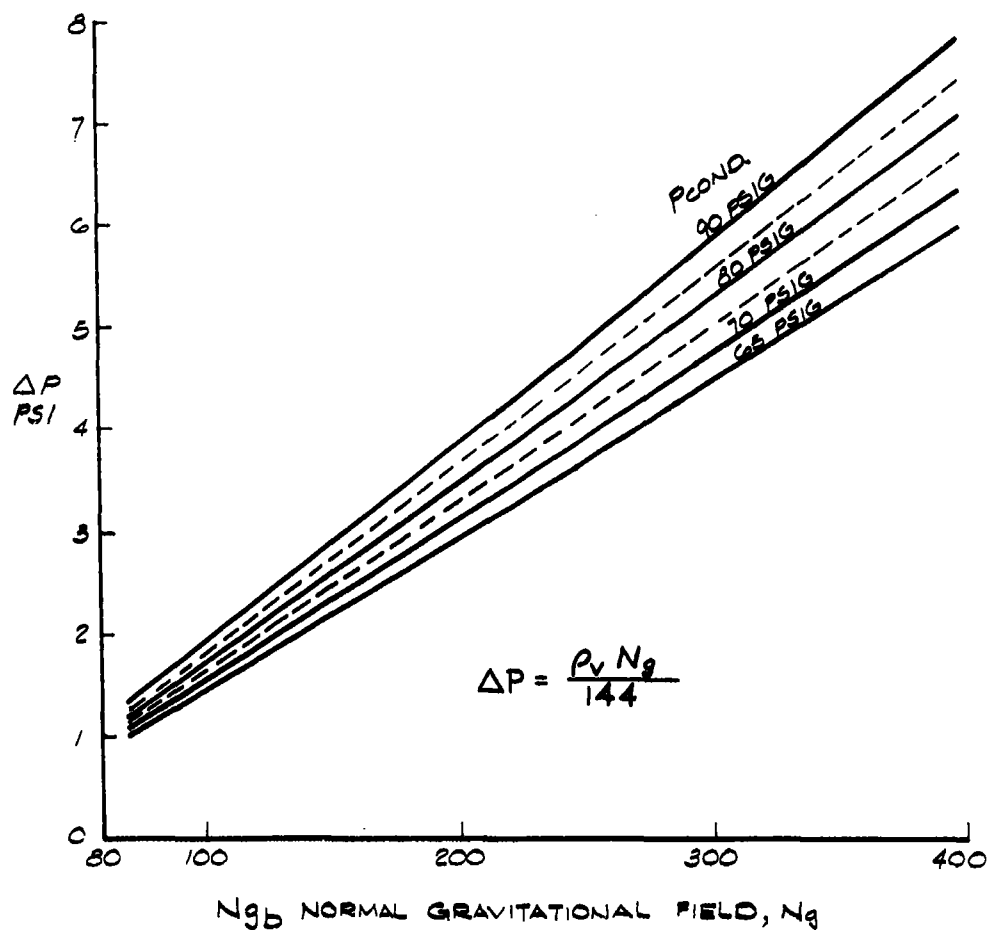


FIG. 84

**CONFIDENTIAL**

C

ASD-TDR-63-665, Part I

$$\begin{aligned} (P_{\text{outlet}} - P_{\text{inlet}})_{\text{boiling passage}} &= (P_{\text{outlet}} - P_{\text{inlet}})_{\text{cond. passage}} \\ &\quad \text{calculated} \\ &\quad + (\Delta P_{\text{inner}} - \Delta P_{\text{outer}})_{\text{transducer}} \end{aligned}$$

All the data taken on the UCON reboiler-condenser was divided into five groups according to the boilup vapor rates. The pressure rise in the boiling passage as a function of normal average centrifugal acceleration is presented in Figure 85. The normal average gravitational field for the boiling passage is defined as follows:

$$\overline{Ng}_b = \frac{\int \omega^2 r \, ds}{\int ds} \quad \text{(Refer to Appendix VII Section 4.5.1 and 4.5.5)}$$

Since the fluid flow in the boiling passage is directed radially outward.  $ds = dr$

$$\therefore \overline{Ng}_b = \frac{\int r \omega^2 \, dr}{\int dr}$$

$$\overline{Ng}_b = \frac{\frac{\omega^2}{2} [r_o^2 - r_i^2]}{r_o - r_i} = \frac{\frac{\omega^2}{2} [r_o + r_i] [r_o - r_i]}{[r_o - r_i]}$$

$$\therefore \overline{Ng}_b = \left( \frac{r_o + r_i}{2} \right) \omega^2 \quad (55)$$

In this case, the mean radius is the arithmetic average of the inner and outer radii. It was observed that for about one third of the runs, the pressure difference between the condensing and boiling streams was considerably less at the 18 in. radial location than at either the 6 in. or 12 in. location. In all the runs, the pressure in the boiling passage increased as the radial distance increased. In most runs, the pressure rise was slightly less than that calculated for a hydrostatic head rise assuming a vapor core having the angular velocity of the rotor. This was consistent with a small amount of slip between the vapor and the rotor, needed to bring the vapor to the angular velocity of the rotor. In the minority of runs mentioned

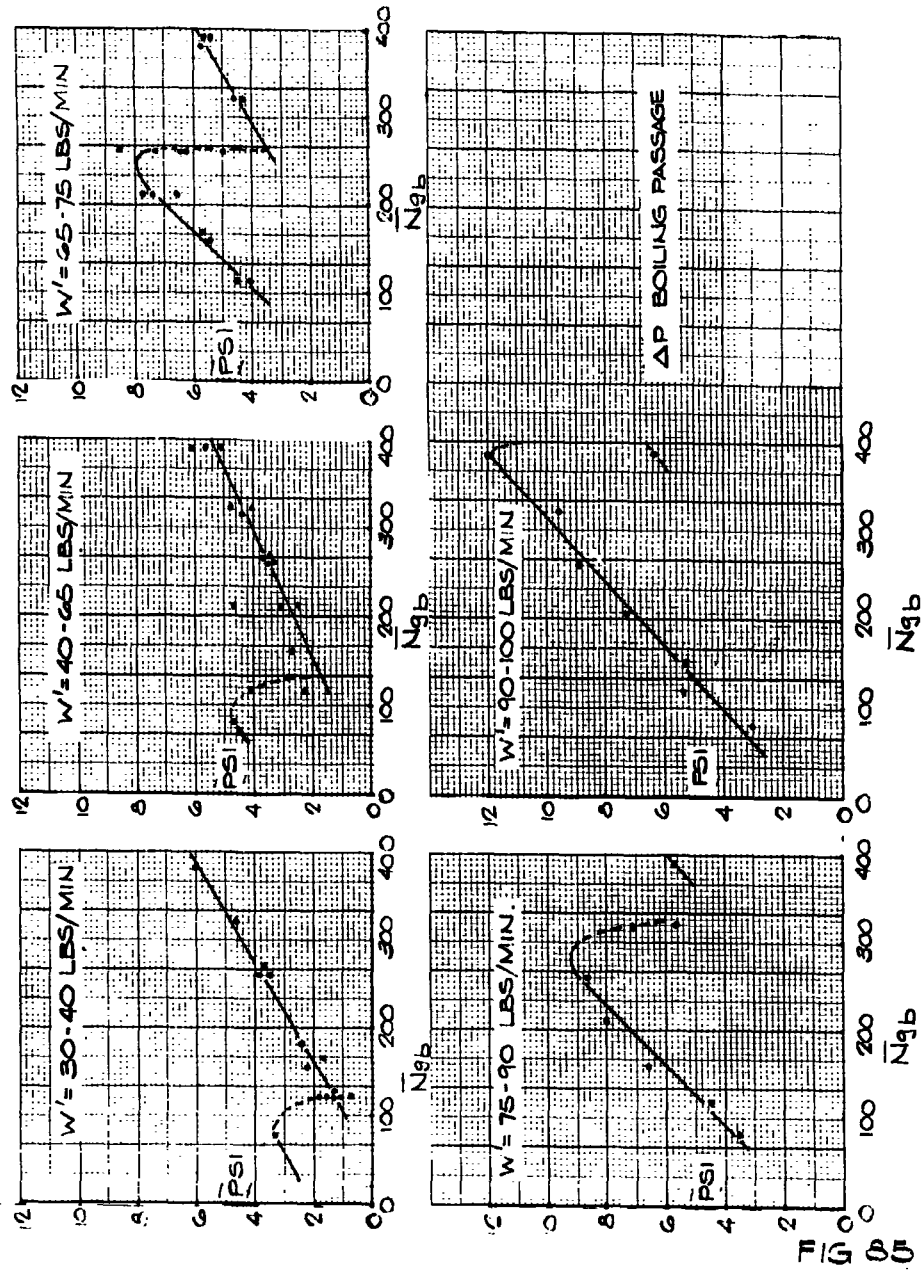
63 ASRP-2391

**CONFIDENTIAL**

CONFIDENTIAL

ASD-TDR-63-665, Part I

PRESSURE RISE IN THE BOILING PASSAGE VERSUS  
BOILUP VAPOR FLOW AND AVERAGE GRAVITATIONAL FIELD



63 ASRP-2391

CONFIDENTIAL

**CONFIDENTIAL**

**ASD-TDR-63-665, Part I**

above, the pressure rise in the outermost part of the rotor became greater than the calculated vapor hydrostatic head.

It was also observed that for each boilup rate, there was a distinct discontinuity in the relation between pressure drop through the boiling passage and  $Ng_b$ , as shown in Figure 85. This transition point occurred at larger accelerations for the higher boilup rates. The runs with a high value of pressure rise in the boiling passage at the outermost part of the rotor were those which established the curve at that side of the transition point at which high over-all  $\Delta P$ 's through the boiling passage occurred. All such runs occurred at low  $Ng_b$  for a given boilup rate.

A suggested explanation for these results is as follows. In most cases, segregated flow was maintained in the boiling passage, with the vapor flowing as a core in the center of the passage, between two films of liquid. Vapor generated as the fluid traveled radially outward tended to entrain liquid, and in some cases enough liquid was entrained to allow development of the bubble or slug modes of two-phase flow at the outer edge of the rotor. The average density of the two-phase mixture was greater than that of vapor, and thus, the hydrostatic head developed was greater. Evidently, higher flow rates tend to favor development of mixed flow and higher  $Ng_b$  tends to oppose it, with the net results shown in Figure 85.

The trend of the transition points in Figure 85 is shown in Figure 86. Smoothed results in the pressure drop through the boiling passage are shown in Figure 87. For the UCON rotor tested, with a spacing of 3/16 in. between crests of opposing tubes in the tube sheets, two-phase mixed flow was encountered for the entire range of centrifugal accelerations at vapor boilup rates of 90 lb. per min., while a segregated vapor core was maintained for practically all accelerations at vapor boilup rates of 30 lb. per min. The intermediate boilup rates exhibited transitions between these two extremes.

Since the reasons for this unusual two-phase flow behavior are not yet understood, it is impossible at this time to predict under what conditions mixed flow (nonsegregated) will occur when boiling oxygen. It should be pointed out that the occurrence of mixed flow at the outer periphery of the rotor is beneficial from a heat transfer standpoint in that it effectively increases the average over-all temperature difference in the reboiler-condenser. Because of this, further work should be done to promote a better understanding and thus allow exploitation.

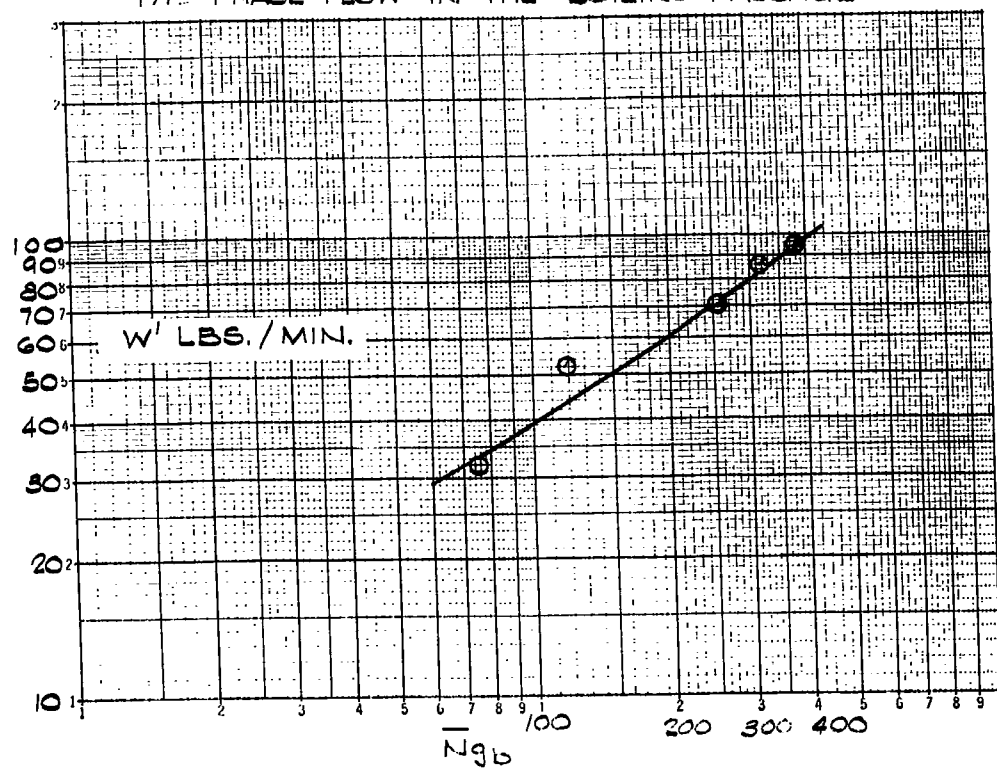
63 ASRP-2391

**CONFIDENTIAL**

CONFIDENTIAL

ASD-TDR-63-665, Part I

PRESSURE RISE TRANSITION POINTS FOR  
TWO-PHASE FLOW IN THE BOILING PASSAGE



NORMAL AVERAGE GRAVITATIONAL FIELD FIG 86

CONFIDENTIAL

**CONFIDENTIAL**

ASD-TDR-63-665, Part I

SMOOTHED DATA ON  
PRESSURE RISE THROUGH  
THE BOILING PASSAGE

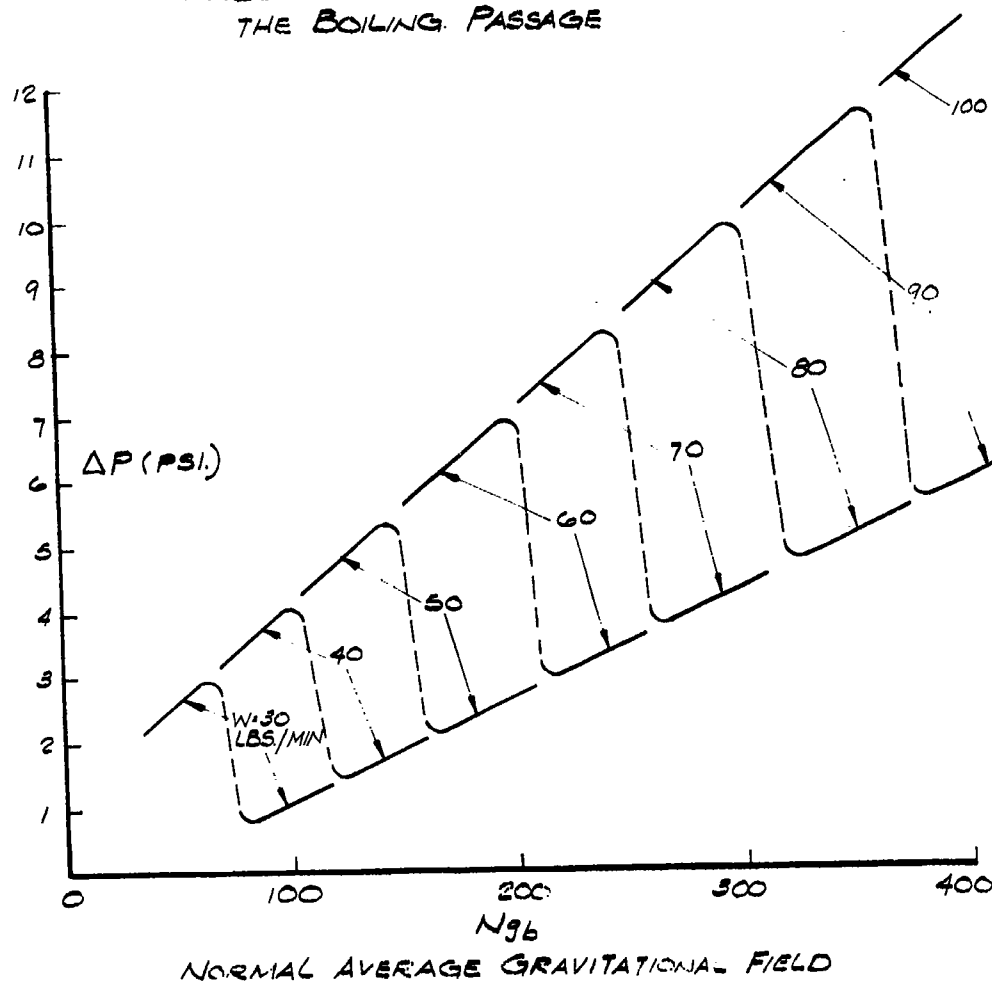


FIG 87

63 ASRP-2391

197  
**CONFIDENTIAL**

**CONFIDENTIAL**

ASD-TDR-63-665, Part I

## 5.0 EXPERIMENTAL PROGRAM IN SUPPORT OF MECHANICAL DESIGN OF BOILERPLATE SEPARATOR

### 5.1 Introduction

In order to design a rotary boilerplate separator it was necessary to undertake supporting experimental work in a number of mechanical areas. Aside from fabrication problems which required solution, the unusual problems encountered in a rotary air separator are associated with the transport of fluids between the various separator components. Examples are the transfer of kettle liquid from the periphery of the high pressure column radially inward against the centrifugal field to the low pressure column and the need for withdrawing liquid from the periphery of the low pressure column into a stationary diffuser. Transfer of kettle liquid has to be accomplished in a controlled fashion to avoid bypassing vapor through the transfer line. Design of a simple, reliable control system required knowledge of the two-phase pressure drop encountered in radial inward flow of a boiling liquid against a gravitational field, and experimental work on the operation of control components in a high gravitational field. Withdrawal of liquid at the periphery of the low pressure column required design of an effective peripheral seal to avoid excessive loss of liquid and a peripheral diffuser capable of recovering part of the kinetic energy of the liquid stream in the form of static pressure. Effort in both areas, the peripheral seal and diffuser, was required to arrive at a workable design.

Consequently, the work described in this section covers two-phase flow transfer control systems, peripheral seals and diffusers, and fabrication techniques for mass transfer and heat transfer elements.

### 5.2 Summary

Experimental data have indicated that a satisfactory centrifugal seal can be designed for peripheral liquid withdrawal. The seal can tolerate pressure differences close to the theoretical maximum without significant leakage.

The objective of the peripheral diffuser is to convert the kinetic energy, which is contained in liquid streams removed at the rotor periphery, into static pressure. Experimental and analytical work with some design innovations led to the prediction that 25 per cent of the kinetic energy would be recovered in a unit designed to separate 100 lb./sec. of air. This relatively small recovery is characteristic of small flow passages

63 ASRP-2391

**CONFIDENTIAL**



**SECRET**

**ASD-TDR-63-665, Part I**

because of large boundary layer losses. It is predicted that the large flow rates and enlarged passage geometry of the full-scale 2000 lb./sec. unit will greatly improve diffuser performance.

Experimental and analytical work yielded a working relationship to calculate pressure drop encountered in two-phase flow against a gravitational field. A computer program was developed to apply this correlation to radial inward flow of a boiling liquid.

A control valve system to be completely contained inside a rotating system was developed and successfully tested. This valve system will be used to control kettle and shelf liquid transfers from the high pressure column to the low pressure column.

Laboratory testing has shown that the Pace Variable Reluctance Transducer would be suitable for pressure measurement in high gravitational fields and at cryogenic temperatures.

Investigation in the area of reboiler-condenser fabrication led to the conclusion that the most practical method of construction is to assemble the unit from 45 individual disks. Each disk consists of individual curved tubes which are aligned side by side and brazed. Construction details are similar to the UCON fluid test rotor, described in Appendix VIII.

Experimental and analytical work in mechanical areas has fulfilled the primary purpose of laying the foundations for design, fabrication, and test of a 100 lb./sec. boilerplate separator. By virtue of the boilerplate mission (establishment of functional feasibility, parametric functional testing, suitability for testing of different heat transfer and mass transfer modules) lightweight design features had to be subordinated to other requirements in the design of the boilerplate model. The next logical step in establishing feasibility of a rotating high capacity distillation separator is design, construction and test of a small scale lightweight unit. It is recommended that future analytical and experimental mechanical work concentrate upon the necessary foundations for design and construction of such a lightweight model.

Specifically work is recommended in the area of lightweight fabrication techniques to effect integration of the present functional

63 ASRP-2391

**SECRET**

**CONFIDENTIAL**

ASD-TDR-63-665, Part I

design concepts with lightweight mechanical construction and to provide for maximum structural utilization of functional elements. Many lightweight fabrication techniques are currently available for large stationary equipment as well as for small to medium sized rotating machinery. However, the former frequently lack the precision required for maintaining necessary force balances in a rotating apparatus with internal circulation of two fluid phases while the latter are largely unapplicable because of size and nature of the structure under consideration.

A second area which is recommended for intensive future study is concerned with internal transport of fluids within the separator, since operational and mechanical stability of the separator will largely depend upon how well transfer and distribution of fluids are accomplished inside the separator. For this reason additional effort is recommended on refinement of two-phase pressure drop correlations and design of the internal control valve and signal systems.

Another area recommended for additional work is concerned with the radial inward transport of saturated liquid from the periphery where only a small pressure driving force is available. Currently, two alternate approaches appear applicable; 1) withdrawal of liquid from the rotor through a stationary diffuser and transport to the center of the device in a stationary line, and 2) generating the required pressure for radial inward transport of liquid by means of pumps located at the rotor periphery. It is recommended to subject the two competing systems to further experimental and analytical study to refine applicable designs and determine which system offers more promise for future use in flight-weight models. In the case of pumps this will require evaluation of possible drive means and design penalties due to location of the pump in a high gravitational field.

Finally, work is recommended in the area of large rolling contact bearings since it may be necessary to develop special design bearings which will accommodate large rates of differential thermal contraction between the structural support elements (e.g. aluminum) and the bearing races which have to be made from hardenable steels for adequate load carrying capacity and life.

5.3.1 Peripheral Seal Design Considerations

Two basic types of seals were considered to fill the requirement of dynamically sealing liquid at a large diameter against a moderate pressure differential. They were:

63 ASRP-2391

**CONFIDENTIAL**

**CONFIDENTIAL**

**C ASD-TDR-63-665, Part I**

a. A centrifugal type seal consisting of blades attached to the rotor wall which generate a head equal in magnitude and opposite in direction to the pressure differential across the seal.

b. A family of contact type seals which seal by virtue of rubbing contact between a rotating, low-friction seal face and a stationary surface.

The general configuration of the centrifugal type seal is shown in Figure 88. It consists of thin radial blades attached to the rotor side walls near the periphery of the rotor. A close clearance has to be maintained between the blades and the stationary surface for the seal to be effective. To reduce the risk due to periodic contact between the blades and the stationary wall and also the accuracy required in axial alignment, the blades are fabricated from a filled Teflon material. Thus, periodic contact will not seriously damage either the blades or the stationary wall.

A centrifugal seal is theoretically capable of developing a head of

$$\Delta P_{\text{seal}} = \frac{\rho L \omega^2}{2 g_c} (r_l^2 - r_{i_{\text{seal}}}^2)$$

for a blade length of  $r_l - r_{i_{\text{seal}}}$ . Since a liquid level exists at the periphery of the rotor, the active seal depth does not extend to the outside of the rotor but only to the liquid level  $r_l$ . Thus, the inside radius of the seal blades must be:

$$r_{i_{\text{seal}}} = \left[ (R_o - h_{\text{seal}})^2 - \frac{2g_c}{\rho \omega^2} \Delta P_{\text{seal}} \right]^{1/2}$$

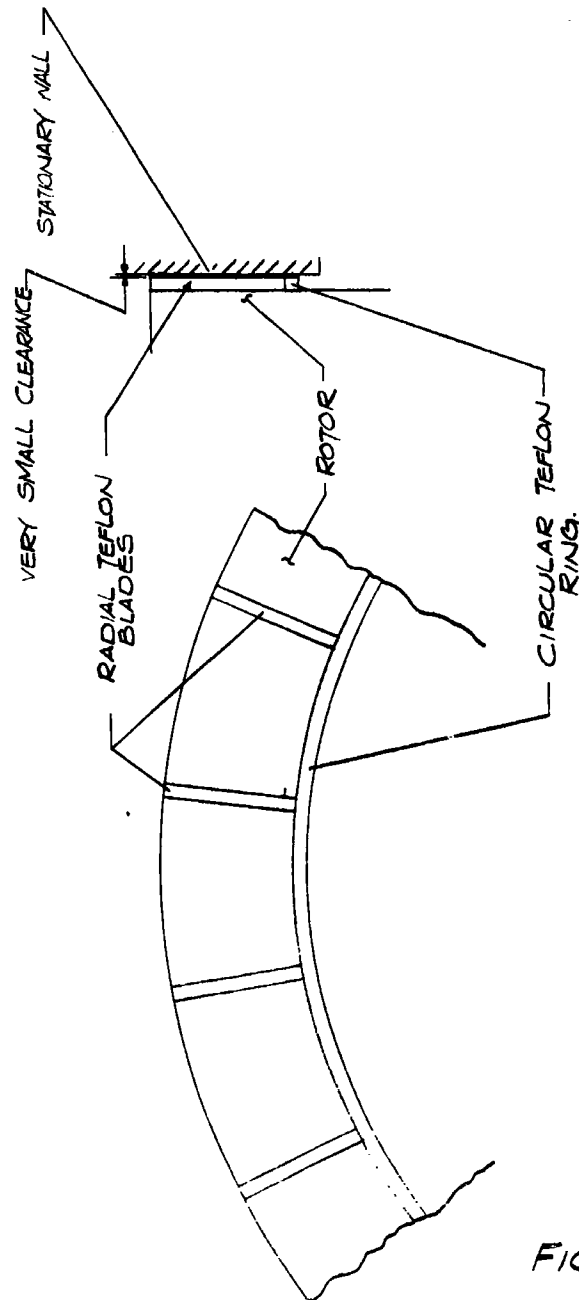
as shown in the theoretical discussion of the centrifugal seal presented in Appendix X.

The contact-type mechanical seal is illustrated by several designs as shown in Figures 89 and 90. The major problem encountered in the operation of such a seal is the excessively high surface speeds at the contact face. The large rotor diameters and moderate rotational

63 ASRP-2391

**CONFIDENTIAL**

ASD-TDR-63-665, Part I

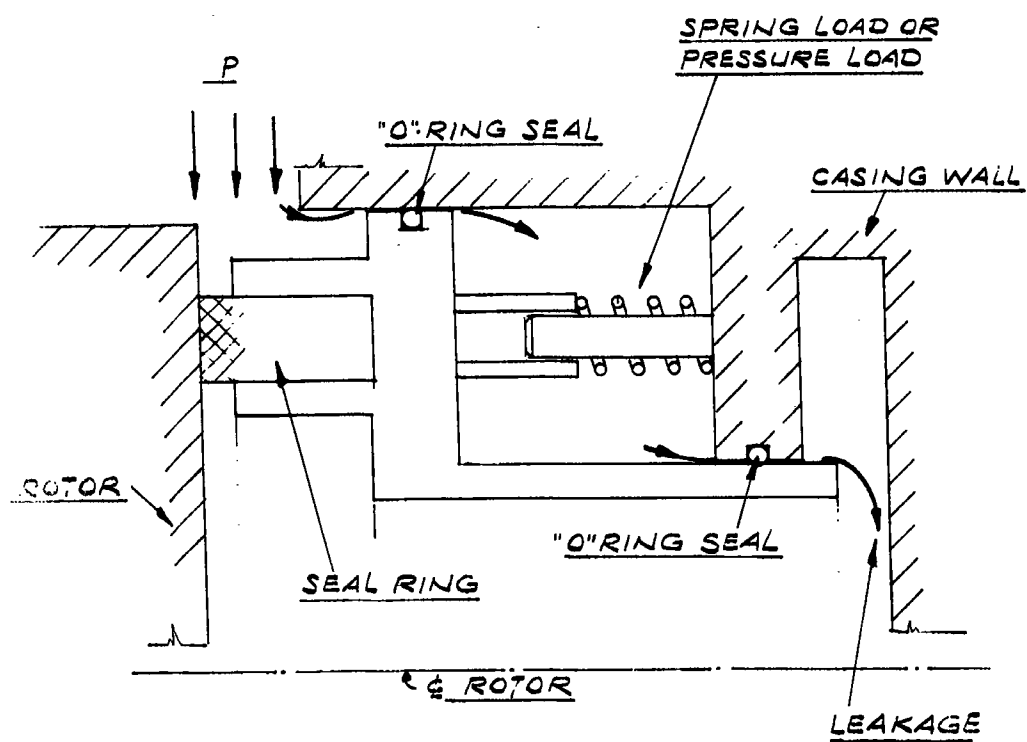


CENTRIFUGAL SEAL CONFIGURATION

FIG. 88

63 ASRP-2391

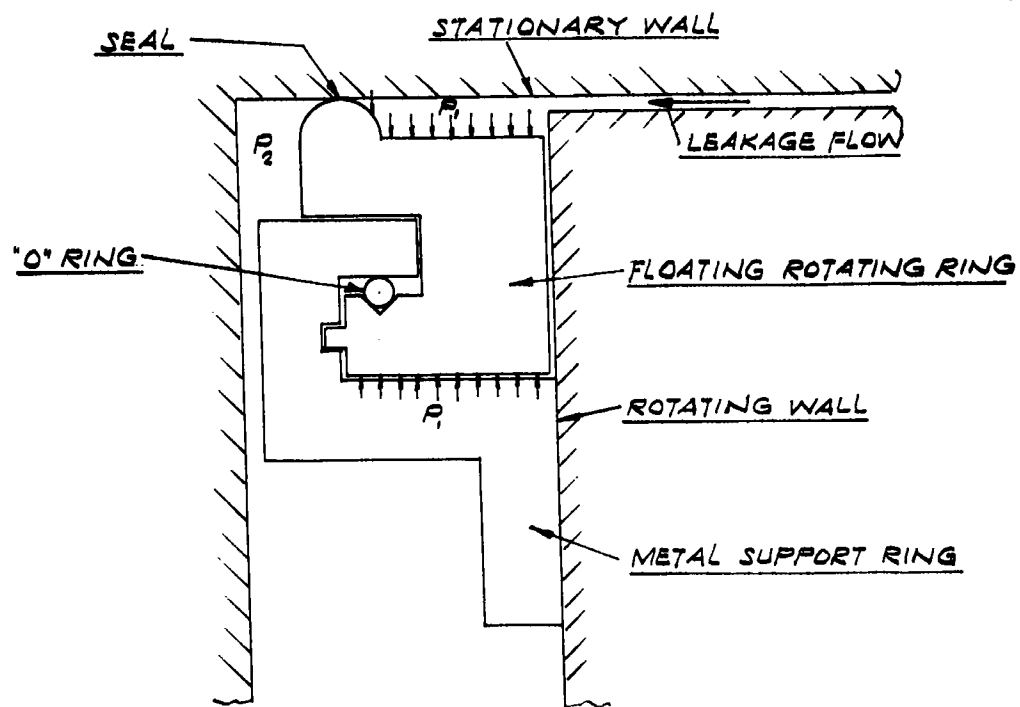
ASD-TDR-63-665, Part I



CONTACT TYPE PERIPHERAL SEAL DESIGN

FIG. 89

63 ASRP-2391



CONTACT - TYPE PERIPHERAL SEAL DESIGN

FIG. 90

63 ASRP-2391

**CONFIDENTIAL**

**ASD-TDR-63-665, Part I**

speeds couple to give surface speeds of 300 fps or 18,000 fpm which is considerably higher than those of the present state-of-the-art experience. Data for various combinations of wear surface materials operating at cryogenic temperatures exists for surface speeds an order of magnitude lower than those of the present design. Another problem with the contact-type seal is that in the ultimate design the stationary mating surface must be aluminum due to the differential thermal expansion problems encountered if another material is used. In general, the aluminum alloys, even if anodized, provide poor wear surfaces in cryogenic service.

In the light of the relative lack of knowledge concerning wear and friction at these excessive surface speeds, it was decided to concentrate most of the research effort on the more readily feasible centrifugal type seal, although some investigations were carried out concerning the high speed wear characteristics of a filled-Teflon seal running against an anodized aluminum surface.

To generate design information for the detailed design of a large diameter seal, an experimental program was carried out.

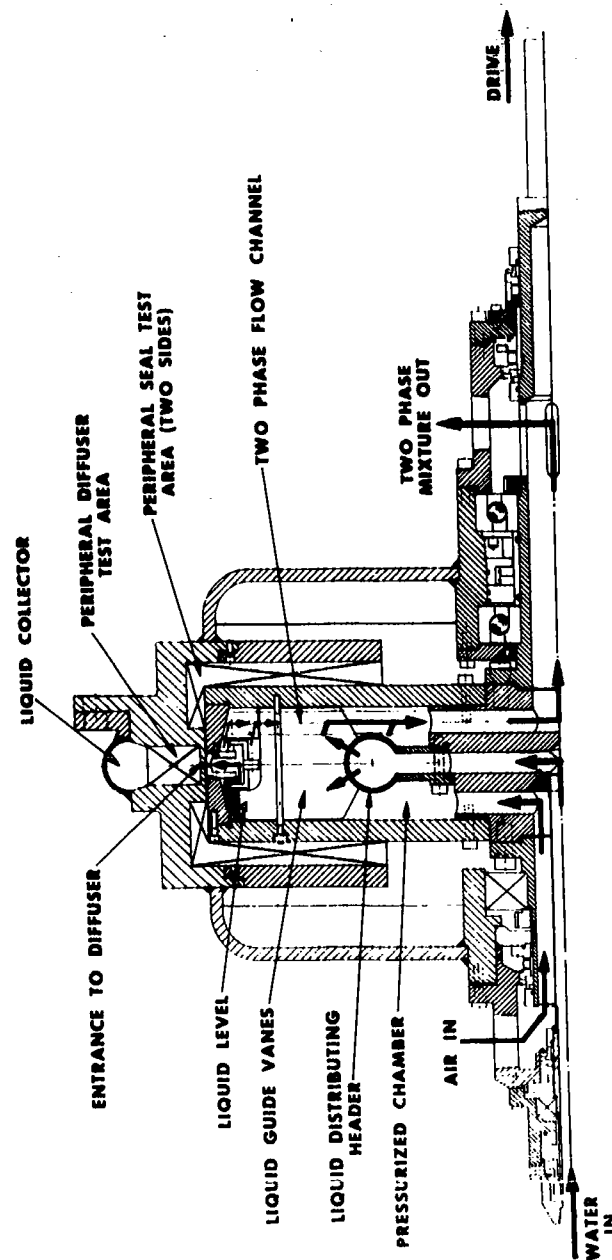
**5.3.2 Peripheral Seal Experimental Apparatus**

A rotating air-water tester was designed to serve as a test device for examining both peripheral seal and diffuser designs and to study the phenomena associated with two-phase flow against a gravitational field. A layout of the device is shown in Figure 91. The function of the machine is to accelerate fluids (air and water), which are introduced at the shaft centerline, to the tip speed of the rotor. At the rotor periphery, the fluid is ejected through an orifice slot into the clearance between the rotor and the casing at which point a seal is required to prevent the fluid from passing into the casing. Ample test areas were provided in the machine to facilitate the investigation of different seal configurations.

The flow and instrumentation diagram for the apparatus as used in both the seal and diffuser tests is shown in Figure 92. A closed water system was employed with a 1000 gallon tank serving as water storage. Water was circulated by a Turbocraft 1 x 2 x 6 series 2000 centrifugal pump located between tank and tester. The water flow rate was controlled manually with a valve at the rotor inlet. With the pump by-pass valve slightly open, a wide range of flow rates could be obtained by manipulating the inlet valve. The main water circuit was

63 ASRP-2391

**CONFIDENTIAL**

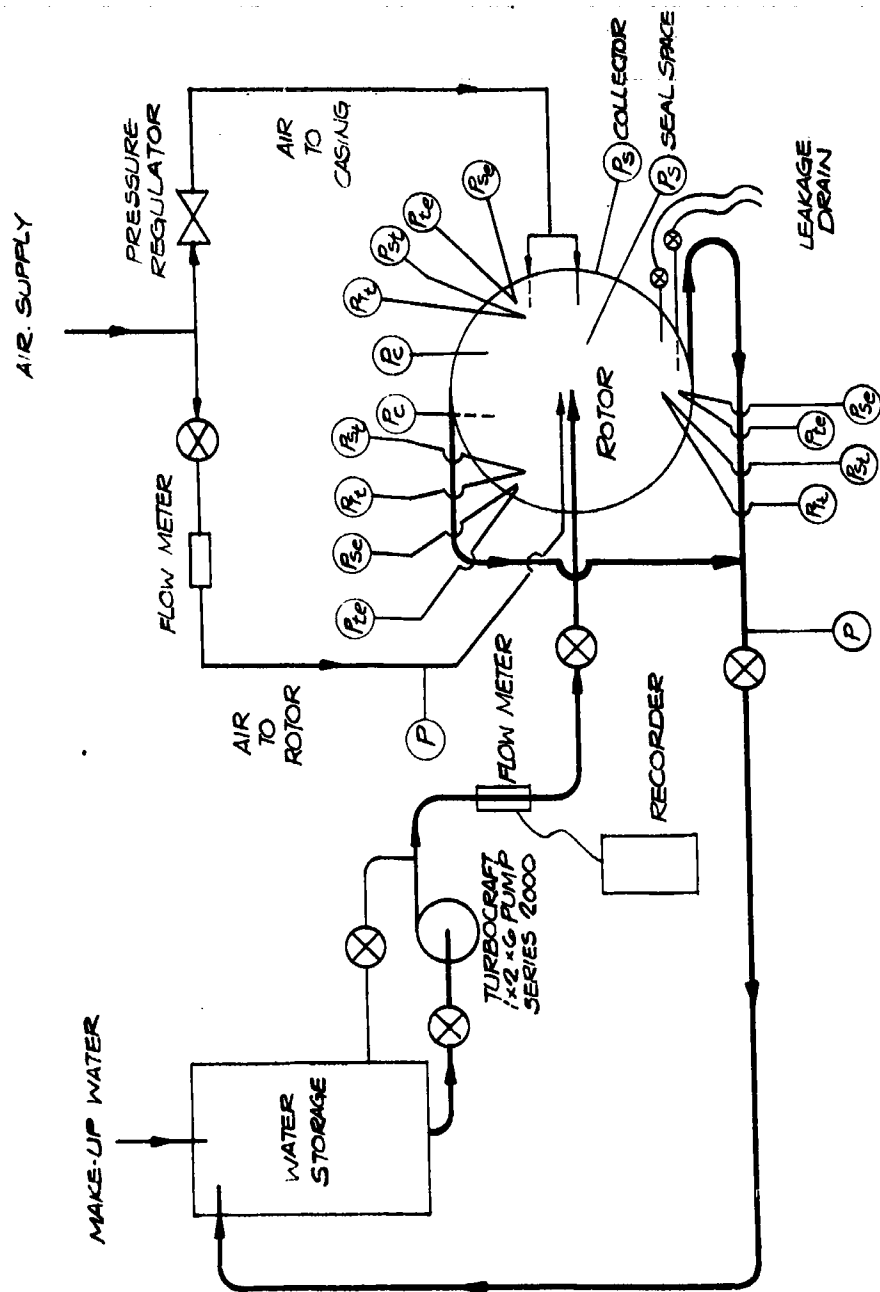


LAYOUT OF PERIPHERAL DIFFUSER AND ROTARY SEAL TESTER

FIG. 91

63 ASRP-2391





FLOW CIRCUIT & INSTRUMENTATION  
FOR SEAL AND DIFFUSER TESTS

FIG. 92

63 ASRP-2391

**CONFIDENTIAL**

**ASD-TDR-63-665, Part I**

also provided with a globe valve located downstream from the rotor to control diffuser back pressure. The water flow was measured by a Potter turbine flow meter located between the pump and the control valve. The recorder receiving the signal from the flow meter was situated so that the setting of the manual control valve could be adjusted as a function of the recorder reading. Air was supplied to the rotor for pressurization and to the casing as a source of casing pressure control.

The tester was powered by a 15 HP variable speed drive. A motor analyzer was attached to the electrical input to obtain readings of the power consumed by the device at various rotational speeds.

**5.3.3 Peripheral Seal Experiments**

Initial tests for peripheral seal development were conducted using a contact type seal. The seal consisted of glass-filled Teflon three-segment tangentially cut rings with a 26-inch inside diameter as shown in Figure 93. It was manufactured by the Double Seal Ring Company. The use of pressure-balancing grooves resulted in a 1/8 inch contact surface. The stationary mating surface was hard coat anodized aluminum. During initial operation, the unpinned segments rotated and as a result the seal "bunched", i.e., the entire gap became concentrated at one of the tangential cuts and the other two spaces were closed. This problem, coupled with improper axial alignment of the seal space, made it difficult to achieve a running fit. Springs were fitted into the spaces between the rings to aid in maintaining the proper gap; though helpful, they proved to be inadequate.

During the short running period the seal performed reasonably well with relatively small leakage rates. The seal was inspected after approximately 15 minutes of running time had been accumulated. It was found that the hard coat aluminum surface had been severely scored and the Teflon rings had begun to gall. This appeared to substantiate the opinion that the aluminum surface was a poor wear surface even at the low test surface speed (~60 fps). Attention was then turned to the centrifugal type seal.

The initial centrifugal type seal configuration which was investigated is shown in Figure 94 (original configuration). It consists of twelve glass-filled Teflon blades mounted on an aluminum backing ring with screwed tabs. One of these seals was attached to each side of the rotor. The blades were 1/2 inch deep and approximately 4-1/2 inches long

63 ASRP-2391

**CONFIDENTIAL**

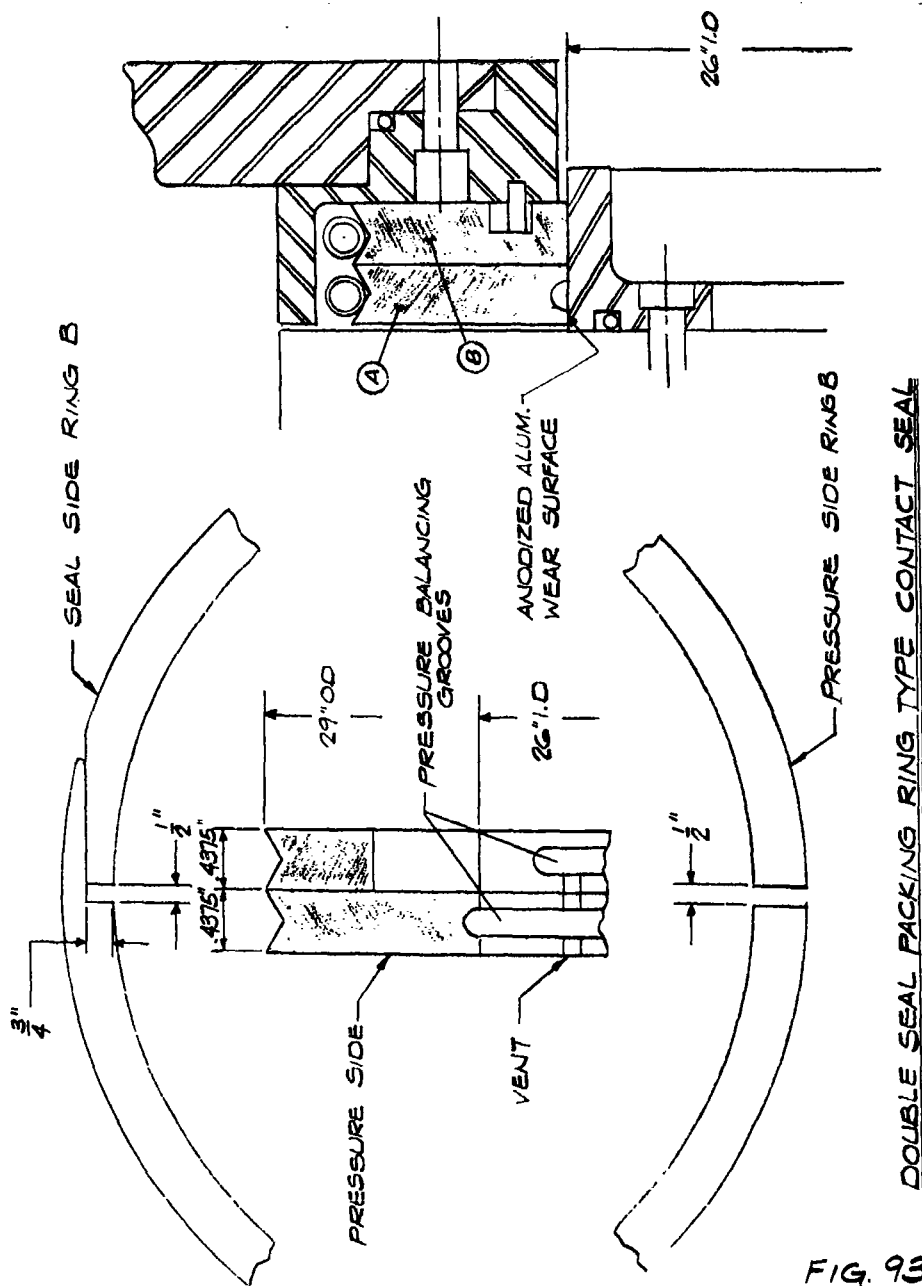


FIG. 93

63 ASRP-2391

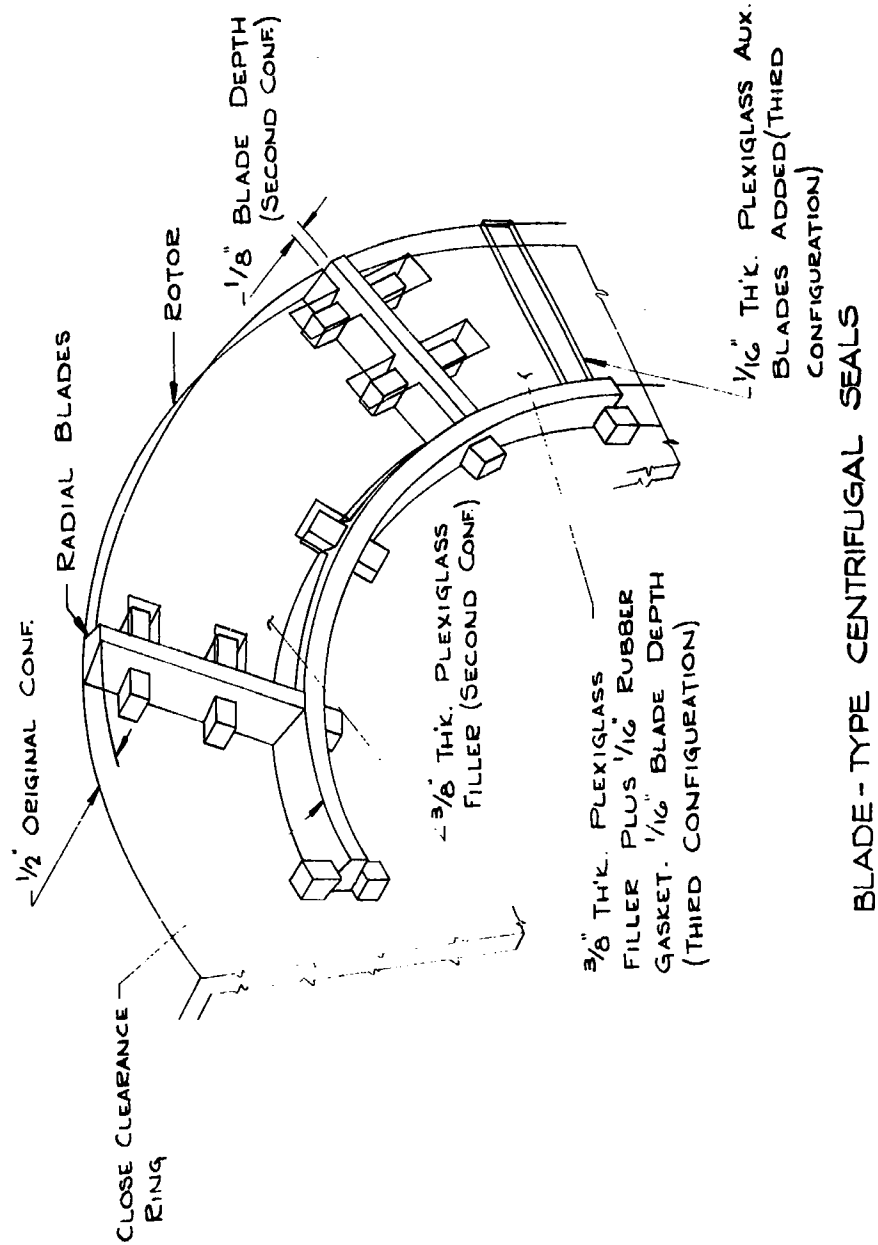


FIG. 94

63 ASRP-2391

# CONFIDENTIAL

## ASD-TDR-63-665, Part I

with a trapezoidal cross-section. The smallest surface of the trapezoid was designed to be nearest to the stationary plate, such that any contact caused by misalignment would occur only on a small surface. Great care was taken in aligning the seals and in obtaining a small axial clearance.

During experimental operation of the first seal configuration, measurements were taken of the pressure across the seal and the power input to the drive at various speeds and flow rates, while visually observing leakage. The pressure developing capability of the seal is shown in Figure 95. The horsepower data is plotted in Figure 96.

The seal blade depth was then changed to 1/8 inch by placing Plexiglas fillers between the Teflon blades as shown in Figure 94 (second configuration). Again the pressure difference across the seal and power requirements were recorded (Figures 95 and 96) and the leakage was measured. Figure 97 shows the percent leakage flow rate for the 1/8 inch depth as a function of the dimensionless pressure differential across the seal. It should be noted that the theoretical maximum pressure differential across the seal is represented by

$$\Delta P_{\text{seal}} / \frac{\rho L \omega^2}{2 g_c} (R_o^2 - r_{i \text{ seal}}^2) = 1$$

when the pressure differential equals the developed liquid head. Figure 97 indicates that leakage starts to increase substantially when the above factor approaches and exceeds the value of 1 and that liquid leakage can be maintained at very small values by operating at values for

$$\Delta P_{\text{seal}} / \frac{\rho L \omega^2}{2 g_c} (R_o^2 - r_{i \text{ seal}}^2) < .8$$

Later the seal blade depth was reduced to 1/16 inch by placing rubber gaskets beneath the Plexiglas fillers as shown in Figure 94 (third configuration). Auxiliary blades were also added by placing two radial Plexiglas strips on each filler. The tests were repeated. The pressure capability of this seal configuration is plotted in Figure 95, and the power requirements in Figure 96. The leakage data for the 1/16 inch depth is shown in Figure 98.

63 ASRP-2391

CENTRIFUGAL SEAL PRESSURE CAPABILITY

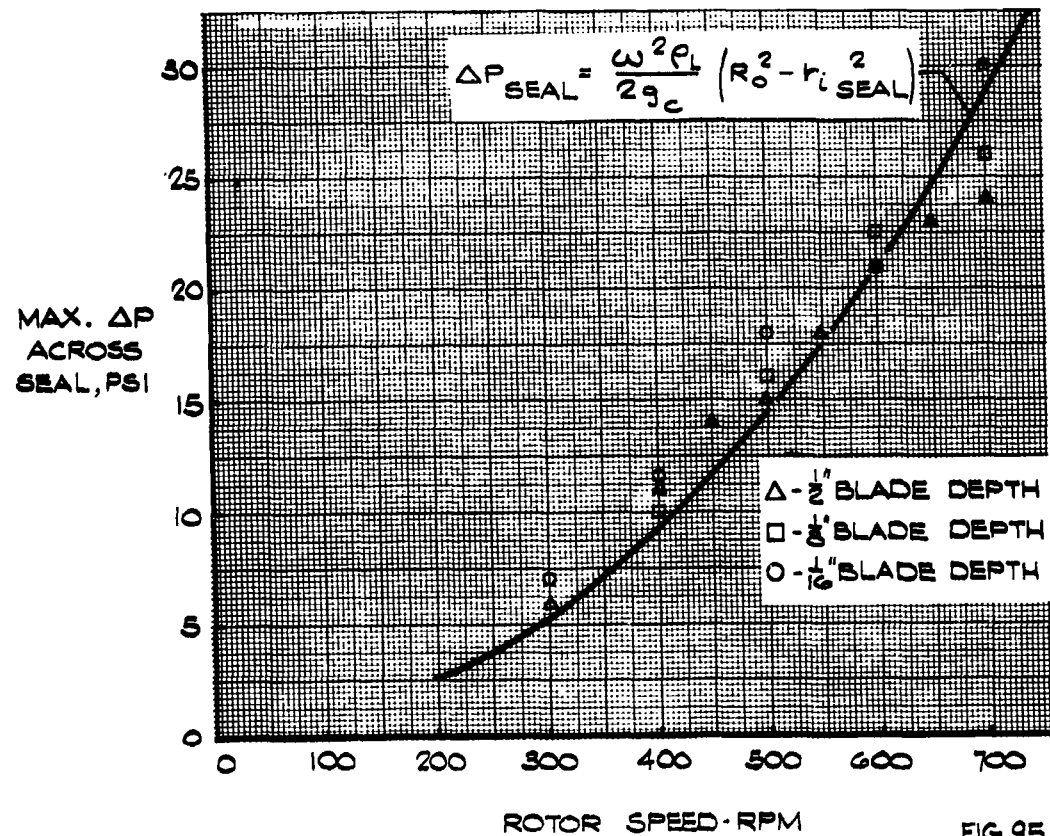
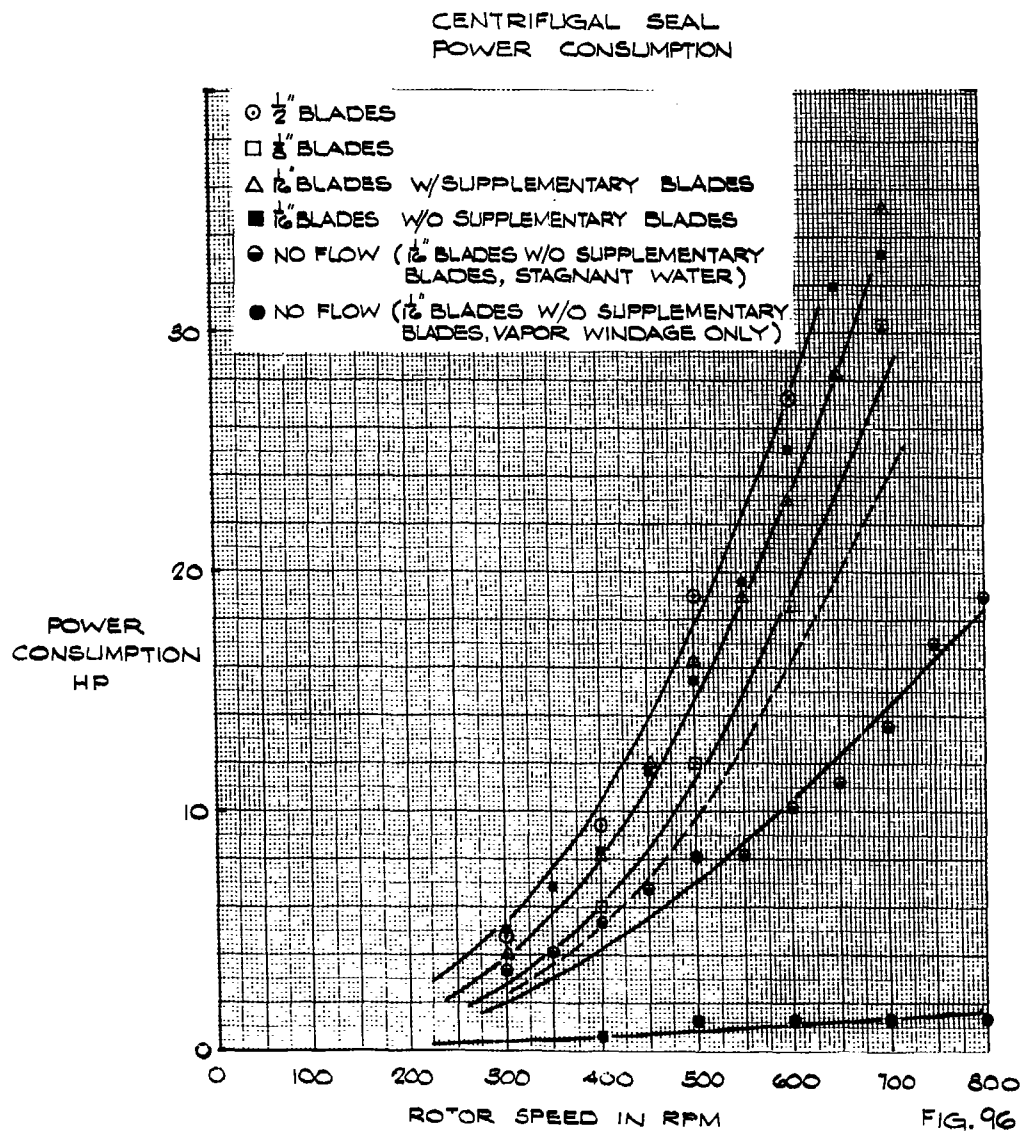


FIG. 95

63 ASRP-2391



63 ASRP-2391

SEAL LEAKAGE,  $\frac{1}{8}$  INCH BLADE DEPTH

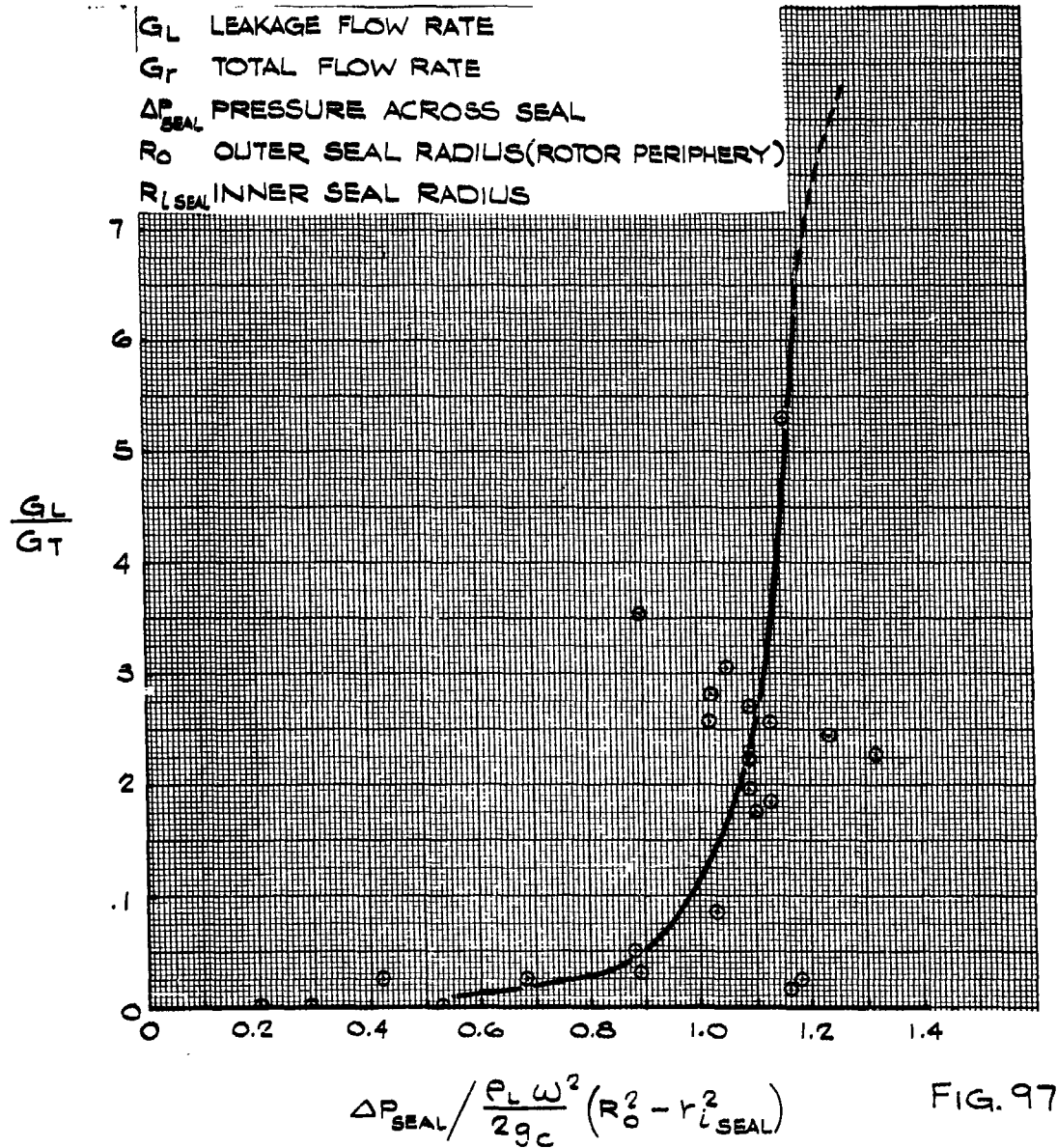
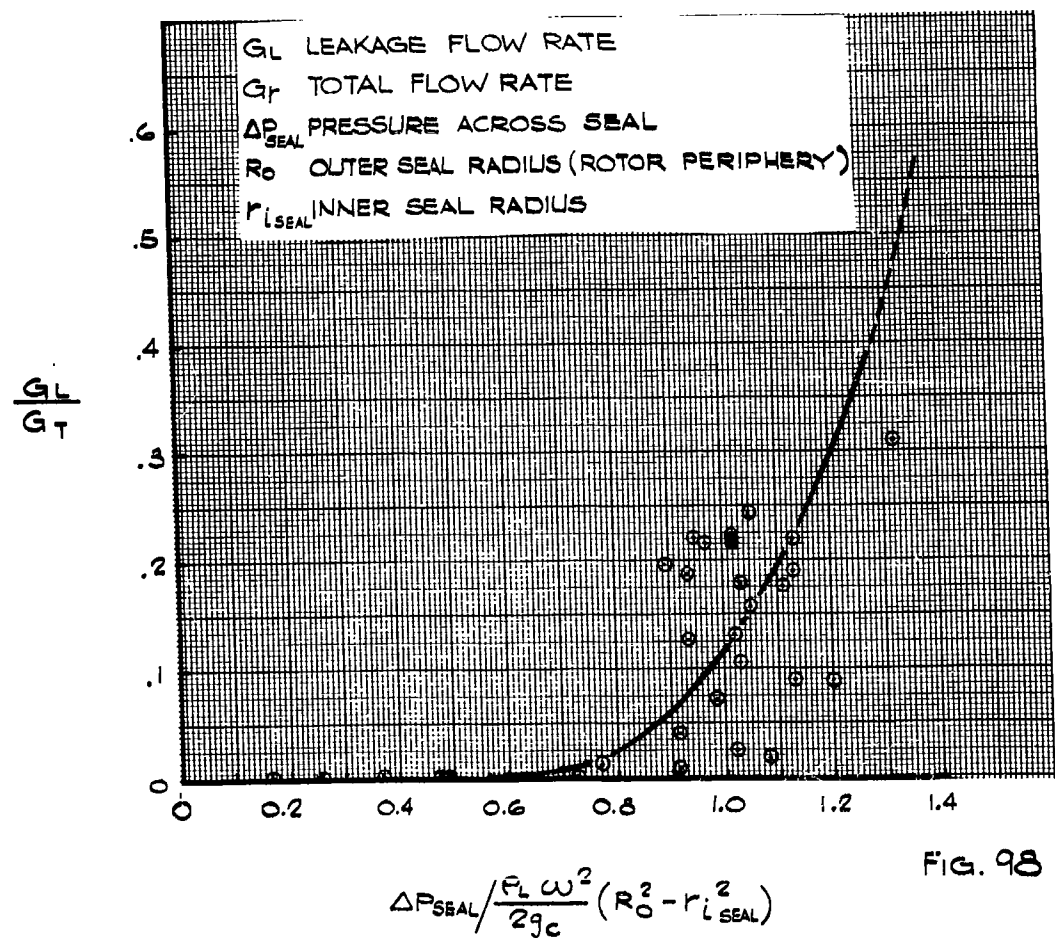


FIG. 97

63 ASRP-2391



SEAL LEAKAGE  $\frac{1}{2}$  INCH BLADE DEPTH



**CONFIDENTIAL**

**ASD-TDR-63-665, Part I**

Because of the power requirement rise between the 1/8 inch blade depth and the 1/16 inch blade depth, the auxiliary blades were removed and power tests conducted. The results appear in Figure 96.

Figures 99 and 100 afford additional views of the installed seals.

**5.3.4 Results**

The experimental data indicate that the seal is capable of approaching its theoretical capability before leakage becomes significant. In Figure 95, the data points lie nearly on the calculated curve. Furthermore, Figures 97 and 98 show that only relatively small leakage rates occur even when the pressure across the seal exceeds the theoretical capability of the seal. Thus the pressure and leakage data indicate that the seal is capable of very satisfactory performance.

The fact that the periphery of the rotor is immersed in liquid with a centrifugal type seal means that windage power losses will be somewhat larger. Thus, data concerning the power requirements is important. The results of the seal experiments, as shown in Figure 96, indicate that the power losses were largest with the 1/2 inch blade depth seal. It was felt that the reason for this was that the large space between blades allowed constant recirculation of the leakage fluid in the seal space. This opinion appeared to be borne out by the reduced power losses in the 1/8 inch blade configuration. No explanation was readily available for the fact that the power losses also increased for the 1/16 inch blade depth. Evidently there exists a depth minimum below which the power losses again increase. At first, it was thought that this was due to the surface roughness created by the addition of the auxiliary blades, but the removal of these blades did not result in a reduction of the power losses. Thus, the optimum blade depth appears to be near 1/8 inch.

**5.4 Peripheral Diffuser**

**5.4.1 Stationary Diffuser Study**

**5.4.1.2 Design and Operation**

Since liquid is withdrawn from the separator at the peripheries of the low pressure column and reboiler-condenser, diffusers are required at these locations to recover the kinetic energy of the liquid by converting the same into potential energy. An experimental test program was carried out to obtain design parameters in support of the design of

63 ASRP-2391

**CONFIDENTIAL**

ASD-TDR-63-665, Part I

**CENTRIFUGAL SEALS MOUNTED ON ROTOR**

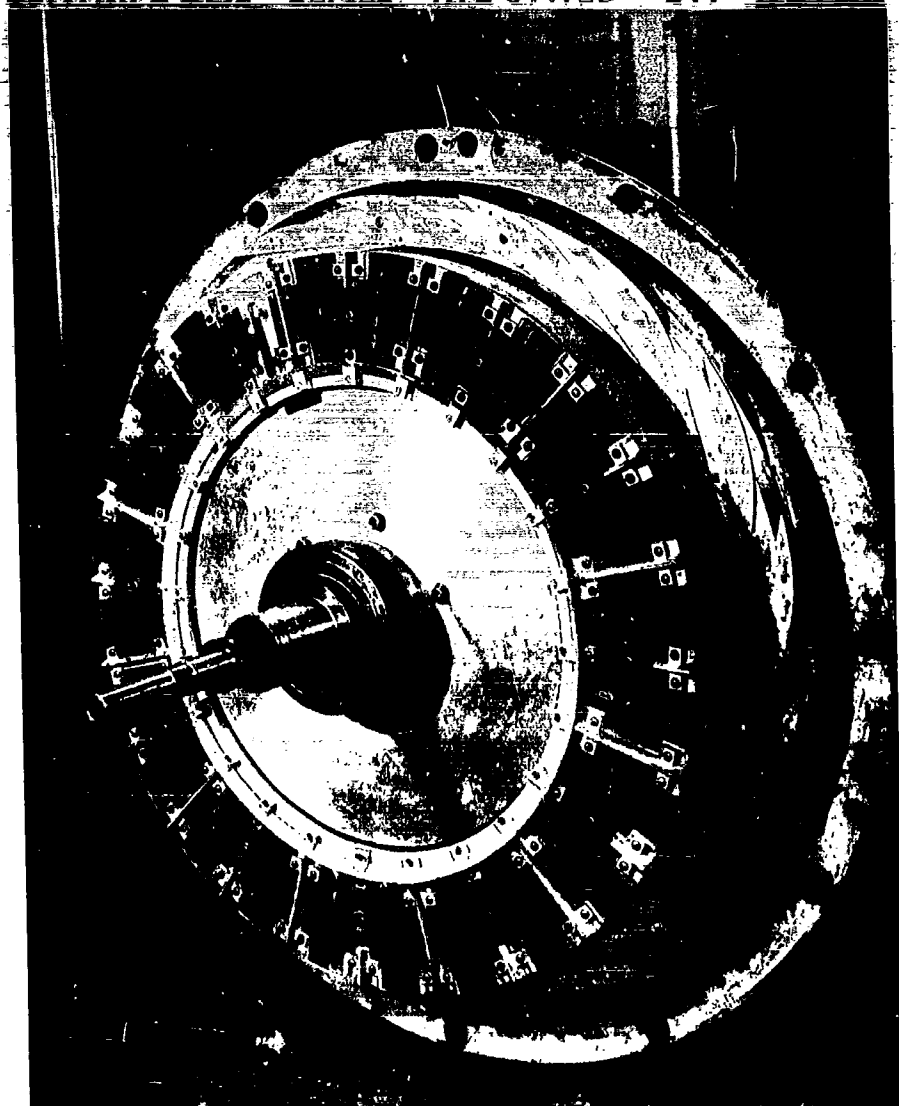


**FIG. 99**

63 ASRP-2391

ASD-TDR-63-665, Part I

## CENTRIFUGAL SEALS MOUNTED ON ROTOR

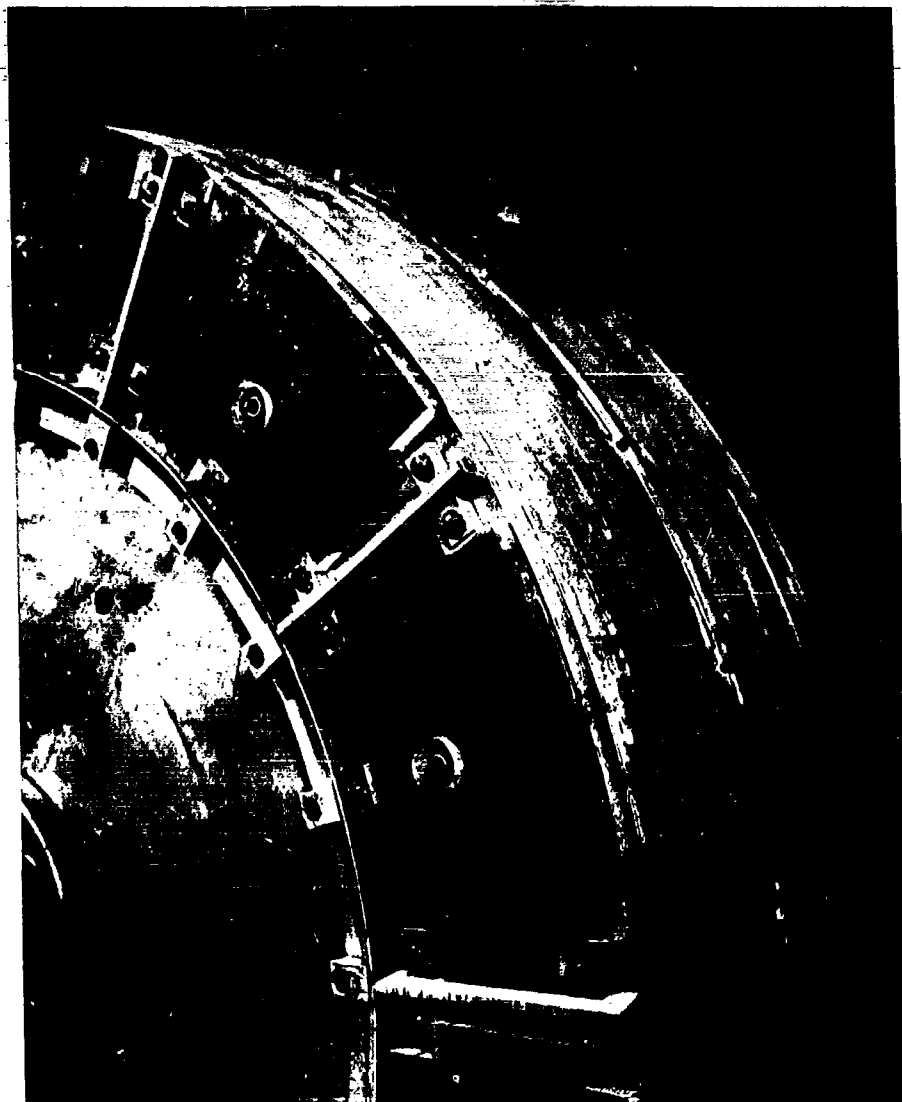


FIG. 100

63 ASRP-2391

**CONFIDENTIAL**

ASD-TDR-63-665, Part I

a diffuser system for the boilerplate air separator. Tests were first conducted on a stationary diffuser and then on a radial annular diffuser system which received flow issuing from the peripheral orifice slot of a rotating chamber. The latter tests are described in Section 5.4.2. The flow diagram of the test apparatus used in the stationary tests is presented as Figure 101.

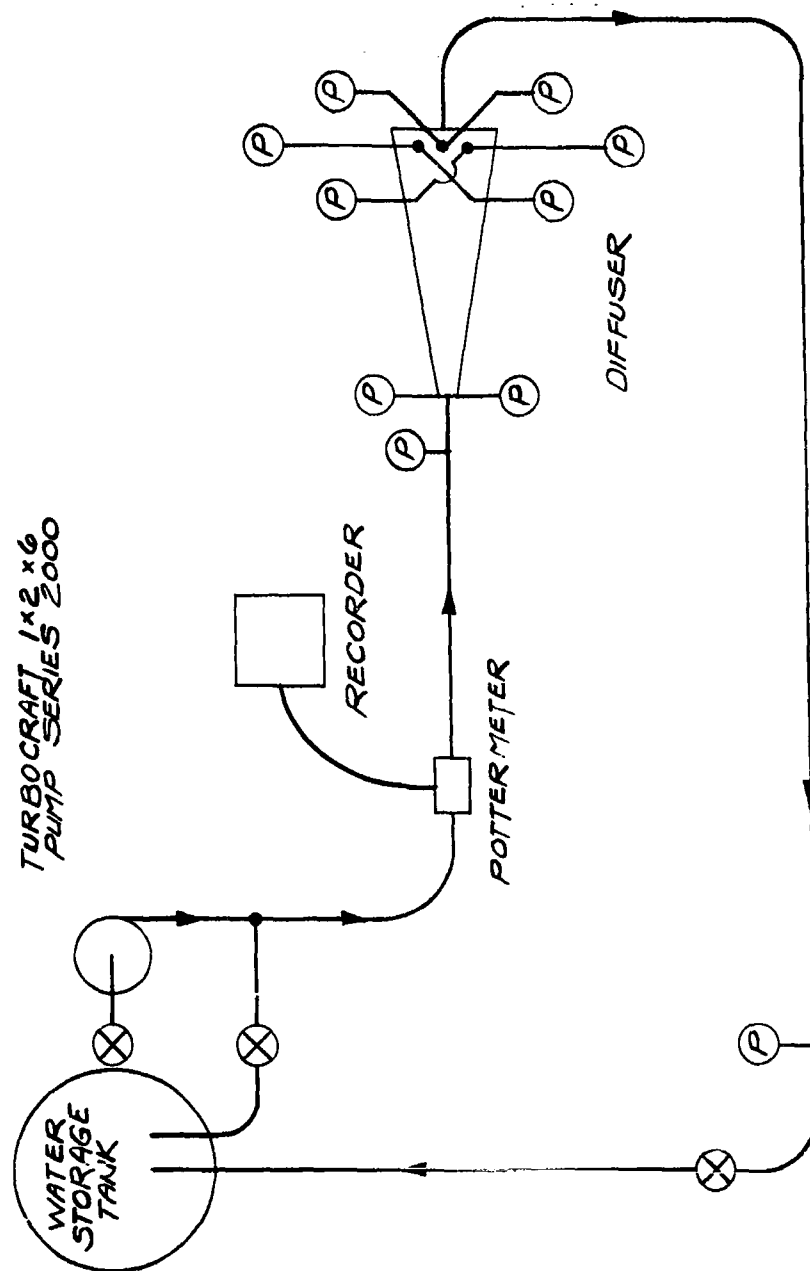
Investigation of the anticipated flow and mechanical limitations of a rotary device formed the basis for selecting the configuration of the stationary diffuser. It was designed to simulate the conditions encountered in the rotary tester. A rotor discharge velocity angle of approximately one degree was indicated. A review of the available literature revealed that optimum efficiency is normally obtained with an included angle of six or seven degrees and a length-to-throat width ratio of approximately 25. Based on these values, the stationary diffuser was originally designed as shown in Figure 102. Initial operation led to modifications of the diffuser to reduce the inlet pressure drop and accommodate larger flows. The original nozzle was replaced with a constriction which tapered from the inlet pipe to the 1/8 inch by 3/4 inch diffuser throat. Most of the 1/8 inch by 3/4 inch passage was removed resulting in the test diffuser as shown in Figure 103. The throat was then defined as the 1/8 inch by 3/4 inch area and static pressure taps were placed at intervals along the diffuser. Tests were then conducted which indicated that the major part of the recovery occurred between the throat (Section 1) and the first static measurement (Section 2). This revealed that much shorter diffuser lengths may be used. The additional length did not provide sufficient additional recovery to justify the bulkier construction.

At Section 2, a total of 3 pressure taps were inserted at the top and bottom of the channel. They all indicated the same pressure even when cavitation was occurring at the throat. It was therefore concluded that continuity flow is established in a short distance after separation. Cavitation occurred at a limiting flow rate of approximately 46 GPM and the minimum efficiency occurred at high velocities as shown in Figure 104 which presents the results of the stationary diffuser tests.

The results of the described tests indicate that efficient diffusion can be obtained for viscous, incompressible flow in a three-dimensional diffuser with a trapezoidal cross-section. Diffusion efficiencies of 80-90 per cent were observed with short length and small divergence angles.

63 ASRP-2391

**CONFIDENTIAL**



FLOW DIAGRAM  
STATIONARY DIFFUSER TEST

FIG. 101

63 ASRP-2391

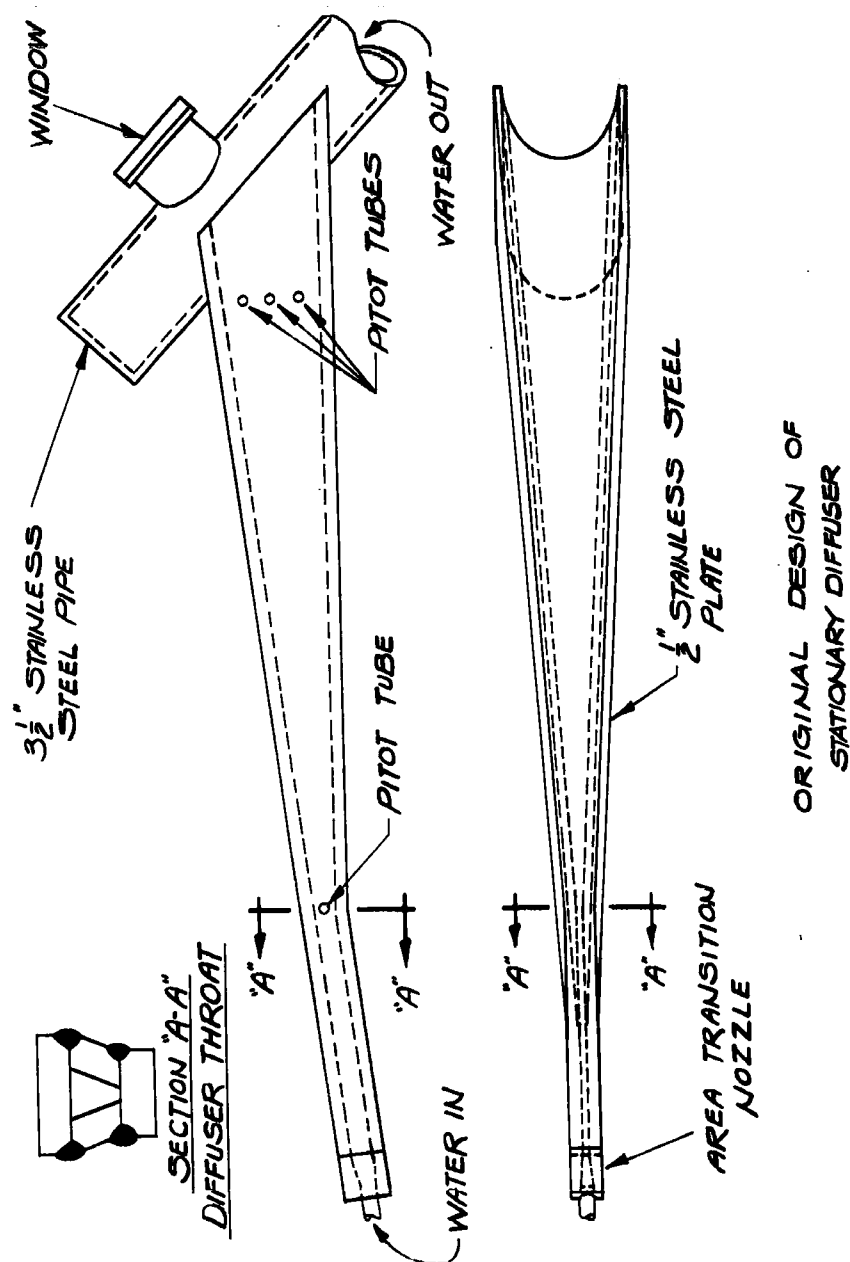
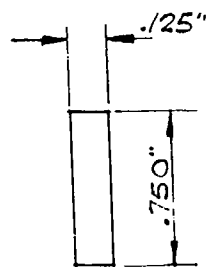
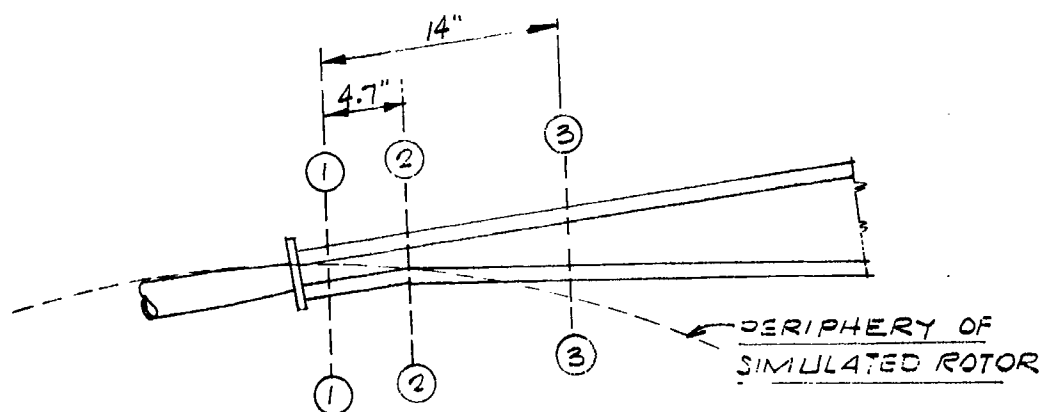
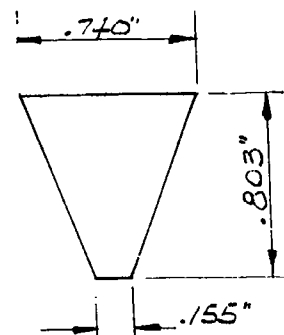


FIG. 102

63 ASRP-2391



SECTION ①  
FLOW AREA



SECTION ②  
FLOW AREA

FINAL STATIONARY DIFFUSER CONFIGURATION

FIG. 103

63 ASRP-2391



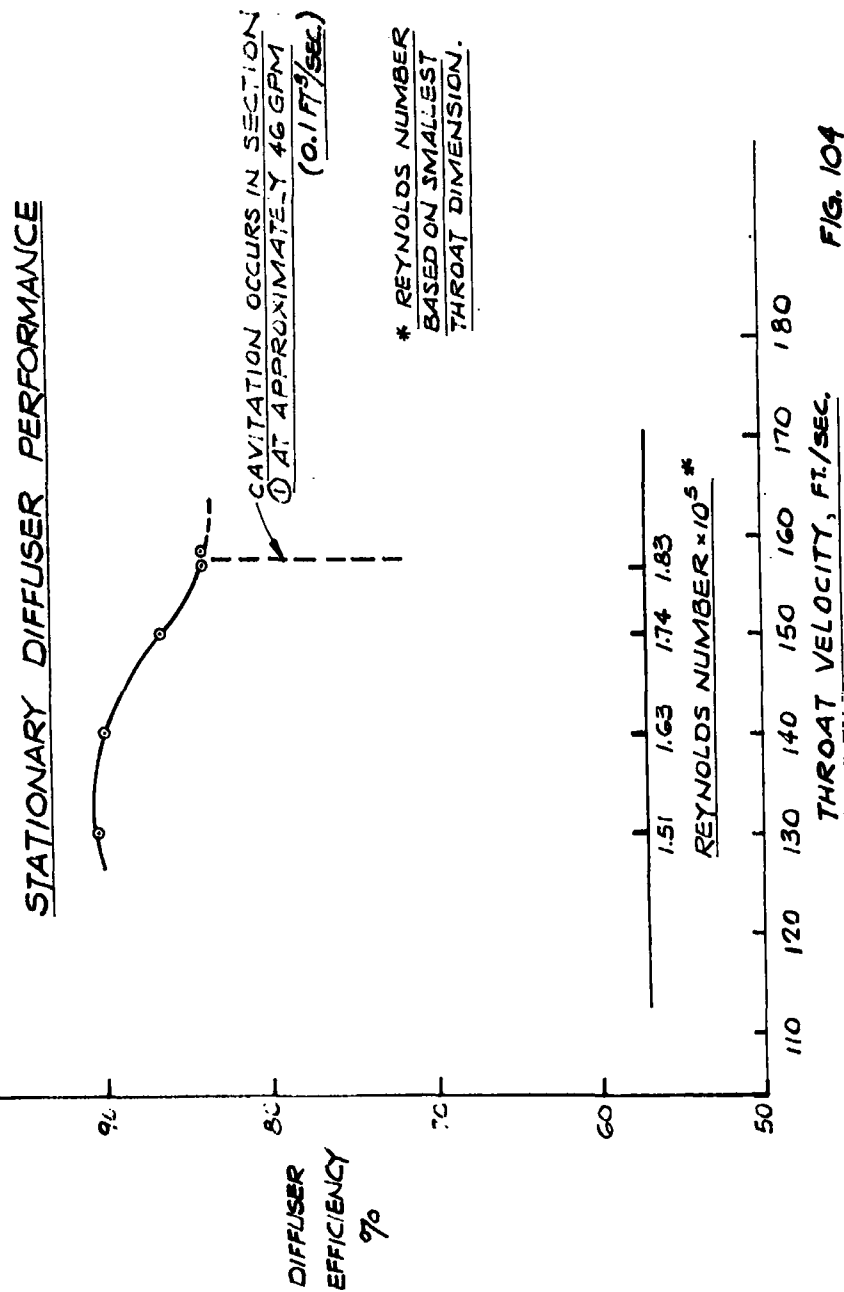


FIG. 104

# CONFIDENTIAL

ASD-TDR-63-665, Part I

Friction losses, with water as the fluid under consideration are reasonably small. These losses amounted to less than 20 per cent of the available head and appeared to occur in the first part of the diffuser. This is to be expected, of course, since the flow velocities were highest in this region. The evidence of low losses in the stationary tests indicate that a square cross-section, which has a more favorable hydraulic radius than the trapezoidal cross-section, is not necessary to achieve efficient diffusion.

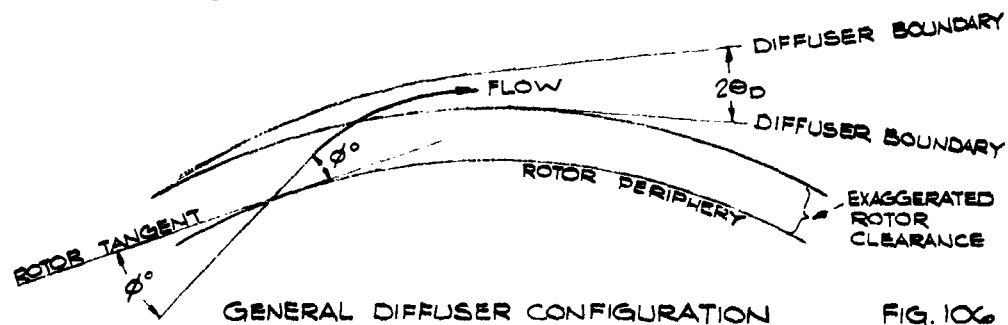
Although cavitation occurs at the throat at high flow rates, the flow re-establishes itself, and continuous flow exists only a short distance downstream from the throat.

## 5.4.2 Rotating Diffuser Study

### 5.4.2.1 Peripheral Diffuser Design

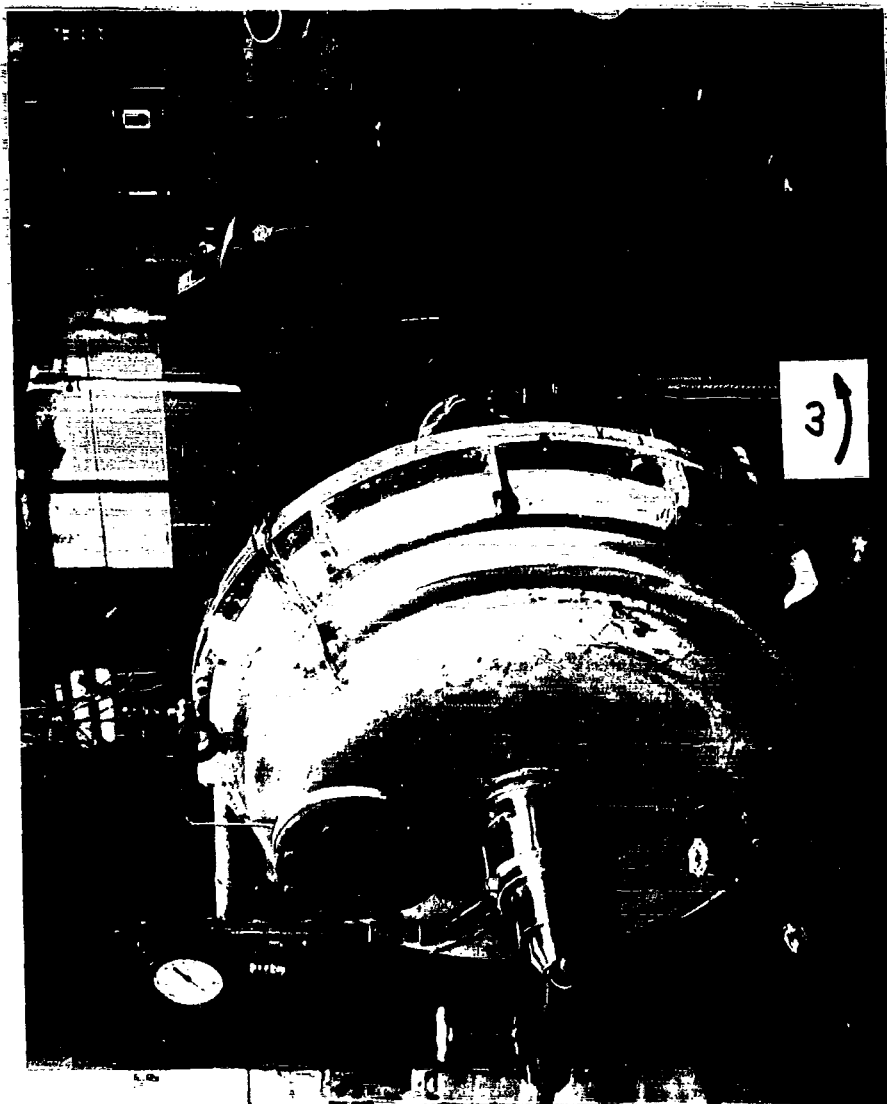
The annular peripheral diffusers were designed to accept a liquid stream from the periphery of a rotating chamber and recover the kinetic energy imparted to the liquid by the rotor. The test apparatus shown in Figure 105 was designed to accommodate various annular diffuser configurations and to simulate the flow conditions for a 100 lb./sec. air separator. Five series of tests were carried out, one on free vortex diffusion and the rest on diffusers with different blade configurations.

Several diffuser geometries were considered, but the two-dimensional flat diffuser (diffusion occurring in two dimensions) was ultimately selected. Such a system is more efficient and requires less space than the free-vortex vaneless diffuser system and is less complex and easier to fabricate than a three-dimensional diffuser system. The general diffuser configuration is shown in Figure 106.



63 ASRP-2391

ASD-TDR-63-665, Part I



ROTARY TESTER FOR PERIPHERAL SEAL AND DIFFUSER TESTS

FIG. 105

63 ASRP-2391

# CONFIDENTIAL

## ASD-TDR-63-665, Part I

From the literature and the results of the stationary diffuser tests, a divergence angle of  $2\theta_D = 7^\circ$  was selected and it was decided to extend the diffuser blades approximately two inches in the radial direction. Fluid flow conditions at the orifice slot indicated a flow angle ( $\phi^\circ$ ) of between one and two degrees from the rotor tangent. This angle  $\phi^\circ$  formed by the exit velocity of the fluid with the rotor tangent is tabulated in Table 15 for various speeds and flow rates. The angle  $\phi^\circ$  incorporated in the diffuser design was selected based upon these calculations. The diffuser width was selected to be somewhat larger than the orifice slot width based upon information in the literature concerning the diffusion of free jets (Ref. 40). Layout streamlining resulted in the basic design diffuser system shown in Figure 107 (blade type 1) with the following configuration:

Diffuser throat	$1/8 \text{ in.} \times 1/8 \text{ in.}$
Divergence angle	$2 \theta_D = 7^\circ$
Area ratio	$A_e/A_t = 6.63$
Length-to-throat width ratio	$L/W = 47.5$
Passage shape	Rectangular
Hydraulic radius:	
Throat	$R'_{Ht} = 0.0312 \text{ in.}$
Exit	$R'_{He} = 0.054 \text{ in.}$
No. of vanes	16
Inside radius	$R'_i = 15-7/32 \text{ in.}$
Outside radius	$R'_o = 17 \text{ in.}$

The blades were machined from aluminum on a pantograph machine. Figure 108 shows the diffuser as mounted on the annular ring, and Figure 109 shows the diffuser exit as formed by the rings. The diffuser is shown mounted in the tester in Figure 110. Close-up views of the diffuser passage are shown in Figures 111 and 112.

The tester was capable of accelerating the fluid to a speed which gave an ideal velocity head in the diffuser throat as plotted in Figure 113. For the design geometry, this corresponded to a throat Reynolds number as given in Figure 114. It was initially expected that the small diameter Pitot tube pressure taps in the diffuser passage would yield little or no reading. This suspicion was later confirmed.

63 ASRP-2391

# CONFIDENTIAL

ASD-TDR-63-665, Part I



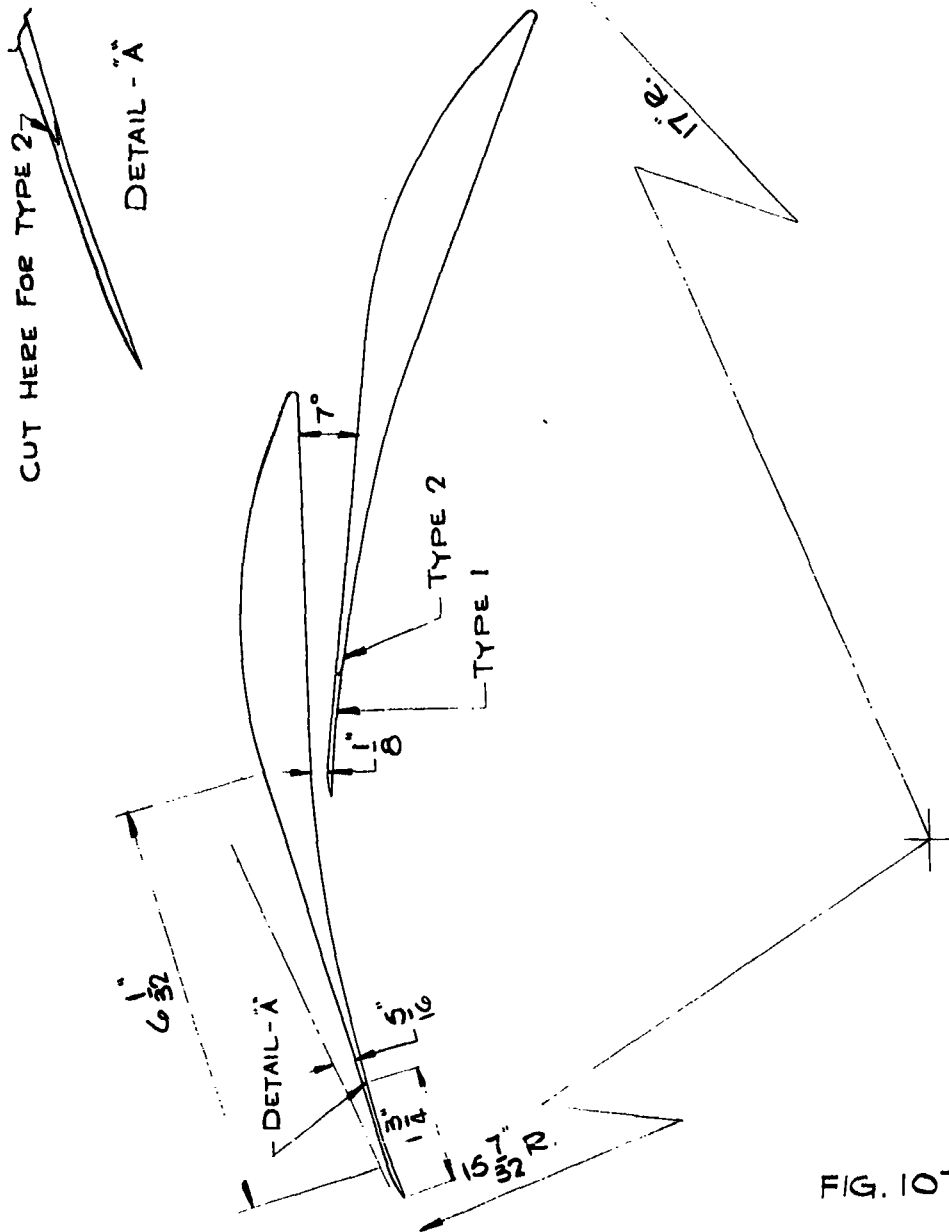
TABLE 15

ANGLE BETWEEN FLUID VELOCITY VECTOR  
AND ROTOR TANGENT

$N, \text{rpm}$	$U, \text{ft./sec.}$	$G_D, \text{gpm}$	$V_f^\circ, \text{ft./sec.}$	$\tan \phi^\circ$	$\phi^\circ, \text{deg.}$
300	39.3	10	.34	.00865	0.5
		20	.68	.01730	1.0
		30	1.02	.0266	1.5
		40	1.36	.0365	2.1
		50	1.70	.0432	2.5
400	52.5	10	.34	.00648	0.37
		20	.68	.01295	0.75
		30	1.02	.01942	1.17
		40	1.36	.0259	1.48
		50	1.70	.0324	1.85
500	65.5	10	.34	.00519	0.29
		20	.68	.01039	0.59
		30	1.02	.01558	0.89
		40	1.36	.0208	1.19
		50	1.70	.0260	1.48
600	78.7	10	.34	.00432	0.25
		20	.68	.00864	0.50
		30	1.02	.01297	0.75
		40	1.36	.0173	0.99
		50	1.70	.0216	1.23
700	91.8	10	.34	.00370	0.22
		20	.68	.00741	0.43
		30	1.02	.01111	0.64
		40	1.36	.0148	0.85
		50	1.70	.0185	1.07

63 ASRP-2391

ASD-TDR-63-665, Part I



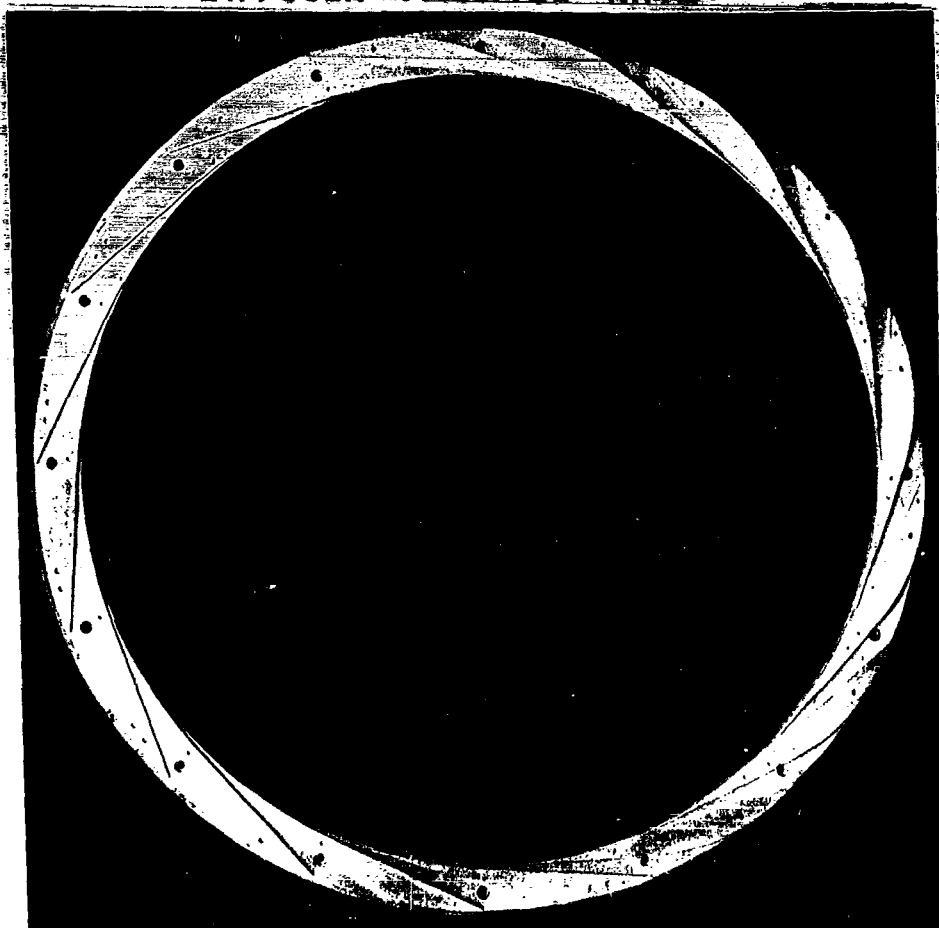
DIFFUSER CONFIGURATIONS

FIG. 107

63 ASRP-2391

ASD-TDR-63-665, Part I

DIFFUSER PASSAGE RING



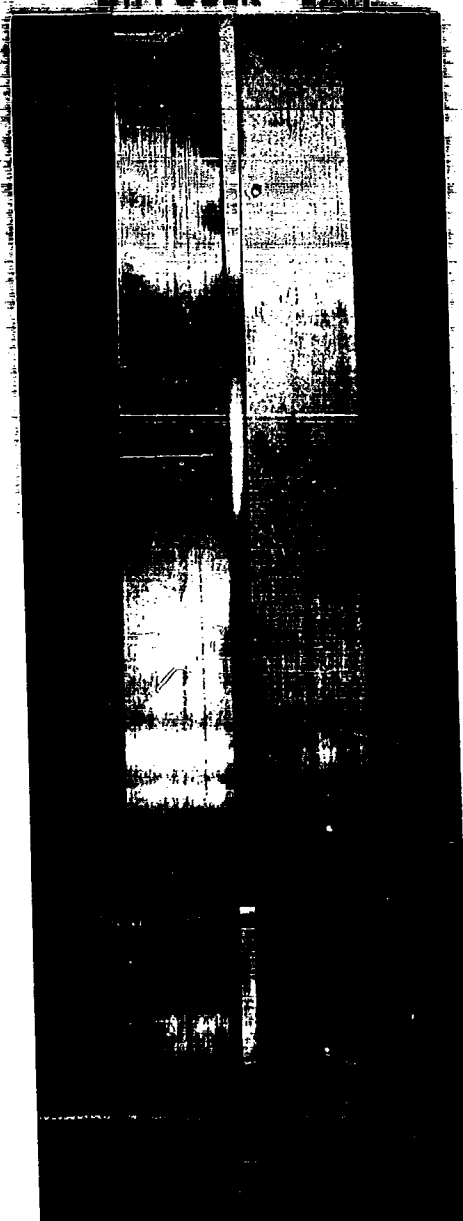
3

FIG. 108

63 ASRP-2391

ASD-TDR-63-665, Part I

**DIFFUSER EXH**



**FIG. 109**  
63 ASRP-2391



ASD-TDR-63-665, Part I

**DIFFUSER MOUNTED ON TESTER**



**FIG. 110**

63 ASRP-2391

ASD-TDR-63-665, Part I

**DIFFUSER PASSAGE**



3

**FIG. 111**

63 ASRP-2391

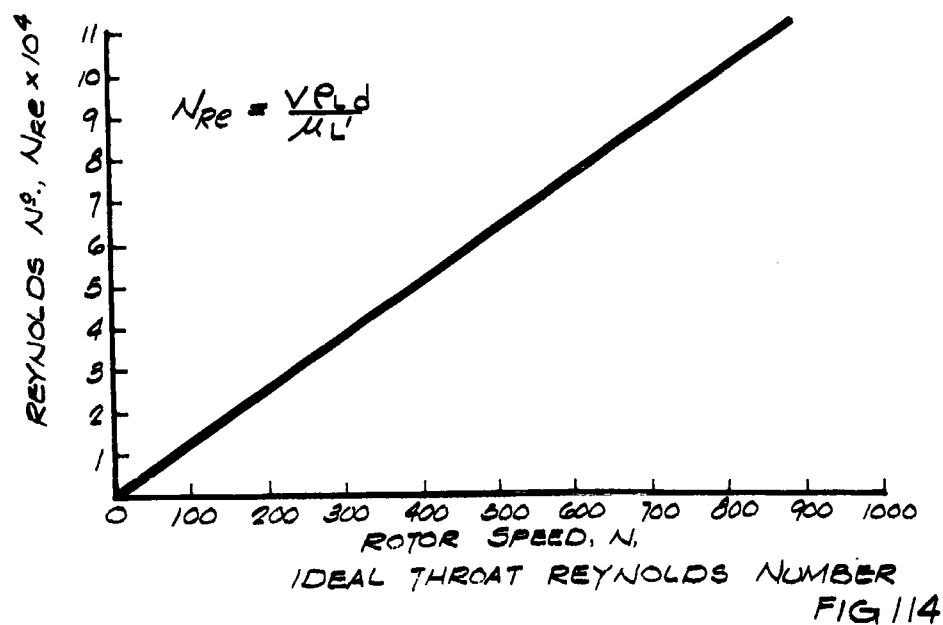
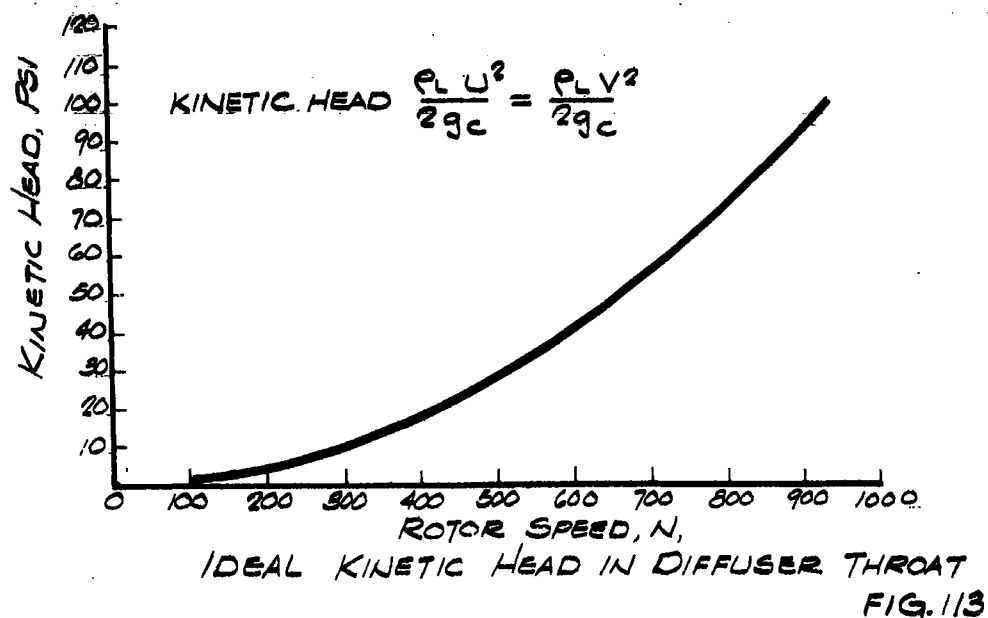
ASD-TDR-63-665, Part I

**DIFFUSER PASSAGE**



**FIG. 112**

63 ASRP-2391



**CONFIDENTIAL**

**ASD-TDR-63-665, Part I**

**5.4.2.2 Peripheral Diffuser Tests**

**5.4.2.2.1 Free Vortex Diffusion**

Although it was recognized that the diffuser passage was much too short for efficient vaneless diffusion, the initial tests were conducted without the diffuser blades. This was done to obtain a cursory picture of the free vortex diffusion process and compare its capabilities with that of an ideal free vortex diffuser occupying the same radial space. Tests were conducted at speeds ranging from 300 to 700 rpm and at flow rates ranging from 5 to 60 gpm. As shown in Figure 115, the result was a vaneless diffuser with an efficiency of approximately 40 per cent based on the ideal recovery possible for free-vortex diffusion in the available space. This indicated early in the tests the magnitude of the losses at the rotor orifice. If the free-vortex process was considered as being relatively free of friction losses, the amount of available kinetic head which was lost at the rotor orifice slot (not including blade passage entrance losses) must have been considerable according to this data. Figure 116 represents the overall energy recovery of the free vortex diffuser.

Changes in flow rate at constant speed for the vaneless diffuser tests and all subsequent tests produced very little change in the pressure rise across the diffuser, since as expected, nearly all of the kinetic energy of the fluid at the rotor exit was contained in the tangential velocity component. The results of the vaneless diffuser tests confirmed the opinion that an efficient free-vortex process would require a prohibitively large radius.

**5.4.2.2.2 Diffusion System With Eight Blades**

To progressively study the effects of the diffuser blades, the next tests were conducted with only eight blades. Such a configuration corresponds to that shown in Figure 108 with every other blade eliminated. In anticipation of the excessive inlet losses, small blades were attached to the rotor at the orifice slot to aid in propelling the liquid into the diffuser passage. These blades are shown in Figure 117. The results of these tests as plotted in Figure 118 show a marked improvement in performance over the free-vortex system plotted in Figure 116. Since adjacent blades did not overlap, a close approach to the expected efficiency of a blade type diffuser was not expected. Only an enhancement of the vaneless diffusion process was indicated demonstrating the ability of the blades to guide and smooth the flow. Again, no trend was shown by changing flow rates at constant speed.

63 ASRP-2391

**CONFIDENTIAL**

VANELESS, FREE VORTEX DIFFUSION  
(WITHOUT INCLUSION OF INLET EXIT  
EXPANSION LOSS)

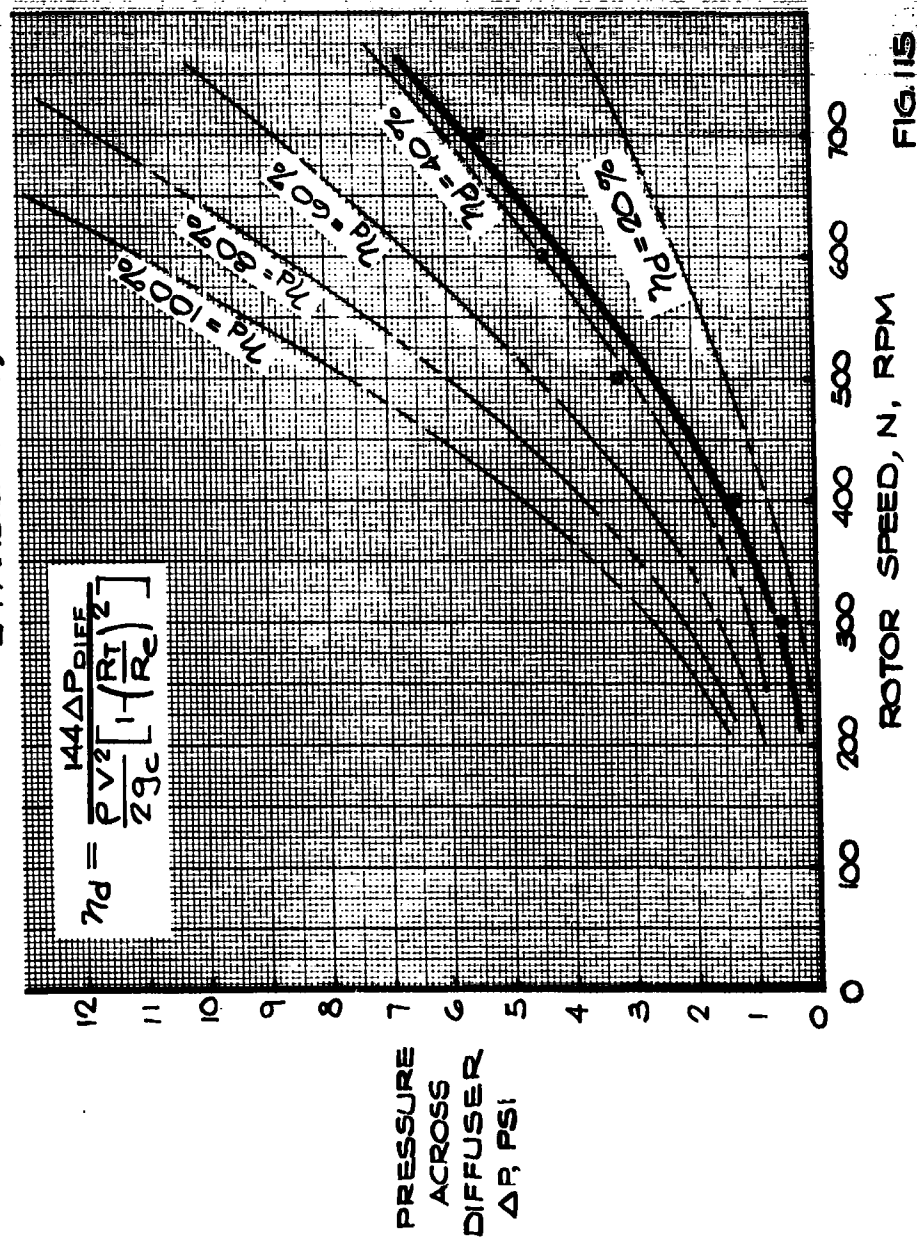


FIG. 115

# VANELESS FREE VORTEX DIFFUSION

NOTE:  
OUTSIDE DIFFUSER DIA. TOO SMALL  
FOR PROPER FREE-VORTEX DIFFUSION  
TESTS CONDUCTED FOR COMPARISON  
ONLY.

$$\eta_o = \frac{P_2 - P_1}{\frac{\rho_1 V^2}{2g_c}}$$

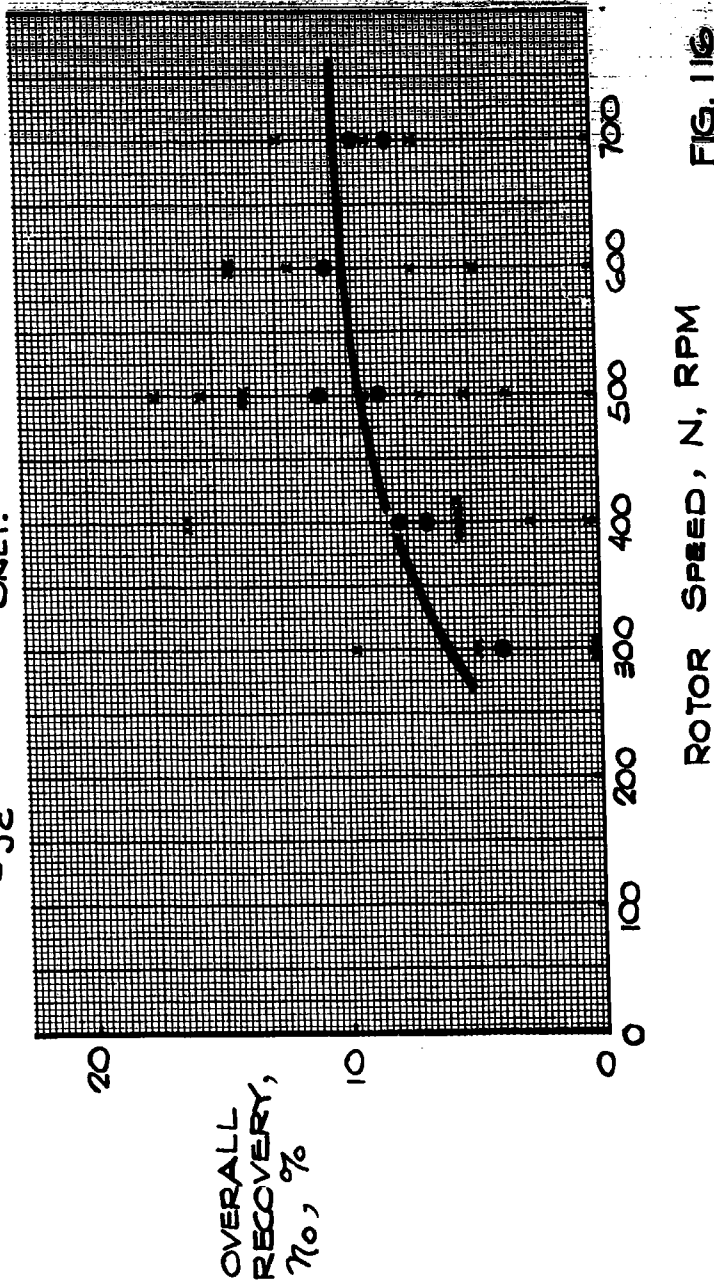


FIG. 116

63 ASRP-2391

ASD-TDR-63-665, Part I

# ORIFICE SLOT PROPELLING BLADES



FIG. 117

63 ASRP-2391



MODIFIED FREE-VORTEX DIFFUSION  
(8 BLADES)

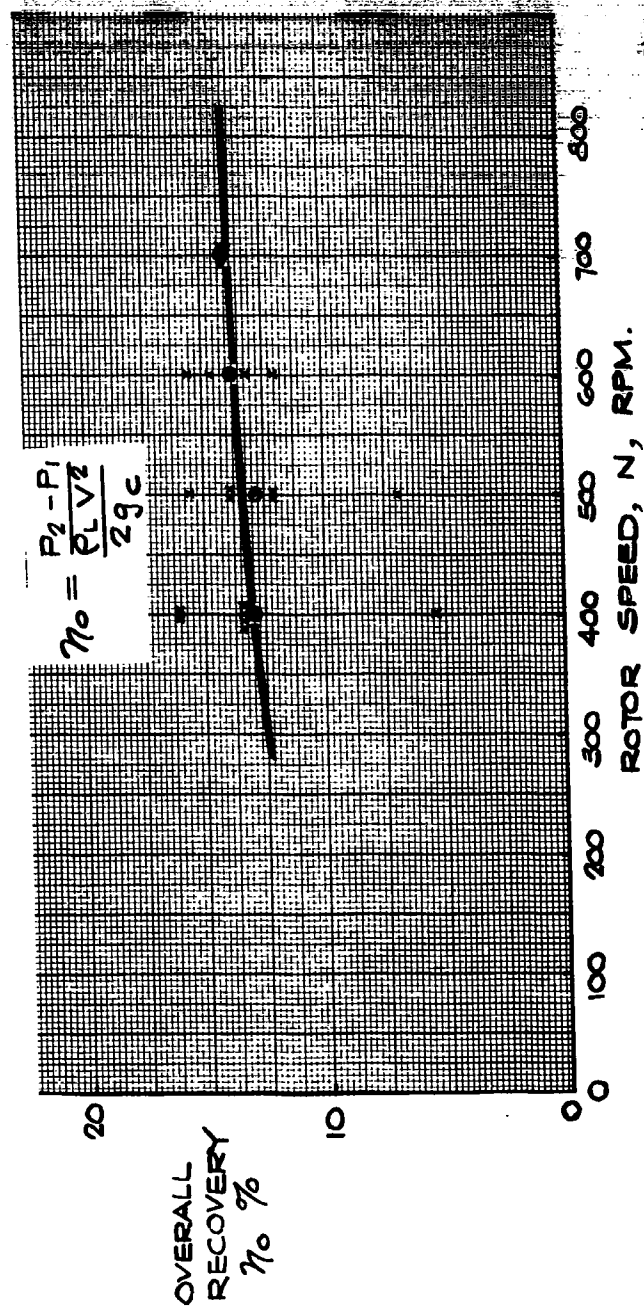


FIG. 116

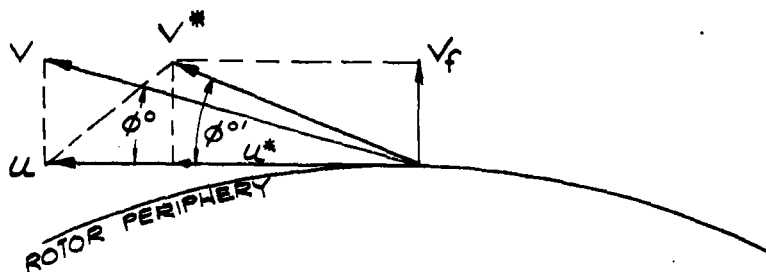
**CONFIDENTIAL**

ASD-TDR-63-665, Part I

5.4.2.2.3 Diffuser System as Designed - Type 1

The third series of tests were conducted with the designed blade and diffuser configuration of Figure 107, blade type one. The efficiency and overall recovery are plotted against speed in Figure 119. In these tests, the huge losses encountered at the rotor orifice became quite evident. A slight deterioration of diffuser performance was observed in spite of the addition of the small blades at the orifice slot in the preceding set of tests. It became evident that as the liquid was ejected from the orifice slot, it encountered very large resistance in the form of liquid trapped between the rotor and the stationary shell. As a result, it was postulated that a large percentage of the available kinetic energy was dissipated before the liquid reached the diffuser throat by the action in the boundary layer between the flowing and stationary liquids. This is shown schematically in Figure 120.

It was also felt that excessive inlet losses were being encountered as the liquid approached that extreme portion of the blade which was nearly concentric with the rotor. If, as was expected, slip was high, then the flow streamline would tend to strike this portion of the blade and be diverted into the diffuser passage as shown in Figure 121. As shown in the following figure, tangential slip thus represents the deviation in the tangential velocity vector from its theoretical value and is expressed as a percentage of the peripheral speed.



VECTOR REPRESENTATION OF SLIP

FIG 122

63 ASRP-2391

**CONFIDENTIAL**

DIFFUSER PERFORMANCE  
CONFIGURATION AS DESIGNATED  
TYPE 1

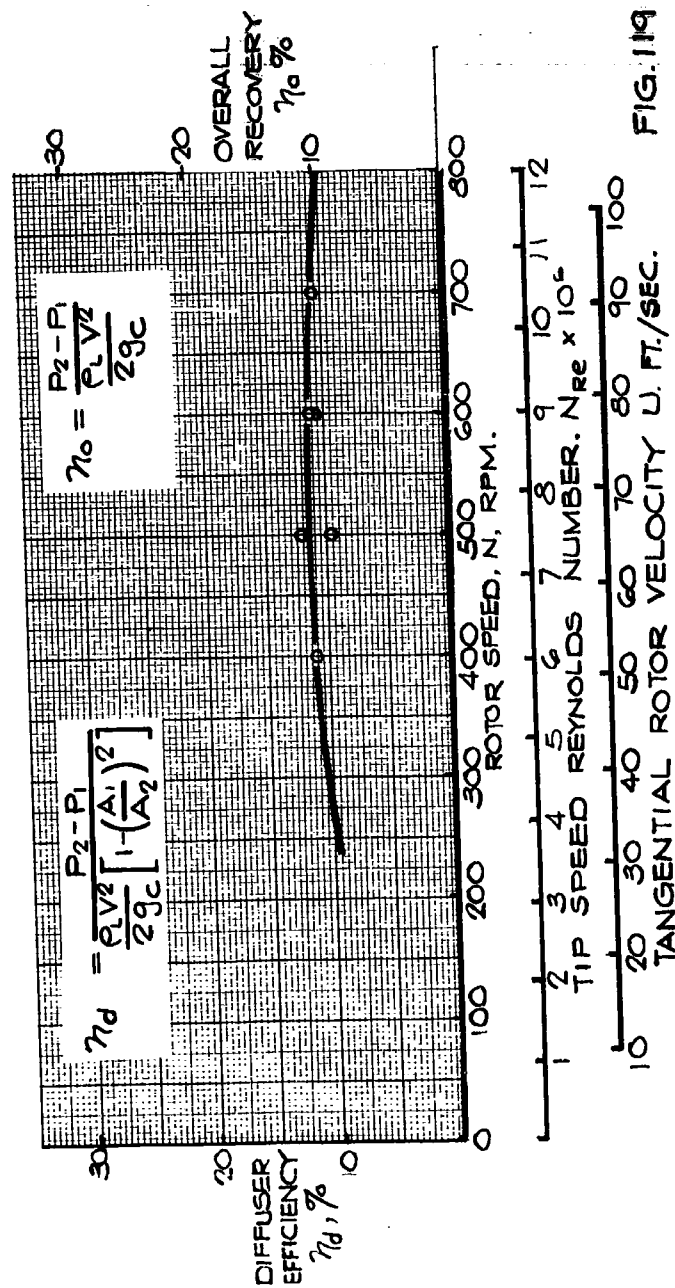
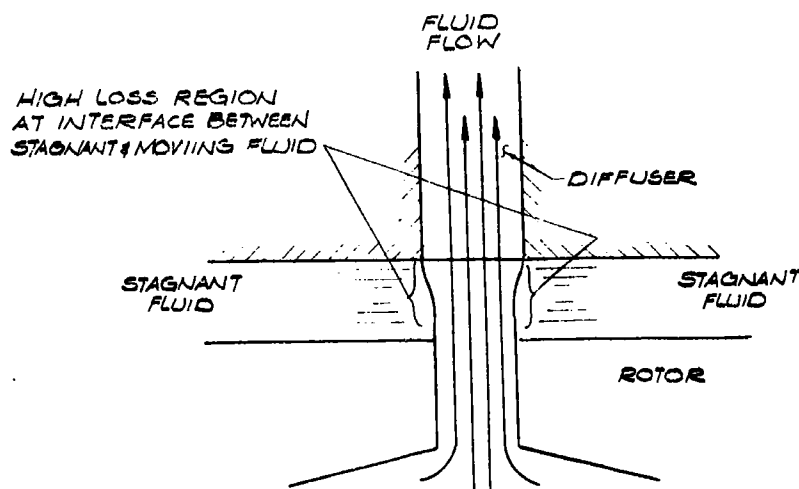


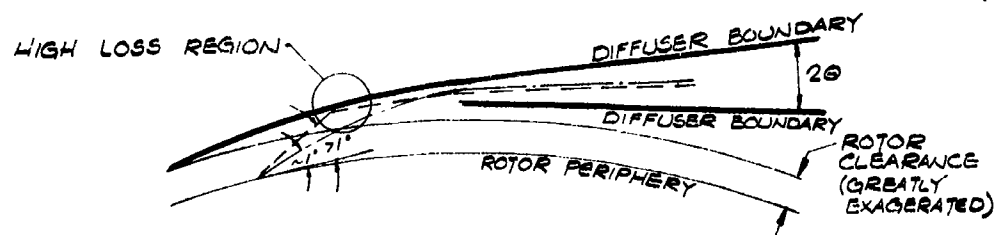
FIG. 119



HIGH LOSS REGION AT ORIFICE SLOT

FIG. 120

————— IDEAL FLOW (ANGLE  $\phi^\circ$  FOR NO SLIP)  
 - - - - - APPARENT HIGH SLIP FLOW (ANGLE  $\phi^\circ$  FOR HIGH SLIP)



INLET CONDITIONS WITH SLIP

FIG. 121

**CONFIDENTIAL**

**ASD-TDR-63-665, Part I**

**5.4.2.2.4 Diffuser System Type 2 with Removal of Inside Blade Ends of Type 1**

To alleviate the slip situation, the inside ends of the blades were cut off giving a diffuser configuration as shown in Figure 107 (blade type two). The fourth series of tests were conducted using these blades.

The diffuser geometry was significantly altered by modifying the blades. The throat width was increased to 0.3 inches. The length-to-throat width ratio was decreased to 13.28. The area ratio was decreased to 2.68 which yields an ideal static pressure rise of 86 per cent of the available kinetic head, i.e.

$$\eta_d = \frac{P_2 - P_1 (100\%)}{\rho_L \frac{V^2}{2g_c} \left[ 1 - \frac{A_1^2}{A_2^2} \right]} = \frac{P_2 - P_1 (100\%)}{\rho_L \frac{V^2}{2g_c} (.86)}$$

The divergence angle remained  $2\theta_D = 7^\circ$ . A significant improvement in diffuser performance was observed in the fourth series of tests with the shorter blade. The data as plotted in Figure 123 shows efficiencies twice as high as in previous tests. The post orifice losses remained excessive and in spite of the two-fold improvement in performance, energy recovery remained somewhat low.

**5.4.2.2.5 Diffuser System of Type 2 with Increase in Angle Between Diffuser Axis and Rotor Tangent**

The fifth series of tests were conducted to measure the effect of changing the angle between the diffuser passage axis and the rotor tangent. It was postulated that an increase in this angle ( $\phi^\circ$ ) would improve performance because of the apparently excessive slip. As shown in Figure 121, an increase in slip requires an increase in the angle  $\phi^\circ$  to allow the liquid to pass unimpeded directly along the axis of the passage. To increase this angle, the blades were respaced to allow installation of 17 blades and then pivoted about the inside end as shown in Figure 124. The result was a passage with a throat width of 0.66 inch, an area ratio of 1.50, an L/W ratio of 5.5, and a divergence angle of  $5.4^\circ$ . The tangent angle  $\phi^\circ$  was increased to  $5^\circ$ . The results appear in Figure 125. Substantial enhancement was noted indicating that slip was, indeed, excessive and that the angle  $\phi^\circ$  should be somewhat larger than the value obtained from the ideal flow conditions. It is also very important to note that an increase in slip results in a marked decrease in the available kinetic energy. This is

63 ASRP-2391

**CONFIDENTIAL**

# DIFFUSER PERFORMANCE CONFIGURATION TYPE 2 SHORTENED BLADE ENDS

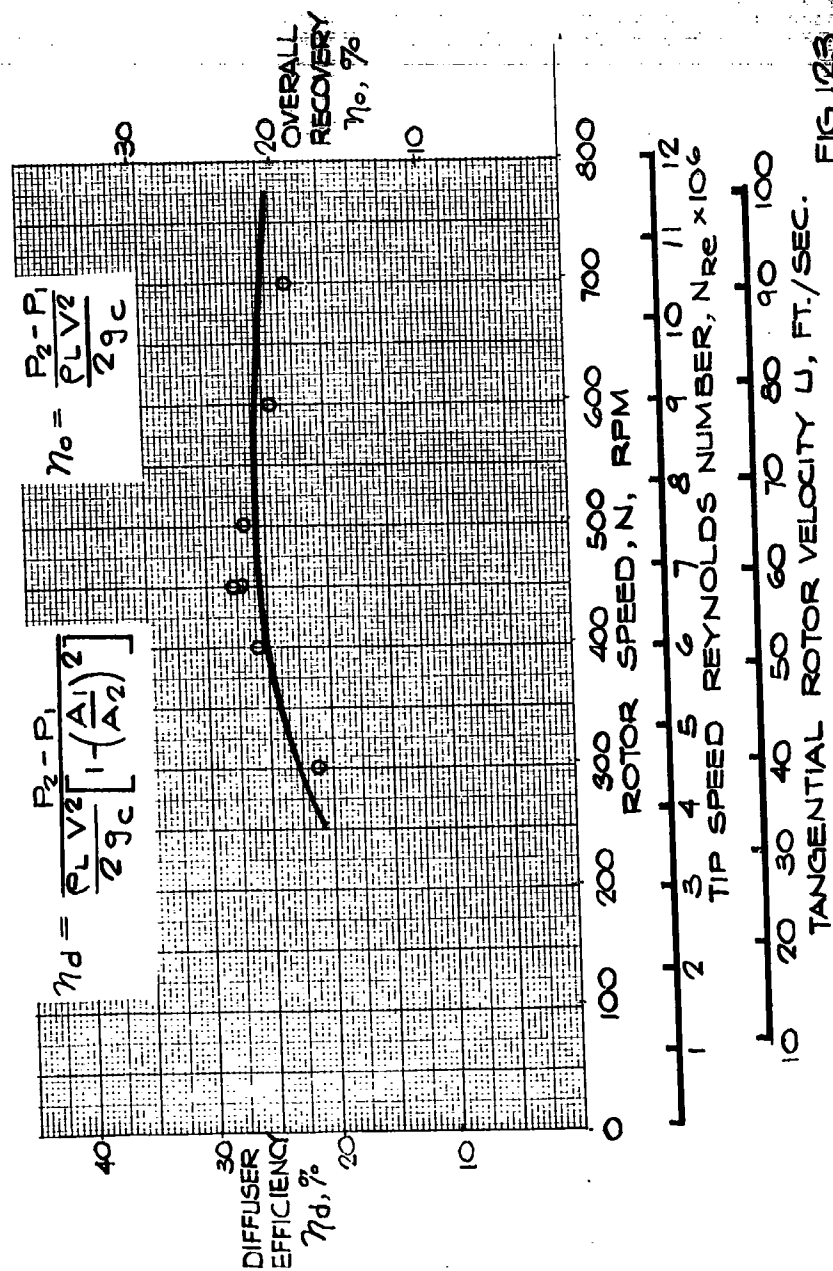


FIG 123

ASD-TDR-63-665, Part I

# PIVOTED DIFFUSER BLADE INSTALLATION



FIG. 124

63 ASRP-2391

DIFFUSER PERFORMANCE  
CONFIGURATION TYPE 2  
WITH INCREASE IN SLIP

$$\eta_o = \frac{P_2 - P_1}{\frac{\rho_L V^2}{2g_c}}$$

$$\eta_d = \frac{P_2 - P_1}{\frac{\rho_L V^2}{2g_c} \left[ 1 - \left( \frac{A_1}{A_2} \right)^2 \right]}$$

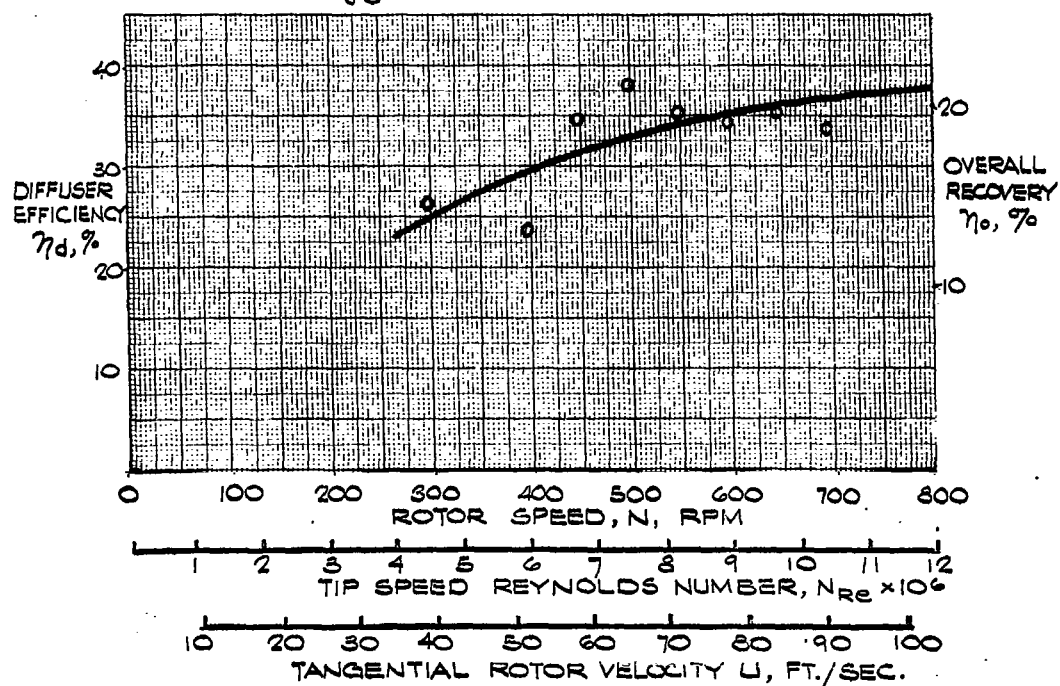


FIG. 125



**CONFIDENTIAL**

ASD-TDR-63-665, Part I

demonstrated in Figure 126 which shows the required increase in  $\phi^\circ$  and the inevitable decrease in kinetic head as slip increases. Thus, if slip is excessive, the diffuser system is operating much more efficiently than indicated since the value of  $V$  is less than the no-slip value. The size of the diffuser throat limited the size of the pressure taps which could be inserted, and it was found that no reliable reading of the total head at the diffuser throat could be obtained. The actual value of  $V$  was, therefore, unknown and all efficiencies had to be based on the rotor tip speed, i.e., no slip conditions.

5.4.2.3 Rotating Diffuser Results

Each series of tests conducted in this study emphasized the extent of the energy losses encountered between the orifice slot and the actual diffuser passage. Based upon the rotor tip speed, which does not account for these losses, diffuser efficiencies ranging between 20 and 40 per cent and overall recoveries approaching 25 per cent were obtained. Thus, in applications of this type of diffuser system with no provisions to reduce the losses, approximately 20 per cent of the total kinetic head available at the rotor periphery may be converted to static pressure.

Several design innovations were considered to enhance the energy recovery for the diffuser. Since high losses are encountered as the fluid leaves the orifice slot (i.e., between the orifice slot and the diffuser throat), a system of blades is proposed (as shown in Figure 127) to propel the flowing fluid past the stationary liquid at the rotor periphery. The blades accelerate the fluid through the high loss region and the guard eliminates the boundary layer between the moving liquid and the stationary liquid. The blades discharge the fluid directly into the diffuser passage. The magnitude of these boundary layer losses would also be considerably reduced in a system with a wider flow passage where the thickness of the boundary layer is much smaller compared to the width of flow. Secondly, the angle between the diffuser axis and the rotor tangent should be increased to compensate for slip at the rotor periphery. This is limited somewhat by dimensional boundaries, but it was felt that an increase in the divergence angle,  $2\theta_D$ , would allow a sufficient increase in  $\phi^\circ$  with no noticeable deterioration in diffuser performance. In addition, the diffuser inlet profile should be as simple and smooth as possible to minimize inlet losses. Comparison of smaller losses and larger flow areas of the stationary tests with the larger losses

63 ASRP-2391

**CONFIDENTIAL**

CALCULATED SLIP CHARACTERISTICS  
ROTARY AIR-WATER TESTER

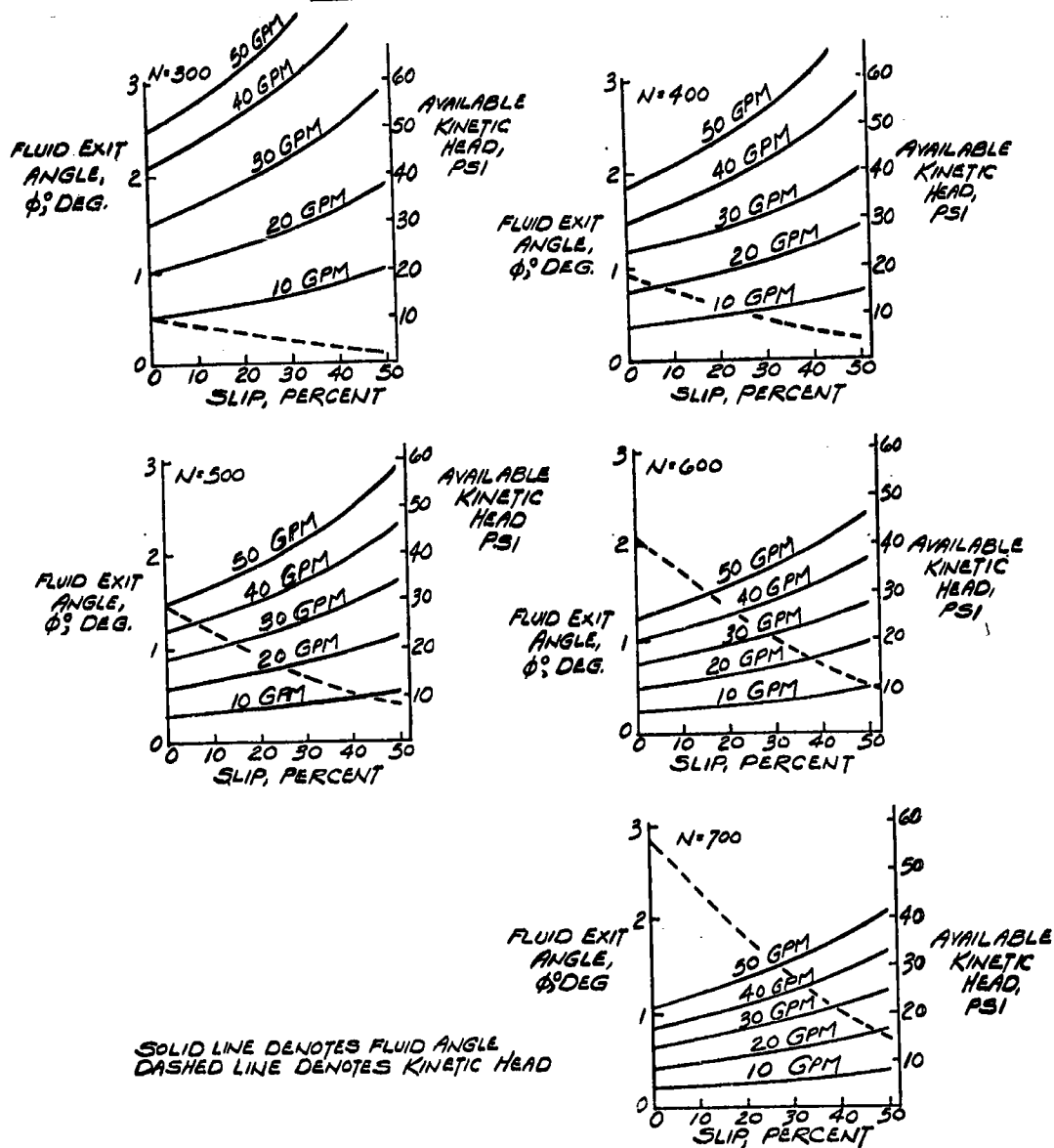
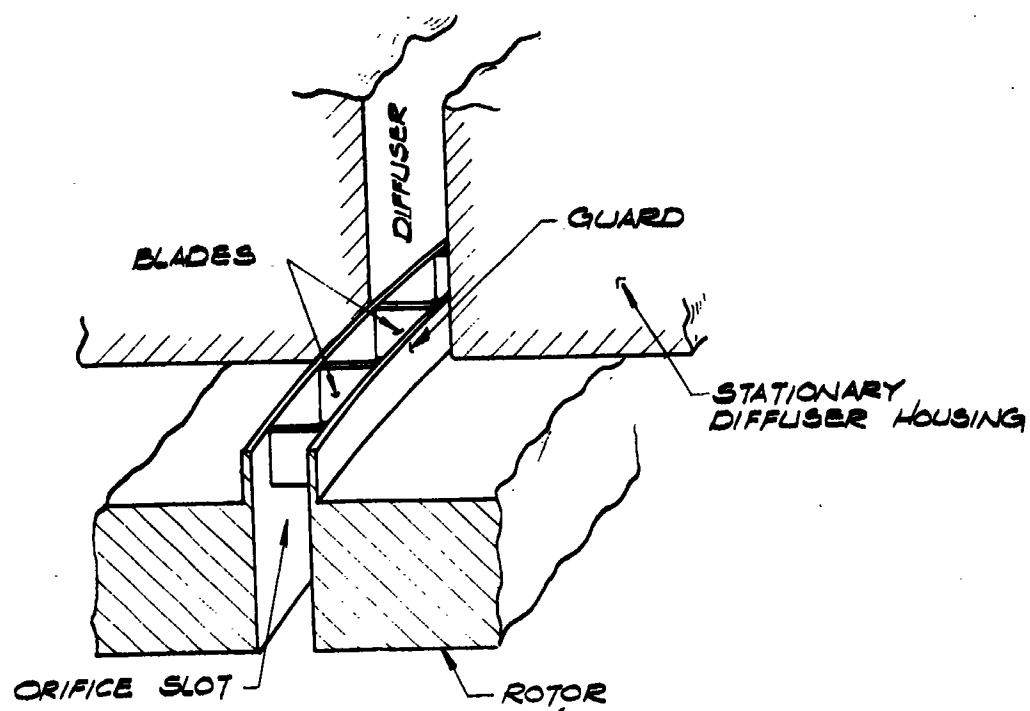


FIG. 126



ORIFICE SLOT PROPELLING BLADES

FIG. 127

**CONFIDENTIAL**

**ASD-TDR-63-665, Part I**

and smaller flow areas of the rotary tests appears to substantiate the opinion that increased flow areas reduce friction losses.

All of these design innovations can be incorporated in a rotating air separator.

Based upon the results of the tests, it is reasonable to assume that overall recoveries of over 25 per cent, including all inlet losses, may be expected for a 100 lb./sec. unit.

It should be emphasized that the relatively large losses encountered in these experimental tests are characteristic of the small flow passages and large boundary layer losses inherent in the system. It is felt that the large flow rates and enlarged passage geometry of a full scale machine will greatly enhance diffuser performance.

**5.5 Pressure Drop in Two-Phase Flow Against a Gravitational Field**

**5.5.1 Analysis**

The problem of two-phase flow is encountered in the transfer of kettle and shelf liquid in a rotating double column separator. Since from these locations saturated liquid has to be transported radially inward against a gravitational field, it will flash and form a two-phase mixture. Because of the high gravitational field acting upon the fluid, pressure drop due to gravitational head differences represents by far the predominant portion of the overall pressure drop experienced. An accurate prediction of this pressure drop is essential to proper design of control components and to define possible limitations in operating speed for the separator since at high speeds the required pressure drop can approach the pressure difference available between kettle and low-pressure column.

A great deal of work has been concentrated recently on the field of two - phase flow by a number of investigators. To discuss or compare all the various attempts would be extremely lengthy and is not the purpose of this report. Basically a number of methods have been tried by many investigators in an effort to predict the two-phase frictional pressure drop and the volumetric liquid fraction,  $R_L$ . In the majority of cases, the primary interest was in the frictional pressure drop multiplier that would allow prediction of two-phase pressure drop from a knowledge of

63 ASRP-2391

**CONFIDENTIAL**

**CONFIDENTIAL**

ASD-TDR-63-665, Part I

the liquid phase pressure drop. Perhaps the most well known, Lockhart-Martinelli, (Ref. 36), originally developed a parameter  $X$  which did precisely that. They then used this same parameter to correlate  $R_L$ . A number of reasons negated the use of this parameter. Previous work done at Linde on two-phase flow in vertical heat exchangers showed that Lockhart-Martinelli generally predict an  $R_L$  that is too low for vertical flow. In addition, it was felt that a more fundamental parameter was necessary since  $X$  did not include a gravitational term and since the friction factor ratio was of negligible influence in the case under study where the frictional pressure drop was negligible compared to the "hydrostatic" head.

By dimensional reasoning, it was deduced that  $R_L$  should be primarily a function of the gravitational field and fluid properties as shown in the following expression:

$$R_L = F [ Ng^{C_3}, \left(\frac{1-X}{X}\right)^{C_4}, \left(\frac{\rho_v}{\rho_L}\right)^{C_5}, V_L^{C_6} ]$$

where:

$$C_3 = F [ \left(\frac{1-X}{X}\right)^{C_7}, \left(\frac{\rho_v}{\rho_L}\right)^{C_8}, V_L^{C_9} ]$$

In addition to the properties listed, viscosities and probably surface tension should have some influence upon  $R_L$ . However, they were neglected in the work under discussion, since other investigators had shown the effect of these properties to be relatively insignificant.

Assuming that frictional pressure drop can be neglected, the pressure drop encountered between two radii of a rotating device is:

63 ASRP-2391

**CONFIDENTIAL**

~~CONFIDENTIAL~~

ASD-TDR-63-665, Part I

$$\Delta P_{R_1 - R_2} = \int_{R_1}^{R_2} \frac{r \omega^2}{g} \rho_{TP} dr$$

where:

$$\rho_{TP} = \rho_L R_L + \rho_V (1 - R_L)$$

$\rho_L$  and  $\rho_V$  are functions of the pressure at location  $r$ . In the case at hand, the densities were defined by assuming isentropic expansion for the fluid flowing radially inward.

In order to compute pressure drop in radial inward flow, it is necessary to know the liquid volume fraction  $R_L$  at each location  $r$ . Since in flow against a gravitational field, the liquid moves slower than the cocurrent vapor, the amount of slip experienced between liquid and vapor will determine the magnitude of  $R_L$ . As it is not possible to set up a sufficiently accurate physical model for two-phase flow,  $R_L$  cannot be derived analytically, but has to be determined by an experimental correlation.

#### 5.5.2 Air-Water Experimental Program

With the above general expression in mind, a test program was planned for a rotating air-water test apparatus constructed for this work as well as for peripheral seal and diffuser tests. A detailed description of the tester is given in the section describing diffuser and seal test work. For two-phase flow work, the tester contained a 3/4 in. I.D. or 3/8 in I. D. radial Plexiglas tube with orifices drilled around the "bottom" circumference of the tube (see Figures 128 and 129.) When air was introduced to the rotor, the resulting pressure differential through the orifices caused the water rotating at the periphery to flow co-currently with the air counter to the gravitational field to the center of the rotor, from where it was discharged. The air pressure and flow, as well as the water flow could be varied, as could be the rotational speed. Pressure drop across the 3 in. long test section was measured with a transducer mounted on the rotor.

63 ASRP-2391

~~CONFIDENTIAL~~

ASD-TDR-63-665, Part I

**TWO PHASE FLOW TEST SECTION**

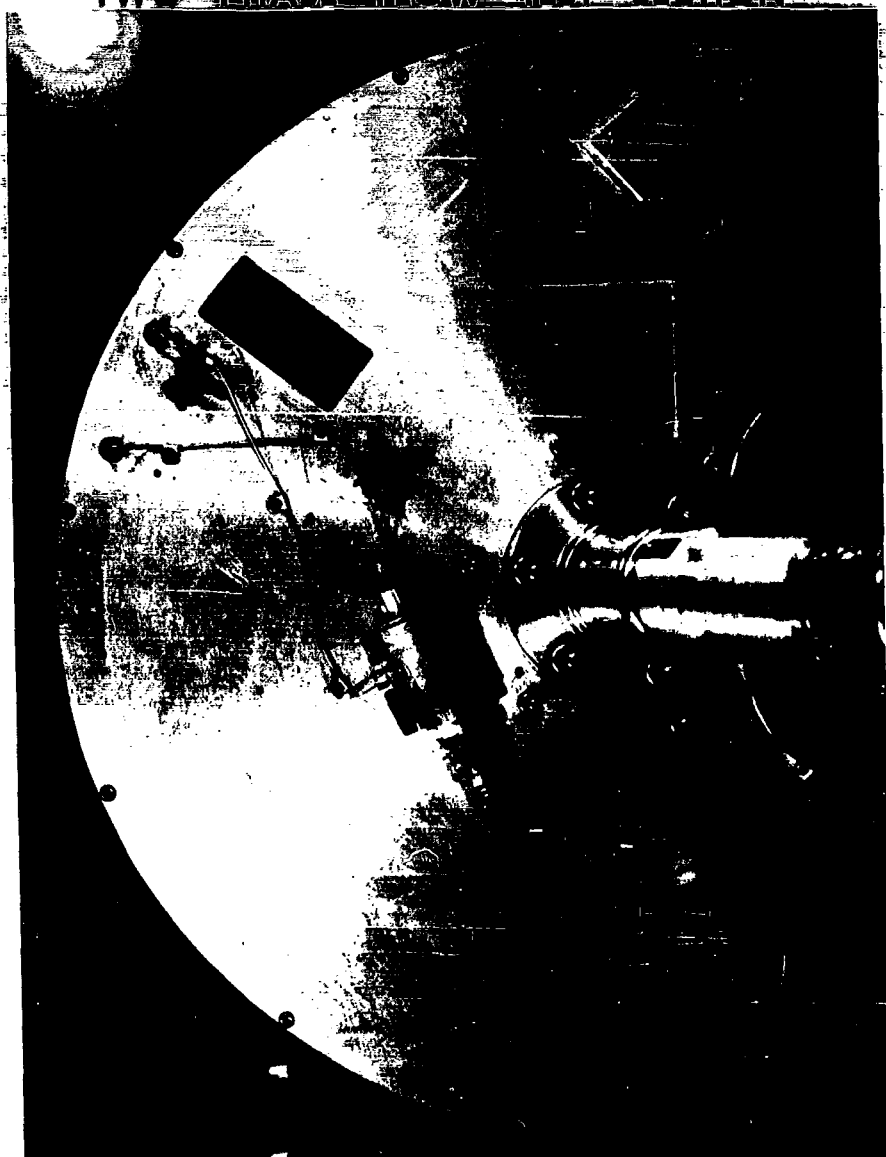
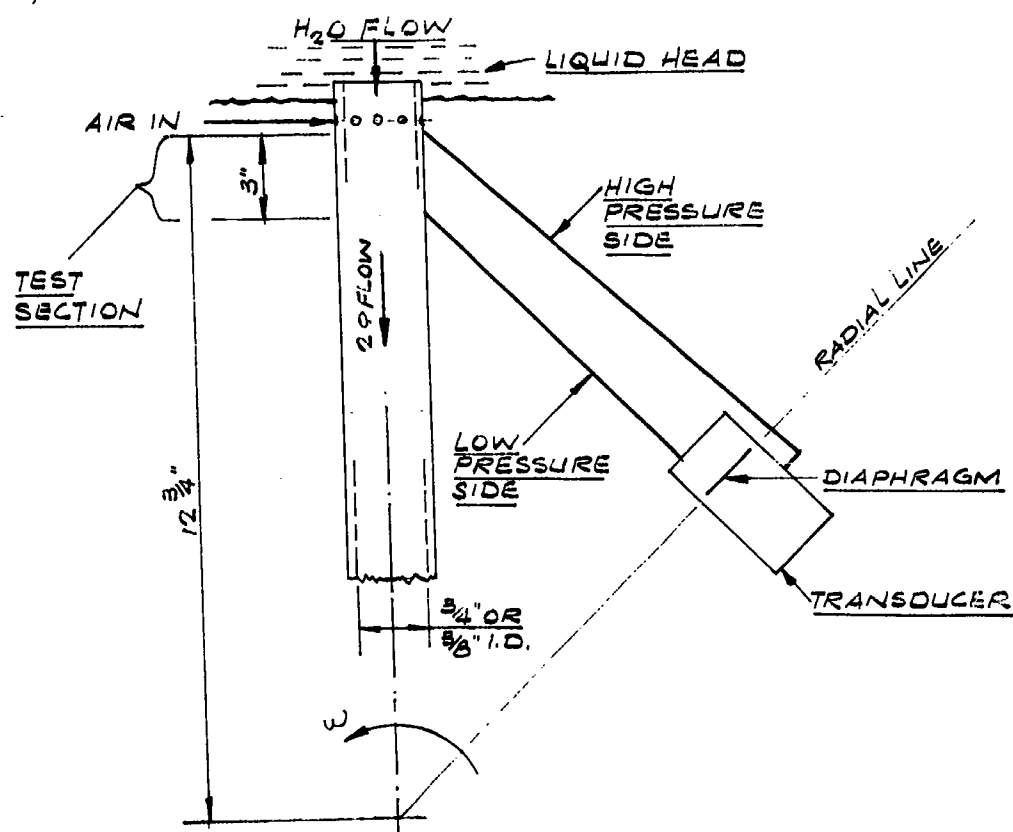


**FIG. 128**

63 ASRP-2391



TWO PHASE FLOW TEST SECTION SCHEMATIC

FIG. 129



**CONFIDENTIAL**

**ASD-TDR-63-665, Part I**

After an initial period in which trouble was encountered with flooding of transducers, a series of data was taken, using a 3/4 in. diameter tube and a 3/8 in. diameter tube. Since no noticeable effect of tube diameter upon pressure drop was detected, this parameter was eliminated from further consideration. The actual effects may have been hidden by the experimental inaccuracies, but for practical purposes they are not important as long as they do not influence the flow regime. This effect of flow regime is accounted for by the  $\frac{1-x}{x}$  term and the  $V_L$  term. Since the primary area of interest was in the bubble and slug flow regime, the majority of data points were taken there. In bubble flow, the air seems to be suspended as bubbles, while in slug flow the liquid is carried along in slugs and large drops. Some points were taken in the annular flow regime. This regime occurs when the ratio of vapor to liquid is so high that the vapor forms a core that forces the liquid to run down the sides of the tube in an annular ring cross section. In this regime, a fairly sharp decrease in pressure drop is realized compared to the mixed flow regimes. This was experimentally confirmed with air-water.

A number of photographs of the flow pattern were taken. Unfortunately, the majority of these are unclear since the Strobe-light used did not have a sufficiently fast response time. At speeds above 300 rpm, the photographs are blurred but at 300 rpm or less, the photographs are very clear and various flow effects can be deduced. As seen in Figures 130 and 131, taken for the 3/4 inch and 3/8 inch diameter tubes, the flow consists of a foam or slug flow in which the liquid is carried along in the fast moving vapor stream. It can be seen that for the smaller diameter tube, as well as for lower g fields, the flow tends to be more of the slug type. The effect of the Coriolis force is also apparent. This force tends to crowd the liquid to the leading edge of the tube.

When the initial series of data were taken, it was correlated using a linear regression technique. Since  $Ng$  was a function of the other variables, it was examined first. By plotting  $R_L$  versus  $Ng$  on log-log coordinate paper, the trend of  $d(\ln R_L)/d(\ln Ng)$  was determined and used as input for the correlating of the remaining parameters; i.e.,  $Ng^{c_3}$  and  $R_L$  were used as the dependent variables with  $\frac{1-x}{x}$ ,  $(\rho_v/\rho_L)$ , and  $V_L$  as the independent variables.

The resulting parameter, which was essentially linear, was so strongly dependent on the weight L/V ratio that more data points were needed to adequately cover the kettle flow range

63 ASRP-2391

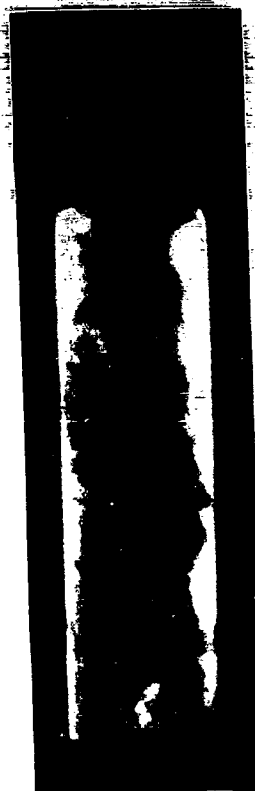
**CONFIDENTIAL**

ASD-TDR-63-665, Part I



$\omega$

$\overline{N_g} = 29$   
 $L/V = 0.06$   
 $\rho_v = 0.25$   
 $\Delta P = 0.4 \text{ psi}$



$\omega$

$\overline{N_g} = 116$   
 $L/V = 0.06$   
 $\rho_v = 0.25$   
 $\Delta P = 4.25 \text{ psi}$



$\omega$

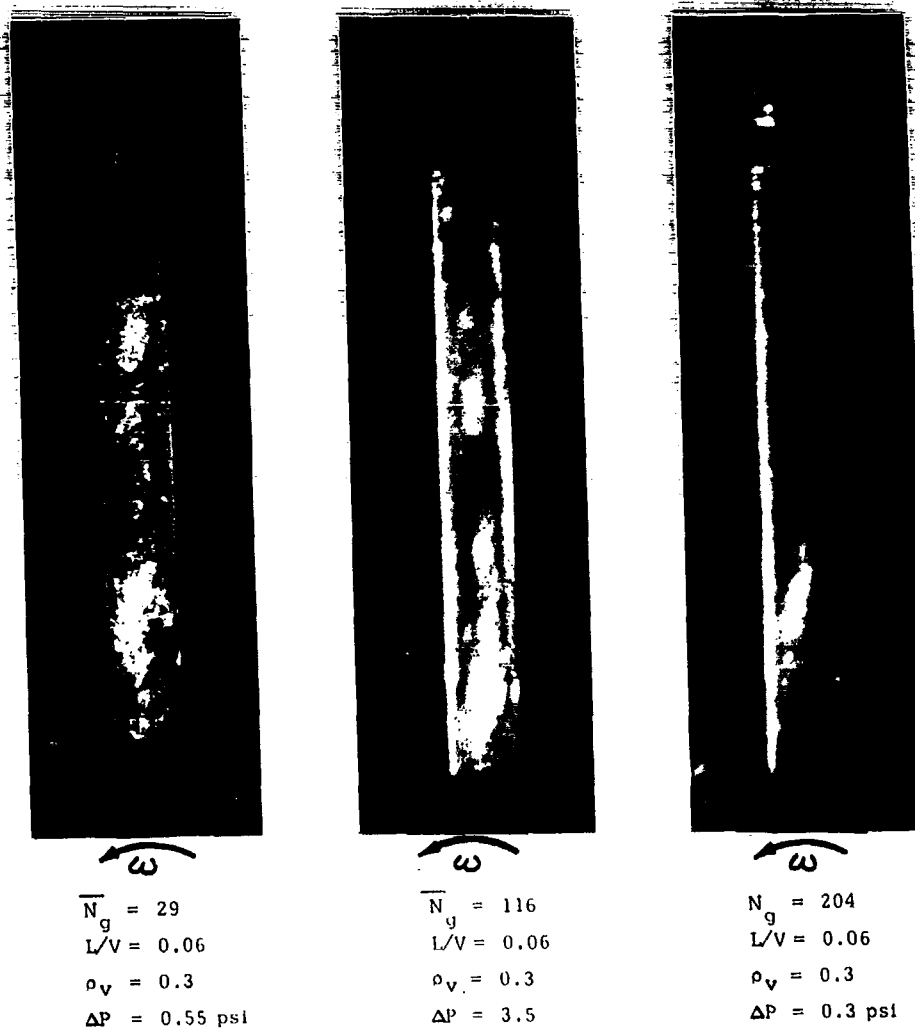
$\overline{N_g} = 156$   
 $L/V = 0.128$   
 $\rho_v = 0.25$   
 $\Delta P = 8.25 \text{ psi}$

TWO PHASE FLOW

FIG. 130

63 ASRP-2391

ASD-TDR-63-665, Part I



TWO PHASE FLOW

FIG. 131

63 ASRP-2391

**CONFIDENTIAL**

ASD-TDR-63-665, Part I

(relatively high L/V). With these points, the finalized correlation was established for air-water mixtures.

The new points, taken at relatively high L/V, confirmed the prediction that the curve (See Figure 132) would bend and level off from the initially sharp slope at lower L/V ratios. The correlating parameter used was:

$$\gamma = \frac{V_L^{1/2} \left( \frac{x}{1-x} \right)^{3/2} \frac{\rho_L}{\rho_v}}{(Ng)^Z}$$

where:

$$Z = \left[ .038 \left( \frac{x}{1-x} \right)^{1/2} \left( \frac{\rho_L}{\rho_v} \right)^{1/3} \right]$$

This parameter predicted the  $R_L$  with about  $\pm 20\%$  error. However, it contained several inadequacies. The Ng exponent was difficult to establish with certainty since the effect of this variable on  $R_L$  in the range of interest is not very large. This was reflected in the poor correlation coefficient realized in the linear regression of the Ng term. However, the major trend is correct, and the Ng term will give satisfactory results in consideration of the modest test program undertaken.

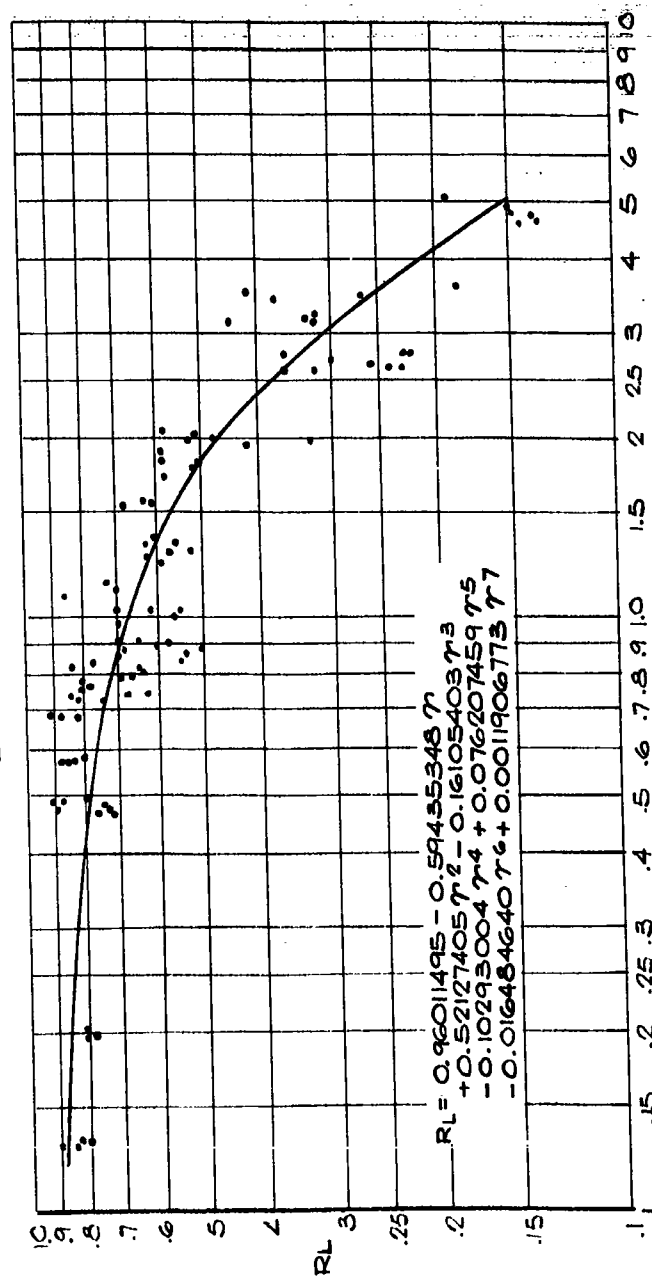
The major conclusions that could be drawn from the air-water tests are the following:

- a. Most significantly for the design of the 100 lb./sec. unit, the increase in slip between the phases and consequently two-phase density due to the high gravitational field is relatively small.
- b. A change in pipe diameter has little influence upon the observed pressure drop for identical flow patterns, except that it can lead to a change in flow pattern in which case the pressure drop changes.
- c. For very low vapor to liquid ratios  $x/1-x$  and density ratios  $\rho_L/\rho_v$ , two-phase density is essentially independent of Ng. As these ratios are decreased  $d\rho_{Tp}/dNg$  becomes larger.

63 ASRP-2391

**CONFIDENTIAL**

TWO PHASE VOLUMETRIC LIQUID FRACTION  
RL AIR WATER DATA



$$\gamma = \frac{V_L \frac{1}{2} \left( \frac{x}{1-x} \right)^{\frac{1}{2}} \left( \frac{\rho_L}{\rho_V} \right)}{N_g \left[ 0.38 \left( \frac{x}{1-x} \right)^{\frac{1}{2}} \left( \frac{\rho_L}{\rho_V} \right)^{\frac{1}{2}} \right]}$$

Fig. 132

**CONFIDENTIAL**

ASD-TDR-63-665, Part I

Utilizing the derived correlation for predicting the two-phase density, a computer program was written which allows computation of the pressure drop experienced in flow of a flashing liquid through a tube against a gravitational field. Upon input of the necessary data, the computer proceeds along the tube in increments of any desired length and by trial and error solution converges upon the correct pressure drop. It then prints out, for each segment, the vapor quality, pressure, two-phase density,  $R_p$ , pressure drop, liquid density, vapor density, and  $\Gamma$ . A short format allows print out of only the first three quantities. The flowsheet for this program is presented in Appendix XI.

5.5.3 UCON Fluid Experimental Program

To test the established correlation with a different fluid system and possibly detect the influence of new parameters on  $R_p$ , experiments were run in conjunction with the control valve tests using UCON 12 as a test fluid. A description of the test rotor is available in the discussion of control system tests.

Saturated UCON liquid was supplied to the test rotor and moved to the periphery where it established a liquid level. This liquid level could be controlled. Pressure difference was used to drive the liquid radially inward through two 5/8 inch diameter tubes. On one of the tubes two pressure taps were located at radii of 12-1/8 inch and 9-1/8 inch respectively. A Pace transducer was used to measure the resultant pressure drop.

A total of fourteen runs were made over an RPM range of 480 to 800, a velocity range of 1.5 to 8.2 ft./sec., and an inlet pressure range of 125 to 145 psia.

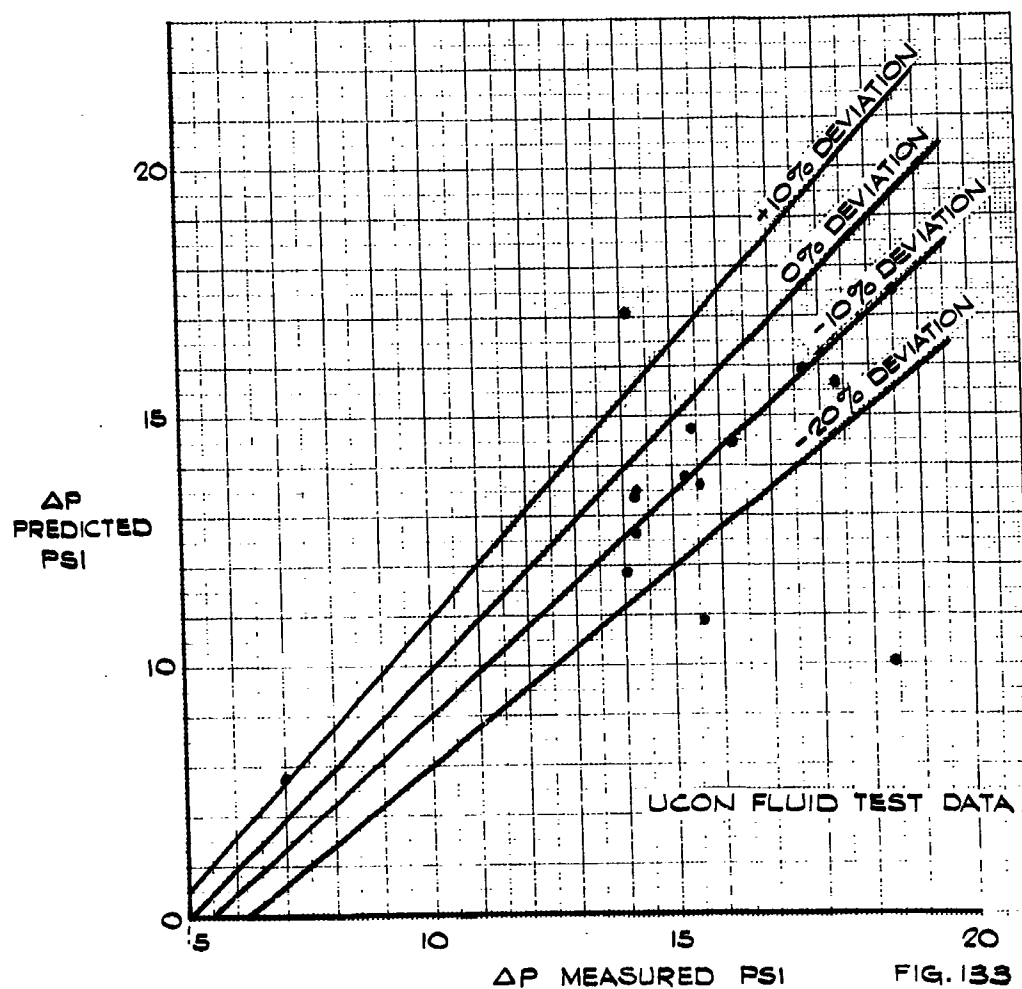
For each run, using the measured inlet conditions, the two-phase computer program was run and the "predicted" pressure drop calculated. This  $\Delta P$  was compared with the measured  $\Delta P$  as shown in Figure 133. Results were very satisfactory, the average absolute error being equal to 10.7%.

Because the deviation between predicted and measured pressure drop was so small, changing the correlating parameter could not be justified. Undoubtedly, the chosen parameter could be improved upon, but this would require a more elaborate test program than the one undertaken.

63 ASRP-2391

**CONFIDENTIAL**

TWO PHASE FLOW AGAINST GRAVITATIONAL FIELD  
PREDICTED VS. MEASURED  $\Delta P$   
FOR UCON FLUID



**CONFIDENTIAL**

#### ASD-TDR-63-665, Part I

As can be seen in Figure 133, twelve of the fourteen points had negative deviation. This is explainable by the fact that a group of air-water data points with much lower  $R_L$  values than the main body of points were included in the least squares fit of  $R_L = f(\gamma)$ . The lever effect of these points was responsible for a predicted  $R_L$  that is lower than measured in that region. Therefore, the UCON fluid data points were added to the air-water points and a new least squares fit calculated. The result is shown, along with the data points in Figure 134. Since the coefficients of this curve are input data to the computer program, it was a simple matter to make allowance for this change. The lower data scatter experienced with UCON is attributed to the fact that a more reliable pressure transducer was used during the UCON runs.

Since the UCON physical properties are very close to the properties of liquid air, it is felt that the pressure drop in the boilerplate model transfer lines can be predicted with an average accuracy of  $\pm 10\%$  and a fair degree of confidence in the calculations.

#### 5.5.4 Pressure Drop Results for Two Phase Flow

The proposed correlation was compared with the results of Lockhart-Martinelli. For the range of  $R_L$  greater than .7, Lockhart-Martinelli predicts much lower values than this correlation. Below  $R_L = .7$ , this correlation approaches Lockhart-Martinelli. The correlation can only be applied down to an  $R_L$  of about .15 since no data was taken below this range. As pointed out earlier examination of the data will reveal that the  $Ng$  influence is small at high  $L/V$  values and becomes larger as the  $L/V$  decreases.

#### 5.6 Internal Control System

##### 5.6.1 Control System Description and Analysis

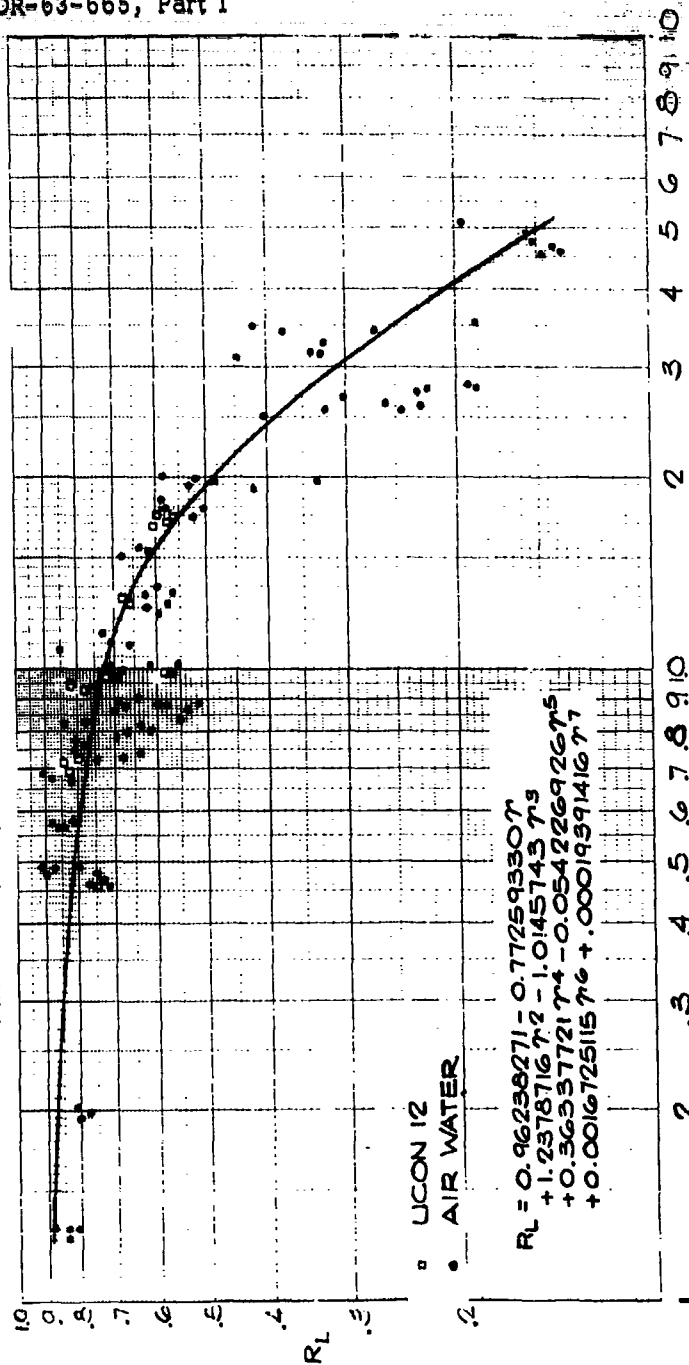
As discussed earlier, two high pressure liquid streams on the boilerplate separator have to be transferred radially inward to the low pressure column. These are the kettle and the shelf liquid streams. In order to avoid bypassing of high pressure vapor to the low pressure column on the one hand and excessive liquid buildup in respective collector spaces on the other, it is necessary to control liquid transfer to maintain a constant liquid level in the kettle and shelf liquid collectors. Since it is difficult and complicated to use a combination of internal sensing device, and control valve operator and an external controller, it was decided to provide a control system completely contained inside of the

63 ASRP-2391

**CONFIDENTIAL**



TWO PHASE VOLUMETRIC LIQUID FRACTION -  $R_L$   
AIR WATER AND UCON FLUID DATA



63 ASRP-2391

$$r = \frac{\left(\frac{x}{1-x}\right)^2 \left(\frac{p_L}{p_V}\right)^{\frac{1}{2}} v_{Lr}^{\frac{1}{2}}}{N_g \left[ \frac{0.08}{1-x} \right]^2 \left(\frac{p_L}{p_V}\right)^{\frac{1}{2}}}$$

FIG. 134

~~CONFIDENTIAL~~

ASD-TDR-63-665, Part I

separator rotor. Because of the critical influence of control system operation, it was felt that a prototype system should be tested in a rotating device simulating the actual separator application.

The simplest control system appeared to consist of a pneumatic control valve which is operated directly by the pressure differential due to liquid level. A schematic of the conceived control system is shown on Figure 135. It consists of a bellows operated valve, the bellows of which are connected to respective liquid level taps. To generate a signal the liquid level tap is connected via an electrically heated reservoir.

An analysis was made on a simplified control system model to obtain some indications of control response times. As shown in Appendix XII, the time constant for the simplified system can be shown to be

$$T_1 = \frac{k_1 k_3}{k_2 k_4}$$

and

$$h_L(t) = \frac{\alpha_1 W_o}{k_1} e^{-t_1/T_1}$$

here

$$k_1 = \rho_L 2 \pi b_k (r_{0k} - H_o)$$

$$k_2 = (2 g_c \Delta P \rho_L)^{1/2}$$

$$k_3 = \frac{2 (k_s + k_b) g_c}{A_B \rho_L \omega^2 r_{ok}}$$

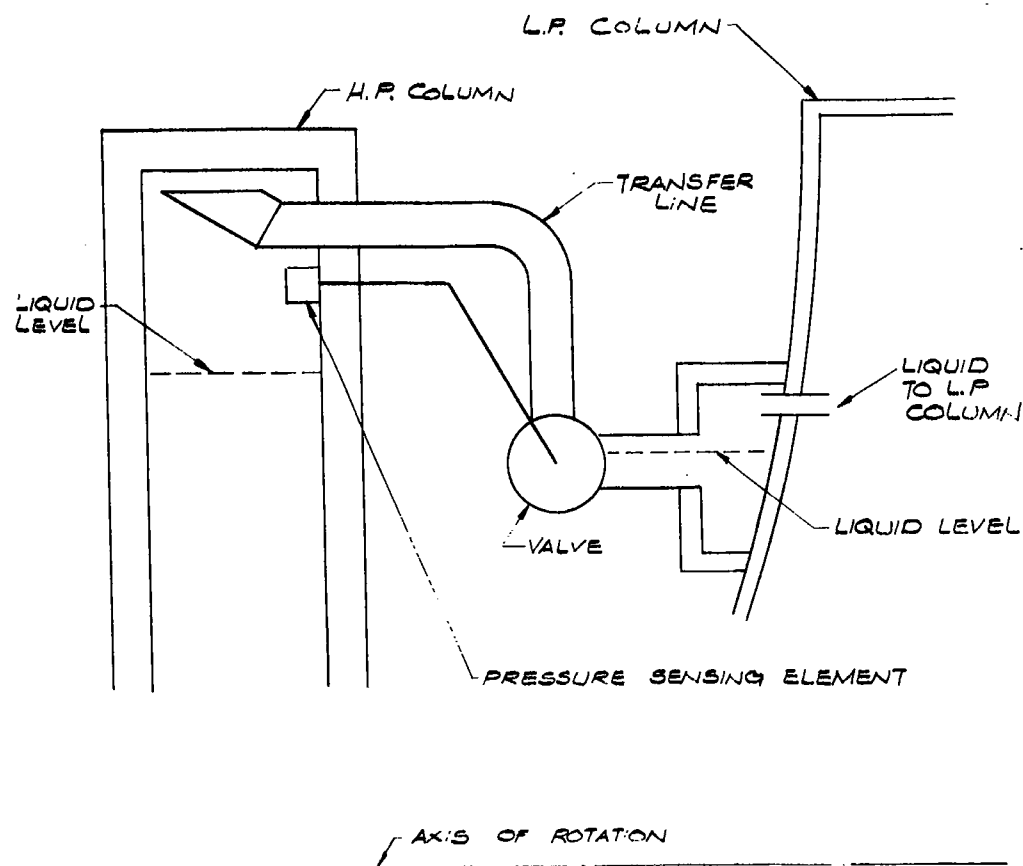
$$k_4 = 0.59 \pi R_{orf}.$$

Basically the k factors describe the various control system elements,  $\frac{\alpha_1 W_o}{k_1}$  describes the magnitude of the delta function or impulse disturbance and  $h_L(t)$  describes the liquid level as a function of time. The latter function is plotted on Figure 136.

63 ASRP-2391

CONFIDENTIAL

ASD-TDR-63-665, Part I



SCHEMATIC OF KETTLE LIQUID LEVEL CONTROL SYSTEM

FIG. 135

63 ASRP-2391

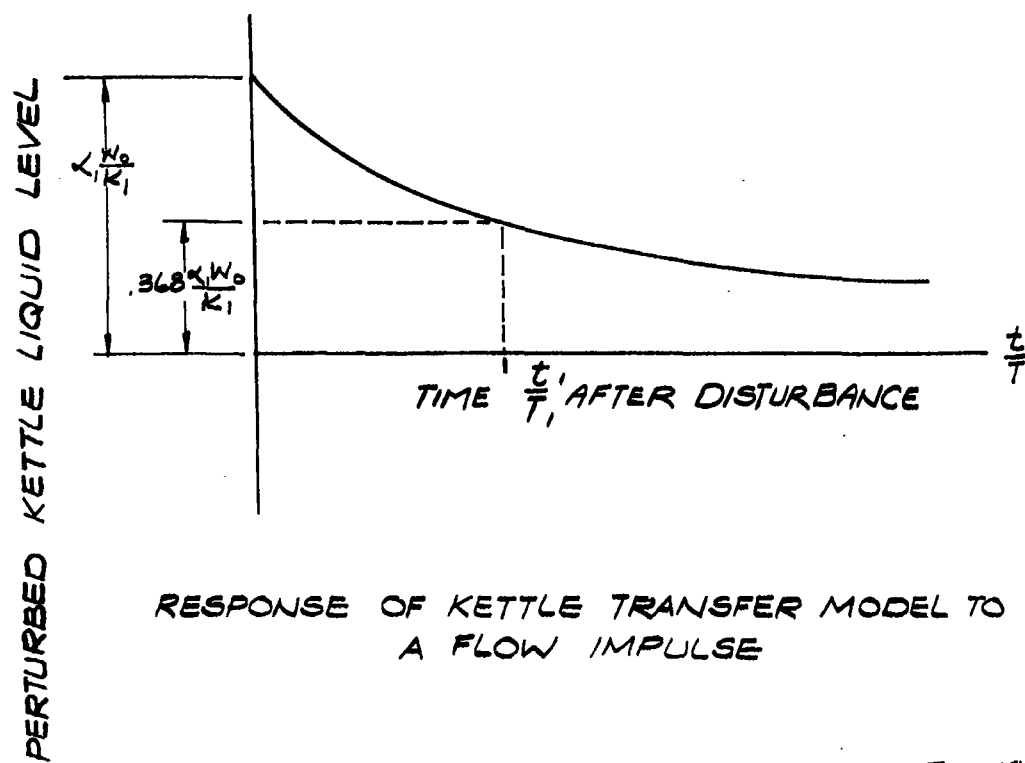


FIG. 136

**CONFIDENTIAL**

**ASD-TDR-63-665, Part I**

From inspecting the above expressions, it is obvious that for a fast response,  $k_2$  and  $k_4$  should be as large and  $k_3$  as small as possible. In reality,  $k_2$  is fixed since the pressure drop across the control valve is given. To make  $k_4$  large requires a maximum change in valve orifice area for as short a stroke as possible. For the case where intersecting circles are used to provide the orifice, this means selecting large diameter circles. There are practical limitations as to how far  $k_4$  can be increased since with very short control strokes a valve tends to become unstable, especially if any hysteresis is present.

$k_3$  can be made small by selecting a low spring constant or large area operating bellows for the control valve. The latter approach appears to be the most feasible way of obtaining a fast response time.

$k_1$  appears in the exponent as well as in the constant multiplier. While a small  $k_1$  (meaning width of the liquid buildup volume) results in a fast response, it also has the effect of increasing the magnitude of the liquid level disturbance and is therefore undesirable.

It should be noted that the simplified model is subject to limitations since pressure drop, flow dynamics through the transfer line, signal time lags, friction in the valve and dynamic effects of valve travel were neglected. For this reason the analysis can serve as a general guide only rather than as a detailed description of system behavior.

**5.6.2 Detail Design of Control System for UCON Fluid Test**

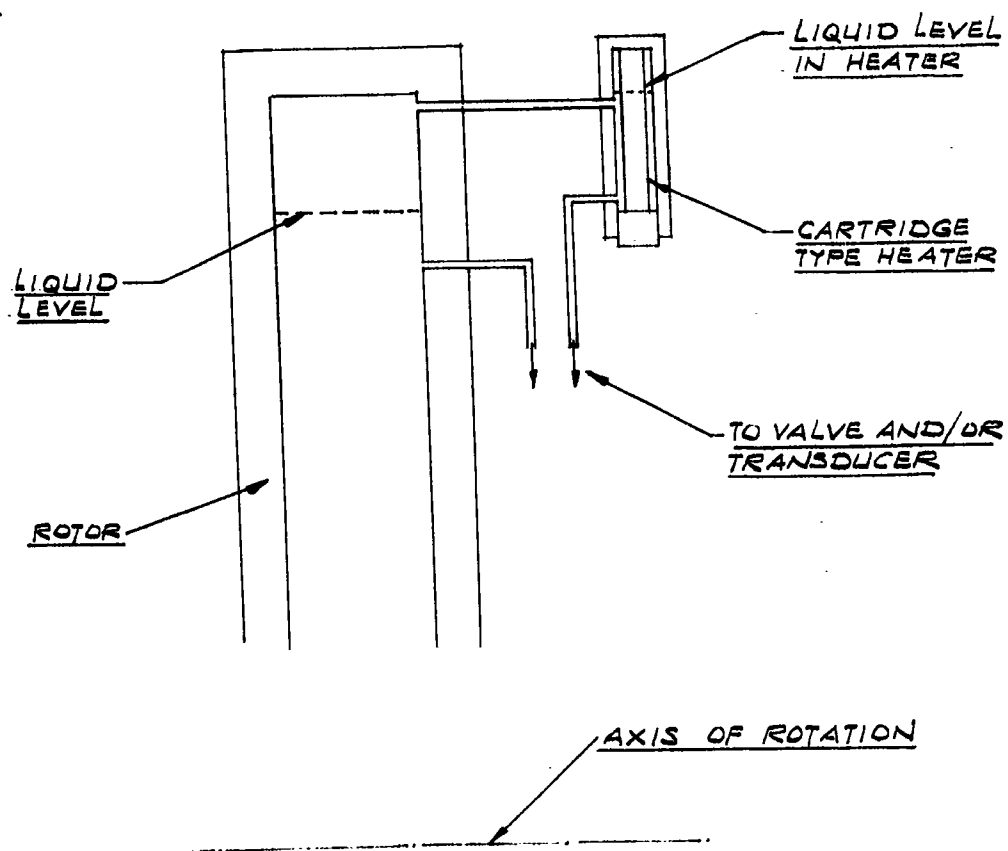
Design of this system was approached with the philosophy of obtaining a scale model of the kettle liquid transfer control system which was capable of being tested in UCON fluid service under conditions simulating kettle operation.

In designing a suitable control valve, the following criteria have to be met: The unit should be of small overall size and weight, g forces must not hinder operation or cause unbalance of the valve, pressures upstream and downstream from the valve should not affect the position of the valve piston, and finally the unit must be capable of operating in a cryogenic environment.

To furnish a control signal and operating force for the bellows, it is necessary to measure the static head of the liquid. Figure 137 shows a typical system for accomplishing this. A heater continuously

63 ASRP-2391

**CONFIDENTIAL**



SCHEMATIC OF MODIFIED HEATER  
DESIGN FOR UCON FLUID ROTOR

FIG. 137

~~CONFIDENTIAL~~

ASD-TDR-63-665, Part I

vaporizes a small amount of liquid that collects at the bottom of a signal chamber. This results in a small vapor flow bubbling back into the column or rotor. Should an increase in column liquid level occur due to a flow surge, some liquid will be forced into the horizontal liquid leg due to the increased pressure in the signal line. All that is required of the heater is to provide sufficient heat to vaporize liquid before it can collect in the radial leg of the signal line. The heater chamber is made sufficiently massive so that stored heat is available for vaporizing these liquid surges.

Since no commercially available valves were found which could meet requirements, the design shown in Figure 138 was developed. This design features a double ported piston operated by two bellows. Fluid enters the valve through parallel inlet ports, is throttled through the matched orifice openings and exits through the single outlet port. This arrangement coupled with the two actuating bellows balances the internal pressure forces and thereby materially reduces the driving force necessary to open or close the valve. This decreases the overall control operator size and makes auxiliary signal amplification unnecessary.

The valve body and pistons are made of aluminum to avoid thermal expansion problems with respect to the separator assembly. To prevent high wear and reduce friction forces, the bore of the valve is ground, hard coat anodized and honed and the pistons are ground and coated with Teflon.

The actuating bellows are made of Type 316 stainless steel. Using the bellows back to back avoids thermal expansion problems here.

Auxiliary springs are used with each bellows to allow set-point adjustment of the valve, reduce the effect of normal tolerances in bellows spring rate and achieve greater linearity in the actuator assembly.

A typical orifice opening versus signal pressure calibration curve for the prototype is shown in Figure 139. Flow calibration with water for the prototype valve is depicted in Figure 140. An exploded view of the prototype valve is shown in photograph, Figure 141.

63 ASRP-2391

~~CONFIDENTIAL~~

ASD-TDR-63-665, Part I

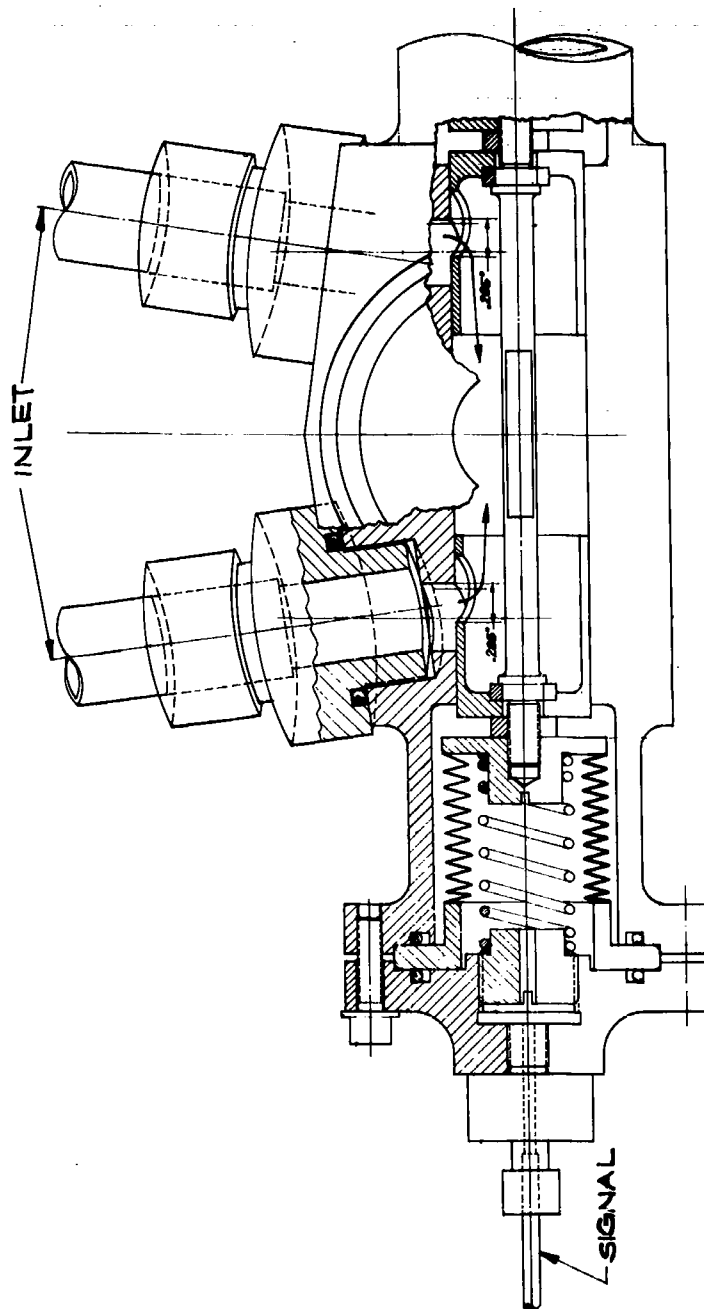


FIG. 136

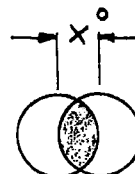
PROTOTYPE CONTROL VALVE

63 ASRP-2391

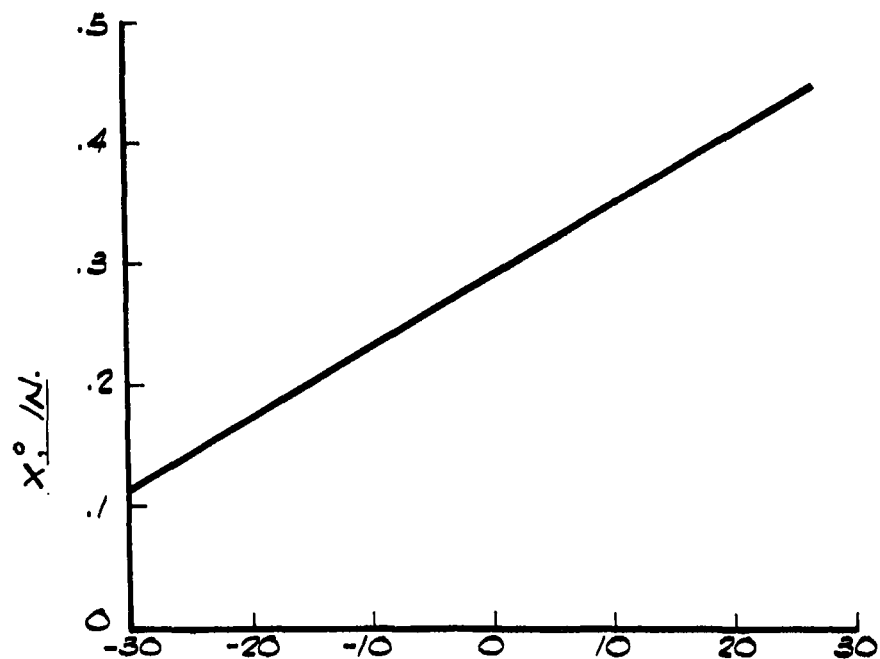


0

ASD-TDR-63-665, Part I



X° VS SP  
FOR 1ST GENERATION  
VALVE



SP, IN HG

CONTROL VALVE ORIFICE OPENING  
VS.  
SIGNAL PRESSURE CALIBRATION CURVE

FIG. 139

63 ASRP-2391

PROTOTYPE VALVE FLOW  
CALIBRATION WITH WATER

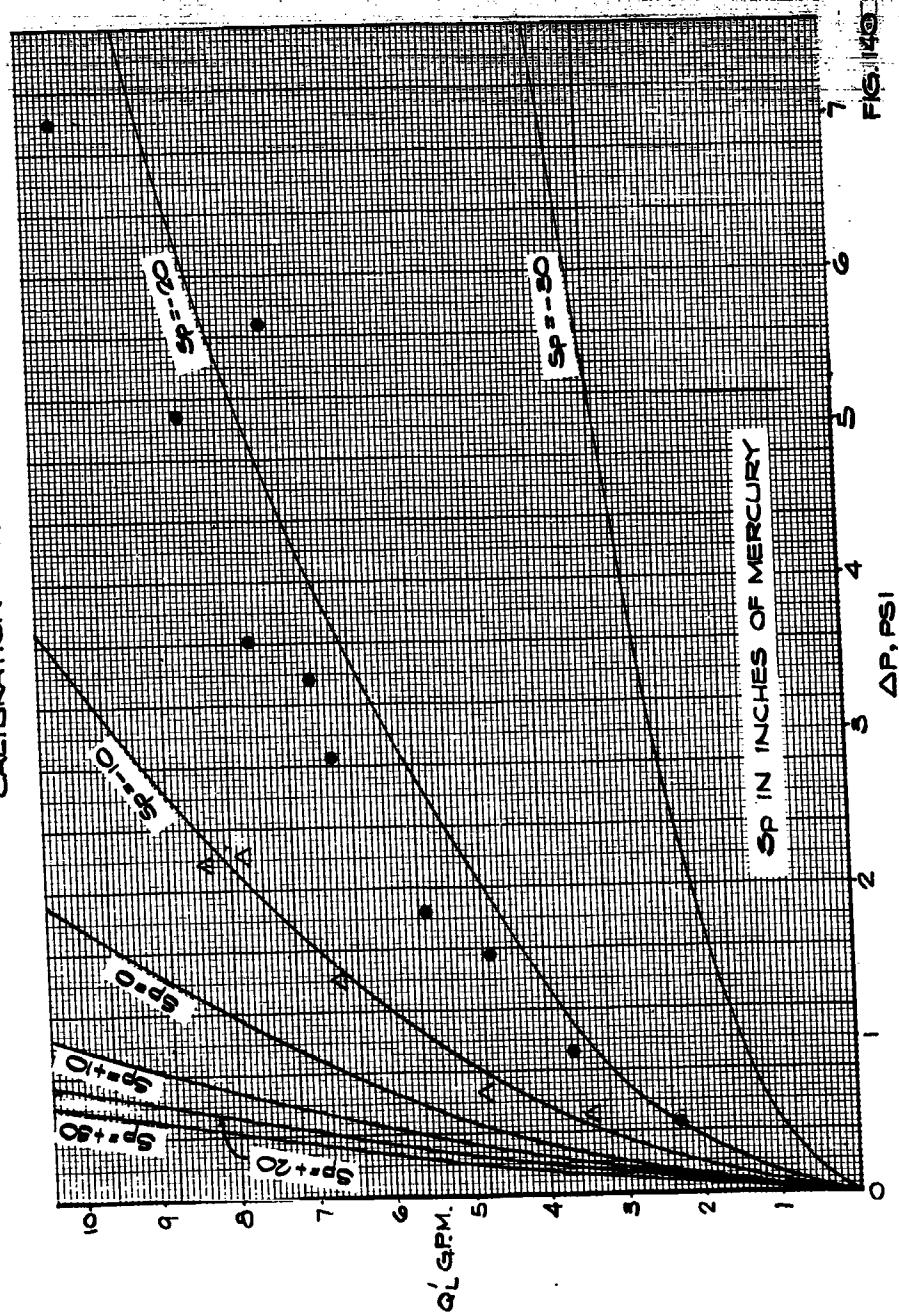
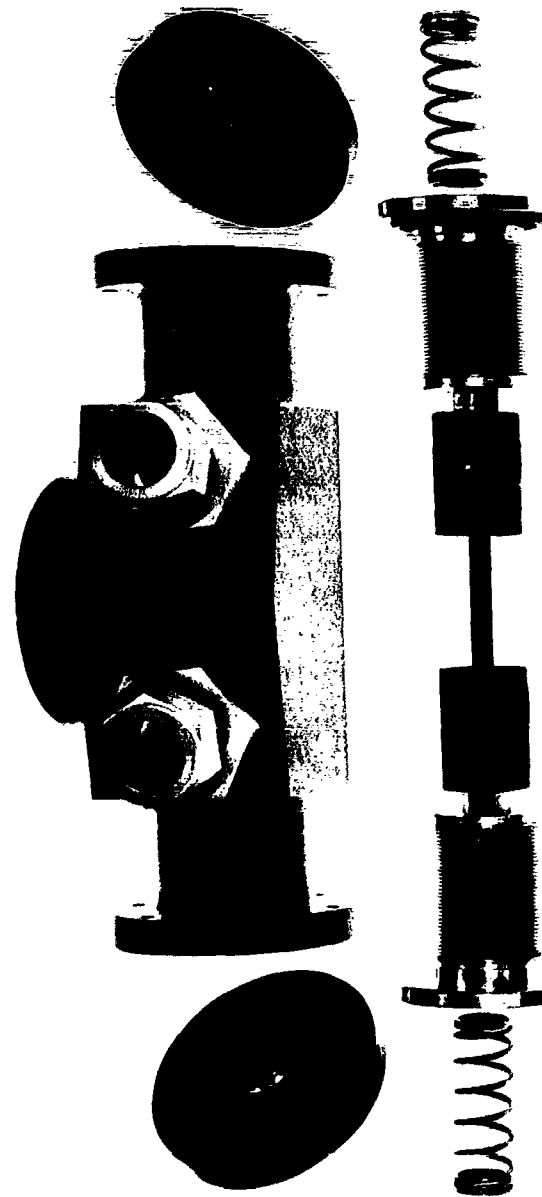


FIG. 140

ASD-TDR-63-665, Part I



EXPLODED VIEW OF PROTOTYPE CONTROL VALVE

FIG. 141

63 ASRP-2391

# CONFIDENTIAL

## ASD-TDR-63-665, Part I

### 5.6.3 Design of UCON Fluid Control System Test Rotor

The UCON fluid test rotor was designed to serve several purposes: check two-phase pressure correlations with a flashing two-phase fluid, evaluate the functional and mechanical design of the control valve, examine the performance of the simulated control loop, and check the operation of the phase separator design.

The functional design of the UCON fluid control system rotor is shown in Figure 142. Saturated UCON 12 liquid enters the rotor through the shaft, is guided into the hub, and radially outward to the holdup chamber located at the periphery. By proper adjustment of the temperature in the system, liquid in the holdup chamber is saturated. From the periphery, saturated liquid is transferred radially inward through a test line and the control valve to a phase separator located close to the center of the rotor. Here the flow is split, vapor returns through the center of the shaft and exits to the main condenser, and the liquid flows radially outward to the casing.

The rotor was designed to simulate conditions existing in the kettle transfer line of a 100 lb./sec. air separator. The holdup chamber had a nominal 3 sec. holdup at a design flow rate of 15 gpm. The response time computed from the theoretical model was in the order of 4 sec. The control system was sized to accommodate 50 percent changes in flow rate while maintaining liquid level control.

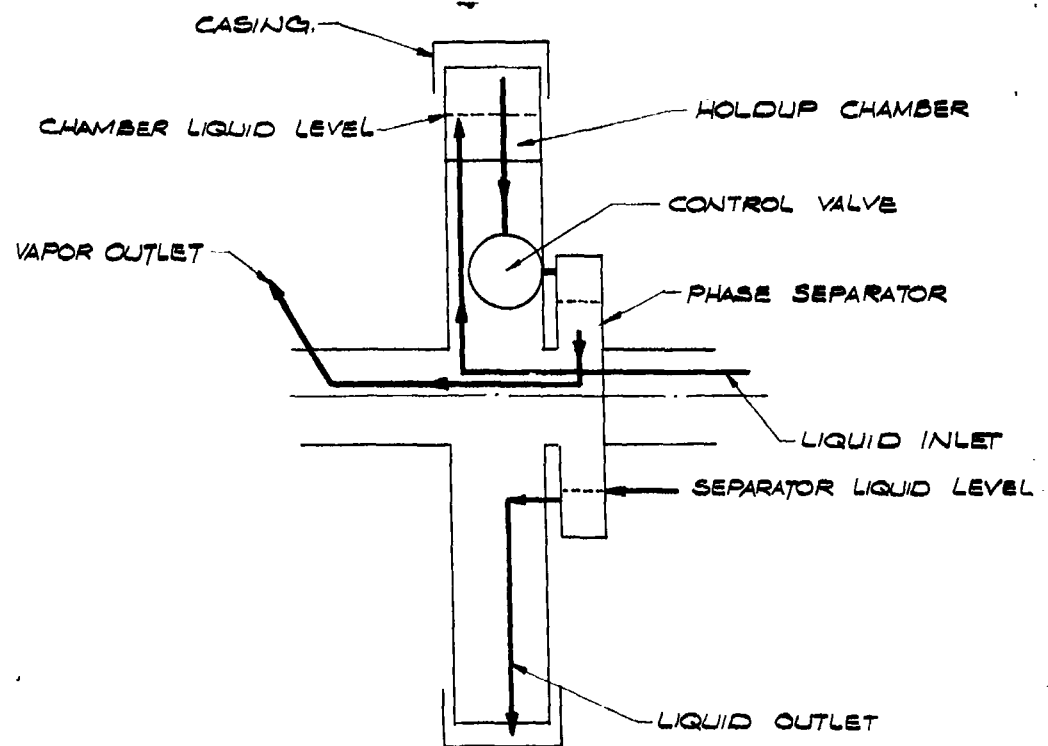
Orientation of the valve in the rotor is such that the gravitational forces will not influence the position of the pistons. This results in an increase in the friction forces between the pistons and the valve body. However, the use of Teflon coated pistons reduced friction forces to tolerable levels.

The phase separator was designed as a separate chamber with a liquid seal preventing bypassing of vapor to the rotor periphery.

Adjustable counterweights were installed in the rotor to compensate for the unbalanced liquid holdup at the periphery.

Instrumentation of the rotor included a Pace P-7 differential pressure transducer to measure pressure drop across a 3-inch segment of tube from the chamber to the valve, a Satham PM-222 differential pressure transducer to measure pressure drop across the valve, a resistance thermometer to determine the temperature in the holdup chamber, and a Satham transducer to monitor signal pressure to the valve.

63 ASRP-2391



UCON FLUID CONTROL SYSTEM  
TEST ROTOR SCHEMATIC

FIG 142

**CONFIDENTIAL**

ASD-TDR-63-665, Part I

5.6.4 UCON Fluid Control System Tests

A total of 16 test runs at various combinations of operating speed and liquid flow rates were completed with the test rotor. Much of the test time was spent observing operation of the system under various conditions rather than taking data, since this procedure appeared to yield considerably more insight into the behavior of the control system.

Basically the tests indicated that the control system operated successfully for a wide range of conditions even though some shortcomings in the system design became apparent. On the basis of the test results, it should be possible to design satisfactory control systems for the boilerplate separator.

In detail the following observations were made during the tests:

- a. Within the design range of the system, adequate liquid level control was maintained.
- b. Response time of the system appeared to be somewhat better than the predicted 4 seconds.
- c. The friction forces between the pistons and valve body introduce some hysteresis into the valve positioning mechanism. Because of the apparent hysteresis, it was sometimes difficult to control liquid level when increasing rotor speed. It should be possible to eliminate hysteresis in future designs by providing larger operating bellows, reducing piston weight, and improving bellows alignment.
- d. When not plagued by hysteresis or apparent stick slip valve travel, effective liquid level control was maintained for a wide range of flow conditions and a speed range from 300 - 650 RPM.
- e. Under certain off-design conditions (usually lower flows and speeds) periodic oscillations in liquid level were observed. Periods of oscillation were 32 seconds. No satisfactory explanation was found for this phenomena other than that most likely these oscillations were due to circuit elements outside the test rotor.
- f. The phase separator worked well during the tests.

63 ASRP-2391

**CONFIDENTIAL**

**CONFIDENTIAL**

**ASD-TDR-63-665, Part I**

g. Test results confirmed that liquid level variations are damped by changes in pressure drop across the radial two-phase transfer line ahead of the valve since increasing liquid level height decreases pressure drop through the line, increasing mass flow through the line reduces pressure drop, and reduction in holdup chamber pressure reduces line pressure drop.

h. Pressure drop data taken during UCON fluid tests indicated that a correlation developed by Hoopes (Ref. 41) yields the most satisfactory prediction for pressure drop of two-phase mixtures through valves.

A detailed data analysis is presented in Appendix XII.

**5.7 Instrumentation**

**5.7.1 Pressure Transducers**

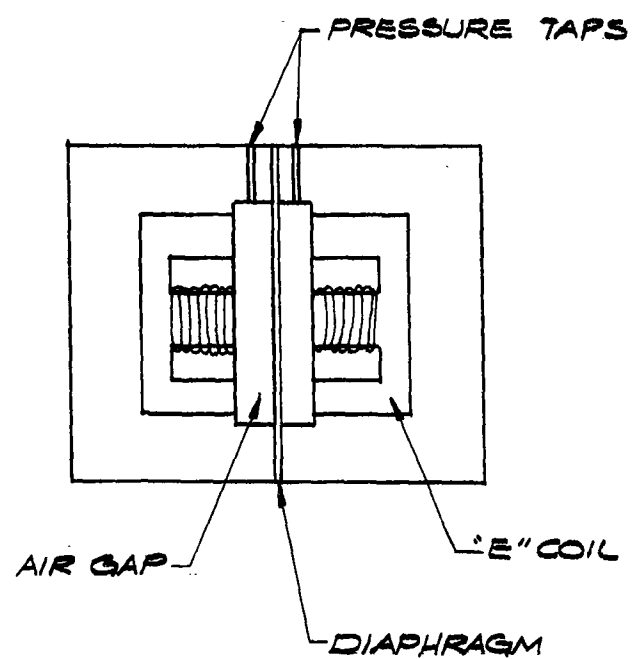
The bulk of the internal instrumentation of the boilerplate separator consists of pressure transducers. Since in previous test work available strain gauge transducers were found to be unsuitable for service in a high gravitational field, it was necessary to find a more reliable transducer capable of operating within a high gravitational field and at cryogenic temperatures.

A suitable transducer was found to be a Pace variable reluctance transducer as shown schematically in Figure 143. It consists of two "E" coils with air gaps separated by a diaphragm to complete the magnetic circuit. When a differential pressure is applied to the taps, the diaphragm is deflected. This changes the inductance of the circuit for each coil. The two coils coupled with a pair of precision resistors form a bridge circuit which is generally excited with a 400 cps or higher frequency oscillator. The bridge output is directly proportional to the pressure differential. The transducer is extremely sensitive,  $\Delta L/L$  being about 5 per cent at full scale. This type of transducer configuration is very attractive for applications involving high gravitational forces since the effect of the acceleration can be practically eliminated by orienting the transducer in such a manner that the plane of the diaphragm is in the direction of the acceleration.

63 ASRP-2391

**CONFIDENTIAL**

ASD-TDR-63-665, Part I



SCHEMATIC OF VARIABLE RELUCTANCE DIFFERENTIAL  
PRESSURE TRANSDUCER

FIG. 143



**CONFIDENTIAL**

**ASD-TDR-63-665, Part I**

The Pace Model P-7 (Figure 143) was selected for evaluation in cryogenic conditions. The Sanborn 150 system with a carrier preamplifier was used for signal readout. A typical hook-up is shown in Figure 144. The test fluid was helium with the entire transducer submerged in liquid nitrogen. A calibration curve for the transducer is shown in Figure 145.

The conclusions from the test were:

- a. The variable reluctance transducer performed very well at cryogenic temperatures.
- b. The transducer is extremely sensitive and requires that an L-pad attenuator must be inserted into the circuit.
- c. There is a sensitivity shift from ambient to cryogenic temperatures, but this is easily compensated for.
- d. It is clear that all traces of moisture must be purged from the transducer cavity to obtain accurate data at cryogenic temperatures.

The same transducer was used for measuring pressure differences in the control test rotor and performed extremely well during all test runs.

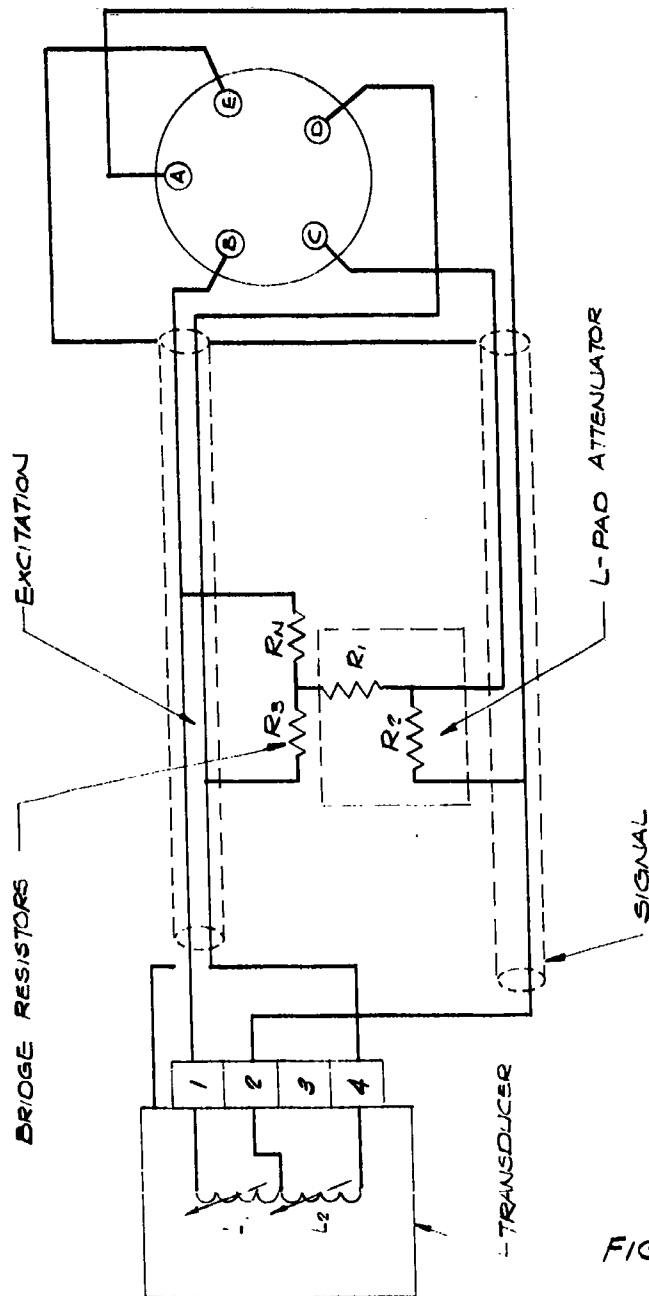
**5.7.2 Experimental Work - Optical Systems**

The necessity of observing tray operation of the cryogenic 100 lb./sec. unit required experimental work to select a suitable mirror. In selecting a mirror, two prime factors were considered: optical quality and suitability for cryogenic use. Two types of mirrors were tested. The first was a first surface mirror constructed of CR-39, a thermal setting optical grade polyester material, coated with a thin layer of aluminum with a quartz overlay. The second was Alcoa 0.032-inch gauge lighting sheet with a special Alzak finish.

The CR-39 mirror had excellent optical quality but cracked in several places when immersed in liquid nitrogen. The aluminum sheet performed well in liquid nitrogen but unfortunately does not have outstanding optical properties. Because of its suitability for cryogenic service, the latter has been used in the design of the 100 lb./sec. separator.

63 ASRP-2391

**CONFIDENTIAL**



TRANSDUCER HOOKUP SCHEMATIC

FIG. 144

ASD-TDR-63-665, Part I

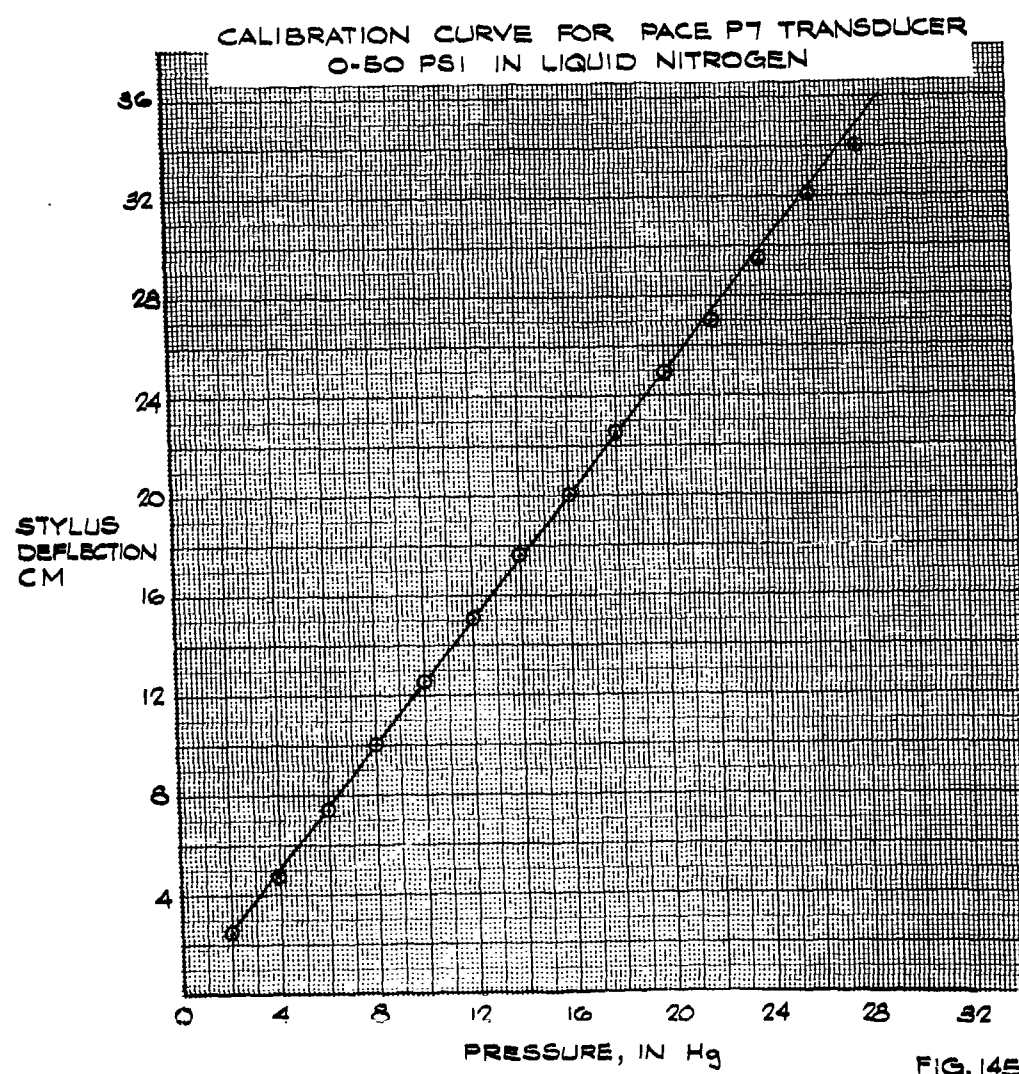


FIG. 145

63 ASRP-2391

# CONFIDENTIAL

## ASD-TDR-63-665, Part I

### 5.7.3 Vibration Monitor

In the 100 lb./sec. unit, it is mandatory to be able to sense excessive shaft unbalance conditions. The rigid design of the casing makes it difficult if not impossible to utilize externally mounted vibration monitoring instrumentation. Since rugged instruments suitable for the cryogenic environment are not readily available, an alternate approach was selected. A strain multiplier will be fastened to the I.D. of the shaft at a point where maximum shaft deflection will occur. A schematic of this arrangement is shown in Figure 146.

Basically, the strain multiplier consists of strain gage mounted on a plate which has been weakened in the region of the gage. Thus the shaft deformation will cause an equal deformation of the multiplier and the strain measured on the multiplier will be approximately  $L_1/L_2$  times the strain occurring in the shaft.

The unit has the advantage that it can be precalibrated at cryogenic conditions and then mounted in the shaft and that the multiplier effect increases the sensitivity of the device.

Experimental work has been concerned with obtaining reliable, reproducible strain gage assemblies for cryogenic use.

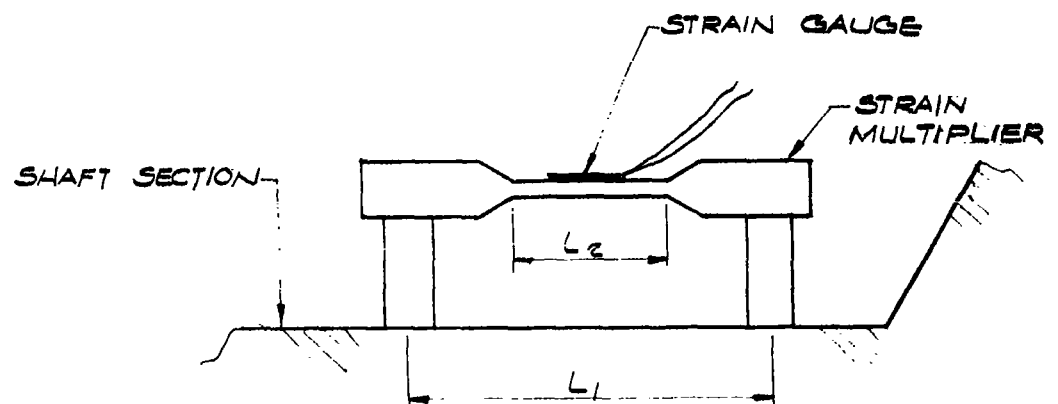
### 5.8 Reboiler-Condenser Fabrication Problems

#### 5.8.1 Basic Considerations

At the outset of work there appeared to be two possible basic manufacturing techniques for fabricating reboiler-condenser heat transfer surfaces. In the first, which was used for construction of the UCON fluid test rotors, the surface is made from curved tubes which are assembled and brazed to form disks. In the second, the surfaces are fabricated from two sheet metal disks which are drawn or stamped into the desired contour - that of a series of curved half tubes - and then permanently joined at the ridges between tube valleys. Since the second method appeared to offer some advantages as to potential weight and cost it was investigated in a brief experimental program.

A second potential problem area in the reboiler-condenser fabrication is the question of assembly and manifolding of individual heat transfer disks to form an integrated reboiler-condenser. Originally it had been planned to stack individual disks together using mechanical

63 ASRP-2391



VIBRATION MONITOR SCHEMATIC

FIG 146

# CONFIDENTIAL

## ASD-TDR-63-665, Part I

fasteners and gaskets to effect assembly. Since in work with the UCON fluid test disks it was shown that with many gasket surfaces, the chances for fluid leakage are considerably increased, it was decided to reduce the number of gaskets required for the reboiler-condenser assembly substantially by permanently assembling up to five disks into integral modules with permanent manifold joints. Furnace soldering was thought to be the most promising method for assembling multiple disk modules. To perfect techniques it was necessary to undertake a small experimental program.

### 5.8.2 Foil Type Heat Exchanger Surface Program

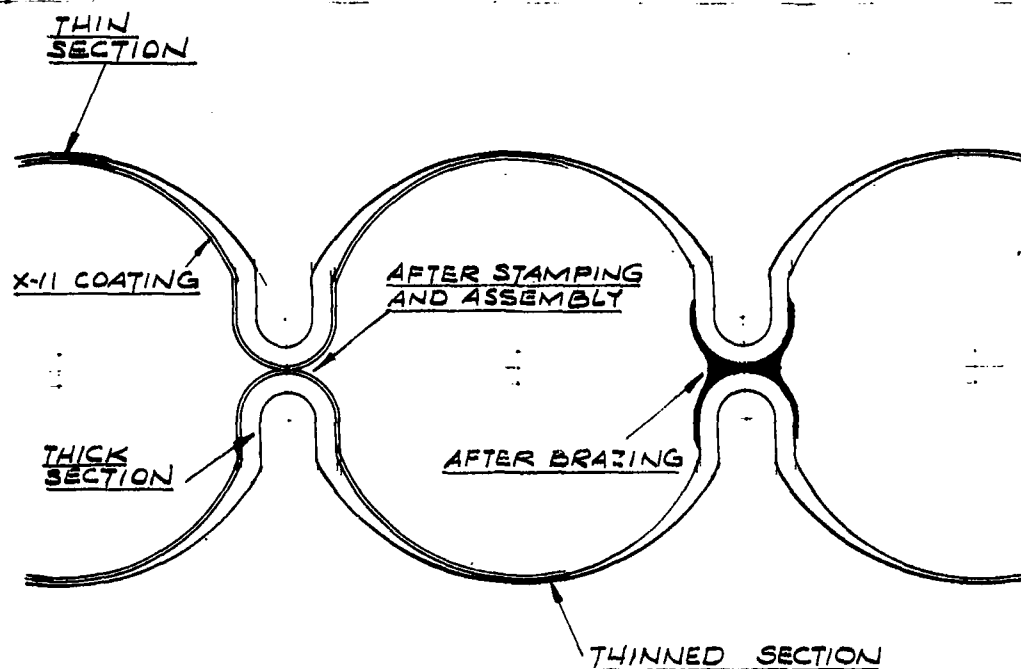
As previously mentioned, during initial development of the reboiler-condenser heat transfer disks it was thought that a lighter weight and less costly design could be achieved by stamping the exchanger in two halves from aluminum foil. The basic concept was to braze the two halves together into a tube bundle as shown in Figure 147. This design has several potential advantages over an exchanger made of tubes. They include:

- a. Considerable weight savings.
- b. Reduction in fabrication time due to ease of mass production.
- c. Cost reduction due to the high price of thin walled aluminum tubing compared to foils of equal thickness.
- d. Increased heat transfer area resulting from decreased brazement areas.
- e. Ease of headering due to the ability of stamping headers as an integral part of the tubes.

An experimental program was launched to determine the feasibility of using a stamping process to produce reboiler-condenser heat transfer disks for the 100 lb./sec. air separator. The foremost problem faced was that the flow passages were curved and could not be formed by a conventional stamping process which uses a combination of plastic deformation and the drawing of metal from the edges of the stamping blank. In order to stamp the desired shape, forming had to be entirely in the plastic range with no flow of material from surrounding areas.

63 ASRP-2391

ASD-TDR-63-665, Part I



STAMPED FOIL HEAT EXCHANGER

FIG. 147

63 ASRP-2391

# CONFIDENTIAL

## ASD-TDR-63-665, Part I

The first stage of the experimental work was designing a die which would permit forming entirely by plastic deformation. Straight passages were used in the die since with plastic deformation, curvature of the flow passages is irrelevant. With only a few passages, metal would tend to be pulled in from the edges, so the die was made for nine passages. In order to reduce costs, a female die (Figure 148) was machined and a rubber pad was used as the male die. The rubber pad had the additional advantage of applying a uniform load over the entire surface of the foil. Grease was used between the rubber pad and foil to reduce friction.

A Baldwin tensile testing machine was used for the stamping press. This made it possible to accurately measure the applied load.

The procedure used in forming was as follows:

- a. Anneal all specimens to insure an "O" temper.
- b. Load a series of specimens to failure to determine the ultimate loading (ultimate strength) of the foil under consideration.
- c. Load a second series of specimens to just under the ultimate load to insure plastic deformation.
- d. Measure the resulting deflection.
- e. Re-anneal the deformed specimens to relieve all work hardening.
- f. Repeat steps 1-5 until the desired deformation (0.125 inches) was achieved.

Table 16 indicates the foil samples used and the recommended annealing temperatures (Ref. 42).

63 ASRP-2391

# CONFIDENTIAL



ASD-TDR-63-665, Part I

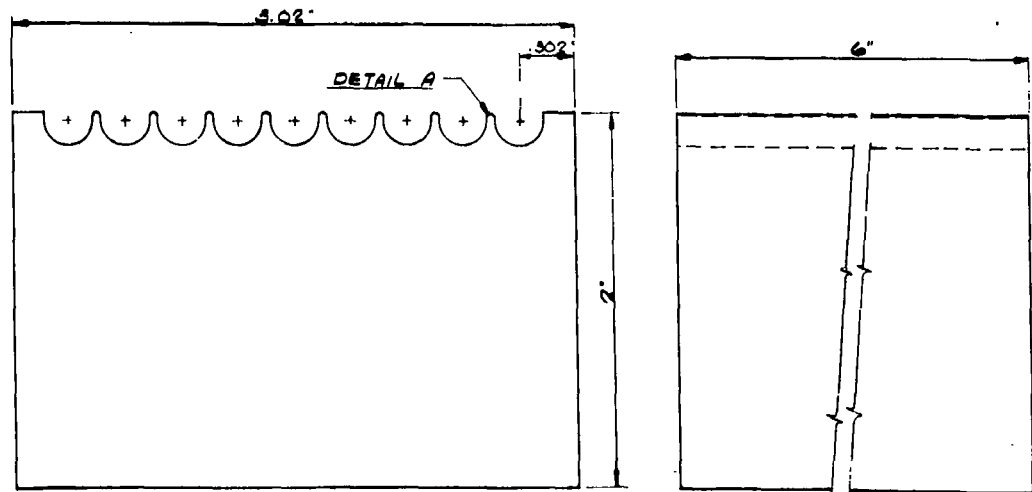
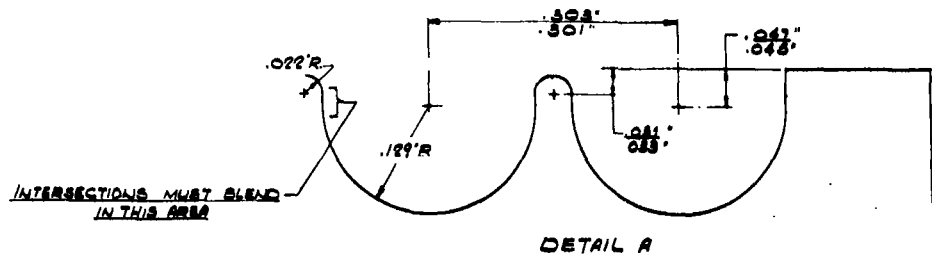


FIG. 148

DIE FOR STAMPING PROCESS

63 ASRP-2391

# CONFIDENTIAL

ASD-TDR-63-665, Part I

TABLE 16

## ANNEALING TEMPERATURES OF FOIL SAMPLES

<u>Materials</u>	<u>Foil Thickness</u>	<u>Recommended Annealing Temperature</u>	<u>Annealing Temperature Used</u>
3003	0.003 in.	775° F.	600°F. 700°F. 800°F. 900°F.
3003 with x-12 braze coating	0.006 in.	775°F.	850-900°F.
1100	0.010 in.	650°F.	600°F. 650°F. 750-800°F.

Table 17 below indicates the data taken by following the procedure stated above for the first drawing operation.

TABLE 17

## EXPERIMENTAL DATA FOR FIRST DRAWING OF FOIL

<u>Materials</u>	<u>Foil Thickness</u>	<u>Points of Failure Observed lb./in.<sup>2</sup> pressure on the foil*</u>	<u>Deformation of Surviving Samples</u>
3003	0.003 in.	103.1 - 155.6	0.029 - 0.064 in.
3003 with x-12 braze coating	0.006 in.	230 - 310	0.050 - 0.075 in.
1100	0.010 in.	405 - 515	0.063 - 0.080 in.

\*no apparent relation between annealing temperature and ultimate load observed.

63 ASRP-2391

# CONFIDENTIAL

## ASD-TDR-63-665, Part I

A typical failure of the 0.003 in. foil may be seen in the attached photograph, Figure 149.

Table 18 presents the results of a second drawing step.

TABLE 18

### EXPERIMENTAL DATA FOR SECOND DRAWING OF FOIL

<u>Materials</u>	<u>Foil Thickness</u>	Points of Failure Observed <u>lb./in.<sup>2</sup> pressure on the foil</u>	<u>Change in Deflection from The First Drawing</u>
3003	0.003	73.6 - 125	0.011 - 0.020
1100	0.010	394 - 416	0.020 - 0.025

The reduction in the pressure required to avoid failure in the specimens was the result of a decrease in the ultimate strength of the material due to improper annealing and due to the thinning of the material during the first drawing.

After a third drawing operation it was found that the possible additional deformation amounted to only about 0.005 inches. In no case did additional drawing operations result in total deformations above 0.110 inches. Specimens tended to fail like cast iron indicating that the yield point and ultimate strength were very close together. Considerable grain growth was observed after the second drawing operation. Failure of specimens of the 0.010 inch foil resulted from end defects on the edges of the specimen rather than from exceeding the ultimate strength at the center of the transfer passages.

63 ASRP-2391

ASD-TDR-63-665, Part I



FOIL FAILURE DURING STAMPING

FIG. 149

63 ASRP-2391

# CONFIDENTIAL

C ASD-TDR-63-665, Part I

Data for light gauge copper was found which indicated that for consecutive stages of plastic deformation, annealing temperatures tend to decrease as shown in Figure 150. This suggested that incorrect annealing temperatures were responsible for the premature failure of the aluminum foil. This opinion was substantiated by the large observed grain growth indicative of excessive annealing temperatures as can be seen in Figure 150.

No extensive annealing data on aluminum similar to the one available for copper could be found in the time available. For this reason it can be assumed that considerable work is required to develop the stamping process. Because of lack of time and cost incentive for using the stamping process in the construction of the disks, for the boilerplate reboiler-condenser, the experiments were terminated.

The stamping method appears to have promise for future lightweight hardware because of weight advantages and, therefore, appears worthy of further development work. More advanced forming processes such as explosive or magnetic forming may offer more promising results and should be explored. The actual weight advantages obtained would be shown in future work.

## 5.8.3 Soldering Experiments

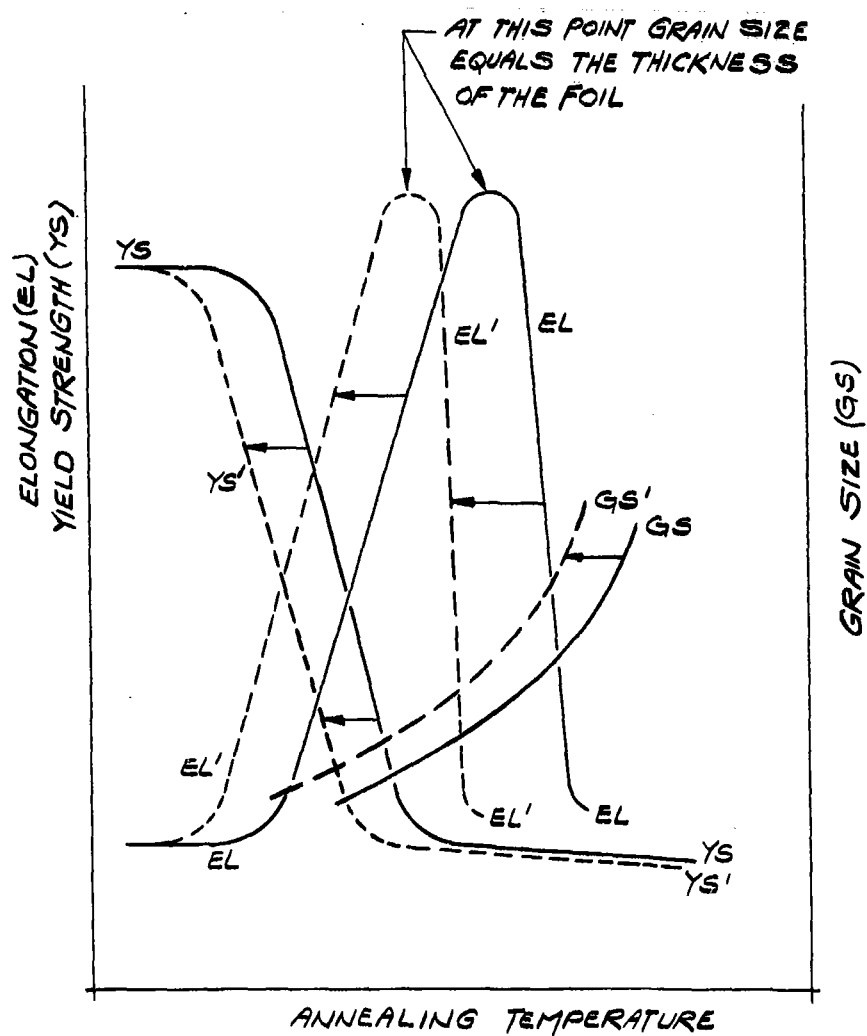
In order to reduce the number of gaskets required and consequently the chance for gasket leakage, it was decided to group the tube disks into modules of five with permanently soldered joints replacing the gasket seals between individual disks. Aside from reducing the number of gaskets required the use of multi-disk modules also allows considerable savings in manufacturing cost due to much simpler machining specifications for individual disks.

To develop necessary soldering techniques and reduce the risk of high scrap rates, it was necessary to study furnace soldering techniques in an experimental program.

The study showed that aluminum soldering is a nearly irreversible process because the oxide formed during the initial soldering acts as a stop-off during subsequent attempts to repair defects. It was found that the majority of defects were caused by insufficient capillary action.

63 ASRP-2391

# CONFIDENTIAL



— BEFORE PLASTIC DEFORMATION  
--- AFTER PLASTIC DEFORMATION

EFFECT OF PLASTIC DEFORMATION ON PROPERTIES  
OF THIN GAGE COPPER V.S. ANNEALING  
TEMPERATURE

FIG. 150

63 ASRP-2391

# SECRET

## ASD-TDR-63-665, Part I

The hypothesis was put forward that if one or both of the surfaces to be soldered together were coated with the soldering material a sealing joint could be obtained by heating the coated surfaces while they were in contact. An appropriate flux would be required to remove the oxide on the coating in order to achieve fusion.

Initial experiments conducted with a commercial silver cadmium aluminum solder resulted in successful solder joints. This solder was expensive, however, and could not be plated on aluminum using conventional plating processes. Pure zinc which can be plated on aluminum parts was later used with success, as was pure cadmium. Cadmium was found not only to give better joints than zinc, but also to be superior at low temperatures because its elongation is much higher than that of zinc (18% vs. 0.6%). Soldering temperatures for pure cadmium are between 610 and 650°F. which is advantageously low for the disks coated with the Linde boiling surface. In soldering, care must be taken that the furnace is preheated to the soldering temperature before the work piece is placed into the furnace to prevent long heating periods during which the flux would become inactive.

Additional experiments have shown that cadmium foil (0.003 in. - 0.006 in. thick), when properly used, can replace the coated surfaces. In the specific application at hand, it is less expensive to use foil on the inner header because of difficulty in coating the latter.

As a by-product of the above mentioned work, it was found that ordinary pencil lead (graphite) can be used as a very effective stop-off for critical areas which are to be protected from solder.

The conclusions drawn from the experimental program are that it should be possible to assemble modules by furnace soldering.

## 6.0 PRELIMINARY DESIGN AND ANALYSIS

### 6.1 Introduction

The preliminary design and analysis projects the mass transfer and heat transfer applied research programs to the ultimate flight-weight air separator. This separator must be capable of operation in a hypersonic aircraft which collects and stores oxidizer in flight. In the single stage concept, following collect, the vehicle accelerates

63 ASRP-2391

# SECRET

**SECRET**

**ASD-TDR-63-665, Part I**

to orbital velocity, and re-enters the earth's atmosphere at the conclusion of its mission. In the two-stage concept, the separator is in the first stage which becomes the launching platform for the orbital vehicle. Thus, in either concept, the separator is a propulsion component in a recoverable booster, and as such must be capable of repeated missions with a minimum of maintenance. Nominally fifty hours of operation between major overhaul has been suggested as a suitable design life.

The scope of the preliminary design study includes the following:

- a. The weight and volume are estimated for a full-size flight-weight separator for several cycle parameters. These studies are then related to propulsion system integration in a brief discussion of separator horsepower and refrigeration requirements.
- b. Optimum arrangements of the major components are determined including the gains and penalties associated with the employment of several small separators.
- c. The scaling effects are examined in extrapolation from the 100 lb./sec. scale model to the full-size flight-weight separator.
- d. Effects of air contaminants on column performance are discussed.
- e. Some of the consequences of operating the unit under off-design conditions are evaluated. Transient conditions of startup and shutdown are also discussed.
- f. Heat transfer surfaces are evaluated to determine their relative merits on a weight and volume basis.
- g. Reliability aspects of the separator are discussed listing the components and methods of calculating overall reliability.

**6.2 Summary**

In the weight and volume analysis of a full-size flight-weight

63 ASRP-2391

**SECRET**



**SECRET**

**ASD-TDR-63-665, Part I**

separator the double column cycle studies are modified from the commercial stationary, vertical column concept to the rotating high gravitational field concept. Using three representative product and waste purity levels, weight and volume estimates were presented each month. These results show that the separator can be produced within the combined weight and volume goal of 5.5 pounds of separator weight per lb./sec. of air throughput, but not under all conditions. In computing the combined goal one cubic foot volume was equated to one pound of separator weight.

A parametric study was first made with a stationary double column cycle. Later, final results of the mass transfer and heat transfer programs were utilized in an expanded parametric study of a rotating separator. This study utilized product purities of 90, 95, and 98 weight per cent oxygen, waste purities of 96, 97, and 98 weight per cent nitrogen, and inlet pressures of 180 to 245 psia; all cases at 56.5 psia waste pressure. Using a near-optimum speed of rotation of 45 radians per second for all cases the results show that minimum separator weight for this waste pressure occurs about 250 to 260 psia. The separator weight increases as inlet pressure decreases since reboiler-condenser  $\Delta T$  is reduced. Similarly, at constant inlet pressure, the separator weight increases as higher product purity and/or waste purity is specified for the separator design because the reboiler-condenser  $\Delta T$  is reduced. Thus it is shown that separator weight is controlled by reboiler-condenser  $\Delta T$  and hence controlled by the parameters affecting this  $\Delta T$ . Other results of these studies show that the refrigeration required at the separator increases as inlet pressure and product oxygen purity decrease and as waste purity increases.

A study of optimum arrangement of components indicates that a single unit or two parallel units would have about the same total weight if total rated air capacity is 2000 lb./sec. The single unit is preferred from the functional and reliability viewpoint since fewer parts are required and flow balancing through parallel separators is eliminated.

Effects of scaling from 1/20 scale (100 lb./sec.) to the full-size 2000 lb./sec. separator were examined for possible functional problems which might be encountered in the full-size unit. Primary interest was in functional problems which would arise in scaling a proven 1/20 scale unit to the full-size separator. None were uncovered since these units are dimensionally similar in diameter.

63 ASRP-2391

**SECRET**

**SECRET**

**ASD-TDR-63-665, Part I**

All major components will therefore be tested within the same general range of gravitational field in the columns and reboiler-condenser.

Possible contaminants in the incoming air were evaluated for their effect on separator performance. If all carbon dioxide and water vapor above the soluble limit are removed from the air stream prior to its entrance into the separator, no problems should arise. If carbon dioxide and water vapor exceed the soluble limit in the inlet air stream, these solids could cause problems in the various orifices of the system. A more detailed analysis of this contaminant problem is now under study under Contract AF 33(657)-11753. These are the only constituents of the upper air which could effect the separator. Combustible materials such as hydrocarbons, which are potentially dangerous in usual air separation plants, are not present in the upper air to any significant degree. Therefore no hydrocarbon problems exist. Precautions must be exercised to exclude hydrocarbons from the preconditioning equipment since these materials provide the same potential hazards as in a ground based oxygen plant.

Transient studies were made and off-design performance was evaluated. Preliminary estimates indicate a total startup time of one minute for the full scale unit. This includes final cooldown, liquid buildup and purity buildup. Cooldown is recommended prior to startup to avoid excessive thermal stresses. This could be done by convection from surrounding hydrogen tankage or by forced convection of cold nitrogen vapor through the separator during preflight checkout. During operation off-design conditions at the air separator due to deviations from the design inlet and waste pressures can be corrected by changes in rotational speed and/or air flow rate. It is recommended that separator shutdown be a gradual process over a period of a minute or two with the air inlet flow rate and rotational speed being gradually lowered to avoid system unbalances such as excessive weeping or vapor flooding. Considerable operating experience, which will be gained in the test of the 1/20 scale separator, can be utilized to obtain much more definitive information for future transient studies.

Future programs should include a continuing evaluation of the separator, relating the technical test programs to the full-size separator, and integrating it with the propulsion system. A major task in this program would include the mapping of separator weight at waste pressures above and below the 56.5 psia case presented in this report.

63 ASRP-2391

**SECRET**

~~SECRET~~

ASD-TDR-63-665, Part I

Additional work should include studies of the refrigeration requirement since this area was treated only as required heat duty. The effect of heat duty on  $\eta$ , pounds of oxidizer per pound of fuel, is a new study, since  $\eta$  is also a function of the hydrogen pressure and expansion ratios used in the reflux condenser interstage turbines.

Further study is also recommended on separator components including the drive. This program would survey currently available hardware and evaluate this with possible new developments in the continuing mechanical program recommended in Section 5.2.

### 6.3 Weight and Volume Analysis

#### 6.3.1 General

The weight and volume of an air separator can be optimized in three areas: the theoretical cycle, the tray dynamics (hydraulics and mass transfer), and the physical arrangement of components. Even with these factors optimized, the separator weight varies widely with boundary conditions such as inlet pressure, waste pressure, waste purity, and product purity. Since the separator is only one component of the propulsion system, and likely the minimum separator weight does not yield minimum propulsion system weight, a weight mapping program was undertaken. With this map, system designers can determine separator weight at various boundary conditions, when determining system weight.

The following weight and volume study program was developed in this contract. Initially, cycle studies for stationary systems were performed for a number of theoretical cycles to indicate means of minimizing refrigeration and weight. Preliminary parametric studies of pressures and purities were made to indicate weight trends. When these studies were completed, attention turned to rotary system analyses. The results of the mass transfer and tray hydraulic and heat transfer experimental programs were utilized for system design. Various mechanical arrangements of the components were investigated for the optimum. Using this optimum arrangement, a weight mapping program was initiated for the boundary conditions of interest. Separator weights were calculated using the general form of the stress equations to make certain that all major components were calculated on the basis of design stress resulting from pressure and rotational speed. Results from a separate heat transfer study (Section 6.8) and optimum component study (Section 6.3.3.8) showed that the

63 ASRP-2391

~~SECRET~~

**SECRET**

**ASD-TDR-63-665, Part I**

separately-rotated reboiler-condenser weight decreases with increasing  $\Delta T$  and increasing rotational speed up to approximately 70 rad./sec. Since the desired speed for the columns is much lower, the column designs for the selected single rotor system used an optimum rotational speed consistent with reasonable column pressure drop (reboiler-condenser  $\Delta T$ ) in developing the weight maps.

Throughout the preliminary design study, a monthly weight estimate was prepared to show the range of weights predicted for the maximum and minimum purity cases at confidence levels of 95%, 50% and 20%.

**6.3.2 Stationary System Cycle Studies**

**6.3.2.1 Parametric Trends in the Stationary System**

In earlier contracts, the basic double column cycle shown in Figure 151 was established as the cycle offering minimum weight and refrigeration. This is the same cycle used commercially for oxygen production. Under this contract this cycle was again found to be the most desirable and hence was the basis for the weight and volume study. Physical property data used in this study were obtained from References 20 and 43.

It was recognized that the stationary system study would provide a useful tool to show the effect of cycle boundary conditions on the number of theoretical trays and system heat duties. These two items are the important parameters which determine system weight and volume. The number of trays influences column pressure drop and therefore the  $\Delta T$  across the reboiler-condenser. Also, rotor diameter and, hence, volume, is determined by the number of trays. System heat duties, the other parameter, include the reboiler-condenser duty which strongly influences the separator weight, and two refrigeration duties which determine the liquid hydrogen required to produce a pound of oxidizer. These refrigeration duties are the reflux-condenser duty which is a rigid thermodynamic requirement of the design conditions and the product subcooler duty which depends on the desired product storage pressure. This pressure may be varied independent of the other boundary conditions.

The results of this system study are summarized in Table 19 and individual point data are included in Appendix XIII. The resulting trends are presented as follows:

**63 ASRP-2391**

**SECRET**

# DOUBLE COLUMN AIR SEPARATOR

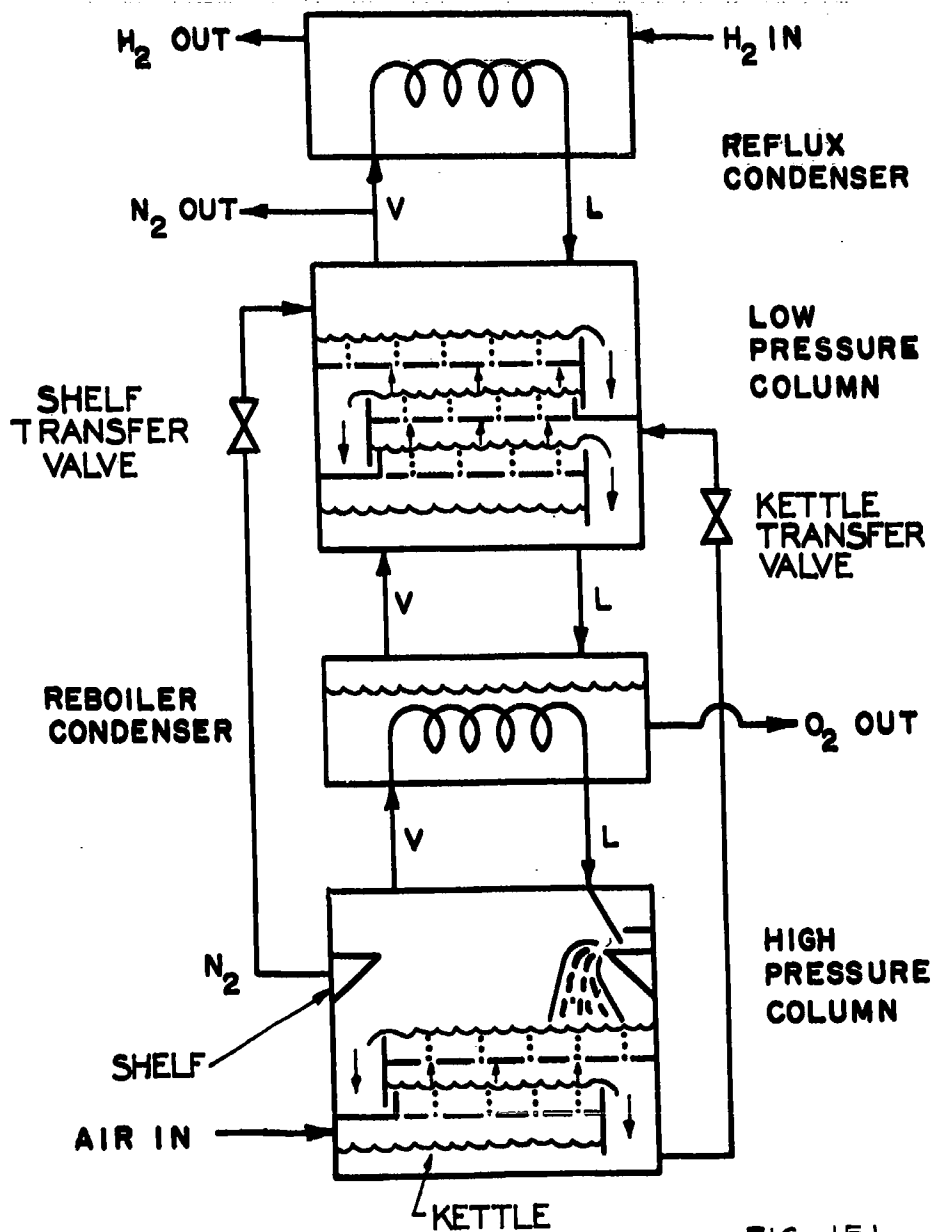


FIG. 151

63 ASRP-2391

**SECRET**

**ASD-TDR-63-665, Part I**

TABLE 19  
AIR SEPARATOR CYCLE STUDY SUMMARY  
(NON-ROTATING SYSTEM)

Point No.	Pressure		Feed Air Super Heat	Heat Exchanger Duties B.t.u./Lb.-mole feed			Theoretical Trays			O <sub>2</sub> Mole Fraction	
	High Pressure Column Psia	Low Pressure Column Psia	B.t.u. Lb.-mole feed	OR	QC	QS	LPC Enriching Section I	LPC Stripping Section II	HPC Section III	Waste	Product
1	234	56.5 to 76.5	0	1765	691	69	9.6	6.1	10	0.01755	0.8874
2	225	56.5 to 76.5	0	1795	694	69	9.0	5.9	10	0.01755	0.8874
3	265	65 to 98	0	1660	623	87	18.9	12.5	15	0.01755	0.9433
4	265	65 to 95	0	1660	656	88	15.4	7.0	15	0.01755	0.8874
5	265	65 to 82.3	0	1662	720	57	4.2	3.0	7	0.044	0.7243
6	225	56.5 to 76.5	0	1795	616	69	9.3	5.8	10	0.01755	0.8874
7	225	56.5 to 76.5	0	1795	656	69	9.4	5.9	10	0.01755	0.8874
8	225	56.5 to 76.5	0	1795	579	69	9.51	5.87	10	0.01755	0.8874
9	234	65 to 95	0	1765	663	88	11.34	7.49	10	0.01755	0.8874
10	245	65 to 95	0	1725	661	88	12.1	8.6	10	0.01755	0.8874
11	265	65 to 95	0	1660	656	88	17.2	11.0	10	0.01755	0.8874
12	245	65 to 95	0	1725	638	88	7.6	7.1	10	0.02636	0.8874
13	245	65 to 95	0	1725	613	88	5.2	6.5	10	0.03636	0.8874
14	265	65 to 95	0	1661	634	88	8.7	8.9	10	0.02636	0.8874
15	225	56.5 to 76.5	0	1795	671	69	6.34	5.12	10	0.02636	0.8874
16	245	40 to 75	0	1725	718	67.5	8.5	6.0	10	0.01755	0.8874
17	245	70 to 105	0	1725	644	98.4	14.9	9.1	10	0.01755	0.8874

63 ASRP-2391

**SECRET**

**SECRET**

**ASD-TDR-63-665, Part I**

The number of low pressure column theoretical trays will decrease with:

- a. Decreasing high pressure column pressure.
- b. Decreasing low pressure column pressure.
- c. Decreasing waste nitrogen purity.
- d. Decreasing product oxygen purity.

The number of high pressure column theoretical trays will decrease:

- a. With decreasing high pressure column pressure.
- b. Indirectly with decreasing low pressure column pressure.
- c. Indirectly with decreasing waste nitrogen purity.
- d. Indirectly with decreasing product oxygen purity.

The indirect relationship results because the number of high pressure column trays is a direct function of the purities in the kettle and shelf streams which are transferred from the high pressure column to the low pressure column. The purities required of these streams are in turn partially determined by low pressure column pressure and purities.

The reboiler-condenser heat load, QR, will decrease:

- a. With increasing high pressure column pressure.
- b. Indirectly with increasing or decreasing low pressure column pressure where the changes required in kettle and shelf stream purities determine the dependence.
- c. Indirectly with increasing waste nitrogen purity because of the probable increase in shelf stream nitrogen purity.
- d. Indirectly with decreasing product oxygen purity because of the probable decrease in kettle stream oxygen purity.

The system refrigeration load, QC, will decrease with:

- a. Increasing high pressure column pressure.
- b. Increasing low pressure column pressure.
- c. Increasing product oxygen purity due to the resultant increase in waste stream flow.
- d. Decreasing waste nitrogen purity due to the resultant increase in waste stream flow.

63 ASRP-2391

**SECRET**

**SECRET**

**ASD-TDR-63-665, Part I**

The product subcooling heat load,  $Q_S$ , will decrease:

- a. With increasing product oxygen purity.
- b. With decreasing low pressure column pressure.
- c. Indirectly with decreasing high pressure column pressure which leads to a resultant drop in low pressure column pressure because of the reduced number of low pressure column theoretical trays.
- d. Indirectly with decreasing waste nitrogen purity which leads to a resultant drop in low pressure column pressure because of the reduced number of low pressure column theoretical trays.

This study established a foundation for future rotary system analysis as it indicated the basic cycle trends. These results are not numerically directly applicable to the rotary system because of the additional variable of rotational speed. This variable will influence the cycle study in the following manner.

- a. The stationary system analysis is based on a constant pressure level in the high pressure column but a rotating system will cause a substantial non-linear variation in high pressure column pressure.
- b. The stationary system pressure level in the low pressure column changes in a linear fashion whereas the rotating system pressure changes non-linearly.

This non-linear variation in pressure level will affect the theoretical tray counts and the system heat duties. The nature of the variation is presented in Section 6.3.3.6.

**6.3.2.2 Cycle Improvements for the Stationary System**

Having established that the double column cycle was the most efficient, some effort was devoted to improving this cycle by reducing the refrigeration load,  $Q_C$ , in the stationary system. The first item considered was subcooling the reflux liquid nitrogen before it passes through the shelf transfer valve (Figure 151) to the low pressure column. Point No. 6 shows the result of this modification of Point No. 2. The hydrogen refrigeration requirements can be reduced by addition of a heat exchanger to subcool the shelf liquid transferred from the high pressure column to the low pressure column. Total refrigeration requirements of the system are not changed, but  $Q_C$  is reduced by 11% to 616 Btu/lb.-mole feed since 78 Btu/lb.-mole feed can be supplied by

63 ASRP-2391

**SECRET**



**SECRET**

**ASP-TDR-63-665, Part I**

subcooling the shelf transfer liquid with the refrigeration in the colder waste vapor stream. The heat exchanger could be a separate unit containing only these streams, or the subcooling coil could be supplied as an accessory in the preconditioning section. It is complicated by the removal of the liquid stream and its return to the rotating column.

The tray requirements of the low pressure column have a net increase of 0.2 theoretical trays since more reflux is supplied from the lower purity shelf transfer stream. This replaces a portion of the higher purity waste vapor which is condensed in the reflux condenser. Consequently, total reflux purity decreases, requiring slightly more trays to achieve the same waste purity.

The next improvement investigated was the use of liquid transfer turbines in place of valves where pressure is reduced in transfer of the shelf and kettle streams from the high pressure column to the low pressure column.

To reduce the external refrigeration requirements at the reflux condenser, it is desirable to approach the reversible cycle by utilizing isentropic rather than isenthalpic expansion of the high pressure liquid streams. Point No. 7 assumes 60% efficiency on this isentropic expansion. Total refrigeration is reduced from 694 to 656 Btu/lb.-mole feed, a net saving of 38 Btu/lb.-mole feed, at the cost of 0.4 theoretical trays in the low pressure column.

The combined effect of reflux subcooling and liquid turbines is shown in Point No. 8. Essentially the refrigeration saving is the sum of that available from the individual steps. No additional improvement was found by combining the two features. Therefore, the transfer turbine feature appears attractive on its own to effect about a 5.5% reduction of refrigeration. It was learned there is no refrigeration excess at warmer levels in the heat exchangers. Therefore, there is no incentive to use the subcooling feature. This work indicated that turbine expansion will affect considerable savings in hydrogen refrigeration with very slight theoretical tray penalties. (Where this cycle is translated to the rotating system it is shown that turbine expansion can be achieved in the rotor without the penalty of turbine hardware.)

63 ASRP-2391

**SECRET**

~~SECRET~~

ASD-TDR-63-665, Part I

6.3.3 Rotary System Studies

6.3.3.1 Process Description of Rotary Air Separator

In Figure 151 the basic double column cycle was presented for stationary column design. This cycle was then adapted to the rotating column where centrifugal effects are added to the usual cycle. The resultant mass flowsheet, Figure 152, was developed. This flowsheet is based on a rotational speed of 60 rad./sec. and recovery of one-half of the inlet air superheat which results from rotational field compression of the inlet air vapor in passing from the inlet shaft to the periphery of the high pressure column. Later studies use a different speed and assume complete recovery of inlet air superheat. A pictorial view of the current flight-weight air separator design is presented in Figure 153.

Referring again to the flowsheet, Figure 152, the separator inlet air vapor enters the separator at the shaft (right side) and flows to the periphery of the high pressure column, being compressed and superheated in the process, which adds 52 Btu/lb.-mole to the feed air. It enters the high pressure column and passes radially inward through the column where for this cycle half of this energy is returned to the rotor. It contacts the liquid on each tray where distillation (mass transfer and heat transfer) is achieved. Distillation occurs here in pressure ranges of 200 to 300 psia depending on the cycle used. The refrigeration for the high pressure column is provided by the reboiler-condenser which absorbs the heat load by totally condensing the high pressure column nitrogen-rich vapor stream. A portion of this condensate is transferred to the low pressure column as reflux. The balance flows through the high pressure column where it becomes richer in oxygen and is collected at the periphery for transfer to the low pressure column. This is the "kettle" liquid which contains a high percentage of oxygen. These two streams undergo nearly isentropic expansion as in a turbine when moving radially inward to the control valves where the expansion to the low pressure column is completed. The "shelf" liquid enters at the radially innermost portion and the "kettle" enters between the enriching and stripping sections at the kettle separator. This expansion was calculated as an 80% efficient isentropic process to allow for piping friction and throttling in the valves.

The low pressure column consists of a nitrogen-rich enriching section mounted next to the shaft, and an oxygen rich stripping section surrounding the enriching section. Distillation in this column occurs in a much lower pressure range than the high pressure column, nominally

63 ASRP-2391

~~SECRET~~

ASD-TDR-63-665, Part I

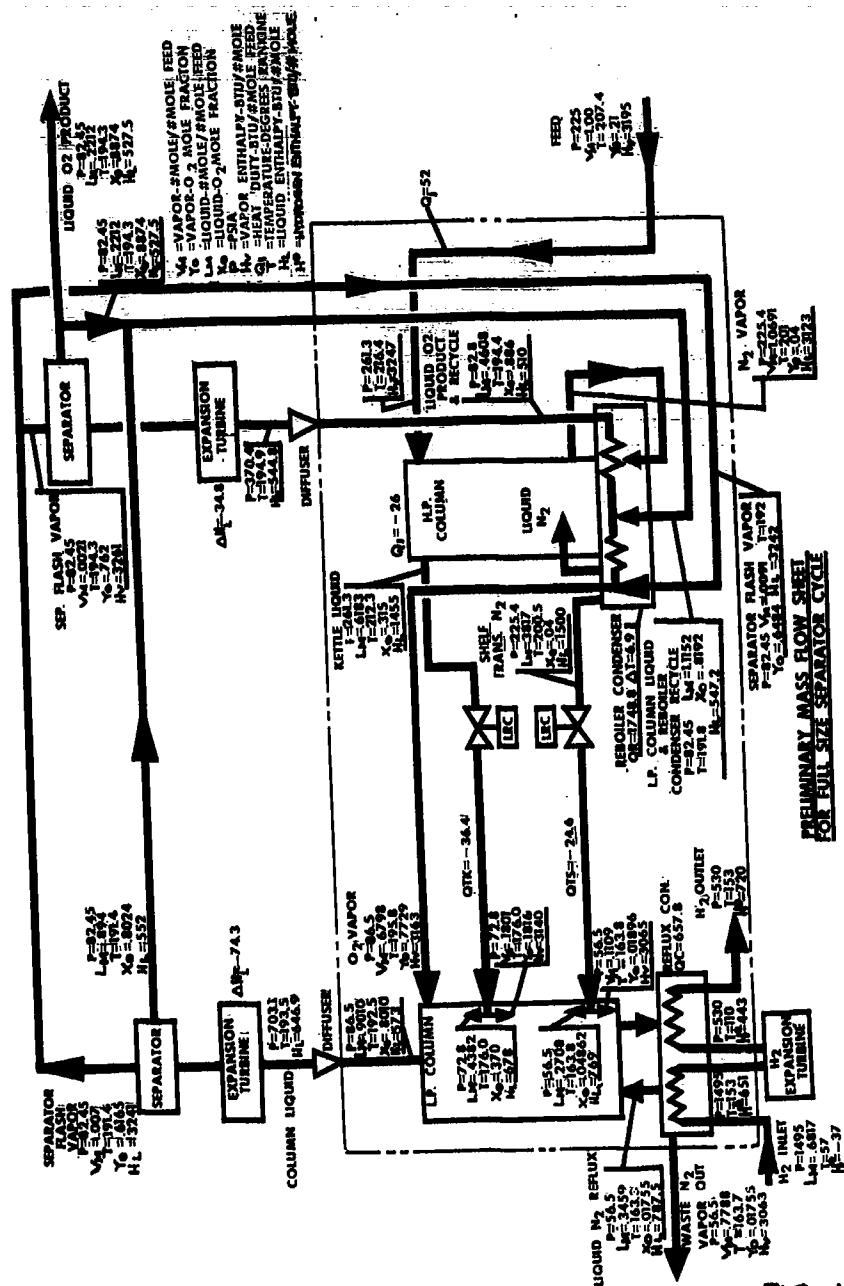


FIG. 152

63 ASRP-2391

**SECRET**

**SECRET**

ASD-TDR-63-665, Part I

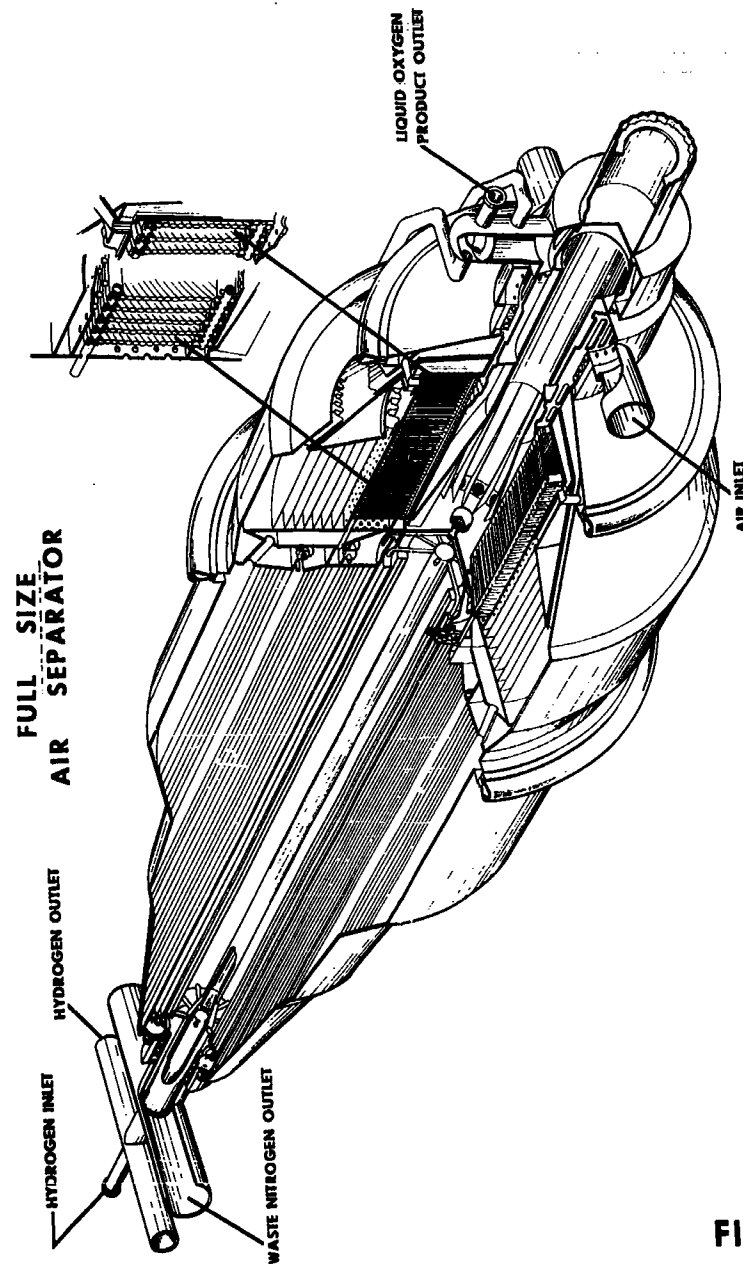


**FIG. 153**

63 ASRP-2391

**SECRET**

**SECRET**

**ASD-TDR-63-665, Part I**

45 to 100 psia. The results of the distillation in the low pressure column yield a waste vapor stream of almost pure nitrogen, which leaves the enriching section through the shaft, and an oxygen-rich liquid stream leaving the stripping section at the periphery.

The source of refrigeration for the low pressure column and the entire air separator system is the reflux condenser which condenses a portion of the waste nitrogen vapor leaving the low pressure column to provide additional liquid reflux. Refrigeration is provided by high pressure hydrogen supplied external to the air separator system. The hydrogen conditions represented in this cycle are not recommended as an optimum but are typical of some propulsion cycles.

The oxygen-rich liquid stream leaves the rotating low pressure column through a diffuser which converts its kinetic energy to static pressure. It is then expanded through an expansion turbine into a liquid-vapor separator where the liquid is enriched slightly in oxygen content. The liquid leaving this separator blends with an oxygen-rich recycle stream from a second separator and enters the rotating reboiler-condenser through the shaft. This liquid stream boils, absorbing the high pressure column heat load. In the boiling it undergoes an equilibrium distillation enriching the oxygen content in the residual liquid which leaves the rotating system through another diffuser. This oxygen-rich liquid is expanded through a turbine which discharges into the second liquid-vapor separator previously mentioned. The liquid stream resulting from this expansion is enriched to the desired product oxygen purity. Part of it is withdrawn as product liquid which then passes through a subcooler and turbine to storage probably at 1 atm. saturation. The remainder is blended with the liquid stream from the first separator, and both liquid streams are recirculated through the reboiler-condenser. The vapor streams from the first and second separators are blended and introduced into the rotating system through the shaft, mixed with the vapor from the boiling side of the reboiler-condenser and sent to the periphery of the low pressure column.

63 ASRP-2391

**SECRET**

~~SECRET~~

ASD-TDR-63-666, Part I

6.3.3.2 Computer Analysis

The rotary system analysis incorporated the use of three computer programs because of the complexity of the rotary system design. The low pressure column and high pressure column each require a design program to develop the physical dimensions and process data. A third computer program utilizes the column information to compute weight and volume of the separator.

A low pressure column design program was written utilizing tray dynamics and mass transfer correlations presented in Section 3.0 of this report. This program uses iterative optimization procedures. It is based on the results of the low pressure column theoretical tray counts obtained in the stationary system cycle studies, but with a pressure correction to take the gravitational field into account. Basically, given the low pressure column boundary conditions, the program will size the column for a specified rotational speed based on optimum superficial vapor velocity. This program is presented in detail in Appendix XIV.

The next computer program was developed for design of the high pressure column. It also utilizes the tray dynamics and mass transfer correlations presented in Section 3, but performs theoretical tray counting as a function of gravitational field pressure level. The distillation process is completely analyzed, tray by tray. This program also uses iterative optimization procedures to find the best superficial vapor velocity for a given rotational speed and column boundary conditions. This program is presented in detail in Appendix XV.

The technique for closure on the optimum superficial vapor velocity is presented in Appendix XVI. (Ref. 39, pg. 447). This technique is used in both column programs.

Finally, the results of the low and high pressure column computer programs were utilized in basic stress and process requirement equations making up an air separator weight and volume program. The results of this program formed the basis for the weight and volume mapping. The weight program is presented in Appendix XVII.

6.3.3.3 Optimum Rotational Speed

Optimum rotational speed is that speed which produces minimum separator weight and volume. It was recognized that the reboiler-condenser

63 ASRP-2391

~~SECRET~~

**SECRET**

**ASD-TDR-63-665, Part I**

would be the governing weight and volume item for the cycles of interest. so cycles were selected to span the maximum to minimum  $\Delta T$  cases. As shown in Section 4.0 of this report, the reboiler-condenser condensing side film assumes the major portion of the overall temperature drop. Both the condensing film coefficient and the overall coefficient,  $U_o$ , rise with increasing rotational speed. Since the overall  $\Delta T$  is a function of column pressure drop, which increases as rotational speed increases, an increase in speed reduces the overall  $\Delta T$ . It is therefore necessary that the product  $U_o \Delta T$ , which is equal to the reboiler-condenser heat flux  $Q/A$ , be maximized for minimum weight and volume.

Figure 154 was developed to find a single speed that would be an approximate optimum for the range of the cycles of interest. In this figure, the weight and volume of three cycles representing high, medium and low  $\Delta T$ 's are plotted against rotational speed. As shown, the cycle with the small  $\Delta T$  (200-95-97) has a sharp optimum, and the optimum range broadens as the cycles with the larger  $\Delta T$ 's are considered. The dotted line illustrates that 45 rad./sec. appears to be the best single speed to represent the optimum speeds for the cycles of interest and it was used in the weight, volume and parametric trend studies of this report.

**6.3.3.4 Inlet Pressure Perturbation**

Figures 155, 156, and 157 represent the first parametric studies at the optimum speed of 45 rad./sec. where parameters influencing system weight and refrigeration are studied. As shown, all three figures are concerned with a perturbation on separator inlet pressure. Figures 155 and 156 are essentially weight parameter studies. Figure 155 shows the number of low pressure column trays increases with a rise in separator inlet pressure because the high pressure column performance is reduced, shifting the load to the low pressure column (because of lower shelf and kettle stream purities).

Reboiler-condenser heat transfer area decreases as inlet pressure increases to 245 psia, due to increased  $\Delta T$ , as shown in Figure 156. The increase in high pressure column pressure more than compensates for the increased column pressure drop due to the increasing number of trays in both columns. However, when the separator inlet pressure is large enough to cause a substantial increase in low pressure column trays (exceeding 260 psia) the column pressure drop will be controlling, reversing the trend.

63 ASRP-2391

**SECRET**

SECRET

ASD-TDR-63-665, Part I

OPTIMUM ROTATIONAL SPEED

WASTE PRESSURE = 56.5 PSIA

INLET AIR FLOW RATE 2088 LB/SEC.

VOLUME PENALTY = 1 LB/ CU. FT.

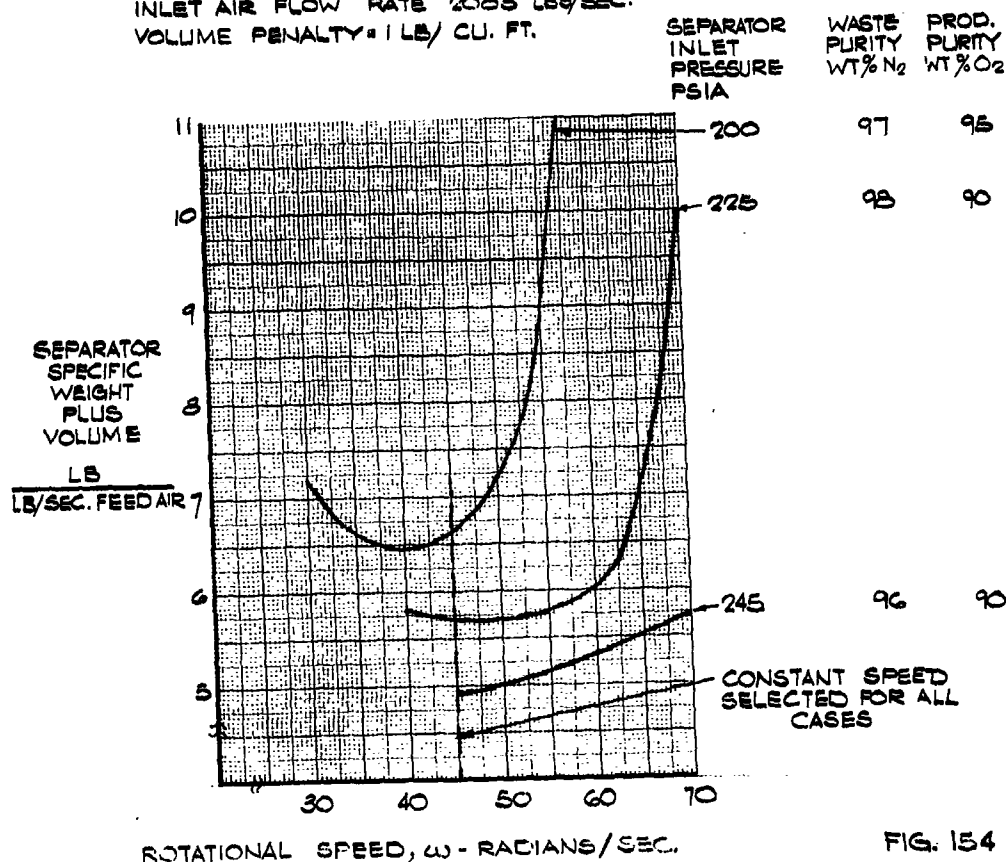


FIG. 154

63 ASRP-2391

SECRET



**SECRET**

ASD-TDR-63-665, Part I

**INLET PRESSURE PERTURBATION  
LOW PRESSURE COLUMN TRAYS**

WASTE PRESSURE = 56.5 PSIA  
ROTATIONAL SPEED = 45 RAD./SEC.

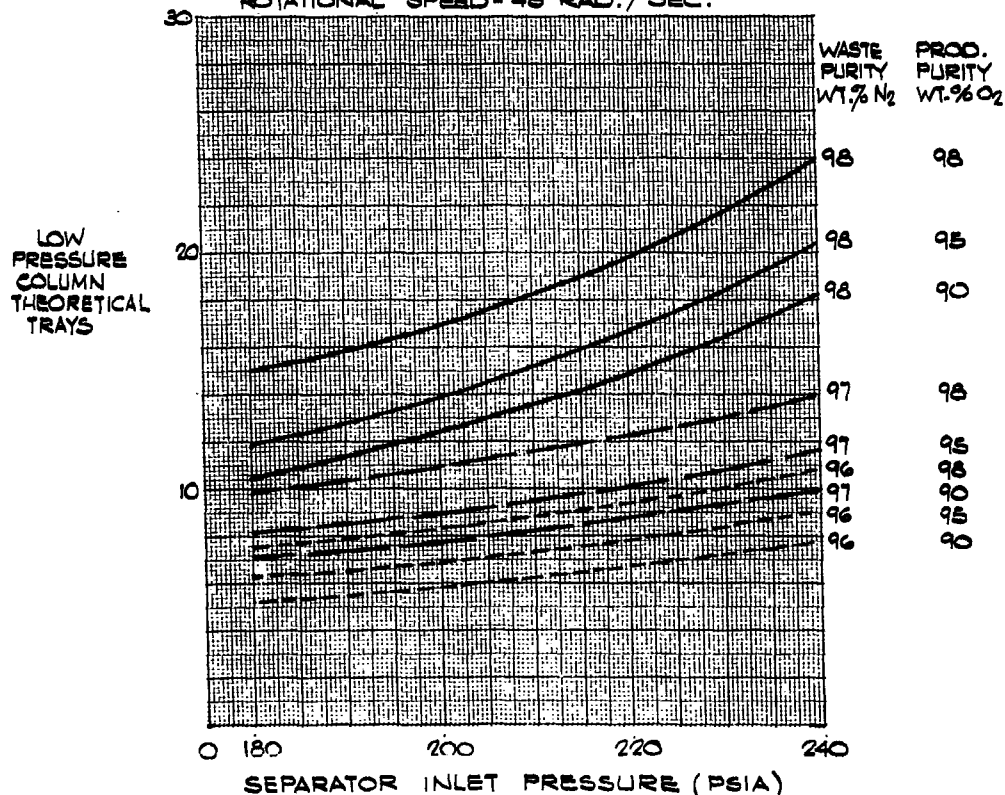


FIG. 155

63 ASRP-2391

**SECRET**

**SECRET**

ASD-TDR-63-665, Part I

INLET PRESSURE PERTURBATION  
REBOILER CONDENSER HEAT TRANSFER AREA

WASTE PRESSURE = 56.5 PSIA  
ROTATIONAL SPEED = 45 RAD./SEC.  
INLET AIR FLOW RATE = 2083 LBS/SEC.

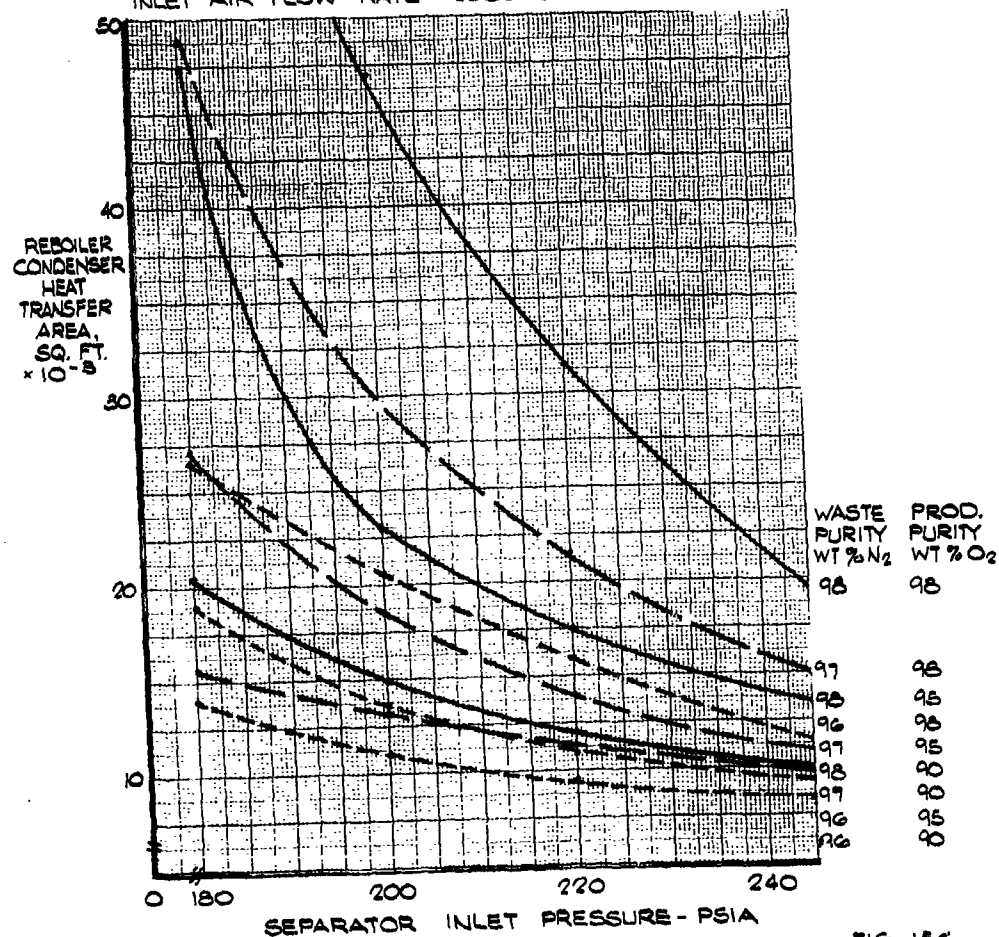


FIG. 156

63 ASRP-2391

**SECRET**

**SECRET**

ASD-TDR-63-665, Part I

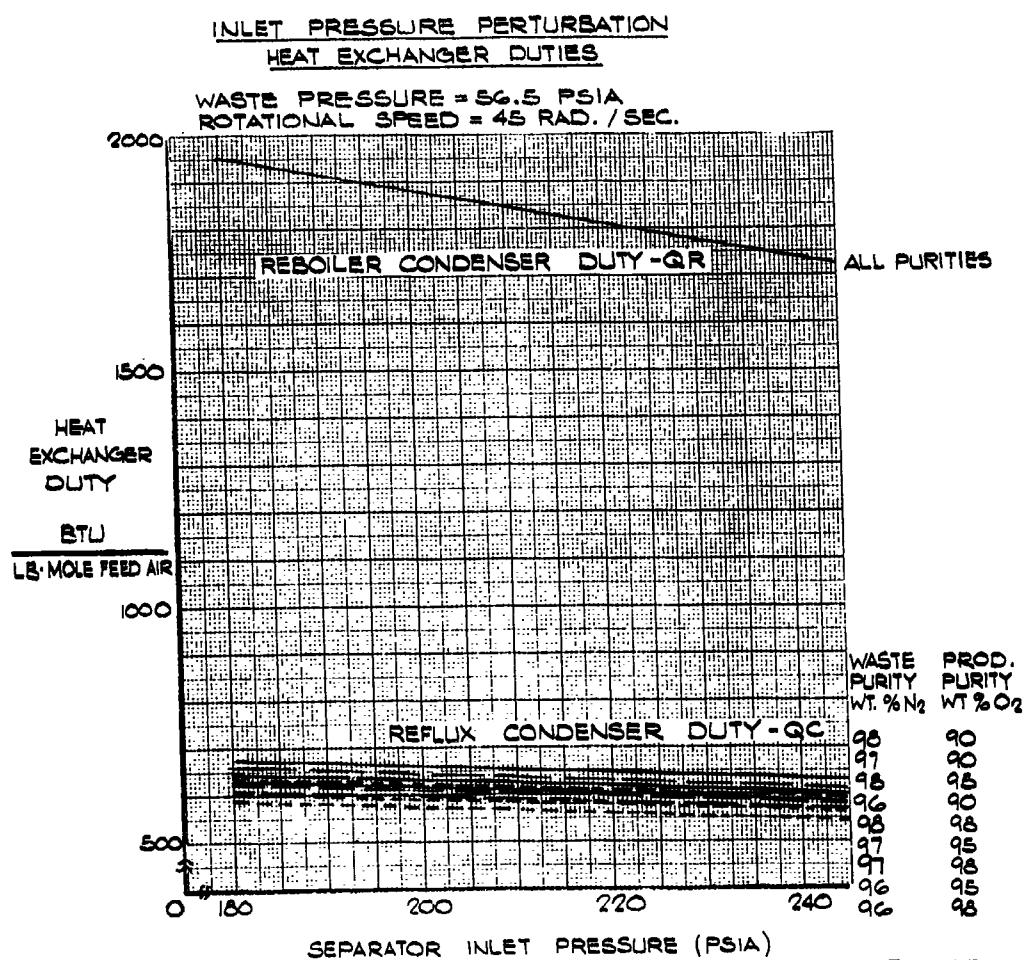


FIG. 157

63 ASRP-2391

**SECRET**

**SECRET**

#### ASD-TDR-63-665, Part I

Figure 157 shows the trend of the heat duty of the reboiler-condenser and is essentially independent of the required purity. This demonstrates the important principle that reboiler-condenser size in a constant pressure study is solely a function of reboiler-condenser  $\Delta T$  as determined by column pressure drop. The reflux condenser duty also decreases as inlet pressure increases, but the change is less pronounced. The decrease in reboiler-condenser and reflux condenser heat duties with increasing separator inlet pressures support the use of higher separator inlet pressures for minimum air separator weight, volume and refrigeration.

#### 6.3.3.5 Waste Purity Perturbations

In Figure 158 the tray requirements for a rotating column are shown to increase with increasing waste nitrogen purity due to the usual pinch condition in attaining high purities in fractional distillation. A similar trend in reboiler-condenser area is shown in Figure 159. As the waste purity increases, the required reboiler-condenser area also increases. This is due to the increased number of low pressure column trays and therefore reduced  $\Delta T$ . The column pressure drop increases with the increased number of trays leaving less pressure difference between high and low pressure sides of the reboiler-condenser. This determines the  $\Delta T$ . Consequently, increasing waste purity will increase both the column weights and the reboiler-condenser weight.

The reboiler-condenser heat duty shown in Figure 160 is independent of waste nitrogen purity. Refrigeration requirement at the reflux condenser increases when waste purity increases. This results from the lower mass flow in the waste stream and increased flow in the product stream. Thus, the waste stream heat content decreases as nitrogen content increases, requiring more refrigeration from the hydrogen in the reflux condenser.

#### 6.3.3.6 Low Pressure Column Pressure Perturbation

The low pressure column pressure level is essentially determined by the waste pressure and the rotational speed. Since the waste pressure for the rotary system studies was fixed at 56.5 psia and an optimum speed of 45 rad./sec. was used, no actual perturbation data for low pressure column pressure could be presented. However, pertinent trends are revealed from the earlier studies of stationary columns. As shown in Figure 161, the low pressure column theoretical tray requirement will increase due to distillation occurring at higher pressures. The reboiler-

63 ASRP-2391

**SECRET**

**SECRET**

**O**

ASD-TDR-63-665, Part I

WASTE PURITY PERTURBATION  
LOW PRESSURE COLUMN TRAYS

WASTE PRESSURE = 56.5 PSIA  
ROTATIONAL SPEED = 45 RAD./SEC.

LOW  
PRESSURE  
COLUMN  
THEORETICAL  
TRAYS

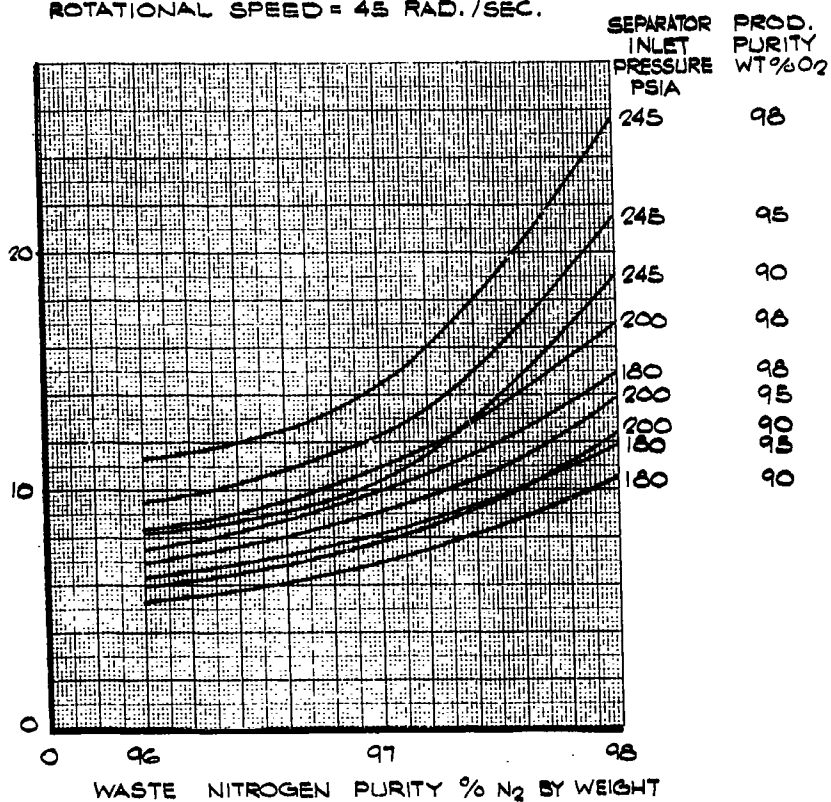


FIG 158

**SECRET**

SECRET

ASD-TDR-63-665, Part I

WASTE PURITY PERTURBATION  
REBOILER CONDENSER HEAT TRANSFER AREA

WASTE PRESSURE = 56.5 PSIA  
ROTATIONAL SPEED = 45 RAD./SEC.  
INLET AIR FLOW RATE = 2083 LBS/SEC.

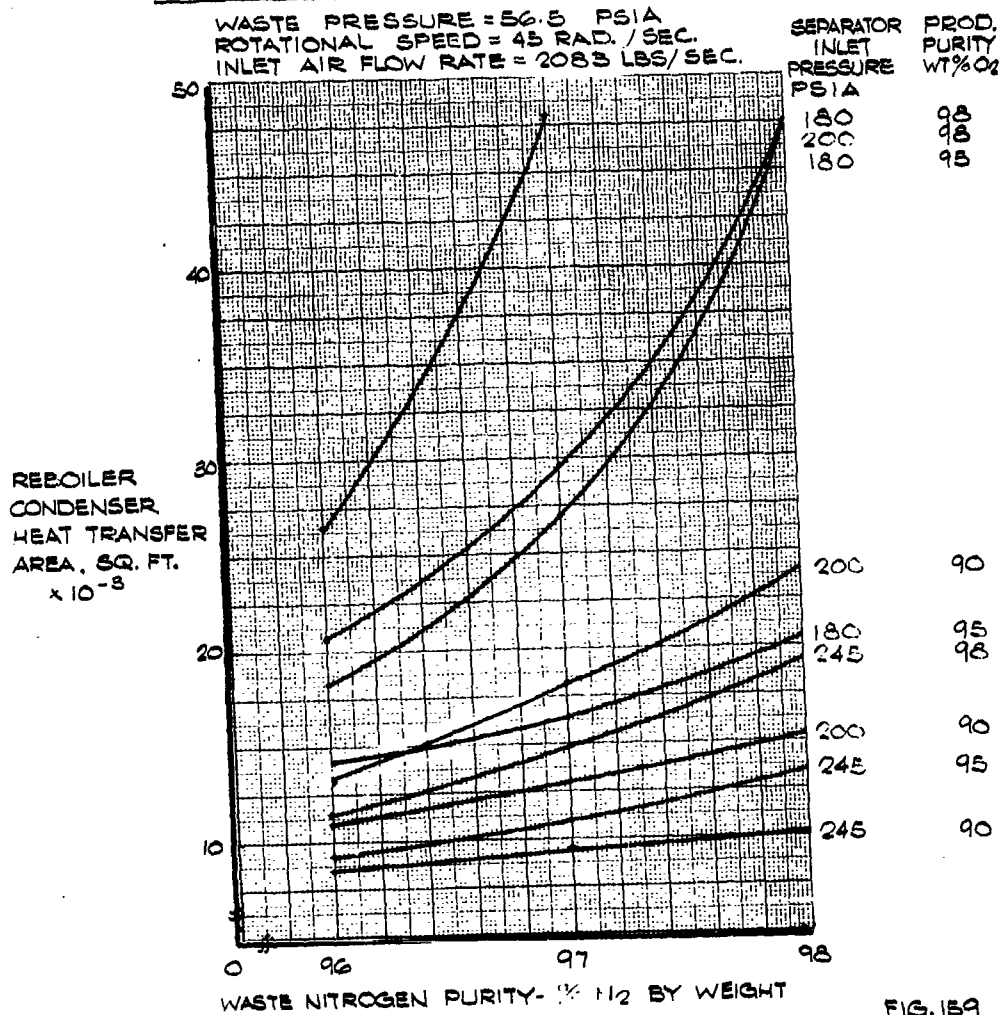


FIG. 159

63 ASRP-2391

SECRET

**SECRET**

ASD-TDR-63-665, Part I

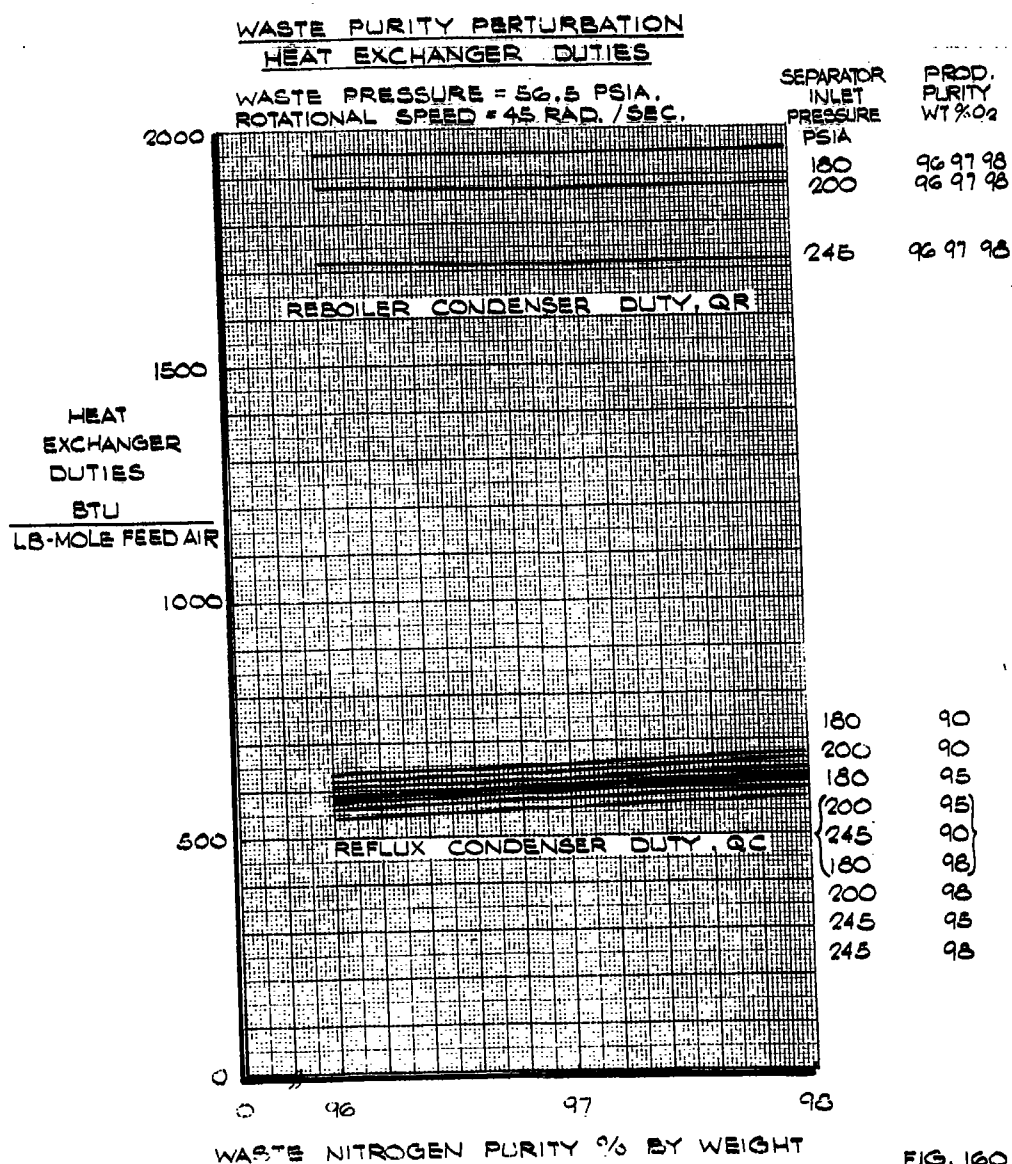


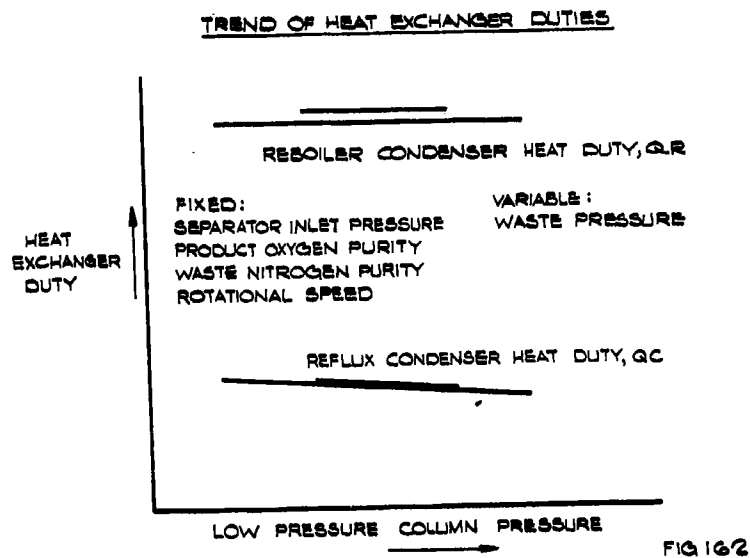
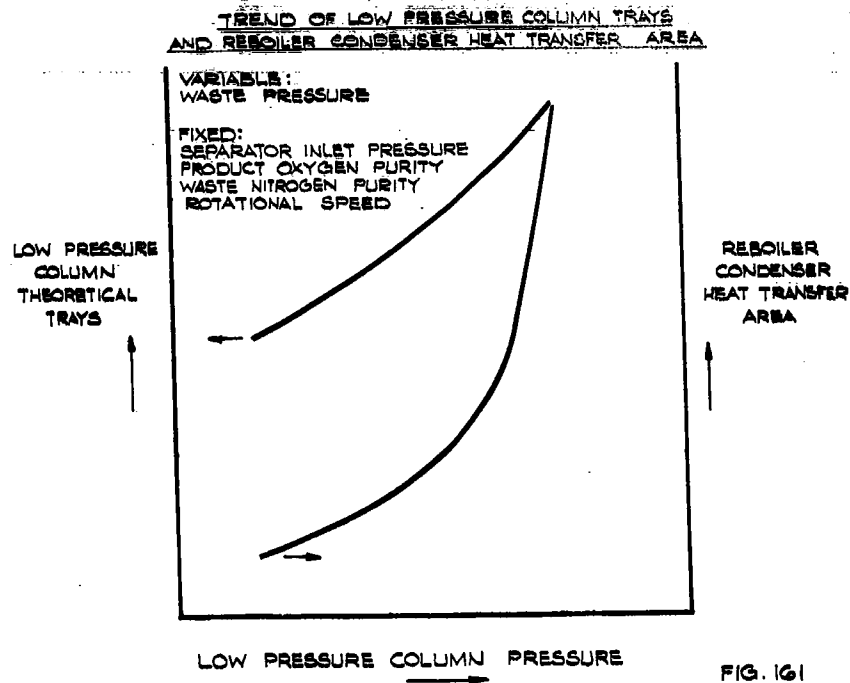
FIG. 160

63 ASRP-2391

**SECRET**

**CONFIDENTIAL**

ASD-TDR-63-665, Part I



63 ASRP-2391

**CONFIDENTIAL**



**SECRET**

**ASD-TDR-63-665, Part I**

condenser area will increase due to reduced  $\Delta T$  resulting from increased low pressure column pressure. Note that the area requirement of the reboiler-condenser increases sharply as the low pressure column pressure level rises against a fixed inlet pressure. This demonstrates the  $\Delta T$  squeeze. The reboiler-condenser heat load, shown in Figure 162, is independent of low pressure column pressure. This follows the earlier studies which show reboiler-condenser duty is only a function of inlet pressure. The reflux condenser heat load will decrease with increasing waste pressure due to more system heat leaving with the waste stream.

The second approach to a perturbation on low pressure column pressure is to let rotational speed vary. Thus, at constant waste pressure, the peripheral pressure becomes a direct function of rotational speed. Figures 163, 164 and 165 illustrate trends for fixed waste pressure and variable rotational speed where the peripheral low pressure column pressure is determined by these quantities. Figure 163 shows that as the low pressure column pressure level increases, the theoretical tray requirement also increases. In Figure 164 the reboiler-condenser heat transfer area shows a minimum which is characteristic of the inter-relation between  $\Delta T$  and heat flux as functions of rotational speed. Note the similarity to Figure 154 in Section 6.3.3.3. The heat duties in Figure 165 decrease as peripheral pressure increases. The reboiler-condenser heat duty is not a direct function of low pressure column pressure but a function of rotational speed which determines the peripheral pressure. The reboiler-condenser duty decreases with increasing rotational speed because the enthalpy of the kettle and shelf streams increases, removing more heat from the high pressure column and thus relieving the reboiler-condenser of this duty. The reflux condenser duty also decreases with increasing rotational speed primarily because of the resultant higher product pressure and, therefore, higher product enthalpy.

**6.3.3.7 Product Purity Perturbations**

A product purity perturbation was made for the rotating separator. In Figure 166 the trend shows more low pressure column trays are required to achieve higher product purity, and at extremely high product purities a pinch occurs analogous to the waste purity pinch. The reboiler-condenser area requirement in Figure 167 shows the area must also increase. The pinch condition is even more dramatic in this figure. The reboiler-condenser area change is strictly a  $\Delta T$  effect since Figure 168 shows that the reboiler-condenser duty

63 ASRP-2391

**SECRET**

**SECRET**

ASD-TDR-63-665, Part I

LOW PRESSURE COLUMN PRESSURE PERTURBATION  
LOW PRESSURE COLUMN TRAYS

WASTE PRESSURE = 56.5 PSIA  
ROTATIONAL SPEED = INDEPENDENT VARIABLE WHICH  
DETERMINES COLUMN PERIPHERAL PRESSURE

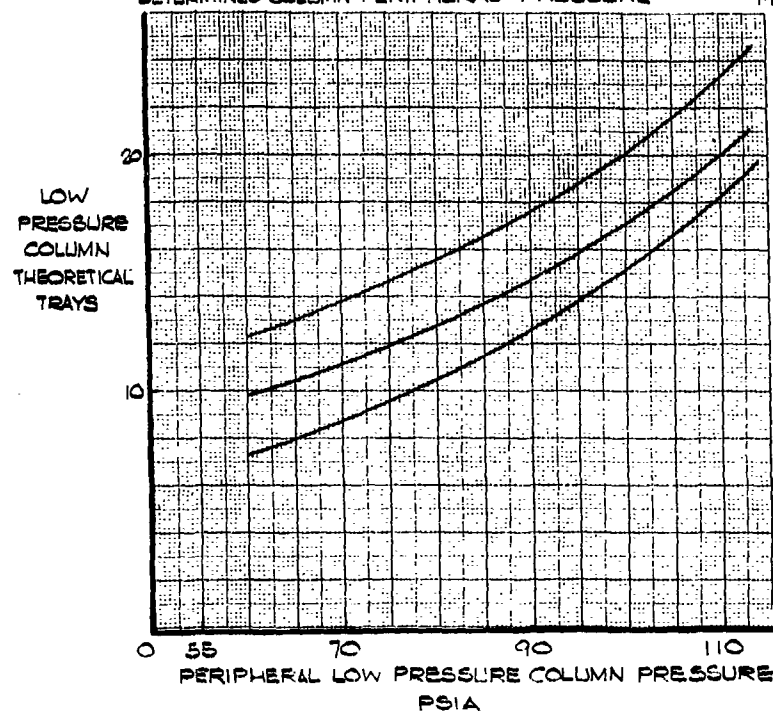


FIG. 163

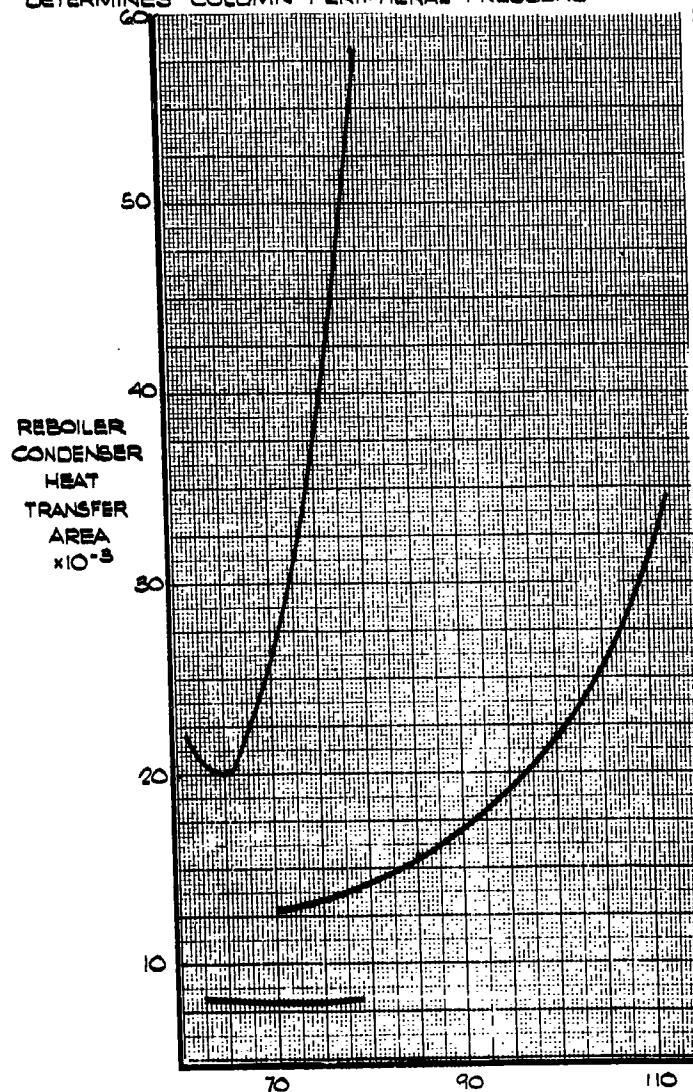
**SECRET**

**SECRET**

ASD-TDR-63-665, Part I

LOW PRESSURE COLUMN PRESSURE PERTURBATION  
REBOILER-CONDENSER HEAT TRANSFER AREA

WASTE PRESSURE = 54.5 PSIA  
ROTATIONAL SPEED = INDEPENDENT VARIABLE WHICH  
DETERMINES COLUMN PERIPHERAL PRESSURE



SEPARATOR INLET PRESSURE PSIA	WASTE PURITY WT % N <sub>2</sub>	PROD. PURITY WT % O <sub>2</sub>
200	97	95

225	96	90
-----	----	----

245	96	90
-----	----	----

PERIPHERAL LOW PRESSURE COLUMN PRESSURE (PSIA)

FIG. 164

63 ASRP-2391

**SECRET**

**SECRET**

ASD-TDR-63-665, Part I

LOW PRESSURE COLUMN PRESSURE PERTURBATION  
HEAT EXCHANGER DUTIES

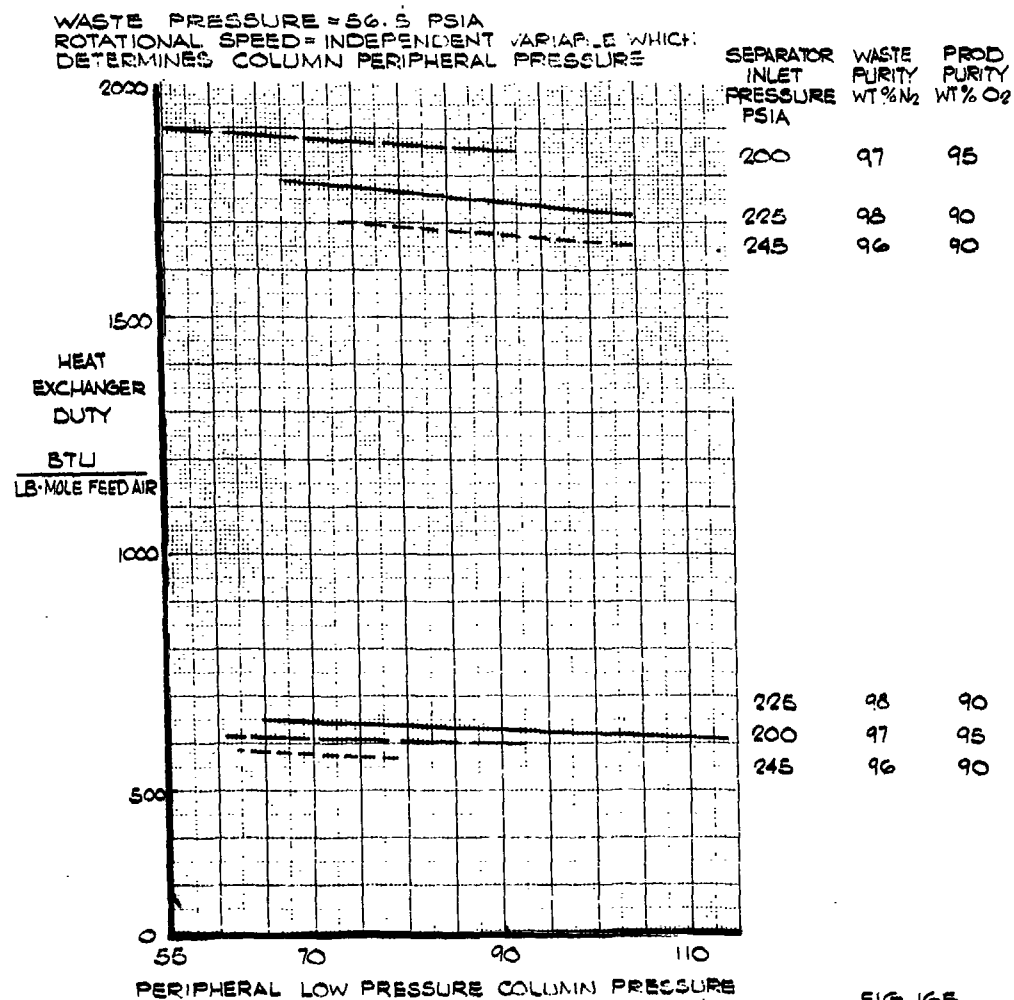


FIG 165

**SECRET**

**SECRET**

ASD-TDR-63-665, Part I

PRODUCT PURITY PERTURBATION  
LOW PRESSURE COLUMN TRAYS

WASTE PRESSURE = 66.5 PSIA  
ROTATIONAL SPEED = 45 RAD./SEC.

LOW PRESSURE  
COLUMN  
THEORETICAL  
TRAYS

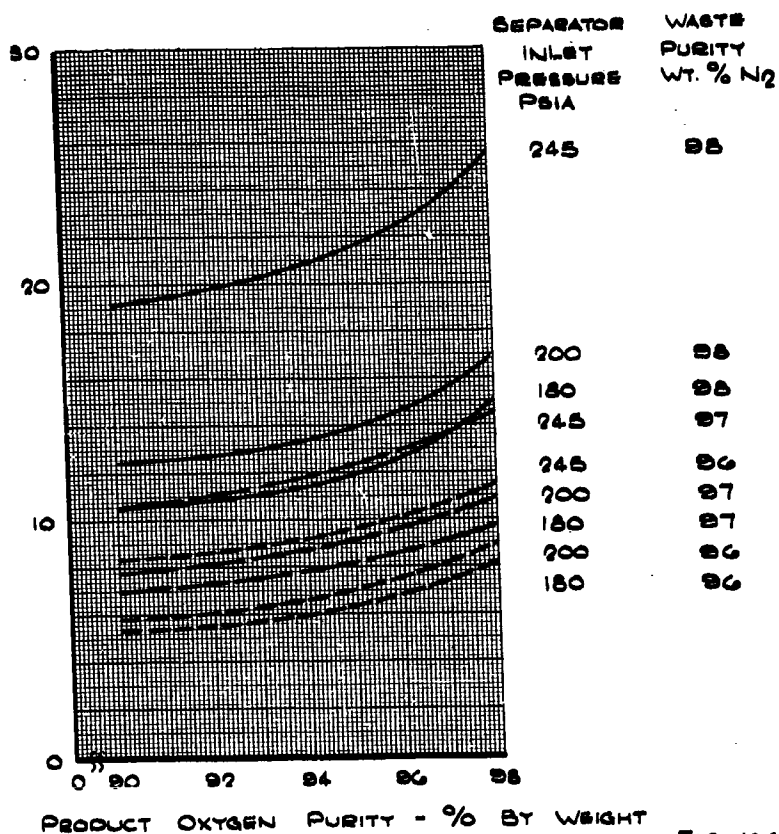


FIG. 166

63 ASRP-2391

**SECRET**

**SECRET**

ASD-TDR-63-665, Part I

PRODUCT PURITY PERTURBATION  
REBOILER CONDENSER HEAT TRANSFER AREA

WASTE PRESSURE = 26.5 PSIA  
ROTATIONAL SPEED = 45 RAD./SEC.  
INLET AIR FLOW RATE = 2083 LBS/SEC.

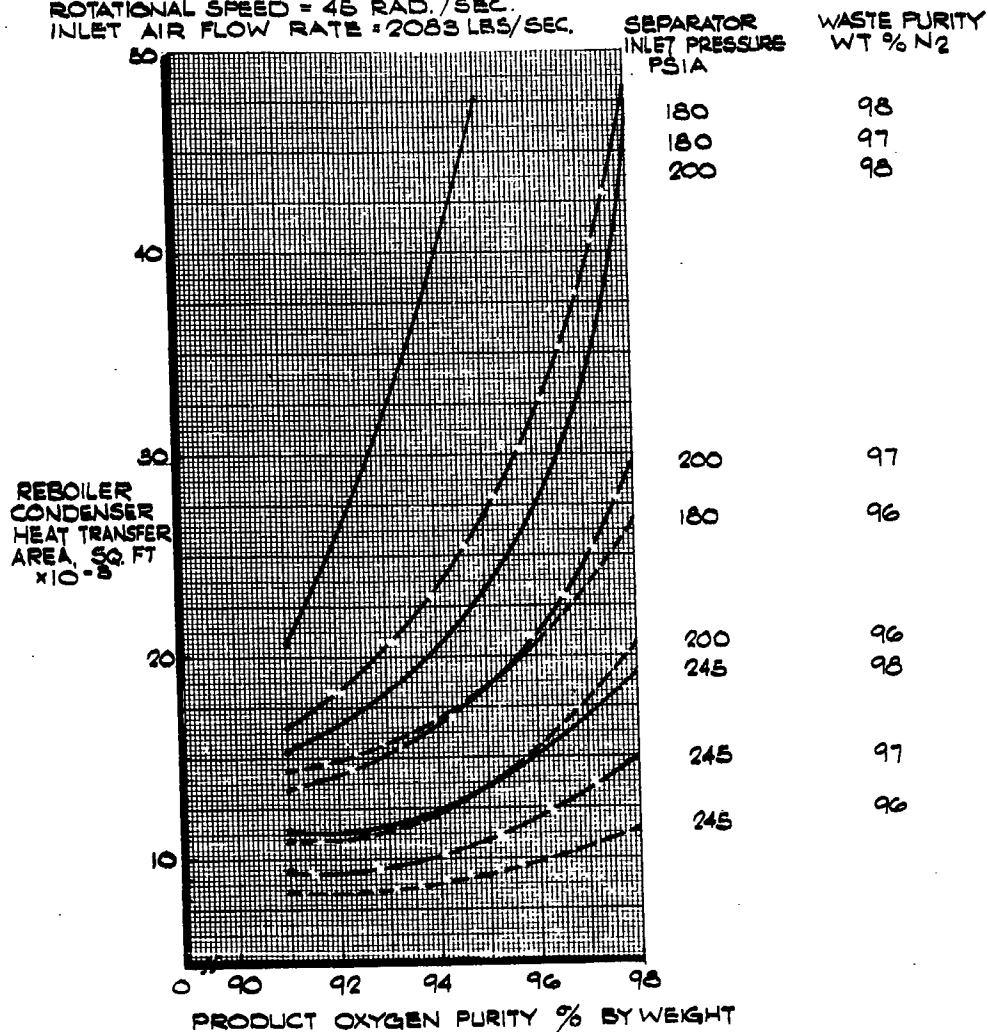


FIG. 167

63 ASRP-2391

**SECRET**

**SECRET**

ASD-TDR-63-665, Part I

PRODUCT PURITY PERTURBATION

HEAT EXCHANGER DUTIES

WASTE PRESSURE = 56.6 PSIA  
ROTATIONAL SPEED = 45 RAD./SEC.

SEPARATOR  
INLET  
PRESSURE  
PSIA

WASTE  
PURITY  
WT. % N<sub>2</sub>

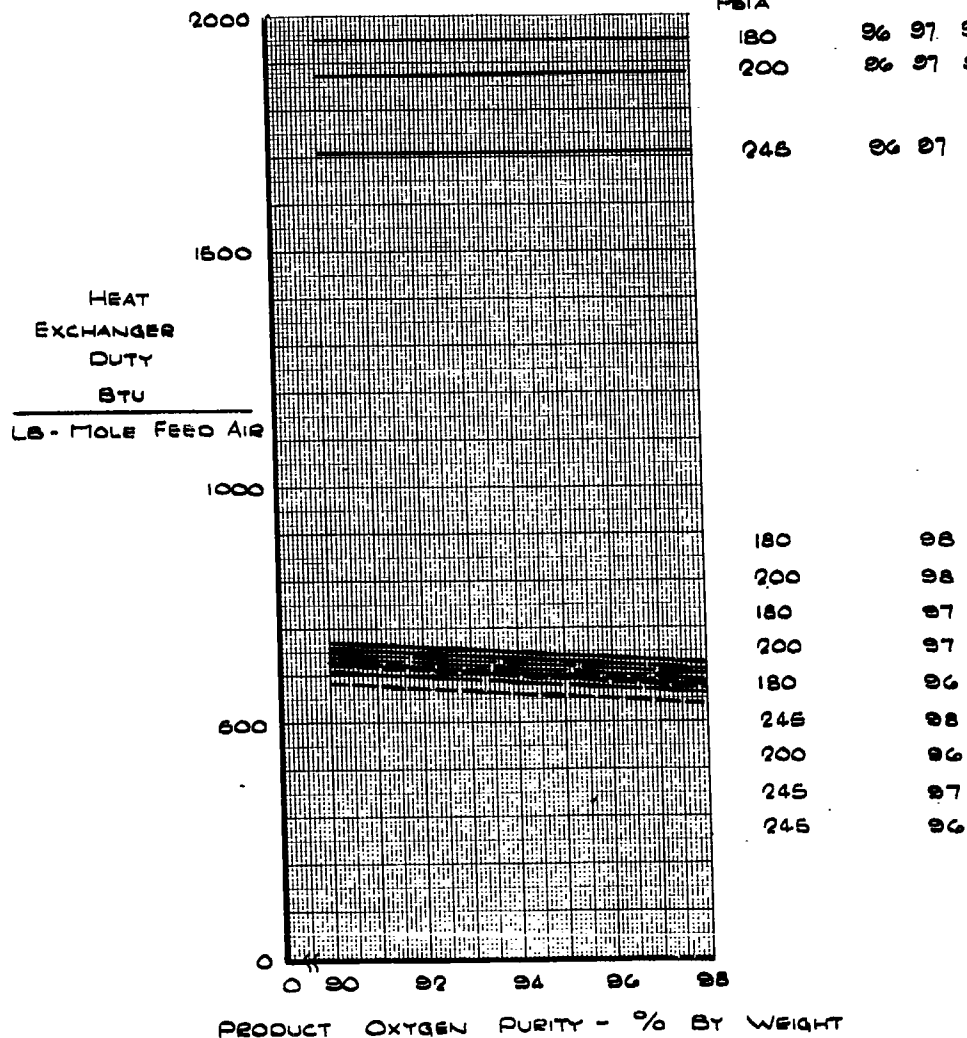


FIG. 10B

63 ASRP-2391

**SECRET**

**SECRET**

**ASD-TDR-63-665, Part I**

is not a direct function of product oxygen purity. Reflux condenser duty decreases as the product purity increases because the product quantity decreases, requiring less refrigeration to make the reduced quantity of liquid.

Summarizing the perturbation studies, both the tray requirements and reboiler-condenser area minimize by reducing waste purity, reducing product purity, and reducing low pressure column pressure. The inlet pressure, however, shows counter trends where the controlling parameter, reboiler-condenser area, decreases with increasing inlet pressure, up to about 245 psia. Higher inlet pressures will gradually increase system weight due to decline in distillation performance, increased pressure drop and reduced  $\Delta T$ . External refrigeration in the form of hydrogen supplied to the reflux condenser can be minimized by decreasing waste purity and increasing inlet pressure, increasing product purity, increasing waste pressure, and increasing rotational speed.

**6.3.3.8 Optimum Arrangement of Components**

Investigation of the optimum physical arrangement of the separator was undertaken early in the program to provide one optimum common configuration for the various weight and volume studies later in the program. Arrangements considered were a single rotor containing all components, separate major components to permit each to revolve at its individual optimum speed, and finally multiple parallel units. In this last case each rotor is a completely integrated single rotor, but of smaller scale than in the first case. Multiples of these smaller separators would be operated in parallel to achieve the desired total flow capacity.

To achieve the best physical arrangement, the functional considerations of each component were noted and then they were combined in the fashion which minimizes the fluid entrance and exit problems from the rotor. The arrangement selected for the single rotor configuration is shown in Figure 152 and 153. This side-by-side arrangement of the columns, fitted around the curved tube reboiler-condenser, was conceived and proposed by Linde.

This single rotor configuration is the recommended approach because it offers the best potential for minimum weight. The reboiler-condenser is mounted near the hub so that the high pressure liquid nitrogen streams can be transferred within the rotor to the two columns. The reflux stream flowing from the reboiler-condenser to the high pressure

63 ASRP-2391

**SECRET**



**SECRET**

**ASD-TDR-63-665, Part I**

column moves radially outward to avoid any pressure loss. The shelf portion transferred to the low pressure column undergoes nearly isentropic expansion as it flows radially inward. Some additional pressure drop is added in the control valve. Kettle liquid is transferred in the same manner from the periphery of the high pressure column. These transfers are polytropic, approximated by an 80% efficient isentropic process between columns. The oxygen vapor from the reboiler-condenser is also transferred within the rotor in the most direct manner to the periphery of the low pressure column. The relative position of these components enhances the reboiler-condenser  $\Delta T$ .

One of the most difficult problems is transfer of liquids from the periphery to the hub of the rotor. There is not sufficient head to move these liquids against the "g" field so they are removed in diffusers and returned to the hub in an external circuit. This configuration presents the low pressure liquid streams for transfer from the periphery thus minimizing the head on the diffuser seals. This too minimizes weight.

From the above it is concluded that the relative position of components recommended in the single rotor offers minimum weight and the most efficient package from the process viewpoint.

Alternatives to the single rotor design were investigated. Each full scale component was analyzed to determine its minimum weight as a function of rotational speed. Hopefully some total weight saving could be achieved by mounting each component on a separate shaft rotating at its optimum speed. The results are plotted on Figure 169 where individual component weights are shown without drive, bearings, and shafts. These auxiliaries are added to the total weights for single and two rotor designs.

Since the single rotor reboiler-condenser weight is minimum around 50 rad./sec. this provides minimum separator weight for a single rotor. Column weights are relatively insensitive to rotational speed but this speed has great effect on pressure drop and  $\Delta T$ . Hence, single rotor reboiler-condenser weight increases sharply above 60 rad./sec.

63 ASRP-2391

**SECRET**

SECRET

ASD-TDR-63-665, Part I

SEPARATE COMPONENT WEIGHT TREND

SEPARATOR INLET PRESSURE 225 PSIA  
WASTE PRESSURE = 56.5 PSIA  
PRODUCT OXYGEN PURITY = 90 WEIGHT %  
WASTE NITROGEN PURITY = 98 WEIGHT %

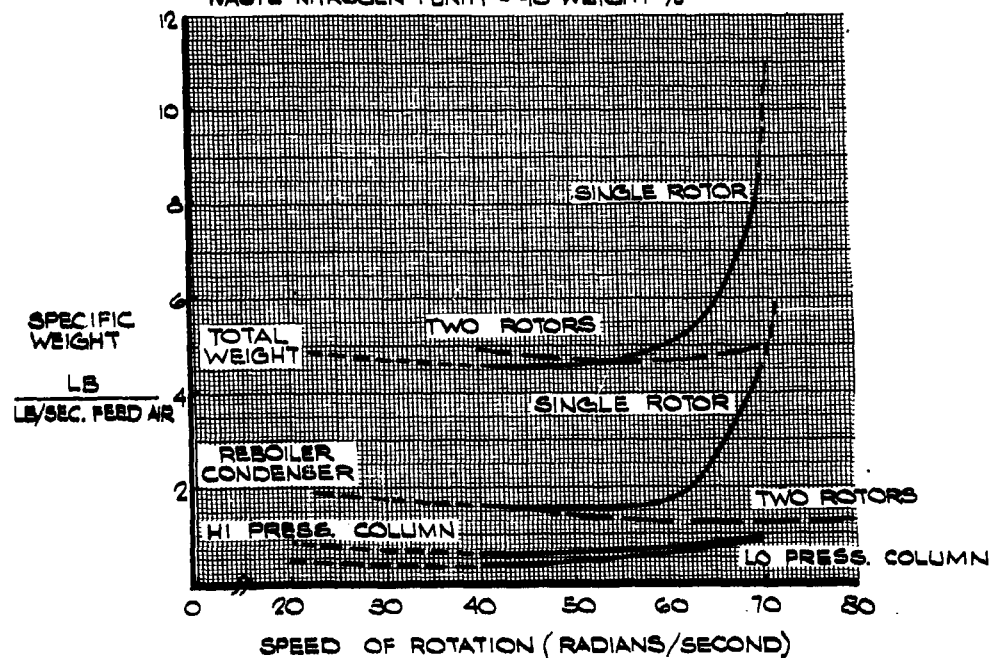


FIG. 169

63 ASRP-2391

SECRET

**SECRET**

**ASD-TDR-63-665, Part I**

Now if the columns are mounted together on a shaft rotating at 40 rad./sec. where column weights are minimum, this large  $\Delta T$  may be applied to the separate reboiler-condenser rotating at its optimum speed. The broken line on Figure 169 shows this separate reboiler-condenser and the total weight of the two modules. The optimum speed of the separate reboiler-condenser is 70 rad./sec. Weight saved on the reboiler-condenser, before adding the bearings, piping and drive which must be duplicated for the second rotor, is 700 lbs. It is unlikely that detailed design could achieve a net saving in the two-rotor concept since this requires that a third full flow vapor stream ( $O_2$  vapor to the low pressure column) be introduced to the column package.

In conclusion, the two rotor concept offers only marginal weight saving, if any, compared to the single rotor. Volume is greater in the two rotor concept since the separate rotor for the reboiler-condenser is a direct volume penalty. The single rotor is equal in volume to the column package of the two rotor designs since the reboiler-condenser in the single rotor concept fits within the high pressure column.

**6.3.3.9 Multiple Unit Assessment**

Multiple parallel separators were considered as a means of decreasing weight or improving performance or reliability. This would employ multiples of the single rotor, each being a complete separator in itself.

In the first case the single rotor separator was investigated to show the variation in weight as a function of mass throughput. No manifold weights are included. Typical weight and volume trends are presented in Figure 170 to indicate the change in specific weight as a function of mass throughput. This curve was made at the 50% confidence level earlier in the program but recent improvements in heat transfer permit this same weight at the 95% confidence level. Design conditions used in this study are for the cycle suggested by General Dynamics/Astronautics.

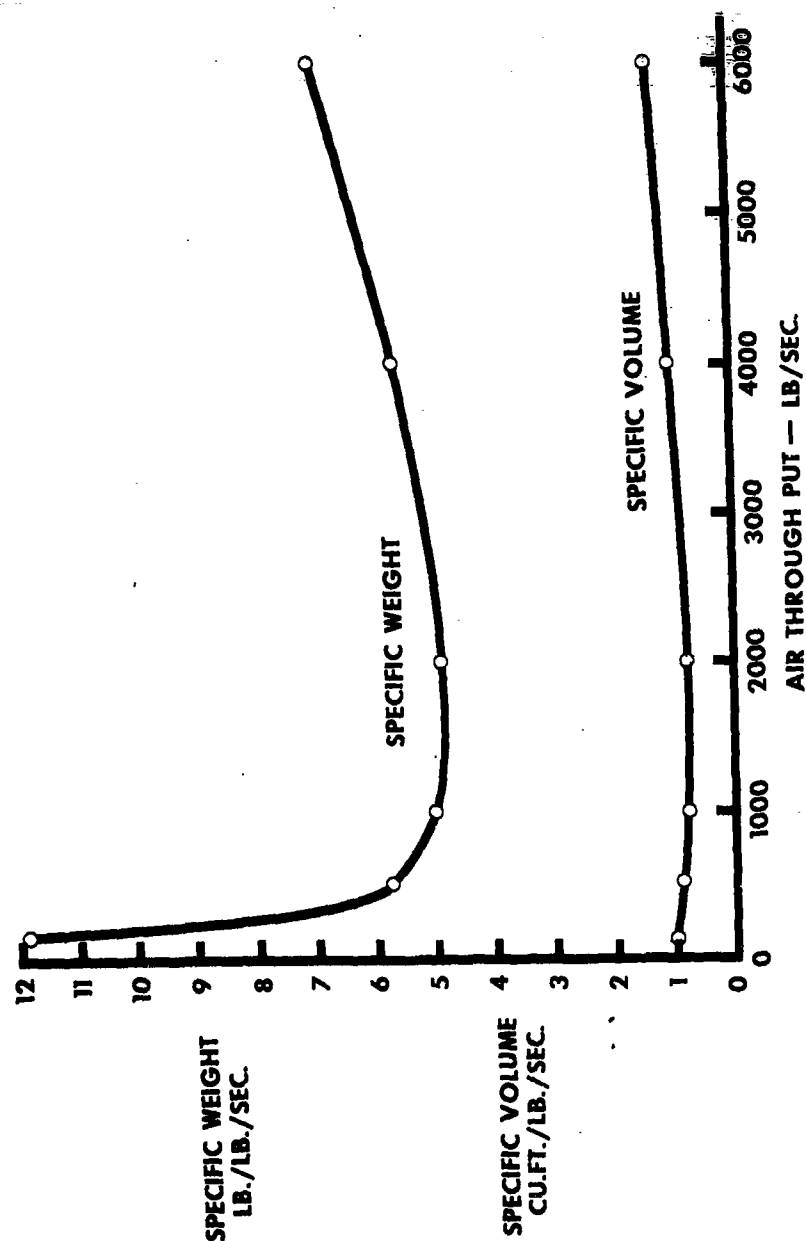
Inlet Pressure	225 psia
Product Purity	90% $O_2$
Waste Purity	98% $N_2$
Waste Pressure	56.5 psia

Figure 170 was developed for a single rotor separator with the  
63 ASRP-2391

**SECRET**

SECRET

ASD-TDR-63-665, Part I



SPECIFIC WEIGHT AND VOLUME OF SINGLE SEPARATOR  
VERSUS AIR THROUGH PUT CAPACITY

FIG. 170

63 ASRP-2391

SECRET

**SECRET**

**ASD-TDR-63-665, Part I**

side-by-side column arrangement as in Figure 153. The outer diameter is adjusted only by the incremental changes necessary in the inner shaft diameter to accommodate the feed air. Column radial thickness is constant and column width is changed to accommodate the changing flowrate.

The minimum separator specific weight occurs between 1000 lb./sec. and 2000 lb./sec. air throughput. This should be typical for most cycles although extreme changes in purity will shift this minimum. As flow increases above 2000 lb./sec. the specific weight increases since most items increase in length directly with flow. In addition, the diameter also increases, influencing the weight of sides and shell as the square of the diameter. Thus, to provide double or triple the 2000 lb./sec. separator capacity, multiples of the 2000 lb./sec. separator would permit the least total separator weight.

At the opposite end of the scale, the nominally constant weight items become controlling at very low throughputs. The column sides, for example, have a minimum diameter of twice the radial column thickness which is determined by the trays necessary to make the desired purity. This is independent of flow requirements. In the extreme, at zero flow, sides and shaft stubs would be required for both columns and the reboiler-condenser, with no trays or shell between them. The scaling effects study in Section 6.4 show that the 100 lb./sec. separator is about the smallest practicable separator which can be constructed in this physical design. Figure 170 shows the weight penalty incurred by this flight weight scale of 100 lb./sec. compared to the projected full size, 2000 lb./sec. separator. Different configurations would be considered if the design flow changes significantly from 2000 lb./sec.

Using the above results, multiple parallel units were plotted in Figure 171. There is no weight reduction apparent from the multiple unit calculations of one, two or four units for a total mass air feed of 2000 lb./sec. The primary weight increase results from the additional supports, bearings, and drives required for multiple smaller scale units. A slight upward trend was found in the rotating sections of multiple units so all factors show increased weight when multiple units were employed. The volume also increases as noted in Figure 171.

Reliability is not particularly enhanced by multiple units. Although the effect of seal and bearing failure on one unit can be minimized by using multiples and shutting down the faulty unit, the added complications of shutoff valves negates this gain. Since failure of a single full scale air separator only requires the mission be aborted, and no flight safety is involved, a single unit is preferred.

63 ASRP-2391

**SECRET**

**SECRET**

ASD-TDR-63-665, Part I

**SPECIFIC WEIGHT AND VOLUME OF  
MULTIPLE PARALLEL SEPARATORS  
(INCLUDING INTERCONNECTING PIPING)**

**INLET AIR FLOW RATE = 2000 LBS/SEC**

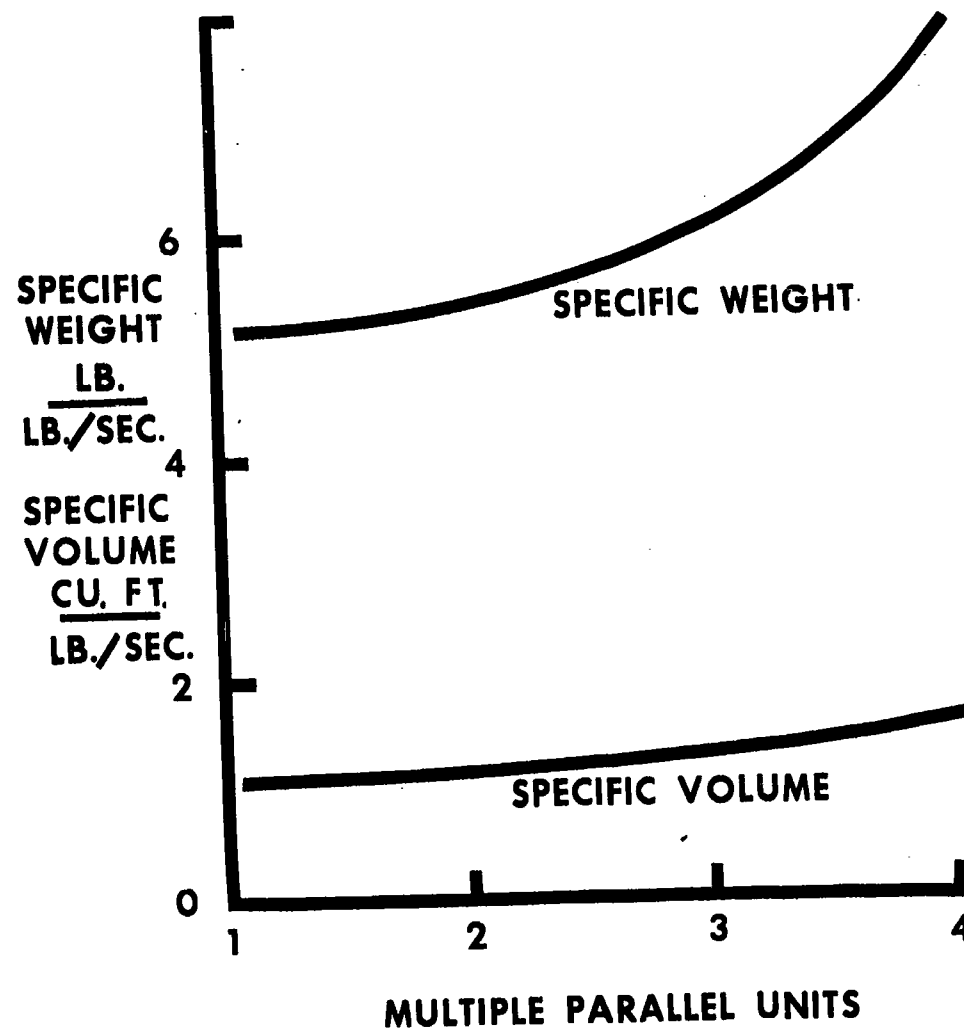


**FIG. 171**

63 ASRP-2391

**SECRET**

**SECRET**

**ASD-TDR-63-665, Part I**

Performance of multiple units may suffer unless special and rather sophisticated equipment is provided to exactly distribute the flows to match the individual unit characteristics such as pressure drop and heat transfer capabilities. Fabrication and maintenance of precisely matched separators would be unnecessarily expensive. If throttling the inlet pressure and the hydrogen pressure is employed to balance the flows through unmatched separators, an unnecessary waste of energy is incurred and reliability is reduced.

In summary the single, full size rotor concept offers the least weight at this time. Using separate full size components has some merit.

**6.3.4 Determination of System Weight and Volume**

**6.3.4.1 Component Process and Stress Requirements**

This Section presents system weight and volume estimates thus reducing the parametric studies discussed in Section 6.3.3 to finite values of weight and volume.

In Appendix XVII of this report, the sample calculations are presented for the weight and volume of the GD/A case at 95% confidence level. It should be noted that these calculations are developed for parametric studies based on the general considerations of design stress produced by pressure and centrifugal loads. They are not intended to replace the detail design formulas used in the ultimate design.

The following description of the program denotes the prime considerations in designing each component leaving the detailed mathematical analysis to be discussed in Appendix XVII.

**a. High Pressure Column**

The high pressure column is designed to contain full pressure since this provides the smallest pressure shell and minimum windage power loss. The air surrounding the rotating shell should be at the lowest density possible to minimize windage.

The shell sides must also withstand the centrifugal stress of the trays and the kettle liquid collected at the

**63 ASRP-2391**

**SECRET**

~~SECRET~~

ASD-TDR-63-665, Part I

periphery. This liquid adds substantially to the required shell weight. In refining the calculations, the 20% strength improvement experienced in aluminum at cryogenic temperature is utilized where the stress results from a cryogenic liquid load. Stress concentrations are also included in the refinements to provide a realistic calculation.

b. Low Pressure Column

The calculations for the Low Pressure Column apply as used for the high pressure column. Some predesign is required to smooth the two sections of the low pressure column into a continuous column side wall which can efficiently carry the loads radially to the shaft and bearings. Here again, the liquid loads add substantially to the required shell weight.

c. Kettle Separator

The low pressure column is further complicated by the kettle feed separator which adds a liquid load near the midpoint of the column. This separator and its support system are calculated separately from the low pressure column. The actual design may integrate this separator with the column but the weights would be additive regardless.

d. Reboiler-Condenser

Weight of the reboiler-condenser is composed of the primary heat transfer area and the shell. Fluid flow requirements are particularly critical in the design of this unit since excess pressure loss may adversely affect the  $\Delta T$ . Thus, the heat transfer area calculation must be made for a specific configuration and mass flow per unit area.

Since recirculation of the liquid oxygen is planned, this liquid weight must be carried through the shell calculation. This liquid plus the condensed nitrogen adds some weight to the shell but not as severely as the columns because the reboiler-condenser radius is smaller.

63 ASRP-2391

~~SECRET~~



**SECRET**

**ASD-TDR-63-665, Part I**

e. Shaft

A central shaft is used to join the columns and carry their weight to the bearings. The columns provide a large section modulus to limit deflection. The shaft is designed for shear and bending stresses. For the present, a 1/4 in. wall thickness is used. This metal in the column hubs will likely be distributed through the columns as rigidizing members.

f. Diffuser

Where liquids leave the rotor, kinetic energy is recovered in diffusers to conserve power and refrigeration. The diffuser weight is nominal since it consists of a collector ring and thin blades nearly tangential to the rotor.

g. Piping and Seals

The piping and seals are introduced as constants. The primary sizing of the rotor stems from the allowable diameter of the inner piping used to introduce and expel fluids (i.e., inlet air and waste nitrogen). Diameter of these lines is based on the allowable velocity consistent with the pressure loss permitted. A full scale unit should have a minimum of a 35 in. diameter central air inlet and waste nitrogen exit. Preferably these should be 40 in. to achieve a nominal head loss. The 40 in. diameter is used in these calculations.

These same principles apply in sizing the other pipes to gradually reduce velocity to minimize head loss at each change in flow direction.

h. Outer Casing

An outer casing or shroud is provided to streamline the rotor surface to reduce windage power loss. This light casing was deleted from the final calculations. The formulas are retained in the computer program for alternate designs which may utilize a stationary casing to minimize pressure drop across the diffuser seal and collect the seal leakage.

i. Bearing Supports

The bearing supports are used to transmit the separator

63 ASRP-2391

**SECRET**

**SECRET**

**ASD-TDR-63-665, Part I**

weight to the vehicle. They are calculated as a function of the separator weight.

**j. Bearings**

The individual bearing weight is multiplied times the separator weight and divided by the bearing load capacity. Commercial aircraft bearing weights are used.

**k. Product Separator**

Primary concern in sizing a product separator is to provide sufficient liquid volume to compensate for momentary upsets and sufficient vapor disengagement from this liquid. The liquid product is withdrawn at the separator and the balance is recirculated through the reboiler-condenser.

**l. Turbines**

The weight of the turbines used to extract power from the liquid streams from the diffusers is estimated from their power requirements. Only rough sizing calculations were made.

**m. Drive**

Weight of the separator drive is estimated from net driving power required to accelerate the fluids removed from the rotor. Work extracted in the hydrogen turbines is returned to the separator.

**n. Volume**

The separator volume is calculated as the volume of a right cylinder with truncated conical ends. The controlling diameter of the cylinder usually is the high pressure column located outside the reboiler-condenser. This procedure is different from the initial calculations where the ellipsoid of revolution was used to describe the displaced volume. As the preliminary design evolved it was shown that the superficial vapor velocity must be lower than desired. Consequently the length increased, changing the shape from the ellipsoid to a cylinder.

63 ASRP-2391

**SECRET**

**SECRET**

**ASD-TDR-63-665, Part I**

**6.3.4.2 System Weight and Volume Mapping**

Figures 172, 173, and 174 show the results of the weight mapping study for three product oxygen purities as a function of separator inlet pressure and waste nitrogen purity. The rotational speed was maintained at the previously determined optimum speed of 45 rad./sec. and the waste pressure maintained at 56.5 psia. Figure 175 presents the volumes for the cycles presented in Figures 172, 173, and 174. As shown previously, the extremely low  $\Delta T$  case (180 psia and 98% waste nitrogen purity,) has zero  $\Delta T$  at 45 rad./sec. and 98% product oxygen purity, and therefore, is non-operable.

These results which are summarized in Table 20 indicate that weight decreases with increasing inlet pressure in the range calculated. This results from the increasing reboiler-condenser  $\Delta T$  as inlet pressure increases at a fixed waste pressure. These curves are the left hand side of a family of parabolas approaching a minimum weight at the upper limit of the inlet pressures investigated. As inlet pressure increases further the reduced volatility in the high pressure column becomes controlling. This causes a rapid increase in the number of trays in the low pressure column. The upper limit is reached when the high pressure column cannot supply the quantity and purity of "kettle" and "shelf" liquids necessary to operate the low pressure column. Low pressure column trays become infinite and the reboiler-condenser  $\Delta T$  approaches zero.

The effect of waste purity and product purity is evident since separator weight rises strongly with an increase in purities. This, too, is a result of more trays which consume more pressure drop within the columns, therefore, reducing the reboiler-condenser  $\Delta T$ . Volume studies in Figure 175 show the strong relationship purities also have on the volume. The upper curve is for the 98% O<sub>2</sub> product purity case which requires so many trays that the diameter exceeds the typical range of the other cases and has a much longer reboiler-condenser.

Figures 176, 177 and 178 illustrate the combined effect of weight and volume where the volume penalty is taken as one pound per cubic foot. The same trends prevail except penalties of extremely low inlet pressure and high waste and product purities are further accentuated.

Finally, the combined effect of separator inlet pressure, waste nitrogen purity, and product oxygen on separator weight and volume for  
63 ASRP-2391

**SECRET**

SECRET

ASD-TDR-63-665, Part I

SEPARATOR WEIGHT

PRODUCT OXYGEN PURITY = 90 WT. %  
 WASTE PRESSURE = 56.5 PSIA  
 INLET AIR FLOW RATE = 2085 LBS./SEC.  
 ROTATIONAL SPEED = 45 RAD./SEC.

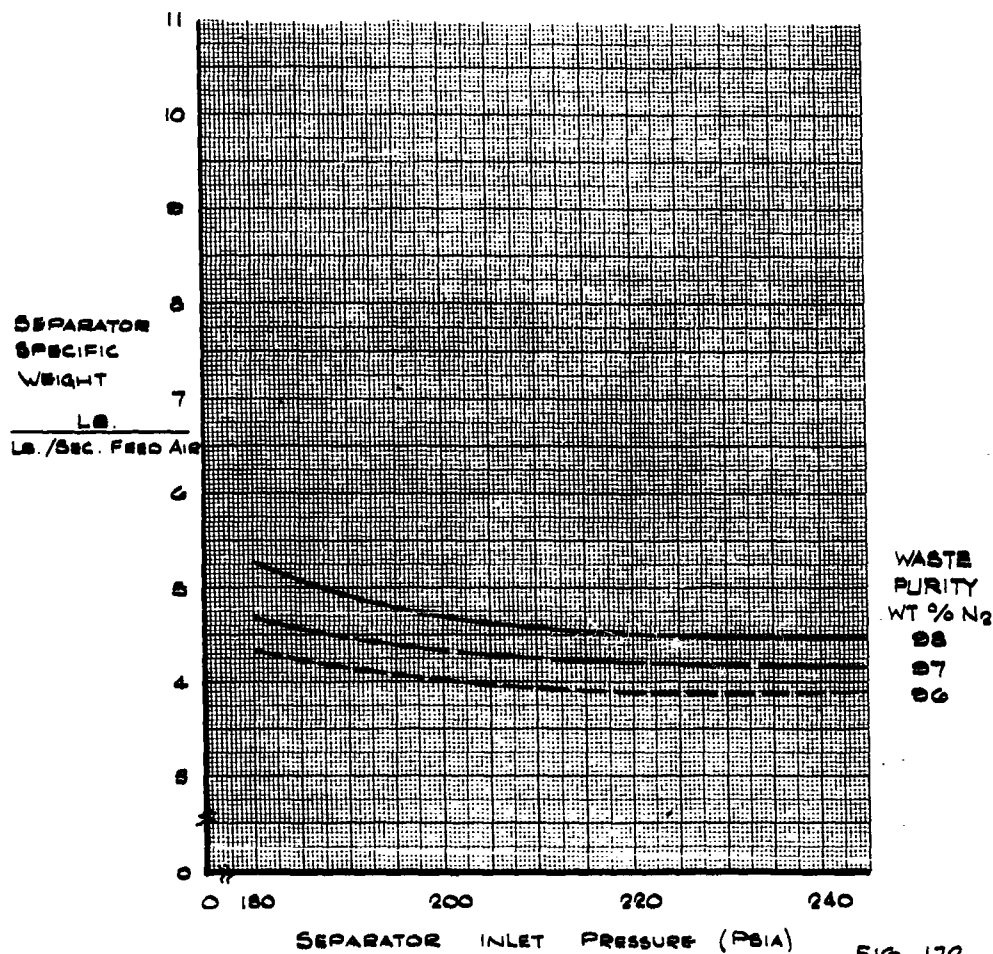


FIG. 172

63 ASRP-2391

SECRET

SECRET

ASD-TDR-63-665, Part I

SEPARATOR WEIGHT

PRODUCT OXYGEN PURITY = 98 WT. %  
WASTE PRESSURE = 54.5 PSIA  
INLET AIR FLOW RATE = 2085 LBS./SEC.  
ROTATIONAL SPEED = 45 RAD./SEC.

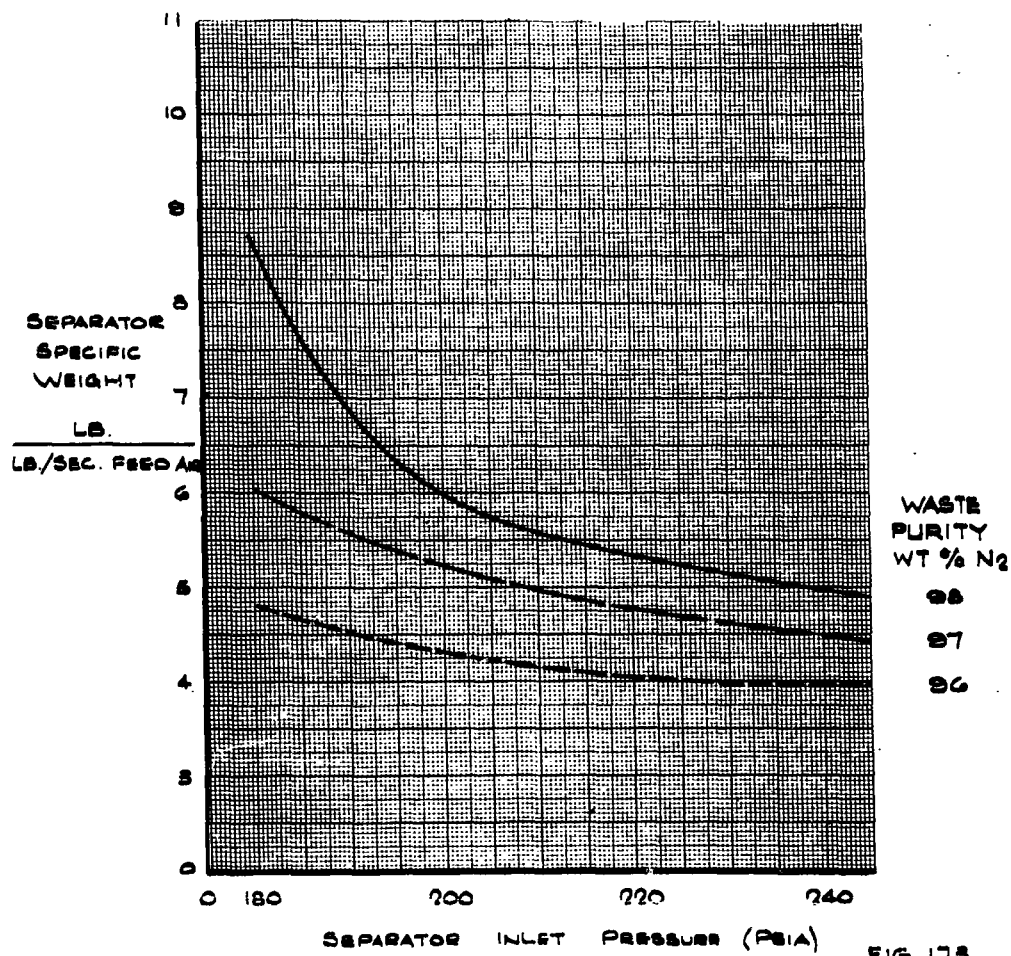


FIG. 178

SECRET

~~SECRET~~

ASD-TDR-63-665, Part I

SEPARATOR WEIGHT

PRODUCT OXYGEN PURITY = 98 WT %  
WASTE PRESSURE = 56.5 PSIA  
INLET AIR FLOW RATE = 2085 LB/SEC.  
ROTATIONAL SPEED = 45 RAD/SEC.

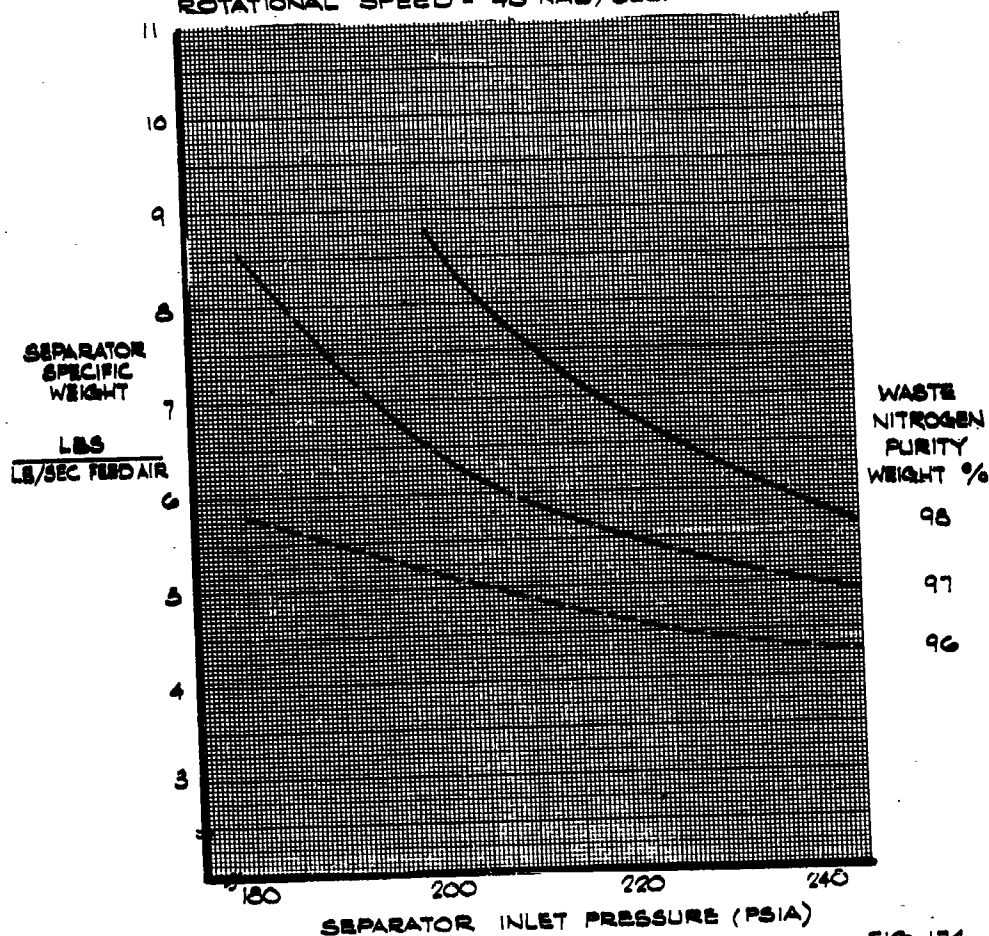


FIG. 174

SECRET

SECRET

ASD-TDR-63-665, Part I

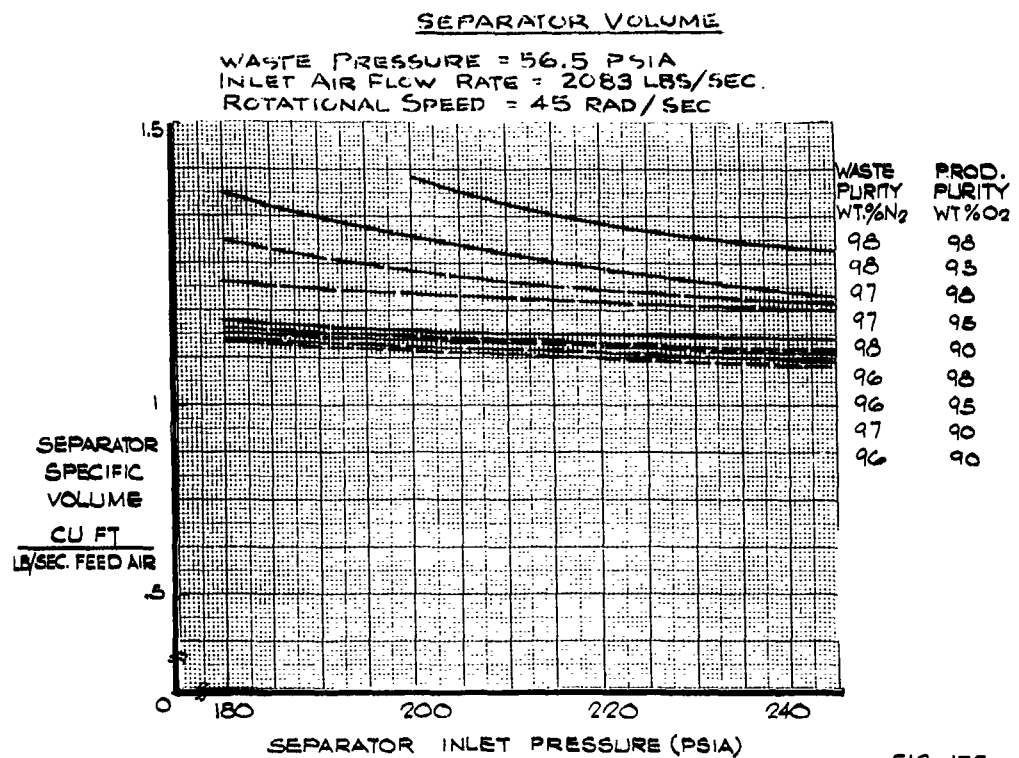


FIG. 175

63 ASRP-2391

SECRET

**SECRET**

ASD-TDR-63-665, Part I

TABLE 20  
WEIGHT AND VOLUME MAPPING SUMMARY  
ROTATIONAL SPEED = 45 RAD./SEC.

<u>Separator</u> <u>Inlet Pressure</u> <u>Psia</u>	<u>Waste</u> <u>Pressure</u> <u>Psia</u>	<u>Product</u> <u>Purity</u> <u>Weight Percent</u>	<u>Waste</u> <u>Purity</u> <u>Weight Percent</u>	<u>Specific</u> <u>Weight</u> <u>Lb.</u> <u>Lb./Sec.</u>	<u>Specific</u> <u>Volume</u> <u>Cu.Ft.</u> <u>Lb./Sec.</u>
180	56.5	90	98	5.28	1.07
200	56.5	90	98	4.70	1.06
225	56.5	90	98	4.62	1.04
245	56.5	90	98	4.45	1.04
180	56.5	90	97	4.67	1.04
200	56.5	90	97	4.37	1.02
245	56.5	90	97	4.18	.99
180	56.5	90	96	4.34	1.03
200	56.5	90	96	4.02	1.01
245	56.5	90	96	3.90	.98
180	56.5	95	98	8.73	1.35
200	56.5	95	98	5.97	1.26
245	56.5	95	98	4.91	1.13
180	56.5	95	97	6.00	1.16
200	56.5	95	97	5.58	1.14
245	56.5	95	97	4.45	1.10
180	56.5	95	96	4.84	1.05
200	56.5	95	96	4.32	1.04
245	56.5	95	96	3.98	1.01
180	56.5	98	98	Non-Operable	
200	56.5	98	98	8.83	1.38
245	56.5	98	98	5.68	1.23
180	56.5	98	97	8.65	1.32
200	56.5	98	97	6.48	1.18
245	56.5	98	97	4.94	1.09
180	56.5	98	96	5.85	1.06
200	56.5	98	96	5.21	1.03
245	56.5	98	96	4.31	1.01

63 ASRP-2391

**SECRET**



SECRET

ASD-TDR-63-665, Part I

SEPARATOR WEIGHT AND VOLUME

PRODUCT OXYGEN PURITY = 90 % BY WEIGHT  
WASTE PRESSURE = 56.5 PSIA  
INLET AIR FLOW RATE = 2083 LBS/SEC.  
VOLUME PENALTY = 1 LB/CU. FT.  
ROTATIONAL SPEED = 45 RAD/SEC

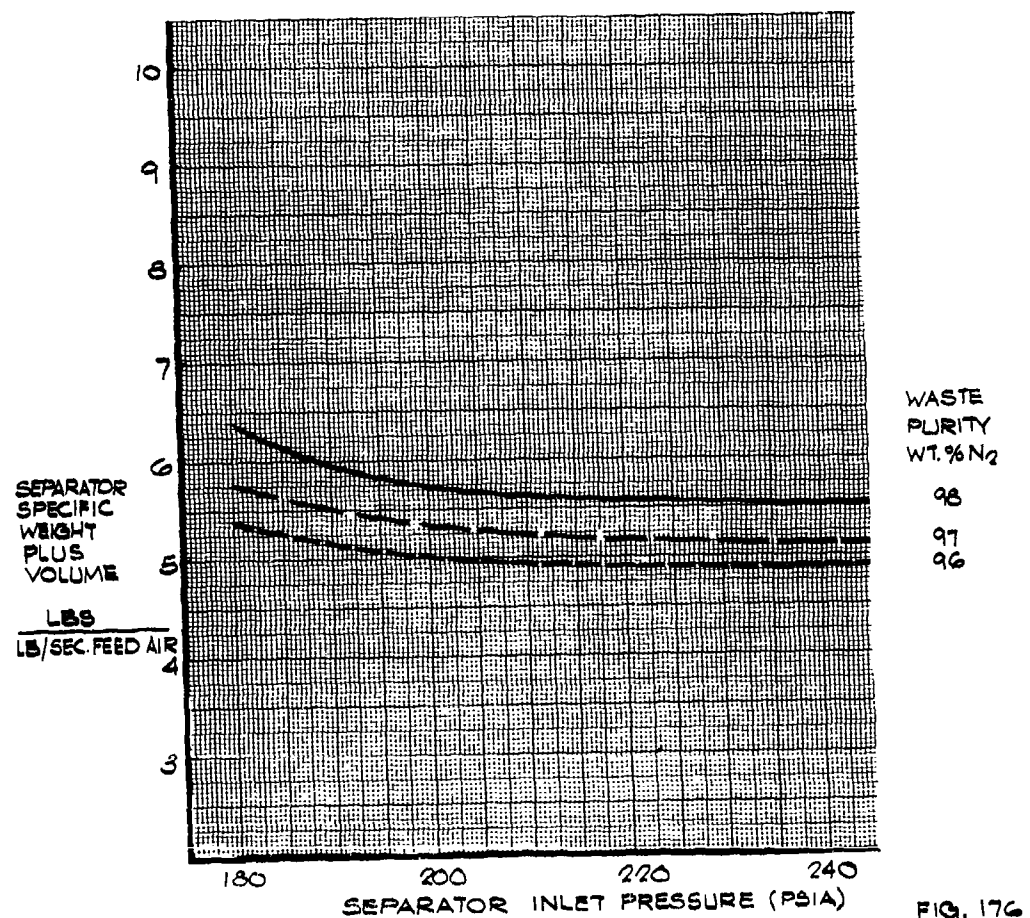


FIG. 176

63 ASRP-2391

343

SECRET

SECRET

ASD-TDR-63-665, Part I

SEPARATOR WEIGHT AND VOLUME

PRODUCT OXYGEN PURITY = 95 % BY WEIGHT  
WASTE PRESSURE = 56.5 PSIA  
INLET AIR FLOW RATE = 2088 LBS/SEC.  
VOLUME PENALTY = 1 LB / CU FT  
ROTATIONAL SPEED = 45 RAD/SEC.

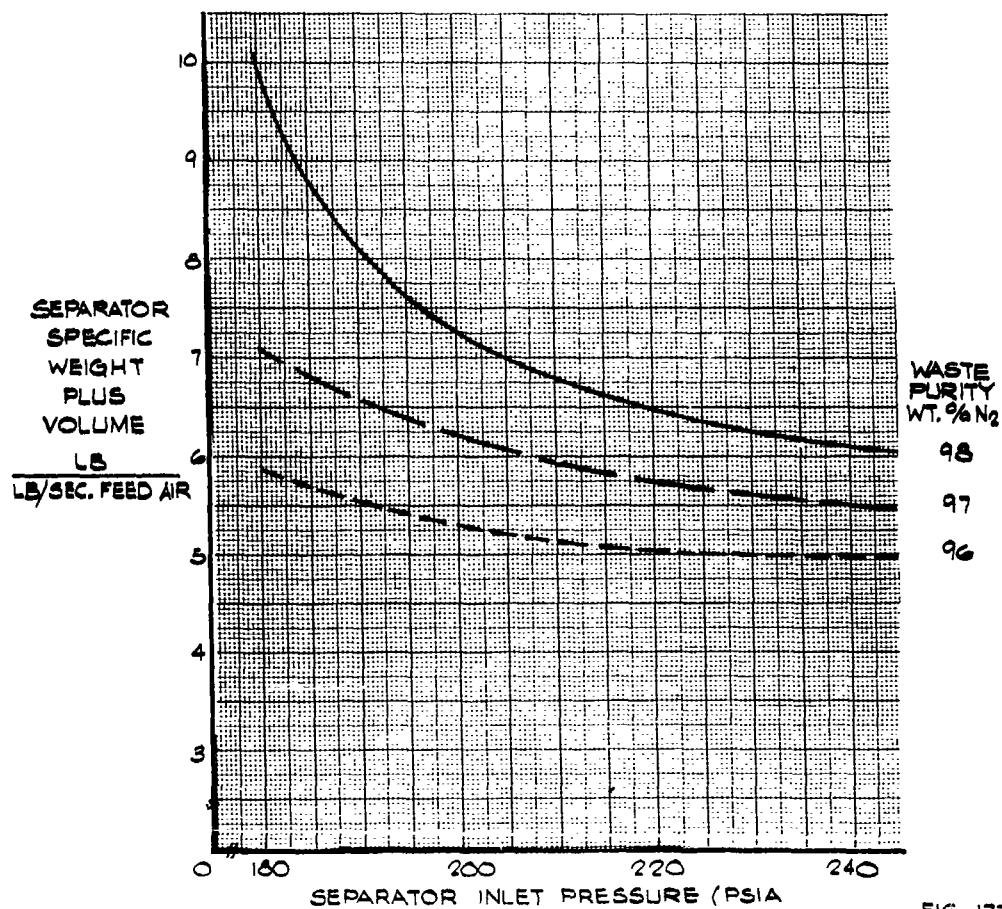


FIG. 177

63 ASRP-2391

SECRET

SECRET

ASD-TDR-63-665, Part I

SEPARATOR WEIGHT AND VOLUME

PRODUCT OXYGEN PURITY = 98% BY WEIGHT  
 WASTE PRESSURE = 56.5 PSIA.  
 INLET AIR FLOW RATE = 2083 LB/SEC.  
 VOLUME PENALTY = 1 LB/CU. FT.  
 ROTATIONAL SPEED = 45 RAD./SEC.

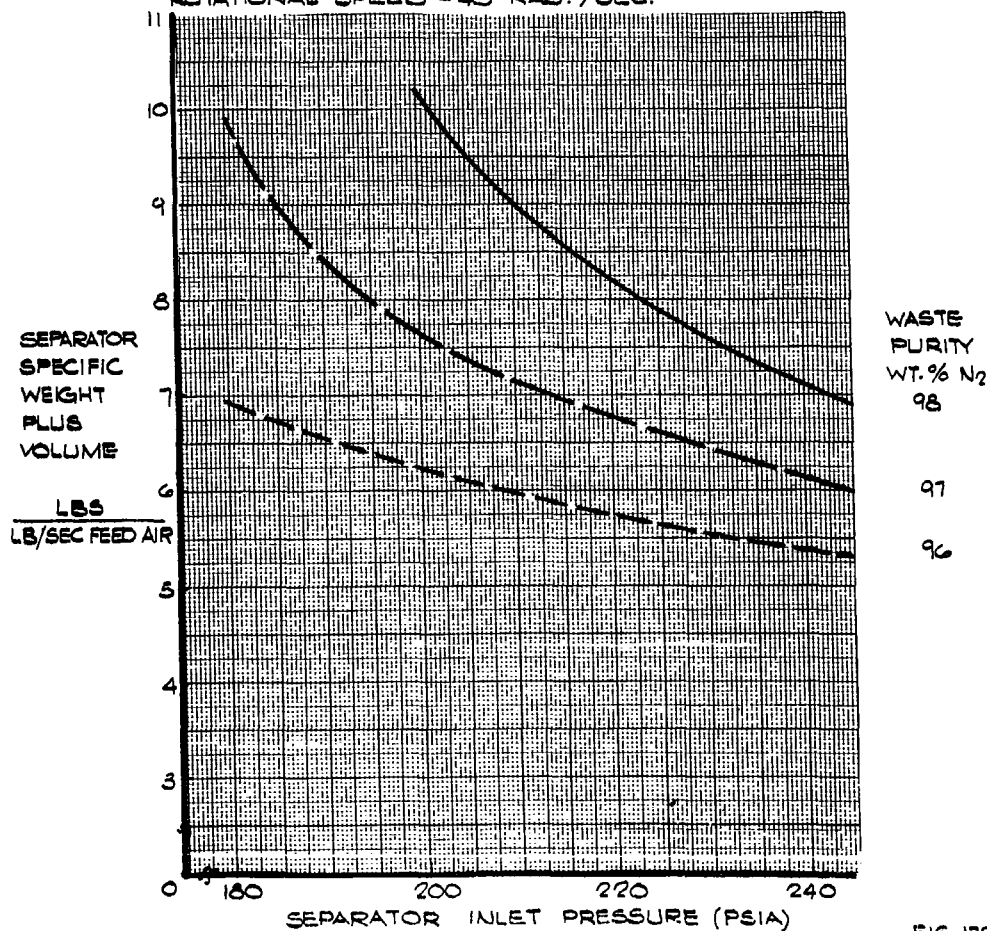


FIG. 178

63 ASRP-2391

SECRET

**SECRET**

**ASD-TDR-63-665, Part I**

a fixed waste pressure and rotational speed is presented in the three dimensional map shown in Figure 179. Separator weight including the volume penalty is plotted against separator inlet pressure and waste nitrogen purity for each product purity studied thus giving three product purity surfaces. The vertical planes cut through at constant inlet pressures of 180, 200, 225, and 245 psia shown clearly that minimum weight coincides with minimum purity at approximately 245 psia inlet pressure.

The extreme cases of low inlet pressure and higher purity cause the reboiler-condenser  $\Delta T$  to approach zero and separator weight, therefore, approaches infinity. A similar phenomenon occurs as inlet pressure increases beyond the scale of this map. The extreme number of column trays will cause excess pressure drop, and therefore  $\Delta T$  approaches zero.

Constant waste purity planes have been replotted separately in Figures 180-182. Constant inlet pressure planes are replotted in Figures 183-185.

**6.3.4.3 Weight and Volume Confidence Level Estimates**

Using the basic double column cycle, it was necessary to establish a basis for monthly weight and volume estimates. Since the work statement covered a broad range of waste and product purities, no single condition would adequately describe the range of weight and volume possible under the work statement. For this reason the associate contractor, General Dynamics/Astronautics, was asked to specify boundary conditions of interest in their studies, and the maximum and minimum purity conditions of the work statement were utilized to provide three specific purity levels for the monthly weight and volume estimate. These three conditions are summarized in Table 19 as Point Nos. 2, 3, and 5 respectively. Specified conditions for the GD/A cycle are given in Appendix XVIII.

The three purity levels were investigated to demonstrate the total range of separator weight and volume possible within the purities specified in the work statement. Each of these cases was calculated at 95%, 50% and 20% confidence level to indicate the present state of the art, and two degrees of reduction in weight and volume which could result from continued applied research on the air separator at these various purity conditions.

63 ASRP-2391

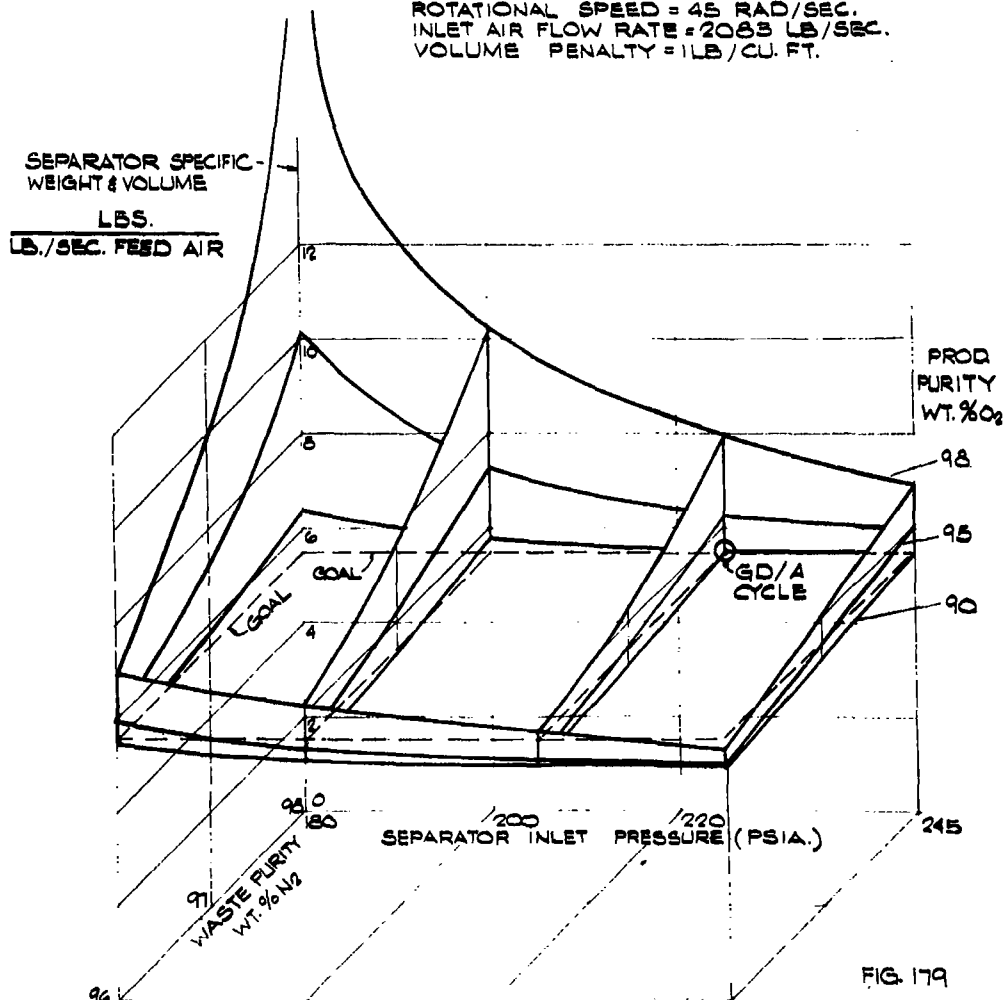
**SECRET**

**SECRET**

ASD-TDR-63-665, Part I

SEPARATOR WEIGHT FUNCTIONS  
(VOLUME PENALTY INCLUDED)

WASTE PRESSURE = 56.6 PSIA.  
ROTATIONAL SPEED = 45 RAD/SEC.  
INLET AIR FLOW RATE = 2083 LB/SEC.  
VOLUME PENALTY = 1 LB/CU. FT.



63 ASRP-2391

**SECRET**

SECRET

ASD-TDR-63-665, Part I

SEPARATOR WEIGHT AND VOLUME

WASTE PRESSURE = 56.5 PSIA  
WASTE NITROGEN PURITY = 96% BY WEIGHT  
INLET AIR FLOW RATE = 208.9 LB/SEC  
VOLUME PENALTY = 1.8 CU FT  
ROTATIONAL SPEED = 45 RAD/SEC

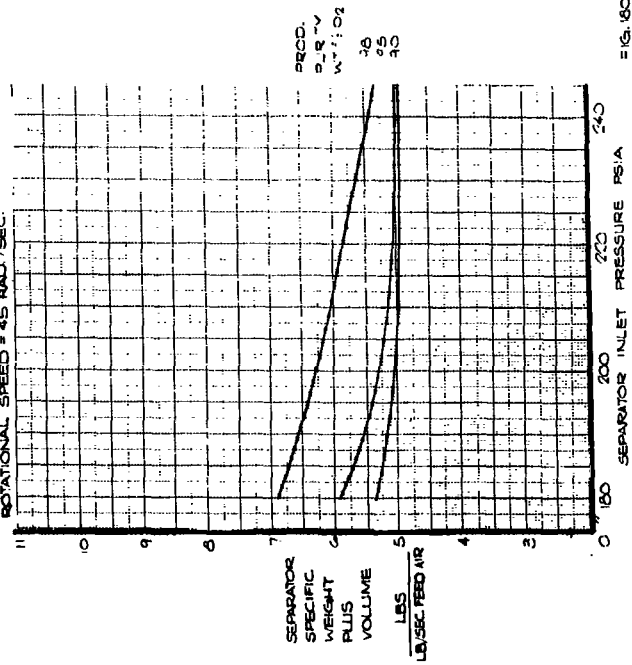


FIG. 180

SEPARATOR WEIGHT AND VOLUME

WASTE PRESSURE = 56.5 PSIA  
WASTE NITROGEN PURITY = 97% BY WEIGHT  
INLET AIR FLOW RATE = 208.9 LB/SEC  
VOLUME PENALTY = 1.8 CU FT  
ROTATIONAL SPEED = 45 RAD/SEC

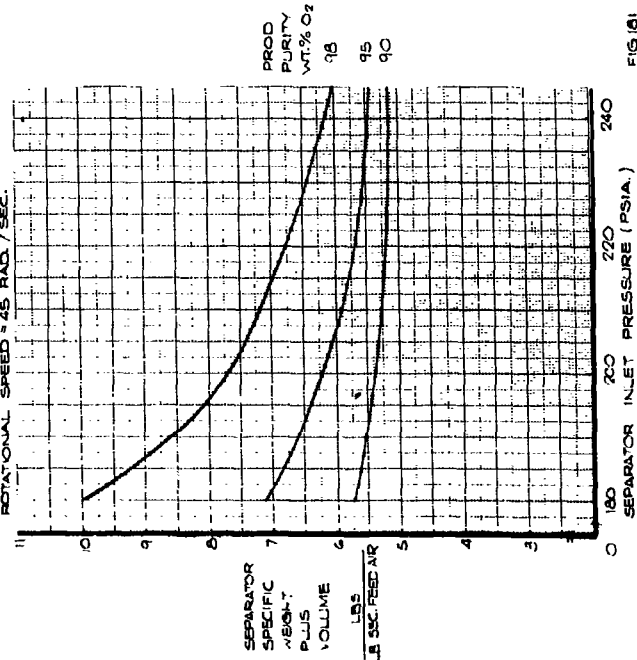


FIG. 181

63 ASRP-2391

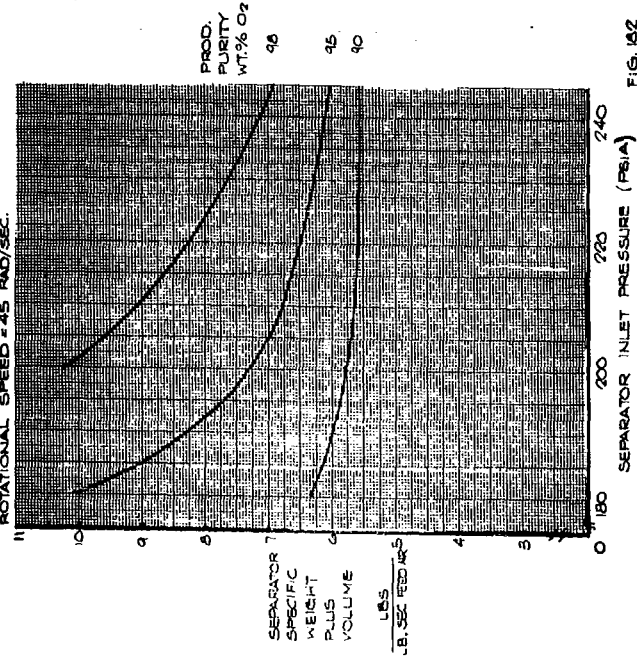
SECRET

SECRET

ASD-TDR-63-665, Part I

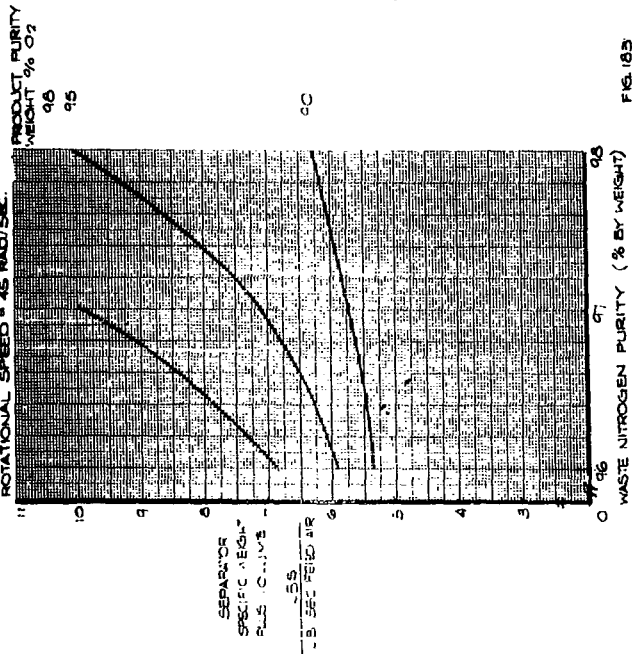
SEPARATOR WEIGHT AND VOLUME

WASTE PRESSURE = 54.5 PSIA  
WASTE NITROGEN PURITY 90% BY WEIGHT  
INLET AIR FLOW RATE = 2085 LB/SEC.  
VOLUME FLOW RATE = 115 CU. FT.  
ROTATIONAL SPEED = 45 RAD/SEC.



SEPARATOR WEIGHT AND VOLUME

SEPARATOR INLET PRESSURE = 180 PSIA  
WASTE PRESSURE = 54.5 PSIA  
INLET AIR FLOW RATE = 2085 LB/SEC.  
VOLUME FLOW RATE = 115 CU. FT.  
ROTATIONAL SPEED = 45 RAD/SEC.



63 ASRP-2391

SECRET

SECRET

ASD-TDR-63-665, Part I

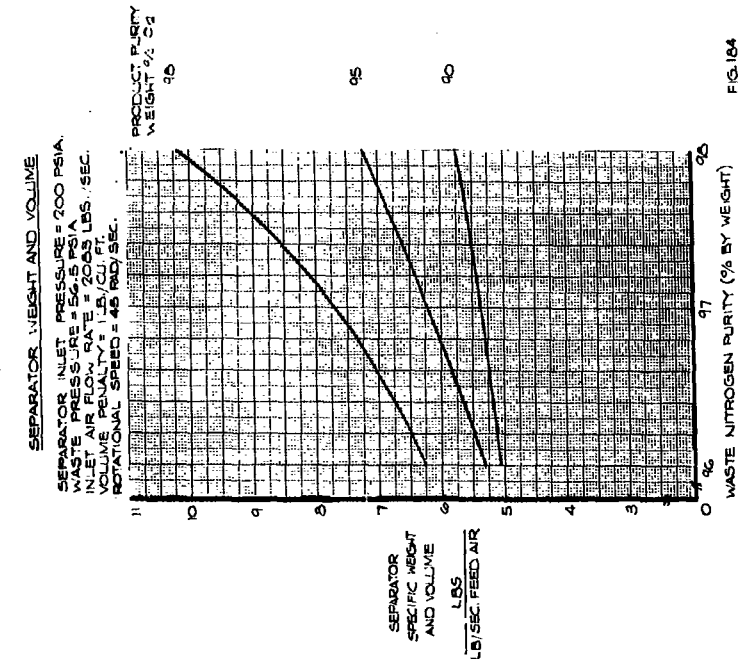


FIG. 184

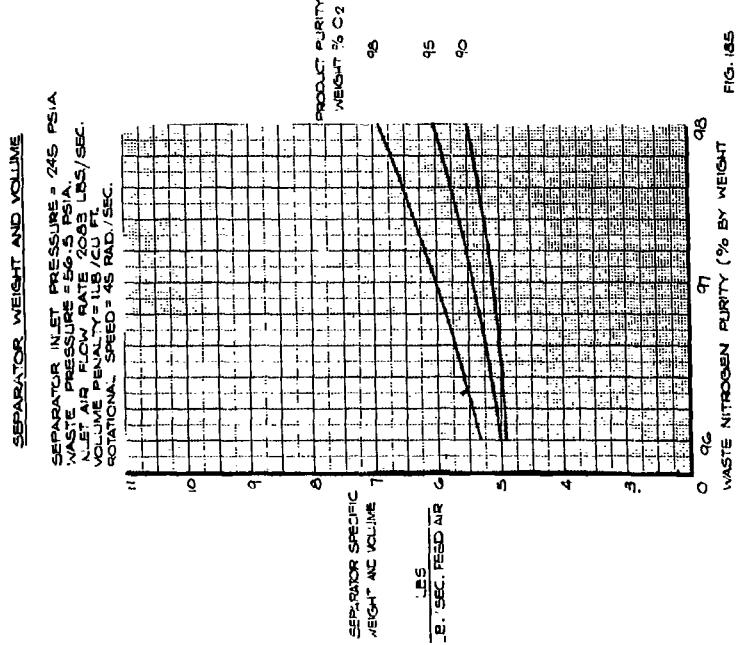


FIG. 185

63 ASRP-2391

SECRET



**SECRET**

ASD-TDR-63-665, Part I

Table 21 incorporates these design criteria for the 95% confidence level with more optimistic values for reduced confidence levels. Assumptions for improved heat transfer and column performance are also presented. The column performance is improved at reduced confidence levels by increasing the superficial vapor velocity with no decrease in tray efficiency.

The monthly weight and volume estimates are presented in Figure 186, based on the above criteria. The single rotor, side-by-side column configuration of Figure 153 is used in this study. Considerable spread is noted from the maximum to minimum purity cases as expected since the tray requirements and reboiler-condenser  $\Delta T$  vary substantially. Major downward steps in the weight at the 5th and 12th months result from introduction of the porous condensing surface in the reboiler-condenser; first in the results with a copper specimen and finally with the porous aluminum surface. All cases meet the weight goal of 5 lb./lb./sec. except the 95% confidence level estimate of the maximum purity case.

The volume estimate shows a major change in the 6th month due to the same improvement in heat transfer. Where the tray dynamic results were applied to the confidence level estimate in the 12th month it was shown the envelope model and column vapor velocities assumed initially were too optimistic. For this reason the volumes were adjusted upwards in the 12th month in spite of a reduction in the reboiler-condenser size. Initially the volume was based on an ellipsoid of revolution where the minor axis was the column diameter and the sum of the low pressure column width and reboiler-condenser length was the major axis. Column vapor superficial velocity was assumed 50% greater than proved to be practicable later in the program. The latest envelope model includes a central section which is a right cylinder; with ends approximated by frustrums of cones. The right cylinder section has a diameter equal to the larger of the column diameters. Its length is the sum of the outer tray widths plus two-foot spacing between the columns. The conical ends are reduced to four-foot diameter at the end, and includes the bearings and inlet piping sections, inboard of the bearings. It seems the volume requirement cannot be met under any purity condition at 95% confidence level. It is likely that only the minimum purity case will approach the volume goal at reduced confidence level. The final confidence level estimates of weight and volume are summarized in Table 22.

63 ASRP-2391

**SECRET**

**SECRET**

ASD-TDR-63-665, Part I

TABLE 21

CONFIDENCE LEVEL DESIGN CRITERIA

	<u>Confidence Level</u>		
	<u>95%</u>	<u>50%</u>	<u>20%</u>
Design stress - Aluminum, psi	33,333	56,500	56,500*
Design stress - Stainless Steel, psi	120,000	180,000	180,000*
Design stress - Titanium, psi	100,000	168,500	168,500*
Heat transfer equivalent wall thickness, mil	13**	8.3	6.8
Heat transfer coefficient multiplier	1	1.2	1.5
Column superficial vapor velocity multiplier	1	1.3	1.7

\* Optional fabrication techniques such as ultra-high strength filament wrapping, etc. will also be applied at the 20% confidence level.

\*\* Revised wall thickness for final calculations is 13 mil. Earlier calculations were based on 9.8 mil.

63 ASRP-2391

**SECRET**

SECRET

ASD-TDR-63-665, Part I

FULL SCALE FLIGHT WEIGHT AIR ENRICHMENT UNIT  
ESTIMATED UNIT WEIGHT AND VOLUME

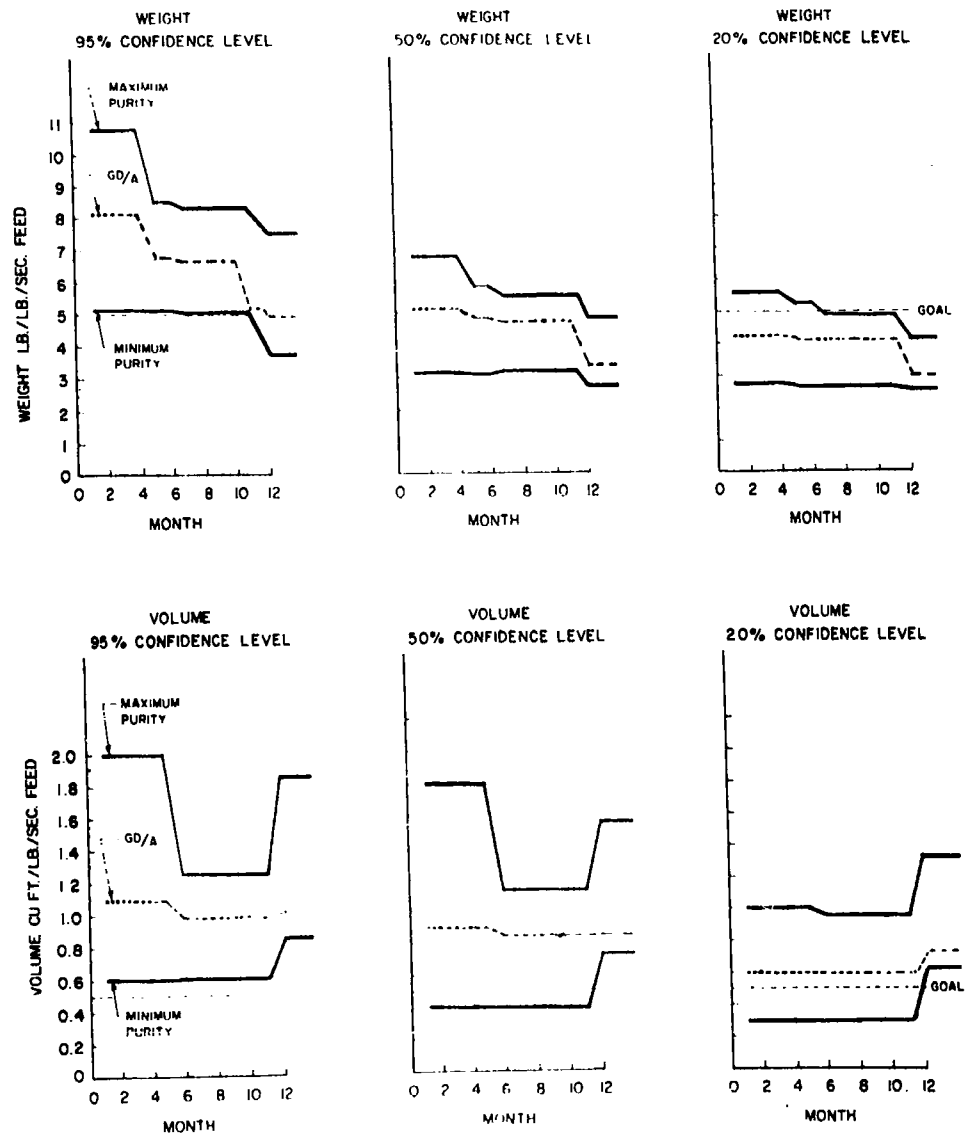


FIG. 186

63 ASRP-2391

SECRET

**SECRET**

ASD-TDR-63-665, Part I

TABLE 22

FINAL CONFIDENCE LEVEL ESTIMATES OF WEIGHT AND VOLUME

	<u>Maximum Purity</u>	<u>Minimum Purity</u>	<u>GD/A</u>
Inlet pressure - psia	265	265	225
Waste pressure - psia	65	65	56.5
Product purity - % oxygen	95	75	90
Waste purity - % nitrogen	98	95	98
Weight, lb./lb./sec.			
95% Confidence	7.53	3.75	4.62
50% Confidence	4.87	2.77	3.32
20% Confidence	4.1	2.54	2.94
Volume, cu. ft./lb./sec.			
95% Confidence	1.86	0.865	1.04
50% Confidence	1.56	0.727	0.847
20% Confidence	1.33	0.624	0.723

63 ASRP-2391

**SECRET**

**SECRET**

**ASD-TDR-63-665, Part I**

**6.3.4.4 Separator Design Optimization**

The ultimate design must be optimized to produce maximum payload in orbit. Each design point would be optimized to balance pressure drop between columns and to trade off column pressure drop against reboiler-condenser  $\Delta T$ . This determines minimum separator weight. This procedure was approximated in each of the points on the weight map previously discussed. The other major trade off is separator weight against volume by adjusting speed of rotation to minimize the combined equivalent weight. A more precise volume trade off penalty will be needed. Figure 187 is an example of this trade off which shows the pre-selected speed of 60 rad./sec. was not the optimum for the General Dynamics/Astronautics cycle. Now that the aluminum porous condensing surface has shown less dependence on rotational speed, the minimum weight, and hence maximum payload due to separator weight, is at 45 rad./sec. The volume, however, is minimum at 55 rad./sec. Their combined effect shows minimum equivalent separator weight occurs between 45 and 50 rad./sec. The change in net separator weight is about -100 lb.

In conclusion, this weight and volume study has shown that the weight goal can be achieved even with some penalty for excess volume in the GD/A cycle.

**6.3.4.5 Separator Heat Load and the Reflux Condenser**

No analytical investigations of the reflux-condenser were performed under this contract although it logically fits within the separator and therefore should be included in future separator studies. However, study of the heat load results and rotational speed dependence leads to some important conclusions.

- a. QC decreases with increasing rotational speed and inlet pressure whereas the weight and volume show optimums with speed and inlet pressure.
- b. QC decreases with increasing product oxygen purity and increasing inlet pressure, counter to the weight and volume trend.

For immediate use in total vehicle integration, the reflux condenser duty in Figure 160 should be used with the weight map, Figure 179. These are at constant rotational speed of 45 rad./sec.

63 ASRP-2391

**SECRET**

SECRET

ASD-TDR-63-665, Part I

### OPTIMUM SEPARATOR SPEED OF ROTATION

SEPARATOR INLET PRESSURE = 225 PSIA  
SEPARATOR WASTE PRESSURE = 56.5 PSIA  
PRODUCT PURITY = 90 WEIGHT PERCENT  
WASTE PURITY = 98 WEIGHT PERCENT  
FLOW RATE = 2083 LB/SEC.  
WEIGHT PENALTY = 1 LB PER LB IN EXCESS OF GOAL  
VOLUME PENALTY = 1 LB PER CU.FT. IN EXCESS OF GOAL

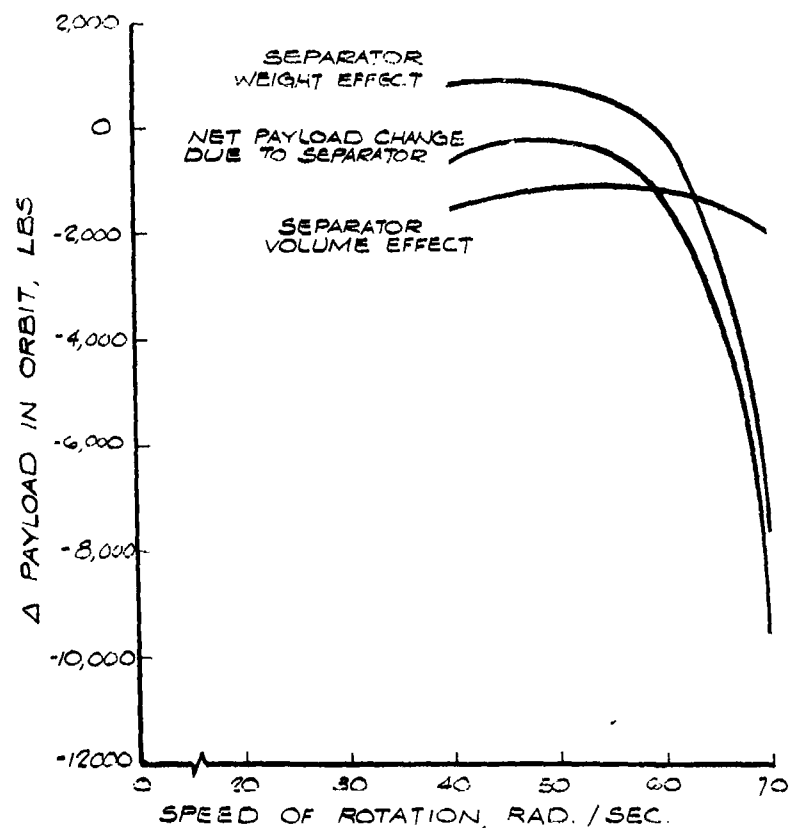


FIG 187

63 ASRP-2391

SECRET

# SECRET

## ASD-TDR-63-665, Part I

When the optimum design conditions have been determined on this basis, a more precise optimum could be achieved by detailed study by Linde using rotational speed as a third parameter.

### 6.4 System Horsepower

This section presents a sample analysis of the system horsepower for the General Dynamics/Astronautics cycle where the rotational speed is constant at 45 rad./sec.

As shown later in Table 24, the following are the approximate horsepower requirements for the air separator.

#### Horsepower Required

a.	Fluid Acceleration Horsepower	=	3900
b.	Seal Fluid Power	=	1000
c.	Windage Friction Power	=	20
d.	Bearing Friction Power	=	50
<hr/>			
Total Horsepower Required		=	4970

Assume the hydrogen stream in the reflux condenser to be as shown in Figure 152 except for the hydrogen flow rate. For the GD/A cycle rotated at 45 rad./sec., the reflux condenser heat load, QC, is 643.3 Btu/10-mole feed air. A heat balance across the reflux condenser yields the hydrogen flow rate and a further calculation yields the hydrogen turbine energy output.

The energy output of the low pressure column and recirculation turbines are based on the assumption of 80 per cent recovery of the total kinetic energy available at the respective rotor peripheries as a result of diffuser operation and subsequent expansions into chambers maintained at pressures approximately equal to the peripheral column and reboiler-condenser pressures respectively.

The horsepower available for work is given as follows:

#### Available Horsepower

a.	Hydrogen Turbine Power	=	14,750
b.	Low Pressure Column Turbine Power	=	1,658
c.	Recirculation Turbine Power	=	448

63 ASRP-2391

**SECRET**

**ASD-TDR-63-665, Part I**

Total Available Horsepower = 16,856

Excess Horsepower Available

16,856 - 4,970 = 11,886

The equations for calculation of the various horsepower items are presented in Appendix XVII.

**6.5 Scaling Effects**

**6.5.1 General**

A study of scaling effects was requested in the work statement to compare the ultimate full scale flight-weight air separator with the 1/20 scale boilerplate air separator now being designed. From this study it is concluded that there are no appreciable scaling effects since the 100 lb./sec. capacity of the boilerplate demonstration model was selected to minimize these effects. The boilerplate 1/20 scale unit is a more conservative design functionally as well as mechanically. It is designed to demonstrate feasibility as well as explore various operating characteristics. The flight-weight full scale unit, however, is designed for minimum weight and will not necessarily be identical to the boilerplate unit.

Primary considerations in selecting the 1/20 scale unit were to limit wall effects on the columns and diffuser. Since the design purity and pressure determine the theoretical trays required, the rotor diameter in this configuration is essentially the same regardless of scale. Thus, with the column diameter fixed by tray requirements, the scale selection was based on the narrowest outer tray which could be fabricated and operated without detrimental effects from the column walls. Scale units smaller than 100 lb./sec. would be possible by sacrificing performance or by altering the configuration. However, results from such smaller units could not be extrapolated as reliably as desired to the flight-weight 2,000 lb./sec. unit.

The following discussion compares the size of the major components in scale and full size separators. Power, speed of rotation, and performance are also discussed. A weight and volume comparison is also made for full scale and 1/20 scale separator. Reliability data which may be gained from the scale tests is also noted.

**63 ASRP-2391**

**SECRET**



~~SECRET~~

## ASD-TDR-63-665, Part I

### 6.5.2 Separator Size

The dimensions of a full scale and 1/20 scale separator are compared in Table 23. The rotor outside diameters are nearly the same, differing by the inner diameters which are sized for the respective feed air quantities. Radial thicknesses of the rotors are 4.00 ft. and 3.95 ft., respectively.

Column diameters are also nearly, equal, but widths are nominally in direct proportion to scale. Deviation from this proportion is due to the slight difference in radii and superficial vapor velocity. The outermost tray widths are 3.25 in. and 40.4 in. in the 1/20 scale and full size high pressure columns. This was the critical scaling dimension since the 3.25 in. wide tray is the narrowest tray which could be fabricated and operated with reasonable freedom from wall effects. This permits 1/8 in. inactive width on each side of the tray with approximately 7% loss of active area.

Dimensions of the reboiler-condenser are proportionately similar in full scale and 1/20 scale units. The radial thicknesses are 18 in. and 15.5 in., respectively, providing nearly the same condensate flow channel length. The radii differ by the inner diameter which is sized to accommodate the required feed air.

### 6.5.3 Separator Performance

#### 6.5.3.1 Cycle

The performance characteristics which are compared in Table 24 show the cycle conditions are identical in waste and product purity. Inlet pressure for the 1/20 scale unit is higher to permit more flexibility in operation of this experimental unit. The waste pressure is lower for the same reason. Tests of the boilerplate 1/20 scale unit would permit duplication of the full scale inlet pressure and waste pressure but not necessarily at the same purity. Furthermore, the design conditions for the full scale unit may be revised toward a lower inlet pressure, possibly as low as 200 psi. The 1/20 scale unit will be operating in the general range of the full scale separator, and no scaling effect is expected from the cycle differences.

63 ASRP-2391

~~SECRET~~

**SECRET**

ASD-TDR-63-665, Part I

TABLE 23

SEPARATOR SIZE COMPARISON

	<u>Full Scale</u> <u>(GD/A Cycle)</u>	<u>1/20 Scale</u>
<u>Rotor</u>		
Outside diameter, ft.	11.4	8.9
Inside diameter, ft.	3.4	1.00
Length, ft.	33.42	8.70
<u>Low Pressure Column</u>		
Outer tray radius, in.	44.45	46.0
Inner tray radius, in.	26.0	12.0
Inner tray width, in.	237.4	32.5
Outer tray width, in.	94.3	4.25
<u>High Pressure Column</u>		
Outer tray radius, in.	57.18	46.0
Inner tray radius, in.	44.0	32.0
Inner tray width, in.	58.6	4.5
Outer tray width, in.	40.4	3.25
<u>Reboiler-Condenser</u>		
Outside radius, in.	42.0	25.0
Inside radius, in.	24.0	9.5
Length, in.	79.7	21.0

63 ASRP-2391

**SECRET**

**SECRET**

ASD-TDR-63-665, Part I

TABLE 24

SEPARATOR PERFORMANCE COMPARISON

	Full Scale (GD/A Cycle)	1/20 Scale
<u>Cycle</u>		
Inlet pressure, psia	225.0	240.0
Waste pressure, psia	56.5	45.0
Waste purity, % nitrogen	98.0	98.0
Product purity, % oxygen	90.0	90.0
<u>Rotor</u>		
Rotor speed, rad./sec.	45	60.0
Fluid acceleration power, hp	3900	232.0
Seal fluid power	1000	325
Windage friction power, hp	20	19
Bearing friction power, hp	50	30
<u>Low Pressure Column-Enriching Section</u>		
Tray number, theoretical	8.5	7.57
Tray number, actual	8	11
Tray spacing, in.	1.25-1.42	1.75-2.25
Foam height, in.	0.95-1.12	0.78-1.44
Superficial vapor velocity, ft./sec.	7.6	7.9-8.6
Column section $\Delta P$ , psi	7.2	12.0
<u>Low Pressure Column-Stripping Section</u>		
Tray number, theoretical	5.5	5.6
Tray number, actual	5	7
Tray spacing, in.	1.12-1.21	1.75
Foam height, in.	0.82-0.91	0.72-1.2
Superficial vapor velocity, ft./sec.	7.4	8.18-9.77
Column section $\Delta P$ , psi	7.1	18.6
<u>High Pressure Column</u>		
Tray number, theoretical	10	8.93
Tray number, actual	9	9
Tray spacing, in.	1.78-1.98	1.75
Foam height, in.	1.48-1.68	0.735-1.30
Superficial vapor velocity, ft./sec.	5.5	4.2-5.2
Column section $\Delta P$ , psi	20.4	33.4

63 ASRP-2391

**SECRET**

**SECRET**

## ASD-TDR-63-665, Part I

### 6.5.3.2 Rotor

Rotor speeds are 45 rad./sec. for the full size separator and 60 rad./sec. for the 1/20 scale separator, producing slightly higher accelerating forces in the 1/20 scale columns and nearly identical acceleration forces in the reboiler-condenser. The power requirements to accelerate the fluid are in proportion to the throughput and acceleration forces but the seal fluid power on the 1/20 scale unit is one-third of that expected on the full size separator. This results from different rotor speeds, nearly equal diameters, different liquid levels and casing pressures. Consequently, this produces a serious refrigeration balance problem on the 1/20 scale unit. Frictional horsepower in the 1/20 scale unit is 10% of the cycle refrigeration requirement, while on the full scale separator, it is only 1.5%. Seal friction heat in the 1/20 scale separator will be removed in sensible heat in the waste nitrogen which will be vented to the atmosphere to minimize this energy input to the rotor. No separate seal cooling is expected on the full scale unit. It would only be used on the 1/20 scale unit to approximate full scale conditions.

### 6.5.3.3 Low Pressure Column

Comparison of this column section in scale and full size shows the two columns are designed to operate consistent with the preliminary tray dynamic correlations, but at different foam heights resulting from slight differences in superficial vapor velocity and gravitational field. Tray efficiency differs substantially due to the basic difference in design philosophy. The full size separator design presumes some enhancement over the known tray efficiency in the projected design available five years hence. (Enhancement is the improvement in overall tray efficiency, assuming limited liquid mixing on the tray. Theory is explained in Perry (Ref. 23, p. 550-552) and other sources (Ref. 17, 44, 45, 46 and 47.) On the other hand the 1/20 scale separator is conservatively designed based on present tray efficiency with no enhancement credited to the design. Future tests with this experimental model and subsequent models will determine the degree of enhancement possible. Murphree tray efficiency may exceed 100%. (Ref. 23, p. 550-552).

There is a slight difference in the number of theoretical trays. Since the column pressure levels are approximately the same due to the 1/20 scale unit having a lower waste pressure and higher rotational speed than the flight-weight unit, the difference occurs in the 1/20 scale unit being designed to separate a binary mixture which requires approximately one less theoretical tray.

63 ASRP-2391

**SECRET**

**SECRET**

#### ASD-TDR-63-665, Part I

Tray spacing is conservative in the 1/20 scale separator to permit off-design performance at higher than normal foam heights. Therefore, disengagement space (tray spacing less foam height) appears larger than necessary and the column outside diameters are about equal in spite of the smaller 1/20 scale inside diameter. There are no significant scaling effects in this column section.

##### 6.5.3.4 High Pressure Column

The high pressure columns of both separators are very similar. However, the full scale unit uses a higher superficial vapor velocity and foam height. The average gravitational field in the column is less because of lower rotational speed despite the larger radii. The gravitational field effect causes a higher pressure drop in the 1/20 scale separator. There is some improvement in column efficiency due to enhancement credited to the full size separator, whereas the 1/20 scale separator uses the point efficiency directly as tray efficiency with no enhancement. There is a 1.1 theoretical tray difference which is due to the slightly lower purity kettle used in the 1/20 scale unit design.

##### 6.5.3.5 Reboiler-Condenser

Designs of the full size and 1/20 scale reboiler-condenser are similar in construction. The full size condenser contains more tubes per disk and longer tubes per disk by virtue of the greater diameters. Since the 1/20 scale unit turns at a faster speed, resulting gravitational fields for the two units are approximately the same with a slightly greater field in the full scale unit. Therefore since the overall  $\Delta T$ 's are approximately equal, the condensing coefficients are approximately the same. No scaling effects are expected since these differences can be calculated from heat transfer correlations.

##### 6.5.4 Weight and Volume

Direct comparison of the weight of a 1/20 scale boilerplate unit with a full scale flight-weight separator has little practical significance other than comparing bearing loads. The full scale rotor with operating fluids will weigh about three times the 1/20 scale unit. Operating experience with the 1/20 scale bearings should provide an experimental confirmation of the bearing designs. Similar bearings are planned for the full scale flight-weight separator.

63 ASRP-2391

**SECRET**

**SECRET**

**ASD-TDR-63-665, Part I**

Volume of the two units is best described by the envelope dimensions. The length of the full scale separator is 33.4 ft., 3.8 times the 1/20 scale unit length of 8.7 ft. Rotor diameters are 11.4 ft. and 8.9 ft., respectively.

**6.5.5 Reliability**

An indication of bearing and seal operating life and reliability will be gained from the boilerplate test of the 1/20 scale unit. Bearing diameters of the full scale unit will be more than double the 1/20 scale unit. Seal outside diameters are approximately the same since the low pressure column diameters are nearly equal. However, seal radial depth may vary due to differences in column peripheral liquid level, rotational speed and casing pressure. These differences are exemplified by the following comparison of the GD/A cycle full scale separator and the 1/20 scale unit.

	<u>Full Scale</u>	<u>1/20 Scale</u>
Peripheral Low Pressure Column Liquid Holdup	3.8 in.	2 in.
Rotational Speed	45 rad./sec.	60 rad./sec.
Casing Pressure	14.7 psia	60 psia

With these conditions seal leakage could be severe in the full scale unit due to the lower casing pressure. This leakage would also be accentuated by the greater liquid depth and slower rotational speed.

The reboiler-condenser seal in the full scale unit will receive the benefit of the same gravitational field as the 1/20 scale unit but will have the same large differential pressure to overcome, as in the column seal just discussed.

Further mechanical applied research is needed in this area. The alternatives apparent now, are to either add a pressure casing or to develop the pumps and pump drive as discussed in Section 5.3. The pressure casing requirement can be evaluated in the cryogenic tests of the 1/20 scale unit using the one seal design built into the rotor. Further seal development and cryogenic tests will determine the effectiveness and reliability of the seals. This performance can be extrapolated to the full size separator.

**63 ASRP-2391**

**SECRET**

**SECRET**

**ASD-TDR-63-665, Part I**

**6.6 Minor Constituent Effects**

**6.6.1 General**

The effect of carbon dioxide and water vapor on column performance was investigated. In general, the major portion of these materials will remain in the preconditioning section, since they will freeze on the heat transfer surfaces. Only that portion which is soluble in the saturated air feed to the separator should enter the distillation separator. It is possible that one or two ppm solid carbon dioxide or water ice will be carried through in addition to the soluble quantities. This discussion is only concerned with these quantities. It is presumed the preconditioning section is carefully designed to limit solid carry-over and promote self-cleaning.

**6.6.2 Water Vapor**

Saturated air entering the distillation separator would contain much less than 1 part per million water vapor. Extrapolation of data from 350°R to 210°R indicates the soluble water vapor content is in the range of  $10^{-4}$  ppm. This amounts to a total of 0.00023 lb. water in 30 minutes of continuous operation, when processing 2083 lb./sec. of air.

Since the solubility limit of water is low, it will wash through the separator and concentrate in the product liquid stream. No adverse effect is expected from this minute quantity of water vapor. Large amounts of water present in the separator during cooldown could cause difficulty; hence, adequate purging procedures will be required during pre-flight checkout.

**6.6.3 Carbon Dioxide**

The incoming air will contain 2 ppm carbon dioxide if it is at 225 psia and saturation temperature. This dissolved quantity is approximately 15 lb. in 30 minutes when processing 2083 lb./sec. of air.

This quantity will remain dissolved and will wash into the kettle liquid. Since the mole fraction of kettle liquid is less, the carbon dioxide will concentrate to 3.3 ppm which is well below the saturation limit of 12 ppm. Kettle liquid is transferred to the low pressure column where the

63 ASRP-2391

**SECRET**

**SECRET**

## ASD-TDR-63-665, Part I

carbon dioxide flows with the oxygen and other less volatile constituents to the reboiler-condenser. Carbon dioxide will be recycled with the excess liquid oxygen and the oxygen vapor fed to the low pressure column. However, the carbon dioxide in the vapor will be washed back into the liquid and returned to the reboiler-condenser. Carbon dioxide therefore can leave the separator only in the product stream. Calculations were made using the carbon dioxide content in the air. For this case, 9.4 ppm carbon dioxide in the product will balance the 2 ppm in the air feed. Since the carbon dioxide saturation limit in the liquid product is about 9 ppm, there is a possibility that traces of solid carbon dioxide will be formed. More than likely the solids would be carried out of the separator in the product liquid.

It is quite possible that some solid carbon dioxide will be carried through the heat exchanger. The amount depends on the efficiency and characteristics of the preconditioning section, but several ppm, corresponding to a total of 20 - 30 lb., can be expected. It is difficult to predict how much of this solid would migrate through the separator. Some will probably plate out in the air ducts, some will dissolve in the kettle liquid and be transferred to the low pressure column where it will concentrate as solids floating in the product and be carried out of the separator.

It should be noted that careful design of the preconditioning section is essential to insure reliable operation of the separator. Excessive carry-over of solids is undesirable since it could plug some of the two-phase distribution orifices, causing liquid unbalance, for example.

At present, the amount of dissolved and solid carbon dioxide expected in the feed air to the separator should have no effect on separator performance. Some solid will probably be present in the product liquid which, if desired, can be removed by a small filter. Should the feed air contain much more carbon dioxide than anticipated, steps will have to be taken to prevent this carbon dioxide from entering the separator. This can be done with conventional means, but would require some extra equipment.

### 6.7 Transient Study and Off-Design Performance

#### 6.7.1 General

Start-up, shutdown, and off-design operation were examined for

63 ASRP-2391

**SECRET**



~~SECRET~~

#### ASD-TDR-63-665, Part I

a full scale flight-weight separator which is designed for the GD/A case. Off-design performance is treated analytically since the first operating experience will be gained during operation of the boiler-plate 1/20 scale unit. Start-up and shutdown procedures will be refined from this experience.

##### 6.7.2 Start-up Performance

Start-up of the separator occurs in three phases: cooldown, liquid build-up, and purity build-up. Cooldown could be achieved in 15.7 seconds from the time hydrogen is first introduced to the warm reflux condenser. This procedure would introduce excessive stress from non-uniform cooldown. It is therefore recommended that the separator be precooled either by convection from the surrounding hydrogen tankage or by forced convection of saturated oxygen or nitrogen vapor within the separator during pre-flight checkout. This latter procedure would also provide the necessary exclusion of moisture and carbon dioxide.

When the flight has progressed to the collect period, hydrogen would be admitted to the reflux condenser. By this time the rotor should be turning at design speed. If the rotor is at operating temperature, it will require about 20 sec. to accumulate the operating liquids within the separator. Some rectification will occur in this period. It is conservatively estimated that an additional 40 sec. will be required to achieve design purities, which is a maximum of one minute from the time hydrogen is introduced to the reflux condenser.

##### 6.7.3 Off-Design Operation

This same separator was analyzed for performance at  $\pm 10$  psi deviation from the 225 psi inlet design pressure, and  $\pm 5$  psi deviation from the 56.5 psi waste design pressure.

The results in Table 25 show that decreasing separator inlet pressure to 215 psi reduces the product and feed throughputs. There is a slight improvement in high pressure column performance as shown by the rise in kettle oxygen purity. Low pressure column performance is also improved as shown by the drop in waste oxygen purity and the rise in product oxygen purity. However, the reboiler-condenser and reflux condenser heat loads increase substantially, reducing the product and feed air throughputs as noted in Table 26. Consequently, net pounds of oxygen collected per second are decreased.

63 ASRP-2391

~~SECRET~~

**SECRET**

ASD-TDR-63-665, Part I

TABLE 25

THEORETICAL CYCLE STUDY WITH  
SEPARATOR INLET PRESSURE DEVIATION

	<u>Inlet Pressure (Psia)</u>		
	<u>215</u>	<u>225</u>	<u>235</u>
Product Pressure (psia)	76.5	76.5	76.5
Waste Pressure (psia)	56.5	56.5	56.5
Product Oxygen Purity (Mole Fraction)	0.9212	0.8874	0.8450
Waste Oxygen Purity (Mole Fraction)	0.01579	0.01755	0.01933
Low Pressure Column Theoretical Trays	14.9	14.9	14.9
High Pressure Column Theoretical Trays	10.0	10.0	10.0
Shelf Oxygen Purity (Mole Fraction)	0.04	0.04	0.04
Kettle Oxygen Purity (Mole Fraction)	0.319	0.315	0.311
Reboiler-Condenser Heat Load (B.t.u./lb.-mole feed)	1835.0	1795.0	1762.0
Reflux Condenser Heat Load (B.t.u./lb.-mole feed)	702.0	694.0	691.0
Kettle Liquid Flow Rate (lb./moles/lb.-mole feed)	0.6098	0.6183	0.6270
Shelf Liquid Flow Rate (lb./moles/lb.-mole feed)	0.3902	0.3817	0.3730
Product Liquid Flow Rate (lb./moles/lb.-mole feed)	0.2145	0.2212	0.2309

63 ASRP-2391

**SECRET**

**SECRET**

ASD-TDR-63-665, Part I

TABLE 26

SEPARATOR PERFORMANCE WITH  
INLET PRESSURE DEVIATION

	<u>Inlet Pressure (Psia)</u>		
	<u>215</u>	<u>225</u>	<u>235</u>
Column Frictional Pressure Drop (psia)	11.0	11.0	11.0
Reboiler-Condenser Condensing Pressure (psia)	204.0	214.0	224.0
Reboiler-Condenser Boiling Pressure (psia)	76.5	76.5	76.5
Reboiler-Condenser $\Delta T$ ( $^{\circ}R$ )	5.0	6.6	7.9
Available Heat Transfer Area Reboiler-Condenser (sq. ft.)	14,600	14,600	14,600
Maximum Separator Air Inlet Feed (lb./sec.) at Speed of 65 rad./sec.	1,834	2,083	2,310
Rotational Speed Adjustment to Restore Original Feed	lower speed	65	raise speed

63 ASRP-2391

**SECRET**

**SECRET**

**ASD-TDR-63-665, Part I**

The increase in separator inlet pressure to 235 psi tends to increase throughput, although there is a slight reduction in the high pressure and low pressure column performances as evidenced by the rise in waste oxygen purity and the drop in product oxygen purity. Net pounds of oxygen are increased at the increased inlet pressure in spite of the reduced product purity.

Corrective measures were investigated to restore the normal feed air throughput at these new inlet pressures. Since the heat transfer area at the reboiler-condenser is constant, the rotational speeds should be adjusted to change the reboiler-condenser  $\Delta T$  and the condensing coefficient. As inlet pressure increases, rotational speed should be increased. Decreased inlet pressure requires lower rotational speed. Changes in speed affect system pressure drop and can therefore correct purities or pressure levels. Table 26 was developed for 65 rad./sec. design speed. Substitution of 45 rad./sec. would change numbers but not the basic conclusion that separator inlet pressure deviations can be compensated for by changes in rotational speed.

Variations in waste pressure were investigated to determine the effect of a malfunction of the waste recompression system. The results in Table 27 show that a drop in waste pressure would improve the theoretical column performance since the distillation is easier at the reduced pressure. Consequently waste and product purities are improved. The reflux condenser heat load is increased but the reboiler-condenser load is constant for the same throughput. However, in actual operation the reboiler-condenser  $\Delta T$  becomes larger, permitting a larger throughput at this point. Throughput will increase until both column pressure drops and the reboiler-condenser  $\Delta T$  have absorbed the drop in waste pressure. Tray hydraulics and mass transfer cannot be analyzed at this time, although it is known that some increase in rotational speed would be needed to prevent flooding of the inner column trays.

If waste pressure increases to 61.5 psia the waste and product purities are decreased. The reflux condenser heat load is also lower than at the design pressure of 56.5 psia. In actual operation a  $\Delta T$  squeeze occurs at the reboiler-condenser although the head load remains constant. By reducing the rotational speed and throughput, the operation could be continued at some intermediate purity.

63 ASRP-2391

**SECRET**

~~SECRET~~

ASD-TDR-63-665, Part I

TABLE 27

THEORETICAL CYCLE STUDY WITH  
SEPARATOR WASTE PRESSURE DEVIATION

	<u>Waste Pressure (Psia)</u>		
	<u>51.5</u>	<u>56.5</u>	<u>61.5</u>
Product Pressure (psia)	76.5	76.5	76.5
Separator Inlet Pressure (psia)	225.0	225.0	225.0
Product Oxygen Purity (Mole Fraction)	0.9050	0.8874	0.878
Waste Oxygen Purity (Mole Fraction)	0.01650	0.01755	0.01890
Low Pressure Column Theoretical Trays	14.9	14.9	14.9
High Pressure Column Theoretical Trays	10.0	10.0	10.0
Shelf Oxygen Purity (Mole Fraction)	0.04	0.04	0.04
Kettle Oxygen Purity (Mole Fraction)	0.315	0.315	0.315
Reboiler-Condenser Heat Load (B.t.u./lb.-mole feed)	1795.0	1795.0	1795.0
Reflux Condenser Heat Load (B.t.u./lb.-mole feed)	704.0	694.0	684.0
Kettle Liquid Flow Rate (lb.-moles/lb.-mole feed)	0.6183	0.6183	0.6183
Shelf Liquid Flow Rate (lb.-moles/lb.-mole feed)	0.3817	0.3817	0.3817

63 ASRP-2391

~~SECRET~~

SECRET

ASD-TDR-63-665, Part I

6.7.4 Shutdown

When collect has been accomplished the separator may be shut down by shutting off the hydrogen refrigeration at the reflux condenser. Experience in the boilerplate model tests will determine if it is desirable to continue a partial air flow through the separator. Liquids on the trays will be vaporized by the incoming air if the air flow is reduced gradually, except in the stripping section of the low pressure column. Here the oxygen vapor flow will fall off rapidly permitting the trays to weep. At this time it is believed that the air should not be shut off completely until all liquids are vaporized. Otherwise an excess of fluid might concentrate at the column periphery.

6.8 Boiling Surface and Condensing Surface Treatments

6.8.1 General

Evaluation of the Linde boiling surface treatment was requested to determine its overall value compared to a plain untreated boiling surface. Subsequent to this request in the work statement, the porous condensing surface has shown even greater improvement. Both surfaces are discussed.

6.8.2 Surface Treatment Evaluation

Design conditions used for the boiling and condensing surface evaluation are as follows:

	Condensing N <sub>2</sub> Rich Stream (tubes)	Boiling O <sub>2</sub> Rich Steam (shell)
Flow Rate, Lb./-Mole/Lb.-Mole Feed	1.069	1.1152
Temperature, R°	199.7	192.8
Pressure, Psia	218.8	80.6
Rotational Speed, Rad./Sec.	60.0	
Reboiler-Condenser Heat Duty, Btu/Lb.- Mole Feed	1748.8	

The heat exchanger is assumed to consist of 1/4" O.D. aluminum tubes arranged in the form of a disk. Nitrogen is condensed inside the tubes and boiling oxygen flows between the disks or rotors. The outside radius is assumed to be 42 in. and the inside radius 24 in. with the rotors on a 1/2" pitch.

63 ASRP-2391

SECRET

~~SECRET~~

# ASD-TDR-63-665, Part I

Three cases are considered in the boiling surface evaluation:

- Case 1. Special boiling surface and porous condensing surface
- Case 2. Special boiling surface and smooth condensing surface
- Case 3. Untreated boiling and smooth condensing surfaces

For the first case, in which the special boiling surface and porous condensing surface are used, a minimum weight and volume are obtained. The boiling side heat transfer coefficient correlation for the special copper boiling surface from Section 4.0, Figure 40, is:

$$h_b = B \Delta T_b^{1.2} \quad \text{where } B = 7100$$

For a porous surface inclined to a "g" field, the condensing side heat transfer coefficient is:

$$h_{CM} = .726 \left[ \frac{\rho_L^2 \lambda k_L^3}{\mu_L} \right]^{1/4} (\omega')^2 \left[ \frac{r_{\text{mean}}}{\Delta T_c d_t} \right]^{1/4} \frac{(hc)_{\text{EXP}}}{(hc)_{\text{THEO}}} @ 1 \text{ atm}$$

$$\text{where } r_{\text{mean}} = \frac{2}{3} \left[ \frac{(r_o^2 - r_{fic}^2)^{3/2} - (r_i^2 - r_{fic}^2)^{3/2}}{r_o^2 - r_i^2} \right]$$

$$h_{CM} = .726 R^o \left[ \frac{(hc)_{\text{EXP}}}{(hc)_{\text{THEO}}} \right] (\omega')^2 \left[ \frac{r_{\text{mean}}}{\Delta T_c d_t} \right]^{1/4} (1 - A\phi)$$

When a heat balance is made across a tube the heat flux,  $Q/A$ , is expressed as:

63 ASRP-2391

~~SECRET~~

**SECRET**

ASD-TDR-63-665, Part I

$$Q/A = .726 \left[ \frac{(h_c)_{EXP}}{(h_c)_{THEO @ 1 \text{ atm}}} \right] R^{\circ} \left[ (\omega')^2 \frac{r_{mean}}{d_t} \right]^{1/4} (1 - A_{\phi})$$

$$\Delta T_c^{3/4} = B \Delta T_b^{2.2}$$

In Case 2, where a special boiling surface and smooth condensing surface are considered, the condensing side heat transfer coefficient enhancement factor,

$$\frac{(h_c)_{EXP}}{(h_c)_{THEO @ 1 \text{ atm.}}}$$

obtained with a porous condensing surface is lost.

This decreases heat transfer performance and results in:

$$\frac{\text{Weight Case 2}}{\text{Weight Case 1}} = 3.0 \text{ and } \frac{\text{Volume Case 2}}{\text{Volume Case 1}} = 3.7$$

In Case 3, when a plain tube without surface treatment on either side is considered heat transfer performance further declines resulting in:

$$\frac{\text{Weight Case 3}}{\text{Weight Case 1}} = 4.0 \text{ and } \frac{\text{Volume Case 3}}{\text{Volume Case 1}} = 8.0$$

### 6.8.3 Reboiler-Condenser Sizing

This study presents the effect of rotational speed at several arbitrary  $\Delta T$  conditions. Table 28 shows the variation of individual heat transfer coefficient, overall heat transfer coefficient and unit heat flux with overall temperature difference and rotational speed. Since the configuration radii are fixed, rotational speed variation is a convenient means of varying the gravitational forces; Ng. As rotational speed increases it can be seen that the condensing side heat transfer coefficient increases while the boiling side heat transfer coefficient decreases. As  $\Delta T$  increases, the condensing side heat transfer coefficient decreases, with a corresponding increase in boiling side heat transfer coefficient.

63 ASRP-2391

**SECRET**



**SECRET**

ASD-TDR-63-665, Part I

TABLE 28

REBOILER-CONDENSER HEAT TRANSFER CHARACTERISTICS

<u>Assumed Overall <math>\Delta T</math></u>	<u>Film Coefficients*</u>		<u>Overall Coefficient</u>	<u>Unit Heat Flux</u>
	$h_b$	$h_{CM}$	$U_o$	$Q/A$
	<u>Btu</u>	<u>Btu</u>	<u>Btu</u>	<u>Btu</u>
	<u>hr.ft.<sup>2</sup>°R</u>	<u>hr.ft.<sup>2</sup>°R</u>	<u>hr.ft.<sup>2</sup>°R</u>	<u>hr.ft.<sup>2</sup></u>
Rotational Speed = 35 rad./sec.			Ng = 102.5	
2.0	7,512	8,643	4,019	8,038
4.0	10,292	5,542	3,602	14,409
6.0	12,138	4,414	3,237	19,420
Rotational Speed = 43 rad./sec.			Ng = 155	
3.0	9,955	8,145	4,480	13,439
3.5	10,678	7,377	4,363	15,270
4.8	12,176	6,088	4,059	19,482
Rotational Speed = 60 rad./sec.			Ng = 302	
2.0	9,268	15,781	5,839	11,678
4.0	13,201	9,858	5,643	22,574
6.9	16,531	7,085	4,959	34,219

\* Data for Aluminum porous condensing surface and special copper boiling surface.

63 ASRP-2391

**SECRET**

**SECRET**

### ASD-TDR-63-665, Part I

The combination of boiling side and condensing side heat transfer resistances determine the overall heat transfer resistance ( $1/U_o$ ) although the wall resistance is becoming effective at the higher flux. It can be seen that the overall heat transfer resistance decreases as  $\Delta T$  increases, and increases as rotational speed increases.

Finally, the unit heat flux equal to the product of the overall heat transfer coefficient and the  $\Delta T$  increases with increase in rotational speed and with  $\Delta T$ .

For minimum reboiler-condenser weight the unit heat flux should be a maximum. Thus the product,  $U_o \Delta T$  must be a maximum. It can be seen that the maximum unit heat flux in Table 28 occurs at a  $\Delta T$  of 6.9 °R and a rotational speed of 60 rad./sec. and thus yields the minimum reboiler-condenser weight of the cases presented in this table. where arbitrary  $\Delta T$ 's were assigned. In designing a separator with fixed inlet and waste pressures, however,  $\Delta T$  is dependent on rotational speed which determines column pressure drop. The result is that most cycles will produce a maximum  $U_o \Delta T$  at speeds less than 60 rad./sec. This results from the strong effect rotational speed exercises over column pressure drop and hence reboiler-condenser  $\Delta T$ .

#### 6.9 Reliability

##### 6.9.1 General

This reliability study is the first in an extensive reliability program which will be required to achieve the final performance reliability data for a full scale flight-weight air separator. The scope of this study includes a look at the number of parts in the preliminary design and the probability calculations with assumed reliability values. Extensive tests will be required on each component to develop the probability data needed for the ultimate reliability analysis.

The reliability of a full scale flight-weight air separator is assessed in three general categories. First and most important is the design and manufacture of the separator. This determines the inherent product reliability. Secondly is the operational reliability which is related to installation, maintenance and servicing of the separator. The third category is mission reliability. Modes of failure are discussed in their relation to the overall mission reliability.

63 ASRP-2391

**SECRET**

**SECRET**

ASD-TDR-63-665, Part I

6.9.2 Product Reliability

A product can only perform as well as its design will permit. To assure a high degree of inherent product reliability it is necessary to specify performance goals and reliability standards at the inception of the design of the flight-weight separator. The preliminary design is evaluated in relation to the performance goals outlined in the work statement. Reliability standards are not specified since this program is still in the applied research phase. However, the low number of moving components inherently provides a high degree of reliability.

6.9.2.1 General Design Requirements

It is required that a full scale flight-weight air enrichment unit be capable of:

- a. "A unit weight of 5.0 lb./lb./sec. of throughput air." This weight goal can be achieved with the minimum desired purity of 90% oxygen product purity and 98% nitrogen waste purity at the 95% confidence level weight estimate on Figure 186. Therefore the weight goal can be met within the purity limitations established for oxidizer product and nitrogen waste streams.
- b. "A unit volume of 0.5 cu.ft./lb./sec. of throughput air." Present realistic evaluation of the system volume indicates that the lowest unit volume possible would be 1.04 cu.ft./lb./sec. at the minimum desired purity at 95% confidence level in Figure 186. The limiting criteria is the superficial vapor velocity which, in current technology, must be under 10 ft./sec. in the columns to obtain reasonable mass transfer efficiency. At minimum desired purity, the separator will incur an 0.54 lb./lb./sec. weight penalty to compensate for the 0.54 cu.ft./lb./sec. volume excess beyond the goal.
- c. "Performance":-
  - (1) "Oxidizer Effluent Purities: 90-95% desired  
75-95% acceptable."
  - (2) "Nitrogen Effluent Purities: 98% desired  
95-98% acceptable."

63 ASRP-2391

**SECRET**

**SECRET**

**ASD-TDR-63-665, Part I**

Purity goals will be met as noted in the weight and volume discussion. With average return from continued research it should be possible to achieve the maximum desired purities within the weight goal.

d. "Satisfactorily accepting air at pressures up to 250 psig at qualities from a few degrees of superheat to saturated liquid, and containing constituents normally found at altitudes between 70,000 and 100,000 ft." The separator will be able to accept air, which has been properly cleansed of impurities, at pressures up to 250 psig and at qualities from a few degrees of superheat to a few percent liquid. The minimum weight separator will probably operate at the upper limit of the pressure levels under investigation, although this also is a strong function of the waste pressure. The saturated liquid feed condition is not compatible with the double column cycle since the high pressure column depends on the vapor feed to achieve separation. A different cycle, probably a less efficient one, would be required if saturated liquid must be separated. The separator will satisfactorily accept air found at 70,000 to 100,000 feet although proper procedures must be established to handle some constituents. The effects of minor constituents is examined in Section 6.6.

e. "Providing satisfactory operation under off-design conditions; e.g. start-up, shutdown, and other transients." The separator will perform at conditions slightly different from the nominal design conditions by adjusting the speed of rotation or throughput. Since the columns contain a fixed number of trays it is not practicable to change radically from the design point without some other compensating change. Start-up and shutdown procedures will be simple, primarily in opening and closing the hydrogen refrigeration supply and the feed air supply. It is planned to protect the separator from a catastrophic failure from excess pressure by installing bursting disks. This will avoid an extreme weight penalty from over design or other relief devices. Off-design performance has been discussed in detail in Section 6.7 of this report.

f. "Not less than fifty (50) flight hours of maintenance-free operation." Maintenance-free operation depends on the performance of the seals, bearings and valves, which are the only parts of the separator which are subject to wear. The following discussion of components confirms that the design should provide the required hours of operation.

63 ASRP-2391

**SECRET**

**SECRET**

ASD-TDR-63-665, Part I

6.9.2.2 Design Reliability of Components

To analyze the reliability of the entire separator, it is necessary to determine the inherent reliability of the individual components. Since these components are in series, the resultant product of the component reliabilities will be the inherent design reliability of the separator. The major separator components, the two columns and the reboiler-condenser, are sections of a single rotor in the current preliminary design. Consequently the only moving parts are the bearings which support this rotor, the shaft seals, diffuser seals, and the control valves which regulate liquid transfer between columns. Drive turbines were not a part of this study.

a. Bearings

Design criteria in the work statement specify a minimum of 50 hours of maintenance-free operation. If each bearing has a 99.5% probability of successful operation in the 50 hour period, the resultant bearing reliability can be calculated using the Weibull function (Ref. 48), the ratio of operating time, to design life at 90% reliability, equals 0.1 at 99.5% reliability. Minimum design life thus should be 500 hours. Using a typical bearing of 35 in. diameter, it would be rated for 12,830 lb. radial load at 100 RPM and 3000 hours average life (4.08 x design life) (Ref. 49).

$$\text{Allowable Bearing Load} = \frac{(\text{Rated Load}) (\text{Speed Factor})}{(\text{Life Factor})}$$

$$\text{Rated Load} = 12,830 \text{ lb.}$$

$$\text{Speed Factor} = .526 \text{ at } 685 \text{ RPM}$$

$$\text{Life Factor} = .88 \text{ at } 500 \times 4.08 \text{ hours}$$

$$\text{Allowable Bearing Load} = \frac{(12,830) (.526)}{(.88)}$$

The above load is the fatigue life capacity which will permit 99.5% reliability of each bearing when properly lubricated and cooled. It is presumed that the design will provide proper lubrication and cooling.

Six bearings will be required to support a 10,000 lb. rotor containing 32,000 lb. of fluid. Therefore total bearing

63 ASRP-2391

**SECRET**

**SECRET**

**ASD-TDR-63-665, Part I**

reliability is  $(99.5\%)^6 = 97.5\%$ . This is the inherent bearing reliability.

**b. Seals**

Design alternatives on the diffuser seal will permit: a pressure balanced contact seal, a close-clearance vane seal, or a pressure shell with minimum seal differential pressure. The design is not sufficiently defined to permit an evaluation of its performance in terms of absolute reliability. Regardless, reliability assumptions may be made for purposes of estimating the overall product reliability.

The two diffuser seals are the most difficult since they encompass the larger diameters. A design life of 50 hours at 98% reliability on each seal is used in their evaluation. Tests of the 1/20 scale unit will provide data for determination of the actual component reliability.

Shaft seals can be assumed to have a 99% reliability for the 50 hour life. There are five of these units.

Combined seal reliability is 91.5%.

**c. Control Valves**

There are two control valves within the rotor. One valve is for kettle liquid transfer; the other is shelf liquid transfer. Reliability of each valve is assumed to be 99.5% in the 50 hour design life. Numerous test results will be required to develop reliability data for these controls.

Inherent design reliability of the total separator is the product of the components, or 88.5% overall reliability based on the assumptions for each component. This study indicates there are only 3 types of components which affect design reliability; a total of 15 individual items. When the cost of a mission effort is calculated it will then be possible to evaluate the degree of separator reliability required and the optimum funding for studies to develop this reliability.

**6.9.2.3 Fabrication Reliability**

As the design progresses from the very preliminary phases it will

**63 ASRP-2391**

**SECRET**

**SECRET**

#### ASD-TDR-63-665, Part I

be possible to develop the detail component drawings and dimensions. Probabilities of manufacturing and assembling parts within tolerances can then be calculated. Since large brazed, soldered or welded assemblies will be required, some probabilities of successful manufacture could be developed to determine the number of duplicate components required to achieve one completely sound structure. The reliability of the components which pass the manufacturing inspection would be determined from a series of reliability tests. Results of these tests would be combined with the component design reliability to provide the inherent reliability of the separator.

#### 6.9.3 Operation Reliability

When the quality control tests have been completed on the manufactured product, the separator must be packaged for shipment. Operational reliability of the separator begins at this point and continues through its installation in the vehicle and its maintenance between missions.

During shipment and storage the separator must be protected from water vapor. Moisture would cause corrosion of the bearings and other parts. Sealing techniques developed for overseas shipment will be adequate for the shipment and storage of the separator. In addition some protection must be provided against the permeation of moisture through the wrapping materials. A positive purge system or desiccant is recommended. No oil or grease may be used for protection since these combustibles are hazardous in an oxygen production facility.

During installation no special atmosphere is required although high humidity or corrosive atmosphere should be avoided. When the separator is in place it is suggested that a dry gas purge be resumed to remove any moisture accidentally introduced into the system.

Following operation of the separator the system should be warmed by purging with a warm dry gas to positively exclude moisture in this critical period when frost will form on the cold heat exchange surfaces and bearings.

With strict adherence to the above procedures no reduction in separator reliability is anticipated from the time it passes quality control tests at the factory.

63 ASRP-2391

**SECRET**

**SECRET**

**ASD-TDR-63-665, Part I**

**6.9.4 Mission Reliability**

The mission reliability is examined in two respects. First, the functional reliability during the mission, and secondly the modes of failure and the consequences.

To determine the functional reliability, the separator and auxiliaries were listed functionally in a logic sequence. Since all are series functions, tabular form was used.

**Mission Functional Reliability Logic**

The separator will produce the quantity and purity of product

- |        |  |
|--------|--|
| IF     | it receives the design air inlet pressure, temperature and volume                            |
| AND IF | the drive delivers the necessary power and speed control                                     |
| AND IF | the hydrogen refrigeration is delivered at specified design conditions                       |
| AND IF | the hydrogen interstage expansion turbine performs as specified                              |
| AND IF | the low pressure column expansion turbine performs as specified                              |
| AND IF | the reboiler-condenser product and recirculation expansion turbine performs as specified     |
| AND IF | the separator performs at the inherent design reliability                                    |
| AND IF | the waste recompression system performs as specified   |
| IF     | all of the above are achieved, the separator contribution to the mission will be successful. |

Applying a uniform 99% reliability to each of these sequences, except the inherent design reliability which was already estimated at 88.5%, the mission reliability would be 82.5% for 50 hours of operation. This is nominally 100 missions. The reliability of the earlier missions would be considerably improved. In the ultimate analysis, an economic justification should be made for the design goal reliabilities.

Modes of failure are also important. If the failure is catastrophic

63 ASRP-2391

**SECRET**



~~SECRET~~

ASD-TDR-63-665, Part I

it naturally would require a much higher reliability than if it only requires aborting a mission with a recoverable vehicle. The only catastrophic failure anticipated would result from an explosion caused by contamination of the system with combustibles. There could be oil or grease introduced in some section of the system during manufacture or possibly volatiles from lubricated equipment at the warm end of the system.

Malfunctions of the separator would include drive failure or bearing failure which would prevent rotation of the separator. Seal failure would permit excess leakage which would reduce system pressure below an operable level. Hydrogen leakage at the reflux condenser would only be serious if the leakage were substantial. Minor hydrogen leaks would be washed into the nitrogen waste stream through the heat exchanger to the engine combustion chamber.

63 ASRP-2391

~~SECRET~~

ASD-TDR-63-665, Part I

(THIS PAGE IS INTENTIONALLY BLANK.)

63 ASRP-2391

**CONFIDENTIAL**

ASD-TDR-63-665, Part I

APPENDIX I

"UCON" FLUID EXPERIMENTAL EQUIPMENT AND  
SEGMENTAL TRAY ROTORS

1. Description

The "UCON" fluid test rotors have been designed so that trays can be inserted at various distances from the hub to form a simple distillation column being rotated about its axis. The purpose of the tester is to investigate the fluid dynamics and mass transfer characteristics of a column in a high gravitational field. The apparatus is arranged so that the rotational velocity (and thus the gravitational force on the trays), the liquid and vapor rates, the column pressure and the inlet temperatures of the gas and reflux streams can all be varied independently. By this means, a wide range of operating conditions can be studied to determine the effect of each variable on the operation of the column. In addition, the number and configuration of the trays can be changed and their behavior studied under various conditions. A stroboscopic light arrangement permits visual observation of the trays through plexi-glas windows on the tester, enabling high-speed photographs to be taken.

In addition to the tester itself, a variety of tanks, condensers, a boiler, pumps, heat exchangers, controls and instruments are required. The schematic flow sheet (Figure 2) illustrates the entire system which is described in some detail below.

The UCON fluid is stored in a 300 gallon tank equipped with a liquid nitrogen cooling coil. A temperature controller on the tank regulates the flow of nitrogen from a standard Linde AT-25 cold converter. The liquid UCON fluid from the tank is fed through a strainer to the suction side of a Turbocraft centrifugal pump. A valving arrangement on the discharge side of the pump allows a portion of the liquid to pass either through the remotely operated boiler feed bypass valve to the condenser, or back to the storage tank. The rest of the liquid passes through the vapor feed control valve, through a turbine-type flowmeter and into the shell side of a standard shell-and-tube boiler manufactured by Basco, Inc. Steam is condensed in the tubes to vaporize the UCON fluid, the amount of

63 ASRP-2391

**CONFIDENTIAL**

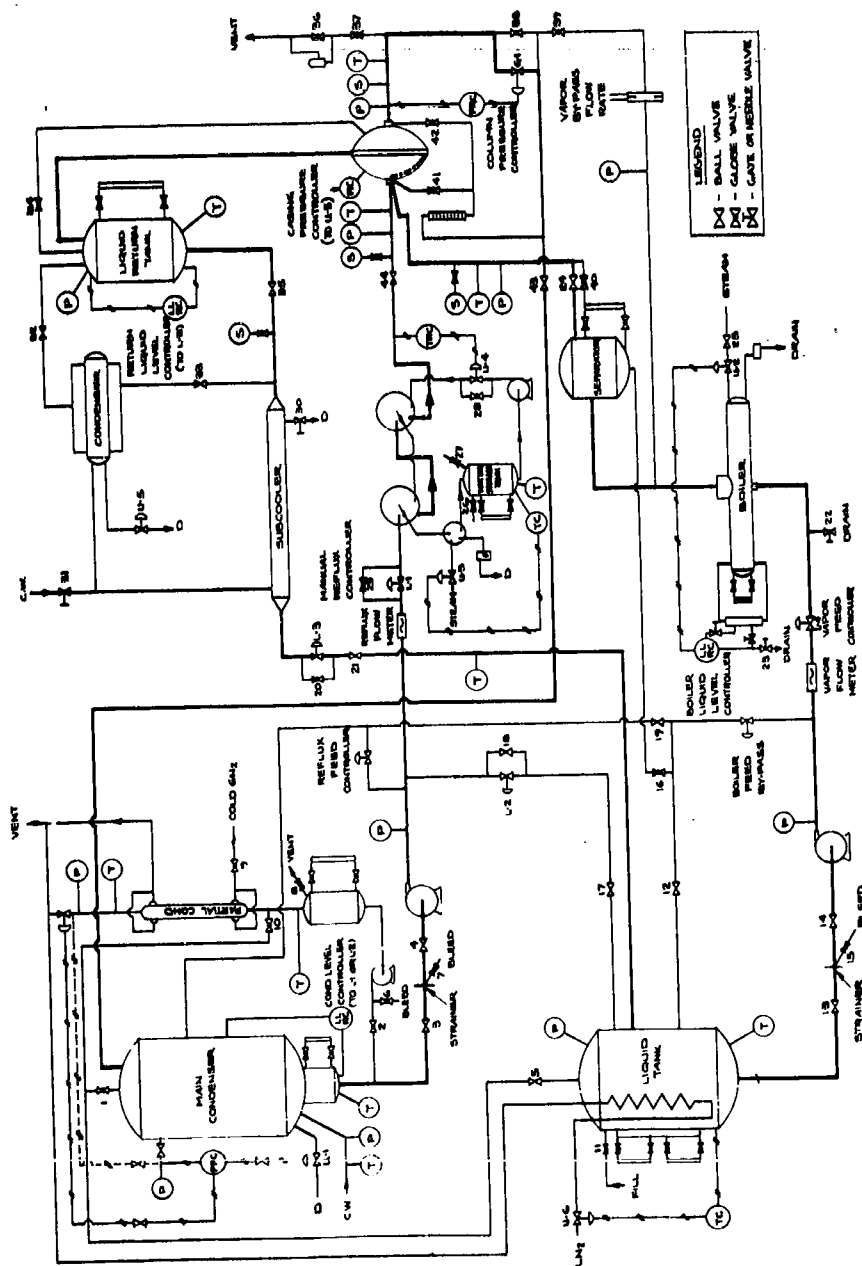


FIG. 2

UCON FLUID TEST SET UP

**CONFIDENTIAL**

**ASD-TDR-63-665, Part I**

steam being regulated by a liquid-level controller on the boiler. The vapor then issues through a separator and into the tester.

Figures 188 and 189 show the disassembled rotor indicating the general configuration of the tester.

The vapor enters the rotor through the outer passage of the concentric tube center shaft and is passed through a pipe to the "bottom" of the chamber column, i.e., the periphery of the rotor. The vapor then passes up through the chamber, out a hole in the hub, and leaves the tester through the center of the shaft behind the rotor, passing out through a header. Reflux liquid enters the tester by way of the center tube of the front shaft and is sprayed into the chamber through two nozzles, one on either side of the chamber near the "top" or center of the rotor. After passing outward through the column, the liquid is discharged centrifugally from the periphery of the rotor into a passage within the rotor casing. It leaves the tester through the bottom, tangentially to the rotor.

In addition to the chamber passage, the impeller has a counter-balancing device to minimize vibration caused by static imbalance. A pressure controller on the casing maintains a present pressure differential between the outer casing and the inner column. This protects the plexiglas windows and prevents backleakage of fluids through the rear shaft seals of the tester. The slight gas leakage through the shaft seals passes through a rotometer and into the vapor outline line to the condenser.

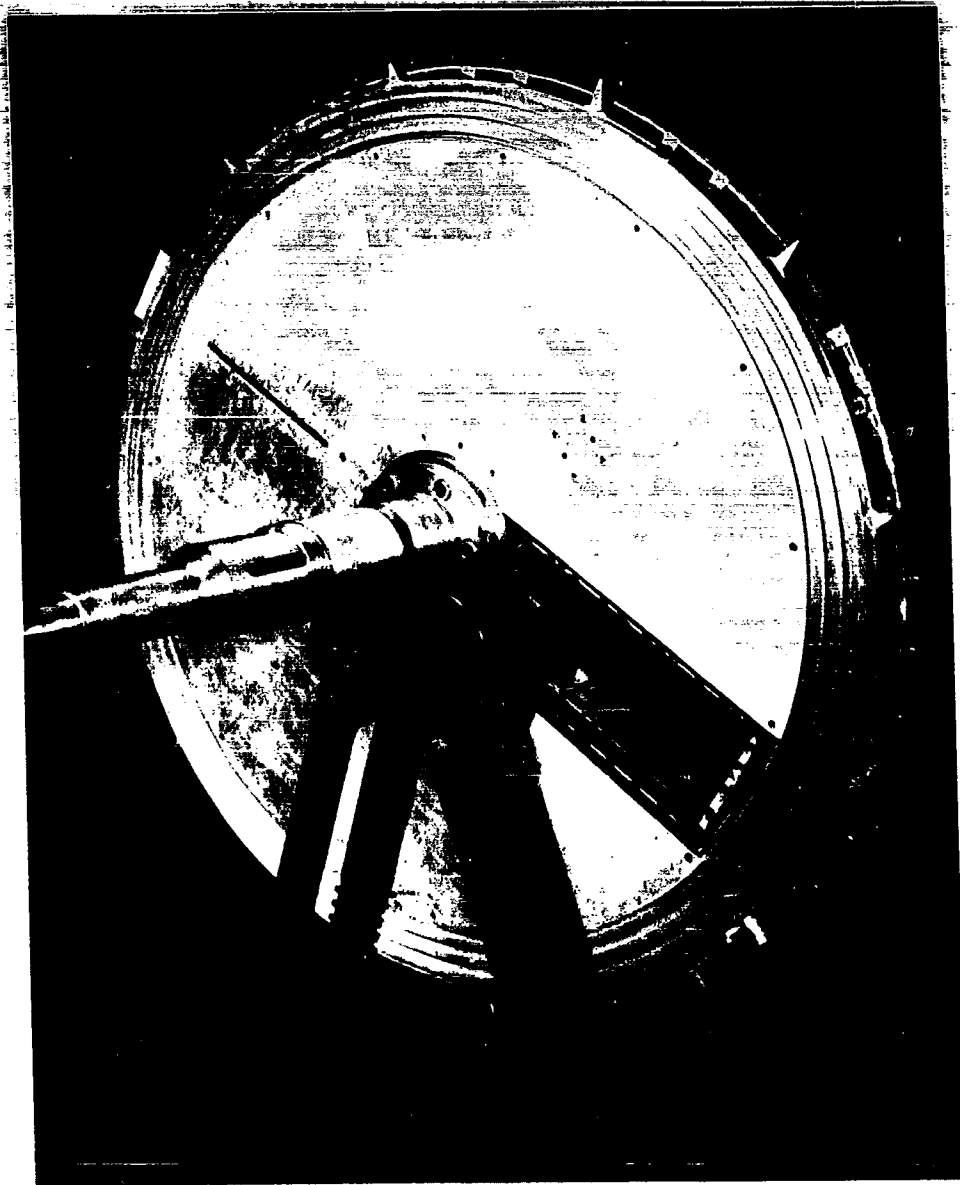
The gas leaving the tester flows through an automatic valve, controlling the pressure within the column, and into the condenser. The condenser is a specially designed cylindrical steel vessel. The upper portion contains four coils of extended surface copper tubing stacked vertically and piped in parallel. Cold water from the supply main flows through the coils and condenses the UCON vapor. The UCON liquid thus formed flows by gravity to the bottom of the tank. Protruding from the bottom is a second cylinder of smaller diameter where the liquid is held. The purpose of the smaller diameter is to facilitate liquid-level control and to minimize the amount of liquid held in the tank. The flow of cold water to the coils is controlled by the pressure within the condenser.

The condensate, or reflux, runs by gravity from the bottom of the condenser, through a strainer and into the suction side of a

63 ASRP-2391

**CONFIDENTIAL**

ASD-TDR-63-665, Part I

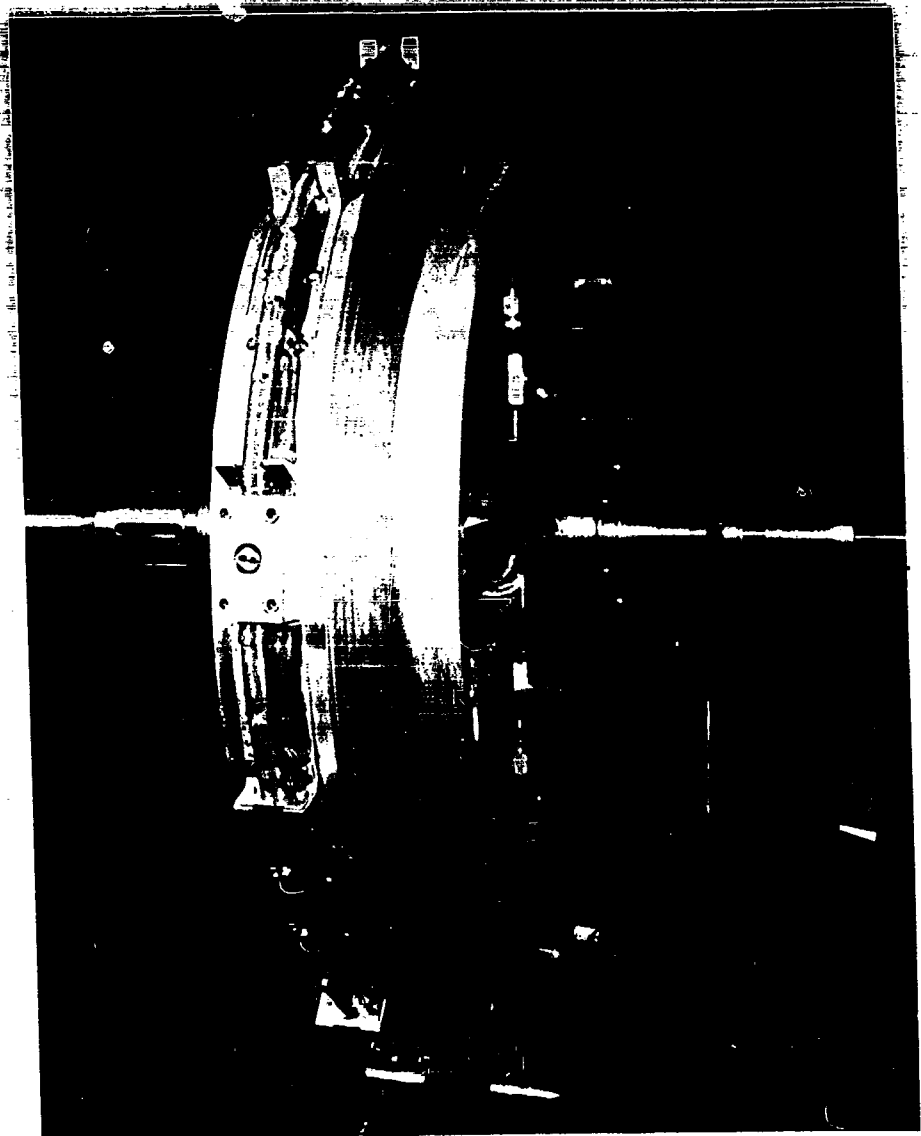


UCON FLUID TEST ROTOR

FIG. 188

63 ASRP-2391

ASD-TDR-63-665, Part I



UCON FLUID TEST ROTOR

FIG. 189

63 ASRP-2391

**CONFIDENTIAL**

**ASD-TDR-63-665, Part I**

pump identical to the boiler feed pump previously mentioned. A portion of the pumped liquid may flow directly to the storage tank, the rate being controlled manually or by the liquid level in the condenser. A remotely operated bypass valve, labeled "Reflux Feed Controller," is provided to aid in priming the pump. The UCON liquid not run to storage passes through a flowmeter and two Heliflow exchangers wherein hot water warms the reflux.

A separate system circulates the hot water from a storage tank, through a pump and the two UCON-water exchangers. Before flowing back to storage, the water passes through a small Heliflow steam heater. A temperature probe in the hot water tank controls the flow of steam to this exchanger and a temperature sensor on the reflux line controls the heating water rate.

Reflux flows into the center of the tester and out the periphery as previously described and then drains into a liquid return holdup tank. A small, water-cooled shell and tube condenser mounted over this tank controls the pressure within the tester casing. The UCON fluid then passes through the tube side of a water-cooled subcooler and returns to the storage tank. The flow rate of this return stream is controlled by a liquid level controller on the liquid return tank.

When the unit is shut down or opened for tray changes, there are numerous points at which air can enter. Any such leakage eventually collects in the condenser or the storage tank and can adversely affect the operation of the system. To remove this air, a partial condenser circuit is provided as shown on the flow sheet. A small Trane core is mounted vertically on one side of the condenser. The air-UCON vapor mixture from the storage tank and the condenser is passed up through the core while cold nitrogen gas is blown through in parallel flow. The UCON condenses and runs, by gravity, into a pot while the air is vented. The condensate is pumped back to the main condenser by a small pump mounted under the pot.

For ease of evaluating the overall magnitude of the equipment, several sizes of the more important pieces of equipment are listed in Table 29.

**2. Test Capabilities**

**a. General**

The equipment has been designed with flexibility in mind so that

**63 ASRP-2391**

**CONFIDENTIAL**



~~CONFIDENTIAL~~

ASD-TDR-63-665, Part I

TABLE 29

UCON Fluid Flow System  
Significant Sizes

Condenser - 4,000 sq. ft.

Collection Pot - 16 in. O.D. x 25 in.

Storage Tank - 300 gal.

Boiler - 47 sq. ft.

Liquid Return Tank - 30 gal.

Subcooler - 64 sq. ft.

Tester - 44 in. diameter

Chamber dimensions - 3 in. x 4 in.

Tray radii - every 1-1/4 in. from 9 in. to 15-1/4 in.

63 ASRP-2391

CONFIDENTIAL

~~CONFIDENTIAL~~

### ASD-TDR-63-665, Part I

a wide variety of tests can be run with little or no change in the system. For the present program, the studies were concerned primarily with the hydraulic characteristics of rotating sieve trays and with their separation efficiency. Various provisions have been made to obtain the desired data for these studies and a detailed discussion of these instruments and associated techniques are described below.

Because of the increased throughput demanded for the circumferential tray tests, several minor piping changes were necessary; most of them to reduce pressure drop between the tester and condenser. For this reason, G-1, the column pressure controller, was eliminated from the system.

The increased feed to the boiler was likely to result in considerable entrainment in the vapor feed stream. To enable measurement of this entrainment, a liquid level control was installed on the separator which regulated an automatic valve in the separator return to storage line. A flowmeter was also installed in this line to measure the amount of entrained liquid sent back to the storage tank.

The schematic flow diagram described previously indicates the various points throughout the system where pressure and temperature sensors are located. These indicators and the flowmeters mentioned before enable the determination of the operating conditions at any time.

#### b. Pressure Drop

To determine the pressure drop through a tray or groups of trays, two differential pressure cells are provided, the output signals of which are fed to a recorder. One cell measures the  $\Delta P$  across the entire tester, the probes for which are located on the inlet and exit vapor lines. A calibration curve based on the empty column pressure drop has been made.

A second cell is located on the rotor itself and the probes may be placed in a number of positions to measure the  $\Delta P$  across one tray or the entire column. The output signal from this unit is affected by the gravitational field. Therefore, a calibration curve of transducer reading versus rotor RPM has been drawn.

#### c. Mass Transfer

For efficiency studies, it is necessary to know the compositions of the various streams entering and leaving the column. To determine

63 ASRP-2391

**CONFIDENTIAL**

**CONFIDENTIAL**

**ASD-TDR-63-665, Part I**

these compositions, sample taps are provided on the appropriate lines into and out of the tester. These taps are indicated by the symbol (S) on the flow diagram and are run to a Beckman GC-2A Gas Chromatograph equipped with an integrating readout device. By various valving techniques samples of any of the four streams may be analyzed.

The GC-2A must first be calibrated by running samples of the pure components through the chromatograph. Cylinders of these gases are provided for this purpose.

**d. Tray Operation**

The successful operation of a program of this nature requires visual observation of the column in operation. For this purpose the chamber and the walls of the tester are equipped with plexiglas windows behind which a stroboscopic light is mounted. An electronic trip mechanism flashes the light at the exact time that the windows are in view. With this arrangement, the following parameters may be observed.

1. Foam height and stability.
2. Amount of weeping from the tray.
3. Downcomer action.
4. Qualitative degree of entrainment.
5. Rangeability, or the maximum range over which the flow rates, RPM, vapor densities, etc. may be varied with the column still operating properly.

63 ASRP-2391

**CONFIDENTIAL**

ASD-TDR-63-665, Part 1

(THIS PAGE IS INTENTIONALLY BLANK.)

63 ASRP~2391

~~CONFIDENTIAL~~

ASD-TDR-63-665, Part I

APPENDIX II

"UCON" FLUID PROPERTIES

In the body of this report, the selection of various UCON fluids as operating fluids for these studies was discussed. They were chosen in order to simulate as many of the physical properties of liquid air as possible while operating at near-ambient temperatures. Included in this appendix are graphs presenting the best available data on the properties of the three UCON fluids used, and a table listing the references from which these properties were obtained.

1. Vapor-Liquid Equilibrium Data

To investigate the efficiency of a column, a binary system was used.

A brief search of the literature, conducted at the outset of this program, revealed a complete lack of equilibrium data for these UCON systems. A series of experimental measurements were consequently made over a moderate pressure range and using a modified bomb method. Based upon this data, liquid activity coefficients could then be determined and utilized in the evaluation of equilibrium data at other pressures.

The results obtained with UCON-12 UCON-114 indicated that this particular system represents an almost ideal liquid phase, that is, ideal enough such that the activity coefficient may be taken as unity. It was found, furthermore, that deviations from vapor phase idealities may be adequately corrected by means of generalized fugacities. The vapor-liquid equilibrium data (Figure 31) was therefore machine computed at various operating pressures using the following relationship written here for the more volatile Component 1.

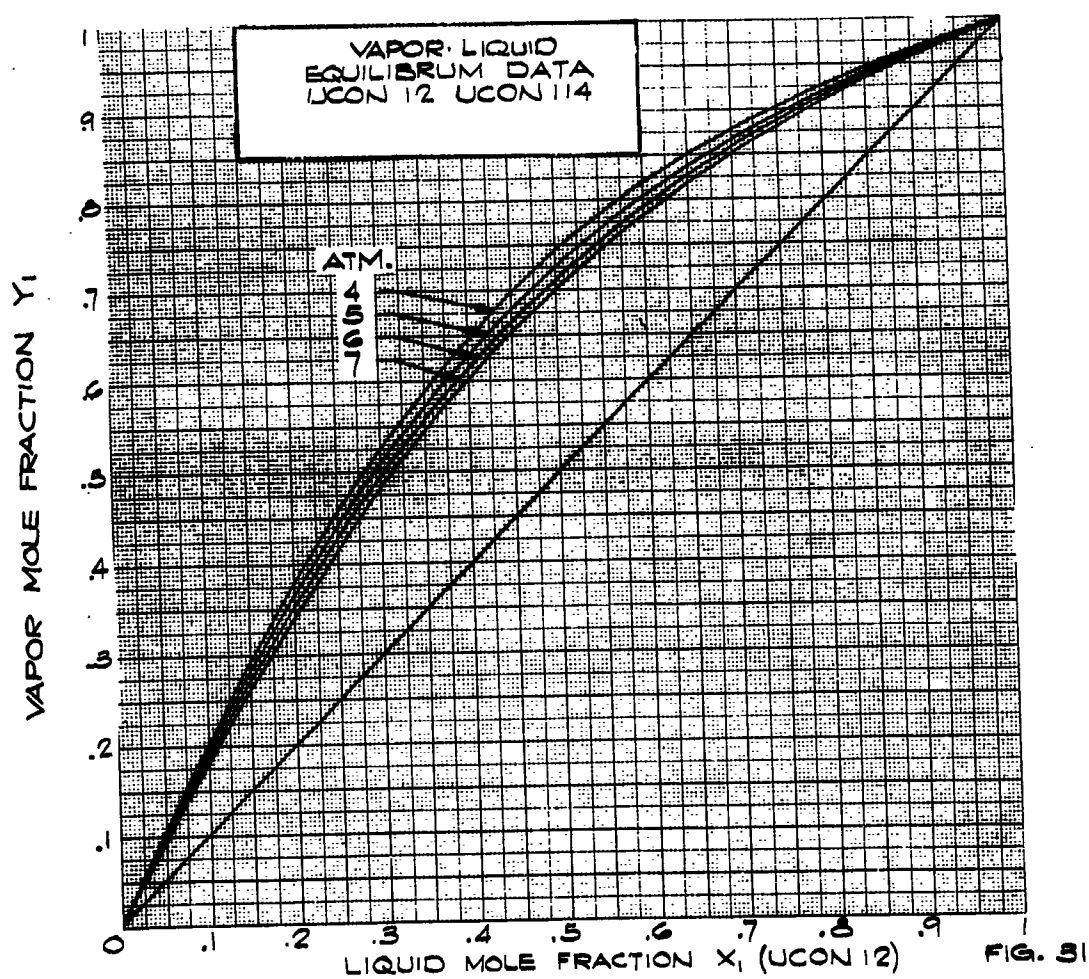
$$K = \frac{Y_1}{X_1} = \frac{\gamma_1^* (\eta_1^\circ P_{v1}) e^{\frac{V_m (P - P_{v1})}{R_c T}}}{\eta_{v1} P} \quad (56)$$

63 ASRP-2391

CONFIDENTIAL

CONFIDENTIAL

ASD-TDR-63-665, Part I



CONFIDENTIAL

**CONFIDENTIAL**

**ASD-TDR-63-665, Part I**

The agreement between computed and experimental results was generally to within about 5%.

For the circumferential tray tests, UCON-21 was a necessary fluid because of its low vapor density. To enable the efficiency runs to be made, a binary system of UCON-21 with UCON-114 was selected because of the availability of UCON-114 with its relatively similar vapor pressure curve. This characteristic is desirable because it usually indicates a narrow "lens" on an x-y, or liquid-vapor equilibrium plot. This allows a constant enrichment on each tray and makes the data less sensitive to errors in the analyzing equipment.

With these considerations in mind, liquid vapor equilibrium data for the system composed of UCON-21 and UCON-114 was taken at three different pressures. A typical plot of this data is shown and illustrates the fact that the system forms a minimum-boiling azeotrope at about 0.66 mole fraction 114. This in no way hindered the use of the system in these tests since the separation was run between the azeotropic composition and that of pure UCON-21. This data was taken only at compositions up to the azeotrope since the remainder of the curve is not required for the purposes of this test program.

Using the laboratory liquid-vapor equilibrium data, Figure 190, the activity coefficient was calculated and plotted for each component. Using this smoothed plot, vapor-liquid equilibrium curves were drawn for various system pressures. The relationship of activity coefficients versus liquid phase composition and a typical X-Y diagram are included (Figure 191).

**2. Physical Properties**

Physical property data are presented in Figure 192 through Figure 199. They are obtained from the following references.

- a. UCON-114 Properties (Ref. 50)
  - (1) Vapor Pressures
  - (2) Liquid & Vapor Viscosity
  - (3) Liquid & Vapor Density
- b. UCON-12 Properties (Ref. 51)
  - (1) Vapor Pressures
  - (2) Liquid & Vapor Viscosity
  - (3) Liquid & Vapor Density
  - (4) Surface Tension

63 ASRP-2391

**CONFIDENTIAL**

~~CONFIDENTIAL~~

ASD-TDR-63-665, Part I

c. UCON-21 Properties

- (1) Vapor Pressures (Ref. 52)
- (2) Liquid & Vapor Density (Ref. 52)
- (3) Liquid & Vapor Viscosity (Ref. 23, p. 790-794)

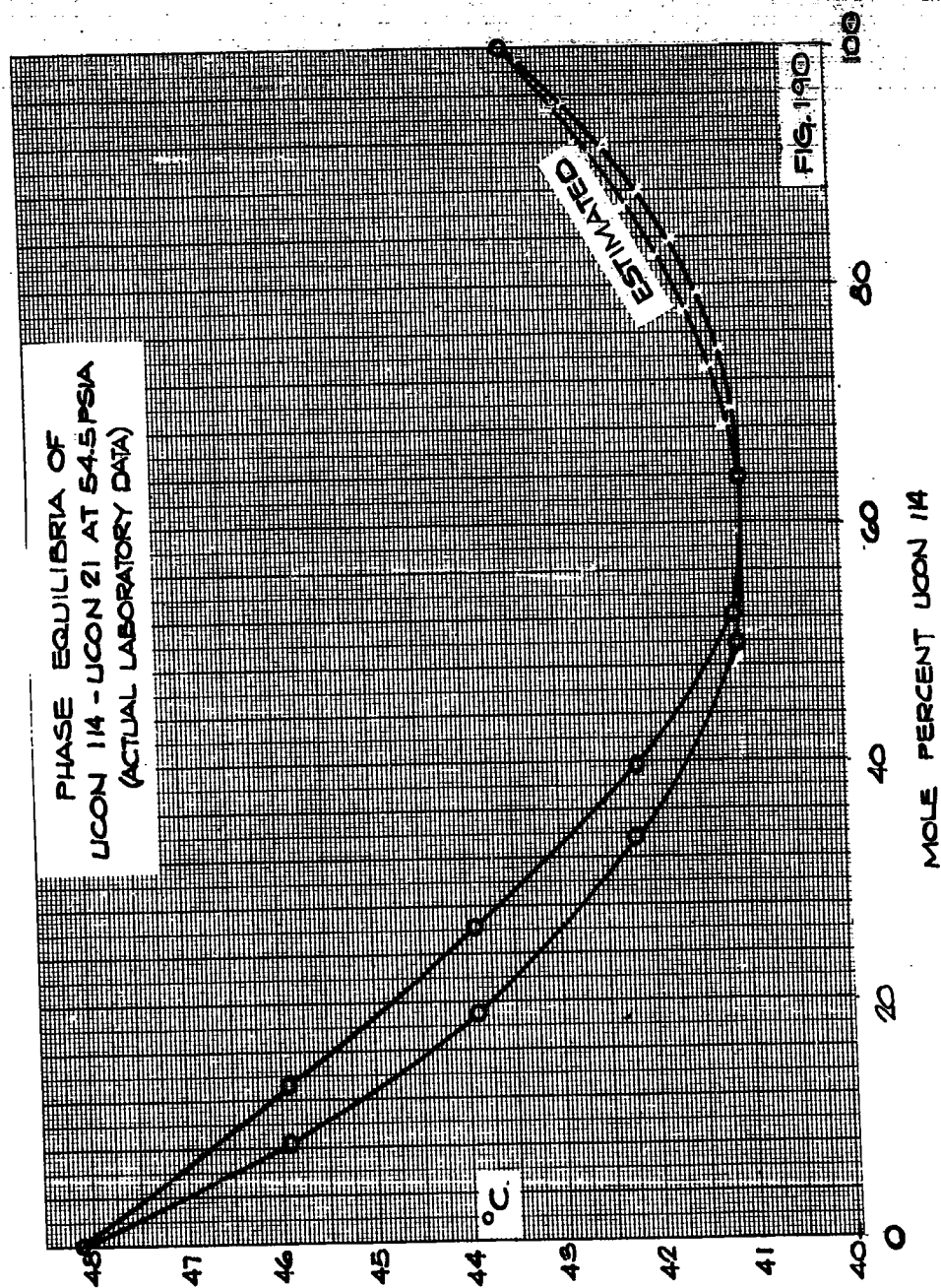
d. Calculated Properties

- (1) Activity Coefficients (Ref. 53)
- (2) Surface Tension (Ref. 53)
- (3) Diffusion Coefficient
  - Vapor - Original Method (Ref. 54)
  - Improved Method (Ref. 55)
  - Liquid (Ref. 54, p. 26)

63 ASRP-2391

CONFIDENTIAL



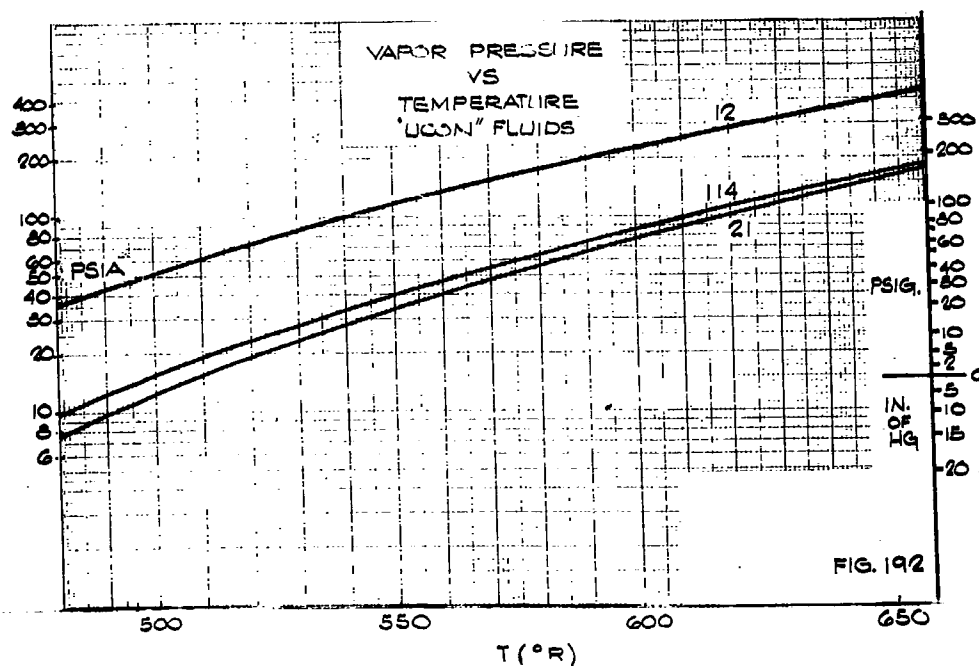
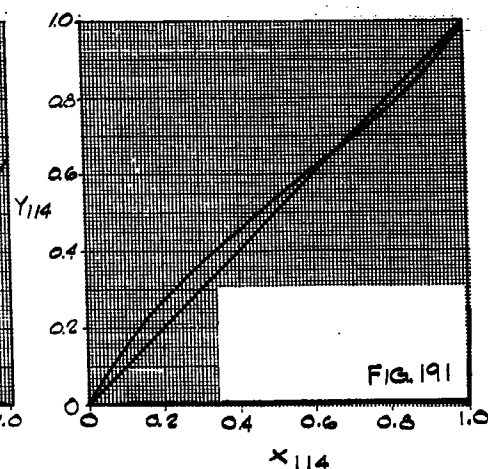
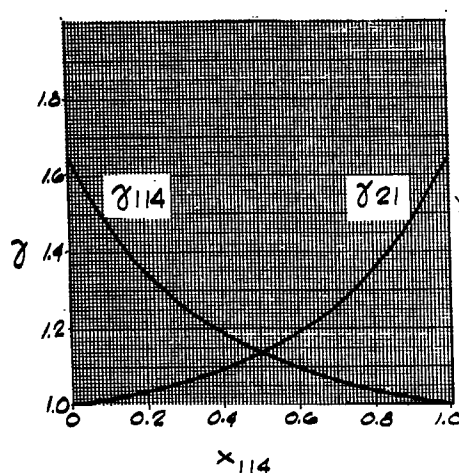


63 ASRP-2391

ASD-TDR-63-665, Part I

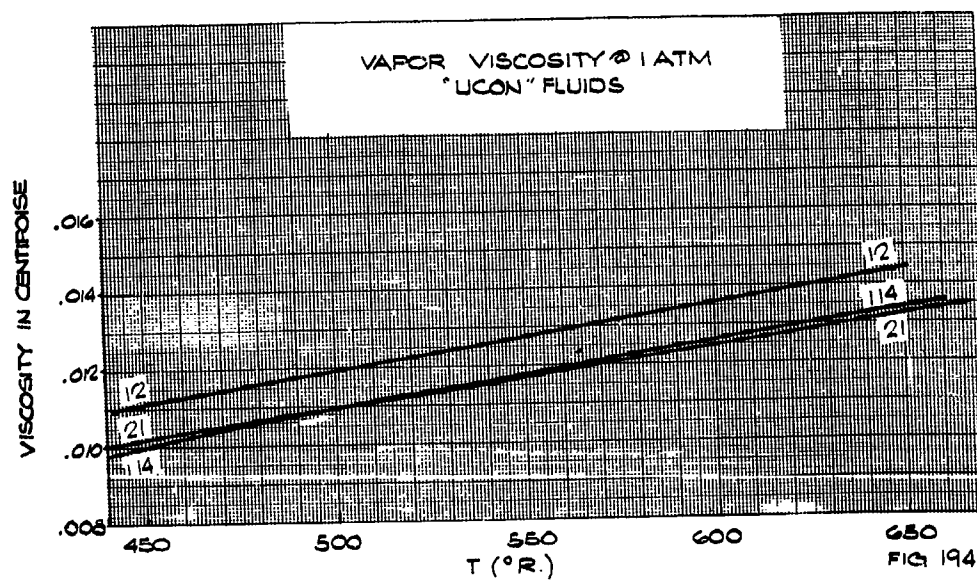
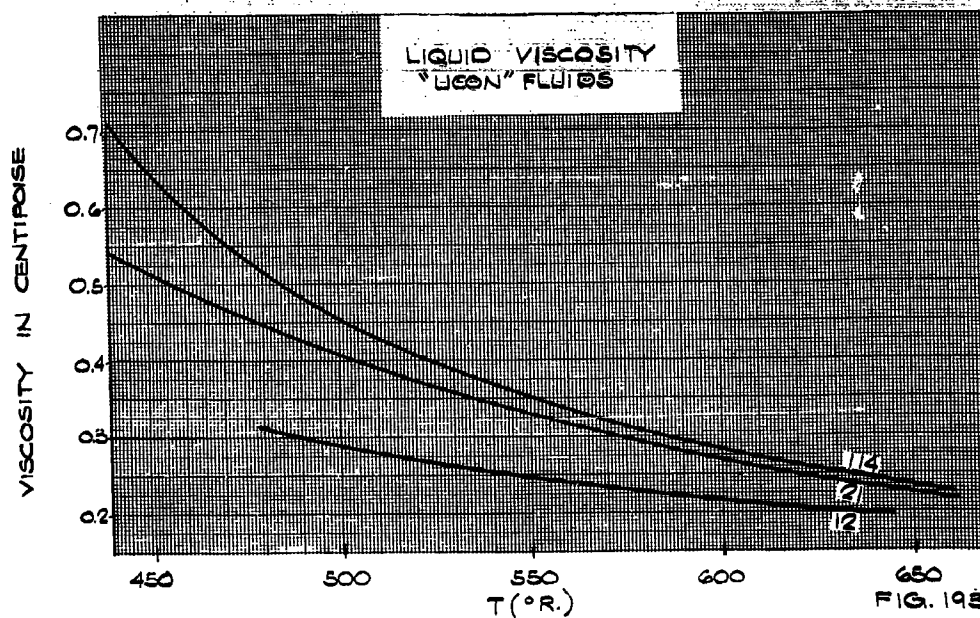
ACTIVITY COEFFICIENT  
VS  
MOLE FRACTION 114

X-Y DIAGRAM  
P = 60 PSIA



63 ASRP-2391

ASD-TDR-63-665, Part I



63 ASRP-2391

ASD-TDR-63-665, Part I

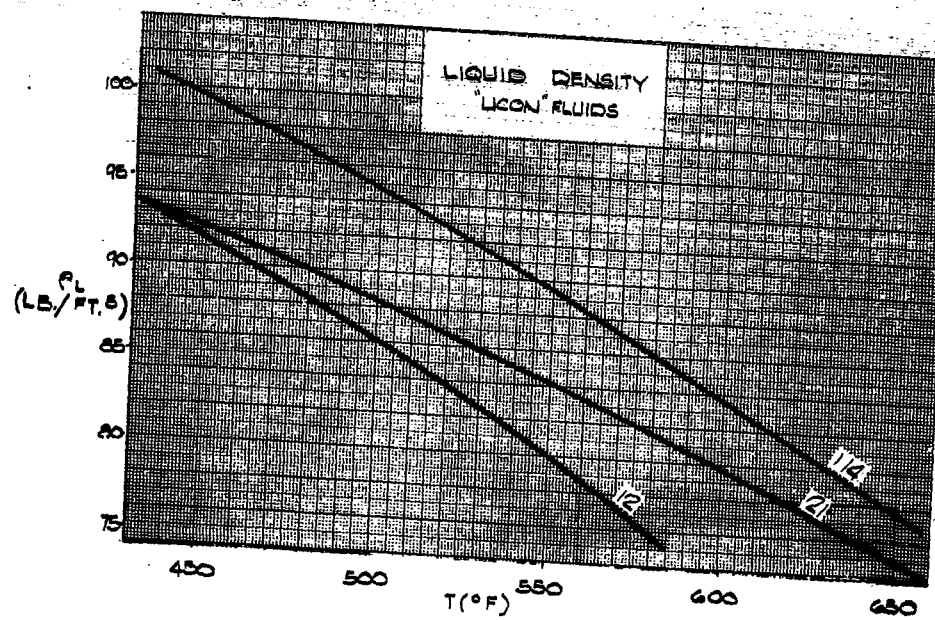


FIG. 195

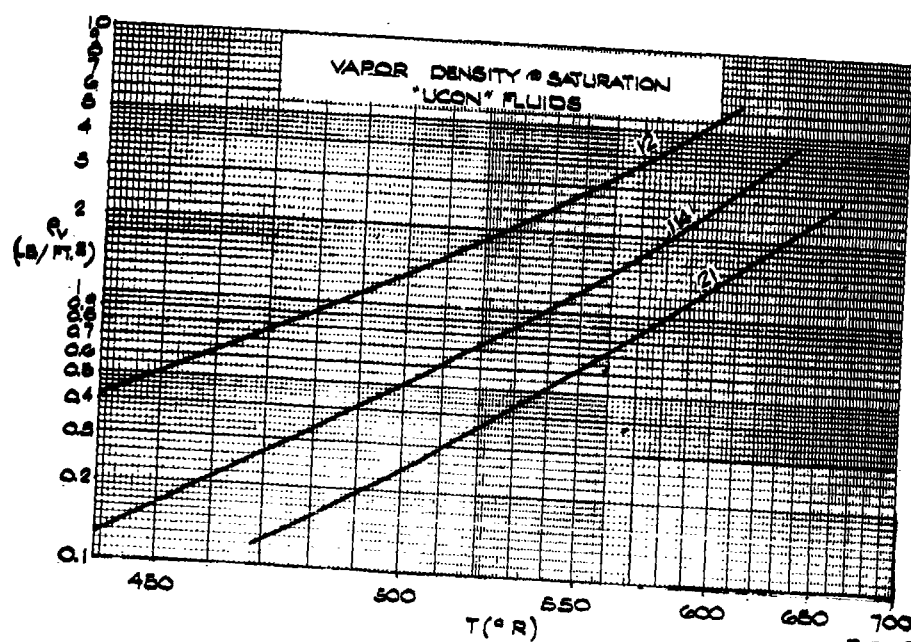


FIG. 196

63 ASRP-2391

ASD-TDR-63-665, Part I

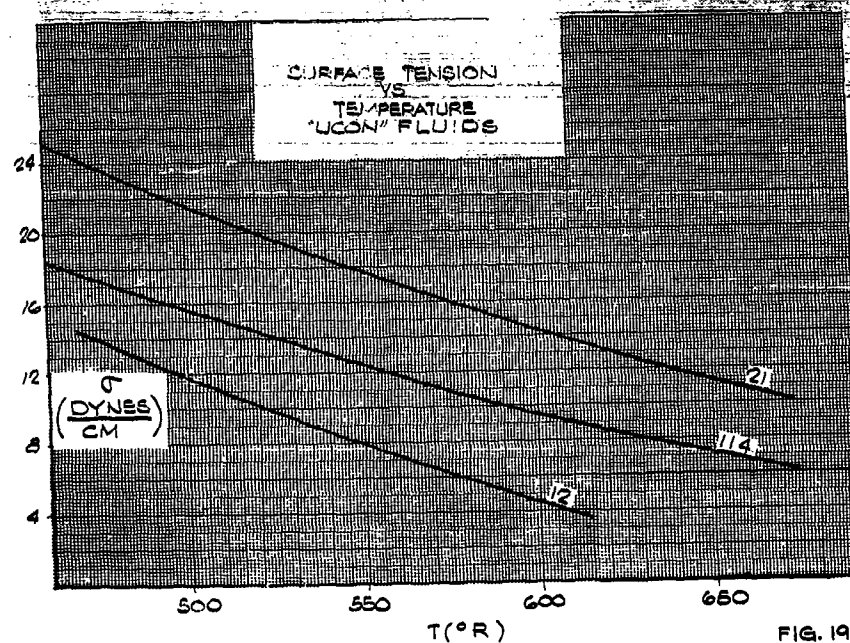


FIG. 197

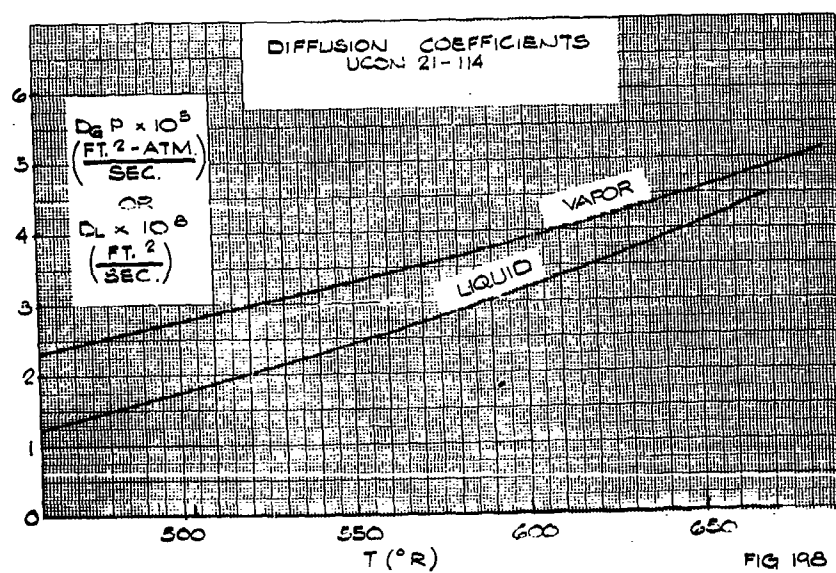


FIG. 198

63 ASRP-2391

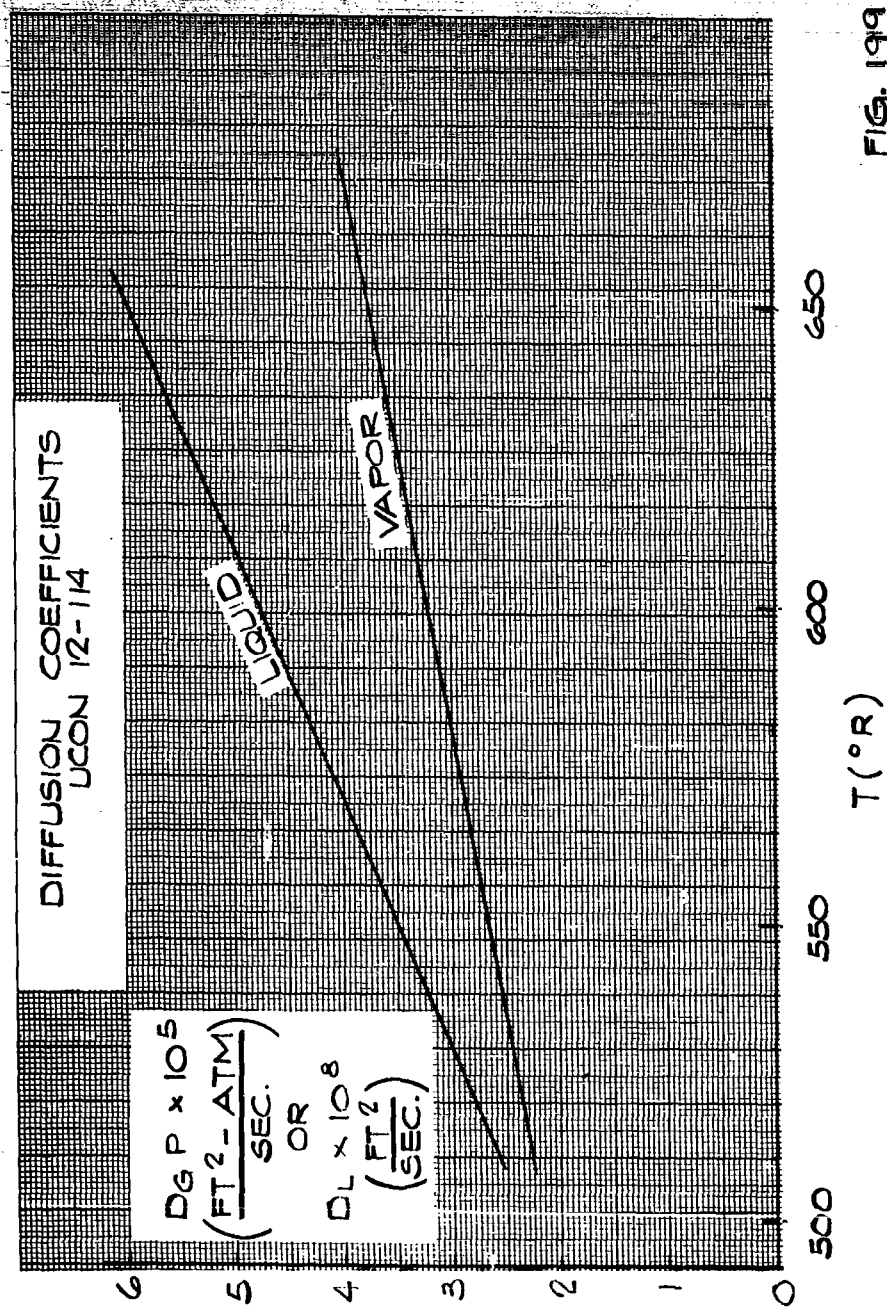


FIG. 199

63 ASRP-2391

**CONFIDENTIAL**

ASD-TDR-63-665, Part I

APPENDIX III

SEGMENTAL TRAY DATA

TABLE 30

SERIES A

<u>Run</u>	<u><math>\rho_v</math></u>	<u><math>V_s</math></u>	<u><math>N_g</math></u>	<u><math>L/V</math></u>	<u><math>Q_L</math></u>	<u><math>h_f</math></u>	<u><math>\Delta P_T</math></u>
1	1.94	11.3	285		0.064	1.6	1.5
2			285		0.112	1.6	1.6
3			285		0.168	2.3	2.3
4			285		0.244	2.8	3.4
5			198		0.056	2.1	1.4
6			198		0.112	2.6	1.8

63 ASRP-2391

**CONFIDENTIAL**

**CONFIDENTIAL**

ASD-TDR-63-665, Part I

TABLE 31

SERIES B

Run	$\bar{v}_v$	$\bar{v}_s$	$N_d$	$L/V$	$\bar{Q}_L$	$h_f$	$\Delta P_T$
1	2.25	5.06	90	0.69	0.056	1.8	0.9
2			90	0.98	0.081	2.0	1.0
3			90	1.45	0.119	2.5	1.2
4			90	1.72	0.141	2.9	1.3
5			164	1.86	0.153	1.8	1.5
6			164	1.45	0.119	1.6	1.4
7			164	0.97	0.079	1.3	1.3
8			171	0.69	0.056	1.0	1.1
9			250	0.63	0.054	0.8	1.8
10			250	1.00	0.082	1.0	1.4
11			250	1.41	0.116	1.3	1.5
12			250	1.72	0.141	1.3	1.6
13		7.75	209	0.44	0.056	1.6	1.6
14			209	0.73	0.093	1.9	1.8
15			209	1.00	0.127	2.3	1.9
16			209	1.44	0.183	2.5	2.3
17			264	0.48	0.061	1.6	1.7
18			264	0.72	0.092	1.8	1.9
19			264	1.02	0.130	1.9	2.0
20			264	1.40	0.178	2.1	2.4
21			264	2.04	0.259	2.3	2.9
22			377	0.62	0.079	1.4	2.0
23			377	1.06	0.134	1.5	2.4
24			359	1.71	0.217	1.8	2.9
25			359	2.29	0.290	2.0	3.6
26			435	2.29	0.290	1.6	4.1
27			435	1.35	0.175	1.4	3.0
28			450	0.96	0.121	1.3	2.8
29		11.9	412	1.42	0.267	2.5	3.8
30			431	1.04	0.197	2.4	3.3
31			431	0.61	0.115	2.3	3.2
32	2.67	5.88	85	0.50	0.056	1.4	0.7
33			85	0.88	0.101	1.6	0.8
34			85	1.16	0.137	1.8	0.9
35			85	1.68	0.193	2.0	1.1
36			155	2.03	0.233	1.5	1.1

63 ASRP-2391

**CONFIDENTIAL**



**CONFIDENTIAL**

ASD-TDR-63-665, Part I

TABLE 31 (Cont'd.)

Run	$\bar{p}_v$	$V_s$	$N_g$	$L/V$	$\bar{Q}_L$	$h_f$	$\Delta P_T$
37	2.67	5.88	160	1.28	0.147	1.1	1.2
38			160	0.80	0.092	0.9	0.9
39			160	0.50	0.058	0.6	0.7
40			209	1.00	0.115	0.8	1.0
41			209	2.30	0.265	1.3	1.9
42		8.79	210	1.45	0.250	1.9	2.3
43			210	0.90	0.155	1.4	1.7
44			210	0.65	0.112	1.3	1.3
45			210	0.41	0.071	1.0	1.1
46			326	0.60	0.104	0.8	1.5
47			326	1.03	0.179	1.1	2.1
48			326	1.45	0.250	1.3	2.8
49			313	2.00	0.345	1.5	3.8
50			402	2.00	0.345	1.3	3.9
51		12.2	252	0.39	0.092	2.0	1.9
52			252	0.79	0.193	2.3	2.5
53			377	0.80	0.193	1.8	3.4
54			377	1.15	0.279	2.0	4.2
55			402	0.55	0.132	1.5	2.3
56			300	0.56	0.135	1.8	2.2
57			294	0.86	0.207	2.0	2.6
58			294	1.19	0.287	2.3	3.3
59	1.52	23.1	339	0.61	0.161	-	3.8
60		23.8	450	0.63	0.163	-	4.1
61		21.2	342	0.52	0.113	-	3.1
62	1.32	16.3	159	0.70	0.105	1.6	1.2
63			159	1.03	0.152	1.9	1.3
64		13.4	159	1.45	0.213	2.0	1.5
65		15.6	159	1.89	0.273	2.0	1.8
66			270	1.89	0.273	1.3	2.4
67			270	1.41	0.204	1.0	1.9
68			288	0.96	0.139	0.9	1.6
69			288	0.57	0.083	0.8	1.4
70		22.2	359	0.37	0.080	1.3	1.9
71			359	0.65	0.141	1.9	2.6
72			359	1.03	0.221	2.0	2.9
73			359	1.69	0.358	2.3	4.0
74	1.49	26.4	359	1.33	0.369	2.5	3.9
75			359	0.80	0.220	2.4	3.1
76			431	0.80	0.220	2.4	3.4

**CONFIDENTIAL**

**CONFIDENTIAL**

ASD-TDR-63-665, Part I

TABLE 32

SERIES C

<u>Run</u>	<u><math>\bar{P}_v</math></u>	<u><math>\bar{V}_s</math></u>	<u><math>N_g</math></u>	<u><math>L/V</math></u>	<u><math>\bar{Q}_L</math></u>	<u><math>h_f</math></u>	<u><math>\Delta P_T</math></u>
1	1.67	8.20	52	0.57	0.055	1.9	0.3
2			52	1.03	0.099	2.1	0.4
3			52	1.43	0.138	2.4	0.4
4			117	0.57	0.055	1.0	0.5
5			117	1.01	0.098	1.4	0.7
6			117	1.74	0.168	1.6	1.0
7		11.7	183	0.57	0.077	1.6	1.1
8			183	0.82	0.113	1.8	1.2
9			183	1.46	0.202	2.0	1.5
10			264	1.46	0.201	1.8	1.9
11			264	2.0	0.276	1.8	2.0
12			264	0.88	0.121	1.4	1.3
13			264	0.47	0.065	1.3	1.0
14		16.1	359	1.43	0.276	2.1	2.9
15			359	0.99	0.190	2.0	2.5
16			359	0.64	0.124	2.0	2.0
17			454	1.43	0.276	1.8	3.2
18			454	1.00	0.193	1.6	2.7
19			454	0.74	0.143	1.5	2.2
20	1.44	19.0	462	1.43	0.276	1.9	2.8
21			462	1.00	0.193	1.8	2.1
22			462	0.71	0.138	1.8	2.0
23	1.34	15.0	264	0.94	0.135	1.8	1.3
24			264	1.61	0.226	1.9	1.8
25			264	0.67	0.094	1.6	1.1
26	2.25	5.25	29	0.63	0.052	1.5	0.4
27			29	1.08	0.091	2.3	0.5
28			90	0.66	0.056	0.8	0.6
29			90	0.95	0.079	0.8	0.6
30			90	1.4	0.118	1.3	0.7
31			164	1.47	0.124	0.8	0.8
32			164	6.67	0.563	1.0	1.2
33		7.96	164	0.96	0.124	1.4	1.3
34			164	1.52	0.197	1.8	1.7
35			164	0.62	0.080	1.3	1.0
36			117	0.61	0.079	1.5	0.8
37			117	0.87	0.112	1.6	1.0

**CONFIDENTIAL**

**CONFIDENTIAL**

ASD-TDR-63-665, Part I

TABLE 32 (Cont'd.)

Run	$\bar{P}_v$	$\bar{V}_s$	$N_q$	$L/V$	$\bar{Q}_L$	$h_f$	$\Delta P_T$
38	2.25	7.96	117	1.51	0.191	2.1	1.3
39		11.25	264	0.49	0.090	1.8	2.7
40			264	0.77	0.140	1.9	2.1
41			264	1.00	0.182	2.0	2.4
42			264	1.34	0.244	2.3	2.9
43			359	1.68	0.311	1.8	3.6
44			359	0.95	0.177	1.5	2.7
45			359	0.62	0.112	1.4	2.0
46			454	0.65	0.121	1.1	1.9
47			454	0.98	0.182	1.3	2.4
48			454	1.49	0.281	1.4	2.9
49		14.00	394	0.46	0.108	2.0	2.3
50			394	0.96	0.224	2.0	3.2
51			394	1.47	0.342	2.0	3.7
52			454	1.51	0.350	1.8	3.6
53			454	1.05	0.241	1.6	3.4
54			454	0.62	0.143	1.5	2.2
55			454	0.43	0.098	1.0	2.0
56			326	0.68	0.157	2.1	2.2
57	2.86	11.03	209	0.50	0.112	1.9	1.4
58			209	0.85	0.193	2.3	2.3
59			326	0.85	0.194	1.4	2.5
60			326	0.50	0.114	1.3	1.7
61			413	0.59	0.145	2.0	2.2
62		13.43	413	1.11	0.250	2.0	3.2

63 ASRP-2391

**CONFIDENTIAL**

**CONFIDENTIAL**

ASD-TDR-63-665, Part I

TABLE 33

SERIES D

<u>Run</u>	<u><math>\bar{p}_v</math></u>	<u><math>\bar{V}_s</math></u>	<u><math>N_q</math></u>	<u><math>L/V</math></u>	<u><math>\bar{Q}_L</math></u>	<u><math>h_f</math></u>	<u><math>\Delta P_T</math></u>
1	1.38	10.01	117	1.27	0.122	1.4	0.7
2				0.86	0.082	1.3	0.6
3				1.86	0.178	1.8	1.0
4			183	1.03	0.099	0.8	0.8
5				1.51	0.145	0.9	0.9
6				2.37	0.228	1.3	1.1
7		13.83	250	1.10	0.151	1.4	1.2
8				1.41	0.189	1.5	1.4
9				1.94	0.266	1.8	1.8
10			326	0.96	0.131	1.0	1.3
11				1.52	0.208	1.1	1.6
12				2.10	0.288	1.4	1.9
13	1.49	17.78	394	0.87	0.161	1.8	2.2
14				1.09	0.202	1.9	2.3
15				1.53	0.284	2.0	2.8
16			462	1.53	0.284	1.6	2.6
17			462	0.99	0.183	1.4	2.0
18	2.26	10.29	198	0.62	0.103	1.5	0.9
19				0.90	0.151	1.5	1.1
20				1.22	0.204	1.9	1.5
21				1.75	0.294	1.9	1.8
22			264	1.75	0.294	1.4	1.4
23			264	2.00	0.168	0.8	0.8
24			138	1.00	0.168	2.0	1.0
25			138	0.67	0.112	1.9	0.8

63 ASRP-2391

**CONFIDENTIAL**

**CONFIDENTIAL**

ASD-TDR-63-665, Part I

TABLE 34

SERIES E

<u>Run</u>	<u><math>P_v</math></u>	<u><math>\bar{V}_s</math></u>	<u><math>N_g</math></u>	<u><math>L/V</math></u>	<u><math>\bar{Q}_L</math></u>	<u><math>h_f</math></u>	<u><math>\Delta P_T</math></u>
1	1.67	7.76	90		0.116	1.7	0.1
2					0.157	2.0	0.1
3					0.237	2.0	0.1
4					0.330	2.3	0.3
5					0.392	2.7	0.4
6			160		0.091	-	0.1
7			160		0.162	1.5	0.2
8		18.38	469		0.029	2.0	1.2
9			469		0.316	2.5	1.3
10			264		0.148	1.5	0.6
11		13.85			0.206	2.0	0.6
12					0.288	2.5	0.6
13			359		0.288	1.8	0.7
14					0.192	1.5	0.9
15					0.140	1.5	0.9
16		10.18	138		0.124	2.5	0.2
17					0.184	2.0	0.3
18					0.256	2.0	0.4
19			236		0.162	1.3	0.5
20					0.242	1.5	0.4
21					0.352	1.5	0.5
22			359		0.440	1.0	0.6
23					0.250	0.7	0.8
24					0.343	1.0	0.7
25	2.27	9.51	102		0.140	1.8	0.4
26					0.198	2.2	0.5
27					0.319	3.0	1.5
28			160		0.325	2.0	0.6
29			160		0.161	1.3	0.4

63 ASRP-2391

**CONFIDENTIAL**

**CONFIDENTIAL**

ASD-TDR-63-665, Part I

TABLE 35

SERIES F

Run	$\bar{P}_v$	$\bar{V}_s$	$N_q$	$L/V$	$\bar{Q}_L$	$h_f$	$\Delta P_T$
1	1.47	7.07	52.2	0.62	0.057	2.0	0.3
2				0.85	0.079	2.1	0.4
3				1.18	0.109	2.3	0.5
4				1.50	0.139	2.5	0.5
5			81.5	1.50	0.139	1.3	0.4
6				1.18	0.109	1.5	0.4
7			117	0.91	0.085	0.6	0.4
8				1.18	0.109	0.8	0.5
9				1.53	0.142	0.9	0.5
10				1.85	0.172	1.1	0.6
11		9.34	183	0.67	0.085	1.4	0.4
12				0.96	0.120	1.4	0.6
13				1.41	0.178	1.6	0.7
14				1.76	0.221	1.8	0.9
15			236	1.76	0.221	1.1	0.8
16				1.39	0.175	1.0	0.7
17				1.00	0.123	1.0	0.6
18			294	1.02	0.126	0.6	0.5
19				1.38	0.169	0.8	0.7
20				1.93	0.238	0.9	0.8
21		12.2	264	0.77	0.125	1.8	0.7
22				1.00	0.164	1.9	0.8
23				1.47	0.240	2.0	1.1
24				1.92	0.314	2.0	1.3
25			326	1.92	0.314	1.6	1.4
26				1.25	0.205	1.6	0.9
27				0.97	0.152	1.5	0.7
28			394	0.80	0.131	0.9	0.8
29				1.02	0.166	1.3	0.7
30				1.48	0.243	1.4	1.1
31				2.00	0.327	1.4	1.3
32			462	2.00	0.327	1.1	1.4
33			387	1.27	0.207	1.1	1.0
34			469	0.90	0.147	1.0	1.3
35		15.4		1.09	0.232	1.8	1.6
36				1.35	0.286	1.9	1.7

**CONFIDENTIAL**

**CONFIDENTIAL**

ASD-TDR-63-665, Part I

TABLE 35 (Cont'd.)

Run	$\bar{P}_v$	$\bar{V}_s$	$N_g$	$L/V$	$\bar{Q}_L$	$h_f$	$\Delta P_T$
37	1.47	15.4	469	1.60	0.335	2.1	1.7
38	1.47	15.4	469	1.88	0.395	2.1	2.0
39	2.30	9.60	264	0.57	0.119	1.8	0.7
40				0.82	0.173	1.8	1.1
41				1.11	0.232	1.9	1.2
42			↓	1.55	0.326	1.9	1.4
43			326	1.55	0.326	1.6	1.5
44			↓	1.12	0.235	1.5	1.3
45				0.80	0.167	1.4	1.2
46			↓	0.59	0.125	1.4	0.7
47			394	0.59	0.125	1.1	0.5
48			↓	1.22	0.255	1.4	1.4
49			↓	1.55	0.326	1.5	1.5
50			450	1.55	0.326	1.4	1.5
51			454	1.23	0.258	1.1	1.3
52			469	0.86	0.181	1.0	1.0
53			469	0.68	0.142	0.9	0.9
54		11.7	394	0.50	0.127	1.8	1.3
55		11.6	↓	1.00	0.246	1.8	1.2
56			↓	1.25	0.311	1.9	1.5
57			↓	1.72	0.438	2.1	1.7
58			454	1.72	0.438	1.8	1.8
59			454	1.00	0.254	1.5	1.4
60			469	0.69	0.175	1.5	0.8
61		6.60	117	0.55	0.076	1.0	0.2
62			↓	0.80	0.113	1.4	0.4
63				1.20	0.170	1.8	0.5
64			↓	2.00	0.283	2.0	0.6
65			160	2.00	0.283	1.5	0.6
66			↓	1.40	0.198	1.1	0.5
67			↓	1.00	0.142	0.9	0.3
68			209	1.00	0.142	0.6	0.3
69			↓	1.50	0.212	1.0	0.4
70			↓	2.00	0.283	1.3	0.5

63 ASRP-2391

**CONFIDENTIAL**

**CONFIDENTIAL**

ASD-TDR-63-665, Part I

TABLE 36

SERIES G

Run	$\bar{P}_v$	$\bar{V}_s$	$N_g$	$L/V$	$\bar{Q}_L$	$h_f$	$\Delta P_T$
1	1.37	7.92	81.5	0.71	0.069	2.0	0.5
2		↓		1.03	0.099	2.1	0.7
3		7.64		1.31	0.126	2.3	0.8
4		7.66		1.74	0.168	2.5	0.8
5		7.66		2.00	0.193	2.5	0.8
6		7.70	117	0.74	0.071	1.0	0.5
7		↓		1.00	0.96	1.1	0.6
8				1.31	0.127	1.3	0.7
9				1.69	0.162	1.4	0.7
10		↓		2.00	0.193	1.8	0.9
11		7.71	160	2.00	0.193	1.1	0.8
12		↓		1.54	0.149	1.0	0.7
13				1.00	0.096	0.6	0.5
14			209	1.03	0.099	0.4	0.5
15				1.46	0.140	0.5	0.6
16				1.86	0.179	0.8	0.6
17				2.11	0.204	0.9	0.6
18	1.47	10.2	394	0.60	0.082	1.8	1.3
19	↓	↓		1.90	0.123	1.9	1.6
20				1.24	0.170	2.0	2.0
21				1.48	0.203	2.3	2.1
22				2.10	0.288	2.3	2.2
23			469	2.00	0.274	2.0	2.2
24				1.48	0.203	1.8	2.1
25				1.00	0.137	1.6	1.8
26				0.74	0.101	1.5	1.5
27				0.58	0.079	1.5	1.4
28	2.90	8.41	209	0.44	0.064	1.8	0.5
29	↓	↓		0.82	0.119	1.9	1.1
30				1.20	0.174	2.0	2.6
31				1.64	0.238	2.0	1.7
32			264	1.66	0.241	1.6	1.6
33				1.20	0.174	1.5	1.3
34				0.80	0.116	1.3	0.9
35				0.60	0.087	1.1	0.8
36			326	0.80	0.116	1.0	0.8
37			↓	1.04	0.151	1.1	1.0

**CONFIDENTIAL**



# CONFIDENTIAL

ASD-TDR-63-665, Part I

TABLE 36 (Cont'd.)

Run	$\bar{p}_v$	$\bar{v}_s$	$N_q$	$L/V$	$\bar{Q}_L$	$h_f$	$\Delta P_T$
38	2.90	8.41	326	1.50	0.218	1.3	1.2
39	↓	↓	↓	2.00	0.291	1.4	1.5
40	↓	7.24	↓	0.51	0.105	1.8	0.8
41	2.85	7.36	↓	0.73	0.148	1.8	1.8
42	↓	↓	↓	1.00	0.203	2.0	2.2
43	↓	↓	↓	1.43	0.291	2.4	2.2
44	↓	↓	394	1.71	0.349	1.4	2.4
45	↓	↓	394	1.21	0.247	1.5	2.1
46	↓	↓	402	0.86	0.174	1.4	1.8
47	↓	↓	↓	0.57	0.116	1.4	0.9
48	2.26	4.65	117	0.77	0.077	1.4	0.8
49	2.27	4.63	↓	1.00	0.100	1.5	0.8
50	↓	↓	↓	1.29	0.129	1.6	0.9
51	2.28	4.62	↓	1.57	0.157	1.6	1.0
52	↓	↓	↓	2.00	0.200	1.6	1.0
53	↓	↓	66.0	2.00	0.200	2.3	0.8
54	↓	↓	↓	1.51	0.152	1.5	0.5
55	↓	↓	↓	1.14	0.114	1.5	0.4
56	2.31	6.48	264	0.60	0.085	1.5	1.3
57	↓	↓	↓	1.00	0.143	1.8	1.6
58	↓	↓	↓	1.44	0.205	1.9	2.0
59	↓	↓	↓	2.00	0.285	2.1	2.2
60	↓	↓	326	2.00	0.285	1.8	2.0
61	↓	↓	↓	1.40	0.200	1.6	1.7
62	↓	↓	↓	1.00	0.143	1.5	1.7
63	↓	↓	↓	0.54	0.077	1.3	1.2
64	↓	↓	394	0.56	0.080	0.9	1.0
65	↓	↓	↓	1.00	0.143	1.3	1.4
66	↓	↓	↓	1.40	0.200	1.5	1.5
67	↓	↓	↓	2.00	0.285	1.6	1.7
68	↓	↓	454	2.00	0.285	1.3	1.8
69	↓	↓	462	1.40	0.200	1.1	1.5
70	↓	↓	462	0.96	0.137	1.0	1.3
71	↓	9.07	454	0.59	0.117	1.8	1.9
72	↓	↓	↓	0.84	0.168	1.9	2.6
73	↓	↓	↓	1.04	0.208	2.1	2.7
74	↓	↓	↓	1.43	0.285	2.1	2.8

63 ASRP-2391

**CONFIDENTIAL**

ASD-TDR-63-665, Part I

TABLE 37

SERIES H

<u>Run</u>	<u><math>P_v</math></u>	<u><math>\bar{V}_s</math></u>	<u><math>N_g</math></u>	<u><math>L/V</math></u>	<u><math>\bar{Q}_L</math></u>	<u><math>h_f</math></u>	<u><math>\Delta P_T</math></u>
1	1.37	7.67	160	0.97	0.093	1.0	0.8
2	↓	↓	↓	1.37	0.131	1.1	0.9
3	↓	↓	↓	1.60	0.153	1.3	0.9
4	↓	↓	↓	2.00	0.192	1.4	1.1
5	↓	↓	209	2.00	0.192	0.9	0.9
6	↓	↓	↓	1.54	0.148	0.9	0.8
7	↓	↓	↓	1.29	0.123	0.8	0.8
8	↓	↓	↓	1.00	0.096	0.5	0.5
9	↓	↓	117	1.00	0.096	1.8	0.7
10	↓	↓	↓	1.43	0.137	1.5	0.8
11	↓	↓	↓	1.74	0.167	1.5	0.9
12	↓	↓	↓	2.00	0.192	1.8	0.9
13	1.39	10.8	264	1.00	0.137	1.8	1.3
14	↓	↓	↓	1.30	0.178	1.5	1.5
15	↓	↓	↓	1.54	0.211	1.6	1.7
16	↓	↓	↓	2.00	0.273	1.8	1.9
17	↓	↓	326	2.00	0.273	1.5	1.7
18	↓	↓	326	1.32	0.180	1.4	1.4
19	1.45	10.4	326	1.00	0.137	1.5	1.2
20	↓	↓	394	1.00	0.137	1.0	1.1
21	↓	↓	↓	1.44	0.197	1.3	1.4
22	↓	↓	↓	2.00	0.273	1.4	1.7
23	↓	↓	469	2.00	0.273	0.8	1.7
24	↓	↓	↓	1.50	0.205	0.8	1.5
25	↓	↓	↓	1.00	0.137	0.6	1.1
26	1.54	13.7	↓	1.79	0.342	1.9	3.0
27	↓	↓	↓	1.29	0.246	1.9	2.3
28	↓	↓	↓	1.00	0.191	1.9	2.1
29	2.31	6.35	117	1.92	0.134	1.8	1.1
30	↓	↓	↓	1.00	0.134	1.5	1.0
31	↓	↓	↓	0.51	0.068	1.3	0.6

23 ASRP-2391

**CONFIDENTIAL**

**CONFIDENTIAL**

ASD-TDR-63-665, Part I

TABLE 38

SERIES S-A

Run	$\overline{p_v}$	$\overline{v_s}$	$N_a$	$h_f$	$\Delta P_T$
1	1.43	7.29	39	2.0	0.4
2			52	1.5	0.4
3			81	1.0	0.5
4			95	0.8	0.5
5			37	2.0	0.4
6			39	1.5	0.4
7			45	1.0	0.4
8			52	0.8	0.3
9			54	2.0	0.5
10			63	1.5	0.6
11			81	1.0	0.6
12			98	0.8	0.6
13		9.36	78	2.0	0.5
14			98	1.5	0.5
15			121	1.0	0.5
16			164	0.8	0.5
17			84	2.0	0.6
18			102	1.5	0.6
19			142	1.0	0.7
20			178	0.8	0.6
21			98	2.0	0.7
22			121	1.5	0.7
23			164	1.0	0.8
24			222	0.8	0.6
25			113	2.0	0.7
26			138	1.5	0.8
27			196	1.0	0.8
28			270	0.8	0.9
29	1.44	11.4	98	2.0	0.6
30			117	1.5	0.6
31			142	1.0	0.6
32			209	0.8	0.6
33			146	2.0	0.7
34			171	1.5	0.7
35			209	1.0	0.6
36			282	0.8	0.7
37			183	2.0	0.9
38	1.46		222	1.5	0.8
39			310	1.0	1.1
40			377	0.8	1.1
41			196	2.0	1.0
42			235	1.5	1.1
43			326	1.0	1.1
44			401	0.8	1.3
45			209	2.0	1.2
46			252	1.5	1.2
47			342	1.0	1.2
48			431	0.8	1.2

63 ASRP-2391

**CONFIDENTIAL**

**CONFIDENTIAL**

ASD-TDR-63-665, Part I

TABLE 38 (Cont'd)

Run	SERIES S-A				
	$\overline{p_v}$	$\overline{V_p}$	$N_g$	$h_f$	$\Delta P_T$
49	1.46	13.4	161	2.0	0.8
50			247	1.0	0.7
51			310	0.8	0.8
52			178	1.5	0.6
53			209	2.0	0.9
54			279	1.5	0.9
55	1.52	12.7	252	2.0	1.2
56			294	2.0	1.8
57			359	2.0	2.6
58			359	1.5	1.6
59			294	1.5	1.2
60			235	1.5	0.8
61			294	1.0	0.8
62			52	-	0.6
63			294	2.0	1.2
64			326	2.0	1.4
65	1.57	14.4	359	2.0	2.1
66			394	2.0	2.1
67			454	2.0	3.0
68			454	1.5	1.8
69			394	1.5	1.2
70			359	1.5	1.1
71			209	2.0	1.1
72			235	2.0	1.2
73			264	2.0	1.5
74			294	2.0	1.9
75	2.28	10.6	326	2.0	1.9
76			359	2.0	2.7
77			359	1.5	1.7
78			326	1.5	1.0
79			294	1.5	1.0
80			359	1.0	1.0
81			431	1.0	1.2
82			81	2.0	0.6
83			98	2.0	0.7
84			117	2.0	0.9
85	2.25	6.54	138	2.0	1.2
86			160	2.0	1.4
87			160	1.5	1.0
88			138	1.5	0.8
89			117	1.5	0.6
90			98	1.5	0.5
91			81	1.5	0.4
92			81	0.8	0.3
93			98	0.8	0.3
94			117	0.8	0.4
95	2.25		138	0.8	0.5
96			160	0.8	0.7
97			264	0.8	0.9

63 ASRP-2391

**CONFIDENTIAL**

**CONFIDENTIAL**

ASD-TDR-63-665, Part I

TABLE 39

SERIES 8-B

<u>Run</u>	<u><math>\rho_v</math></u>	<u><math>V_a</math></u>	<u><math>N_g</math></u>	<u><math>h_f</math></u>	<u><math>\Delta P_T</math></u>	<u><math>Q_L</math></u>
1	1.43	8.41	58	2.0	0.3	0.013
2			73	2.0	0.6	0.055
3			89	2.0	0.7	0.085
4			108	2.0	0.9	0.110
5			81	1.5	0.5	0.019
6			98	1.5	0.6	0.053
7			117	1.5	0.7	0.074
8			117	1.0	0.5	0.009
9			138	1.0	0.5	0.026
10			160	1.0	0.7	0.056
11			160	0.8	0.5	0.016
12			183	0.8	0.6	0.028
13			209	0.8	0.7	0.049
14	1.45	11.4	160	2.0	0.7	0.012
15			183	2.0	1.0	0.047
16			209	2.0	1.2	0.088
17			235	2.0	1.6	0.143
18			235	1.5	1.1	0.052
19			209	1.5	0.7	0.017
20			183	1.5	0.6	-
21			160	1.5	0.4	-
22			160	1.0	0.4	-
23			183	1.0	0.5	-
24			209	1.0	0.5	-
25			235	1.0	0.7	0.012
26			264	1.0	0.7	0.016
27			294	1.0	0.8	0.023
28			326	1.0	1.0	0.027
29			394	1.0	1.1	0.085
30			469	1.0	1.6	0.143
31			326	1.5	1.7	0.143
32			279	1.5	1.9	0.099
33			394	1.5	1.9	0.248
34			264	2.0	1.7	0.168
35			294	2.0	2.1	0.248
36		14.5	209	2.0	0.6	0.010
37			249	2.0	1.3	0.018
38			279	2.0	1.5	0.041
39			310	2.0	1.4	0.062
40			342	2.0	1.6	0.066
41			377	2.0	2.1	0.149
42			412	2.0	2.6	0.228
43			423	1.5	1.7	0.080

63 ASRP-2391

**CONFIDENTIAL**

**CONFIDENTIAL**

ASD-TDR-63-665, Part I

TABLE 39 (Cont'd)

SERIES S-B

Run	$\overline{v_v}$	$\overline{v_a}$	$N_g$	$h_f$	$\Delta P_T$	$\overline{Q_L}$
44	1.45	14.5	394	1.5	1.4	0.054
45	1.45	14.5	377	1.5	1.1	0.039
46	2.32	9.07	0	-	0.2	-
47	↓	↓	183	2.0	0.8	0.021
48			209	2.0	1.1	0.062
49			235	2.0	1.5	0.102
50			264	2.0	1.8	0.179
51			294	2.0	2.1	0.275
52			294	1.5	1.6	0.125
53			264	1.5	1.3	0.056
54			235	1.5	0.9	0.035
55			209	1.5	0.7	0.021
56			235	1.0	0.7	0.015
57			264	1.0	1.0	0.032
58			294	1.0	1.0	0.035
59			326	1.0	1.3	0.064
60			359	1.0	1.5	0.088
61			394	1.0	1.6	0.114
62			431	1.0	1.8	0.142
63			394	1.5	2.1	0.305
64			359	1.5	2.0	0.204
65			326	1.5	1.9	0.182
66	2.38	11.1	326	2.0	1.1	0.016
67	↓	↓	359	2.0	1.2	0.028
68			394	2.0	1.9	0.085
69			450	2.0	3.0	0.264
70			326	1.5	0.9	0.015
71			359	1.5	0.9	0.016
72	2.32	6.45	84	2.0	0.5	0.060
73	↓	↓	98	2.0	0.7	0.088
74			117	2.0	0.9	0.148
75			138	2.0	1.1	0.236
76			81	1.5	0.3	0.027
77			98	1.5	0.6	0.057
78			117	1.5	0.8	0.082
79			138	1.5	0.9	0.122
80			160	1.5	1.0	0.173
81			183	1.5	1.2	0.284
82			235	1.0	1.1	0.284
83			209	1.0	1.0	0.187
84			183	1.0	0.9	0.097
85			160	1.0	0.7	0.054
86			138	1.0	0.5	0.028
87			117	1.0	0.4	0.011

63 ASRP-2391

**CONFIDENTIAL**

**CONFIDENTIAL**

ASD-TDR-63-665, Part I

TABLE 40

Run	SERIES 8-C					
	$\bar{a}_v$	$\bar{V}_s$	$N_g$	$h_f$	$\Delta p_T$	$Q_L$
1	1.64	13.1	49	-	1.1	
2			200	1.6	1.4	0.0033
3			225	1.6	1.4	
4			253	1.5	1.5	
5			281	1.3	1.4	
6			312	1.0	1.5	
7			377	0.8	1.4	
8			377	1.5	2.2	0.033
9			344	1.8	2.2	
10			312	2.0	2.2	
11			412	1.4	2.3	
12			412	1.6	2.8	0.072
13			377	1.8	2.6	
14			344	2.1	2.8	
15			312	2.2	2.7	
16			344	2.4	3.4	0.137
17			377	2.1	3.4	
18			412	1.8	3.4	
19			412	2.0	3.5	0.216
20			449	1.8	3.4	
21			377	2.4	4.1	
22	1.64	10.2	49	-	0.5	
23			112	2.5	1.2	0.013
24			153	1.8	1.2	
25			200	1.5	1.2	
26			225	1.3	1.3	
27			253	1.1	1.3	
28			281	1.0	1.3	
29			175	2.4	1.8	0.052
30			200	2.0	1.7	
31			225	1.8	1.8	
32			253	1.6	1.8	
33			281	1.3	1.8	
34			312	1.1	1.7	
35			200	2.4	2.2	0.104
36			225	2.1	2.2	
37			253	1.8	2.2	
38			281	1.5	2.1	
39			312	1.3	2.2	
40			344	1.3	2.2	
41			377	1.0	2.1	
42			225	2.3	2.6	0.166
43			281	1.8	2.5	
44			312	1.5	2.5	
45			377	1.3	2.2	
46			253	2.4	2.8	0.228
47			312	1.6	2.7	
48			377	1.4	2.3	
49			449	1.1	-	
50			281	2.0	3.1	0.333
51			344	1.8	2.9	
52			377	1.5	2.8	
53			449	1.3	-	
54	1.64	7.83	49	-	0.3	

**CONFIDENTIAL**

**CONFIDENTIAL**

ASD-TDR-63-665, Part I

TABLE 40 (Cont'd)

SERIES B-C						
Run	$\rho_v$	$V_s$	$N_g$	$h_f$	$\Delta P_r$	$Q_v$
55	1.63	7.83	78	2.0	0.8	0.023
56			94	1.6	0.8	
57			112	1.5	0.9	
58			132	1.3	0.9	
59			153	1.1	1.0	
60			112	1.8	1.1	0.068
61			132	1.5	1.1	
62			153	1.3	1.1	
63			175	1.0	1.2	
64			112	2.4	1.5	0.127
65			132	1.9	1.5	
66			153	1.6	1.4	
67			175	1.4	1.4	
68			200	1.3	1.4	
69			225	1.0	1.4	
70			132	2.3	1.8	0.189
71			153	1.9	1.7	
72			175	1.6	1.7	
73			200	1.4	1.5	
74			225	1.3	1.5	
75			253	1.0	1.5	
76	2.65	8.27	49	-	0.4	-
77			94	2.0	0.9	0.017
78			112	1.8	0.9	
79			132	1.4	1.0	
80			153	1.3	1.0	
81			175	1.0	1.1	
82			132	2.0	1.6	0.095
83			153	1.8	1.5	
84			175	1.5	1.6	
85			200	1.3	1.5	
86			225	1.0	1.5	
87			153	1.9	1.8	0.174
88			175	1.6	1.6	
89			200	1.4	1.7	
90			225	1.3	1.8	
91			253	1.1	1.9	
92			175	2.4	-	0.307
93			200	1.9	2.2	
94			225	1.5	2.1	
95			253	1.4	2.1	
96			281	1.3	2.1	
97	2.66	8.45	49	-	0.7	-
98			225	1.9	2.2	0.068
99			253	1.8	2.1	
100			281	1.5	2.1	
101			312	1.3	2.2	
102			253	2.4	3.1	0.181
103			281	1.9	3.0	
104			312	1.8	3.0	
105			377	1.4	3.0	
106			312	2.1	3.6	0.325
107			281	1.9	3.5	
108			431	1.4	-	
109	2.20	7.25	200	1.8	2.1	0.174
110	2.20	7.26	312	1.1	2.2	0.174

63 ASRP-2391

**CONFIDENTIAL**



**CONFIDENTIAL**

ASD-TDR-63-665, Part I

TABLE 41

SERIES S-D

Run	$\overline{v}_v$	$\overline{v}_s$	$N_g$	$h_f$	$\Delta P_T$	$\overline{Q}_L$
1	1.43	8.39	66	2.0	0.6	0.057
2			↓	1.5	0.3	0.025
3				1.0	0.3	0.012
4			81	0.8	0.3	0.012
5			↓	1.0	0.4	0.025
6				1.5	0.4	0.032
7			↓	2.0	0.6	0.083
8			98	2.0	0.9	0.146
9			↓	1.5	0.6	0.070
10				1.0	0.5	0.183
11			↓	0.8	0.4	0.012
12			117	0.8	0.5	0.027
13			↓	1.0	0.6	0.042
14				1.5	0.7	0.099
15			↓	2.0	0.9	0.196
16			138	1.8	0.9	0.250
17			↓	1.5	0.9	0.183
18				1.0	0.6	0.063
19			↓	0.8	0.5	0.037
20			160	0.8	0.6	0.055
21			↓	1.0	0.7	0.094
22				1.5	0.9	0.245
23	1.51	10.9	↓	2.0	1.1	0.060
24				1.5	0.6	0.151
25			↓	1.0	0.5	0.070
26			183	0.8	0.5	0.007
27			↓	1.0	0.6	0.012
28				1.5	0.7	0.027
29			↓	2.0	1.0	0.065
30			209	2.0	1.4	0.151
31			↓	1.5	1.0	0.070
32				1.0	0.7	0.044
33			↓	0.8	0.5	0.012
34			235	0.8	0.6	0.020
35			↓	1.0	0.8	0.047
36				0.8	0.6	0.015
37			264	0.8	0.7	0.027
38			↓	1.0	1.0	0.063
39				1.5	1.3	0.104
40			↓	2.0	1.7	0.235
41	1.64	12.8	325	1.0	0.7	0.010

**CONFIDENTIAL**

~~CONFIDENTIAL~~

ASD-TDR-63-665, Part I

TABLE 41 (Cont'd.)

SERIES S-D

Run	$\rho_v$	$\frac{V}{s}$	$N_g$	$h_f$	$\Delta P_r$	$\frac{Q}{L}$
42	1.64	12.8	326	1.5	1.1	0.055
43				2.0	1.5	0.091
44			↓	2.3	2.3	0.211
45			359	2.0	3.1	0.182
46			↓	1.5	1.4	0.065
47			394	1.5	1.6	0.091
48			↓	1.8	1.9	0.148
49			↓	2.0	2.3	0.307
50			469	1.8	2.4	0.307
51			↓	1.5	2.2	0.182
52			↓	1.1	1.6	0.091
53	2.32	10.3	294	1.0	1.2	0.039
54			↓	1.5	1.4	0.053
55			↓	2.0	2.1	0.114
56			294	2.3	2.1	0.177
57			326	2.0	2.3	0.278
58			↓	1.5	2.1	0.187
59			↓	1.0	1.5	0.076
60			↓	0.8	1.3	0.048
61			359	0.8	1.2	0.048
62			↓	1.0	1.3	0.053
63			↓	1.5	1.9	0.129
64			↓	2.0	2.2	0.304
65			394	2.0	2.5	0.380
66			↓	1.5	2.1	0.253
67			↓	1.0	1.6	0.104
68			↓	0.8	1.2	0.053
69	2.25	6.66	81	2.0	0.7	0.114
70			↓	1.5	0.5	0.066
71			↓	1.0	0.3	0.036
72			117	0.8	0.4	0.036
73			↓	1.0	0.6	0.061
74			↓	1.5	0.8	0.170
75			↓	2.0	0.9	0.253
76			160	1.5	1.0	0.253
77			↓	1.0	0.9	0.177
78			↓	0.8	0.7	0.063
79			98	2.0	0.8	0.127
80			160	1.0	0.8	0.127
81			209	0.8	0.9	0.127
82			326	0.5	1.0	0.127
83			469	0.3	1.2	0.127

~~CONFIDENTIAL~~

**CONFIDENTIAL**

ASD-TDR-63-665, Part I

**TABLE 42**

**SERIES S-E**

Run	$\rho_v$	$V_s$	$N_g$	$h_f$	$\Delta T$	$\bar{Q}_L$
1	1.67	9.49	112	1.8	1.1	0.085
2			132	1.5	1.1	
3			153	1.3	1.1	
4			175	1.1	1.2	
5			200	1.0	1.2	
6			132	1.8	1.2	0.125
7			153	1.5	1.3	
8			175	1.3	1.4	
9			200	1.1	1.4	
10			225	1.0	1.5	
11			153	2.1	1.9	0.217
12			175	1.8	1.8	
13			200	1.5	1.7	
14			225	1.3	1.7	
15			253	1.1	1.7	
16			312	1.0	1.9	
17	1.70	12.2	200	2.0	1.6	0.088
18			225	1.9	1.7	
19			253	1.6	1.8	
20			281	1.4	1.8	
21			312	1.3	1.9	
22			200	2.1	1.9	0.164
23			225	1.9	1.9	
24			253	1.6	2.1	
25			281	1.5	2.1	
26			312	1.4	2.2	
27			344	1.3	2.3	
28			253	2.3	2.9	0.255
29			281	1.9	2.8	
30			312	1.8	2.8	
31			344	1.6	2.7	
32			377	1.4	2.6	
33			449	1.3	-	
34	1.69	15.2	395	1.8	2.8	0.105
35			449	1.4	-	
36			395	1.8	3.0	0.200
37			412	1.5	3.0	
38			449	1.5	-	
39	2.71	6.46	64	1.8	0.7	0.076
40			78	1.5	0.7	
41			94	1.3	0.8	
42			112	1.0	0.9	
43			132	0.9	1.0	
44			225	0.5	1.2	

63 ASRP-2391

**CONFIDENTIAL**

**CONFIDENTIAL**

ASD-TDR-63-868, Part I

TABLE 42 (Cont'd.)

SERIES B-E

Run	$\overline{p}_v$	$\overline{V}_s$	$N_g$	$h_f$	$\Delta P_T$	$\overline{Q}_L$
45	2.71	6.46	78	1.9	0.9	0.144
46			94	1.5	1.0	
47			112	1.3	1.1	
48			132	1.1	1.1	
49			153	1.0	1.2	
50			132	1.8	1.6	0.240
51			183	1.8	1.6	
52			178	1.3	1.6	
53			200	1.0	1.5	
54		9.50	175	1.9	1.8	0.152
55			200	1.6	1.8	
56			225	1.5	1.9	
57			253	1.4	2.0	
58			281	1.3	2.1	
59			312	1.1	2.2	
60			200	2.1	2.5	0.243
61			225	1.8	2.4	
62			253	1.6	2.3	
63			281	1.4	2.3	
64			312	1.3	2.4	
65			344	1.1	2.5	
66	3.74	4.68	49	1.8	0.7	0.090
67			64	1.5	0.7	
68			78	1.3	0.7	
69			94	1.0	0.9	
70			112	1.1	0.9	
71			153	0.8	1.0	
72			64	1.9	0.9	0.181
73			78	1.5	0.8	
74			94	1.3	1.0	
75			112	1.1	1.0	
76			132	1.0	1.1	
77			153	0.8	1.2	
78			175	0.6	1.1	
79			94	2.3	1.7	0.237
80			112	1.9	1.6	
81			132	1.5	1.4	
82			153	1.3	1.5	
83			175	1.0	1.4	
84	3.73	7.11	183	2.3	2.0	0.232
85			175	1.8	2.0	
86			200	1.6	2.0	
87			225	1.4	2.0	
88			253	1.3	2.1	
89			281	1.1	2.1	

**CONFIDENTIAL**

CONFIDENTIAL

ASD-TDR-63-665, Part I

TABLE 43

SERIES S-F

Run	$\overline{D}_v$	$\overline{V}_s$	$N_a$	$h_f$	$\Delta P_T$	$\overline{Q}_L$
1	1.66	9.75	132	1.8	1.7	0.079
2	↓	↓	153	1.6	1.8	↓
3			175	1.5	1.8	
4			200	1.4	1.8	
5			225	1.3	1.9	
6			153	1.8	1.9	
7			175	1.5	2.0	
8			200	1.4	1.9	
9			225	1.3	2.0	
10			253	1.3	2.1	
11			153	1.8	2.0	0.177
12	↓	↓	175	1.5	2.0	↓
13			200	1.4	2.0	
14			225	1.3	2.0	
15			253	1.1	2.1	
16			253	1.9	3.1	
17			281	1.8	3.2	
18			312	1.8	3.3	
19			344	1.5	3.3	
20			377	1.3	3.3	
21			281	1.9	3.3	0.164
22	↓	↓	312	1.6	3.4	↓
23			344	1.5	3.4	
24			377	1.4	3.3	
25			449	1.4	-	
26			312	1.6	3.7	
27			344	1.4	3.6	
28			377	1.3	-	
29			449	1.1	-	
30			49	-	2.0	
31			377	2.0	4.9	0.210
32	↓	↓	412	1.9	5.3	↓
33			449	1.9	-	
34			412	1.8	3.3	
35			49	-	1.0	
36	2.58	7.13	78	2.0	1.2	0.076

63 ASRP-2391

CONFIDENTIAL

**CONFIDENTIAL**

ASD-TDR-63-665, Part I

TABLE 43 (Cont'd)

SERIES S-F

<u>Run</u>	<u><math>\rho_v</math></u>	<u><math>V_B</math></u>	<u><math>N_G</math></u>	<u><math>h_f</math></u>	<u><math>\Delta P_T</math></u>	<u><math>Q_L</math></u>
37	2.58	7.13	94	1.8	1.3	0.076
38			112	1.5	1.3	
39			132	1.4	1.4	
40			153	1.3	1.4	
41			94	1.9	1.5	0.146
42			112	1.8	1.5	
43			132	1.5	1.5	
44			153	1.3	1.6	
45			175	1.0	1.7	
46			132	1.8	2.0	0.212
47			153	1.5	1.9	
48			175	1.3	1.8	
49			200	1.0	1.8	
50			50	-	2.0	-
51			253	-	1.8	-
52	2.61	11.2	253	2.0	4.0	0.232
53			281	1.8	3.9	
54			312	1.6	4.0	
55			344	1.5	3.9	
56			377	1.4	4.1	
57			449	1.3	-	
58	3.55	5.16	64	1.9	1.0	0.152
59			78	1.5	1.0	
60			94	1.3	1.1	
61			112	1.0	1.2	
62			132	0.9	1.2	
63			94	1.5	1.4	0.188
64			281	0.8	1.5	
65	3.60	7.29	153	2.1	2.6	0.219
66			175	1.8	2.6	
67			200	1.5	2.6	
68			225	1.4	2.6	
69			253	1.3	2.8	
70			253	1.8	5.0	0.288

**CONFIDENTIAL**

~~CONFIDENTIAL~~

ASD-TDR-63-665, Part I

TABLE 44

SERIES M-A

<u>Run</u>	<u>PV</u>	<u>PL</u>	<u>N<sub>G</sub></u>	<u>h<sub>f</sub></u>	<u>V<sub>a</sub></u>	<u>Q<sub>L</sub></u>	<u>L/V</u>	<u>ΔP<sub>T</sub></u>
1	1.65	88.6	386	1.9	14.7	0.133	0.74	2.3
2	1.69	88.7	386	2.1	14.4	0.179	1.00	2.6
3	1.69	88.7	386	2.3	14.4	0.206	1.15	2.7
4	1.72	88.4	459	1.8	14.2	0.207	1.15	2.9
5	1.72	88.4	459	1.8	14.2	0.179	1.00	2.9
6	1.70	88.4	459	1.6	14.3	0.132	0.74	2.5
7	1.54	88.8	288	1.	12.1	0.068	0.50	1.2
8	1.58	88.9	288	1.6	11.8	0.137	1.0	1.7
9	1.57	88.8	288	1.8	11.9	0.206	1.5	1.9
10	1.57	89.2	319	1.4	11.9	0.137	1.0	1.7
11	1.57	89.2	352	1.3	11.9	0.137	1.0	1.8
12	1.57	89.2	386	1.3	11.9	0.137	1.0	1.8
13	1.57	89.2	459	1.1	11.9	0.137	1.0	1.8
14	1.57	89.0	258	1.8	11.9	0.137	1.0	1.6
15	1.57	89.0	231	2.0	11.9	0.137	1.0	1.4
16	1.42	89.3	51	1.6	7.85	0.081	1.0	0.6
17	1.42	89.2	96	1.3	7.84	0.082	1.0	0.6
18	1.42	89.2	115	1.1	7.85	0.082	1.0	0.6
19	1.42	89.2	156	1.0	7.85	0.082	1.0	0.8

CONFIDENTIAL

**CONFIDENTIAL**

ASD-TDR-63-665, Part I

TABLE 45

SERIES M-B

Run	$\pi$	$\rho_v$	$\rho_L$	$N_g$	$h_f$	$\bar{V}_s$	$\bar{Q}_L$	$L/V$	$\bar{E}_{mv}$	$(NTU)_g$	$\Delta P_T$
1	4.5	1.9	86.2	65	1.2	5.32	0.083	1.0	0.843	1.843	0.5
2	4.5	1.9	86.0	39	1.5	5.32	0.083	1.0	0.911	2.428	0.4
3	5.1	2.2	85.5	319	1.6	11.6	0.199	1.0	0.575	0.856	2.2
4	5.1	2.2	85.1	386	1.4	11.6	0.200	1.0	0.517	0.728	2.2
5	5.1	2.2	85.3	258	2.0	11.7	0.199	1.0	0.700	1.206	2.0
6	5.1	2.2	85.4	96	2.0	8.15	0.141	1.0	0.804	1.63	0.9
7	5.0	2.2	85.4	141	1.6	8.15	0.140	1.0	0.820	1.716	1.0
8	5.1	2.2	85.5	422	2.0	13.7	0.228	1.0	0.673	1.118	2.8
9	7.8	3.3	80.7	231	2.0	8.91	0.241	1.0	0.637	1.014	1.7
10	7.8	3.3	80.7	386	1.5	9.01	0.243	1.0	0.337	0.411	1.0
11	6.4	2.8	83.2	44	1.7	5.21	0.113	1.0	0.686	1.161	0.3
12	6.5	2.8	83.0	131	1.7	7.93	0.175	1.0	0.672	1.114	1.0
13	6.5	2.8	83.0	100	2.2	7.93	0.174	1.0	0.706	1.226	0.9
14	6.6	2.8	83.0	261	2.1	11.8	0.259	1.0	0.483	0.659	2.0

TABLE 46

SERIES M-C

Run	$\pi$	$\rho_v$	$\rho_L$	$N_g$	$h_f$	$\bar{V}_s$	$\bar{Q}_L$	$L/V$	$\bar{E}_{mv}$	$(NTU)_g$	$\Delta P_T$
1	5.08	2.22	85.4	51	0.9	4.31	0.113	1.0	0.245	0.281	0.23
2	5.08	2.21	85.2	36	1.8	4.25	0.114	1.0	0.402	0.515	0.23
3	5.20	2.26	85.3	155	1.9	7.47	0.199	1.0	0.376	0.472	0.67
4	5.03	2.20	85.3	199	1.5	7.78	0.200	1.0	0.309	0.369	0.55
5	5.05	2.20	85.3	253	1.0	7.76	0.201	1.0	0.277	0.325	0.65
6	5.08	2.22	85.5	344	2.0	11.2	0.287	1.0	0.301	0.358	1.17
7	5.08	2.23	85.6	412	1.5	11.3	0.286	1.0	0.263	0.305	1.25
8	6.51	2.79	82.9	74	2.0	5.21	0.174	1.0	0.425	0.553	0.25
9	6.65	2.85	82.9	201	1.8	8.52	0.288	1.0	0.408	0.524	1.20

63 ASRP-2391

**CONFIDENTIAL**



CONFIDENTIAL

ASD-TDR-63-665, Part I

TABLE 47

SERIES M-D

Run	$\overline{P}$	$\overline{p_v}$	$\overline{p_L}$	$N_g$	$h_f$	$\overline{V_s}$	$\overline{Q_L}$	$L/v$	$\overline{E_{mv}}$	$\overline{(NTU)}_g$	$\Delta P_T$
1	5.09	2.20	85.2	156	2.0	9.85	0.166	1.0	0.706	1.227	1.48
2	5.10	2.20	85.2	204	1.5	9.91	0.168	1.0	0.632	1.000	1.45
3	5.00	2.17	85.2	459	1.3	12.6	0.210	1.0	0.533	0.762	2.35
4	5.01	2.17	85.3	386	1.6	12.8	0.211	1.0	0.580	0.869	2.20
5	5.10	2.21	85.2	306	1.8	12.5	0.210	1.0	0.581	0.871	2.15
6	5.06	2.19	85.2	259	1.3	9.96	0.167	1.0	0.673	1.118	1.44
7	5.05	2.19	85.3	80	1.8	7.29	0.124	1.0	0.815	1.688	0.70
8	5.06	2.19	85.2	135	1.3	7.50	0.131	1.0	0.748	1.378	0.83
9	7.12	3.01	81.7	180	1.3	7.34	0.176	1.0	0.738	1.343	1.16
10	7.07	2.98	81.8	123	1.9	7.49	0.178	1.0	0.772	1.482	1.09
11	6.10	2.61	83.3	93	1.9	6.83	0.143	1.0	0.846	1.877	0.78
12	6.10	2.61	83.3	121	1.3	6.89	0.146	1.0	0.921	2.545	0.85
13	6.03	2.57	83.5	369	1.8	12.3	0.245	1.0	0.551	0.801	2.49
14	6.03	2.56	83.1	204	1.9	9.86	0.201	1.0	0.630	0.995	1.75
15	6.07	2.57	83.1	288	1.5	9.82	0.200	1.0	0.576	0.858	1.84
16	5.97	2.53	83.3	386	1.3	10.0	0.204	1.0	0.467	0.629	1.85
17	7.12	3.00	81.4	288	1.8	10.2	0.248	1.0	0.650	1.049	2.09
18	7.12	3.00	81.4	319	1.6	10.2	0.248	1.0	-	-	2.18

63 ASRP-2391

CONFIDENTIAL

**CONFIDENTIAL**

ASD-TDR-63-665, Part I

**TABLE 48**  
SERIES M-E

Run	P	$\overline{p_v}$	$\overline{p_L}$	$N_a$	$h_f$	$\overline{V_s}$	$\overline{Q_L}$	L/V	$\overline{E_{mv}}$	$(NTU)_a$	$AP_T$
1	5.00	2.16	85.0	175	1.9	10.7	0.173	1.0	0.532	0.759	1.31
2	5.05	2.18	85.0	225	1.6	10.6	0.173	1.0	0.515	0.724	1.32
3	5.05	2.19	85.2	200	1.9	10.5	0.173	1.0	0.748	1.379	1.30
4	5.05	2.19	85.2	253	1.3	10.5	0.173	1.0	-	-	1.39
5	5.05	2.20	85.3	282	1.3	10.8	0.175	1.0	0.474	0.643	1.44
6	5.08	2.19	85.1	223	1.8	10.5	0.269	1.65	0.845	-	1.63
7	5.08	2.19	85.1	315	1.9	13.2	0.218	1.0	0.509	0.713	2.22
8	5.08	2.18	85.1	381	1.6	13.1	0.215	1.0	0.461	0.618	2.04
9	5.08	2.18	85.1	449	1.4	13.1	0.215	1.0	-	-	1.80
10	5.03	2.18	85.3	91	1.8	7.76	0.123	1.0	0.643	1.032	0.83
11	5.08	2.20	84.6	112	1.4	7.87	0.132	1.0	0.652	1.066	0.68
12	5.10	2.19	84.6	121	1.8	7.77	0.212	1.76	-	-	1.08
13	-	2.25	85.4	181	1.4	7.82	0.214	1.67	-	-	0.93
14	-	2.25	85.4	174	1.3	7.82	0.214	1.67	-	-	0.91
15	-	2.25	85.4	198	1.1	7.82	0.214	1.67	-	-	1.0
16	-	2.25	85.4	251	1.0	7.82	0.214	1.67	-	-	1.1
17	-	2.69	83.3	198	1.6	10.4	0.104	0.51	-	-	1.0
18	-	2.69	83.3	281	1.4	10.4	0.104	0.51	-	-	1.04
19	-	2.69	83.3	310	1.1	10.4	0.104	0.51	-	-	1.03
20	-	2.69	83.3	198	2.1	10.4	0.204	1.0	-	-	1.40
21	-	2.69	83.3	251	1.6	10.4	0.204	1.0	-	-	1.49
22	-	2.69	83.3	279	1.5	10.4	0.204	1.0	-	-	1.64
23	-	2.69	83.3	310	1.4	10.4	0.204	1.0	-	-	1.58
24	-	2.69	83.3	375	1.1	10.4	0.204	1.0	-	-	1.15
25	-	2.69	83.3	375	1.4	10.4	0.316	1.56	-	-	1.10
26	-	2.69	83.3	310	1.6	10.4	0.316	1.56	-	-	1.98
27	-	2.69	83.3	251	1.9	7.50	0.316	1.56	-	-	1.99
28	-	2.69	83.7	251	1.1	7.50	0.233	1.59	-	-	1.19
29	-	2.69	83.7	224	1.3	7.50	0.233	1.59	-	-	1.12
30	-	2.69	83.7	198	1.3	7.50	0.233	1.59	-	-	1.10
31	-	2.69	83.7	174	1.5	7.50	0.233	1.59	-	-	1.01
32	-	2.69	83.7	152	1.6	7.50	0.233	1.59	-	-	1.03
33	-	2.69	83.7	131	1.8	7.50	0.233	1.59	-	-	0.98
34	-	2.69	83.7	131	1.5	7.50	0.147	1.0	-	-	0.73
35	-	2.69	83.7	112	1.6	7.50	0.147	1.0	-	-	0.63
36	-	2.69	83.7	94	1.8	7.50	0.147	1.0	-	-	0.67
37	-	2.69	83.7	198	0.8	7.50	0.147	1.0	-	-	0.85
38	-	2.69	83.7	78	1.6	7.50	0.074	0.50	-	-	0.40
39	-	2.69	83.7	63	1.8	7.50	0.074	0.50	-	-	0.35
40	-	2.69	83.7	49	1.9	7.50	0.074	0.50	-	-	0.33

**TABLE 49**

SERIES M-F

Run	P	$\overline{p_v}$	$\overline{p_L}$	$N_a$	$h_f$	$\overline{V_s}$	$\overline{Q_L}$	L/V	$\overline{E_{mv}}$	$(NTU)_a$	H <sub>log</sub>
1	5.15	2.24	84.2	173	1.25	6.3	0.170	1	0.244	0.280	5.43
2	5.20	2.27	84.1	372	1.25	8.0	0.217	1	0.242	0.277	5.43

63 ASRP-2391

**CONFIDENTIAL**

~~CONFIDENTIAL~~

ASD-TDR-63-665, Part I

APPENDIX IV

CIRCUMFERENTIAL TRAY DATA

TABLE 50  
HYDRAULIC DATA

<u>Run</u>	<u>Psig</u>	$\rho_V$ (lb./ft. <sup>3</sup> )	$\rho_L$ (lb./ft. <sup>3</sup> )	$V_b$ (ft./sec.)	$\frac{Q_L}{b}$	$N_g$	$h_{f\text{ obs}}$	$\Delta P_{\text{ obs}}$
1.2	38	.94	84.0	6.58	.0237	34.0	0.8	
1.3	38	.94	84.0	6.70	.0200	29.0	0.9	
2.2	37	.94	84.0	6.53	.0242	15.0	1.5	
2.3	37	.94	84.0	6.65	.0204	12.6	1.8	
3.2	38	.94	84.0	6.53	.0232	60.0	0.6	.57
3.3	38	.94	84.0	6.65	.0196	51.0	0.5	
4.2	46	1.08	81.5	7.42	.0115	34.0	0.9	.25
4.3	46	1.08	81.5	7.56	.0097	29.0	1.0	
5.2	47	1.08	81.5	7.42	.0304	34.0	1.2	.27
5.3	47	1.08	81.5	7.56	.0256	29.0	1.4	
6.2	49	1.14	81.5	6.86	.0319	34.0	1.5	.30
6.3	49	1.14	81.5	6.98	.0269	29.0	1.7	
7.2	50	1.16	81.5	6.75	.0319	60.0	0.7	.51
7.3	50	1.16	81.5	6.87	.0269	51.0	0.9	
8.2	50	1.16	82.0	6.56	.0317	93.0	0.4	.69
8.3	50	1.16	82.0	6.68	.0268	79.0	0.7	
9.2	46	1.09	82.0	6.91	.00874	34.0	1.0	.40
9.3	46	1.09	82.0	7.04	.00740	29.0	1.2	
10.2	47	1.11	82.2	7.01	.00874	94.0	0.2	.42
10.3	47	1.11	82.2	7.14	.00740	80.0	0.4	

63 ASRP-2391

CONFIDENTIAL

**CONFIDENTIAL**

**ASD-TDR-63-665, Part I**

**TABLE 91**  
**EFFICIENCY DATA**

Run	Psig	$\rho_v$ lb./ft. <sup>3</sup>	$\rho_L$ lb./ft. <sup>3</sup>	$V_a$ ft./sec.	$\frac{Q_L}{b}$	$N_a$	$h_f$	$E_c$	$K$	$E_{MV}$	(NTU) <sub>a</sub>	$D_g$
101.2	43	1.07	84.7	5.58	.0256	34	0.7	.525	1.09	.51	.71	$9.18 \times 10^{-6}$
101.3	43	1.07	84.7	5.68	.0216	29	0.9	.525	1.09	.51	.71	9.18
102.2	46	1.11	83.9	5.50	.0275	21.5	1.2	.525	1.12	.50	.69	8.82
102.3	46	1.11	83.9	5.60	.0232	18.2	1.5	.525	1.12	.50	.69	8.82
103.2	47	1.16	83.9	5.26	.0275	63	0.5	.550	1.13	.53	.75	8.70
103.3	47	1.16	83.9	5.36	.0232	53.5	0.5	.550	1.13	.53	.75	8.70
104.2	54	1.26	83.5	6.45	.0358	34	1.6	.415	1.14	.40	.51	8.03
104.3	54	1.26	83.5	6.57	.0302	29	1.8	.415	1.14	.40	.51	8.03
105.2	57	1.27	83.3	6.31	.0359	76	0.7	.620	1.17	.60	.92	7.73
105.3	57	1.27	83.3	6.43	.0303	64	0.8	.620	1.17	.60	.92	7.73
106.2	53	1.26	83.2	6.34	.0364	212	0.1	.585	1.17	.56	.82	8.11
106.3	53	1.26	83.2	6.45	.0307	178	0.3	.585	1.17	.56	.82	8.11

**HYDRAULIC DATA**

Run	Psig	$\rho_v$ (lb./ft. <sup>3</sup> )	$\rho_L$ (lb./ft. <sup>3</sup> )	$V_a$ (ft./sec.)	$\frac{Q_L}{b}$	$N_a$	$h_{f\text{ obs}}$	$\Delta P_{\text{ obs}}$
11.2	50	1.16	82.6	6.82	.0237	86.0	0.4	.53
11.3	50	1.16	82.6	6.94	.0200	73.0	0.6	
12.2	52	1.19	82.6	6.71	.0234	34.0	0.9	.45
12.3	52	1.19	82.6	6.83	.0198	29.0	1.3	
13.2	52	1.19	81.6	7.56	.0229	60.0	0.7	1.00
13.3	52	1.19	81.6	7.70	.0194	52.0	0.9	
14.2	52	1.19	81.7	7.44	.0229	94.0	0.5	.60
14.3	52	1.19	81.7	7.57	.0194	80.0	0.7	
15.2	53	1.21	81.9	7.34	.0225	36.0	1.0	.60
15.3	53	1.21	81.9	7.47	.0191	31.0	1.2	
16.2	54	1.23	82.0	7.23	.0343	34.0	1.1	.60
16.3	54	1.23	82.0	7.36	.0230	29.0	1.1	
17.2	55	1.24	82.2	7.16	.0345	60.0	0.8	.58
17.3	55	1.24	82.2	7.29	.0292	52.0	1.1	
18.2	55	1.24	82.6	7.17	.0351	94.0	0.5	.63
18.3	55	1.24	82.6	7.30	.0297	80.0	0.6	
19.2	36	0.92	83.5	5.87	.0174	15.0	1.0	.54
19.3	36	0.92	83.5	5.97	.0147	12.6	1.2	
20.2	35	0.89	83.5	6.07	.0165	34.0	0.5	.17
20.3	35	0.89	83.5	6.19	.0139	29.0	0.7	

63 ASRP-2391

**CONFIDENTIAL**

**CONFIDENTIAL**

ASD-TDR-63-665, Part I

APPENDIX V

CIRCUMFERENTIAL TRAY UCON FLUID TEST ROTOR

1. Introduction

Since the UCON fluid mass transfer test rotor, constructed under Contract AF 33(616)-7646, permitted only tests of segmental tray sections, it was necessary to fabricate a new test rotor capable of receiving complete circumferential trays and suitable for installation in the existing tester casing. Primary purpose of the rotor was to obtain comparative results on hydraulic behavior of complete circumferential trays and to examine the possibility of liquid maldistribution on trays and the resulting mechanical effects due to rotor unbalance.

2. Rotor Design

Design of the circumferential tray rotor was approached with a dual goal: (1) to arrive at the most suitable test rotor from a functional and mechanical point of view, and (2) to simulate, if possible fabrication techniques which would be later encountered in the fabrication of trays for the 100 lb./sec. boilerplate separator.

As seen in Figure 200, the test rotor consists basically of a radial chamber housing four concentric trays. The tray chamber was designed to give a constant radial superficial vapor velocity. Since four trays were used, the inner face of the tray chamber walls was designed with four different tapered sections. The intersection of adjacent tapered sections fixes the location for the trays.

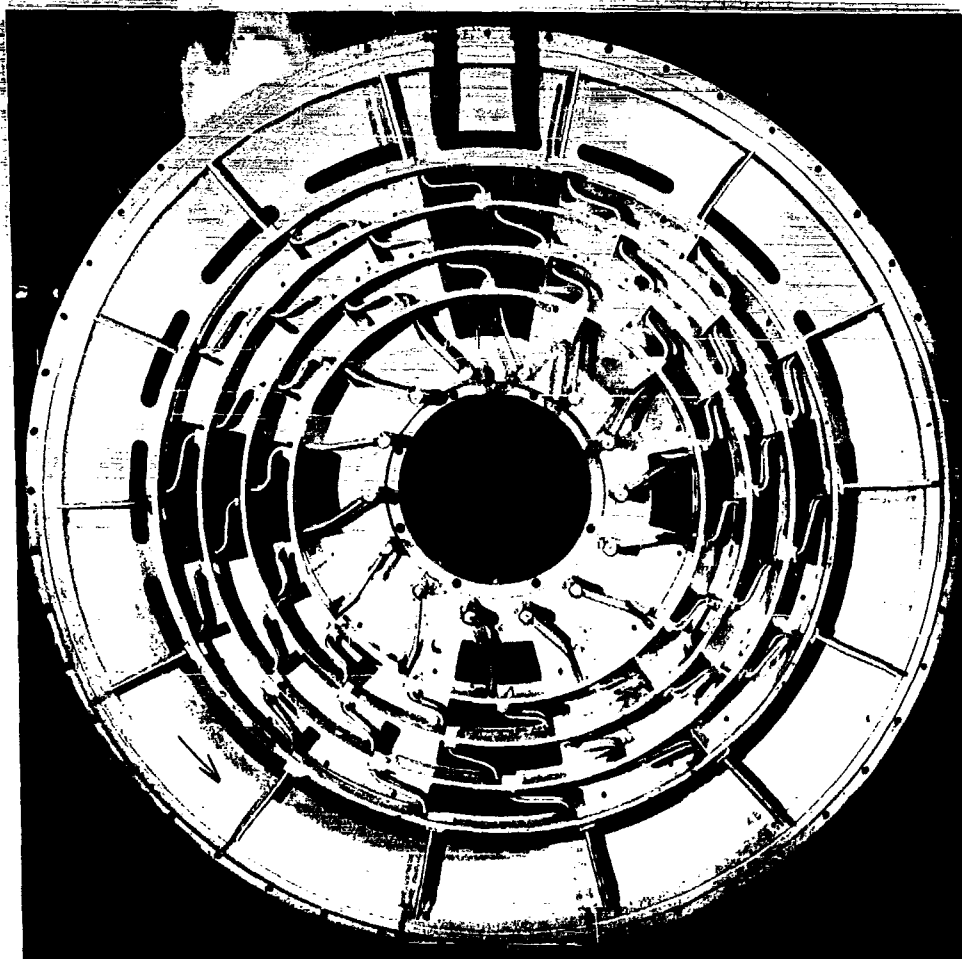
The following tray ring widths with their respective radial positions specify the tray chamber configurations.

63 ASRP-2391

**CONFIDENTIAL**

**CONFIDENTIAL**

ASD-TDR-63-665, Part I



**CIRCUMFERENTIAL TRAY UCON TEST ROTOR**

**FIG. 200**

63 ASRP-2391

**CONFIDENTIAL**

**CONFIDENTIAL**

ASD-TDR-63-665, Part I

<u>Tray No.</u>	<u>Width (in.)</u>	<u>Radius (in.)</u>
1	2-1/2	9.25
2	2-1/32	11.25
3	1-23/32	13.25
4	1-1/2	15.25

To ease installation and removal of different tray configurations, trays are fixed to rings which are inserted into grooves in the rotor walls and held in place by a number of J-bolts. Test fluids (liquid and vapor) are introduced into the hollow front shaft. A center tube located within the shaft and manifolded to radial channels in the hub carries the liquid to an annular chamber on the outer surface of the hub. From here the liquid is transferred to the inlet weirs of tray No. 1 by header tubes.

Each header tube discharges into two downcomer tubes through 1/8 inch orifices.

The annular space between the liquid channel and the shaft I.D. guides the vapor to a second set of radial holes in the hub leading to a radial chamber on the outside of the rotor wall. The vapor is introduced to the outer periphery of the tray chamber through annular ports in the chamber wall.

Liquid is discharged at the rotor periphery through radial tubes. Vapor is discharged at the drive end of the shaft.

### 3. Tray Ring Design and Fabrication

Figure 201 shows a circumferential tray ring assembly of the UCON tester. As evident from this picture the tray rings consist of a circumferential perforated strip representing the active tray area with a number of inlet weirs and downcomer troughs equally spaced around its periphery. The sides of the strip are inserted into the annular grooves of the edge rings as shown. Downcomer tubes transfer liquid from the downcomer trough of one tray to the inlet weir of an adjacent tray.

The downcomer troughs with the downcomer tubes and the inlet weirs were fabricated as individual components. The preformed components were then positioned on the tray strip as

63 ASRP-2391

**CONFIDENTIAL**

**CONFIDENTIAL**

ASD-TDR-63-665, Part I

**CIRCUMFERENTIAL TRAY RING ASSEMBLY**

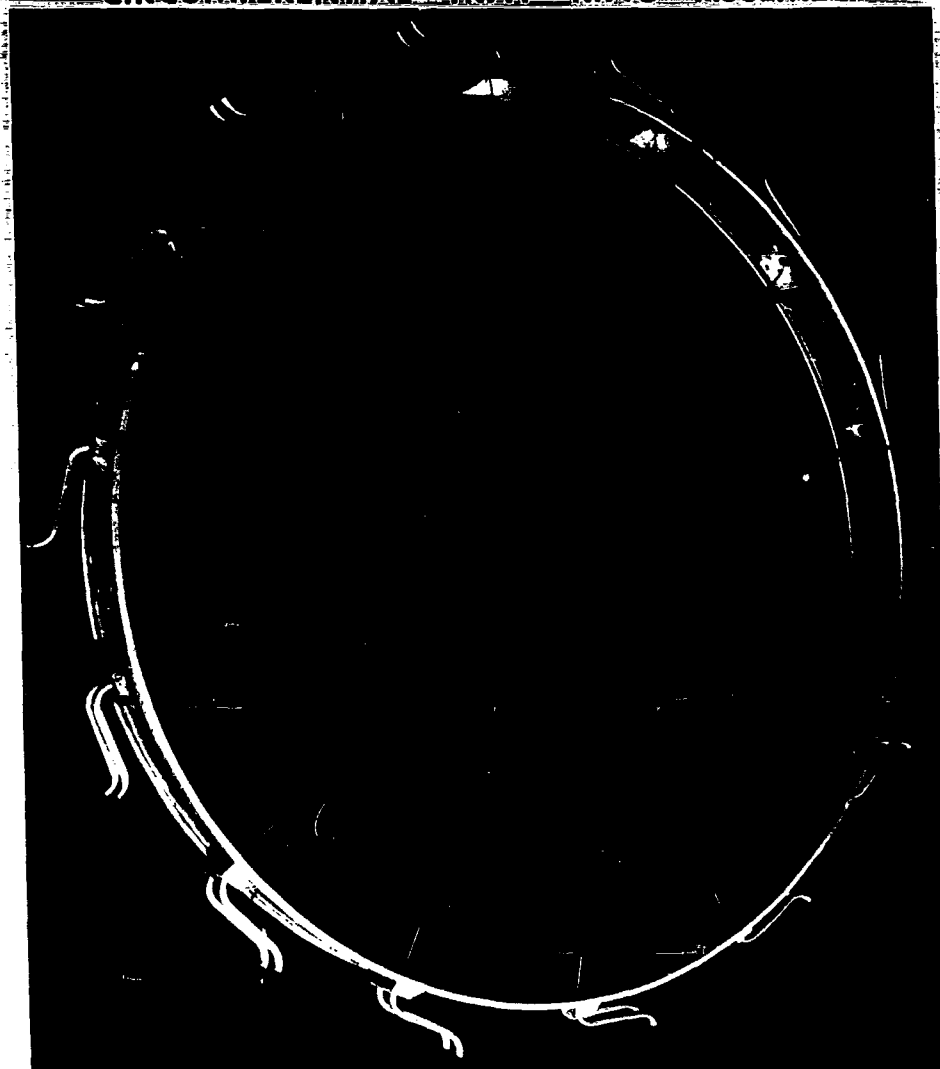


**FIG. 201**

63 ASRP-2391

**CONFIDENTIAL**



**CONFIDENTIAL**

**ASD-TDR-63-665, Part I**

shown on Figure 202 and permanently attached in a furnace brazing operation. For an all aluminum construction, the downcomers and inlet weirs were folded from Alcoa No. 11 brazing sheet (3003 aluminum clad with 4303 aluminum) and the perforated tray material was specified as 3003 aluminum. This material combination made the tray ring assembly furnace brazeable at a temperature range from 1120-1140°F. Because of the lightweight construction of the tray ring assembly, no difficulty was encountered in bringing it to brazing temperatures, nor was a great deal of fixturing required even through the strength of aluminum is considerably reduced at these elevated temperatures. The assembly to be brazed was introduced into the furnace which had been preheated to the required temperature. A five-minute heating period was adequate to obtain complete flow of the clad brazing surface.

Following brazing the perforated strip downcomer assembly was inserted into the grooves of the edge rings (Figure 203) and permanently joined to the rings in a furnace soldering operation using cadmium silver solder with a melting range of 640 to 740°F.

To effect assembly of the individual tray rings in the tray chamber, concentric circumferential grooves were machined on the inner face of the rotor walls. The tray rings were positioned in the grooves on one side wall of the rotor and bolted from the inside. After relative alignment of the various ring trays, the other side wall was "dropped" into position to form the tray chamber. Fastening of the tray rings to the blind side wall was accomplished from the outside through the use of specially designed J-bolts sealed on the outer face of the rotor wall.

The areas of difficulty in the design and fabrication of the circumferential tray rings included fixturing of each component for the brazing and soldering operation and the cleaning procedure after brazing and soldering.

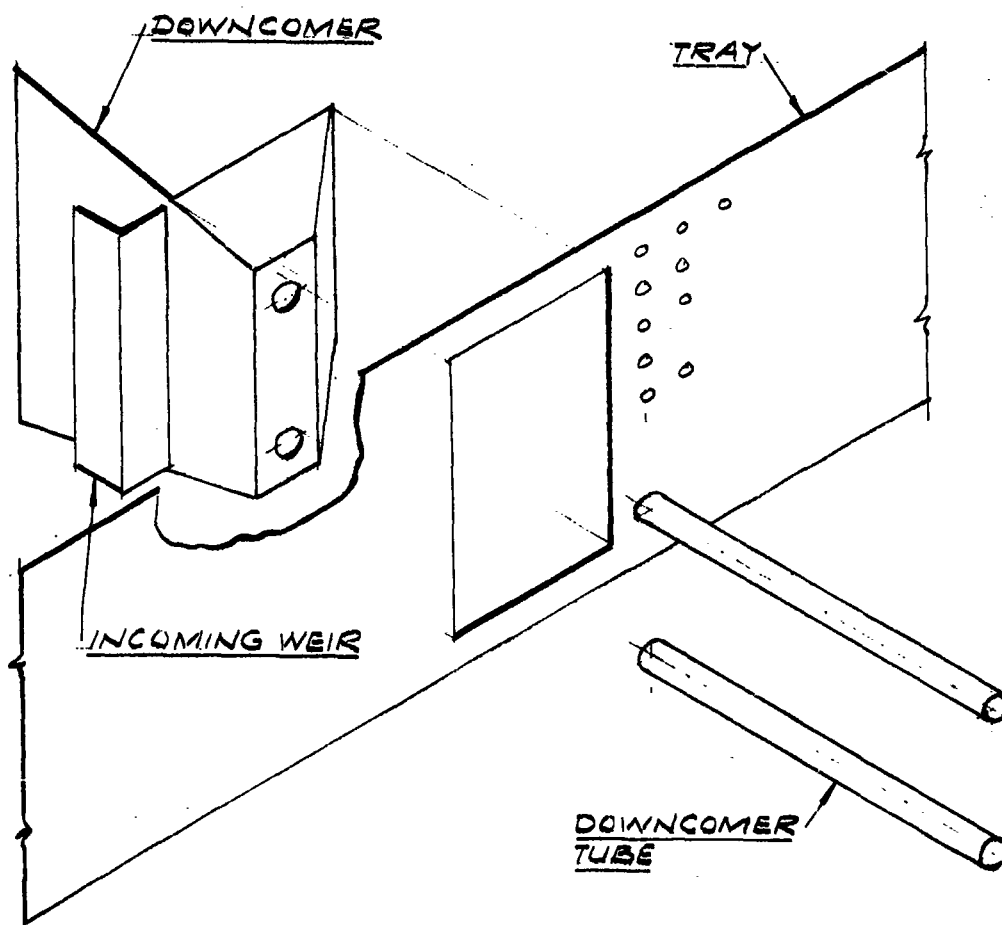
In the first area of difficulty, a single tack weld proved inadequate to position the downcomer uniformly on the tray strip. Also, the wires used to position the inlet weir on the tray and to hold the solder wire in position resulted in local hot spots and stress risers which led to the enlargement of the tray perforations in the vicinity of the wires.

63 ASRP-2391

**CONFIDENTIAL**

**CONFIDENTIAL**

ASD-TDR-63-665, Part I



ASSEMBLY OPERATION  
CIRCUMFERENTIAL TRAY

FIG. 202

63 ASRP-2391

**CONFIDENTIAL**

**CONFIDENTIAL**

ASD-TDR-63-665, Part I

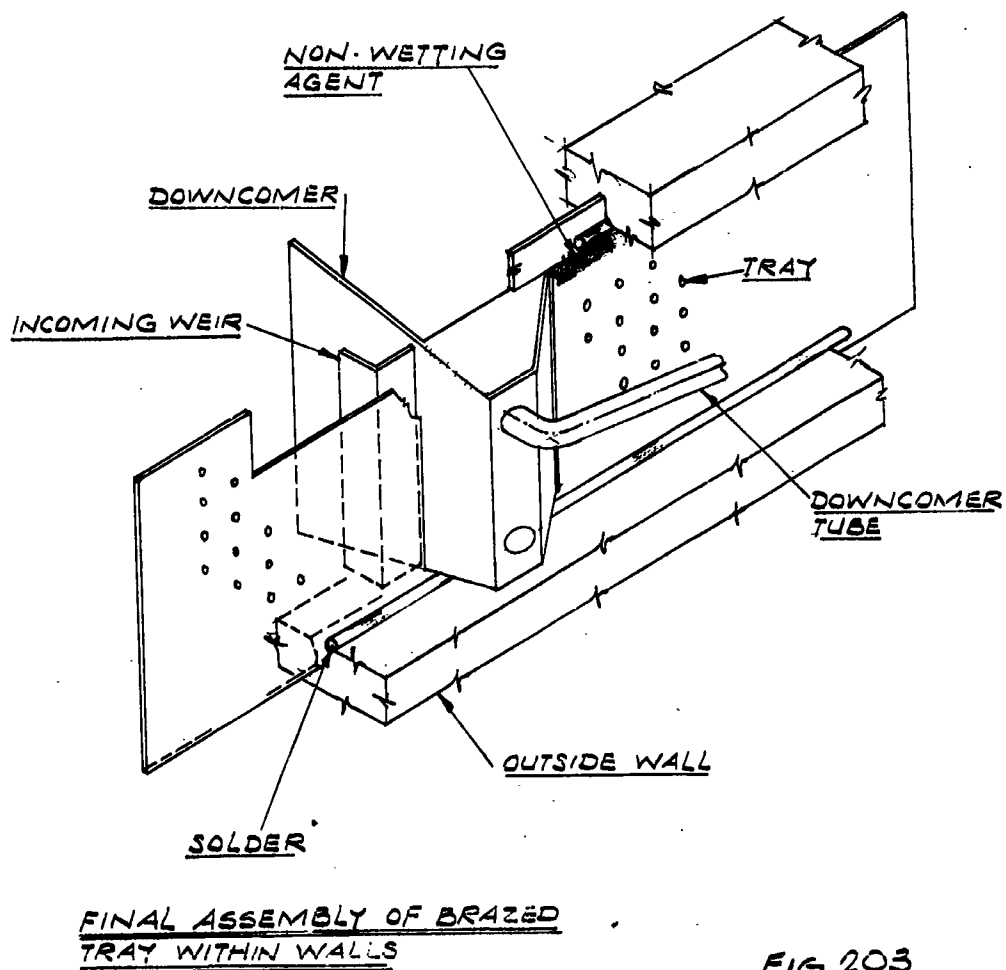


FIG 203

63 ASRP-2391

**CONFIDENTIAL**

~~CONFIDENTIAL~~

ASD-TDR-63-665, Part I

The second area of difficulty arising from the various pickling stages for the prefabricated and finished assembly presented a more serious problem. Chemical attack enlarged the size of perforations with a critical resultant increase of approximately 20 per cent in the free area of the trays. To compensate for the open area increase, a small portion of tray area was blocked off along the edges.

Although during the fabrication of the tray rings two 5 to 10 minute immersions in a mild phosphoric acid solution (10 per cent  $H_3PO_4$ ) were used, one before brazing and one before the soldering operation; they were of small consequence to the final dimensions. The final pickling in a nitric-hydrofluoric solution (14 per cent  $HNO_3$ , 3-4 per cent HF) required to remove the soldering flux was most detrimental. The last pickling operation will be eliminated in all future tray fabrication.

4. Instrumentation and Visual Observation.

The rotor was instrumented with three 0-50 psi pressure transducers. One transducer was positioned to determine individual tray pressure drop across Tray No. 2; the second transducer was installed to pick up total pressure drop across the four trays; and the third transducer was used to reference the tray chamber pressure to casing pressure.

For visual observation of the tray performance, four plexi-glas windows spaced 90° apart were provided on each face of the rotor. Strong solvent action upon the plexiglas windows by the UCON 21 test fluid during initial test runs required a material substitution. An adequate substitution was found in a clear Polyester material commercially known as CR-34 plastic.

5. Mechanical Operation of Test Rotor

Mechanical operation of the test rotor was satisfactory. No severe mechanical vibrations which would have been encountered in case of maldistribution of liquid on trays, were observed during extended operation of the unit.

63 ASRP-2391

CONFIDENTIAL

**CONFIDENTIAL**

ASD-TDR-63-665, Part I

APPENDIX VI

DERIVATION OF EQUATION FOR CALCULATION OF  
CONDENSATE DRAINAGE BLANKETING

The velocity of flow through an open channel of any cross section can be expressed by the Chezy formula. (Ref. 23, p. 377)

$$V = C_2 \sqrt{\frac{R_H F}{L^0}} \quad (\text{ft./sec.}) \quad (57)$$

The coefficient  $C_2$  equal to  $\sqrt{2g_C/f}$  can be expressed by the Manning formula (Ref. 21, p. 383) for open channels

$$C_2 = \frac{1.486 R_H^{1/6}}{n} \left( \frac{1b_m - ft}{1b_f - sec^2} \right)^{1/2} \quad (58)$$

Since the velocity of flow can be expressed as:

$$V = \frac{W}{A \rho_L}$$
$$\therefore \frac{W}{A \rho_L} = \left[ \frac{1.486 R_H^{1/6}}{n} \right] \left[ \sqrt{\frac{R_H F}{L^0}} \right]$$

$$\text{or } \frac{W}{A \rho_L} = \frac{1.486 R_H^{2/3} F^{1/2}}{n (L^0)^{1/2}}$$

Rearranging the equation,

$$(1) \quad \frac{1}{A R_H^{2/3}} = \frac{1.486 \rho_L F^{1/2}}{n (L^0)^{1/2} W} \quad (59)$$

63 ASRP-2391

**CONFIDENTIAL**

**CONFIDENTIAL**

ASD-TDR-63-665, Part I

This is an expression for flow of condensate drainage along the bottom of the tube and now it must be expressed in terms of the condensate blanketing angle,  $\phi$ , (See Figure 53).

The cross-section (A) of the condensate equals the area of the circular sector bounded by  $r_t$  and  $\phi$  minus the area of the triangle abc.

$$\begin{aligned} \therefore A &= \frac{\phi}{2\pi} [\pi r_t^2] - [r_t \sin \frac{\phi}{2}] [r_t \cos \frac{\phi}{2}] \\ A &= \frac{\phi}{2} r_t^2 - r_t^2 \sin \frac{\phi}{2} \cos \frac{\phi}{2} \\ A &= r_t^2 \left[ \frac{\phi}{2} - \sin \frac{\phi}{2} \cos \frac{\phi}{2} \right] \end{aligned} \quad (60)$$

The hydraulic radius ( $R_H$ ) is defined as the cross-section area over the wetted perimeter where contact with the wall defines the wetted perimeter.

$$\begin{aligned} \therefore R_H &= \frac{A}{w.p.} = \frac{r_t^2 \left[ \frac{\phi}{2} - \sin \frac{\phi}{2} \cos \frac{\phi}{2} \right]}{r_t \phi} \\ R_H &= \frac{r_t}{\phi} \left[ \frac{\phi}{2} - \sin \frac{\phi}{2} \cos \frac{\phi}{2} \right] \end{aligned} \quad (61)$$

Substituting into Equation (59) for A and  $R_H$  :

$$\begin{aligned} &\frac{1}{(r_t^2 \left[ \frac{\phi}{2} - \sin \frac{\phi}{2} \cos \frac{\phi}{2} \right]) \left( \frac{r_t}{\phi} \left[ \frac{\phi}{2} - \sin \frac{\phi}{2} \cos \frac{\phi}{2} \right] \right)^{2/3}} = \\ &\frac{1.486 \rho_L F^{1/2}}{W n(L^\circ)^{1/2}} \end{aligned}$$

combining terms:

63 ASRP-2391

**CONFIDENTIAL**

**CONFIDENTIAL**

ASD-TDR-63-665, Part I

$$\frac{\phi^{2/3}}{r_t^{8/3} [\phi/2 - \sin \phi/2 \cos \phi/2]^{5/3}} = \frac{1.486 \rho_L F^{1/2}}{W n (L^0)^{1/2}}$$

squaring both sides of the equation and rearranging:

$$\frac{\phi^{4/3}}{[\phi/2 - \sin \phi/2 \cos \phi/2]^{10/3}} = (F/L^0)^2 \left[ \frac{1.486}{n} \right]^2 \rho_L^2 \frac{r_t^{16/3}}{W^2}$$

The frictional energy loss must equal the change in potential energy in order that flow may occur:

$$\therefore \frac{F}{L^0} = \frac{g N g}{g_c} \sin \alpha^\circ \quad (62)$$

Since  $\psi$  is the complement of  $\alpha^\circ$

$$\frac{F}{L^0} = \frac{g N g}{g_c} \cos \psi$$

Letting  $n$  (smooth tube) = 0.011 (Ref. 23, P. 384)

$$f(\phi) = \frac{\phi^{4/3}}{[\phi/2 - \sin \phi/2 \cos \phi/2]^{10/3}} = \left( \frac{1.486}{.011} \right)^2 \frac{g}{g_c} N g \cos \psi \frac{\rho_L^2 r_t^{16/3}}{W^2} \quad (63)$$

63 ASRP-2391

**CONFIDENTIAL**

ASD-TDR-63-665, Part I

(THIS PAGE IS INTENTIONALLY BLANK.)

63 ASRP-2391



~~CONFIDENTIAL~~

ASD-TDR-63-665, Part I

APPENDIX VII

DERIVATION OF CONDENSER TUBE EQUATION

This appendix presents the derivation of the equation describing the shape of the tubes in the reboiler-condenser. The final formula was previously presented as equation (43) in Section 4.5 of this report.

Referring to Figure 204,

$$\text{at } r_1, d t_1 = r_1 d \Theta_1$$

$$\text{at } r, d t = r d \Theta$$

Let  $d\Theta_1 = d\Theta$  since tubes are assumed to be in lateral contact everywhere along the tube lengths or curvature is such that the subtended angles of the radial arcs along the tube are equal.

$$\text{Therefore: } \frac{d t_1}{r_1} = \frac{d t}{r}$$

Since the subtended radial arcs of the actual tube are small, it can be assumed that  $dt_1 \sim t_1$  and  $dt \sim t$ .

$$\text{Therefore: } \frac{t_1}{r_1} = \frac{t}{r}$$

$$\text{and } \frac{t_1}{t} = \frac{r_1}{r}$$

Defining  $\Psi$  as the angle between the radius vector of the rotor and the axis of the tube and assuming the length  $t$  is small enough such that the radius vector is perpendicular to it, therefore:

$$\cos \Psi = \frac{t_1}{t} \text{ as shown in Figure 204.}$$

and

$$\cos \Psi = \frac{r_1}{r}$$

63 ASRP-2391

~~CONFIDENTIAL~~

DERIVATION OF CONDENSER TUBE EQUATION

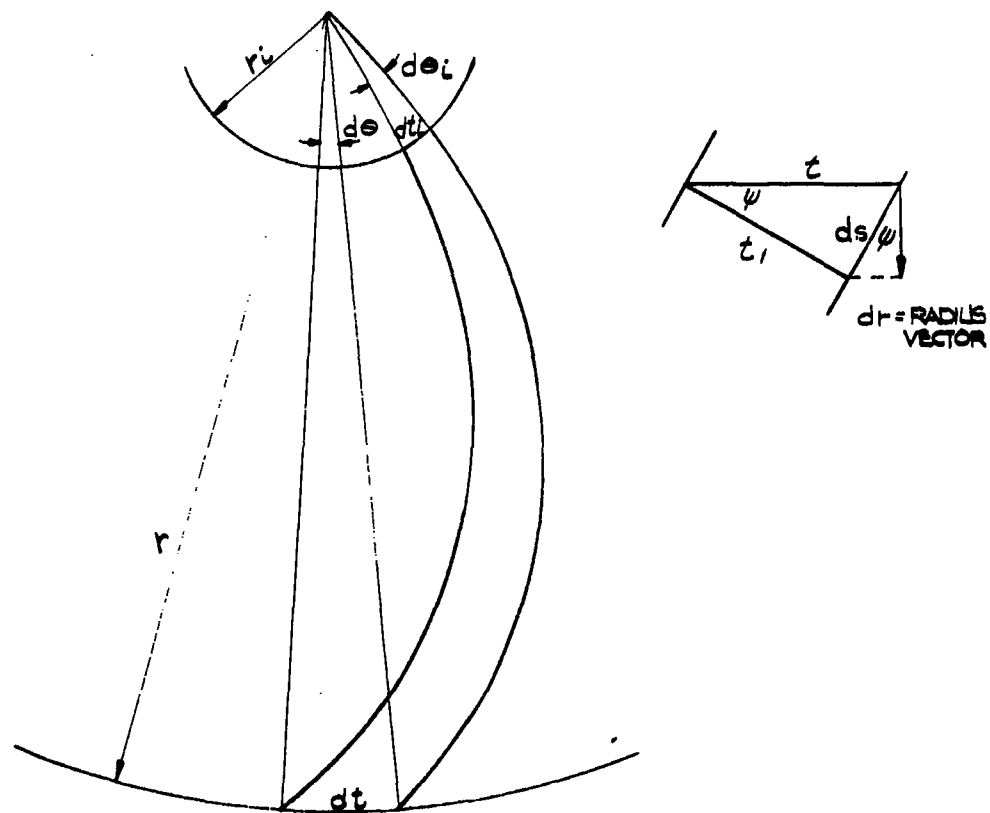


FIG. 204

**CONFIDENTIAL**

ASD-TDR-63-665, Part I

From the definition of the differential of an arc in polar coordinates,

$$\cos \psi = \frac{dr}{ds}$$

and

$$ds = \left[ r^2 + \left( \frac{dr}{d\Theta} \right)^2 \right]^{1/2} d\Theta$$

$$\text{since } \frac{r_1}{r} = \frac{dr}{ds}$$

Therefore:

$$\frac{r}{r_1} dr = \left[ r^2 + \left( \frac{dr}{d\Theta} \right)^2 \right]^{1/2} d\Theta$$

or

$$\left( \frac{dr}{d\Theta} \right)^2 \left[ \left( \frac{r}{r_1} \right)^2 - 1 \right] = r^2$$

Since the angle  $\Theta$  is normally considered to be positive in a counter-clockwise direction, the final differential is:

$$-d\Theta = \frac{1}{r_1} \frac{\sqrt{r^2 - r_1^2}}{r} dr$$

Integration of this differential equation results in the following equation for a single tube in the tube disc in polar coordinates:

$$\Theta = \arccos \left( \frac{r_1}{r} \right) - \sqrt{\left( \frac{r}{r_1} \right)^2 - 1} \quad (64)$$

63 ASRP-2391

**CONFIDENTIAL**

ASD-TDR-63-665, Part I

(THIS PAGE IS INTENTIONALLY BLANK.)

63 ASRP-2391

**CONFIDENTIAL**

ASD-TDR-63-665, Part I

APPENDIX VIII

DESIGN AND FABRICATION OF  
UCON FLUID HEAT TRANSFER TEST ROTOR

1. Introduction

In order to test the functional and mechanical concepts for the reboiler-condenser heat transfer surfaces, a special test rotor capable of being installed into the housing of the existing UCON test facility was designed and fabricated. This rotor was to include on a somewhat reduced scale a typical heat transfer passage of the conceived heat transfer surface configuration consisting of one boiling and two condensing passes in the form of two disks assembled from spirally curved 5/16 O.D. tubes.

Design of the rotor was approached from two goals: (1) to arrive at a suitable test device, and (2) to provide some opportunity for developing and testing fabrication techniques which would find later application in the construction of a reboiler-condenser for the boiler-plate separator.

2. General Design

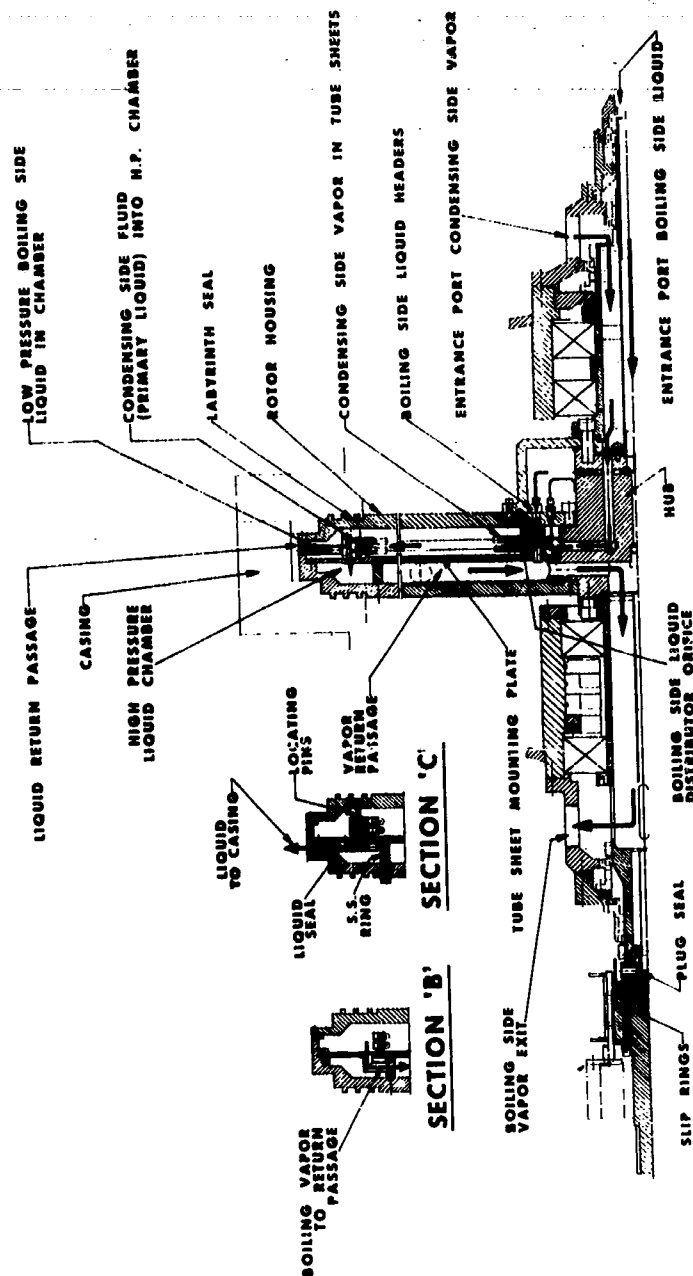
As can be seen from Figure 205, the rotor provides for a cylindrical chamber into which two tube disks can be assembled to form two condensing passages within the tubes, and a boiling passage between the tube disks. Liquid enters the rotor at the centershaft at the right of the figure, flows to the hub from which it travels radially outward to a liquid hold up chamber. From the chamber, liquid is guided through 16 equally spaced headers to an annular spacer. From here the liquid is throttled through a series of small orifices located in the distributor orifice ring, shown in more detail in Figure 206. Pressure drop through the orifices effectively distributes the liquid around the circumference of the tube sheets. Part of the liquid is vaporized on its path to the periphery. This vapor is returned to the axis through the boiling vapor return chamber, shown in Section "B" of Figure 205. The remaining liquid collects in the chamber at the periphery and is discharged via the liquid seal to the casing and from there to the storage tank.

63 ASRP-2391

**CONFIDENTIAL**

CONFIDENTIAL

ASD-TDR-63-665, Part I

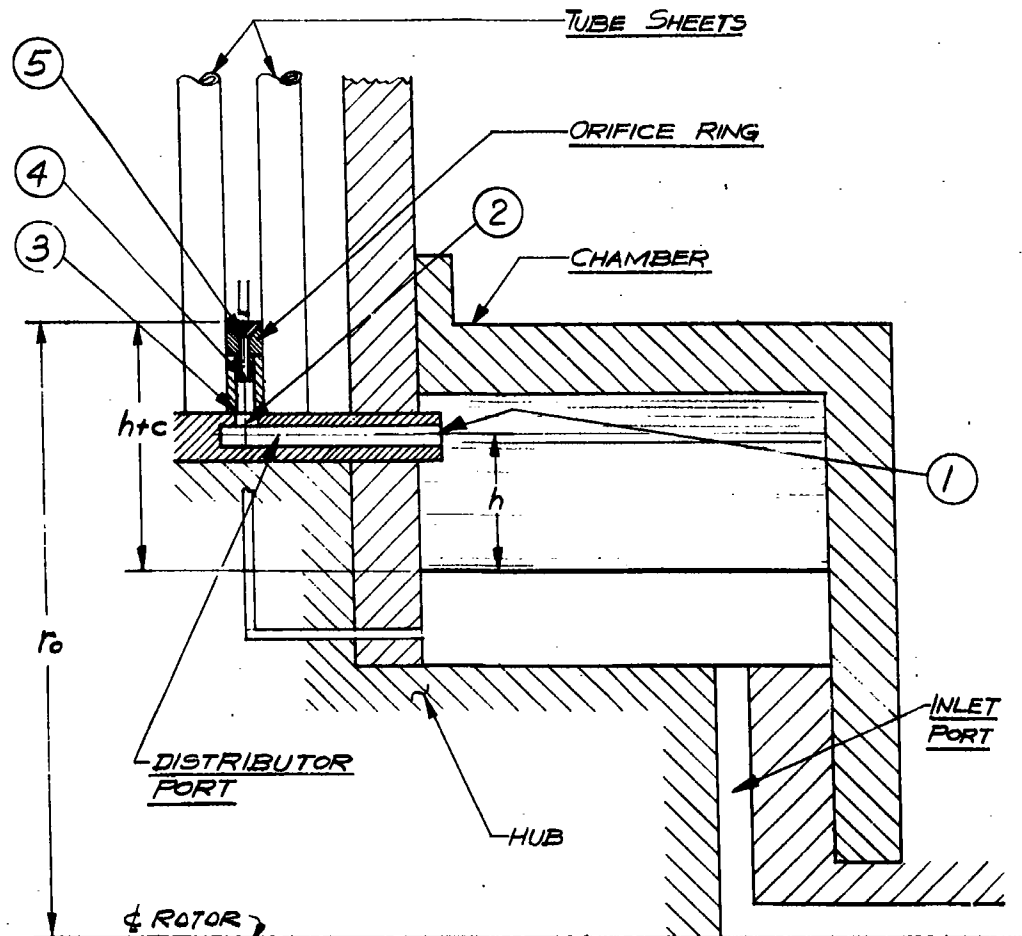


UCON HEAT TRANSFER TEST ROTOR

FIG. 205

63 ASRP-2391

CONFIDENTIAL



DISTRIBUTOR ORIFICE  
CONFIGURATION

FIG. 206

63 ASRP-2391

**CONFIDENTIAL**

ASD-TDR-63-665, Part I

The condensing side vapor enters through the side port, and passes down the annular shaft passage to the hub. It then travels radially outward to the inside of the tube sheets. Flowing through the tubes, it is condensed and transmitted to the high pressure liquid chamber. From this chamber the collected liquid flows into the casing and out to storage, as shown in Section "C" of Figure 205. By providing a greater radial depth on the lower pressure liquid seal (boiling side) it was possible to operate the condensing side at higher pressures. The differential liquid column balances the pressure differential.

Pressure transducers were installed at various points in the tube disks to measure the pressure difference between boiling side and condensing side. Another transducer measured liquid level in the inlet liquid chamber.

### 3. Tube Disk Design and Fabrication

From functional considerations reported in Section 4.0 of the report, it was established that the heat transfer surface should be provided in the form of spirally curved tubes assembled to form disks which are rotated around their axis. High pressure vapor is condensed inside the tubes and low pressure liquid is boiled outside.

The mechanical requirements for the heat transfer disk were analyzed by considering the worst possible case from the point of view of strength, namely a uniform rotating disk without the support provided by the tube headering. By use of References (56) and (57), estimates of the maximum stress and shear in the disks were calculated to be 4,125 psi and 1,900 psi respectively, at the inside diameter of the disk at the maximum speed of the UCON fluid tester, 1250 RPM.

Since the yield strength of Type 3003-0 Aluminum is 6000 psi and the shear strength is 11,000 psi, the conservative estimate of the two stresses is evidence of a large safety factor.

The disks were subjected to spin tests as described at the end of this appendix to insure structural integrity and adequate strength.

After considering several different materials of construction for the various disk components, Type 3003 Aluminum was selected on the basis of availability, strength to weight ratio, and ease of fabrication.

63 ASRP-2391

**CONFIDENTIAL**



**CONFIDENTIAL**

ASD-TDR-63-665, Part I

The tubes chosen had an 0.280 in. inside diameter and an 0.016 in. wall thickness. The reason for using an 0.016 in. wall thickness was that 0.016 in. was the thinnest wall which was readily available. Calculations on primary and shear stresses indicated that thinner walls could be used safely if available.

Welding and soldering were discarded as methods for joining tubes after laboratory tests showed that both of these techniques gave poor results. Brazing appeared to offer considerable promise for joining tubes to each other and to headers while welding could be employed in fabricating the outer header since material here is fairly thick and joints easily accessible. Consequently torch brazing was tried and found to be successful in the laboratory. Since hand brazing proved time-consuming, it was decided to follow a suggestion made by Alcoa and salt bath dip braze preassembled and fixtured disks.

The final mechanical design of the UCON fluid heat transfer elements has already been shown in Figure 37. The disks contain 121 tubes which lie side-by-side. The tubes are squared at the ends to obtain good braze joints between the tube ends and headers. Section A-A of Figure 37 shows a cross-section through the outer header and one cross header. The header is notched to assure concentric alignment when assembling individual disks in the tester. Sealing between cross headers is accomplished by O-rings. The bolt hole, not shown in Section A-A but shown in the front elevation accommodates the clamping bolt which applies the required pressure to seal the cross headers. Section B-B shows a typical cross section through the inner header. The selected design permitted any number of disks to be stacked together into as large a heat exchanger as desired.

Fabrication techniques and disk assembly were the next step. The tubing was purchased in 12 foot lengths. The necessary length of each tube on a disk was found to be 24 inches from the equation in Section 4.5.1. Seeing that the tubes must be bent, squared, and trimmed, the tubing was cut into 28.75 inch lengths. After cutting, all the tube segments were annealed for one hour at 850°F. to make sure that all material was of "O" temper prior to forming. A plexiglas die for bending the tubes was fabricated. By a cut and try method this die was shaped to correct for spring back until the tubes made with it complied with the desired curve. After the tubes had been bent to the desired shape, a rubber round (0.275 dia.) was inserted into the tube and the ends were compressed into a square aluminum die. While the tube was still compressed the rubber was withdrawn. Only then was

63 ASRP-2391

**CONFIDENTIAL**

**CONFIDENTIAL**

**ASD-TDR-63-665, Part I**

the squared tube taken from the die. The inside edges of the die were rounded so that a smooth transition zone between the round and square tube sections was obtained. To facilitate withdrawal of the compressed rubber, it was lubricated with machine oil. The purpose of withdrawing the rubber before opening the die was to maintain the dimensions of the square as closely as possible ( $\pm 0.001$  in. was obtained). Following squaring both ends were trimmed to exact dimensions and deburred. The result of these operations is shown in Figure 207.

All components of the headering were cut from standard 3003 aluminum sheet, plate, or tubing and machined to rough dimensions. Some difficulty was encountered in machining the aligning grooves into the outside header rings because of poor rigidity of these parts.

The major problem during assembly was to fit 121 tubes into a disk. The tubes had become slightly elliptical in the process of bending. In order to form a full disk it was necessary to reduce the minor diameter further. This was accomplished by forcing tubes into place in groups of six while annealing them with a torch to relieve compressive stresses. It was found that by following a careful annealing procedure all 121 tubes could be placed into the proper position. Heavy tape was then used to hold the tube disk together for shipment to the brazing vendor for final assembly, fixturing, and brazing.

The dip brazing of all disks was accomplished by the Benson Manufacturing Company of Kansas City, Missouri. To fixture disks, including headers, for brazing, individual tubes were joined to each other and the headers by tack welding. For brazing No. 718 was laid in hoops on top of the tubes at radii of 6, 7, 9, 11, 13, 15, 17, and 18 in. Following this the bundles were preheated to 1050°F. for 45 minutes and then dipped for 4 minutes into a salt bath at 1100°F. Results as previously shown in Figure 69 were excellent for all disks. It should be noted that the outer header was left open to allow brazing salt to escape from the tubes when the disks were taken from the molten salt bath. Washing with hot water and nitric acid completely removed all traces of salt.

Following brazing, the outer header wall was closed by welding and the manifold blocks were welded into place.

The next step in the manufacturing procedure was to apply the special boiling surface on to the boiling side of the disks. This was accomplished with some technical difficulties which developed because of the

63 ASRP-2391

**CONFIDENTIAL**

**CONFIDENTIAL**

ASD-TDR-63-665, Part I

**CURVED HEAT TRANSFER TUBE FOR  
UCON TEST ROTOR**

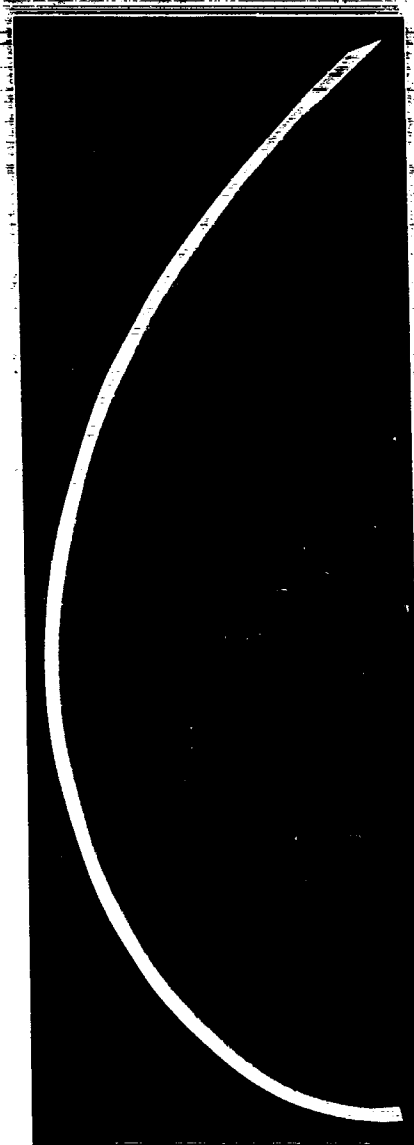


**FIG. 207**

63 ASRP-2391

**CONFIDENTIAL**

**CONFIDENTIAL**

ASD-TDR-63-665, Part I

configuration of the surface to be coated. However, the difficulties were overcome and a very satisfactory special boiling surface was applied to several disks.

Following this, all parts were finish machined.

The completed disks were subjected to a spin test. The object of this test was to insure structural integrity of the disks. In the first part of the spin test the disks were run dry at 2200 RPM, without any visible damage or yielding of parts. At a speed of 1600 RPM with the disk filled with water, the tests were equally successful with no indication of yielding. Factor of safety of this design was considered adequate since the maximum speed of the tester was to be 1250 RPM. The minimum actual safety factor at the worst possible condition of total flooding is  $(1600/1250)^2$  or 1.65 as the stress is proportional to the square of the rotational speed. However, as previously mentioned, calculations indicated much greater safety factors specifically since the disks would receive much structural support from the headering.

To accurately calculate the minimum wall thickness necessary from strength considerations requires a lengthy and complicated analysis not justified for the design of the UCON experimental disks.

63 ASRP-2391

**CONFIDENTIAL**

**CONFIDENTIAL**

ASD-TDR-63-665, Part I

APPENDIX IX

COMPUTER PROGRAM FOR INTEGRATION OF SYSTEM OF  
FOUR DIFFERENTIAL EQUATIONS DESCRIBING HEAT TRANSFER  
IN UCON FLUID ROTOR

The system of four differential equations that are derived on pages 170-177 is a boundary value problem. A systematic procedure of trial and error was required to obtain a solution for a given set of parameters.

The configuration and environment of a condenser tube section is shown in Figure 208. Over the left half of the tube there was no heat transfer taking place on the exterior of the tube. At the top and bottom of the tube there was a brazing fillet which also prohibited heat transfer on the exterior of the tube. In addition there was a condensate trough on the bottom of the tube across which no heat transfer took place.

The integration of the differential equations proceeded in three segments starting at two different points. The solution for a given set of parameters was obtained by matching the results at the points where there was overlapping between segments. On the right side of the tube where boiling heat transfer took place, there was a sizable portion of the tube where the circumferential gradient ( $\partial/\partial\phi$ ) in the wall was zero, meaning the heat transfer was transverse only. This was true due to the high performance of the special boiling surface where the heat conducted through the tube wall from the condensation taking place on the opposite side of the tube was rapidly dissipated before progressing very far into the region where the boiling fluid contacted the exterior of the tube. This fact was used in matching the values of the variables that were integrated starting from the two different points.

The integration of the four differential equations was started at two different points in three directions. These three integration segments were at  $\phi_1 = 0$ , proceeding clockwise; at  $\phi_1 = 0$ , proceeding counterclockwise; and  $\phi_1 = \pi$ , proceeding counterclockwise. Since the four functions  $\frac{d\theta}{d\phi_1}$ ,  $\frac{dz}{d\phi_1}$ ,  $\frac{dy}{d\phi_1}$  and  $\frac{dQ}{d\phi_1}$  were thus treated as

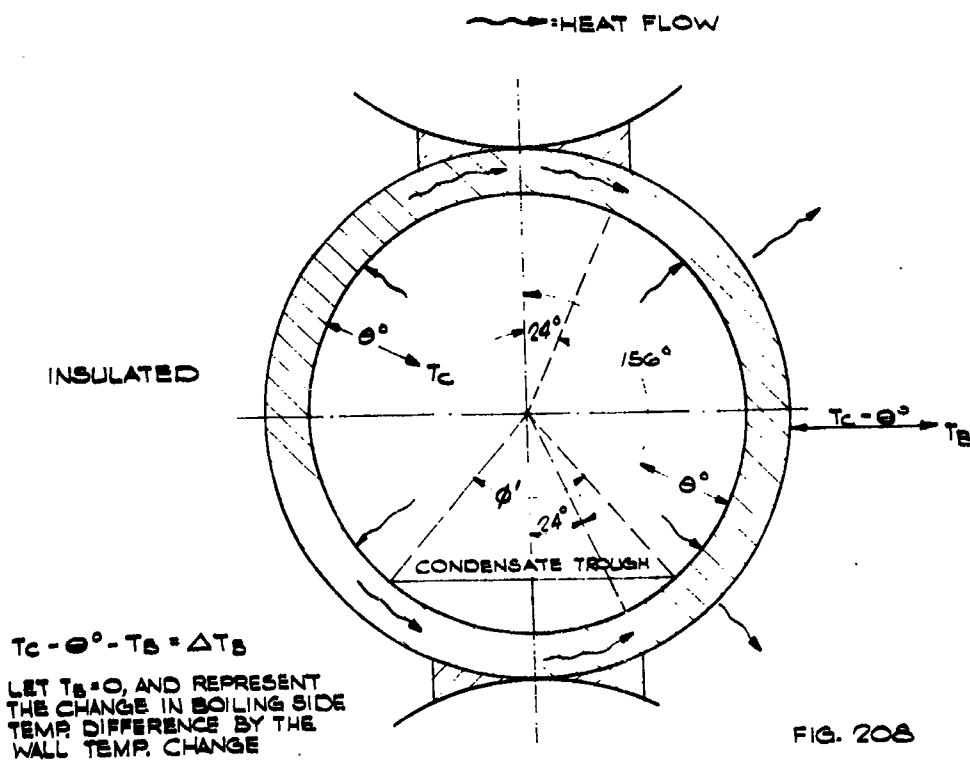
63 ASRP-2391

**CONFIDENTIAL**

CONFIDENTIAL

ASD-TDR-63-665, Part I

CONDENSER TUBE SECTION  
UCON FLUID TESTER



CONFIDENTIAL

**CONFIDENTIAL**

**ASD-TDR-63-665, Part I**

initial value problems, sets of initial values of  $\Theta$ ,  $Z$ ,  $Y$ , and  $\bar{Q}$  must either be known or assumed to start the solution.

The initial value of  $\bar{Q}$  for all segments was zero. At the top of the tube ( $\Phi'_1 = 0$ ) for an assumed temperature difference on the condensing side ( $\Theta^\circ$ ) the value of  $Y$  was calculable.

The first step in a solution consisted of obtaining mutually consistent pairs of  $\Theta^\circ$  and  $Z$  starting from  $\Phi'_1 = 0$  and integrating in a clockwise direction. The criteria for a mutually consistent pair of  $\Theta^\circ$  and  $Z$  was that the value  $\Theta^\circ$  be equal to  $\Theta_s^\circ$  (transverse condensing side heat transfer temperature difference) at the point where  $Z$  was first equal to zero. The value of  $\Theta_s^\circ$  was obtained from the heat balance on an element of the wall where:

$$Q_1 = Q_2 = 0.$$

$$Q_c = Q_b \quad (\text{See Figure 75})$$

$$\Theta_s^\circ = \frac{h_b}{h_{c1}} (T_c - T_b - \Theta_s^\circ)$$

If the initial value of  $Z$  was too large,  $\Theta^\circ = \Theta_s^\circ$  before  $Z = 0$ . Similarly, if the initial value of  $Z$  was too small,  $\Theta^\circ$  would reach the value  $\Theta_s^\circ$  after  $Z$  became zero. Through this procedure of trial and error, pairs of  $\Theta^\circ$  and  $Z$  were obtained which consist of all possible solutions starting the integration at the top of the tube and proceeding downward to the right. The integration was terminated at  $\Phi'_1 = \pi$ . The line of solutions is shown in Figure 209.

**SOLUTIONS FOR TOP OF TUBE**

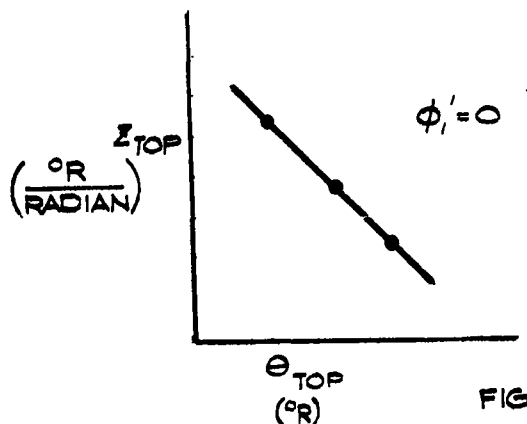


**FIG. 209**      63 ASRP-2391

**CONFIDENTIAL**

CONFIDENTIAL

ASD-TDR-63-665, Part I

The second step consisted of using pairs of  $\Theta^\circ$  and  $Z$  obtained from the line of solution for the top, Figure 209, for starting the integration at  $\phi' = 0$ , and proceeding in a counterclockwise direction to  $\phi' = \pi$ . The complete range of possible solutions for the point at  $\phi' = \pi$ , in the form of pairs of values of  $\Theta^\circ$  and  $Z$  at  $\phi' = \pi$ , were thus obtained as shown in Figure 210.

SOLUTION FOR BOTTOM OF TUBE

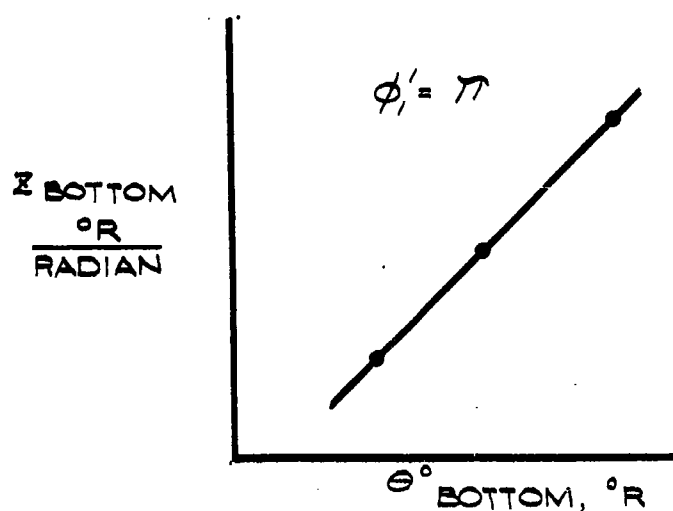


FIG. 210

The final step consisted of starting the solution at the bottom and proceeding in a counterclockwise direction. By trial sets of values of  $\Theta^\circ$  and  $Z$  for an assumed  $Y$  at  $\phi' = \pi$  were found which were possible solutions in that  $\Theta^\circ = \Theta_s^\circ$  when  $Z = 0$ . Assumption of a good value for  $Y$  was obtained from experience in running the program. This  $Y$  value was held constant as pairs of  $\Theta^\circ$  and  $Z$  were found.

For the given  $Y$ , this resulted in a crossplot on Figure 210 for solutions for the bottom of the tube as shown in Figure 211.

63 ASRP-2391

CONFIDENTIAL



**CONFIDENTIAL**

ASD-TDR-63-665, Part I

**CROSSPLOT OF SOLUTIONS FOR BOTTOM OF TUBE**

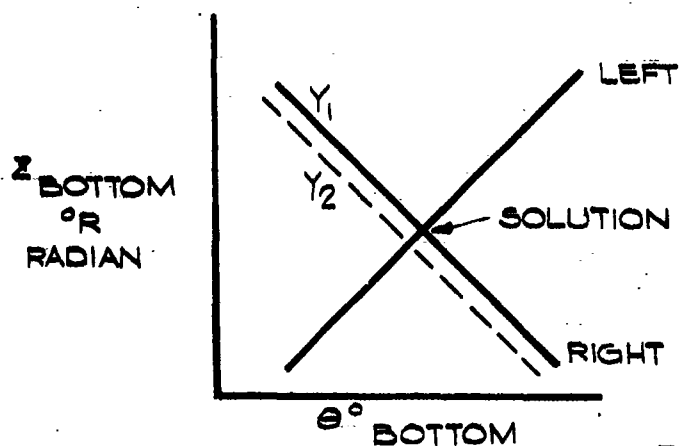


FIG. 211

The solution occurs at the intersection of the two lines on Figure 211. The effect of changing the solution by changing  $Y$  assumed at the bottom, was investigated and found to be an insensitive variation having a limited range as shown by the dotted line in Figure 211. Interpolation between the lines of  $Y_1$  and  $Y_2$  was used to obtain the exact solution.

After obtaining the exact solution, a final run was made using the known values previously determined.

The necessary data input and the output of the program are presented as follows:

Data Input

$Z$	Initial
$\theta$	Initial
$Y$	Initial
$\frac{\phi}{2}$	(Determined as functions of $Q/A$ and $Ng$ as shown earlier in this report.)
$B$	(Determined from Figures 41 and 42)

63 ASRP-2391

**CONFIDENTIAL**

~~CONFIDENTIAL~~

ASD-TDR-63-665, Part I

Data Input (Con't)

$C_1$   
 $g \cdot Ng$   
 $k_f$  (Determined from Ref . 51)  
 $k_m$   
 $u$  (Determined from Figures 41 and 42)  
 $r_t$   
 $t_t$   
 $T_c$   
 $\alpha^\circ$   
 $\lambda$   
 $\rho_L$   
 $\mu_L$   
 $\Delta\phi_1$  (Normally  $10^\circ$ )

Output of Program

The following are determined as functions of the angle around the tube circumference for the tube left half (0-180°) and right half (0-180°).

$z$   
 $\Theta^\circ$   
 $Y$   
 $\bar{Q}$

where at  $180^\circ$ ,  $z$  left =  $-z$  right and  $\Theta^\circ$  left =  $\Theta^\circ$  right.

The flowsheet for the computer program is presented as Figure 212. The Runge-Kutta Technique is standard and is shown as a subroutine (Ref. 39). Subroutine A illustrates the application of this particular system to the Runge-Kutta technique. The use of the equations in subroutine A is generalized as follows,

63 ASRP-2391

CONFIDENTIAL

**CONFIDENTIAL**

ASD-TDR-63-665, Part I

where:

$$f_1 = \bar{z} = \frac{d\bar{\Theta}^\circ}{d\phi_1}, \quad f_2 = \frac{d\bar{z}}{d\phi_1} = \frac{d^2\bar{\Theta}^\circ}{d\phi_1^2}, \quad f_3 = \frac{d\bar{Y}}{d\phi_1}, \quad f_4 = \frac{d\bar{Q}}{d\phi_1}$$

Left Half of Tube

$$\text{for: } 0 < \phi_1 < (180^\circ - \frac{\phi_1'}{2})$$

$$f_1 = -\bar{z}$$

$$f_2 = \frac{k_f C_1 r_t^2}{k_m t_t} \cdot \frac{\Theta^\circ}{Y}$$

$$f_3 = \frac{\mu_L k_f r_t}{\rho_L^2 g N g \lambda \cos \alpha^\circ \sin \phi_1} - \frac{Y}{3} \cot \phi_1'$$

$$f_4 = k_f r_t \frac{\Theta^\circ}{Y}$$

$$\text{for: } (180^\circ - \frac{\phi_1'}{2}) < \phi_1 < 180^\circ$$

$$f_1 = -\bar{z}$$

$$f_2 = 0 = \frac{d\bar{z}}{d\phi_1}$$

$$f_3 = 0 = \frac{d\bar{Q}}{d\phi_1}$$

$f_4$  is meaningless, set to zero

Right Half of Tube

$$\text{for: } 0 < \phi_1 < 24^\circ$$

$$f_1 = \bar{z}$$

$$f_2 = - \frac{k_f C_1 r_t^2}{k_m t_t} \cdot \frac{\Theta^\circ}{Y}$$

$$f_3 = \frac{\mu_L k_f r_t}{\rho_L^2 g N g \lambda \cos \alpha^\circ \sin \phi_1} \cdot \frac{\Theta^\circ}{Y^3} - \frac{Y}{3} \cot \phi_1'$$

$$f_4 = k_f r_t \frac{\Theta^\circ}{Y}$$

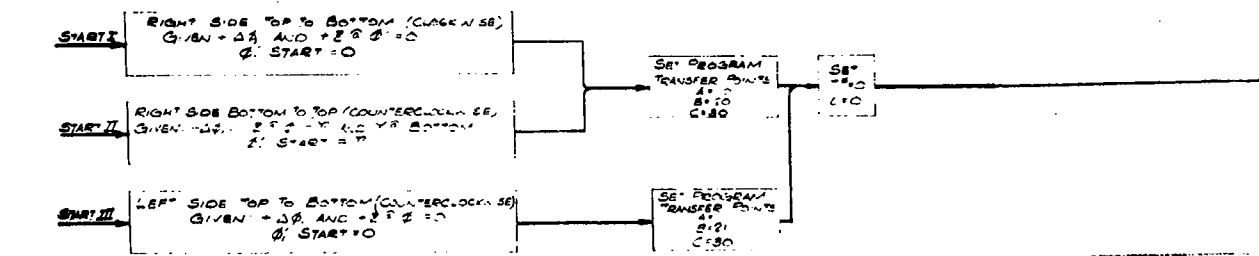
63 ASRP-2391

**CONFIDENTIAL**

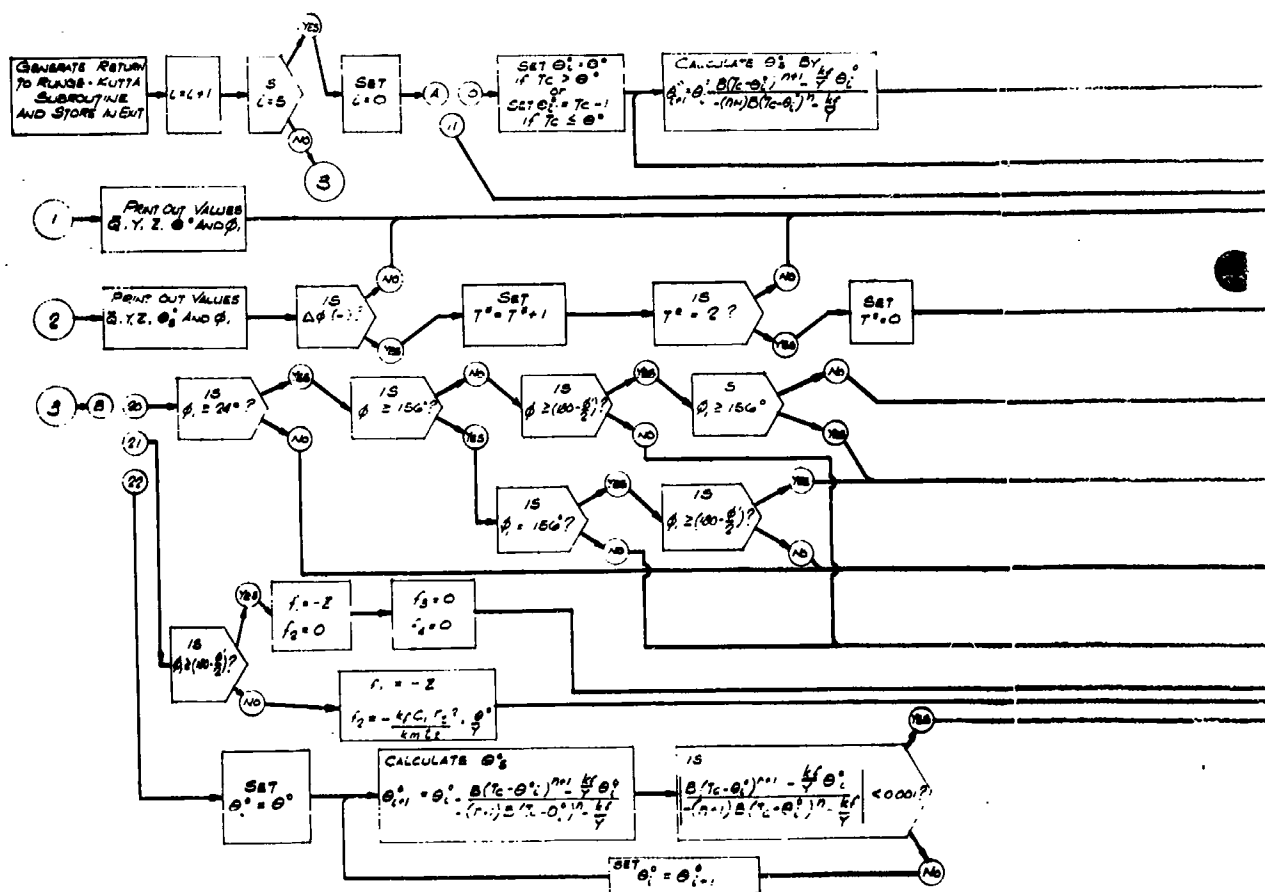
# CONFIDENTIAL

## ASD-TDR-63-665, Part I

COMPUTER PROGRAM FOR INTEGRATION OF SYSTEM OF FOUR DIFFERENTIAL  
MAIN



CONTENTS OF



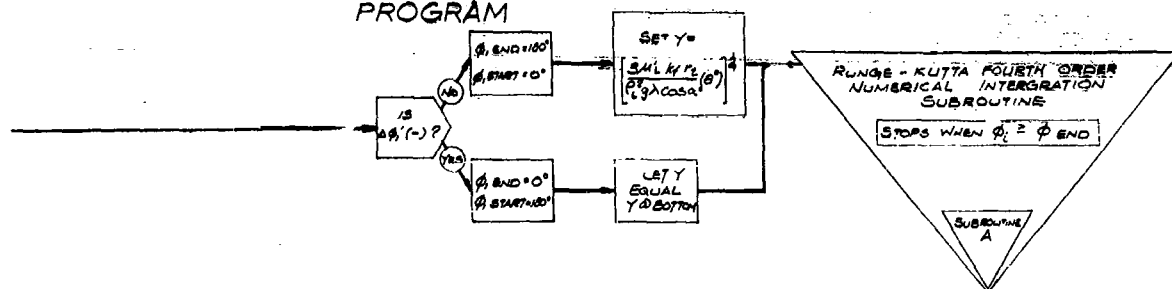
63 ASRP-2391

# CONFIDENTIAL

**CONFIDENTIAL**

ASD-TDR-63-665, Part I

EQUATIONS DESCRIBING HEAT TRANSFER IN UGEN FLUID ROTOR  
PROGRAM



SUBROUTINE A

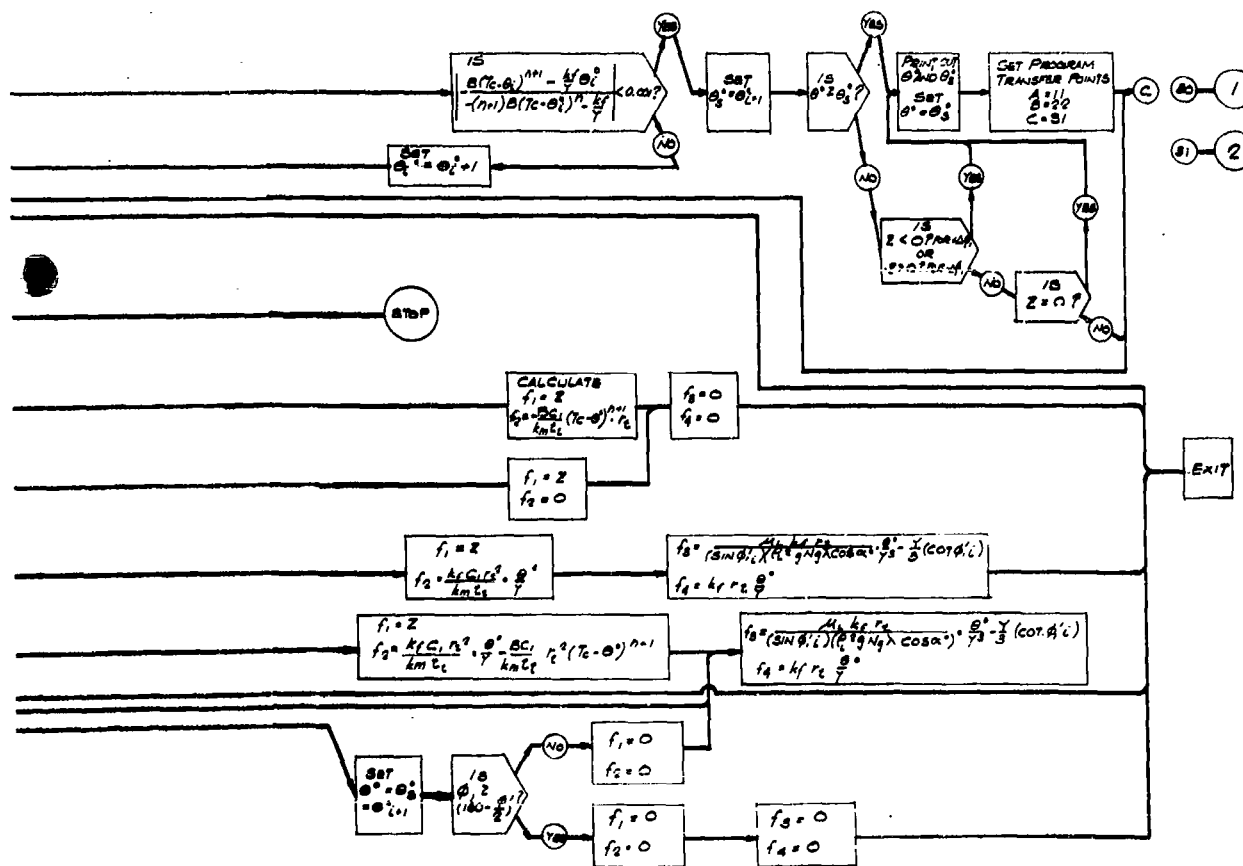


FIG. 212

63 ASRP-2391

**CONFIDENTIAL**

**CONFIDENTIAL**

ASD-TDR-63-665, Part I

Case I  $\frac{\phi'}{2} > 24^\circ$

for:  $24^\circ < \phi_1 < (180 - \frac{\phi'}{2})$

$$f_1 = Z$$

$$f_2 = \frac{k_f C_1 r_t^2}{k_m t_t} \cdot \frac{\Theta^0}{Y} - \frac{BC_1}{k_m t_t} r_t^2 (T_c - \Theta^0)^{n+1}$$

$$f_3 = \frac{\mu_L k_f r_t}{\rho_L^2 g N g \lambda \cos \alpha^\circ \sin \phi_1} \cdot \frac{\Theta^0}{Y^3} - \frac{Y}{3} \cot \phi_1$$

$$f_4 = k_f r_t \frac{\Theta^0}{Y}$$

for:  $(180 - \frac{\phi'}{2}) > \phi_1 < 156$

$$f_1 = Z$$

$$f_2 = \frac{B C_1 r_t^2}{k_m t_t} (T_c - \Theta^0)^{n+1}$$

$$f_3 = 0$$

$$f_4 = \text{is meaningless, set to zero}$$

for:  $156 < \phi_1 < 180^\circ$

$$f_1 = Z$$

$$f_2 = 0$$

$$f_3 = 0$$

$$f_4 = \text{is meaningless, set to zero}$$

Case II  $\frac{\phi'}{2} < 24^\circ$

for:  $24^\circ < \phi_1 < 156^\circ$   
 same as Case I For:  $24^\circ > \phi_1 < (180 - \frac{\phi'}{2})$

63 ASRP-2391

**CONFIDENTIAL**

**CONFIDENTIAL**

ASD-TDR-63-665, Part I

for:  $156^\circ \leq \phi_1 < (180^\circ - \frac{\phi_1'}{2})$

same as For:  $0 \leq \phi_1 < 24^\circ$

for:  $(180^\circ - \frac{\phi_1'}{2}) \leq \phi_1 \leq 180^\circ$

same as Case I  $156 \leq \phi_1 \leq 180^\circ$

As shown in the flowsheet (fig. 212), there are three starting positions depending on the tube segment being studied. The computation path next goes to subroutine A and is controlled by computer logic. Flow into the exit indicates flow into the Runge-Kutta integration and from there back to the beginning of subroutine A. Path 22 was utilized to force  $Z$  to stay at zero in calculations continuing to  $\pi$  after appropriate determination of  $Z = 0$  and  $\Theta^\circ = \Theta_s^\circ$  on the right side of the tube. This avoided unreal buildups in  $Z$  in the computation beyond the matching point over the circumferential length where  $Z$  is zero.

63 ASRP-2391

**CONFIDENTIAL**

ASD-TDR-63-665, Part I

(THIS PAGE IS INTENTIONALLY BLANK.)

63 ASRP-2391



# CONFIDENTIAL

ASD-TDR-63-665, Part I

## APPENDIX X

### THEORETICAL DISCUSSION OF THE CENTRIFUGAL SEAL

Consider the following configuration and its related nomenclature:

#### SKETCH OF CENTRIFUGAL SEAL

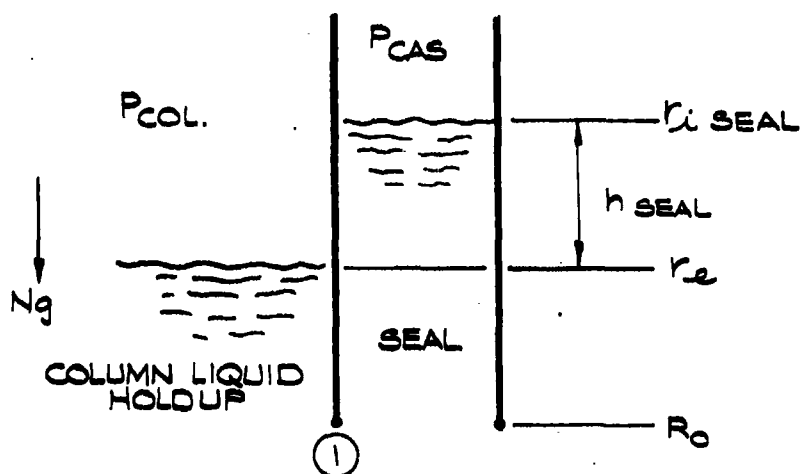


FIG 213

The pressure at point (1) resulting from the conditions in the column is the sum of the column pressure  $P_{COL}$ , and the pressure created by the liquid head in the centrifugal field which is given as follows: the centrifugal force on an infinitesimal body of fluid of mass  $dm$  at radius  $r$  is  $dm \omega^2 r$ . But the mass is

$$dm = dA dr \rho_L$$

where  $\rho_L$  is the liquid density. The centrifugal force gives rise to a

63 ASRP-2391

# CONFIDENTIAL

ASD-TDR-63-665, Part I

pressure difference  $dP$  across  $dr$  and hence a differential force  $dPdA$  where  $dA$  is the area normal to  $dr$ . Equating for equilibrium conditions:

$$dPdA = dm\omega^2 r = dA r \frac{\rho_L}{g_c} \omega^2 r$$

$$\text{and } \frac{dP}{\rho_L} = \frac{\omega^2}{g_c} r dr$$

In the present case the limits of integration are  $r_1$  and  $R_o$ . Thus

$$\begin{aligned} dP &= \frac{\omega^2 \rho_L}{g_c} r dr \\ P_i - P_{col} &= \frac{\omega^2 \rho_L}{g_c} \int_{r_1}^{R_o} r dr \\ &= \frac{\omega^2 \rho_L}{2 g_c} (R_o^2 - r_1^2) \end{aligned}$$

Thus:

$$P_i = P_{col} + \frac{\omega^2 \rho_L}{2 g_c} (R_o^2 - r_1^2)$$

Similarly on the casing side with  $r_{i\text{seal}} < r < R_o$

$$P_i = P_{cas} + \frac{\omega^2 \rho_L}{2 g_c} (R_o^2 - r_{i\text{seal}}^2)$$

Thus:

$$\begin{aligned} \Delta P_{\text{seal}} = P_{col} - P_{cas} &= \frac{\omega^2 \rho_L}{2 g_c} (R_o^2 - r_{i\text{seal}}^2) - \frac{\omega^2 \rho_L}{2 g_c} (R_o^2 - r_1^2) \\ &= -\frac{\omega^2 \rho_L}{2 g_c} (r_1^2 - r_{i\text{seal}}^2) \end{aligned}$$

63 ASRP-2391

CONFIDENTIAL

**CONFIDENTIAL**

ASD-TDR-63-665, Part I

or

$$r_{i\text{seal}} = \left[ r_1^2 - \frac{2 g_c \Delta P_{\text{seal}}}{\omega^2 \rho_L} \right]^{1/2} \quad (65)$$

Now if the casing pressure is raised such that

$$P_{\text{cas}} > P_{\text{col}}$$

The picture becomes:

**CENTRIFUGAL SEAL - RISE IN CASING PRESSURE**

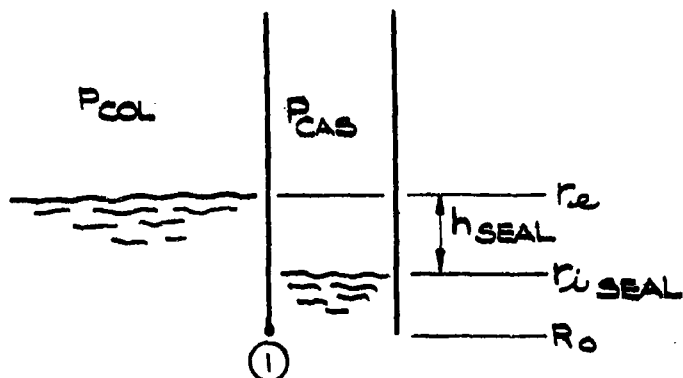


FIG. 2/4

Defining  $h_{\text{seal}}$  as shown, the total depth of immersion now becomes:

$$R_O - r_1 - [h_{\text{seal}}]$$

63 ASRP-2391

**CONFIDENTIAL**

# CONFIDENTIAL

ASD-TDR-63-665, Part I

where  $h_{\text{seal}} = r_{1\text{seal}} - r_1$

(keep in mind that  $h_{\text{seal}}$  may be positive or negative as follows:

$$h_{\text{seal}} \text{ is neg. for } P_{\text{col}} > P_{\text{cas}}$$

$$h_{\text{seal}} = 0 \quad \text{for } P_{\text{col}} = P_{\text{cas}}$$

$$h_{\text{seal}} \text{ is pos. for } P_{\text{col}} < P_{\text{cas}})$$

Hence:

$$r_{1\text{seal}}^2 = h_{\text{seal}}^2 + 2 r_1 h_{\text{seal}} + r_1^2$$

Since  $h_{\text{seal}} \ll r_{1\text{seal}}$  the term  $h_{\text{seal}}^2$  may be neglected, thus

$$r_{1\text{seal}}^2 = r_1^2 + 2 r_1 h_{\text{seal}}$$

and

$$\begin{aligned} \Delta P_{\text{seal}} &= \frac{\omega^2 \rho_L}{2 g_c} (r_1^2 - r_{1\text{seal}}^2 - 2 r_1 h_{\text{seal}}) \\ &= \frac{\omega^2 \rho_L}{2 g_c} (-2 r_1 h_{\text{seal}}) \end{aligned}$$

or

$$h_{\text{seal}} = - \frac{\Delta P_{\text{seal}} g_c}{\rho_L r_1 \omega^2} \quad (66)$$

Note that this conforms with the definition of  $h_{\text{seal}}$  as outlined above in terms of sign.

To be mathematically rigorous,

$$R_o - r_1 + h_{\text{seal}} = (R_o - r_1) - \frac{(\Delta P_{\text{seal}}) g_c}{\rho_L r_1 \omega^2} \quad (67)$$

since when  $h_{\text{seal}}$  is positive  $\Delta P_{\text{seal}}$  is negative.

63 ASRP-2391

**CONFIDENTIAL**

ASD-TDR-63-665, Part I

However, if the control valve is designed such that the liquid level is maintained at approximately 2 in. regardless of casing pressure, the last term of the above equation has  $r_1 \approx R_o$ . Thus  $R_o$  can be used with sufficient accuracy in the term defining  $h_{\text{seal}}$ .

63 ASRP-2391

**CONFIDENTIAL**

ASD-TDR-63-665, Part I

(THIS PAGE IS INTENTIONALLY BLANK.)

63 ASRP-2391

# CONFIDENTIAL

ASD-TDR-63-665, Part I

## APPENDIX XI

### COMPUTER PROGRAM FOR EVALUATION OF TWO-PHASE PRESSURE DROP AGAINST A GRAVITATIONAL FIELD

This program was written to use correlations developed from experimental data presented in Tables 52, 53 and 54 to evaluate two-phase flow directed against a gravitational field. The results are pertinent to study of the shelf and kettle transfer lines and their control valves. The flowsheet for the computer program is presented as Figure 215.

Assumptions involved in this program are as follows:

- a. Complete isentropic expansion with neglect of frictional losses.
- b. Pipelines are radially directed. Deviation from the radial direction would necessitate expressing  $\Delta R$  as a function of pipeline slope.
- c. Linear variation in liquid density from pipeline inlet to outlet.
- d. Variation in vapor density is in accordance with the Ideal Gas Law.
- e. Vapor quality is a function of pipeline inlet pressure to a power times the logarithm of the pipeline segment boundary pressure ratios.

Values for the constants  $a_1$  and  $a_2$  were obtained by calculation using data obtained from Reference (20).

Series A and B, air-water data, are omitted because experimental equipment problems during testing made these results unreliable.

63 ASRP-2391

# CONFIDENTIAL

# CONFIDENTIAL

ASD-TDR-63-665, Part I

TABLE 52

Two-Phase Flow of Air and Water Against Gravitational Field

Series "C"

Run	Aver. N g	G <sub>L</sub> H <sub>2</sub> O lb./Sec.	G <sub>g</sub> Air lb./Sec.	P <sub>v</sub> lb./Cu. Ft.	ΔP Psi	L/V Vol.
298	28.5	0.139	0.0123	0.30	0.55	0.055
299	51.0				1.48	
300	80.0				4.15	
302	116.0				4.25	
303	156.0				5.50	
305	204.0				7.15	
307	258.0				12.4	
309	320.0				14.6	
310	28.5	0.278	0.0123		1.05	0.110
311	51.0				2.45	
313	80.0				5.2	
317	116.0				7.75	
318	156.0				8.25	
319	204.0				11.65	
320	258.0				16.7	
321	28.5	0.417			1.87	0.165
322	51.0				3.15	
323	80.0				5.5	
325	116.0				6.55	
326	156.0				10.0	
327	204.0				13.3	
328	258.0				16.3	
329	29.5	0.556			2.25	0.220
330	51.0				3.37	
331	80.0				5.5	
332	116.0				6.55	
334	156.0				9.45	
335	204.0				15.0	
344	28.5	0.139	0.0246		0.25	0.0275
346	51.0				0.50	
347	80.0				0.90	
348	116.0				1.25	
349	156.0				1.75	
350	204.0				2.35	
351	258.0				3.1	
352	320.0				3.9	
356	28.5	0.278			0.25	0.055
357	51.0				0.50	
358	80.0				0.90	
359	116.0				1.25	
360	156.0				1.75	
362	204.0				2.35	
364	258.0				3.10	
365	51.0	0.417			0.75	0.0825
367	80.0				1.00	
368	116.0				1.75	
369	156.0				3.5	

63 ASRP-2391

# CONFIDENTIAL



# CONFIDENTIAL

ASD-TDR-63-665, Part I

TABLE 52 (Cont'd.)

Two-Phase Flow of Air and Water Against Gravitational Field

Series "C"

Run	Aver. N g	G <sub>L</sub> H <sub>2</sub> O lb./Sec.	G <sub>g</sub> Air lb./Sec.	p <sub>v</sub> lb./Cu.Ft.	ΔP Psi	L/V Vol.
370	204.0	0.417	0.0246	0.30	9.0	0.0825
371	258.0	↓	↓	↓	9.4	↓
372	51.0	0.556	↓	↓	1.25	0.110
373	80.0	↓	↓	↓	2.60	↓
374	116.0	↓	↓	↓	4.90	↓
375	156.0	↓	↓	↓	6.20	↓
377	204.0	↓	↓	↓	9.10	↓
378	258.0	↓	↓	↓	12.70	↓
380	51.0	0.695	↓	↓	2.38	0.1375
381	28.5	↓	↓	↓	2.38	↓
383	80.0	↓	↓	↓	5.87	↓
384	116.0	↓	↓	↓	7.65	↓
385	156.0	↓	↓	↓	9.40	↓
386	204.0	↓	↓	↓	12.65	↓
387	80.0	↓	↓	↓	1.15	↓
389	51.0	0.417	0.0369	↓	0.75	0.055
390	116.0	↓	↓	↓	1.40	↓
393	156.0	↓	↓	↓	1.62	↓
394	204.0	↓	↓	↓	1.65	↓
395	258.0	↓	↓	↓	5.80	↓
396	28.5	0.556	0.0369	↓	0.62	0.0733
397	51.0	↓	↓	↓	0.87	↓
398	80.0	↓	↓	↓	1.30	↓
399	116.0	↓	↓	↓	1.62	↓
400	156.0	↓	↓	↓	2.25	↓
401	204.0	↓	↓	↓	3.25	↓
409	80.0	0.417	0.0123	0.35	5.95	0.182
410	116.0	↓	↓	↓	6.55	↓
412	156.0	↓	↓	↓	9.15	↓
413	204.0	↓	↓	↓	12.1	↓
414	258.0	↓	↓	↓	14.5	↓
415	320.0	↓	↓	↓	23.3	↓
420	28.5	↓	0.012	0.20	2.0	0.110
423	51.0	↓	↓	↓	3.6	↓
425	80.0	↓	↓	↓	6.2	↓
428	116.0	↓	↓	↓	8.1	↓
430	156.0	↓	↓	↓	9.0	↓
432	28.5	0.556	↓	↓	2.25	0.147
434	51.0	↓	↓	↓	3.75	↓
435	80.0	↓	↓	↓	5.6	↓
437	116.0	↓	↓	↓	7.1	↓

479

63 ASRP-2391

# CONFIDENTIAL

# CONFIDENTIAL

ASD-TDR-63-665, Part I

TABLE 53

Two-Phase Flow of Air and Water Against Gravitational Field

Series "D"

<u>Run</u>	<u>Aver. N<sub>g</sub></u>	<u>G<sub>L</sub> H<sub>2</sub>O Lb./Sec.</u>	<u>G<sub>g</sub> Air Lb./Sec.</u>	<u>ρ<sub>v</sub> Lb./Cu.Ft.</u>	<u>ΔP Psi</u>	<u>L/V Vol.</u>
481	28.5	0.139	0.006	0.30	0.6	0.110
482	51.0				2.25	
484	80.0				2.0	
485	116.0				3.25	
486	156.0				4.1	
488	204.0				7.1	
492	258.0				10.0	
521	28.5		0.0123		0.4	0.055
522	51.0				0.8	
525	80.0				1.1	
526	116.0				1.6	
527	156.0				2.0	
529	204.0				2.3	
530	258.0				2.35	
533	320.0				4.5	

CONFIDENTIAL

CONFIDENTIAL

ASD-TDR-63-665, Part I

TABLE 54  
Two-Phase Flow of UCON-12 Fluid Against a Gravitational Field

Run	RPM	Average $X$ Lb./Lb.	Average $\rho_v$ Lb./Ft. <sup>3</sup>	Average $\rho_L$ Lb./Ft. <sup>3</sup>	Total Flow Lb./Sec.	Calculated		Measured	
						$\Delta P$	PSI	$\Delta P$	PSI
2	750	.087	2.54	80.5	.647	13.5	13.5	14.2	14.2
3	700	.088	2.54	80.5	.593	13.7	13.7	15.2	15.2
4	775	.091	2.51	80.3	.899	14.4	14.4	16.2	16.2
5	775	.089	2.52	80.2	1.345	12.6	12.6	14.2	14.2
6	775	.086	2.52	80.6	1.80	11.8	11.8	14.0	14.0
7	800	.082	2.58	80.6	1.80	13.6	13.6	15.5	15.5
8	800	.084	2.55	80.8	1.345	14.7	14.7	15.4	15.4
9	800	.088	2.50	82.9	.907	15.9	15.9	17.7	17.7
11	675	.077	2.81	79.6	.656	13.4	13.4	14.2	14.2
12	775	.077	2.82	79.3	.585	17.5	17.5	19.5	19.5
13	740	.081	2.70	79.5	.532	16.2	16.2	18	18
14	750	.092	2.65	79.7	.532	15.6	15.6	18.3	18.3
15	800	.069	2.92	79.1	1.77	17.0	17.0	14.1	14.1
16	480	.036	2.95	80.3	2.84	7.7	7.7	7.0	7.0

Average values taken at 1" below top tap

Tube I.D. = 5/8" Tap 1 = 9-1/8" Tap 2 = 12-1/8"

63 ASRP-2391

CONFIDENTIAL

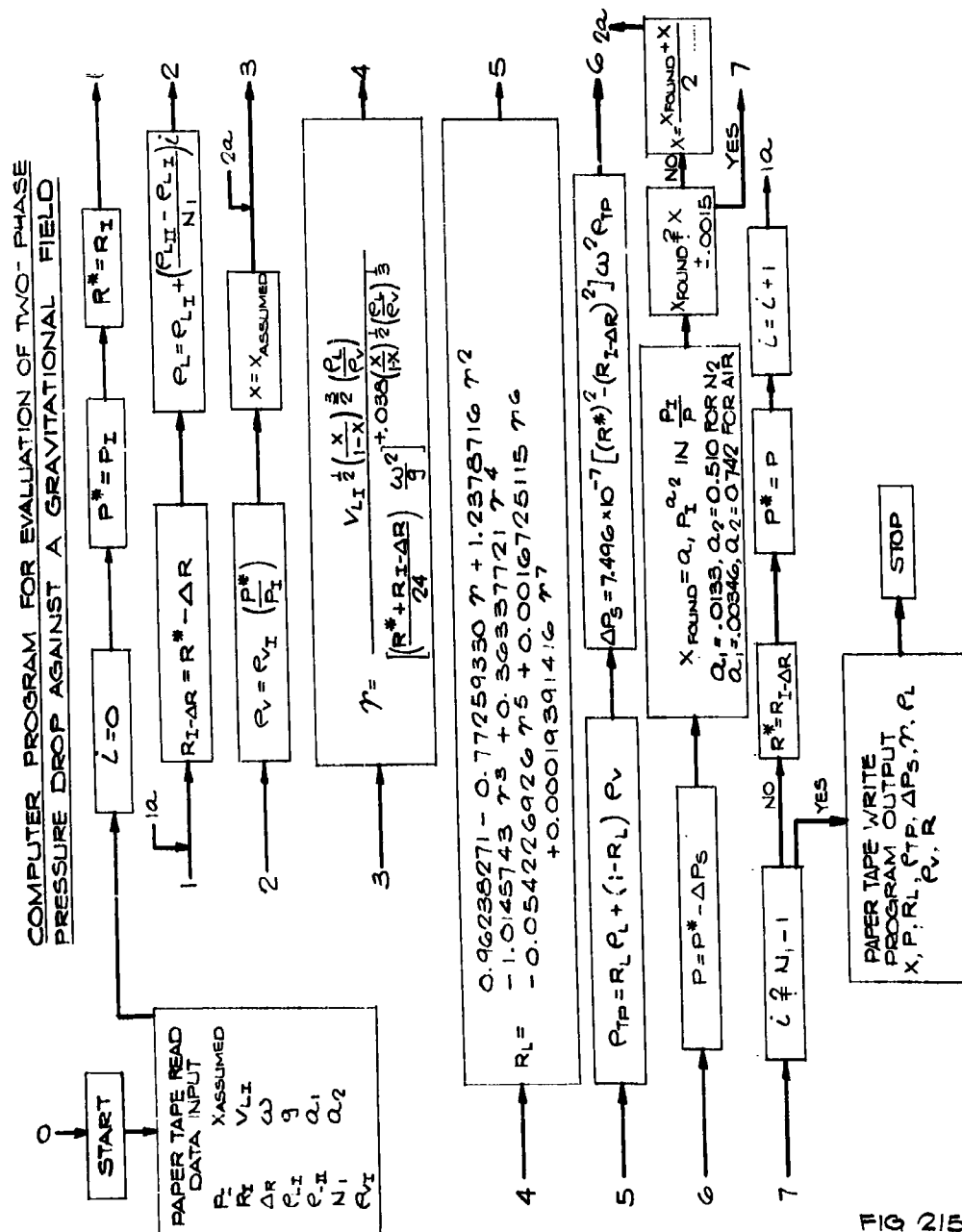


FIG 215

# CONFIDENTIAL

ASD-TDR-63-665, Part I

## APPENDIX XII

### CONTROL VALVE SYSTEM

#### 1. Control Valve System Analysis

As indicated on Figure 135, the basic elements of the kettle transfer system are:

- a. The liquid collector space which acts as a holdup chamber.
- b. The valve which opens or closes depending upon liquid level.
- c. The pressure sensing element which converts the static head of the liquid to a pneumatic signal proportional to liquid level.

These are presented in a conventional block diagram in Figure 216. In this basic model, the effect of the pressure drop through the kettle transfer line has not been included, as this is felt to be of minor importance. In the following, a short analysis on the simplified control system model is presented to obtain some indication of control response times.

The transfer functions for the individual components are derived below.

- a. Holdup chamber transfer function: The geometric configuration is shown in Figure 217.

$$W - W_v = \rho_L \pi (r_{ok}^2 - h_L^2) b_k \frac{dh_L}{dt_1}$$

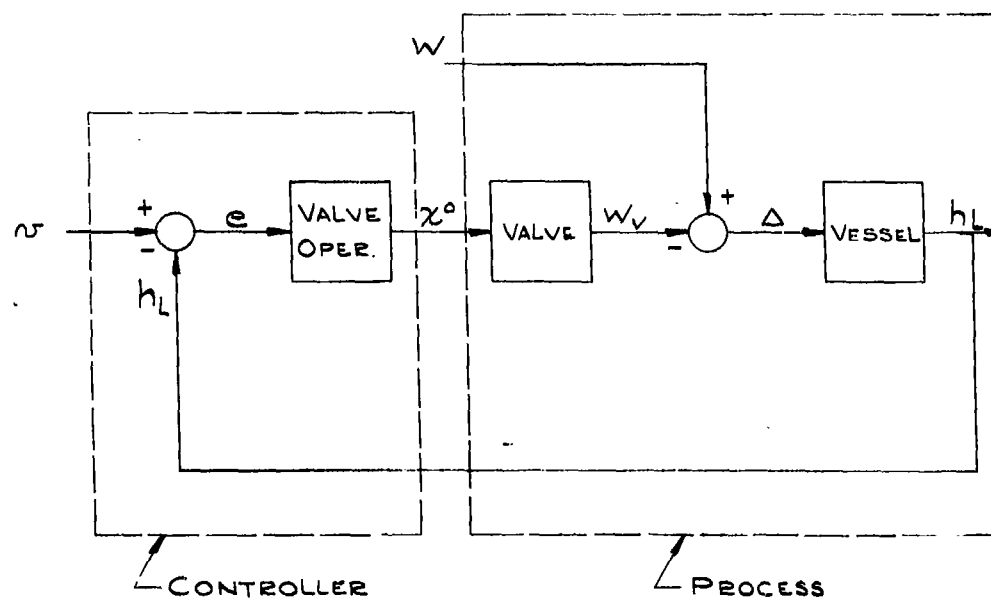
$$W - W_v = \rho_L \pi b_k (r_{ok}^2 - h_L^2) \frac{dh_L}{dt_1}$$

or in operational notation.

63 ASRP-2391

CONFIDENTIAL

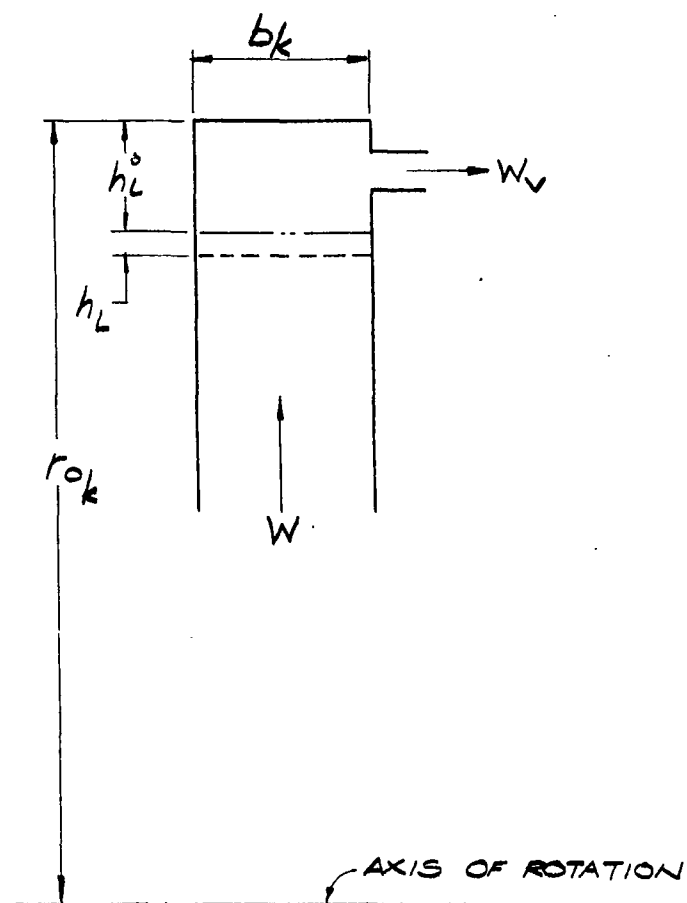
ASD-TDR-63-665, Part I



BLOCK DIAGRAM OF TRANSFER VALVE CONTROL SYSTEM

FIG. 216

ASD-TDR-63-665, Part I



KETTLE SCHEMATIC

FIG. 217.

# CONFIDENTIAL

ASD-TDR-63-665, Part I

$$W(s) - W_v(s) = \rho_L 2 \pi b_k (r_{o_k} - h_L^0) s h_L(s)$$

or,

$$\frac{h_L(s)}{W(s) - W_v(s)} = \frac{1}{k_1 s}$$

$$\text{where, } k_1 = \rho_L 2 \pi b_k (r_{o_k} - h_L^0)$$

$$\text{since, } \Delta(s) = W(s) - W_v(s)$$

$$\frac{h_L(s)}{\Delta(s)} = \frac{1}{k_1 s} \quad (68)$$

b. Valve Transfer Function: for the valve,

$$W_v = A [2g_c \Delta P \rho_L]^{1/2}$$

$$W_v^0 + w_v = (A^0 + a_a) [2g_c \Delta P \rho_L]^{1/2}$$

$$\text{but, } W_v^0 = A^0 [2g_c \Delta P \rho_L]^{1/2}$$

$$\text{thus, } w_v(s) = a_a(s) [2g_c \Delta P \rho_L]^{1/2}$$

$$[2g_c \Delta P \rho_L]^{1/2} = k_2$$

$$\text{or, } w_v(s) = a_a(s) k_2 \quad (69)$$

63 ASRP-2391

# CONFIDENTIAL



# CONFIDENTIAL

ASD-TDR-63-665, Part I

c. Valve Operator Transfer Function: This must be broken down into two parts:

- (1) Signal pressure -  $h_L$  functional relation.

The pressure signal available is found from

$$Sp = \frac{\rho_L}{2g_c} \omega^2 [2 r_{o_k} h_L - h_L^2]$$

This assumes a pressure tap mounted at the periphery,  $r_{o_k}$ . Since  $r_{o_k}$  is large, this can be approximated by,  $r_{o_k}$

$$Sp = \frac{\rho_L}{g_c} \omega^2 [r_{o_k} (h_L^o + h_L)]$$

- (2) Operator position  $x^o$  - Sp relation

$$Sp A_B = 2(k_s + k_b) x^o$$

These two-relationships are combined

$$\frac{\rho_L \omega^2}{g_c} r_{o_k} (h_L^o + h_L) = 2(k_s + k_b)(x_c^o + x_t^o)$$

and

$$A_B \frac{\rho_L \omega^2}{g_c} r_{o_k} h_L^o = 2(k_s + k_b) x_c^o$$

thus,

$$A_B \frac{\rho_L \omega^2}{g_c} r_{o_k} h_L(s) = 2(k_s + k_b) x_t^o(s)$$

63 ASRP-2391

# CONFIDENTIAL

# CONFIDENTIAL

ASD-TDR-63-665, Part I

$$\frac{A_B \frac{\rho_L \omega^2}{g_c} r_{ok}}{2(k_s + k_b)} = A_B \frac{\rho_L \omega^2 r_{ok}}{2g_c (k_s + k_b)} = \frac{1}{k_3}$$

$$\frac{h_L(s)}{x_t^o(s)} = k_3 \quad (70)$$

d. Orifice Area Transfer Function

Figure 218 indicates the orifice configuration used in the design of the control valve.

$$\begin{aligned} \text{Area of Sector} &= \phi'_i R_{\text{orf}}^2 \\ \text{Area of Triangle} &= R_{\text{orf}}^2 \cos \phi'_i \sin \phi'_i \\ \text{Orifice Area} &= 2R_{\text{orf}}^2 [\phi'_i - \cos \phi'_i \sin \phi'_i] \\ x^o &= 2R_{\text{orf}} [1 - \cos \phi'_i] \end{aligned}$$

thus,

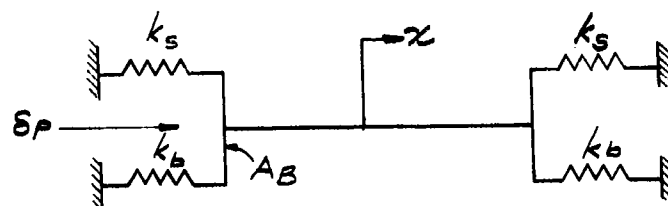
$$\begin{aligned} \frac{x^o}{2R_{\text{orf}}} &= 1 - \cos \phi'_i \\ \frac{A}{\pi R_{\text{orf}}^2} &= \frac{1}{\pi} [2\phi'_i - \sin 2\phi'_i] \\ \phi'_i &\rightarrow 0 \text{ to } \frac{\pi}{2} \end{aligned}$$

This is then linearized to obtain:

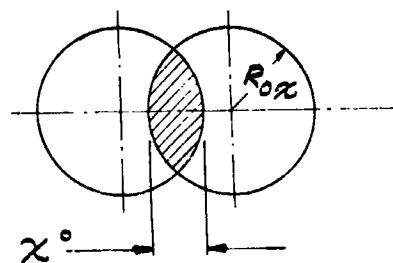
$$\begin{aligned} \frac{A}{\pi R_{\text{orf}}^2} &= 1.18 \frac{x^o}{2R_{\text{orf}}} - .2 \\ \frac{A^o}{\pi R_{\text{orf}}^2} &= \frac{1.18 X_c^o}{2R_{\text{orf}}} - .2 \end{aligned}$$

63 ASRP-2391

# CONFIDENTIAL



SCHEMATIC OF VALVE OPERATOR



ORIFICE OPENING

FIG 2/8

# CONFIDENTIAL

ASD-TDR-63-665, Part I

hence,

$$\frac{a_a}{\pi R_{orf}^2} = \frac{1.18 x_t^o}{2 R_{orf}}$$

or,

$$\frac{a_a}{\pi R_{orf}} = \frac{1.18 x_t^o}{2} = .59 x_t^o$$

$$a_a(s) = .59 \pi R_{orf} x_t^o(s)$$

$$\text{let } .59 \pi R_{orf} = k_4$$

$$a_a(s) = k_4 x_t^o(s) \quad (71)$$

In summary:

$$\text{Kettle Holdup: } \frac{h_L(s)}{(s)} = \frac{1}{k_1 s}$$

$$\text{where: } (s) = W(s) - W_v(s)$$

$$\text{Valve: } W_v(s) = a_a(s) k_2$$

$$\text{Valve Operator: } \frac{h_L(s)}{x(s)} = k_3$$

$$\text{Orifice Area: } a_a(s) = x^o(s) k_4$$

It is desired to examine as a measure of the control effectiveness the response to a delta-function input flow.

$$h_L(s) = \frac{1}{k_1 s} [W(s) - W_v(s)]$$

$$h_L(s) = \frac{1}{k_1 s} [W(s) - a_a(s) k_2]$$

63 ASRP-2391

# CONFIDENTIAL

~~CONFIDENTIAL~~

ASD-TDR-63-665, Part I

$$h_L(s) = \frac{1}{k_1 s} [W(s) - x^0(s) k_2 k_4]$$

$$h_L(s) = \frac{1}{k_1 s} W(s) - h_L(s) k_2 \frac{1}{k_3} k_4$$

or,

$$k_1 s h_L(s) = W(s) - k_2 \frac{1}{k_3} k_4 h_L(s)$$

$$h_L(s) [k_1 s + k_2 \frac{1}{k_3} k_4] = W(s)$$

$$\frac{h_L(s)}{W(s)} = \frac{1}{k_1 s + k_2 \frac{1}{k_3} k_4} = \frac{\frac{k_3}{k_2 k_4}}{\frac{k_1 k_3}{k_2 k_4} s + 1}$$

or,

$$\frac{h_L(s)}{W(s)} = \frac{\frac{1}{k_1}}{s + \frac{k_2 k_4}{k_1 k_3}}$$

let  $W(s) = \alpha_1 W_0$  where  $\alpha_1$  is some constant

then,

$$h_L(s) = \left[ \frac{\frac{1}{k_1}}{s + \frac{k_2 k_4}{k_1 k_3}} \right] \alpha_1 W_0$$

thus,

$$h_L(t_1) = \frac{W_0}{k_1} e^{-\left(\frac{k_2 k_4}{k_1 k_3}\right) t_1}$$

63 ASRP-2391

~~CONFIDENTIAL~~

**CONFIDENTIAL**

ASD-TDR-63-665, Part I

let,

$$\frac{k_1 k_3}{k_2 k_4} = T_1, \text{ the system time constant}$$

$$h_L(t_1) = \frac{\alpha_1 W_o}{k_1} e^{-\frac{t_1}{T_1}} \quad (72)$$

2. Data Analysis for Control System Tests

The following are considered in data analysis for the control system described in section 5.5.

a. Data obtained

- (1) flow ( $Q_L^1$ ) gal/min =  $\frac{W_v}{\rho_L} \left( \frac{7.48 \text{ gal}}{\text{cu.ft.}} \right) \left( \frac{60 \text{ sec}}{\text{min}} \right)$
- (2) speed (N) RPM
- (3) inlet liquid pressure ( $\rho_L^1$ )
- (4) outlet vapor pressure ( $\rho_v^1$ )
- (5) liquid level ( $h_L$ ), ft.

b.  $Q_L^1$ , w,  $\rho_L^1$ , and UCON fluid thermodynamic data used as input data to determine conditions at upstream side of valve. (Air-water correlations enter here.)

c. X downstream of the valve is found from assumption of isenthalpic flow through valve.

d.  $R_L$  downstream is computed from the assumption that for a given X and density ( $\rho_L$ ,  $\rho_v$ ) the kinetic energy is a minimum—no valid reason for this is known, but result compares well with the two-phase correlations.

e.  $R_L$ , X density ratios are used with the Hoopes correlation to find  $\Delta P_{TP}^1 / \Delta P_{LIQ}^1$ .

f.  $\Delta P_{LIQ}$  is determined from standard orifice equation knowing orifice area and standard flows for value.

63 ASRP-2391

**CONFIDENTIAL**

**CONFIDENTIAL**

ASD-TDR-63-665, Part I

g.  $\Delta P_{TP}^1$  is found and compared with pressure drop determined from  $P$  upstream of valve and measured vapor pressure.

Analysis of a typical data point:

$$Q_L^1 = 10 \text{ gpm}$$

$$N = 800 \text{ RPM}$$

$$P_L^1 = 149 \text{ psia}$$

$$P_V^1 = 80 \text{ psia}$$

$$\Delta P_{TP}^1 = 14.1 \text{ psi}$$

$$\text{Valve Operator Signal Pressure} = 15 \text{ psi}$$

The first step is to compute the pressure drop across the valve. Since the correlation to be used utilizes the downstream conditions, these must be found. The downstream pressure is approximately 80 psia (the vapor outlet pressure). The downstream  $X$  was found for isentropic and isenthalpic, the average valve (.160) will be used.

To compute the downstream  $R_L$ , it is assumed that the kinetic energy will be a minimum.

$$K.E. = \frac{G_1^2}{2g_C} \left[ \frac{(1-X)^3}{R_L^2} V_{SL}^2 + \frac{X^3 V_{SV}^2}{(1-R_L)^2} \right] \quad (73), (\text{ref. } 41)$$

$\frac{d K.E.}{d R_L} = 0$ , this will give the value of  $R_L$  for which the kinetic energy is a minimum.

$$\frac{-(1-X)^3 V_{SL}^2}{R_L^3} + \frac{3 V_{SV}^2}{(1-R_L)^3} = 0$$

$$\text{for this case } X = .160 \quad V_{SV} = .506 \quad V_{SL} = .012$$

thus,

$$\frac{-.853 \times 10^{-4}}{R_L^3} + \frac{10.5 \times 10^{-4}}{(1-R_L)^3} = 0$$

63 ASRP-2391

**CONFIDENTIAL**

**CONFIDENTIAL**

ASD-TDR-63-665, Part I

$$-(1 - R_L)^3 .853 + 10.5 R_L^3 = 0$$

$R_L = .3$  minimizes the function.

The Hoopes correlation parameter can now be computed.

$$\frac{(1 - X)^2}{R_L} + \frac{V_{SV}}{V_{SL}} \frac{X^2}{1 - R_L} = \frac{(1 - .160)^2}{.3} + \frac{.506}{.012} \frac{(160)^2}{1 - .3} = 3.89$$

From the correlation  $\Delta P_{TP}^1 / \Delta P_{LIQ} = 3$

$\Delta P_{LIQ}$ , the pressure drop assuming liquid flow is now determined.

$$W = A [ 2g_c \Delta P_{LIQ} \rho_L ]^{1/2}$$

$W = .88 \text{ lb./sec. per tube.}$

The corresponding  $\rho_L = 77.5 \text{ lb./ft.}^3$

The orifice area must be determined from the valve piston position or the valve operator signal pressure = 15 psi.

The orifice area obtained from Figure 218 is  $.0727 \text{ in.}^2$

$\Delta P_L$  is found to be 4.21 psi

thus,

$$\Delta P_{TP}^1 = 4.21 (3.89) = 16.4 \text{ psi.}$$

63 ASRP-2391

**CONFIDENTIAL**



ASD-TDR-63-665, Part I

APPENDIX XIII

STATIONARY COLUMN RESULTS

63-ASRP-2391

**SECRET**

# ASD-TDR-63-665, Part I

TABLE 55

POINT NO. 1

LOW PRESSURE COLUMN PRESSURE - 56.5 S P S 76.5 PSIA\*

HIGH PRESSURE COLUMN PRESSURE - 234 PSIA

FEED AIR SUPERHEAT - 0 B.T.U.

VAPOR MOL FRACTION			LIQUID MOL FRACTION			FLOW QUAN.		
N	A	O	N	A	O	L	V	
<b>TOP SECTION OF LOW PRESSURE COLUMN</b>								
.9782	.004240	.01755	1.000	.0000	.0000	.0000	-.7788	FEED
.9773	.003183	.01951	.9440	.005953	.05001	.2512	.1227	FEED
.9783	.004375	.01730	.9627	.005016	.03226	.5543	.9592	
.9695	.006212	.02427	.9474	.008204	.04441	.5519	.9568	1
.9580	.008089	.03393	.9272	.01148	.06132	.5485	.9534	2
.9432	.009902	.04686	.9012	.01467	.08411	.5440	.9488	3
.9250	.01152	.06345	.8689	.01755	.1136	.5382	.9431	4
.9036	.01278	.08359	.8305	.01985	.1497	.5315	.9364	5
.8799	.01356	.1066	.7874	.02134	.1913	.5243	.9291	6
.8553	.01380	.1309	.7422	.02186	.2359	.5171	.9219	7
.8316	.01352	.1549	.6982	.02146	.2803	.5104	.9153	8
.8104	.01283	.1768	.6585	.02032	.3211	.5048	.9097	9
.7926	.01191	.1954	.6252	.01872	.3561	.5005	.9053	10
			.6317	.01646	.3518			9.6
<b>BOTTOM SECTION OF LOW PRESSURE COLUMN</b>								
.1893	.03365	.7770	.08504	.02756	.8874	-.2212	.0000	FEED
.1893	.03365	.7770	.1627	.03210	.8052	.8671	.6459	
.3286	.03528	.6361	.2674	.03334	.6993	.8803	.6590	1
.4803	.03230	.4874	.3830	.03114	.5859	.8987	.6775	2
.6119	.02664	.3615	.4850	.02686	.4882	.9184	.6972	3
.7056	.02083	.2736	.5586	.02243	.4189	.9344	.7131	4
.7635	.01629	.2203	.6045	.01893	.3765	.9446	.7233	5
.7964	.01322	.1904	.6307	.01656	.3527	.9498	.7285	6
.8145	.01130	.1742	.6453	.01507	.3396	.9540	.7328	7
			.6317	.01646	.3518			6.1
.8104	.009055	.1805	.6234	.01317	.3634	.4485	.1776	FEED
<b>HIGH PRESSURE COLUMN</b>								
.9733	.003564	.02315	.9550	.005044	.04000	-.3739	.0000	FEED
.9550	.005044	.04000	.9550	.005044	.04000	.7297	1.104	
.9349	.006367	.05871	.9244	.007059	.06849	.7155	1.089	1
.9137	.007495	.07881	.8917	.008802	.09950	.7012	1.075	2
.8920	.008396	.09957	.8578	.01022	.1320	.6873	1.061	3
.8707	.009058	.1202	.8240	.01128	.1647	.6743	1.048	4
.8505	.009491	.1400	.7916	.01200	.1964	.6626	1.036	5
.8321	.009720	.1582	.7616	.01240	.2260	.6523	1.026	6
.8158	.009783	.1744	.7349	.01254	.2525	.6437	1.018	7
.8018	.009724	.1885	.7119	.01247	.2757	.6365	1.010	8
.7901	.009585	.2003	.6925	.01228	.2953	.6308	1.005	9
.7806	.009400	.2100	.6765	.01200	.3115	.6261	1.000	10
.7901	.009586	.2003	.6765	.01200	.3115	-.6261	.0000	FEED
.7806	.009400	.2100	1.000	.0000	.0000	.0000	1.000	FEED

HEAT EXCHANGER DUTIES - B.t.u./Lb. mole feed

QR 1765, QC 691, QS 69

\* These calculations account for the variation of the relative volatilities and enthalpies with pressure. All following cases are the same unless otherwise indicated.

**SECRET**

SECRET

ASD-TDR-63-665, Part I

TABLE 56

POINT NO. 2

LOW PRESSURE COLUMN PRESSURE - 56.5 ≤ P ≤ 76.5 PSIA\*

HIGH PRESSURE COLUMN PRESSURE - 225 PSIA

FEED AIR SUPERHEAT - 0 B.T.U.

VAPOR MOL FRACTION			LIQUID MOL FRACTION			FLOW QUAN.		
N	A	O	N	A	O	L	V	
TOP SECTION OF LOW PRESSURE COLUMN								
.9783	.004151	.01755	1.000	.0000	.0000	.0000	-.7788	FEED
.9775	.003135	.01934	.9446	.005864	.04957	.2608	.1209	FEED
.9784	.004278	.01733	.9627	.004942	.03233	.5650	.9620	
.9695	.006083	.02441	.9475	.008023	.04448	.5626	.9596	1
.9577	.007955	.03438	.9271	.01124	.06167	.5590	.9561	2
.9422	.009793	.04796	.9004	.01442	.08522	.5542	.9513	3
.9229	.01145	.06564	.8666	.01733	.1161	.5481	.9451	4
.8999	.01276	.08738	.8258	.01968	.1545	.5408	.9379	5
.8740	.01357	.1124	.7797	.02119	.1992	.5329	.9299	6
.8472	.01379	.1390	.7311	.02170	.2472	.5250	.9221	7
.8214	.01346	.1652	.6838	.02123	.2949	.5178	.9149	8
.7984	.01270	.1889	.6415	.01997	.3385	.5118	.9089	9
.7795	.01170	.2088	.6064	.01825	.3754	.5072	.9043	10
			.6321	.01682	.3510			9.0
BOTTOM SECTION OF LOW PRESSURE COLUMN								
.1887	.03404	.7773	.08472	.02788	.8874	-.2212	.0000	FEED
.1887	.03404	.7773	.1625	.03248	.8051	.8765	.6552	
.3281	.03571	.6361	.2676	.03376	.6986	.8898	.6686	1
.4805	.03269	.4868	.3841	.03152	.5844	.9087	.6874	2
.6129	.02693	.3601	.4871	.02716	.4857	.9289	.7077	3
.7072	.02102	.2718	.5615	.02263	.4159	.9454	.7241	4
.7654	.01640	.2182	.6079	.01905	.3731	.9558	.7346	5
.7985	.01327	.1882	.6342	.01663	.3492	.9612	.7400	6
			.6321	.01602	.3510			5.9
.8091	.009126	.1818	.6216	.01324	.3651	.4490	.1693	FEED
HIGH PRESSURE COLUMN								
.9736	.003537	.02282	.9549	.005060	.04000	-.3817	.0000	FEED
.9549	.005060	.04000	.9549	.005060	.04000	.7193	1.101	
.9345	.006418	.05908	.9234	.007153	.06941	.7052	1.087	1
.9129	.007568	.07953	.8897	.008954	.1014	.6909	1.073	2
.8909	.008478	.1006	.8549	.01040	.1347	.6772	1.059	3
.8694	.009138	.1214	.8203	.01148	.1682	.6645	1.046	4
.8492	.009560	.1413	.7873	.01219	.2005	.6530	1.035	5
.8308	.009773	.1594	.7571	.01257	.2303	.6432	1.025	6
.8147	.009818	.1754	.7305	.01268	.2569	.6349	1.017	7
.8011	.009745	.1892	.7075	.01259	.2798	.6281	1.010	8
.7898	.009594	.2006	.6885	.01237	.2991	.6226	1.004	9
.7806	.009400	.2100	.6730	.01208	.3149	.6183	1.000	10
.7897	.009594	.2007	.6730	.01208	.3150	-.6183	.0000	FEED
.7806	.009400	.2100	1.000	.0000	.0000	.0000	1.000	FEED

HEAT EXCHANGER DUTIES - B.t.u./lb. mole feed  
QR 1795, QC 694, QS 69

\* These calculations account for the variation of the relative volatilities and enthalpies with pressure. All following cases are the same unless otherwise indicated.

SECRET

# SECRET

## ASD-TDR-63-665, Part I

TABLE 57

POINT NO. 3

LOW PRESSURE COLUMN PRESSURE - 65 ≤ P ≤ 98 PSIA\*

HIGH PRESSURE COLUMN PRESSURE - 265 PSIA

FEED AIR SUPERHEAT - 0 B.T.U.

Vapor	Mol	Fraction	Liquid	Mol	Fraction	Flow	Quan.	
N	A	Q	N	A	Q	L	V	
TOP SECTION OF LOW PRESSURE COLUMN								
.9773	.005112	.01755	1.000	.0000	.0000	.0000	-.7921	FEED
.9759	.005690	.02049	.9426	.006670	.05072	.2403	.1321	FEED
.9775	.005318	.01714	.9612	.005835	.03295	.3176	.9374	
.9701	.007483	.02298	.9477	.002739	.04254	.5153	.9352	1
.9613	.009973	.02913	.9315	.01358	.09491	.5129	.9326	2
.9509	.01132	.03799	.9123	.01716	.07050	.5097	.9294	3
.9399	.01324	.04790	.8901	.02094	.08961	.5059	.9256	4
.9283	.01464	.06003	.8648	.02697	.1182	.5018	.9213	5
.9168	.01664	.07376	.8371	.03490	.1580	.4970	.9168	6
.8991	.01822	.08863	.8077	.04506	.1662	.4923	.9120	7
.8796	.01977	.1040	.7780	.05843	.1956	.4877	.9074	8
.8546	.02153	.1192	.7431	.07508	.2248	.4834	.9031	9
.8299	.02350	.1355	.7054	.09315	.2535	.4796	.8993	10
.8047	.02566	.1524	.6687	.02383	.2775	.4764	.8961	11
.8284	.02803	.1706	.6344	.02231	.2992	.4739	.8936	12
.8200	.03118	.1899	.6019	.02075	.3174	.4720	.8917	13
.8133	.03430	.2103	.5728	.01925	.3319	.4706	.8905	14
.8082	.03740	.2318	.5468	.01789	.3435	.4697	.8894	15
.8044	.04048	.2546	.5234	.01671	.3519	.4692	.8889	16
.8016	.04354	.2789	.5022	.01571	.3581	.4690	.8887	17
.7998	.04658	.3047	.4827	.01489	.3624	.4691	.8888	18
.7986	.04960	.3320	.4656	.01422	.3653	.4694	.8891	19
.7980	.05260	.3607	.4507	.01365	.3662			20.54

### BOTTOM SECTION OF LOW PRESSURE COLUMN

.06962	.03342	.8970	.05096	.02574	.9435	-.2079	.0000	FEED
.06962	.03342	.8970	.05094	.03147	.9267	.2212	.6133	
.1298	.03925	.8510	.1049	.03504	.8953	.2446	.6109	1
.2160	.04217	.7818	.1698	.05005	.7922	.2313	.6034	2
.3202	.04138	.6525	.2533	.05752	.7092	.2419	.6040	3
.4458	.03721	.5170	.3491	.05445	.6205	.2561	.6062	4
.5950	.03161	.4125	.4507	.05221	.5391	.2718	.6090	5
.7630	.02539	.3316	.5694	.04947	.4752	.2859	.6180	6
.9042	.02005	.2793	.6481	.04636	.4306	.2965	.6326	7
.9797	.01613	.2402	.7197	.04394	.4020	.3033	.6494	8
.9850	.01350	.2185	.7991	.04161	.3846	.3071	.6692	9
.9825	.01182	.2027	.8605	.03900	.3744	.3089	.6901	10
.9811	.01076	.1901	.9013	.03619	.3656	.3089	.7011	11
.9805	.01011	.1806	.9212	.03369	.3582	.3084	.7006	12
.9803	.009711	.1730	.9355	.03135	.3522	.3075	.6996	13
			.9422	.02915	.3462			14.47

.8017	.009045	.1892	.6239	.01278	.3633	.4306	.1890	FEED
-------	---------	-------	-------	--------	-------	-------	-------	------

### HIGH PRESSURE COLUMN

.9716	.004108	.02427	.9544	.005599	.04000	-.3724	.0000	FEED
.9544	.008599	.04000	.9544	.005599	.04000	.7583	1.111	
.9543	.008599	.04000	.9270	.007589	.06346	.7845	1.097	1
.9177	.007990	.07432	.8905	.009843	.09229	.7109	1.083	2
.8998	.008857	.09197	.8607	.01060	.1197	.6980	1.070	3
.8813	.009904	.1092	.8415	.01168	.1468	.6860	1.058	4
.8644	.009947	.1297	.8148	.01234	.1729	.6732	1.048	5
.8490	.01021	.1468	.7900	.01279	.1978	.6607	1.038	6
.8338	.01053	.1663	.7678	.01301	.2192	.6476	1.050	7
.8190	.01087	.1886	.7386	.01296	.2356	.6307	1.023	8
.8047	.01019	.2132	.7176	.01279	.2554	.6130	1.017	9
.7976	.009999	.2394	.7059	.01271	.2683	.5969	1.009	10
.7919	.009841	.2663	.6954	.01253	.2813	.5815	1.006	11
.7873	.009604	.2930	.6866	.01209	.2953	.5670	1.003	12
.7836	.009356	.3209	.6824	.01187	.3097	.5531	1.002	13
.7806	.009100	.3490	.6773	.01165	.3108	.5396	1.000	14
.7835	.009356	.3209	.6773	.01166	.3109	-.6276	.0000	FEED
.7806	.009100	.3490	1.000	.0000	.0000	.0000	1.000	FEED

HEAT EXCHANGER DUTIES - B.T.U./Lb. mole feed

QP 1660, QC 623, QS 87

\* The calculations account for the variation of the relative volatilities and enthalpies with pressure.

# SECRET

# SECRET

## ASD-TDR-63-665, Part I

TABLE 58

POINT NO. 4

LOW PRESSURE COLUMN PRESSURE -  $65 \leq P \leq 95$  PSIA\*

HIGH PRESSURE COLUMN PRESSURE - 265 PSIA

FEED AIR SUPERHEAT - 0 B.T.U.

Vapor	Mol	Fraction	Liquid	Mol	Fraction	Flow	Quan.	
N	A	Q	N	A	Q	L	Y	
TOP SECTION OF LOW PRESSURE COLUMN								
.9773	.005103	.01753	1.000	.0000	.0000	.0000	-.7768	FEED
.9759	.003650	.02049	.9426	.006670	.05072	.2403	.1321	FEED
.9776	.005308	.01714	.9617	.005811	.03252	.5304	.9388	1
.9697	.007532	.02277	.9477	.009740	.04254	.5504	.9367	2
.9601	.009737	.03019	.9306	.01365	.05378	.5277	.9340	3
.9485	.01185	.03771	.9098	.01740	.07283	.5242	.9306	4
.9343	.01371	.05151	.8851	.02078	.09412	.5201	.9265	5
.9192	.01524	.06559	.8587	.02360	.11197	.5153	.9217	6
.9020	.01653	.08164	.8253	.02566	.14991	.5101	.9165	7
.8840	.01695	.09907	.7919	.02685	.1813	.5048	.9112	8
.8659	.01705	.1170	.7582	.02714	.2147	.4996	.9060	9
.8487	.01671	.1346	.7249	.02661	.2473	.4949	.9013	10
.8331	.01603	.1508	.6964	.02546	.2782	.4906	.8972	11
.8197	.01515	.1652	.6707	.02390	.3094	.4875	.8939	12
.8066	.01417	.1772	.6496	.02214	.3406	.4833	.8896	13
.7999	.01319	.1869	.6350	.02093	.3609	.4822	.8885	14
.7933	.01229	.1944	.6204	.01873	.3715	.4816	.8879	15
.7884	.01149	.2001	.6112	.01727	.3791	.4814	.8876	16
.7850	.01082	.2042	.6048	.01603	.3791	.4814	.8876	15.58
			.6162	.01488	.3609			
BOTTOM SECTION OF LOW PRESSURE COLUMN								
.1863	.02968	.7840	.08808	.02452	.8874	-.2212	.0000	FEED
.1855	.02968	.7840	.1605	.02833	.8111	.8425	.6213	1
.3124	.03133	.6562	.2543	.02957	.7161	.8540	.6328	2
.4488	.02942	.5218	.3571	.02017	.6148	.8699	.6486	3
.5709	.02522	.4039	.4505	.02505	.5245	.8874	.6639	4
.6670	.02035	.3165	.5220	.02153	.4565	.9021	.6808	5
.7242	.01660	.2392	.5700	.01852	.4115	.9125	.6913	6
.7617	.01371	.2046	.5994	.01632	.3843	.9185	.6973	7
.7837	.01179	.2046	.6166	.01484	.3689	.9213	.7001	8
			.6162	.01488	.3689			6.98
.8018	.009040	.1892	.6244	.01277	.3629	.4397	.1879	FEED
HIGH PRESSURE COLUMN								
.9716	.004108	.02427	.9344	.005599	.04000	-.3724	.0000	FEED
.9544	.005599	.04000	.9544	.005599	.04000	.7383	1.111	1
.9363	.006900	.05682	.9270	.007569	.06946	.7243	1.097	2
.9177	.007930	.07432	.8985	.009283	.09229	.7109	1.083	3
.8992	.008857	.09197	.8697	.01060	.11197	.6980	1.070	4
.8815	.009904	.1092	.8415	.01162	.14468	.6860	1.058	5
.8644	.009947	.1257	.8148	.01234	.1729	.6752	1.048	6
.8490	.01021	.1408	.7900	.01279	.1972	.6657	1.038	7
.8352	.01033	.1544	.7678	.01301	.2192	.6576	1.030	8
.8233	.01094	.1663	.7485	.01308	.2386	.6507	1.023	9
.8132	.01027	.1765	.7316	.01296	.2554	.6450	1.017	10
.8047	.01015	.1852	.7176	.01279	.2696	.6403	1.013	11
.7976	.009999	.1924	.7059	.01257	.2815	.6365	1.009	12
.7919	.009841	.1983	.6964	.01233	.2913	.6335	1.005	13
.7873	.009684	.2030	.6886	.01209	.2995	.6310	1.003	14
.7836	.009536	.2069	.6824	.01187	.3097	.6291	1.002	15
.7806	.009400	.2100	.6775	.01165	.3108	.6276	1.0000	16
.7835	.009536	.2069	.6775	.01166	.3109	-.6276	.0003	FEED
.7806	.009400	.2100	1.000	.0000	.0000	.0000	1.000	FEED

HEAT EXCHANGER DUTIES - B.t.u./Lb. mole feed

OR 1660, GC 656, QS 88

\* These calculations account for the variation of the relative volatilities and enthalpies with pressure.

# SECRET

**SECRET**

**ASD-TDR-63-665, Part I**

TABLE 59

POINT NO. 5

LOW PRESSURE COLUMN PRESSURE -  $65 \leq P \leq 82.3$  PSIA\*

HIGH PRESSURE COLUMN PRESSURE - 265 PSIA

FEED AIR SUPERHEAT - 0 B.T.U.

Vapor	Mol	Fraction	Liquid	Mol	Fraction	Flow	Quan.	
<u>N</u>	<u>A</u>	<u>Q</u>	<u>N</u>	<u>A</u>	<u>Q</u>	<u>L</u>	<u>V</u>	
<u>TOP SECTION OF LOW PRESSURE COLUMN</u>								
.9508	.005218	.04400	1.000	.0000	.0000	.0000	.7560	FEED
.9597	.003973	.03637	.9046	.007094	.08832	.2536	.1382	FEED
.9495	.005402	.04313	.9303	.006051	.06370	.5706	.9348	1
.9206	.007495	.07194	.8822	.009518	.1083	.5603	.9245	2
.8848	.009346	.1058	.8219	.01284	.1655	.5482	.9124	3
.8449	.01069	.1444	.7533	.01497	.2318	.5354	.8996	4
.8051	.01135	.1835	.6838	.01620	.3000	.5235	.8877	5
.7701	.01137	.2186	.6215	.01632	.3622	.5138	.8780	4.24
			.6516	.01475	.3337			
<u>BOTTOM SECTION OF LOW PRESSURE COLUMN</u>								
.4572	.02224	.5206	.2533	.02236	.7243	.2440	.0000	FEED
.4572	.02224	.5206	.4005	.02227	.5773	.8767	.6327	1
.6234	.01900	.3576	.5232	.01991	.4569	.9016	.6576	2
.7316	.01514	.2532	.6049	.01705	.3781	.9208	.6767	3
.7923	.01203	.1956	.6512	.01477	.3340	.9321	.6881	4
.8239	.01005	.1660	.6757	.01325	.3110	.9394	.6953	3.01
			.6516	.01475	.3337			
.8105	.008924	.1805	.6296	.01287	.3575	.4111	.1970	FEED
<u>HIGH PRESSURE COLUMN</u>								
.9528	.004440	.04280	.9240	.005993	.07000	.3918	.0000	FEED
.9240	.005993	.07000	.9240	.005993	.07000	.6970	1.089	1
.8955	.007245	.09727	.8730	.007969	.1131	.6768	1.069	2
.8685	.008179	.1233	.8355	.009479	.1550	.6789	1.051	3
.8442	.008817	.1470	.7956	.01054	.1939	.6437	1.036	4
.8232	.009201	.1676	.7606	.01119	.2282	.6314	1.023	5
.8057	.009388	.1849	.7711	.01153	.2573	.6216	1.013	6
.7917	.009438	.1989	.7072	.01164	.2812	.6140	1.006	7
.7806	.009400	.2100	.6882	.01159	.3002	.6082	1.000	
.7916	.009438	.1989	.6882	.01159	.3002	.6082	.0000	FEED
.7806	.009400	.2100	1.000	.0000	.0000	.0000	1.000	FEED

HEAT EXCHANGER DUTIES - B.t.u./lb. mole feed

QR 1662, QC 720, QS 57

\* These calculations account for the variation of the relative volatilities and enthalpies with pressure.

**SECRET**

# SECRET

## ASD-TDR-63-665, Part I

TABLE 60  
POINT NO. 6

LOW PRESSURE COLUMN PRESSURE -  $56.5 \leq P \leq 76.5$  PSIA\*

HIGH PRESSURE COLUMN PRESSURE - 225 PSIA

FEED AIR SUPERHEAT - 0 B.T.U.

78 B.t.u./Lb. Mole Feed Shelf Subcooling

Vapor	Mol	Fraction	Liquid	Mol	Fraction	Flow	Quan.	
H	A	U	H	A	U	L	Y	
TOP SECTION OF LOW PRESSURE COLUMN								
.9702	.004243	.01755	1.000	.0000	.0000	.0000	.7788	FEED
.9789	.003021	.01810	.9479	.005662	.04647	.2947	.08699	FEED
.9787	.004329	.01700	.9633	.004941	.03178	.5651	.9622	1
.9699	.006193	.02393	.9482	.008123	.04366	.5627	.9598	2
.9582	.008132	.03371	.9200	.01145	.06090	.5393	.9563	3
.9429	.01004	.04704	.9016	.01475	.08561	.5545	.9515	4
.9238	.01177	.06442	.8682	.01779	.1140	.5484	.9455	5
.9010	.01313	.08588	.8279	.02027	.1518	.5412	.9385	6
.8737	.01403	.1107	.7821	.02189	.1960	.5333	.9304	7
.8405	.01430	.1372	.7737	.02249	.2439	.5254	.9225	8
.8227	.01399	.1673	.6864	.02206	.2916	.5182	.9153	9
.7996	.01323	.1872	.6438	.02080	.3374	.5122	.9092	10
.7805	.01220	.2073	.6083	.01905	.3727	.5075	.9045	9.27
			.6284	.01699	.3546			
BOTTOM SECTION OF LOW PRESSURE COLUMN								
.1894	.03363	.7770	.08505	.02755	.8874	.2212	.0000	FEED
.1894	.03363	.7770	.1630	.03210	.8049	.8768	.6333	1
.2241	.03527	.6356	.2685	.03335	.6982	.8902	.6690	2
.4816	.03227	.4461	.3351	.03112	.5838	.9092	.6879	3
.6139	.02657	.3595	.4480	.02681	.4852	.9294	.7082	4
.7080	.02073	.2713	.5623	.02233	.4154	.9459	.7246	5
.7660	.01617	.2179	.6004	.01881	.3728	.9563	.7331	6
.7989	.01310	.1880	.6747	.01642	.3489	.9617	.7405	7
			.6284	.01699	.3546			5.76
.8091	.009097	.1818	.6219	.01320	.3649	.4496	.1687	FEED
HIGH PRESSURE COLUMN								
.9736	.003537	.02282	.9549	.005060	.04000	.3817	.0000	FEED
.9549	.005060	.04000	.9549	.005060	.04000	.7193	1.101	1
.9345	.006418	.05900	.9234	.007153	.06941	.7052	1.087	2
.9129	.007568	.07933	.8897	.008954	.1014	.6909	1.073	3
.8909	.008478	.1006	.8549	.01040	.1347	.6772	1.059	4
.8694	.009130	.1214	.8203	.01148	.1682	.6645	1.046	5
.8492	.009560	.1413	.7873	.01219	.2005	.6530	1.035	6
.8308	.009773	.1594	.7571	.01257	.2303	.6432	1.025	7
.8147	.009818	.1754	.7305	.01268	.2569	.6349	1.017	8
.8011	.009745	.1892	.7076	.01259	.2793	.6281	1.010	9
.7898	.009594	.2006	.6886	.01237	.2991	.6226	1.004	10
.7806	.009400	.2100	.6730	.01208	.3149	.6183	1.000	
.7897	.009594	.2007	.6730	.01208	.3150	.6183	.0000	FEED
.7806	.009400	.2100	1.000	.0000	.0000	.0000	1.000	FEED

HEAT EXCHANGER DUTIES - B.t.u./Lb. mole feed

QR 1795, QC 616, QS 69

QSL 78

\* These calculations account for the variation of the relative volatilities and enthalpies with pressure.

# SECRET

**SECRET**

# ASD-TDR-63-665, Part I

TABLE 61  
POINT NO. 7

LOW PRESSURE COLUMN PRESSURE - 56.5 P 76.5 PSIA\*

HIGH PRESSURE COLUMN PRESSURE - 225 PSIA

FEED AIR SUPERHEAT - 0 B.T.U.

50% Efficient Turbine Expansion of Kettle and Shelf Streams

Vapor	Mol	Fraction	Liquid	Mol	Fraction	Flow	Quan.	
N	A	Q	N	A	Q	L	V	
<b>TOP SECTION OF LOW PRESSURE COLUMN</b>								
.9782	.004230	.01755	1.000	.0000	.0000	.0000	.7788	FEED
.9778	.003137	.01905	.9453	.005871	.04884	.2685	.1132	FEED
.9785	.004347	.01712	.9628	.005000	.03222	.5562	.9532	1
.9692	.006183	.02392	.9479	.008154	.04396	.5539	.9509	2
.9585	.008079	.03345	.9281	.01143	.06048	.5505	.9475	3
.9437	.009937	.04636	.9023	.01467	.08301	.5459	.9430	4
.9253	.01162	.06311	.8699	.01763	.1125	.5401	.9372	5
.9033	.01295	.08372	.8309	.02004	.1491	.5332	.9303	6
.8787	.01380	.1075	.7866	.02163	.1917	.5257	.9228	7
.8530	.01407	.1330	.7398	.02223	.2379	.5182	.9152	8
.8280	.01379	.1582	.6939	.02184	.2842	.5112	.9083	9
.8072	.01308	.1814	.6523	.02066	.3271	.5053	.9024	10
.7868	.01210	.2011	.6172	.01898	.3638	.5007	.8978	9.41
			.6316	.01672	.3516			

## BOTTOM SECTION OF LOW PRESSURE COLUMN

.1893	.03369	.7770	.08500	.02760	.8874	.2212	.0000	
.1873	.03369	.7770	.1630	.03215	.8049	.8768	.6595	1
.3290	.03533	.6757	.2684	.03341	.6902	.8902	.6690	2
.4814	.03233	.4862	.3850	.03118	.5839	.9092	.6819	3
.6138	.02663	.3596	.4879	.02686	.4892	.9295	.7082	4
.7078	.02078	.2714	.5621	.02237	.4155	.9460	.7247	5
.7658	.01621	.2180	.6003	.01884	.3728	.9565	.7732	6
.7987	.01313	.1881	.6346	.01645	.3490	.9619	.7407	7.09
			.6516	.01672	.3516			

.8109	.009039	.1800	.6247	.01314	.3622	.4579	.1604	FEED
-------	---------	-------	-------	--------	-------	-------	-------	------

## HIGH PRESSURE COLUMN

.9736	.003537	.02282	.9549	.005060	.04000	.3817	.0000	FEED
.9549	.005060	.04000	.9549	.005060	.04000	.7193	1.101	1
.9345	.006418	.05908	.9234	.007153	.06941	.7052	1.087	2
.9129	.007568	.07953	.8897	.008934	.1014	.6909	1.073	3
.8909	.008478	.1006	.8549	.01080	.1347	.6772	1.059	4
.8694	.009138	.1214	.8203	.01148	.1682	.6645	1.046	5
.8492	.009560	.1413	.7873	.01219	.2005	.6530	1.035	6
.8308	.009773	.1594	.7571	.01257	.2303	.6432	1.025	7
.8147	.009818	.1754	.7305	.01268	.2569	.6349	1.017	8
.8011	.009745	.1892	.7076	.01259	.2798	.6281	1.010	9
.7898	.009594	.2006	.6885	.01237	.2991	.6226	1.004	10
.7806	.009400	.2100	.6730	.01208	.3149	.6183	1.000	
.7897	.009594	.2007	.6730	.01208	.3150	.6183	.0000	FEED
.7806	.009400	.2100	1.000	.0000	.0000	.0000	1.000	FEED

HEAT EXCHANGER DUTIES - B.T.U./Lb. mole feed

QR 1795, QC 656, QS 69

QTS 17, QTK 20

\* These calculations account for the variation of the relative volatilities and enthalpies with pressure.

**SECRET**



SECRET

ASD-TDR-63-665, Part I

TABLE 62  
POINT NO. 8

LOW PRESSURE COLUMN PRESSURE -  $56.5 \leq P \leq 76.5$  PSIA\*

HIGH PRESSURE COLUMN PRESSURE - 225 PSIA

FEED AIR SUPERHEAT - 0 B.T.U.

60% EFFICIENT TURBINE EXPANSION OF KETTLE AND SHELF STREAMS

78 B.T.U./LB. - MOLE FEED SHELF SUBCOOLING

Vapor	Mol	Fraction	Liquid	Mol	Fraction	Flow	Quan.
N	A	U	N	A	U	L	Y
TOP SECTION OF LOW PRESSURE COLUMN							
.9782	.004237	.01755	1.000	.0000	.0000	.0000	.7788 FEED
.9792	.002986	.01784	.9486	.005603	.04581	.3024	.07930 FEED
.9789	.004305	.01678	.9694	.004918	.03104	.5563	.9534
.9704	.006145	.02343	.9486	.008080	.04312	.5541	.9511
.9592	.008051	.03276	.9293	.01137	.05929	.5508	.9478
.9446	.009923	.04343	.9040	.01465	.08138	.5463	.9453
.9265	.01162	.06192	.8720	.01765	.1104	.5405	.9376
.9047	.01299	.08227	.8334	.02009	.1465	.5337	.9308
.8803	.01357	.1095	.7895	.02174	.1897	.5262	.9233
.8546	.01418	.1312	.7428	.02240	.2348	.5187	.9157
.8295	.01393	.1565	.6968	.02206	.2811	.5117	.9087
.8069	.01323	.1798	.6549	.02090	.3242	.5057	.9027
.7879	.01225	.1998	.6194	.01923	.3614	.5010	.8980
			.6311	.01876	.3522		9.51
BOTTOM SECTION OF LOW PRESSURE COLUMN							
.1893	.03366	.7770	.08503	.02757	.8874	.2212	.0000 FEED
.1893	.03366	.7770	.1630	.03212	.8049	.8768	.6955
.3291	.03330	.6356	.2684	.03338	.6982	.8902	.6690
.4815	.03230	.4862	.3850	.03115	.5836	.9092	.6880
.6138	.02660	.3396	.4879	.02683	.4832	.9295	.7083
.7078	.02076	.2714	.5622	.02235	.4135	.9460	.7248
.7658	.01620	.2180	.6084	.01885	.3728	.9565	.7353
.7987	.01311	.1881	.6346	.01644	.3490	.9620	.7407
			.6311	.01676	.3522		5.87
.8109	.009039	.1801	.6247	.01314	.3622	.4580	.1603 FEED
HIGH PRESSURE COLUMN							
.9736	.003537	.02282	.9549	.005060	.04000	.3817	.0000 FEED
.9549	.005060	.04000	.9549	.005060	.04000	.7193	1.101
.9345	.006418	.05908	.9234	.007153	.06941	.7052	1.087
.9129	.007568	.07953	.8897	.008954	.1014	.6909	1.073
.8909	.008478	.1006	.8549	.01040	.1347	.6772	1.059
.8694	.009138	.1214	.8203	.01148	.1682	.6645	1.046
.8492	.009560	.1413	.7873	.01219	.2005	.6530	1.035
.8308	.009773	.1594	.7571	.01257	.2303	.6432	1.025
.8147	.009818	.1754	.7305	.01268	.2569	.6349	1.017
.8011	.009745	.1892	.7076	.01259	.2798	.6281	1.010
.7898	.009594	.2006	.6885	.01237	.2991	.6226	1.004
.7806	.009400	.2100	.6730	.01208	.3149	.6183	1.000
.7897	.009594	.2007	.6730	.01208	.3150	.6183	.0000 FEED
.7806	.009400	.2100	.6730	.01208	.3149	.6183	1.000 FEED

HEAT EXCHANGER DUTIES - B.t.u./Lb. mole feed

QR 1795, QC 579, QS 69, QSL 78, QTS 17, QTK 20

\* These calculations account for the variation of the relative volatilities and enthalpies with pressure.

SECRET

# SECRET

## ASD-TDR-63-665, Part I

TABLE 83

POINT NO. 3

LOW PRESSURE COLUMN PRESSURE -  $65 \leq P \leq 95$  PSIA\*

HIGH PRESSURE COLUMN PRESSURE - 234 PSIA

Vapor		Mol Fraction		FEED AIR SUPERHEAT - O.B.T.U.		Flow		Quan.	
				Liquid	Mol Fraction				
N	A	Q	N	A	Q	L	V		
TOP SECTION OF LOW PRESSURE COLUMN									
.9782	.004271	.01755	1.000	.0000	.0000	.0000	.7788	FEED	
.9770	.003212	.01983	.9450	.005876	.04916	.2572	.1167	FEED	
.9783	.004407	.01727	.9627	.005021	.03226	.5525	.9573		1
.9705	.006173	.02337	.9490	.008088	.04290	.5507	.9555		2
.9605	.007946	.03156	.9316	.01118	.05723	.5480	.9529		3
.9481	.009646	.04222	.9098	.01416	.07599	.5445	.9493		4
.9332	.01117	.05563	.8834	.01687	.09972	.5400	.9448		5
.9158	.01241	.07175	.8524	.01910	.1285	.5347	.9395		6
.8965	.01327	.09019	.8176	.02069	.1617	.5288	.9337		7
.8762	.01368	.1101	.7806	.02151	.1979	.5228	.9277		8
.8539	.01365	.1305	.7433	.02155	.2351	.5170	.9219		9
.8368	.01325	.1500	.7080	.02091	.2711	.5119	.9167		10
.8198	.01258	.1676	.6763	.01977	.3099	.5075	.9124		11
.8056	.01175	.1827	.6498	.01832	.3519	.5042	.9090		12
.7943	.01088	.1948	.6286	.01677	.3946	.5018	.9067		11.34
			.6370	.01550	.4476				
BOTTOM SECTION OF LOW PRESSURE COLUMN									
.1807	.03326	.7861	.08517	.02743	.8874	.2212	.0000	FEED	
.1807	.03326	.7861	.1567	.03180	.8115	.8828	.6615		1
.3060	.03926	.6587	.2514	.03333	.7153	.8945	.6732		2
.4448	.03318	.5220	.3573	.03179	.6107	.9112	.6900		3
.5712	.02838	.4004	.4556	.02816	.5165	.9300	.7088		4
.6676	.02294	.3095	.5314	.02399	.4446	.9465	.7232		5
.7318	.01830	.2499	.5824	.02041	.3571	.9580	.7367		6
.7711	.01492	.2140	.6137	.01779	.3685	.9645	.7433		7
.7940	.01266	.1933	.6319	.01604	.3821	.9674	.7461		8
.8072	.01124	.1816	.6421	.01494	.3929	.9679	.7466		7.49
			.6370	.01550	.4476				
.8073	.009120	.1835	.6308	.01301	.3562	.4642	.1619	FEED	
HIGH PRESSURE COLUMN									
.9733	.003564	.02315	.9550	.005044	.04000	.3739	.0000	FEED	
.9550	.005044	.04000	.9550	.005044	.04000	.7297	1.104		1
.9349	.006367	.05871	.9244	.007059	.06849	.7155	1.089		2
.9137	.007495	.07881	.8917	.008802	.09950	.7012	1.075		3
.8920	.008596	.09957	.8578	.01022	.1320	.6873	1.061		4
.8707	.009058	.1202	.8240	.01128	.1647	.6743	1.048		5
.8505	.009491	.1400	.7916	.01200	.1964	.6626	1.036		6
.8321	.009720	.1582	.7616	.01240	.2260	.6523	1.026		7
.8158	.009783	.1744	.7349	.01254	.2525	.6437	1.018		8
.8018	.009724	.1885	.7119	.01247	.2757	.6365	1.010		9
.7901	.009585	.2003	.6925	.01228	.2953	.6308	1.005		10
.7806	.009400	.2100	.6765	.01200	.3115	.6261	1.000		
.7901	.009586	.2003	.6765	.01200	.3115	.6261	.0000	FEED	
.7806	.009400	.2100	1.000	.0000	.0000	.0000	1.000	FEED	

HEAT EXCHANGER DUTIES - B.t.u./Lb. mole feed

QR 1765, QC 663, QS 88

\* These calculations account for the variation of the relative volatilities and enthalpies with pressure.

# SECRET

# SECRET

## ASD-TDR-63-665, Part I

TABLE 64

POINT NO. 10

LOW PRESSURE COLUMN PRESSURE  $65 \leq p \leq 95$  PSIA\*

HIGH PRESSURE COLUMN PRESSURE - 245 PSIA

FEED AIR SUPERHEAT - O.R.T.U.

Vapor	Mol	Fraction	Liquid	Mol	Fraction	Flow	Quan.	
N	A	Q	N	A	Q	L	V	
TOP SECTION OF LOW PRESSURE COLUMN								
.9782	.004251	.01755	1.000	.0000	.0000	.0000	.7788	FEED
.9767	.003225	.02006	.9444	.005898	.04972	.2449	.1194	FEED
.9784	.004380	.01724	.9628	.004999	.03216	.5393	.9538	1
.9707	.006095	.02322	.9491	.008039	.04281	.5374	.9518	2
.9611	.007784	.03110	.9321	.01105	.05689	.5347	.9492	3
.9495	.009372	.04118	.9111	.01390	.07500	.5313	.9457	4
.9356	.01077	.05364	.8860	.01643	.09754	.5271	.9415	5
.9197	.01190	.06843	.8570	.01850	.1245	.5222	.9366	6
.9022	.01266	.08517	.8248	.01995	.1552	.5168	.9313	7
.8838	.01304	.1032	.7907	.02071	.1885	.5113	.9258	8
.8655	.01303	.1215	.7565	.02077	.2227	.5061	.9205	9
.8458	.01286	.1413	.7192	.02056	.2602	.5005	.9149	10
.8306	.01222	.1572	.6903	.01943	.2902	.4966	.9110	11
.8177	.01145	.1708	.6658	.01806	.3161	.4935	.9079	12
.8074	.01065	.1819	.6461	.01662	.3373	.4912	.9057	13
.8027	.009778	.1875	.6308	.01522	.3539	.4723	.8868	12.05
			.6597	.01483	.3465			
BOTTOM SECTION OF LOW PRESSURE COLUMN								
.1805	.03337	.7861	.08508	.02752	.8874	.2212	.0000	FEED
.1805	.03337	.7861	.1561	.03188	.8120	.8670	.6457	1
.3091	.03537	.6596	.2497	.03339	.7169	.8785	.6572	2
.4424	.03331	.5243	.3540	.03188	.6141	.8948	.6736	3
.5673	.02857	.4041	.4505	.02891	.5212	.9130	.6918	4
.6627	.02310	.3141	.5252	.02416	.4507	.9290	.7078	5
.7265	.01834	.2349	.5756	.02065	.4038	.9403	.7191	6
.7657	.01520	.2191	.6067	.01808	.3753	.9469	.7256	7
.7887	.01296	.1984	.6248	.01632	.3588	.9499	.7286	8
.8019	.01154	.1866	.6351	.01526	.3477	.9506	.7293	9
.8095	.01066	.1798	.6408	.01459	.3446	.9500	.7288	8.65
			.6387	.01483	.3465			
HIGH PRESSURE COLUMN								
.9729	.003596	.02354	.9550	.005022	.04000	.3643	.0000	FEED
.9550	.005022	.04000	.9550	.005022	.04000	.7416	1.106	1
.9354	.006503	.05826	.9237	.006944	.06741	.7217	1.092	2
.9147	.007401	.07789	.8941	.008616	.09723	.7132	1.077	3
.8935	.008288	.09826	.8614	.009990	.1286	.6992	1.063	4
.8724	.008982	.1186	.8286	.01104	.1604	.6860	1.050	5
.8523	.009400	.1383	.7968	.01176	.1913	.6741	1.038	6
.8337	.009649	.1567	.7671	.01219	.2207	.6633	1.028	7
.8171	.009733	.1731	.7404	.01236	.2472	.6545	1.019	8
.8028	.009697	.1875	.7171	.01233	.2706	.6469	1.011	9
.7906	.009574	.1998	.6972	.01216	.2906	.6407	1.005	10
.7806	.009400	.2100	.6807	.01191	.3074	.6357	1.000	
.7906	.009574	.1998	.6807	.01191	.3074	.6357	.0000	FEED
.7806	.009400	.2100	1.000	.0000	.0000	.0000	1.000	FEED

HEAT EXCHANGER DUTIES B.T.U./LB. MOLE FEED

QR 1725, QC 661, QS 88

\* These calculations account for the variation of the relative volatilities and enthalpies with pressure.

# SECRET

# SECRET

## ASD-TDR-63-665, Part I

TABLE 65

POINT NO. 11

LOW PRESSURE COLUMN PRESSURE  $65 \leq P \leq 95$  PSIA

HIGH PRESSURE COLUMN PRESSURE - 265 PSIA

FEED AIR SUPERHEAT - 0 B.T.U.

Vapor	Mol	Fraction	Liquid	Mol	Fraction	Flow	Quan.
H	A	U	H	A	U	L	Y
TOP SECTION OF LOW PRESSURE COLUMN							
.9778	.004662	.01755	1.000	.0000	.0000	.0000	.7788 FEED
.9765	.003857	.02048	.9433	.009992	.05073	.2235	.1229 FEED
.9780	.004866	.01717	.9688	.008232	.03193	.5157	.9481
.9702	.006873	.02295	.9484	.008931	.04264	.5134	.9458
.9609	.008783	.03027	.9313	.01847	.05627	.5106	.9429
.9502	.01052	.03931	.9111	.01572	.07320	.5072	.9395
.9378	.01202	.05014	.8879	.01853	.09359	.5032	.9356
.9242	.01319	.06262	.8619	.02079	.1173	.4989	.9312
.9096	.01400	.07644	.8339	.02238	.1437	.4943	.9266
.8945	.01442	.09100	.8049	.02325	.1719	.4896	.9220
.8796	.01448	.1059	.7739	.02394	.2007	.4852	.9175
.8635	.01422	.1202	.7403	.02303	.2287	.4811	.9135
.8468	.01374	.1335	.7032	.0217	.2547	.4776	.9100
.8297	.01311	.1452	.6635	.02102	.2779	.4747	.9071
.8123	.01243	.1552	.6203	.01974	.2977	.4724	.9048
.7948	.01174	.1635	.5766	.01843	.3140	.4707	.9031
.7773	.01109	.1700	.5339	.01723	.3269	.4696	.9019
.7597	.01032	.1750	.4911	.01613	.3367	.4688	.9012
.7421	.01002	.1787	.4488	.01519	.3440	.4683	.9008
.7245	.009611	.1814	.4064	.01439	.3492	.4684	.9008
.7069	.009273	.1832	.3633	.01374	.3527	.4686	.9010
.6893	.008927	.1832	.3204	.01360	.3510		17.19
BOTTOM SECTION OF LOW PRESSURE COLUMN							
.1834	.03151	.7850	.08699	.02601	.8874	.2212	.0000 FEED
.1834	.03151	.7850	.1580	.03006	.8119	.8424	.6211
.3082	.03332	.6585	.2308	.03142	.7178	.8540	.6327
.4438	.03135	.5248	.3530	.02999	.6170	.8700	.6406
.5689	.02693	.4072	.4464	.02671	.5257	.8876	.6464
.6936	.02200	.3134	.5184	.02298	.4486	.9030	.6518
.7205	.01778	.2617	.5671	.01977	.4132	.9141	.6588
.7386	.01470	.2267	.5971	.01741	.3833	.9207	.6635
.7510	.01263	.2064	.6148	.01583	.3694	.9241	.6688
.7599	.01131	.1940	.6248	.01482	.3604	.9253	.6704
.7614	.01049	.1881	.6304	.01420	.3553	.9252	.6704
.7657	.009992	.1843	.6336	.01383	.3525	.9245	.6702
.7684	.009689	.1819	.6354	.01360	.3510	.9233	.6701
.7706			.6354	.01360	.3510		11.00
.8099	.009031	.1811	.6350	.01291	.3521	.4550	.1986 FEED
HIGH PRESSURE COLUMN							
.9721	.003665	.02427	.9550	.004996	.04000	.2464	.0000 FEED
.9550	.004996	.04000	.9550	.004996	.04000	.7651	1.112
.9364	.006190	.05743	.9278	.006753	.06946	.7509	1.097
.9165	.007243	.07645	.8984	.008301	.09330	.7364	1.083
.8960	.008104	.09991	.8677	.009595	.1227	.7222	1.069
.8754	.008767	.1150	.8365	.01061	.1529	.7089	1.055
.8545	.009294	.1323	.8059	.01134	.1827	.6952	1.042
.8337	.009518	.1500	.7769	.01181	.2113	.6812	1.031
.8127	.009643	.1707	.7502	.01203	.2378	.6677	1.021
.7916	.009643	.1850	.7264	.01206	.2615	.6543	1.013
.7706	.009551	.1989	.7037	.01194	.2823	.6413	1.006
.7506	.009400	.2100	.6882	.01173	.3001	.6286	1.000
.7306	.009240	.2100	.6800	.01173	.3001	.6286	1.000
.7106	.009080	.2100	.6718	.01173	.3001	.6286	1.000
.6906	.008920	.2100	.6636	.01173	.3001	.6286	1.000
.6706	.008760	.2100	.6554	.01173	.3001	.6286	1.000
.6506	.008600	.2100	.6472	.01173	.3001	.6286	1.000
.6306	.008440	.2100	.6390	.01173	.3001	.6286	1.000
.6106	.008280	.2100	.6308	.01173	.3001	.6286	1.000
.5906	.008120	.2100	.6226	.01173	.3001	.6286	1.000
.5706	.007960	.2100	.6144	.01173	.3001	.6286	1.000
.5506	.007800	.2100	.6062	.01173	.3001	.6286	1.000
.5306	.007640	.2100	.5980	.01173	.3001	.6286	1.000
.5106	.007480	.2100	.5898	.01173	.3001	.6286	1.000
.4906	.007320	.2100	.5816	.01173	.3001	.6286	1.000
.4706	.007160	.2100	.5734	.01173	.3001	.6286	1.000
.4506	.007000	.2100	.5652	.01173	.3001	.6286	1.000
.4306	.006840	.2100	.5570	.01173	.3001	.6286	1.000
.4106	.006680	.2100	.5488	.01173	.3001	.6286	1.000
.3906	.006520	.2100	.5406	.01173	.3001	.6286	1.000
.3706	.006360	.2100	.5324	.01173	.3001	.6286	1.000
.3506	.006200	.2100	.5242	.01173	.3001	.6286	1.000
.3306	.006040	.2100	.5160	.01173	.3001	.6286	1.000
.3106	.005880	.2100	.5078	.01173	.3001	.6286	1.000
.2906	.005720	.2100	.4996	.01173	.3001	.6286	1.000
.2706	.005560	.2100	.4914	.01173	.3001	.6286	1.000
.2506	.005400	.2100	.4832	.01173	.3001	.6286	1.000
.2306	.005240	.2100	.4750	.01173	.3001	.6286	1.000
.2106	.005080	.2100	.4668	.01173	.3001	.6286	1.000
.1906	.004920	.2100	.4586	.01173	.3001	.6286	1.000
.1706	.004760	.2100	.4504	.01173	.3001	.6286	1.000
.1506	.004600	.2100	.4422	.01173	.3001	.6286	1.000
.1306	.004440	.2100	.4340	.01173	.3001	.6286	1.000
.1106	.004280	.2100	.4258	.01173	.3001	.6286	1.000
.0906	.004120	.2100	.4176	.01173	.3001	.6286	1.000
.0706	.003960	.2100	.4094	.01173	.3001	.6286	1.000
.0506	.003800	.2100	.4012	.01173	.3001	.6286	1.000
.0306	.003640	.2100	.3930	.01173	.3001	.6286	1.000
.0106	.003480	.2100	.3848	.01173	.3001	.6286	1.000

HEAT EXCHANGER DUTIES - B.T.U./Lb. mole feed

QR 166, QC 656, QS 88

\* These calculations account for the variation of the relative volatilities and enthalpies with pressure.

# SECRET

# SECRET

## ASD-TDR-63-665, Part I

TABLE 66

POINT NO. 12

LOW PRESSURE COLUMN PRESSURE  $65 \leq P \leq 95$  PSIA\*

HIGH PRESSURE COLUMN PRESSURE - 245 PSIA

FEED AIR SUPERHEAT - O.B.T.U.

Vapor	Mol	Fraction	Liquid	Mol	Fraction	Flow	Quan.	
N	A	O	N	A	O	L	Y	
<u>TOP SECTION OF LOW PRESSURE COLUMN</u>								
.9688	.004819	.02636	1.000	.0000	.0000	.0000	-.7867	FEED
.9767	.003225	.02006	.9444	.005898	.04972	.2449	.1194	FEED
.9678	.009019	.02715	.9575	.005319	.03719	.5282	.9507	1
.9495	.007095	.04336	.9245	.009078	.06661	.5286	.9450	2
.9276	.008947	.06342	.8841	.01247	.1034	.5158	.9382	3
.9050	.01042	.08660	.8383	.01522	.1465	.5082	.9306	4
.8772	.01139	.1114	.7898	.01709	.1931	.5005	.9229	5
.8522	.01185	.1359	.7422	.01801	.2398	.4935	.9159	6
.8298	.01185	.1584	.6990	.01809	.2829	.4875	.9100	7
.8111	.01192	.1773	.6628	.01753	.3197	.4830	.9054	8
.7966	.01101	.1923	.6346	.01661	.3488	.4799	.9023	9
			.6382	.01504	.3467			7.61
<u>BOTTOM SECTION OF LOW PRESSURE COLUMN</u>								
.1829	.03187	.7853	.08630	.02630	.8874	-.2133	.0000	FEED
.1829	.03187	.7853	.1589	.03048	.8106	.8592	.6459	1
.3096	.03374	.6566	.2549	.03192	.7132	.8705	.6570	2
.4498	.03168	.5185	.3624	.03039	.6072	.8844	.6751	3
.5772	.02700	.3958	.4614	.02684	.5117	.9043	.6910	4
.6738	.02173	.3045	.5376	.02279	.4396	.9108	.7065	5
.7377	.01727	.2450	.5884	.01934	.3923	.9303	.7170	6
.7767	.01403	.2093	.6193	.01682	.3639	.9358	.7225	7
.7993	.01182	.1888	.6571	.01516	.3477	.9377	.7245	8
.8123	.01053	.1772	.6471	.01411	.3388	.9374	.7241	9
			.6582	.01304	.3467			7.11
.8065	.003032	.1824	.6305	.01302	.3565	.4566	.1791	FEED
<u>HIGH PRESSURE COLUMN</u>								
.9729	.003596	.02354	.9550	.005022	.04000	-.3643	.0000	FEED
.9550	.005022	.04000	.9550	.005022	.04000	.7416	1.106	1
.9354	.006503	.05826	.9257	.006944	.06741	.7275	1.092	2
.9147	.007401	.07789	.8941	.008616	.09725	.7132	1.077	3
.8935	.008288	.09826	.8614	.009990	.1286	.6992	1.063	4
.8724	.008992	.1186	.8286	.01104	.1604	.6860	1.050	5
.8523	.009400	.1383	.7968	.01176	.1915	.6741	1.038	6
.8337	.009649	.1567	.7671	.01219	.2207	.6635	1.028	7
.8171	.009735	.1731	.7404	.01256	.2472	.6545	1.019	8
.8028	.009697	.1875	.7171	.01283	.2706	.6469	1.011	9
.7906	.009574	.1998	.6972	.01216	.2906	.6407	1.005	10
.7806	.009400	.2100	.6807	.01191	.3074	.6357	1.000	
.7906	.009574	.1998	.6807	.01191	.3074	-.6357	.0000	FEED
.7806	.009400	.2100	1.000	.0000	.0000	.0000	1.000	FEED

HEAT EXCHANGER DUTIES - B.t.u./Lb. mole feed

QR 1725, QC 638, QS 88

\* These calculations account for the variation of the relative volatilities and enthalpies with pressure.

# SECRET

# SECRET

## ASD-TDR-63-665, Part I

TABLE 67

POINT NO. 13

LOW PRESSURE COLUMN PRESSURE  $65 \leq P \leq 95$  PSIA\*

HIGH PRESSURE COLUMN PRESSURE - 245 PSIA

FEED AIR SUPERHEAT - O.B.T.U.

Vapor	Mol	Fraction	Liquid	Mol	Fraction	Flow	Quan.	
N	A	O	N	A	O	L	V	
TOP SECTION OF LOW PRESSURE COLUMN								
.9584	.005271	.03636	1.000	.0000	.0000	.0000	-.7960	FEED
.9767	.003225	.02006	.9444	.005898	.04972	.2449	.1194	FEED
.9561	.005529	.03841	.9517	.005569	.04271	.5156	.9473	
.9267	.007833	.06548	.8972	.009838	.09292	.5062	.9379	1
.8937	.009677	.09659	.8350	.01333	.1517	.4959	.9276	2
.8603	.01089	.1288	.7707	.01569	.2136	.4861	.9178	3
.8298	.01145	.1588	.7110	.01684	.2722	.4778	.9094	4
.8045	.01148	.1840	.6611	.01698	.3220	.4715	.9032	5
.7855	.01118	.2033	.6232	.01645	.3604	.4673	.8990	6
			.6422	.01500	.3428			5.17
BOTTOM SECTION OF LOW PRESSURE COLUMN								
.1844	.03089	.7847	.08709	.02551	.8874	-.2040	.0000	FEED
.1844	.03089	.7847	.1611	.02960	.8093	.8501	.6461	
.3132	.03269	.6541	.2596	.03099	.7094	.8609	.6569	1
.4564	.03062	.5130	.3705	.02943	.6001	.8768	.6788	2
.5865	.02593	.3875	.4726	.02584	.5015	.8947	.6907	3
.6847	.02068	.2946	.5507	.02177	.4276	.9099	.7058	4
.7491	.01627	.2347	.6022	.01832	.3795	.9197	.7157	5
.7878	.01309	.1991	.6332	.01583	.3510	.9245	.7204	6
.8102	.01100	.1788	.6508	.01420	.3350	.9255	.7215	7
			.6422	.01500	.3428			6.51
.8089	.009021	.1820	.6294	.01304	.3576	.4541	.1816	FEED
HIGH PRESSURE COLUMN								
.9729	.003596	.02354	.9550	.005022	.04000	-.3643	.0000	FEED
.9550	.005022	.04000	.9550	.005022	.04000	.7416	1.106	
.9354	.006303	.05876	.9257	.006944	.06741	.7275	1.092	1
.9147	.007401	.07789	.8941	.008616	.09725	.7132	1.077	2
.8935	.008288	.09826	.8614	.009990	.1286	.6992	1.063	3
.8724	.008952	.1186	.8286	.01104	.1604	.6860	1.050	4
.8523	.009400	.1383	.7968	.01176	.1915	.6741	1.038	5
.8337	.009649	.1567	.7671	.01219	.2207	.6635	1.028	6
.8171	.009735	.1731	.7404	.01236	.2472	.6545	1.019	7
.8028	.009697	.1875	.7171	.01233	.2706	.6469	1.011	8
.7906	.009574	.1998	.6972	.01216	.2906	.6407	1.005	9
.7806	.009400	.2100	.6807	.01191	.3074	.6357	1.000	10
.7906	.009574	.1998	.6807	.01191	.3074	-.6357	.0000	FEED
.7526	.009400	.2100	1.000	.0000	.0000	.0000	1.000	FEED

HEAT EXCHANGER DUTIES - B.t.u./Lb. mole feed

QR 1725, QC 613, QS 88

\* These calculations account for the variation of the relative volatilities and enthalpies with pressure.

# SECRET

# SECRET

## ASD-TDR-63-665, Part I

TABLE 68

POINT NO. 14

LOW PRESSURE COLUMN PRESSURE -  $65 \leq P \leq 95$  PSIA\*

HIGH PRESSURE COLUMN PRESSURE - 265 PSIA

FEED AIR SUPERHEAT - O.B.T.U.

Vapor	Mol	Fraction	Liquid	Mol	Fraction	Flow	Quan.	
N	A	U	N	A	U	L	V	
TOP SECTION OF LOW PRESSURE COLUMN								
.9689	.004744	.02636	1.000	.0000	.0000	.0000	.7867	FEED
.9763	.003257	.02048	.9433	.005952	.05073	.2235	.1229	FEED
.9679	.004937	.02712	.9576	.005279	.03715	.5048	.9452	1
.9504	.006875	.04268	.9245	.008930	.06655	.4992	.9395	2
.9302	.008538	.06125	.8859	.01211	.1020	.4927	.9330	3
.9082	.009812	.08200	.8433	.01459	.1422	.4858	.9261	4
.8857	.01063	.1036	.7992	.01623	.1845	.4790	.9193	5
.8644	.01101	.1246	.7569	.01703	.2261	.4728	.9131	6
.8454	.01101	.1435	.7189	.01710	.2640	.4676	.9080	7
.8296	.01076	.1596	.6870	.01666	.2964	.4636	.9011	8
.8172	.01035	.1724	.6618	.01591	.3223	.4608	.8993	9
.8080	.009900	.1821	.6431	.01504	.3419	.4590		8.74
			.6406	.01412	.3453			
BOTTOM SECTION OF LOW PRESSURE COLUMN								
.1823	.03221	.7855	.08602	.02658	.8874	.2133	.0000	FEED
.1823	.03221	.7855	.1577	.03077	.8115	.8343	.6210	1
.3077	.03410	.6582	.2518	.03220	.7160	.8452	.6319	2
.4494	.03207	.5225	.3564	.03071	.6129	.8606	.6473	3
.5703	.02746	.4022	.4527	.02724	.5201	.8778	.6645	4
.6653	.02225	.3124	.5269	.02329	.4498	.8927	.6794	5
.7286	.01703	.2335	.5769	.01990	.4032	.9030	.6898	6
.7674	.01460	.2100	.6075	.01741	.3751	.9088	.6955	7
.7902	.01245	.1974	.6254	.01576	.3589	.9112	.6979	8
.8033	.01108	.1856	.6354	.01471	.3499	.9114	.6981	9
.8109	.01024	.1789	.6411	.01407	.3449	.9104	.6971	8.92
			.6406	.01412	.3453			
.8105	.009019	.1805	.6332	.01295	.3539	.4509	.2026	FEED
HIGH PRESSURE COLUMN								
.9721	.003665	.02427	.9550	.004996	.04000	.3464	.0000	FEED
.9550	.004996	.04000	.9550	.004996	.04000	.7651	1.112	+
.9364	.006198	.05743	.9278	.006753	.06948	.7909	1.097	1
.9165	.007243	.07625	.8984	.008301	.09330	.7564	1.083	2
.8960	.008104	.09591	.8677	.009595	.1227	.7222	1.069	3
.8754	.008767	.1150	.8365	.01061	.1529	.7085	1.055	4
.8555	.009234	.1353	.8059	.01134	.1827	.6959	1.042	5
.8367	.009518	.1538	.7769	.01181	.2113	.6846	1.031	6
.8197	.009643	.1707	.7502	.01203	.2378	.6747	1.021	7
.8046	.009643	.1856	.7264	.01206	.2615	.6663	1.013	8
.7916	.009551	.1989	.7057	.01194	.2823	.6593	1.006	9
.7806	.009400	.2100	.6882	.01173	.3001	.6536	1.000	10
.7916	.009551	.1989	.6882	.01173	.3001	.6536	.0000	FEED
.7806	.009400	.2100	1.000	.0000	.0000	.0000	1.000	FEED

HEAT EXCHANGER DUTIES - B.T.U./lb. Mole Feed

QR 1661. QC 634. OS 88

\* These calculations account for the variation of the relative volatilities and enthalpies with pressure.

# SECRET

# SECRET

## ASD-TDR-63-665, Part I

TABLE 69

POINT NO. 15

LOW PRESSURE COLUMN PRESSURE -  $56.5 \leq P \leq 76.5$  PSIA\*

HIGH PRESSURE COLUMN PRESSURE - 225 PSIA

FEED AIR SUPERHEAT - O B.T.U.

Vapor	Mol	Fraction	Liquid	Mol	Fraction	Flow	Quan.	
N	A	O	N	A	O	L	V	
TOP SECTION OF LOW PRESSURE COLUMN								
.9686	.005015	.02636	1.000	.0000	.0000	.0000	.7867	FEED
.9775	.003175	.01936	.9445	.005938	.04961	.2605	.1213	FEED
.9675	.005248	.02725	.9572	.005449	.03730	.5533	.9584	
.9469	.007633	.04540	.9213	.009691	.06902	.5467	.9517	1
.9207	.009972	.06936	.8749	.01373	.1114	.5383	.9433	2
.8896	.01185	.09659	.8191	.01712	.1638	.5285	.9335	3
.8559	.01309	.1310	.7578	.01943	.2228	.5184	.9234	4
.8230	.01359	.1634	.6968	.02045	.2827	.5091	.9142	5
.7939	.01343	.1927	.6424	.02026	.3374	.5015	.9066	6
.7705	.01282	.2167	.5982	.01924	.3826	.4999	.9010	7
			.6243	.01675	.3589			6.34
BOTTOM SECTION OF LOW PRESSURE COLUMN								
.1934	.03117	.7794	.08703	.02557	.8874	.2133	.0000	FEED
.1934	.03117	.7794	.1673	.02980	.8029	.8683	.6550	
.3562	.03262	.6312	.2759	.03091	.6932	.8816	.6683	1
.4916	.02970	.4787	.3958	.02872	.5755	.9006	.6873	2
.6255	.02427	.3503	.5007	.02457	.4747	.9208	.7075	3
.7194	.01877	.2618	.5755	.02032	.4042	.9368	.7235	4
.7767	.01453	.2088	.6213	.01702	.3617	.9465	.7332	5
.8088	.01160	.1796	.6469	.01480	.3383	.9511	.7378	6
			.6243	.01675	.3589			5.12
.8093	.009095	.1816	.6209	.01322	.3650	.4475	.1700	FEED
HIGH PRESSURE COLUMN								
.9736	.003537	.02282	.9549	.005060	.04000	.3317	.0000	FEED
.9549	.005060	.04000	.9549	.005060	.04000	.7193	1.101	
.9345	.006418	.05908	.9234	.007153	.06941	.7052	1.087	1
.9129	.007568	.07953	.8897	.008954	.1014	.6909	1.073	2
.8909	.008478	.1006	.8549	.01040	.1347	.6772	1.059	3
.8694	.009138	.1214	.8203	.01148	.1682	.6645	1.046	4
.8492	.009560	.1413	.7873	.01219	.2005	.6530	1.035	5
.8308	.009773	.1594	.7571	.01257	.2303	.6432	1.025	6
.8147	.009818	.1754	.7305	.01268	.2569	.6349	1.017	7
.8011	.009745	.1892	.7076	.01259	.2798	.6281	1.010	8
.7898	.009594	.2040	.6885	.01237	.2991	.6226	1.004	9
.7806	.009400	.2100	.6730	.01208	.3149	.6183	1.000	10
.7897	.009594	.2007	.6730	.01208	.3150	.6183	.0000	FEED
.7806	.009400	.2100	1.000	.0000	.0000	.0000	1.000	FEED

HEAT EXCHANGER DUTIES - B.t.u./Lb. Mole Feed

QR 1795, QC 671, QS 69

\* These calculations account for the variation of the relative volatilities and enthalpies with pressure.



# SECRET

## ASD-TDR-63-665, Part I

TABLE 70

POINT NO. 16

LOW PRESSURE COLUMN PRESSURE -  $40 \leq P \leq 75$  PSIA\*

HIGH PRESSURE COLUMN PRESSURE - 245 PSIA

FEED AIR SUPERHEAT - O.B.T.U.

Vapor	Mol	Fraction	Liquid	Mol	Fraction	Flow	Quan.	
N	A	Q	N	A	Q	L	Y	
TOP SECTION OF LOW PRESSURE COLUMN								
.9782	.004243	.01755	1.000	.0000	.0000	.0000	-.7788	FEED
.9779	.003133	.01901	.9411	.006169	.05275	.2267	.1376	FEED
.9783	.004405	.01734	.9624	.005064	.03255	.5318	.9462	
.9675	.006438	.02606	.9431	.008692	.04817	.5295	.9439	1
.9530	.008509	.03847	.9171	.01241	.07051	.5259	.9404	2
.9343	.01045	.05525	.8831	.01594	.1010	.5209	.9354	3
.9114	.01207	.07650	.8412	.01892	.1399	.5146	.9290	4
.8854	.01315	.1014	.7930	.02098	.1860	.5074	.9219	5
.8583	.01358	.1281	.7420	.02188	.2361	.5002	.9147	6
.8324	.01337	.1542	.6929	.02162	.2855	.4936	.9081	7
.8099	.01269	.1774	.6498	.02043	.3298	.4883	.9028	8
.7920	.01172	.1963	.6152	.01871	.3661	.4844	.8988	9
			.6263	.01659	.3571			6.50
BOTTOM SECTION OF LOW PRESSURE COLUMN								
.1902	.03365	.7761	.08505	.02755	.8874	-.2212	.0000	FEED
.1902	.03365	.7761	.1629	.03207	.8051	.8506	.6293	
.3300	.03524	.6348	.2671	.03327	.6996	.8619	.6407	1
.4822	.03219	.4856	.3822	.03102	.5868	.8783	.6571	2
.6141	.02646	.3595	.4834	.02673	.4899	.8958	.6745	3
.7077	.02063	.2717	.5562	.02231	.4215	.9094	.6881	4
.7655	.01609	.2184	.6014	.01885	.3797	.9173	.6961	5
.7986	.01303	.1884	.6271	.01682	.3564	.9205	.6993	6
			.6263	.01659	.3571			5.97
.8126	.009006	.1784	.6194	.01326	.3673	.4341	.2016	FEED
HIGH PRESSURE COLUMN								
.9729	.003596	.02354	.9550	.005022	.04000	-.3643	.0000	FEED
.9550	.005022	.04000	.9550	.005022	.04000	.7416	1.106	
.9354	.006303	.05826	.9257	.006944	.06741	.7275	1.092	1
.9147	.007401	.07789	.8941	.008616	.09725	.7132	1.077	2
.8935	.008288	.09826	.8614	.009390	.1286	.6992	1.063	3
.8724	.008952	.1186	.8286	.01104	.1604	.6860	1.050	4
.8523	.009400	.1383	.7968	.01176	.1915	.6741	1.038	5
.8337	.009649	.1567	.7671	.01219	.2207	.6635	1.028	6
.8171	.009735	.1731	.7404	.01236	.2472	.6545	1.019	7
.8028	.009697	.1875	.7171	.01233	.2706	.6469	1.011	8
.7906	.009574	.1946	.6972	.01216	.2906	.6407	1.005	9
.7806	.009400	.2100	1.000	.0000	.0000	.6357	1.000	10
.7906	.009574	.1998	.6807	.01191	.3074	-.6357	.0000	FEED
.7806	.009400	.2100	1.000	.0000	.0000	.0000	1.000	FEED

HEAT EXCHANGER DUTIES - B.t.u./Lb. Mole Feed

QR 1725, QC 718, QS 68

\* These calculations account for the variation of the relative volatilities and enthalpies with pressure.

# SECRET

SECRET

ASD-TDR-63-665, Part I

TABLE 71

POINT NO. 17

LOW PRESSURE COLUMN PRESSURE -  $70 \leq p \leq 105$  PSIA

HIGH PRESSURE COLUMN PRESSURE - 245 PSIA

FEED AIR SUPERHEAT - Q.B.T.U.

Vapor	Mol	Fraction	Liquid	Mol	Fraction	Flow	Quan.
H	A	Q	N	A	Q	L	V
TOP SECTION OF LOW PRESSURE COLUMN							
.9779	.004539	.01755	1.000	.0000	.0000	.0000	.7788
.9765	.003239	.02022	.9449	.005853	.04921	.2485	.1158
.9781	.004697	.01723	.9627	.005145	.03217	.5383	.9528
.9706	.005599	.02276	.9495	.008519	.04202	.5366	.9510
.9616	.008459	.02990	.9334	.01183	.05480	.5342	.9486
.9509	.01020	.03891	.9141	.01496	.07097	.5311	.9456
.9383	.01175	.04991	.8914	.01776	.09085	.5274	.9419
.9241	.01302	.06287	.8655	.02008	.1144	.5232	.9376
.9085	.01394	.07753	.8370	.02179	.1412	.5185	.9329
.8922	.01446	.09336	.8067	.02381	.1705	.5136	.9281
.8757	.01459	.1097	.7761	.02513	.2008	.5089	.9234
.8600	.01437	.1257	.7465	.02680	.2307	.5046	.9190
.8455	.01388	.1406	.7193	.0286	.2587	.5008	.9153
.8329	.01321	.1539	.6953	.03079	.2859	.4977	.9122
.8222	.01245	.1653	.6751	.0334	.3094	.4953	.9098
.8136	.01169	.1747	.6588	.03604	.3232	.4937	.9081
.8069	.01096	.1821	.6461	.03872	.3372	.4926	.9070
.8018	.01031	.1879	.6365	.04152	.3480	.4920	.9065
			.6373	.0436	.3484		14.79
BOTTOM SECTION OF LOW PRESSURE COLUMN							
.1784	.03202	.7896	.08609	.02651	.8874	.2212	.0000
.1784	.03202	.7896	.1551	.03063	.8143	.8768	.6555
.2976	.03406	.6683	.2449	.03218	.7229	.8881	.6669
.4293	.03442	.5383	.3453	.03097	.6257	.9041	.6828
.5510	.02821	.4203	.4394	.02781	.5328	.9221	.7008
.6463	.02324	.3304	.5142	.02401	.4618	.9383	.7171
.7120	.01883	.2691	.5663	.02062	.4131	.9502	.7290
.7536	.01549	.2209	.5994	.01804	.3826	.9575	.7362
.7786	.01320	.2082	.6191	.01526	.3646	.9610	.7397
.7932	.01171	.1951	.6306	.01311	.3543	.9620	.7407
.8018	.01076	.1875	.6371	.01143	.3485	.9615	.7403
.8069	.01018	.1829	.6408	.01094	.3453	.9601	.7389
			.6373	.01436	.3484		9.05
.8065	.009134	.1844	.6360	.01209	.3511	.4692	.1665
HIGH PRESSURE COLUMN							
.9729	.003596	.02354	.9550	.00502	.04000	.3643	.0000
.9550	.005022	.04000	.9550	.005022	.04000	.7416	1.106
.9354	.006303	.05846	.9357	.006944	.06741	.7275	1.092
.9147	.007401	.07789	.8941	.008616	.09725	.7132	1.077
.8935	.008288	.09826	.8614	.009990	.1286	.6992	1.063
.8724	.008952	.1186	.8266	.01104	.1604	.6860	1.050
.8523	.009400	.1383	.7968	.01176	.1915	.6741	1.038
.8337	.009649	.1567	.7671	.01219	.2207	.6633	1.028
.8171	.009733	.1731	.7404	.01236	.2472	.6545	1.019
.8028	.009697	.1875	.7171	.01233	.2706	.6469	1.011
.7906	.009574	.1998	.6972	.01216	.2906	.6407	1.005
.7806	.009400	.2100	.6807	.01191	.3074	.6357	1.000
.7906	.009574	.1998	.6807	.01191	.3074	.6357	.0000
.7806	.009400	.2100	1.000	.0000	.0000	.0000	1.000

HEAT EXCHANGER DUTIES - B.T.U./lb. Mole Feed

OR 1725, QD 411, QD 98

\* These calculations account for the variation of the relative volatilities and enthalpies with pressure.

SECRET

**CONFIDENTIAL**

ASD-TDR-63-665, Part I

APPENDIX XIV

LOW PRESSURE COLUMN DESIGN COMPUTER PROGRAM

1. Description and Criteria

This appendix describes the tray dynamics design program which utilizes iterative optimization procedures and is based on the results of theoretical tray counts obtained from cycle studies and mass transfer research discussed in Section 3.0 of this report. Results from the cycle studies established flows for preselected inlet and waste pressures and product and waste purities. The innermost radius of the column is fixed. The procedure is to solve the enriching section and stripping section separately beginning with the nitrogen rich enriching section near the shaft.

The method of computer solution as shown in Figure 219, is to start at the radially innermost tray and then sum the tray efficiencies as each tray is computed. At the point where the desired final pressure ( $P_{f1}$ , which is the kettle pressure for the enriching section calculation or the peripheral column pressure for the stripping section) equals the tray pressure ( $P_k'$ ), a check is made to see if the summation of the tray efficiencies ( $\sum E^o$ ) equals the theoretical tray number ( $N_p^*$ ). If it does, the computer prints out the answers and stops. If it does not, the starting superficial vapor velocity ( $V_s$  initial) is changed by an increment to approximate the derivative. The column is computed again, this time using ( $V_s$  initial -  $\Delta V_s$ ). At the tray where  $|P_k' - P_{f1}| < 0.1$ , a new superficial vapor velocity is calculated as shown on the flowsheet, Figure 219, line 6. The derivation of the equation which calculates the new superficial vapor velocity is presented in Appendix XVI.

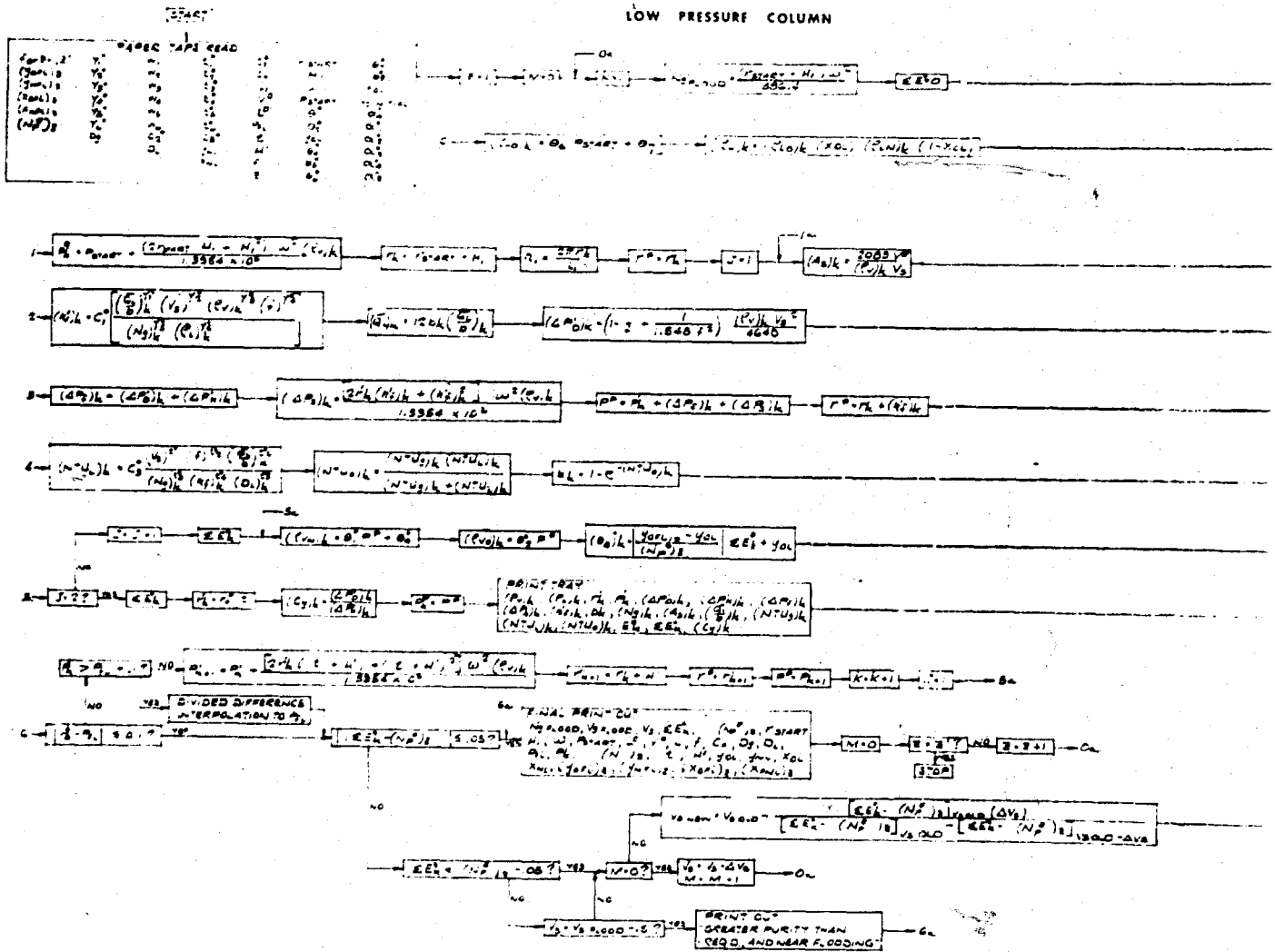
The column section is recomputed with  $V_{s\text{new}}$  and the procedure continued until solution is obtained. The following criteria for enriching and stripping section results must be satisfied. All physical property data used for the program were obtained from Ref. (20).

- a. The ratio of dry plate pressure drop to hydrostatic pressure drop on any tray ( $\Delta P_D / \Delta P_H$ ) called the weeping factor ( $C_y$ ), must be greater than 0.2. This limit is established as the dumping criteria for the flight-

63 ASRP-2391

**CONFIDENTIAL**

ASD-TDR-63-665, Part I



**SECRET**

ASD-TDR-63-665, Part I

### COMPUTER PROGRAM FLOWSHEET

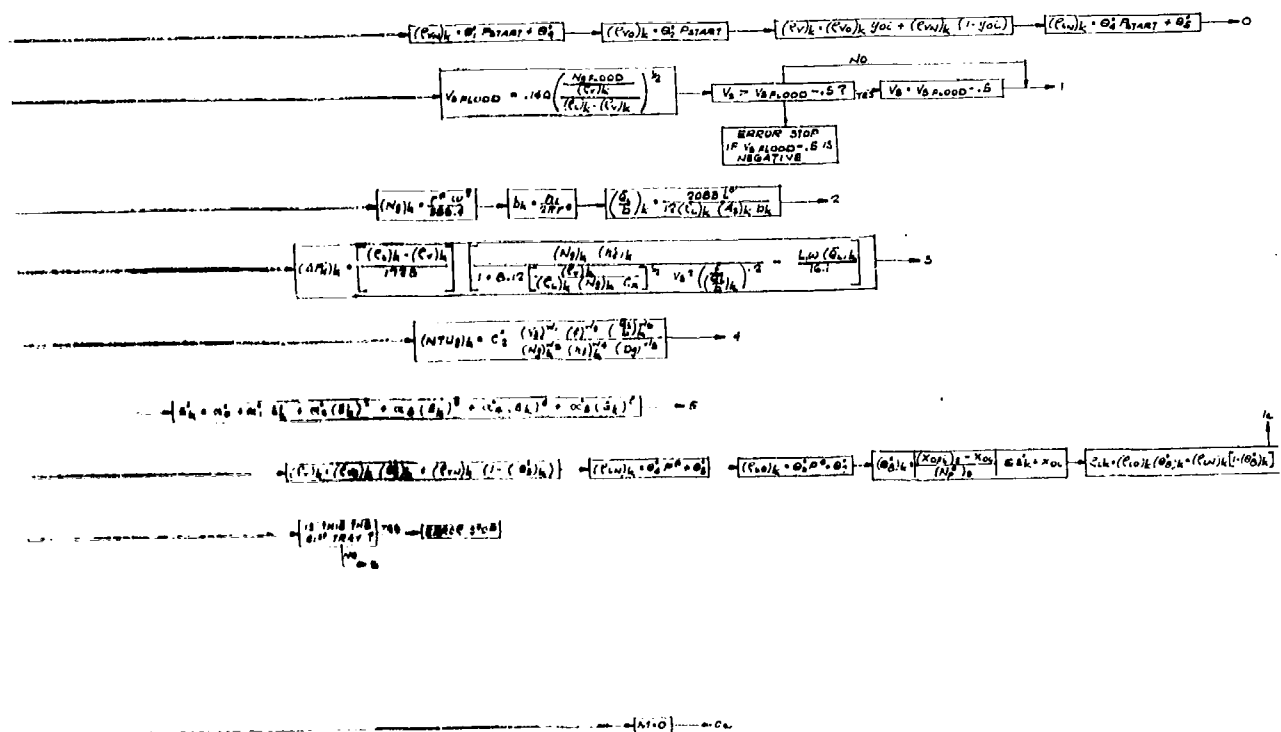


FIG. 219

63 ASRP-2391

515

**SECRET**

**CONFIDENTIAL**

**ASD-TDR-63-665, Part I**

weight separator, below which excessive liquid passes radially through the tray holes instead of along the tray from one downcomer to another. This must be avoided for satisfactory column operation.

b. Tray foam heights in the enriching section must be greater than 0.7 inches, and greater than 0.6 inches in the stripping section. Since the foam heights never were too high, no upper limit was established for this column.

The computer program was written so that the superficial vapor velocity was always maintained at least 0.5 ft./sec. below the flooding value where entrainment of the liquid in the vapor prevents liquid reflux from passing radially outward in the column.

Since the reboiler-condenser and separation chambers in the system improve the purity of the liquid stream leaving the low pressure column, the computer program was written to design the column based on a maximum of five final purities in a given run. Thus, the low pressure column and reboiler-condenser plus separation chambers could be optimized together to give a final desired oxygen purity in the product liquid stream leaving the appropriate separation chamber.

It has been conservatively assumed that the reboiler-condenser and separation chambers improve the oxygen purity in the liquid leaving the low pressure column by one theoretical tray.

**2. Basic Assumptions**

The following were assumed in the low pressure column computer program analysis:

- a.  $N_p^*$  from the low pressure column theoretical tray counts where  $\Delta P$  per tray is constant can be used with correction for pressure profile.
- b. Average column section vapor diffusivity ( $D_g$ ) at average pressure and composition can be used: (Variation in  $D_g$  is minor).
- c. Number of downcomers per tray for a given column section is constant (assumes spacing between downcomers on a tray will not become excessive).

63 ASRP-2391

**CONFIDENTIAL**

## CONFIDENTIAL

### ASD-TDR-63-665, Part I

- d. Iteration for hydrostatic tray pressure drop is avoided as the relationship between  $Ng^\circ$  and  $Ng$  is assumed to be constant.
- e. Liquid and vapor densities are linear functions of temperature and composition (good approximation for regions studied.)
- f. Enhancement in tray efficiency due to the desired non-mixing of the liquid on the tray and non-mixing of the vapor between trays is assumed to be 25 per cent of the theoretical maximum. This is a theoretical prediction, Ref. (17), (23, p. 550-552), (44), (45), (46), and (47), for the rotating column where the gravitational effect is substantial. Experimental programs with the boilerplate cryogenic separator are planned to evaluate the actual enhancement. If the experimental results indicate that enhancement is not possible, optimization of the full-scale unit tray dynamics should nullify the effect of necessary reduction in efficiency.
- g. The free area fraction (f) for the column section is constant. Tray by tray variation in free area will be used at the final design point.
- h. A constant orifice coefficient ( $C_v$ ) for calculation of dry plate pressure drop is assumed. This too will be varied in final designs.
- i. For purposes of the tray dynamics design of the low pressure column, the presence of argon is neglected; however, the theoretical tray counts used are for the ternary system.
- j. Average liquid and vapor flows ( $L^\square$  and  $V^\square$ ) are used for a given column section.
- k. The liquid side mass transfer resistance is taken to be negligible. This is based on earlier experimental evidence under this contract.

63 ASRP-2391

CONFIDENTIAL

# CONFIDENTIAL

## ASD-TDR-63-665, Part I

### 3. Equation Constants for Data Input

The following are constants presently used in the equations presented on the computer program flowsheet:

- a.  $Z' = 1 \text{ to } 5$
- b.  $Y_1^{\circ} = 0.333, Y_2^{\circ} = 1.6, Y_3^{\circ} = 0.5, Y_4^{\circ} = 0.13,$   
 $Y_5^{\circ} = 0.85, Y_6^{\circ} = 0.5$
- c.  $W_1 = -3.12, W_2 = 0, W_3 = 0.75, W_4 = -0.75,$   
 $W_5 = 0.667, W_6 = 0$
- d.  $C_2^{\circ} = 47,700$
- e.  $t_1^{\circ} = 0, t_2^{\circ} = 0, t_3^{\circ} = 0, t_4^{\circ} = 0, t_5^{\circ} = 0, t_6^{\circ} = 0$
- f.  $C_1^{\circ} = 48.7$
- g.  $C_x = 0.9$
- h.  $C_3^{\circ} = 1 \times 10^{10}$
- i.  $\Theta_1^{\circ} = 0.01735, \Theta_2^{\circ} = 0.01762, \Theta_4^{\circ} = -0.04192,$   
 $\Theta_5^{\circ} = 48, \Theta_6^{\circ} = 0.0905, \Theta_7^{\circ} = 72.2, \Theta_9^{\circ} = 0$
- j.  $\alpha_0^{\circ} = -0.0067, \alpha_1^{\circ} = 1.4388, \alpha_2^{\circ} = -3.5691, \alpha_3^{\circ} = 13.4815,$   
 $\alpha_4^{\circ} = -17.1361, \alpha_5^{\circ} = 7.7812$
- k.  $\Delta V_s = 0.01$

63 ASRP-2391



# CONFIDENTIAL

ASD-TDR-63-665, Part I

## APPENDIX XV

### HIGH PRESSURE COLUMN DESIGN COMPUTER PROGRAM

#### 1. Description and Criteria

This program is more refined than the low pressure column program presented in Appendix XIV, in that the theoretical tray count and tray dynamics are analyzed together thus obtaining the exact influence of the gravitational field in a tray by tray computation.

The iterative optimization technique (similar to that for the low pressure column program) is presented in the computer flowsheets, Figures 220 and 221. The method of solution is to match a desired final kettle liquid oxygen purity with a peripheral tray liquid oxygen purity by iterating on the superficial vapor velocity.

The general procedure is to provide sufficient boundary conditions so that overall heat, mass and composition balances can be performed to completely describe the high pressure column boundaries. The column is solved by starting at the radially innermost tray near the shelf and changing purities, pressures and temperatures along with column tray dynamics parameters in climbing radially outward. At the point where the tray pressure equals the specified peripheral pressure, the oxygen purity in the liquid leaving the last tray is checked against the oxygen purity of the kettle liquid (given data input). If it checks, the computer prints out and stops. If it does not check, the column is computed again using  $V_{s\text{initial}} - \Delta V_s$ . At the point where  $|P_K - P_k| \leq 0.1$ , a new superficial vapor velocity is calculated from the equation shown on the flowsheet, Figure 220, line 7. Appendix XVI presents the derivation of this equation. The column is recomputed with the new  $V_s$  and the procedure continued till solution is obtained.

The tray equilibrium subroutine which performs the basic distillation analysis is appended as Figure 221. The basic equations used for the computations leading to  $\alpha_{NO}$  were obtained from Reference (20) and those pertaining to calculation of  $\alpha_{AO}$  were obtained by correlation of argon-oxygen data given in Reference (58).

63 ASRP-2391

# CONFIDENTIAL

1



1

**SECRET**

ASD-TDR-63-665, Part I

COMPUTER PROGRAM FLOWSHEET

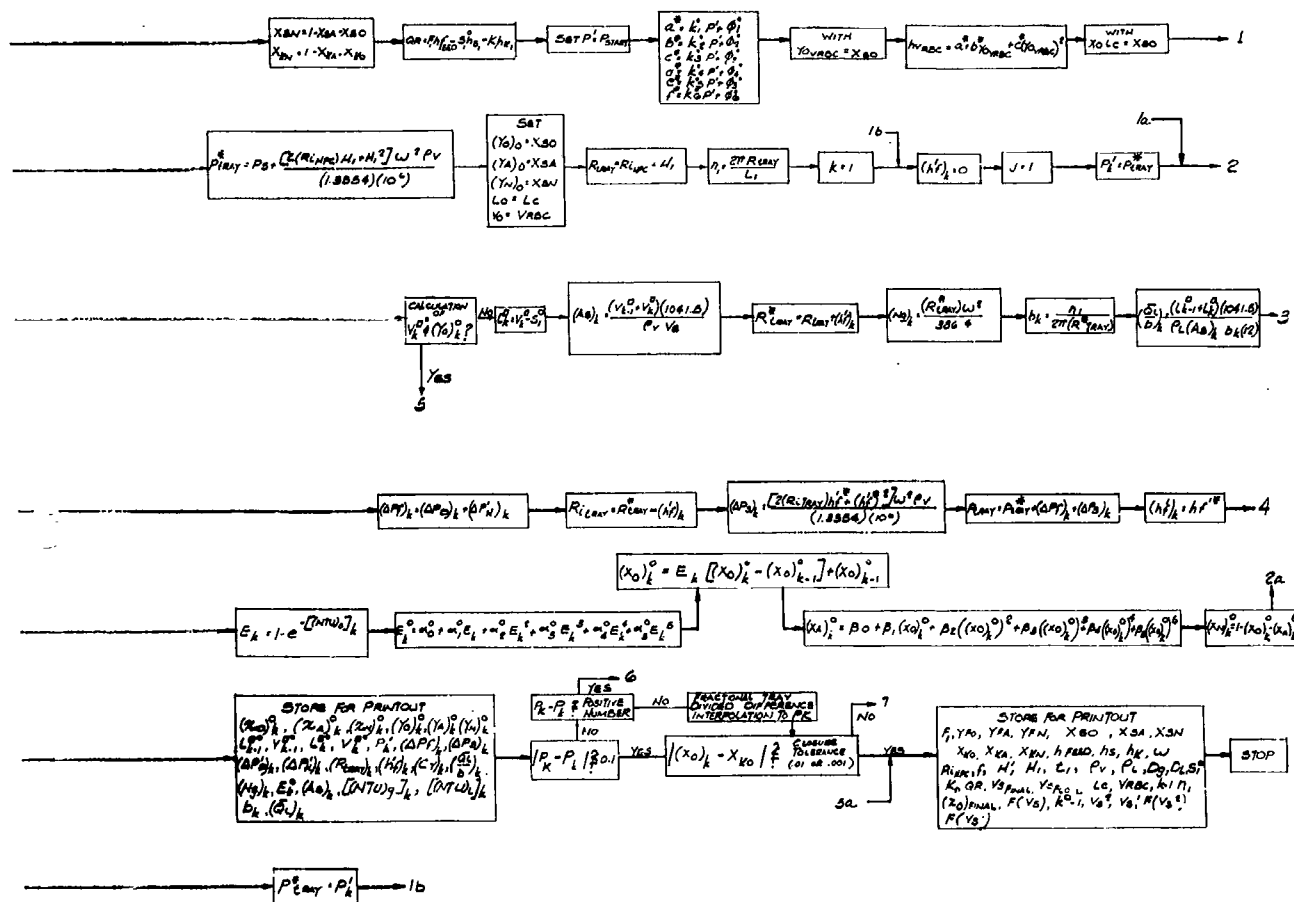


FIG. 220

**SECRET**

ASD-TDR-63-665, Part I

# CONFIDENTIAL

## ASD-TDR-63-665, Part I

The criteria for acceptance of a solution are as follows:

- a. Dumping criteria identical to that for the low pressure column analysis presented in Appendix XIV.
- b. Tray foam heights must be less than 1.9 inches. Low foam heights are no problem in this column because of the high vapor density.
- c. The superficial vapor velocity is kept below the flooding valve in the same manner as described for the low pressure column. (Appendix XIV).

### 2. Peripheral Pressure Computation

The separator inlet air is delivered through the shaft at the specified pressure but is compressed in passing to the periphery of the high pressure column. The derivation and final formula used to calculate this static pressure rise are presented as follows:

It is assumed that the vapor density is a linear function of pressure or

$$\rho_v = d_1 + d_2 P$$

where  $d_1$  and  $d_2$  are known values for a given composition.

The compression of the vapor is determined by the gravitational field change in kinetic energy imparted to the vapor.

Therefore, 
$$dP = \frac{VdV \rho_v}{g_c}$$

substituting 
$$dP = \frac{VdV (d_1 + d_2 P)}{g_c}$$

separating variables,

$$\frac{dP}{d_1 + d_2 P} = \frac{VdV}{g_c}$$

Since  $V = R\omega$  for the rotating system where  $\omega = \text{constant}$ ,

$$\frac{dP}{d_1 + d_2 P} = \frac{R\omega d(R\omega)}{g_c} = \frac{R\omega^2 dR}{g_c}$$

63 ASRP-2391

# CONFIDENTIAL

# CONFIDENTIAL

ASD-TDR-63-665, Part I

Integrating, 
$$\int_{P'_I}^{P'_f} \frac{dP}{d_1 + d_2 P} = \frac{\omega^2}{g_c} \int_{R_i}^{R_o} R dR$$

Therefore: 
$$\frac{1}{d_2} \ln \frac{d_1 + d_2 P'_f}{d_1 + d_2 P'_I} = \frac{(R_o^2 - R_i^2) \omega^2}{2 g_c}$$

Changing form:

$$\frac{d_1 + d_2 P'_f}{d_1 + d_2 P'_I} = e^{\frac{d_2 (R_o^2 - R_i^2) \omega^2}{2 g_c}}$$

Solving for  $P'_f$

$$P'_f = \frac{(d_1 + d_2 P'_I) e^{\left[ \frac{d_2 \omega^2 (R_o^2 - R_i^2)}{2 g_c} \right]} - d_1}{d_2}$$

For the case of the inlet air stream,  $R_i = 0$ ,  $d_1 = -0.853$  and  $d_2 = 0.0001517$ .

Therefore:

$$P'_f = \frac{(-0.853 + 0.0001517 P'_I) e^{\left[ \frac{0.0001517 \omega^2 R_o^2}{2 g_c} \right]} - 0.853}{0.0001517} \quad (75)$$

By assuming  $R_o$ ,  $P'_f$  can be computed for air from the above equation. Frictional pressure drop in the inlet air shaft to the peripheral channel is neglected.

## 3. Basic Assumptions

- a. Use of average vapor diffusivity. (variation in  $D_g$  is minor).
- b. Number of downcomers per tray are constant (assumes spacing between downcomers will not become excessive).
- c. Iteration for hydrostatic pressure drop is avoided as the relationship between  $Ng^\circ$  and  $Ng$  is assumed to be constant.

63 ASRP-2391

**CONFIDENTIAL**

**ASD-TDR-63-665, Part I**

- d. Average liquid and vapor densities are used because of the very slight variation in the high pressure column in contrast to the relatively larger change in the low pressure column.
- e. Enhancement in tray efficiency due to desired non-mixing of liquid on the tray and non-mixing of vapor between trays is assumed to be 25% of the theoretical maximum. The statements in Appendix XIV in regard to experimental attainment of this enhancement in the boilerplate separator apply.
- f. The free area fraction ( $f$ ) is constant for all column trays thus adding a conservative factor to the point efficiency.
- g. A constant orifice coefficient ( $C_v$ ) for calculation of dry plate pressure drop is assumed.
- h. The liquid side mass transfer resistance is assumed to be negligible, based on earlier experimental results under this contract.
- i. Cooling of the column vapor by expansion against the gravitational field is equal to the superheat incurred by the inlet air vapor in passing to the periphery.

**4. Equation Constants for Data Input**

The following are constants presently used in the equations presented on the computer program flowsheets:

- a.  $k_1^\circ - k_6^\circ$  and  $\phi_1^\circ - \phi_6^\circ$  as presented in Table 72.
- b.  $Y_1^\circ = 0.333$ ,  $Y_2^\circ = 1.6$ ,  $Y_3^\circ = 0.5$ ,  $Y_4^\circ = -0.13$ ,  
 $Y_5^\circ = 0.85$ ,  $Y_6^\circ = 0.5$
- c.  $W_1 = -3.12$ ,  $W_2 = 0$ ,  $W_3 = -0.75$ ,  $W_4 = -0.75$ ,  
 $W_5 = -0.667$ ,  $W_6 = 0$
- d.  $t_1^\circ = 0$ ,  $t_2^\circ = 0$ ,  $t_3^\circ = 0$ ,  $t_4^\circ = 0$ ,  $t_5^\circ = 0$ ,  $t_6^\circ = 0$
- e.  $C_1^\circ = 48.7$ ,  $C_2^\circ = 47,700$ ,  $C_3^\circ = 1 \times 10^{10}$
- f.  $C_x = 0.9$

63 ASRP-2391

**CONFIDENTIAL**

**CONFIDENTIAL**

ASD-TDR-63-665, Part I

- g.  $\alpha_0^\circ = -0.0031025555$ ,  $\alpha_1^\circ = 1.11327908$ ,  $\alpha_2^\circ = -0.7473526$ ,  
 $\alpha_3^\circ = 3.0019803$ ,  $\alpha_4^\circ = -3.3589933$ ,  $\alpha_5^\circ = 1.4715685$ ,
- h.  $\beta_0 = 0.0032693939$ ,  $\beta_1 = 0.0463815$ ,  $\beta_2 = 0.30203628$ ,  
 $\beta_3 = -2.9289547$ ,  $\beta_4 = 8.4881099$ ,  $\beta_5 = -9.1778025$
- i.  $\gamma_0 = 0.0018595222$ ,  $\gamma_1 = 0.088622572$ ,  $\gamma_2 = -0.10460442$ ,  
 $\gamma_3 = -2.3210486$ ,  $\gamma_4 = 12.332021$ ,  $\gamma_5 = -22.390105$
- j.  $\Delta V_s = 0.01$ , tolerance on  $W^\circ = 1 \times 10^{-7}$ , tolerance on  $X_0$  (equilibrium calculation) =  $1 \times 10^{-7}$ , column closure tolerance =  $\pm .001$

63 ASRP-2391

**CONFIDENTIAL**



**CONFIDENTIAL**

ASD-TDR-63-665, Part I

TABLE 72

ENTHALPY COEFFICIENTS AS LINEAR FUNCTIONS OF PRESSURE

Coefficients			
$k_1^\circ - 6 = \text{Btu/lb.-mole/psig}$			
$\phi_1^\circ - 6 = \text{Btu/lb.-mole}$			
	Pressure Range (psig)		
	<u>160 - 200</u>	<u>200 - 250</u>	<u>240 - 290</u>
$k_1^\circ$	-0.3	-0.4889	-0.7714
$\phi_1^\circ$	3171	3210	3279
$k_2^\circ$	0.33	1.4875	1.4875
$\phi_2^\circ$	326.2	97	97
$k_3^\circ$	-0.103	-0.9136	-0.7271
$\phi_3^\circ$	-150.5	43.7	-8.4
$k_4^\circ$	2.81	3.04	2.7273
$\phi_4^\circ$	912.4	882	960
$k_5^\circ$	0	1.7125	0.6192
$\phi_5^\circ$	-695	-1034	-767
$k_6^\circ$	0	-1.7	-0.2308
$\phi_6^\circ$	242	578	229

**CONFIDENTIAL**

ASD-TDR-63-665, Part I

(THIS PAGE IS INTENTIONALLY BLANK.)

63 ASRP-2391

**CONFIDENTIAL**

ASD-TDR-63-665, Part I

APPENDIX XVI

DISTILLATION COLUMN SOLUTION AS A  
FUNCTION OF SUPERFICIAL VAPOR VELOCITY

In the column closure functions presented in the flowsheets of Appendices XIV and XV, it is shown that the solution for the low pressure column program occurs where the summation of tray efficiencies equals the number of theoretical trays ( $\Sigma E^\circ = N_p^*$ ) and in the high pressure column where the final column oxygen purity equals the kettle oxygen purity ( $X_O = X_{K_O}$ ). These solutions are obtained by changing the column superficial vapor velocity until the proper value is found which gives  $\Sigma E^\circ = N_p^*$  and  $X_O = X_{K_O}$  plus or minus given tolerances. The equation used to change  $V_s$  is shown on Figures 219 and 220 and is derived as follows:

Let  $f(V_s) = \Sigma E^\circ - N_p^*$  and  $X_O - X_{K_O}$  where a solution occurs at  $f(V_s) = 0$ .

If  $f(V_s)$  occurring at  $V_s$  were lowered by an incremental finite amount,  $\Delta V_s$ , the new  $f(V_s)$  at  $V_s - \Delta V_s$  would be approximately, given by the following:

$$f(V_s)_{V_s - \Delta V_s} = f(V_s)_{V_s} - \left( \frac{\Delta f(V_s)_{V_s}}{\Delta V_s} \right) \Delta V_s$$

rearranging:

$$\frac{f(V_s)_{V_s} - f(V_s)_{V_s - \Delta V_s}}{\Delta V_s} = \frac{\Delta f(V_s)_{V_s}}{\Delta V_s}$$

In the limit as  $\Delta V_s$  approaches zero,

$$\frac{f(V_s)_{V_s} - f(V_s)_{V_s - \Delta V_s}}{\Delta V_s} = \frac{df(V_s)}{dV_s}$$

Assume that  $\Delta V_s \sim dV_s$

Therefore, between  $f(V_s)_{V_s}$  and  $f(V_s)_{V_s - \Delta V_s}$ , we have a straight line.

63 ASRP-2391

**CONFIDENTIAL**

~~CONFIDENTIAL~~

ASD-TDR-63-665, Part I

Let us define this straight line function as  $F(V_s)$ .

Therefore, by definition:

$$F(V_s) = [\text{slope}] V_s + [\text{ordinate intercept}]$$

The slope of this line has been shown to be  $\frac{df(V_s)}{dV_s}$  and the ordinate intercept can be obtained, since at some  $V_{s_{\text{new}}}$ ,

$$F(V_s) = 0$$

Therefore, the ordinate intercept can be calculated as follows:

$$0 = \left[ \frac{df(V_s)}{dV_s} \right] V_{s_{\text{new}}} + [\text{ordinate intercept}]$$

and

$$[\text{ordinate intercept}] = - \left[ \frac{df(V_s)}{dV_s} \right] V_{s_{\text{new}}}$$

Finally,

$$F(V_s) = \left[ \frac{df(V_s)}{dV_s} \right] V_s - \left[ \frac{df(V_s)}{dV_s} \right] V_{s_{\text{new}}}$$

solving for  $V_{s_{\text{new}}}$ :

$$V_{s_{\text{new}}} = V_s - \frac{F(V_s)}{\left[ \frac{df(V_s)}{dV_s} \right]}$$

Since  $V_s$  here is the initial or old superficial vapor velocity and since:

$$\frac{df(V_s)}{dV_s} \sim \frac{f(V_s)_{V_s} - f(V_s)_{V_s - \Delta V_s}}{\Delta V_s}$$

$$\therefore V_{s_{\text{new}}} = V_{s_{\text{old}}} - \frac{F(V_{s_{\text{old}}}) \Delta V_s}{f(V_{s_{\text{old}}}) - f(V_{s_{\text{old}}} - \Delta V_s)}$$

Since  $F(V_{s_{\text{old}}}) = f(V_{s_{\text{old}}})$  as the straight line and curve functions

63 ASRP-2391

CONFIDENTIAL

**CONFIDENTIAL**

ASD-TDR-63-665, Part I

intersect at  $V_{s_{old}}$ , by definition:

$$V_{s_{new}} = V_{s_{old}} - \frac{f(V_{s_{old}})\Delta V_s}{f(V_{s_{old}}) - f(V_{s_{old}} - \Delta V_s)} \quad (76)$$

63 ASRP-2391

**CONFIDENTIAL**

ASD-TDR-63-665, Part I

(THIS PAGE IS INTENTIONALLY BLANK.)

63 ASRP-2391

~~SECRET~~

ASD-TDR-63-665, Part I

APPENDIX XVII

AIR SEPARATOR

WEIGHT, VOLUME, AND HORSEPOWER

COMPUTER PROGRAM AND SAMPLE CALCULATIONS

The following presents the equations and calculation procedures used to obtain air separator weight, volume and horsepower. Sample calculations for the General Dynamics/Astronautics cycle (separator inlet pressure, 225 psia; waste pressure, 56.5 psia; product oxygen purity, 90 per cent by weight; and waste nitrogen purity, 98 per cent by weight) are included. The equations or items incorporated in the weight and volume computer program are numbered or specially noted. All physical property data used were obtained from References(20) and (37).

Dimensional constants appearing in the equations are listed as follows:

3600 sec./hr.  
29 lb./lb.-mole air  
2.016 lb./lb.-mole hydrogen  
20736 in.<sup>4</sup>/ft.<sup>4</sup>  
1728 in.<sup>3</sup>/ft.<sup>3</sup>  
144 in.<sup>2</sup>/ft.<sup>2</sup>  
12 in./ft.  
  
1.818 x 10<sup>-3</sup> hp/ft.-lb./sec.  
1.415 hp/Btu/sec.  
1.285 x 10<sup>-3</sup> Btu/ft.-lb.

1. High Pressure Column

Data Input

$\delta_1$   
 $\delta_2$

Output of Program

bavg  
 $W_T$   
 $W_D$

63 ASRP-2391

~~SECRET~~

~~SECRET~~

# ASD-TDR-63-665, Part I

## Data Input

$R_1$   
 $R_O$   
 $b_1$   
 $b_O$   
 $k_t$   
 $P_p$   
 $\rho_m$   
 $S_1$   
 $C_1$   
 $h_L^{ol}$   
 $\rho_{L-MAX}$   
 $\omega$   
 $g$

## Output of Program

$W_T + W_D$   
 $h$   
 $W_{sh}$   
 $ts$   
 $W_{si}$   
 $W_{HPC}$

Average Column Width

$$A_{avg} = \frac{A_1 + A_O}{2}$$

$$2 \pi (R_{avg}) (b_{avg}) = \frac{2 \pi R_1 b_1 + 2 \pi R_O b_O}{2}$$

$$2 \pi \left( \frac{R_1 + R_O}{2} \right) b_{avg} = \frac{2 \pi R_1 b_1 + 2 \pi R_O b_O}{2}$$

$$b_{avg} = \frac{R_1 b_1 + R_O b_O}{R_1 + R_O} \quad (77)$$

$$b_{avg} = \frac{(42) (58.6) + (68.39) (40.4)}{42 + 68.39}$$

$$b_{avg} = 47.3 \text{ in.}$$

63 ASRP-2391

~~SECRET~~



**SECRET**

# ASD-TDR-63-665, Part I

## Weight of Trays:

The trays are assumed to act as tension support members for the column side walls sustaining the column pressure.

For a given tray:

$$S_1 = \frac{\text{FORCE ON SIDES BETWEEN TRAYS}}{\text{TRAY CROSS-SECTIONAL AREA}} = \frac{2\pi (R_{\text{tray}}) (H') (P_{\text{tray}})}{2\pi (R_{\text{tray}}) (t') (1-f)}$$

$$\therefore t' = \frac{H' (P_{\text{tray}})}{S_1 (1-f)}$$

$$\text{The weight of one tray} = \frac{2\pi (R_{\text{tray}}) (b_{\text{tray}}) (t') (1-f) \rho_m}{1728}$$

Substituting:

$$\text{Weight of one tray} = \frac{2\pi (R_{\text{tray}}) (b_{\text{tray}}) \rho_m (H') (P_{\text{tray}})}{1728 S_1}$$

$$\text{Weight of all trays} = \sum_{i=1}^{\# \text{ trays}} \frac{2\pi (R_{\text{tray}_i}) (b_{\text{tray}_i}) \rho_m (H'_i) (P_{\text{tray}_i})}{1728 S_1}$$

$$\Sigma 2\pi R_{\text{tray}} H' \sim \pi (R_o'^2 - R_1'^2)$$

Let  $P_{\text{tray}} = P_p$  for all trays

Let  $b_{\text{tray}} = b_{\text{avg}}$  for all trays

Insert  $k_t$  for tray perforations

$$\therefore W_T = \frac{\pi (R_o'^2 - R_1'^2) \rho_m b_{\text{avg}} k_t P_p}{1728 S_1} \quad (78)$$

$$W_T = \frac{\pi [(68.39)^2 - (42)^2] (164) (47.3) (1.0) (229.9)}{(1728) (33,333)}$$

$$W_T = 283.5 \text{ lbs.}$$

63 ASRP-2391

**SECRET**

~~SECRET~~

ASD-TDR-63-665, Part I

Weight of Downcomers

$$W_D = \delta_1 W_T \quad (79)$$

$$W_D = (0.5) (283.5)$$

$$W_D = 141.8 \text{ lb.}$$

Weight of Trays plus Weight of Downcomers

$$W_T + W_D = \delta_2 W_T \quad (80)$$

$$W_T + W_D = (1.5) (283.5)$$

$$W_T + W_D = 425.3 \text{ lb.}$$

If ripple trays were used,  $\delta_1 = 0$  and  $\delta_2 = 1$ .

If the downcomer trays used did not take their share of tensile stress on the sides,  $\delta_1 = 1.5$  and  $\delta_2 = 2.5$ .

Since it is assumed that the downcomer trays used will take their share of stress on the side,  $\delta_1 = 0.5$  and  $\delta_2 = 1.5$ .

Shell Thickness (with cryogenic liquid buildup)

Includes increase in design stress due to cryogenic improvement factor,  $C_1 > 1$ .

The column shell must support the peripheral column pressure, and the gravitational field loading of liquid holdup and the shell metal itself. The necessary shell thickness will be made up of contributions from these three factors.

$$h = [\text{pressure contribution}] + [\text{liquid holdup contribution}] \\ + [\text{metal contribution}]$$

63 ASRP-2391

~~SECRET~~

**SECRET**

ASD-TDR-63-665, Part I

$$h = [\text{hoop tension thickness}] + [\text{thickness to support liquid}] \\ + [\text{thickness to support metal}]$$

$$h = \frac{P_p R_o'}{S_1} + \frac{h_L^{ol} \rho_{L-MAX} R_o'^2 \omega^2}{20736 g_c S_1} + \frac{h \rho_m R_o'^2 \omega^2}{20736 g_c S_1}$$

$$h = \frac{R_o' P_p + \frac{h_L^{ol} \rho_{L-MAX} R_o'^2 \omega^2}{20736 g_c}}{S_1 - \frac{\rho_m R_o'^2 \omega^2}{20736 g_c}}$$

with inclusion of  $C_1$  factor:

$$h = \frac{R_o' P_p + \frac{h_L^{ol} \rho_{L-MAX} R_o'^2 \omega^2}{20736 g_c}}{C_1 S_1 - \frac{\rho_m R_o'^2 \omega^2}{20736 g_c}} \quad (81)$$

$$h = \frac{(68.39)(229.9) + \frac{(8.46)(45)(68.39)^2(45)^2}{20736(32.2)}}{(1.2)(33,333) - \frac{(1.64)(68.39)^2(45)^2}{20736(32.2)}}$$

$$h = 0.561 \text{ in.}$$

63 ASRP-2391

**SECRET**

**SECRET**

### ASD-TDR-63-665, Part I

#### Shell Thickness (without cryogenic liquid)

$$h = \frac{R_o' P_P}{S_1 - \frac{\rho_m R_o'^2 \omega^2}{20736 g_c}} \quad (82)$$

$$h = \frac{(63.39)(229.9)}{33,333 - \frac{(164)(68.39)^2(45)^2}{20736(32.2)}}$$

$$h = 0.507 \text{ in.}$$

Selecting the maximum shell thickness,  $0.561 > 0.507$

Therefore,  $h = 0.561 \text{ in.}$

#### Side Thickness (with cryogenic liquid)

Includes increase in design stress due to cryogenic improvement factor,  $C_1 > 1$ .

Assume that the shell is allowed to deflect and therefore the sides need not support it. Therefore the side thickness must be sufficient to support gravitational field loading but the additional metal thickness required to support the gravitational loading on the trays is also added. Support for the column pressure loading on the sides is provided by the trays as previously shown.

$$t_s = \left[ \begin{array}{l} \text{thickness due to} \\ \text{loading on side} \end{array} \right] + \left[ \begin{array}{l} \text{thickness due to load-} \\ \text{ing on the trays} \end{array} \right]$$

$$t_s = \frac{R_o'^2 \omega^2 \rho_m t_s}{20736 g_c S_1} + \frac{k_t P_P b_{avg}}{S_1} + \frac{R_o'^2 \omega^2 \rho_m}{20736 g_c S_1}$$

63 ASRP-2391

**SECRET**

~~SECRET~~

ASD-TDR-63-665, Part I

$$t_s = \frac{k_t P_p \text{ bavg } R_o'^2 \omega^2 \rho_m}{20736 g_c S_1^2 \left( 1 - \frac{R_o'^2 \omega^2 \rho_m}{20736 g_c S_1} \right)}$$

with inclusion of  $C_1$  factor,

$$t_s = \frac{k_t P_p \text{ bavg } R_o'^2 \omega^2 \rho_m}{20736 g_c C_1^2 S_1^2 \left( 1 - \frac{R_o'^2 \omega^2 \rho_m}{20736 g_c C_1 S_1} \right)} \quad (83)$$

$$t_s = \frac{(1.0) (229.9) (47.3) (68.39)^2 (45)^2 (164)}{20736 (32.2) (1.2)^2 (33,333)^2 \left[ 1 - \frac{(68.39)^2 (45)^2 (164)}{20736 (32.2) (1.2) (33,333)} \right]}$$

$$t_s = .017 \text{ in.}$$

Side Thickness (without cryogenic liquid)

$$t_s = \frac{k_t P_p \text{ bavg } R_o'^2 \omega^2 \rho_m}{20736 g_c S_1^2 \left( 1 - \frac{R_o'^2 \omega^2 \rho_m}{20736 g_c S_1} \right)} \quad (84)$$

$$t_s = \frac{(1.0) (229.9) (47.3) (68.39)^2 (45)^2 (164)}{20736 (32.2) (33,333)^2 \left[ 1 - \frac{(68.39)^2 (45)^2 (164)}{(20736) (32.2) (33,333)} \right]}$$

$$t_s = .024 \text{ in.}$$

Selecting the maximum side thickness,

$$.024 > .017$$

$$\text{Therefore, } t_s = .024 \text{ in.}$$

63 ASRP-2391

~~SECRET~~

**SECRET**

ASD-TDR-63-665, Part I

Shell Weight (Cylindrical Shell)

$$W_{sh} = \frac{2\pi R_o' b_o \rho_m h}{1728} \quad (85)$$

$$W_{sh} = \frac{2\pi (68.39) (40.4) (164) (0.561)}{1728}$$

$$W_{sh} = 923.7 \text{ lbs.}$$

Sides Weight (Circular Disks)

$$W_{si} = \frac{\pi (R_o'^2 - R_i'^2) t_s \rho_m}{1728} (\# \text{ sides}) \quad (86)$$

$$W_{si} = \frac{\pi [(68.39)^2 - (42)^2] (.024) (164)}{1728} (2)$$

$$W_{si} = 41.7 \text{ lbs.}$$

Total High Pressure Column Weight

$$W_{HPC} = W_T + W_D + W_{sh} + W_{si} \quad (87)$$

$$W_{HPC} = 283.5 + 141.8 + 923.7 + 41.7$$

$$W_{HPC} = 1390.7 \text{ lbs.}$$

63ASRP-2391

**SECRET**

**SECRET**

ASD-TDR-63-665, Part I

2. Low Pressure Column

Data Input

Output of Program

$\delta_1$

bavg

$\delta_2$

$W_T$

$R_1$

$W_D$

$R'_O$

$W_T + W_D$

$b_1$

h

$b_O$

$W_{sh}$

$k_t$

$t_s$

$P_p$

$W_{si}$

$\rho_m$

$W_{LPC}$

$S_1$

$C_1$

$h_L^{\circ'}$

$\rho_{L \max}$

$\omega$

g

R

$b_k$

$R_k$

Average Column Width

enriching section

$$A_{avg_e} = \frac{A_{ie} + A_{oe}}{2}$$

63 ASRP-2391

**SECRET**

**SECRET**

ASD-TDR-63-665, Part I

$$2\pi R_{av}_e b_{av}_g = \frac{2\pi R_i b_i + 2\pi R_k b_k}{2}$$

$$2\pi \left( \frac{R_i + R_k}{2} \right) b_{av}_e = \frac{2\pi R_i b_i + 2\pi R_k b_k}{2}$$

$$b_{av}_e = \frac{R_i b_i + R_k b_k}{R_i + R_k}$$

stripping section:

$$A_{av}_s = \frac{A_{is} + A_{os}}{2}$$

$$2\pi (R_{av})_s b_{av}_s = \frac{2\pi R_k b_k + 2\pi R'_o b_o}{2}$$

$$2\pi \left( \frac{R_k + R'_o}{2} \right) b_{av}_s = \frac{2\pi R_k b_k + 2\pi R'_o b_o}{2}$$

$$b_{av}_s = \frac{R_k b_k + R'_o b_o}{R_k + R'_o}$$

$$b_{av}_g = \frac{b_{av}_e + b_{av}_s}{2} = \frac{R_i b_i + R_k b_k}{2(R_i + R_k)} + \frac{R_k b_k + R'_o b_o}{2(R_k + R'_o)} \quad (88)$$

$$b_{av}_g = \frac{(24)(237) + (36.7)(136.9)}{2(24 + 36.7)} + \frac{(36.7)(136.9)(57.51)(94.3)}{2(36.7 + 57.51)}$$

$$b_{av}_g = 152.4 \text{ in.}$$

63 ASRP-2391

**SECRET**



**SECRET**

ASD-TDR-63-665, Part I

Weight of Trays

(Same derivation as for high pressure column)

$$W_T = \frac{\pi (R_o^2 - R_i^2) \rho_m b_{avg} k_t P_p}{1728 S_1} \quad (89)$$

$$W_T = \frac{\pi [(57.51)^2 - (24)^2] (164) (152.4) (1.0) (56.16)}{1728 (33,333)}$$

$$W_T = 209.1 \text{ lbs.}$$

Weight of Downcomers

$$W_D = \delta_1 W_T \quad (90)$$

$$W_D = (0.5) (209.1)$$

$$W_D = 104.6 \text{ lbs.}$$

Weight of Trays plus Weight of Downcomers

$$W_T + W_D = \delta_2 W_T \quad (91)$$

$$W_T + W_D = (1.5) (209.1)$$

$$W_T + W_D = 313.7 \text{ lbs.}$$

Shell Thickness (With cryogenic liquid buildup)

Includes increase in design stress due to cryogenic improvement factor,  $C_1 > 1$ .

(Same derivation as high pressure column.)

63 ASRP-2391

**SECRET**

**SECRET**

ASD-TDR-63-665, Part I

$$h = \frac{R_o' P_p + \frac{h_L' \rho_L \max R_o'^2 \omega^2}{20736 g_c}}{C_1 S_1 - \frac{m R_o'^2 \omega^2}{20736 g_c}} \quad (92)$$

$$h = \frac{(57.51)(56.16) + \frac{(3.82)(67)(57.51)^2(45)^2}{20736 (32.2)}}{(1.2)(33,333) - \frac{(164)(57.51)^2(45)^2}{20736 (32.2)}}$$

$$h = 0.151 \text{ in.}$$

Shell Thickness (without cryogenic liquid)

$$h = \frac{R_o' P_p}{S_1 - \frac{m R_o'^2 \omega^2}{20736 g_c}} \quad (93)$$

$$h = \frac{(57.51)(56.16)}{33,333 - \frac{(164)(57.71)^2(45)^2}{20736 (32.2)}}$$

$$h = 0.102 \text{ in}$$

Selecting the maximum shell thickness,

$$0.151 > 0.102$$

Therefore,  $h = 0.151 \text{ in.}$

Side Thickness (with cryogenic liquid)

Includes increase in design stress due to cryogenic improvement factor,  $C_1 > 1$

63 ASRP-2391

**SECRET**

~~SECRET~~

# ASD-TDR-63-665, Part I

(same derivation as high pressure column)

$$t_s = \frac{k_t P_b \text{avg } R_o'^2 \omega^2 \rho_m}{20736 g_c C_1^2 S_1^2 \left(1 - \frac{R_o'^2 \omega^2 \rho_m}{20736 g_c C_1 S_1}\right)} \quad (94)$$

$$t_s = \frac{(1.0)(56.16)(152.4)(57.51)^2(45)^2(164)}{20736 (32.2)(1.2)^2(33,333)^2 \left[1 - \frac{(57.51)^2(45)^2(164)}{20736 (32.2)(1.2)(33,333)}\right]}$$

$$t_s = 0.0092 \text{ in.}$$

Side Thickness (without cryogenic liquid)

$$t_s = \frac{k_t P_b \text{avg } R_o'^2 \omega^2 \rho_m}{20736 g_c S_1^2 \left(1 - \frac{R_o'^2 \omega^2 \rho_m}{20736 g_c S_1}\right)} \quad (95)$$

$$t_s = \frac{(1.0)(56.16)(152.4)(57.51)^2(45)^2(164)}{20736 (32.2) (33,333)^2 \left[1 - \frac{(57.51)^2(45)^2(164)}{20736 (32.2)(33,333)}\right]}$$

$$t_s = 0.0133$$

Selecting the maximum side thickness,

$$0.0133 > 0.0092$$

$$\text{Therefore, } t_s = 0.0133 \text{ in.}$$

Shell Weight

$$W_{sh} = \frac{2\pi R_o' b_o \rho_m h}{1728} \quad (96)$$

63 ASRP-2391

~~SECRET~~

**SECRET**

ASD-TDR-63-665, Part I

$$W_{sh} = \frac{2\pi (57.51)(94.3)(164)(0.151)}{1728}$$

$$W_{sh} = 488.7 \text{ lbs.}$$

Sides Weight

$$W_{si} = \frac{\pi (R_o^2 - R_i^2) t_s \rho_m}{1728} (\# \text{ sides}) \quad (97)$$

$$W_{si} = \frac{\pi [(57.51)^2 - (24)^2] (0.0133) (164)}{1728} (2)$$

$$W_{si} = 21.7 \text{ lbs.}$$

Total Low Pressure Column Weight

$$W_{LPC} = W_T + W_D + W_{sh} + W_{si} \quad (98)$$

$$W_{LPC} = 209.1 + 104.6 + 488.7 + 21.7$$

$$W_{LPC} = 824.1 \text{ lbs.}$$

3. Kettle Separator

<u>Data Input</u>		<u>Output of Program</u>
g	S <sub>1</sub>	h <sub>k</sub>
P <sub>k</sub>	ρ <sub>m</sub>	W <sub>ksh</sub>
R <sub>k</sub>	b <sub>s</sub>	t <sub>ks</sub>
ω	R <sub>i</sub> (low pressure column)	W <sub>ksi</sub>
h <sub>lk</sub>	C <sub>i</sub>	W <sub>ks</sub>
ρ <sub>Lmax</sub>	h <sub>L</sub> <sup>o'</sup>	

63 ASRP-2391

**SECRET**

**SECRET**

# ASD-TDR-63-665, Part I

## Shell Thickness (with cryogenic liquid holdup)

Includes increase in design stress due to cryogenic improvement factor  $C_1 > 1$ .

The kettle separator shell must support the kettle separator pressure, and the gravitational field loading of kettle separator liquid holdup and the shell metal. The necessary shell thickness will be made up of contributions from these three factors.

$$h_k = [ \text{pressure contribution} ] + [ \text{liquid holdup contribution} ] + [ \text{metal contribution} ]$$

$$h_k = [ \text{hoop tension thickness} ] + [ \text{thickness to support liquid} ] + [ \text{thickness to support metal} ]$$

$$h_k = \frac{P_k R_k}{S_1} + \frac{R_k^2 \omega^2 h_{LK} \rho_{L-MAX}}{20736 g_c S_1} + \frac{R_k^2 \omega^2 \rho_m h_k}{20736 g_c S_1}$$

$$h_k = \frac{P_k R_k + \frac{R_k^2 \omega^2 h_{LK} \rho_{L-MAX}}{20736 g_c}}{S_1 - \frac{R_k^2 \omega^2 \rho_m}{20736 g_c}}$$

with inclusion of  $C_1$  factor

$$h_k = \frac{P_k R_k + \frac{R_k^2 \omega^2 h_{LK} \rho_{L-MAX}}{20736 g_c}}{C_1 S_1 - \frac{R_k^2 \omega^2 \rho_m}{20736 g_c}} \quad (99)$$

63 ASRP-2391

**SECRET**

**SECRET**

ASD-TDR-63-665, Part I

$$h_k = \frac{(49.02)(36.7) + \frac{(36.7)^2 (45)^2 (5)(67)}{20736 (32.2)}}{(1.2)(33,333) - \frac{(36.7)^2 (45)^2 (164)}{20736 (32.2)}}$$

$$h_k = 0.0485 \text{ in.}$$

Shell Thickness (without cryogenic liquid)

$$h_k = \frac{P_k R_k}{S_1 - \frac{R_k^2 \omega^2 \rho_m}{20736 g_c}} \quad (100)$$

$$h_k = \frac{(49.02)(36.7)}{33,333 - \frac{(36.7)^2 (45)^2 (164)}{20736 g_c}}$$

$$h_k = 0.054 \text{ in.}$$

Selecting the maximum shell thickness,

$$0.054 > 0.0485$$

$$\text{Therefore, } h_k = 0.054 \text{ in.}$$

Side Thickness

The kettle separator side thickness has been sufficiently small in all cycle weight calculations so that it can be neglected.

$$\text{Therefore, } t_{ks} = 0$$

Shell Weight

(Cylindrical Shell)

63 ASRP-2391

**SECRET**

~~SECRET~~

ASD-TDR-63-665, Part I

$$W_{ksh} = \frac{2\pi R_k b_k h_k \rho_m}{1728} \quad (101)$$

$$W_{ksh} = \frac{2\pi (36.7)(8)(0.054)(164)}{1728}$$

$$W_{ksh} = 9.5 \text{ lbs.}$$

Sides Weight

(circular disk, sides supported by extension to shaft).

$$W_{ksi} = \frac{(R_k^2 - R_i^2) \rho_m t_{ks}}{1728} \quad (102)$$

since  $t_{ks}$  is assumed = 0

$$W_{ksi} = 0$$

Total Kettle Separator Weight

$$W_{ks} = W_{ksh} + W_{ksi} \quad (103)$$

$$W_{ks} = 9.5 + 0$$

$$W_{ks} = 9.5 \text{ lbs.}$$

4. Reboiler-Condenser

Data Input				Output of Program	
$S_1$	$T_o$	$C_i$	$k_L$	$\Delta T_c$	WHTA
$W_L$	$r_i'$	$g$	$\mu_L$	$\Delta T_b$	$W_{rsi}$
QR	$r_o'$	L/A	$r_{mean}$	$U_o$	$W_{RBC}$
$A/\phi$	$t_t'$	$F_{mb}$	$d_t$	LHTA	
$W_a$	$\rho_m$	Ma	$\frac{(h_c)_{EXP}}{(h_c)_{THEO}}$	Q/A	
$\omega$		$\rho_L$		$h_{RBC}$	
$\Delta T_c$ (Starting value)	$P_p$	$\lambda$		$W_{rsh}$	

63 ASRP-2391

~~SECRET~~

~~SECRET~~

# ASD-TDR-63-665, Part I

## Data Input Derivations and Calculations

The derivation of  $r_{\text{mean}}$  for the full scale reboiler-condenser is somewhat different from that presented in Section 4 of this report as the tube axes do not coincide with the radius vectors at the inner radius. A fictitious radius of 10 in. is used as the point where coincidence occurs.

$$\overline{Ng_T} = \frac{\int Ng_T dS'}{\int dS'}$$

$$\frac{r_{\text{mean}} \omega^2}{g} = \frac{\int Ng \sin \psi dS'}{\int dS'} = \frac{\int \frac{r' \omega^2}{g} \sin \psi dS'}{\int dS'}$$

$$r_{\text{mean}} = \frac{\int r' \sin \psi dS'}{\int dS'}$$

$$dS' = \frac{r' dr'}{r'_{\text{fic}}} \text{ and } \cos \psi = \frac{r'_{\text{fic}}}{r'} \text{ (Refer to Appendix VII)}$$

$$\sin \psi = \sqrt{1 - \left(\frac{r'_{\text{fic}}}{r'}\right)^2}$$

$$r_{\text{mean}} = \frac{\int_{r'_{\text{fic}}}^{r'_0} r' \sin \psi dS' - \int_{r'_{\text{fic}}}^{r'_1} r' \sin \psi dS'}{\int_{r'_{\text{fic}}}^{r'_0} dS'}$$

substituting:

$$r_{\text{mean}} = \frac{\int_{r'_{\text{fic}}}^{r'_0} r' \sqrt{1 - \left(\frac{r'_{\text{fic}}}{r'}\right)^2} \left(\frac{r' dr'}{r'_{\text{fic}}}\right) - \int_{r'_{\text{fic}}}^{r'_1} r' \sqrt{1 - \left(\frac{r'_{\text{fic}}}{r'}\right)^2} \left(\frac{r' dr'}{r'_{\text{fic}}}\right)}{\int_{r'_{\text{fic}}}^{r'_0} \left(\frac{r' dr'}{r'_{\text{fic}}}\right)}$$

63 ASRP-2391

~~SECRET~~



**SECRET**

ASD-TDR-63-665, Part I

After Integration and Substitution:

$$r_{\text{mean}} = \frac{2/3 \left[ ([r'_o]^2 - [r'_{fic}]^2)^{3/2} - ([r'_i]^2 - [r'_{fic}]^2)^{3/2} \right]}{(r'_o)^2 - (r'_{fic})^2}$$

$$\text{and } \bar{Ng}_T = \frac{r_{\text{mean}} \omega^2}{12 g}$$

putting in appropriate numerical values,

$$r_{\text{mean}} = \frac{2/3 \left[ ([42]^2 - [10]^2)^{3/2} - ([24]^2 - [10]^2)^{3/2} \right]}{(42)^2 - (10)^2}$$

$$r_{\text{mean}} = 32.4 \text{ in.}$$

$$\bar{Ng}_T = \frac{r_{\text{mean}} \omega^2}{12 g}$$

$$\bar{Ng}_T = \frac{(32.4) (45)^2}{12 (32.2)} = 170$$

The ratio  $(h_c)_{\text{EXP}} / (h_c)_{\text{THEO}}$  represents the improvement in the condensing side film coefficient as a function of  $\bar{Ng}_T$  and  $Q/A$  for the aluminum porous condensing surface. Since  $\bar{Ng}_T @ \omega = 45 \text{ rad./sec.}$  is known, assuming a value for the reboiler-condenser heat flux,  $Q/A$ , a value for  $(h_c)_{\text{EXP}} / (h_c)_{\text{THEO}}$  can be obtained. Since the computer program calculated  $Q/A$ , for certain cases it was necessary to run several times until assumed  $Q/A$  approximately equaled  $Q/A$  from the program output. The reboiler-condenser overall temperature difference is obtained by taking the difference between the boiling and condensing side saturated temperatures at the  $r_{\text{mean}}$  radius.

63 ASRP-2391

**SECRET**

**SECRET**

# ASD-TDR-63-665, Part I

## Overall Heat Transfer Coefficient

As shown by the discussion in section 4 of this report, the condensing side film coefficient for the full scale unit reboiler-condenser is given by the following:

$$h_{c_1} = 0.726 \left[ \frac{\rho_L^2 \lambda k_L^3}{\mu_L \Delta T_c} \right]^{1/4} \left[ \frac{a}{L^c} \right]^{1/4} \left[ \frac{(h_c)_{EXP}}{(h_c)_{THEO}} \right] (1-A\phi)$$

or

$$h_{c_1} = \text{(Nusselt Coefficient)} \quad \text{(coefficient (fraction of improvement) unblanketed area)}$$

substituting with  $L^c \approx dt$

$$h_{c_1} = 0.726 \left[ \frac{\rho_L^2 \lambda k_L^3}{\mu_L \Delta T_c} \right]^{1/4} \left[ \frac{r_{mean} (3,600 \omega)^2}{d_t} \right]^{1/4} \left[ \frac{(h_c)_{EXP}}{(h_c)_{THEO}} \right] (1-A\phi)$$

$$h_{c_1} = 0.726 \left[ \frac{\rho_L^2 \lambda k_L^3}{\mu_L \Delta T_c} \right]^{1/4} (60) \left( \frac{r_{mean}^{1/4} \omega^{1/2}}{d_t^{1/4} \Delta T_c^{1/4}} \right) \left[ \frac{(h_c)_{EXP}}{(h_c)_{THEO}} \right] (1-A\phi)$$

$$\text{Let } D_1 = 0.726 \left[ \frac{\rho_L^2 \lambda k_L^3}{\mu_L} \right]^{1/4} \left( \frac{r_{mean}}{d_t} \right)^{1/4}$$

63 ASRP-2391

**SECRET**

**SECRET**

ASD-TDR-63-665, Part I

Therefore: 
$$h_{c_1} = 60 D_1 \omega^{1/2} \Delta T_c^{-1/4} \left[ \frac{(h_c)_{\text{EXP}}}{(h_c)_{\text{THEO}}} \right] (1 - A_\phi)$$

From Figure 40, 
$$h_b = 7100 \Delta T_b^{1.2}$$

Boiling on the Linde copper boiling surface represents more extensive boiling data than that obtained from the Linde aluminum boiling surface experiments and is used to represent future performance for the full-scale unit. (See Section 4.)

Since the inside area of the reboiler-condenser tubes ~ outside area of the tubes, and the metal resistance is negligible,

$$\frac{1}{U_o} = \frac{1}{h_b} + \frac{1}{h_{c_1}}$$

and

$$U_o = \frac{h_b h_{c_1}}{h_b + h_{c_1}}$$

substituting the appropriate equations for  $h_b$  and  $h_{c_1}$

$$U_o = \frac{(7100 \Delta T_b^{1.2}) (60 D_1 \omega^{1/2} \Delta T_c^{-1/4} \left[ \frac{(h_c)_{\text{EXP}}}{(h_c)_{\text{THEO}}} \right] (1 - A_\phi))}{7100 \Delta T_b^{1.2} + 60 D_1 \omega^{1/2} \Delta T_c^{-1/4} \left[ \frac{(h_c)_{\text{EXP}}}{(h_c)_{\text{THEO}}} \right] (1 - A_\phi)}$$

dividing by  $60 \Delta T_c^{-1/4}$

$$U_o = \frac{7100 \Delta T_b^{1.2} D_1 \omega^{1/2} \left[ \frac{(h_c)_{\text{EXP}}}{(h_c)_{\text{THEO}}} \right] (1 - A_\phi)}{118.3 \Delta T_b^{1.2} \Delta T_c^{-1/4} + D_1 \omega^{1/2} \frac{(h_c)_{\text{EXP}}}{(h_c)_{\text{THEO}}} (1 - A_\phi)} \quad (104)$$

63 ASRP-2391

**SECRET**

**SECRET**

### ASD-TDR-63-665, Part I

#### Bolling and Condensing Temperature Drops

For steady state operation, the heat transferred from the condensing side equals the heat absorbed by the boiling side.

Therefore:  $h_b \Delta T_b = h_c \Delta T_c$  where  $A_b = A_c$

Substituting:

$$(7100 \Delta T_b^{1.2}) \Delta T_b = \left[ 60 D_1 \omega^{1/2} \Delta T_c^{-1/4} \left[ \frac{(h_c)_{EXP}}{(h_c)_{THEO}} \right] (1 - A_\phi) \right] \Delta T_c$$

Therefore:

$$\Delta T_b = .1165 \left( D_1 \left[ \frac{(h_c)_{EXP}}{(h_c)_{THEO}} \right] (1 - A_\phi) \right)^{0.455} \omega^{0.2272} \Delta T_c^{0.341} \quad (105)$$

$$\text{and } \Delta T_o = \Delta T_b + \Delta T_c ;$$

Compute  $\Delta T_b$  and  $\Delta T_c$  by trial and error using an input starting value for  $\Delta T_c$

Inserting numerical values for the GD/A cycle:

$$D_1 = 0.726 \left[ \frac{(39)^2 (58) (0.052)^3}{(0.132)} \right]^{1/4} \left( \frac{32.4}{0.250} \right)^{1/4}$$

$$D_1 = 7.62$$

Assume  $Q/A = 40,000$  Btu/ft.hr. and  $N_{gt} = 170$       Therefore:  $\frac{(h_c)_{EXP}}{(h_c)_{THEO}} = 2.37$  from Fig. 63

Let  $A_\phi = 0.1$  giving  $\bar{\Phi}' = 36^\circ$

Therefore:  $1 - A_\phi = 0.9$

Since  $\omega = 45$  rad./sec.

$$\Delta T_b = .1165 (7.62 [2.37] (0.9))^{0.455} (45)^{0.2272} \Delta T_c^{0.341}$$

$$\Delta T_b = 0.985 \Delta T_c^{0.341}$$

63 ASRP-2391

**SECRET**

~~SECRET~~

ASD-TDR-63-665, Part I

now,

$$\Delta T_o = \Delta T_b + \Delta T_c$$

or

(106)

$$11.5 = \Delta T_b + \Delta T_c$$

By trial and error,

$$\Delta T_c = 9.4 \text{ }^\circ\text{R}$$

$$\Delta T_b = 2.1 \text{ }^\circ\text{R}$$

Substituting into the overall heat transfer coefficient equation (104) previously obtained,

$$U_o = \frac{7100 (2.1)^{1.2} (7.62 (45))^{1/2} (2.37)(0.9)}{118.3 (2.1)^{1.2} (9.4)^{1/4} + (7.62(45))^{1/2} (2.37)(0.9)}$$

$$U_o = 3077 \text{ Btu/ft.}^2\text{-hr.}^\circ\text{R}$$

Heat Flux

$$Q/A = U_o \Delta T_o \quad (107)$$

$$Q/A = (3077)(11.5)$$

$$Q/A = 35,384 \text{ Btu/ft.}^2\text{-hr.}$$

Since  $35,384 \sim 40,000$  calculation is acceptable due to the small variation in  $(h_c)_{\text{EXP}} / (h_c)_{\text{THEO.}}$ .

Length of Heat Transfer Area

$$\text{LHTA} = \frac{\text{feet of length}}{\text{square foot of heat transfer area}} \left( \frac{\text{Heat Transfer rate}}{\text{(heat flux)}} \right)$$

63 ASRP-2391

~~SECRET~~

~~SECRET~~

### ASD-TDR-63-665, Part I

$$LHTA = \frac{(3600 \text{ sec./hr.}) (L/A)(QR) (Wa)}{Ma (Q/A)} \quad (108)$$

$$LHTA = \frac{(3600) (5.1 \times 10^{-4}) (1779.8) (2083)}{(29) (35,384)}$$

$$LHTA = 6.64 \text{ ft.}$$

#### Shell Thickness (with cryogenic liquid holdup)

This includes increase in design stress due to cryogenic improvement factor  $C_1 > 1$ .

The shell thickness must be sufficiently thick to support peripheral pressure and gravitational loading of liquid holdup and shell metal.

$$h_{RBC} = [\text{hoop tension}] + [\text{liquid holdup}] + [\text{metal thickness}]$$

$$h_{RBC} = \frac{P_p r'_o}{S_1} + \frac{(r'_o)^2 \omega^2 W_L}{144 (2\pi r'_o) (LHTA) S_1 g_c} + \frac{\rho_m r'_o{}^2 \omega^2}{20736 g_c S_1} h_{RBC}$$

Solving for  $h_{RBC}$

$$h_{RBC} = \frac{P_p r'_o + \frac{r'_o{}^2 \omega^2 W_L}{288\pi (LHTA) g_c}}{S_1 - \frac{\rho_m (r'_o)^2 \omega^2}{20736 g_c}}$$

63 ASRP-2391

~~SECRET~~

**SECRET**

ASD-TDR-63-665, Part I

Inserting  $C_1$

$$h_{RBC} = \frac{P_p r_o' + \frac{r_o' \omega^2 W_L}{288\pi (LHTA) g_c}}{C_1 S_1 - \frac{\rho_m (r_o')^2 \omega^2}{20736 g_c}} \quad (109)$$

$$h_{RBC} = \frac{(55.09)(42) + \frac{(42)(45)^2 (1964)}{288\pi (6.64)(32.2)}}{(1.2)(33,333) - \frac{(164)(42)^2 (45)^2}{20736 (32.2)}}$$

$$h_{RBC} = 0.081 \text{ in.}$$

Shell Thickness (without cryogenic liquid)

$$h_{RBC} = \frac{P_p r_o'}{S_1 - \frac{\rho_m (r_o')^2 \omega^2}{20736 g_c}} \quad (110)$$

$$h_{RBC} = \frac{(55.09) (42)}{33,333 - \frac{(164)(42)^2 (45)^2}{20736 (32.2)}}$$

63 ASRP-2391

**SECRET**

~~SECRET~~

ASD-TDR-63-665, Part I

$$h_{RBC} = 0.071 \text{ in.}$$

selecting the maximum shell thickness

$$0.081 > 0.071$$

$$\text{Therefore } h_{RBC} = 0.081 \text{ in.}$$

Shell Weight

(cylindrical shell)

$$W_{rsh} = \frac{2 \pi r_o' h_{RBC} (\text{LHTA}) \rho_m}{144} \quad (111)$$

$$W_{rsh} = \frac{2\pi(42)(0.081)(6.64)(164)}{144}$$

$$W_{rsh} = 162.0 \text{ lbs.}$$

Sides Weight (with cryogenic liquid buildup)

(Circular Sides)

Includes increase in design stress due to cryogenic improvement factor,

$$C_1 > 1.$$

63 ASRP-2391

~~SECRET~~



~~SECRET~~

# ASD-TDR-63-665, Part I

A metal weight necessary to support the shell against deflection due to the liquid holdup is added to the metal weight necessary for support of gravitational loading on the sides.

$$W_{rsi} = \frac{\pi (r'_o)^2 \omega^2 W_L \rho_m}{20736 g_c S_1} + \frac{(r'_o)^2 \omega^2 W_{rsi} \rho_m}{20736 S_1 g_c}$$

solving for  $W_{rsi}$

$$W_{rsi} = \frac{\pi (r'_o)^2 \omega^2 W_L \rho_m}{20736 g_c S_1 - (r'_o)^2 \omega^2 \rho_m}$$

inserting  $C_i$  and number of sides

$$W_{rsi} = \frac{\pi (r'_o)^2 \omega^2 W_L \rho_m}{20736 g_c C_i S_1 - (r'_o)^2 \omega^2 \rho_m} \quad (\# \text{ sides}) \quad (112)$$

$$W_{rsi} = \frac{\pi (42)^2 (45)^2 (1964) (164)}{20736 (32.2)(1.2)(83,333) - (42)^2 (45)^2 (164)} \quad (2)$$

$$W_{rsi} = 276.6 \text{ lbs.}$$

63 ASRP-2391

~~SECRET~~

~~SECRET~~

ASD-TDR-63-665, Part I

Heat Transfer Area Weight

(Weight of active heat transfer area on tube disks plus additional area required for manifolding and brazing).

$$WHTA = \frac{(\text{Heat Transfer Rate}) (\text{Metal Thickness}) (\text{Metal Density})}{(\text{Manifolding \& Brazing Factor}) (\text{Heat Flux})}$$

$$WHTA = \frac{(3600 \text{ sec./hr.}) (QR) (W_a) (t_t') \cdot \rho_m}{(12 \text{ in./ft.}) F_{mb} Ma Q/A} \quad (113)$$

$$WHTA = \frac{(3600) (1779.8) (.012974) (164) (2083)}{(12) (0.769) (29) (35,384)}$$

$$WHTA = 2987.3 \text{ lbs.}$$

Total Reboiler-Condenser Weight

$$W_{RBC} = W_{rsh} + W_{rsi} + WHTA \quad (114)$$

$$W_{RBC} = 162.0 + 276.6 + 2987.3$$

$$W_{RBC} = 3425.9 \text{ lbs.}$$

5. Shaft

Data Input

Dsi

Dso

LRC (Normally taken as inner  
width of low pressure column)

LHTA

L<sub>R</sub>

Lext

ρ<sub>m</sub>

Output Program

Ls

W<sub>shaft</sub>

63 ASRP-2391

~~SECRET~~

**SECRET**

### ASD-TDR-63-665, Part I

#### Shaft Length

$$L_s = LRC + 12 (LHTA) + L_R + L_{ext} \quad (115)$$

$$L_s = 237.4 + 12 (6.64) + 24 + 60$$

$$L_s = 401.1 \text{ in.}$$

#### Shaft Weight

(Cylindrical Shaft)

$$W_{\text{shaft}} = \frac{\pi (D_{s_o}^2 - D_{s_i}^2) L_s \rho_m}{4(1728)} \quad (116)$$

$$W_{\text{shaft}} = \frac{\pi [(40.6)^2 - (40.0)^2] (401.0)(164)}{4 (1728)}$$

$$W_{\text{shaft}} = 1445.6 \text{ lbs.}$$

#### 6. Low Pressure Column Diffuser

<u>Data Input</u>		<u>Output of Program</u>
$R'_o$	$\omega$	$W_{\text{blades -c}}$
$t_D$	$\rho_L$	$W_{\text{seal-c}}$
$\rho_m$	$g_c$	$W_{\text{coll-c}}$
$R_D$	$r'_i \text{ seal}$	$W_{\text{PS}}$
$N_{\text{DSI}}$	$t \text{ seal}$	$W_{\text{DIFF-LPC}}$
$R_p$	$N_{\text{ssi}}$	
$S_1$	$b_o$	
$P_p$		

63 ASRP-2391

**SECRET**

**SECRET**

### ASD-TDR-63-665, Part I

#### Diffuser Passage Weight

(thin circumferential ring)

$$W_{\text{blades-c}} = \frac{2\pi R_o' R_D t_D \rho_m N_{DSI}}{1728} \quad (117)$$

$$W_{\text{blades-c}} = \frac{2\pi (57.51)(2)(0.325)(164)(2)}{1728}$$

$$W_{\text{blades-c}} = 73.1 \text{ lbs.}$$

#### Peripheral Seal Weight

(thick circumferential ring)

$$W_{\text{seal-c}} = \frac{\pi [(R_o')^2 - (r_{\text{seal}}')^2] t_{\text{seal}} \rho_m N_{ssi}}{1728} \quad (118)$$

$$W_{\text{seal-c}} = \frac{\pi [(57.51)^2 - (51.51)^2] (0.1875)(164)(2)}{1728}$$

$$W_{\text{seal-c}} = 44.6 \text{ lbs.}$$

#### Collector Rings Weight

(circumferential pipes outside diffuser)

$$\text{Wall thickness of pipe} = \frac{(\text{Pipe Pressure}) R_p}{S_1}$$

$$\text{Pipe Pressure} = P_p + \frac{(R_o')^2 \omega^2 \rho_L}{2 g_c (20736)}$$

$$W_{\text{coll-c}} = \frac{2\pi (R_o' + R_D + R_p) (2\pi R_p) \left( \frac{\text{pipe wall thickness}}{\rho_m} \right)}{1728}$$

**SECRET**

**SECRET**

ASD-TDR-63-665, Part I

$$W_{\text{coll-c}} = \frac{2\pi}{1728} (R'_O + R_D + R_p) (2\pi R_p) \left[ \frac{(\text{pipe pressure}) R_p}{S_1} \right] \rho_m$$

$$W_{\text{coll-c}} = \frac{2\pi}{1728} (R'_O + R_D + R_p) (2\pi R_p) \left[ \frac{\left( P_p + \frac{[R'_O]^2 \omega^2 \rho_L}{(20736) 2g_c} \right) R_p}{S_1} \right] \rho_m \quad (119)$$

$$\text{Since Area of Pipe} = \frac{G_T}{V_L \rho_L} = \frac{\pi R_p^2}{144}$$

$$\text{Therefore: } R_p = 12 \sqrt{\frac{G_T}{\pi V_L \rho_L}}$$

$$\text{Let } V_L = 50 \text{ ft./sec.}$$

$$G_T = (0.8765 \frac{\text{lb.-moles}}{\text{lb.-mole feed}}) (\frac{1 \text{ lb. mole feed}}{29 \text{ lbs.feed}}) (\frac{31.2 \text{ lbs.fluid}}{\text{lb.mole fluid}}) (\frac{2083 \text{ lbs.feed}}{\text{sec.}})$$

$$G_T = 1965 \text{ lbs./sec.}$$

Let the number of collector pipes = 12

$$\text{Flow per pipe} = \frac{1965}{12} = 163.8 \text{ lb./sec.}$$

$$\text{For each pipe } R_p = 12 \sqrt{\frac{163.8}{\pi (50) (67)}} = 1.53 \text{ in.}$$

Substituting numerical values and multiplying by the number of pipes,

$$W_{\text{coll-c}} = (12) \frac{4\pi^2 (164)}{1728 (33,333)} \left[ (57.51) (1.53)^2 + (2) (1.53)^2 + (1.53)^3 \right] \left[ 56.16 + \frac{(57.51)^2 (45)^2 (67)}{(20736) (2) (32.2)} \right]$$

$$W_{\text{coll-c}} = 75.6 \text{ lb.}$$

63 ASRP-2391

**SECRET**

# SECRET

## ASD-TDR-63-665, Part I

### Diffuser Pressure Shell

(not in computer program)

The diffuser pressure shell is mounted at the periphery of the low pressure column and is used to apply a casing pressure equal to the low pressure column peripheral pressure for proper seal operation.

This pressure shell is cylindrically shaped and its weight is determined by hoop tension in the shell wall.

$$\begin{aligned}
 W_{PS} &= (\text{thickness}) (\text{area}) (\text{density}) \\
 W_{PS} &= \left( \frac{P_p R'_O}{S_1} \right) (2\pi R'_O b_O) \left( \frac{\rho_m}{1728} \right) \\
 W_{PS} &= \frac{2\pi (R'_O)^2 b_O P_p \rho_m}{1728 S_1} \quad (120) \\
 W_{PS} &= \frac{2\pi (57.51)^2 (94.3) (56.16)(164)}{1728 (33,333)} \\
 W_{PS} &= 313.4 \text{ lbs.}
 \end{aligned}$$

### Total Low Pressure Column Diffuser Weight

$$\begin{aligned}
 W_{\text{DIFF-LPC}} &= W_{\text{blades-c}} + W_{\text{seal-c}} + W_{\text{coll-c}} + W_{PS} \quad (121) \\
 W_{\text{DIFF-LPC}} &= 73.1 + 44.6 + 75.6 + 313.4 \\
 W_{\text{DIFF-LPC}} &= 506.7 \text{ lbs.}
 \end{aligned}$$

### 7. Reboiler-Condenser Diffuser

Data Input				Output of Program	
$r'_O$	$R_D$	$S_1$	$g_c$	$W_{\text{blades-r}}$	
$t_D$	$N_D$	$P_p$	$r'_l \text{ seal}$	$W_{\text{seal-r}}$	
	$R_p$	$\omega$	$t_{\text{seal}}$	$W_{\text{coll-r}}$	
$\rho_m$		$\rho_L$	$N_{ssi}$	$W_{\text{DIFF-RBC}}$	

63 ASRP-2391

# SECRET

ASD-TDR-63-665, Part I

Diffuser Passage Weight

$$W_{\text{blades-r}} = \frac{2\pi r_o' R_D t_D \rho_m N_{Dsi}}{1728} \quad (122)$$

$$W_{\text{blades-r}} = \frac{2\pi (42) (2) (0.325) (164) (2)}{1728}$$

$$W_{\text{blades-r}} = 52.3 \text{ lbs.}$$

Peripheral Seal Weight

$$W_{\text{seal-r}} = \frac{\pi [(r_o')^2 - (r_{i\text{seal}})^2] t_{\text{seal}} \rho_m N_{ssi}}{1728} \quad (123)$$

$$W_{\text{seal-r}} = \frac{\pi [(42)^2 - (36)^2] (0.1875) (164) (2)}{1728}$$

$$W_{\text{seal-r}} = 32.6 \text{ lbs.}$$

Collector Rings Weight

$$W_{\text{coll-c}} = \frac{4\pi^2 \rho_m}{1728 S_1} (r_o' R_p^2 + R_D R_p^2 + R_p^3) \left[ P_p + \frac{(r_o')^2 \omega^2 \rho_L}{20736 (2 g_c)} \right] \quad (124)$$

Let  $V_L = 50 \text{ ft./sec.}$

$$G_T = (0.4424 \frac{\text{lb.-moles}}{\text{lb.-mole feed}}) (\frac{1 \text{ lb.-mole feed}}{29 \text{ lb. feed}}) (\frac{31.5 \text{ lb. fluid}}{\text{lb mole feed}}) (\frac{2083 \text{ lb. feed}}{\text{sec.}})$$

$$G_T = 1001 \text{ lb./sec.}$$

Let the number of collector pipes = 8

Flow per pipe =  $1001/8 = 125.1 \text{ lb./sec.}$

$$\text{For each pipe: } R_p = 12 \sqrt{\frac{125.1}{\pi (50) (67)}} = 1.31 \text{ in.}$$

63 ASRP-2391

# SECRET

# SECRET

ASD-TDR-63-665, Part I

substituting numerical values and multiplying by the number of pipes,

$$W_{\text{coll-r}} = (8) \frac{4\pi^2(164)}{1728(33,333)} [(42)(1.31)^2 + (2)(1.31)^2 + (1.31)^3] \\ [55.09 + \frac{(42)^2(45)^2(67)}{(20736)(2)(32.2)}]$$

$$W_{\text{coll-r}} = 16.4 \text{ lbs.}$$

(diffuser pressure shell is deleted here)

Total Reboiler-Condenser Diffuser Weight

$$W_{\text{DIFF-RBC}} = W_{\text{blades-r}} + W_{\text{seal-r}} + W_{\text{coll-r}} \quad (125)$$

$$W_{\text{DIFF-RBC}} = 52.3 + 32.6 + 16.4$$

$$W_{\text{DIFF-RBC}} = 101.3 \text{ lbs.}$$

## 8. Piping

(estimate inputed to program)

The system piping is estimated to weigh 870 lbs. and is determined as a linear function of separator inlet pressure.

## 9. Outer Casing

The computer program presently calculates the outer casing surrounding the air separator as a prolate spheroid formed by rotation of an ellipse about its axis. This shroud must sustain the casing pressure. Its weight has been deleted from the weight and volume results presented in this report.

63 ASRP-2391

# SECRET



# SECRET

ASD-TDR-63-665, Part I

## Data Input

$S_1$

$R'_O$  (maximum outer radius  
of rotor)

$P_{ENV}$

$P'_{CAS}$

$\rho_m$

$L_{ext}$

## Output of Program

$A_{CAS}$

AXIS

$t_{CAS}$

$W_{CAS}$

## Calculation Procedure

### Length of Major Axis

$$AXIS = L_s - 24 \quad (126)$$

Outer Casing Mean Surface Area (Ref. 57)

$$A_{CAS} = \frac{2\pi (R'_O + 0.5)^2}{144} + \frac{2\pi (R'_O + 0.5) \left(\frac{AXIS}{2}\right)}{144 \sqrt{1 - \frac{(R'_O + 0.5)^2}{\left(\frac{AXIS}{2}\right)^2}}} \quad (127)$$

$$\text{arc sin} \sqrt{1 - \frac{(R'_O + 0.5)^2}{\left(\frac{AXIS}{2}\right)^2}}$$

[ assumes  $(R'_O + 0.5) < AXIS/2$ , if not, data for  $R'_O + 0.5$  and  $AXIS/2$  must be reversed so that the square root of a negative number will not result, if

$$R'_O + 0.5 = \frac{AXIS}{2} \quad A_{CAS} = \frac{4\pi (R'_O + 0.5)^2}{144} \quad ]$$

63 ASRP-2391

# SECRET

# SECRET

## ASD-TDR-63-665, Part I

Thickness of Outer Casing

(hoop tension in wall of ellipsoid of revolution)

$$t_{CAS} = \frac{(P'_{CAS} - P_{ENV}) \left( \frac{AXIS}{4} \right)}{S_1} \quad (128)$$

Outer Casing Weight

$$W_{CAS} = \frac{A_{CAS} \rho_m t_{CAS}}{12} \quad (129)$$

### 10. Bearing Supports

The bearing supports are estimated to weigh 190.5 lbs.

Computer program is set up to obtain weight of bearing supports as a direct function of the sum of items 1-8.

### 11. Bearings

The bearings are estimated to weigh 190.5 lbs. The bearing weight must equal the weight of the bearing supports.

### 12. Separation Chambers (not rotating)

The separation chambers are estimated to weigh 500 lbs. Computer program is set up to obtain separation chamber weight as a direct function of chamber pressure.

### 13. Turbines (Estimate Inputed to Program)

The turbine weights are estimated as follows:

Product Stream Subcooling Turbine	-	50 lbs.
Recirculation Stream Turbine	-	50 lbs.
Low Pressure Column Turbine	-	50 lbs.

63 ASRP-2391

# SECRET

ASD-TDR-63-665, Part I

## Drive and Horsepower Requirements

<u>Data Input</u>	<u>Output of Program</u>
$L_{LPC}^{\square}$	HPF
$M_{LPC}$	HPT
$L_{RBC}^{\square}$	$W_{DRIVE}$
$M_{RBC}$	HPW
$W_a$	HPB
$Ma$	HPS
$\omega$	$C_{HP}$
	$g_c$

The computer program calculates the total air separator horsepower required and converts the figure to an estimate of drive weight. The fluid acceleration horsepower requirement is based on the power required to accelerate the liquids leaving the low pressure column and the reboiler-condenser to their respective peripheries where the maximum radius (low pressure column or reboiler-condenser) is used as the radial exit point.

### Fluid Acceleration Horsepower Required

(130)

$$HPF = (L_{LPC}^{\square} M_{LPC} + L_{RBC}^{\square} M_{RBC}) \left( \frac{W_a}{Ma} \right) \frac{\omega^2 (R'_O \text{ or } r'_O)^2}{2 g_c}$$

For the GD/A cycle,  $R'_O = 57.51$  in. and  $r'_O = 42$  in.

Therefore  $R'_O = 57.51$  in. is the proper radius.

Substituting numerical values:

$$HPF = [ (0.8765) (31.2) + (0.4424) (31.5) ] \left( \frac{2083}{29} \right) (45)^2 \frac{(57.51)^2}{2 (32.2)} \left( \frac{1 \text{ ft.}^2}{144 \text{ in.}^2} \right) (1.818 \times 10^{-3}) \frac{\text{hp}}{\text{ft.-lb./sec.}}$$

$$HPF = 3,900 \text{ hp}$$

63 ASRP-2391

# SECRET

## ASD-TDR-63-665, Part I

### Estimates of Other Horsepower Requirements

Seal Fluid Horsepower (HPS)	=	1000 hp
Windage Loss (HPW)	=	20 hp
Bearing Friction Loss (HPB)	=	50 hp

Total Horsepower Required:

$$\begin{aligned} HP_{REQ} &= HPF + HPS + HPW + HPB & (131) \\ HP_{REQ} &= 3900 + 1000 + 20 + 50 \\ HP_{REQ} &= 4970 \text{ hp} \end{aligned}$$

Drive Weight

The drive weight is estimated as a function of the air separator horsepower requirements.

$$\begin{aligned} W_{DRIVE} &= C_{HP} (HPT) & (132) \\ W_{DRIVE} &= (0.0345) (4970) \\ W_{DRIVE} &= 144.2 \text{ lbs.} \end{aligned}$$

Section 6 of this report presents the results of an air separator horsepower balance showing that considerable excess horsepower is available for work. As previously shown, the system horsepower requirement is 4970 hp. The available system horsepower calculations are presented as follows:

Low Pressure Column Turbine

$$HP_{LPC-T} = (L_{LPC} M_{LPC}) \left( \frac{W_a}{M_a} \right) \Delta H_T \left( 1.415 \frac{\text{hp-sec}}{\text{Btu}} \right) \quad (133)$$

The peripheral low pressure column pressure = 70.86 psia.

Assuming eighty per cent diffuser thermodynamic efficiency, the pressure at the turbine inlet is given by the following:

$$\begin{aligned} P'_L &= (0.8) \frac{(R'_O)^2 \omega^2 O_L}{(20736) (2g_c)} + 70.86 & (134) \\ P'_L &= (0.8) \frac{(57.51)^2 (45)^2 (67)}{(20736) (2) (32.2)} + 70.86 \\ P'_L &= 339.4 \text{ psia} \end{aligned}$$

Assuming the separation chamber is maintained at 70.86 psia and that the turbine thermodynamic efficiency is eighty per cent, the enthalpy change across the turbine is given by the following: 63 ASRP-2391

# SECRET

ASD-TDR-63-665, Part I

$$\Delta H_T = (0.8) (144) \frac{\Delta P}{\rho_L} (1.285 \times 10^{-3} \frac{\text{Btu}}{\text{ft.-lb.}}) \quad (135)$$

$$\Delta H_T = \frac{(0.8)(144)(339.4-70.86)(1.285 \times 10^{-3})}{67}$$

$$\Delta H_T = 0.595 \text{ Btu/lb.}$$

Therefore:

$$HP_{LPC-T} = [(0.8765)(31.2)] \left( \frac{2083}{29} \right) (0.595)(1.415)$$

$$HP_{LPC-T} = 1658 \text{ hp}$$

Recirculation Turbine

$$HP_{RBC-T} = (L_{RBC} M_{RBC}) \left( \frac{W_a}{M_a} \right) \Delta H_T (1.415 \frac{\text{hp-sec}}{\text{Btu}}) \quad (136)$$

The peripheral reboiler-condenser pressure = 69.79 psia.  
Assuming eighty per cent diffuser thermodynamic efficiency, the pressure at the turbine inlet is given by the following:

$$P'_L = (0.8) \frac{(r'_o)^2 \omega^2 \rho_L}{(20736) (2 g_c)} + 69.79 \quad (137)$$

$$P'_L = (0.8) \frac{(42)^2 (45)^2 (67)}{(20736) (2) (32.2)} + 69.79$$

$$P'_L = 213.0 \text{ psia}$$

Assuming the separation chamber is maintained at 69.79 psia and that the turbine thermodynamic efficiency is eighty per cent, the enthalpy change across the turbine is given by the following:

$$\Delta H_T = (0.8) (144) \frac{\Delta P}{\rho_L} (1.285 \times 10^{-3} \text{ Btu/ft.-lb.}) \quad (138)$$

$$\Delta H_T = (0.8) (144) \frac{(213.0-69.8)}{67} (1.285 \times 10^{-3})$$

$$\Delta H_T = 0.316 \text{ Btu/lb.}$$

63 ASRP-2391

# SECRET

**SECRET**

ASD-TDR-63-665, Part I

Therefore:

$$HP_{RBC-T} = [(0.4424)(31.5)] \left( \frac{2083}{29} \right) (0.316) (1.415)$$

$$HP_{RBC-T} = 448 \text{ hp}$$

Hydrogen Turbine

$$HP_{H-T} = (L_m M_H) \frac{W_a}{M_a} \Delta H_T (1.415 \text{ hp-sec./Btu}) \quad (139)$$

from Figure 152,

$$\Delta H_T \text{ for the hydrogen turbine} = 218 \text{ Btu/lb.-mole}$$

The enthalpy change for the reflux condenser heat exchanger = 965 Btu/lb.-mole

Since QC for the GD/A cycle = 643.3 Btu/lb.-mole feed,

$$L_m = \frac{643.3}{965} = 0.667 \text{ lb.-mole/lb.-mole feed}$$

and

$$\Delta H_T = (218 \text{ Btu/lb.-mole}) \left( \frac{1 \text{ lb.-mole}}{2.016 \text{ lbs.}} \right) = 108.1 \text{ Btu/lb.}$$

substituting:

$$HP_{H-T} = [(0.667)(2.016)] \left( \frac{2083}{29} \right) (108.1)(1.415)$$

$$HP_{H-T} = 14,750 \text{ hp}$$

Total Air Separator Horsepower Output

$$HP_{\text{OUTPUT}} = HP_{LPC-T} + HP_{RBC-T} + HP_{H-T} \quad (140)$$

$$HP_{\text{OUTPUT}} = 1658 + 448 + 14,750$$

$$HP_{\text{OUTPUT}} = 16,856$$

63 ASRP-2391

**SECRET**

**SECRET**

ASD-TDR-63-665, Part I

Net Horsepower

$$HP_{NET} = HP_{OUTPUT} - HP_{REQ} \quad (141)$$

$$HP_{NET} = 16,856 - 4970$$

$$HP_{NET} = 11,886 \text{ hp (EXCESS)}$$

15. Total Air Separator Weight

Sum of component weights, items 1 thru 8, and 10 thru 14.

$$\begin{aligned} WAS = & W_{HPC} + W_{LPC} + W_{KS} + W_{RBC} + W_{SHAFT} \quad (142) \\ & + W_{DIFF-LPC} + W_{DIFF-RBC} + \text{PIPING} + \text{BEARING SUPPORTS} \\ & + \text{BEARINGS} + \text{SEPARATION CHAMBERS} + \text{TURBINES} \\ & + W_{DRIVE} \end{aligned}$$

$$\begin{aligned} WAS = & 1390.7 + 824.1 + 95 + 3425.9 + 1445.6 \\ & + 506.7 + 101.3 + 870 + 190.5 \\ & + 190.5 + 500 + 150 \\ & + 144.2 \end{aligned}$$

$$WAS = 9749 \text{ lbs.}$$

$$\text{Weight/Unit Flow Rate} = WAS/Wa = 9749/2083 = 4.68 \frac{\text{lbs.}}{\text{lb./sec.}}$$

16. Air Separator Volume

The present method for calculating air separator volume is the sum of the volumes of end sections which are two truncated cones, plus a middle section which is a right circular cylinder.

Input

$R'_O$  (maximum column radius)

Output

$V_{cyl}$

63 ASRP-2391

**SECRET**

**SECRET**

ASD-TDR-63-665, Part I

<u>Input</u>	<u>Output</u>
LHTA	Vac
$b_{o\_HPC}$	$V_{wc}$
$b_{i\_LPC}$	VAS
$b_{o\_LPC}$	
$D_{SO}$	
$L_R$	
$L_{ext}$	

Cylindrical Volume

(Air separator right cylindrical volume section bounded by the maximum outer radius and axial distance between the high and low pressure column peripheral width extremities.)

$$V_{cyl} = \frac{\pi (R_o')^2}{1728} [ b_{o\_HPC} + L_R + b_{o\_LPC} ] \quad (143)$$

$$V_{cyl} = \frac{\pi (68.39)^2}{1728} [ 40.4 + 24 + 94.3 ]$$

$$V_{cyl} = 1349.5 \text{ ft.}^3$$

Air Inlet Side Truncated Conical Volume

(Air separator volume section bounded by maximum outer radius, shaft outer radius and distance between point of air inlet and extremity of high pressure column peripheral width.)

$$L_{ext} = 60, 48 \text{ included in } V_{ac} \text{ and } 12 \text{ in } V_{wc}$$

63 ASRP-2391

**SECRET**



**SECRET**

ASD-TDR-63-665, Part I

$$V_{ac} = \frac{\pi [12 (LHTA) - b_{oHPC} + 48]}{3 (1728)} \left[ (R'_O)^2 + \left(\frac{D_{so}}{2}\right)^2 + \left(\frac{D_{so}}{2}\right) R'_O \right] \quad (144)$$

(Ref. 23, p. 57)

$$V_{ac} = \frac{\pi [12 (6.64) - 40.4 + 48]}{3 (1728)} \left[ (68.39)^2 + \left(\frac{40.6}{2}\right)^2 + \left(\frac{40.6}{2}\right) (68.39) \right]$$

$$V_{ac} = 342.7 \text{ ft.}^3$$

Waste Exit Side Truncated Conical Volume

(Air separator volume section bounded by maximum outer radius, shaft outer radius and distance between point of waste exit and extremity of low pressure column peripheral width.)

$$V_{wc} = \frac{\pi [b_{iLPC} - b_{oLPC} + 12]}{3 (1728)} \left[ (R'_O)^2 + \left(\frac{D_{so}}{2}\right)^2 + \left(\frac{D_{so}}{2}\right) (R'_O) \right] \quad (145)$$

$$V_{wc} = \frac{\pi [237.4 - 94.3 + 12]}{3 (1728)} \left[ (68.39)^2 + \left(\frac{40.6}{2}\right)^2 + \left(\frac{40.6}{2}\right) (68.39) \right]$$

$$V_{wc} = 608.9 \text{ ft.}^3$$

Total Air Separator Volume

$$VAS = V_{cyl} + V_{ac} + V_{wc} \quad (146)$$

$$VAS = 1349.5 + 342.7 + 608.9$$

$$VAS = 2301.1 \text{ ft.}^3$$

$$\text{Volume/Unit Flow Rate} = VAS/W_a = 2301.1/2083 = 1.105 \frac{\text{ft.}^3}{\text{lb./sec.}}$$

63 ASRP-2391

**SECRET**

**SECRET**

ASD-TDR-63-665, Part I

(THIS PAGE IS LEFT INTENTIONALLY BLANK)

63 ASRP-2391

576

**SECRET**

**SECRET**

ASD-TDR-63-665, Part I

APPENDIX XVIII

COMMUNICATIONS FROM  
GENERAL DYNAMICS/ASTRONAUTICS

Two communications have been received from General Dynamics/Astronautics, the Associate Contractor responsible for the air frame. The first conveyed their preferred cycle to be used for separator weight calculations and the second contained the recommended design stresses for 95 per cent confidence weight calculations. This information was incorporated into the program.

1. Air Separation Cycle Studies

A theoretical cycle study was made using the General Dynamics/Astronautics boundary conditions for the stationary double column air separation cycle. The following conditions were specified:

- a. Air flow = 2083 lb./sec.
- b. Separator inlet pressure = 225 psia
- c. Product purity = 90% oxygen by weight
- d. Waste purity = 2% of oxygen by weight
- e. Feed air flow is considered a binary mixture of oxygen (20.9 mol per cent) and nitrogen (79.1 mol per cent) at saturated conditions.
- f. Waste pressure should be the highest absolute pressure level possible to avoid incurring large weight penalties in the preconditioning system.

Minor changes were made in the suggested specifications to accommodate the existing computer program and the work statement from ASD. Feed air flow is a ternary mixture to approximate actual conditions expected at the 70,000 to 100,000 ft. altitude. Argon cannot be ignored at the desired high product purity outlined in the work statement. Waste

63 ASRP-2391

**SECRET**

# SECRET

## ASD-TDR-63-665, Part I

pressure was mutually established at 56.5 psia to approximate the 54.5 psia pressure currently used by General Dynamics/Astronautics for one flight trajectory. Existing Linde computer data tapes can be used at this pressure, and this pressure permits an inlet pressure perturbation when compared to similar studies made by Linde for ASD as a subcontractor to The Marquardt Corporation.

### 2. Preliminary Weight and Volume Estimate

For the preliminary weight and volume calculations, General Dynamics/Astronautics suggested the following:

General material (ultimate) strength properties currently used for separator design at 95% confidence.

Titanium	--	150,000 psi
Aluminum	-	50,000 psi
Stainless	-	180,000 psi

Shear strength equals  $2/3$  times tensile strength. Factor of safety equals 1.5 based on ultimate strength. Minimum sheet thickness equals 0.010 in. except in tubular heat exchanger surfaces.

Volume requirements are predominantly fixed by the diameter limitation. Diameters larger than 16 ft. will require a major change in air frame.

63 ASRP-2391

578

# SECRET

LIST OF REFERENCES

1. Elements of Fractional Distillation, R. Robinson, C. S., and Gilliland, E. R., McGraw-Hill Book Company, Inc., 1950.
2. Linde Company Report LCR-61-186 (1961)
3. Linde Company Report LCR 62-17 (1962)
4. Miesse, C. C., Ind. Eng. Chem., 47, 1690 (1955)
5. Frazer, R. P., Eisenklam, P., Dambrowski, N. and Hasson, D., A. I. Ch. E. Journal, 8, 672 (1962)
6. Hinze, J. O., Appl. Sci. Res., A1, 273 (1948)
7. Hinze, J. O., A.I.Ch.E. Journal, 1, 295 (1955)
8. Lane, W. R., Ind. Eng. Chem., 43, 1312 (1951)
9. Ingebo, R. D., N.A.C.A. T.N., 3762 (1956)
10. Consiglio, J. A. and Slepcevic, C. M., A.I.Ch.E. Journal, 3, 413 (1957)
11. Dryden, H. L., J. Washington Acad. Sci., 25, 101 (1935)  
Dryden, H. L., and Kuethe, E., N.A.C.A. T.R., 342 (1929)  
Dryden, H. L., Schubauer, G. B., Mack, W. C. and Skramstad, H. K., N.A.C.A. T.R., 581 (1937)
12. Toro Bin, L. B., and Gauvin, W. H., Can.J. Chem. Eng., 189 (Dec., 1960)
13. Kolodzie, P. A. and Van Winkle, M., A.I.Ch.E. Journal, 3, 305 (1957)
14. Higbie, R., Trans. Am. Inst. Chem. Eng., 31, 365 (1935)
15. Geddes, R. L., Trans. Am. Inst. Chem. Eng., 42, 79, (1946)
16. Griffith, R. M., Chem. Eng. Sci., 12, 198 (1960)

63 ASRP-2391

ASD-TDR-63-665, Part I

17. Lewis, W. K., Ind. Eng. Chem., 28, 399 (1936)
18. Heat Transmission, McAdams, W. H., McGraw-Hill Book Company, Inc., New York, Third Edition, p. 330, 1954.
19. "Saturated Vapors on Inclined Circular Cylinders," Jacob, M., and Hassan, E., Transactions of the ASME, 80, 887-894 (1958)
20. Saturation Properties of Oxygen Nitrogen Mixtures, Yendall, E. F. and Olzewski, W. J., A.S.D. Technical Report 61-536, September, 1961.
21. International Critical Tables, Vol. 4
22. Freon Technical Bulletin B-2, E. I. DuPont de Nemours and Co., Inc., Copyright, 1957
23. Chemical Engineer's Handbook, Perry, J. H., McGraw-Hill Book Company, Inc., New York City, New York, p. 363, (1950)
24. Transport Phenomena, Bird, R. B., Stewart, W. E., and Lightfoot, E. N., John Wiley & Sons, Inc., New York, London, p. 42-47
25. "Promotion of Dropwise Condensation of Several Pure Organic Vapors," Bobco, R. P., ASME paper 57-S-2, 1957
26. "Dropwise Condensation and Heat Transfer Rates," Topper, L. and Baer, E., Journal of Colloid Science, 10, p. 225-226, 1955
27. Merte, H. and Clark, J. A., Journal of Heat Transfer, 83C, p. 233-243, 1961
28. "Heat Exchange Between a Copper Surface and Liquid Hydrogen and Nitrogen", Mulford, R. N., Nigon, J. P., Dash, J. G., Keller, W. E., LAMS-1443, Los Alamos Scientific Laboratory, Los Alamos, New Mexico
29. P. H. D. Thesis, Mikhail, Dept. of Chem. Eng., Imperial College, Royal College of Science, England, 1952
30. "Heat Transfer To Boiling Liquid Oxygen and Liquid Nitrogen," Haselden, G. G., Peters, J. J., Trans. Inst. Chem. Engrs, 27, p. 201-208, 1949

63 ASRP-2391

ASD-TDR-63-665, Part I

31. "The Nucleate and Film Boiling Curve of Liquid Nitrogen at One Atmosphere," Flynn, T. M., Draper, J. W., Roos, J. J., Paper L-6, 1961 Cryogenic Engineering Conference, Univ. of Michigan, Aug. 15-17, 1961.
32. "Echanges Thermiques dans L'azote et L'hydrogene Bouillant sous Pression," Roubeau, R., Service de Physique Corpusculaire a Haute Energie, C. E. N., Saclay, France
33. Linde Data, Outside Vertical Tube (7/8" D x 3 1/8" Long), Eng. Laboratory Memorandum 370
34. Linde Data, Linde Boiling Surface
35. Linde Data, Jenkins, A. C., Boiling on a Vertical Cylinder of Untreated Aluminum (1" D x 6" Long)
36. "Proposed Correlation of Data for Isothermal Two-Phase, Two-Component Flow in Pipes," Lockhart, R. W., Martinelli, R. C., Chemical Eng. Progress, 45, p. 39, 1949
37. A Compendium of the Properties of Materials at Low Temperature (Phase I) - Part I - Properties of Fluids, Johnson, V. J., WADD Report, October, 1960
38. Applied Statistics for Engineers, Volk, W., McGraw-Hill Book Company, Inc., New York, Toronto, London, 1958
39. Introduction to Numerical Analysis, Hildebrand, F. B., McGraw-Hill Publishing Co., Inc., New York, p. 233-239, 1956
40. Diffuser Studies with Single and Two-Phase Flow, Report No. TM-62-1, Schneits, G. R., Jet Propulsion Center, Purdue Univ., April, 1962
41. "Flow of Steam-Water Mixtures in a Heated Annulus and Through Orifices," Hoopes, J., Jr., A.I.Ch.E. Journal, 3, p. 268, June, 1957
42. Materials in Design Engineering, 56, No. 5, p. 104, Oct., 1962
43. National Bureau of Standards Report No. 6791, NBS Project 8130-12-81531
44. Anderson, Sc. D. Thesis, MIT, 1954 63 ASRP-2391

ASD-TDR-63-665, Part I

45. Ruckenstein, Zh. prikl. Khim., 30, p. 1012, 1957
46. Foss, et. al., A.I.Ch.E. Journal, 4, p. 231, 1958
47. Gilbert, Ch. Engr. Sci., 10, p. 243, 1959
48. "Ball Bearing Survival," Shube, E., Machine Design, July 19, 1962
49. Real-Slim Ball Bearing, Kaydon Catalog
50. "Thermodynamic Properties of Freon-114", Benning, A. F., and McHarness, R. C., E. I. DuPont de Nemours & Co., Wilmington, Delaware; 1944
51. "Thermodynamic Properties of Freon-12," E. I. DuPont de Nemours & Co., Wilmington, Delaware; 1955
52. Handbook of Refrigeration Engineering, Woolrich, W. R., and Bartlett, L. H., (Third Edition); D. Van Nostrand Co., Inc., New York; pp. 158-173, 1948
53. "Vapor-Liquid Equilibrium," Hala, E., et. al. Pergamon Press, New York City, New York; p. 38, 1958
54. Mass Transfer Operations, Treybal, R. E., McGraw-Hill Book Company, Inc., New York City, New York, p. 22, 1955
55. "Lennard-Jones Force Constants From Viscosity Data," Flynn and Thodos, A. E. Ch.E. Journal, 8, 3, p. 362 (July, 1962)
56. Strength of Materials. Part II - Advanced Theory and Problems, Timoshenko, S., D. Van Nostrand Co., Inc., Toronto, New York, London, p. 245-253, 1951
57. Elements of Strength of Materials, Timoshenko, S. and MacCullough, G. H., D. Van Nostrand Co., Inc., Toronto, New York, London, p. 57-91, 1949



ASD-TDR-63-666, Part I

- 58. "Vapor-Liquid Equilibria of Nitrogen-Argon-Oxygen Mixtures,"  
Latimer, R. E., A.I.Ch. E. Journal, March, 1947
- 59. Mathematical Tables from Handbook of Chemistry and  
Physics, Hodgman, C. D., Chemical Rubber Publishing Co.,  
Cleveland, Ohio, p. 260, 1941

63 ASRP-2391

**UNCLASSIFIED**

**UNCLASSIFIED**